NASA TECHNICAL NOTE

NASA TN D-3091




NASA TN D-3091

# GODDARD SPACE FLIGHT CENTER CONTRIBUTIONS TO THE COSPAR MEETING - MAY 1965

*Goddard Space Flight Center*
*Greenbelt, Md.*


NATIONAL AERONAUTICS AND SPACE ADMINISTRATION • WASHINGTON, D. C. • JULY 1966

# GODDARD SPACE FLIGHT CENTER

## CONTRIBUTIONS TO THE COSPAR MEETING – MAY 1965

Goddard Space Flight Center
Greenbelt, Md.

NATIONAL AERONAUTICS AND SPACE ADMINISTRATION

For sale by the Clearinghouse for Federal Scientific and Technical Information
Springfield, Virginia 22151 – Price $7.00

GODDARD SPACE FLIGHT CENTER
CONTRIBUTIONS TO THE COSPAR MEETING

MAY 1965

## FOREWORD

The Committee on Space Research (COSPAR) held its fifth International Space Sciences Symposium in May 1965 in Buenos Aires, Argentina. This volume presents a collection of papers co-authored or presented at the meeting by personnel of NASA's Goddard Space Flight Center, Greenbelt, Maryland.

There has been no attempt to arrange the papers in any particular sequence. Their publication within a single NASA Technical Note, rather than as separate ones, was prompted by recognition of the growing need for more inter-disciplinary communication. It is to be hoped, therefore, that the readers of any of these papers will find material of interest in all of them.

Technical Information Division
Goddard Space Flight Center
Greenbelt, Maryland

CONTENTS

# RELATIVE ADVANTAGES OF SMALL AND OBSERVATORY TYPE SATELLITES

by
G. H. Ludwig
*Goddard Space Flight Center*

Both the relatively small Explorer and the large Orbiting Observatory classes of scientific satellites have advantages which need to be considered carefully when a new space experiment is to be performed. The small satellite offers greater choice in tailoring the orbit to the experiments. The orbital, orientation, telemetry, and operational needs of a particular experiment are not usually compromised to as large an extent because fewer experiments are involved. The smaller size simplifies the electrical, magnetic, and radiated interference problem, since fewer operating components are involved. It provides greater ease in testing and scheduling, and permits a shorter pre-launch lead time.

The larger observatory permits the conduct of more complex or larger numbers of related experiments for the more detailed study of the co-relationships between the numerous space phenomena. Since it is less highly integrated, standard experiment/spacecraft interfaces can be defined to simplify the experiment design and integration problems. The larger size permits the use of higher capacity and more flexible data systems and more precise active orientation systems. Operational efficiency is higher, since the data from a large number of experiments can be recorded and processed simultaneously. It is concluded that both types should continue to be used to meet the varied requirements of the space sciences program.

## INTRODUCTION

The earth satellites presently being used for space science investigations can be grouped into two broad classes. The first is the relatively small satellite typified by the Explorer series. It includes the Explorer, Vanguard, Solar Radiation (S.R.), Injun, Traac, Starad, Lofti, Rados, and International Program (Ariel, Alouette, and San Marco) satellites. The second class consists of the larger observatories, and includes the Orbiting Solar Observatories (OSO), Orbiting Geophysical Observatories (OGO) and Orbiting Astronomical Observatories (OAO). An Advanced Orbiting Solar Observatory (AOSO) is also being developed. The relative merits of the two classes have been the subject of many debates. This paper is an attempt to summarize some of the more significant advantages of each type.

and third observatories (OGO-I and OSO-II) have been launched, and it is becoming possible to discuss statistically significant actual experience and performance. To illustrate some of the arguments, reference will be made to several specific satellites. The Interplanetary Monitoring Platform (IMP-I, 1963-46A, or Explorer XVIII) typifies the small Explorer class satellite built within a NASA laboratory. A satellite built at another government laboratory is typified by the Naval Research Laboratory Solar Radiation satellite (1964-01D). The University of Iowa Injun series is the only presently existing satellite series built entirely at a university laboratory, and will be represented by Injun IV (1964-76B). The observatory class will be illustrated by OGO-I (1964-54A).

## WEIGHT AND VOLUME CAPABILITY

The Explorer class satellite weights have ranged from 7 kilograms for the atmospheric drag balloon (Explorer IX) to 14 kilograms for the early energetic particles Explorers, to 184 kilograms for the Atmospheric Structures Explorer XVII. Only three have weighed more than 120 kilograms as is shown in Figure 1. The observatory weights have ranged from 208 kilograms for OSO-I to 488 kilograms, for OGO-I. The first OAO will weigh about 1600 kilograms. Weight has historically been the primary limiting factor when choosing the experiments for each spacecraft mission because of launch vehicle limitation. The large weight carrying capability of the observatories becomes especially significant if individual experiments are very heavy, and if it is necessary to conduct a large number of experiments at the same position in space at the same time to correlate various space phenomena.

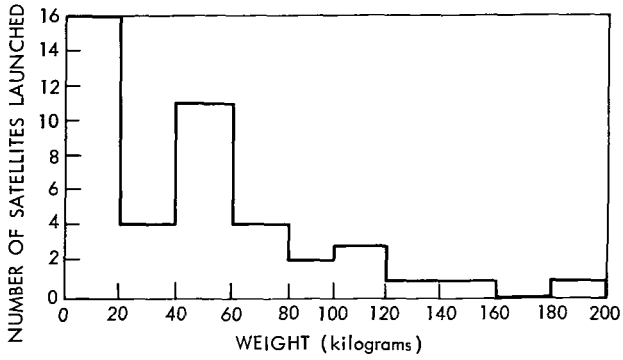


Figure 1—The number of small scientific satellites successfully launched as a function of weight. All space science earth orbiting satellites launched to the end of 1964 for which weights were announced are included. Vanguard I and six tetrahedron satellites, each weighing less than 2.5 kg. are included although they are not normally included in the Explorer class. Communication, navigation, and weather satellites are not included.

Volume for experiments has always been secondary in importance, and will probably continue to be so, except for experiments requiring large optical systems or apertures. Presumably, these large optical, near-optical, and radio-astronomy experiments can be performed only on the larger observatories.

On the other hand, large weight and volume may be a liability for some experiments. When searching for relatively rare elementary particles, the large mass of an observatory can create an unacceptable background flux of secondary particles. A large volume may complicate the outgassing problem, causing a local contamination for atmospheric and ionospheric experiments.

## ATTITUDE CONTROL

Numerous experiments require some form of attitude control. Some of these requirements can be met on both small and large spacecraft, while others are more feasible with one class or the other.

There are many possible types of attitude control, each having interest for certain classes of experiments.

### Non-oriented and Random Orientation

Some experiments are intended to observe an isotropic field, and therefore require no orientation. It is possible to perform some measurements of a non-isotropic field if the instantaneous orientation of the non-oriented spacecraft is known. Other experiments may actually prefer a random tumble to obtain data statistically integrated over the entire sphere. These missions are best performed by small satellites, since all sets of experiments flown on larger observatories will almost always contain sub-sets which require orientation. In addition the problems of providing adequate solar power and acquiring data telemetered to the earth from tumbling spacecraft would be more serious for the larger observatories where higher capacity data systems are normally employed.

### Spin Orientation

Spin orientation is acceptable or preferable for many experiments, and is easy to achieve for small satellites, since most of the smaller unguided final rocket stages require spinning for stability. A separate spin subsystem would have to be added for the observatories. Observatories can be made to spin satisfactorily as demonstrated by the actual operation of OGO-I.

### Earth Orientation

Earth orientation is desired for many spacecraft to permit use of high-gain antennas for high-capacity data transmission; and some experiments require earth orientation either toward or away from the earth. Some techniques, such as gravity-gradient stabilization, can be used on either large or small satellites. Others, such as the use of horizon scanners and active torquers of various types, require use of the larger observatories because of their complexity. This results from the fact that active attitude control system weights do not, in general, scale linearly with total spacecraft weights. The smallest active earth orientation system has a weight which is too large for the smaller satellites.

### Magnetic Field Orientation

Alignment of sensors at an angle fixed relative to the local magnetic field is desirable for certain classes of experiments designed to investigate the low energy particles whose motions

are controlled by the earth's magnetic field. Such experiments can be performed near the earth most easily on small satellites, since the controlling torques are small and can be produced directly by the magnetic field, as was done on the Injun satellites. If experiments of this type are to be performed at higher altitudes, where the earth's field is weaker, active attitude control systems using sensitive magnetic field sensors and active torquing devices would be necessary. The active system would probably require a larger satellite. Actually, these experiments can be performed at the cost of somewhat increased instrumentation and data processing complexity, by appropriate sampling of scanning detectors, if the direction of the field is measured concurrently.

### Direction of Motion Orientation

Orientation with respect to the direction of motion is desirable for experiments which investigate particles whose velocities are lower than or comparable with that of the spacecraft. Of course, some of these experiments can be performed on spinning satellites of all sizes by the use of appropriate time sampling techniques, but continuous orientation of the sensors along the satellite velocity vector or in the orbital plane requires the use of an active orientation system in a larger satellite.

### Sun Orientation

Sun orientation is desirable to simplify the collection of solar energy by solar cells or reflectors, and many experiments require solar orientation. A few solar orientation systems, such as a torqued spin-axis system, are suitable for use on small satellites. Some solar experiments can be performed by careful timing of the observations from a spinning satellite. It is likely, however, that solar experiments requiring medium to high pointing accuracy or solar disc scanning will continue to be located on the larger observatories to take advantage of their higher capability orientation system.

### Celestial Inertial Orientation

Many astronomical experiments require orientation toward a fixed point on the celestial sphere, and a capability for moving to a new point between observations. Small spin-stabilized satellites are acceptable for some experiments requiring low pointing accuracy, for example, gamma ray astronomy, where the sources are very weak and integration over a large solid angle is necessary. Most of these experiments, however, require an active orientation system and, therefore, the larger observatories.

Combinations of several different orientation schemes lead, in general, to greater complexity and larger spacecraft. The OSO is spin and sun oriented. The OGO employs earth, sun, and orbit plane orientation, while OAO will contain a highly accurate directable celestial inertial system and a low accuracy sun orientation system.

In summary, passive orientation techniques are useful on small satellites, and some of them are better suited to small satellites than large ones. A few simple active systems are being used

or considered for small satellites. For example, Iowa has used an active magnetic field orientation system on Injun. Any but the simplest active system requires the use of larger observatories.

## DATA HANDLING, STORAGE, AND TELEMETRY

As in the case of the active attitude control systems, data handling, storage, and telemetry systems do not scale linearly with spacecraft weight. Doubling the number of time multiplexer inputs, for example, requires only one additional stage in the multiplexer counter. In addition, the capability of electronics equipment increases roughly with volume, or the cube of linear dimensions, while the container and other structural weight increases more nearly as the surface area, or the square of linear dimensions. Therefore, doubling the data-handling system weight permits more than doubling the number of functional circuits. For these reasons, the capability of the data system per pound of experiments tends to be larger for larger spacecraft.

Experiments in space are designed to measure fields which may be functions of time and position from a location which is, in turn, moving. The ability to make a meaningful mapping of that field depends almost entirely on the information bandwidth, assuming that adequate freedom in selection of sampling formats and times exists. With present data systems, this freedom usually exists in both large and small satellites. To illustrate, Figure 2 shows the telemetry format for IMP-I and Figure 3 shows the format for the main commutator in OGO-I. In addition to this main commutator, OGO has a 128-word sub-commutator for slowly varying measurements and a flexible format commutator for a relatively few rapidly varying measurements. Both IMP and OGO are able, by proper assignment of the many telemetry words to the various experiments, to meet a very large number of the sampling sequence needs.

Thus, the ability of an experiment to effectively map a field depends most directly on the information bandwidth available for that experiment. Table 1 is a tabulation of the bandwidth per experiment and bandwidth per unit experiment weight for several representative satellites. It can be seen that, from the standpoint of the data system alone, it is presently possible to perform a more comprehensive and detailed mapping of a property of space on the larger spacecraft.

## POWER

The total amount of solar power obtained on a satellite per experiment unit weight is not necessarily a function of satellite size. Power available from an array is very nearly a linear function of both array area and weight. Non-oriented satellites require more area to obtain a given power because the sun does not always illuminate the array normally. On the other hand, the large actively oriented satellites require electrical power to keep the arrays directed toward the sun. Table 2 shows the power available to experiments in the four representative spacecraft.

Since power for long periods of operation has always been expensive in terms of spacecraft weight, considerable effort has been expended to design electronic circuits to operate on very low power. The same techniques have been employed on satellites of all sizes.

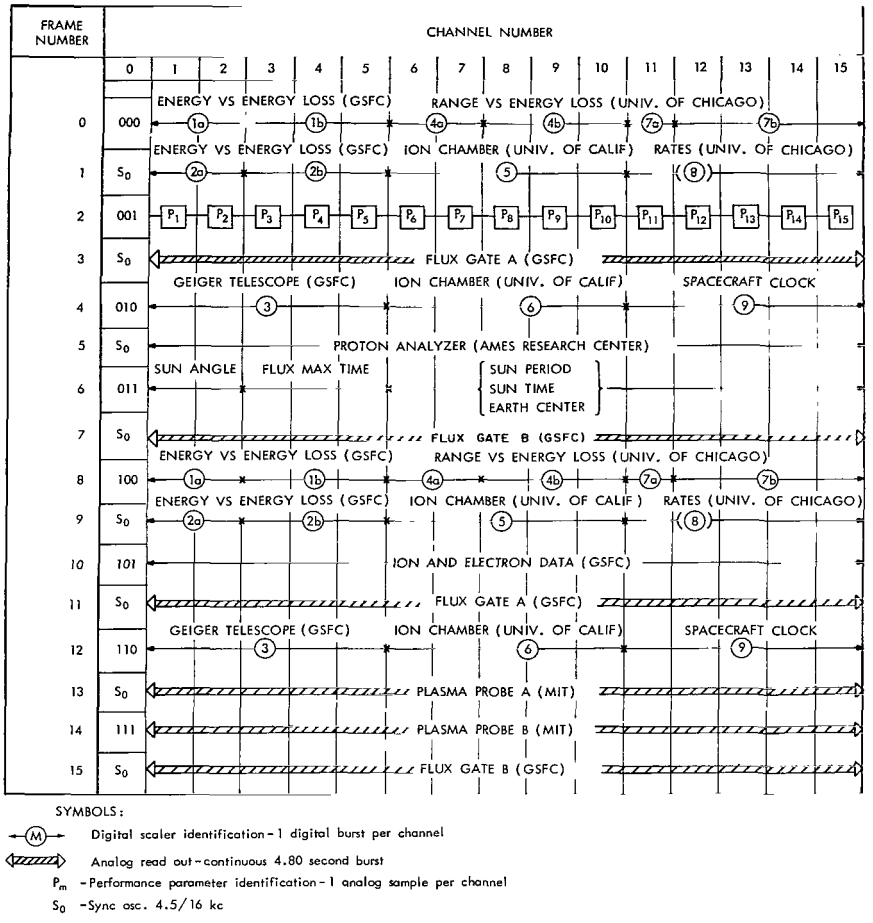


Figure 2—The IMP-I (Explorer XVIII) PFM telemetry data format. This is a modified tone burst-blank system in which the tone frequency contains the information. One burst-blank period (0.32 sec) makes one channel. Sixteen channels (5.12 sec) make one frame. Sixteen frames (81.92 sec) makes one sequence. The tone burst is normally used to send digital information (8 quantizing levels or 3 binary bits per burst) or analog samples (1% accuracy). In six of the frames the blanks are eliminated so that analog quantities can be transmitted continuously for 4.80 second periods.

## INTERFERENCE TO EXPERIMENTS

Many experiments are susceptible to interference from other experiments and from the spacecraft. This includes interference in many forms, such as electrical interference from oscillations and transients in operating systems, magnetic interference from ferromagnetic materials and electrical current loops, mechanical interference from moving masses, radioactive interference from calibrating sources, particle interference from secondary interactions of cosmic rays in the mass of the spacecraft, and interference from the gases released from the spacecraft. Obviously, the smaller the spacecraft and the fewer the experiments, the more manageable is the interference problem. Interference is combated on the larger observatories where many diverse experiments

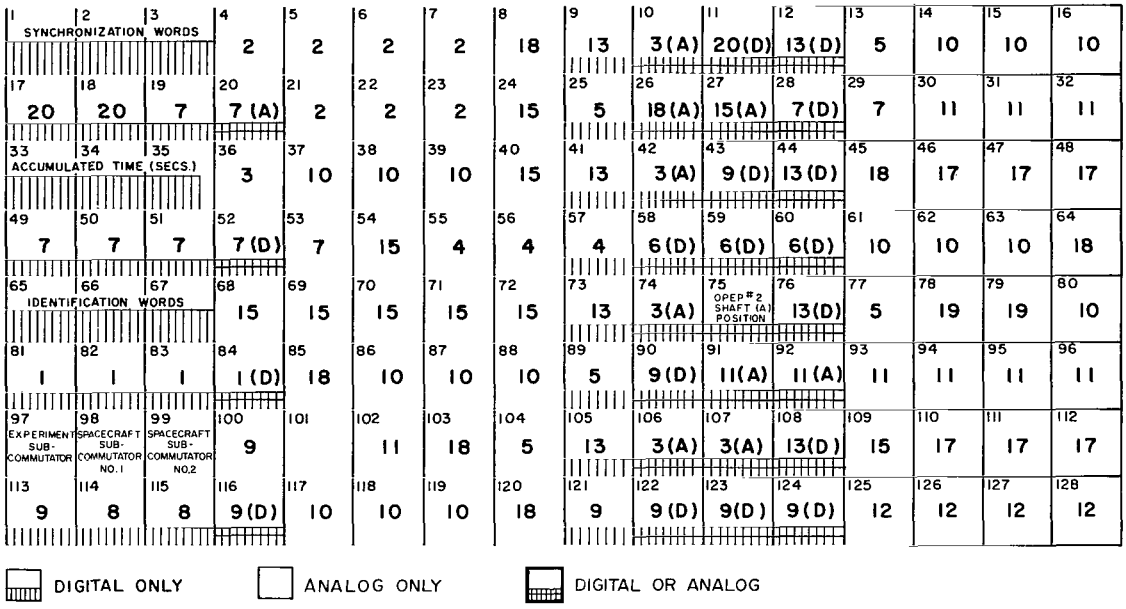


Figure 3—The OGO-I main frame PCM telemetry data format. The number in the upper left hand corner of each box denotes the word number. The number in the center of the box designates the OGO-I experiment number using that word. The letter following some experiment numbers indicates whether the analog or digital option was chosen. Nine binary bits make one word. A total of 128 words make one frame, and 128 frames (128 sub-commutator words) make one sequence. Bit rates are 1000, 8000, or 64,000 bits per second (1, 8, or 64 sequences per 0.868 second).

Table 1

Telemetry Capabilities of Representative Spacecraft.

| Spacecraft Identification | Total Spacecraft Weight (kg) | Experiment Weight (kg) | Experiment/ Spacecraft Weight Ratio | Number of Major Experiments | Maximum Real-Time Equivalent Bit Rate (bits per sec.) | Max. Bit Rate per Experiment (BPS per experiment) | Max. Bit Rate per Experiment Weight (BPS per kg) |
|---|---|---|---|---|---|---|---|
| 1965-76B, Injun IV | 34.6 | 8.4 | 0.243 | 6 | 144 | 26.0 | 17.2 |
| 1964-01D, S.R. | 45.4 | 10.9 | 0.240 | 6 | 280 | 46.7 | 25.7 |
| 1963-46A, IMP-I (Explorer XVIII) | 62.5 | 16.1 | 0.258 | 7 | 23.6 | 3.37 | 1.47 |
| 1964-54A, OGO-I | 488 | 87.0 | 0.178 | 25 | 64,000 | 2560 | 735 |

Note 1. An acceptable error rate can still be obtained if the Injun IV bit rate is increased by a factor of 8 and the IMP-I equivalent bit rate is by a factor of 4.

Note 2. The maximum telemetry ranges for Injun IV and solar radiation satellites are less than 4,000 km. The maximum ranges for IMP-I and OGO-I are 200,000 and 150,000 km respectively. The maximum bit rates quoted are usable at the maximum ranges in all cases.

Table 2

Experiment Power on Representative Spacecraft.

| Spacecraft Identification | Total Spacecraft Power (watts) | Experiment Power (watts) | Power per Experiment (watts) | Power per Experiment Weight (watts per kg) |
|---|---|---|---|---|
| 1965-76B, Injun IV | 5.97 | 2.89 | 0.482 | 0.344 |
| 1964-01D, S.R. | 3.39 | 1.89 | 0.315 | 0.174 |
| 1963-46A, IMP-I | 38.0 | 9.68 | 1.38 | 0.601 |
| 1964-54A, OGO-I | 260.0 | 60.0 | 2.40 | 0.690 |

are carried by the use of booms to isolate detectors from the rest of the observatory, and by careful interference engineering and control. With great care, the interference levels on the larger observatories can be made acceptable for a large number of experiments. Some of the most sensitive ones, however, may have to be performed on special small satellites.

## PROGRAM COORDINATION AND EASE OF INTEGRATION

Small satellites are presently easier to coordinate and integrate, primarily because of the smaller number of individuals involved. The amount of this effort which experimenters are obliged to perform varies considerably, and is influenced strongly by the quality of the design and specification of the electrical, mechanical, and thermal interfaces between the experiments and spacecraft. It is also affected by the interfaces between the operations and data-processing groups and the experimenters. Standardization and careful specification of these interfaces before experiment design begins greatly simplifies the coordination, integration, and operations efforts. In principle, the standard observatory concept could lead to a significant reduction in the liaison requirements, since the same observatory and operational systems are used repeatedly, permitting careful specification and development of familiarity with the system by the experimenters. The smaller spacecraft are unable to achieve this goal because of the continuing pressure to specialize the spacecraft to better meet the needs of the experiments. It is common on these spacecraft to design the experiments, spacecraft, and data processing systems concurrently, so that the interfaces evolve in the process of the work. This leads to a significant amount of additional liaison effort.

This advantage of the larger observatories is more or less offset by the fact that they involve much larger numbers of personnel. This tends to lead toward a breakdown of the personal working relationships and a greater formalization of the liaison. Realization of the advantage outlined above for the observatories depends on the degree to which a personal, informal working relationship can be established between the experimenters and integration and operations groups, while maintaining the coordination necessary to ensure that the scientific objectives of any one experiment are not jeopardized by other experiments or the spacecraft.

The degree of involvement of the experimenter can lie anywhere between two extremes. In the first, that of an experimenter who completely designs, builds, tests, integrates, and launches his own experiments, these efforts are performed within his own organization by personnel under his direct control. This condition is approached in the conduct of many balloon and sounding rocket programs. In the other extreme, the experimenter designs his experiment according to a carefully written set of interface specifications, delivers it to an integration crew at a central laboratory, and appears there occasionally to check the calibration.

Operation after the launch can be divided into two similar extremes. In the former, the experimenter operates his own receivers and other ground equipment and carries his flight records to his own analysis group (or analyzes them completely himself). In the latter, a ground system is established and operated by a central laboratory, and the raw data are delivered to the experimenters in directly usable form.

Most actual satellite programs fall somewhere between these two extremes, and a considerable amount of liaison between the experimenters and other groups is necessary. The arrangement which is preferred by various experimenters depends to some extent on those individuals' personalities and the extent of their other responsibilities. Advantages are often cited for both extremes. The advocates of the completely self-contained operation feel that they can directly influence all aspects of the project, and are less subject to the whims and shortcomings of a large number of strangers or near strangers. In addition, many of the experimenters located at universities feel it desirable to have their students become intimately familiar by direct experience with many different aspects of their projects, including the pre-launch integration and testing and in-flight operations.

The advocates of the central integration, testing, launching, and operations facility, feel that this gives them more time for their primary interest, the development of new experiments and analysis of their data. They feel that they are able to conduct a larger number of experiments and derive more results per unit time than experimenters who concern themselves with all of the technical details of the spacecraft subsystems and ground receiving stations. Since these two different approaches stem from strongly felt genuine differences of opinion on the parts of the members of the scientific community, it is doubtful whether a single method of operating satellite programs can or should ever be found. Presently there seems to be a continued acceptance of both general methods of operation as evidenced by the recent approval of the university small satellite program on the one hand and the continued scheduling of the large observatories on the other.

## ORBITAL REQUIREMENTS

The small satellite offers a definite advantage in meeting the requirements of the experiments for specific individual orbits. A satellite containing a single experiment can be launched into an optimum orbit for that experiment. A large observatory carrying many experiments must be launched into an orbit which best meets the needs of as many experiments as possible. It will, in general, be optimum for less than the entire set of experiments. In the limit, as the number of

spacecraft per year became very large, this distinction would disappear, since large numbers of experiments would require the same orbit. It is doubtful whether this condition will ever be reached. It is true, however, that there are now sufficiently large numbers of experiments requiring roughly similar orbits to justify the use of multi-experiment observatories. But it is also true that small satellites are necessary for some experiments requiring specialized orbits.

## UTILIZATION OF GROUND FACILITIES

The ground facilities, including tracking and data acquisition stations, control centers, orbital computation facilities, and communications and data relay links can be used more efficiently for larger observatories. It requires considerably more equipment and personnel to acquire data from a number of small satellites than from a single large one containing the same experiments. The same holds for tracking and orbit computation. In fact, it may be easier to compute an accurate orbit for a single large satellite than for a single small one, since the large one can include higher powered and higher performance tracking beacons and transponders. The control center and communications links can be operated for a large observatory with less expenditure of resources than for an equivalent number of small satellites, assuming they have comparable command and other operational capabilities.

The data processing facility utilization is not quite as straightforward. It may be argued that the data processing rate would depend only on the telemetered bit rate, in which case a ranking in terms of satellite class would not be meaningful. But this neglects editing, tape evaluation, and computer loading times, which are more nearly proportional to the number of data acquisition station recordings than to the number of telemetered data bits. Therefore, the observatories with their high data rates also offer an advantage in the utilization of the data processing facilities.

## RELIABILITY

The electronic subsystems complexity is higher for large observatories than for small satellites. Thus, it might seem that a small satellite would operate longer than an observatory. And it might appear likely that more data would be obtained before failure from a number of small satellites than from the same number of experiments in an observatory. This seeming advantage of the small satellites is offset by several factors.

1. The more complex observatory subsystems can be divided into partially or completely redundant subsystems, such that a large fraction of the goals can be achieved even if a number of failures occurs.

2. A larger observatory can carry a large capability command system, allowing the correction of many problems as they occur.

3. Since an observatory is not tailored to each load of experiments to as large a degree as the small satellites, its subsystems can be used repeatedly without essential modification.

The reliability of a system increases as it evolves through a long use history, as weaknesses are corrected, and as production, testing, and operational personnel become more familiar with it.

4. Since the observatory systems are designed for repeated use, more effort can be expended per unit complexity in their development.

These factors act in such a manner that there is no clear-cut reliability difference at present between individual small and large observatories. There is some indication, however, that the observatories may emerge as the more reliable of the two.

## CONCLUSIONS

The discussions above have indicated that each of the two main classes of scientific earth satellites has distinct advantages. These are summarized in Table 3. A cross in one column indicates that that satellite class generally has an advantage in the category listed. Where neither class has a clear advantage, a dash is shown. Question marks indicate that insufficient information exists to properly evaluate the category.

It is therefore obvious that the long range space science program will continue to require the use of both the small satellites and large observatories in order to meet the needs of the large variety of experiments and researchers.

Table 3

Comparison between Small Satellites and Large Observatory Stations.

| Category | Small Satellite | Large Observatory |
|---|---|---|
| Ability to launch large or heavy experiments, or many related experiments | | X |
| Applicability of simple orientation techniques | - | - |
| Applicability of high capability active orientation techniques | | X |
| Information rate | | X |
| Availability of electrical power | - | - |
| Experiment interference | X | |
| Ease of integration | ? | ? |
| Program coordination, testing, scheduling | X | |
| Ability to meet orbital requirements of all experiments | X | |
| Utilization of ground facilities | | X |
| Reliability | ? | ? |

# THE NIMBUS I METEOROLOGICAL SATELLITE—GEOPHYSICAL OBSERVATIONS FROM A NEW PERSPECTIVE

by

W. Nordberg

*Goddard Space Flight Center*

The Nimbus I meteorological satellite which was launched into a nearly polar sunsynchronous orbit and was fully earth oriented carried a set of very high resolution television cameras, a directly transmitting television camera of lesser resolution and a High Resolution Infrared Radiometer. The observations of detailed cloud features during daytime, the direct transmission of such observations to local weather station via an Automatic Picture Transmission system and the measurement and pictorial presentation of earth, water and cloud temperatures from orbital altitudes at nighttime with the infrared radiometer have provided geophysical and meteorological measurements from a truly global perspective. Temperatures of ice surfaces of Antarctica and Greenland were presented in high resolution radiation pictures with accuracies of about ±2°K. Pictorial maps of cloud cover and of cloud top heights were obtained during nighttime permitting a three-dimensional analysis of the global cloud structure and inferences regarding the dynamics of weather fronts, severe storms and atmospheric circulation cells. Measurements of sea surface temperatures were made in many areas of the world. Radiation patterns observed over terrain in cloudless conditions indicate the temperatures of the soil and permit inferences, in certain cases, of these parameters which determine the thermal properties of the soil, namely moisture, vegetation and rock formations. The data are available for further analysis by the scientific community and a catalog of all Nimbus observations is contained in Reference 9.

## INTRODUCTION

The first photographs of the earth's surface and of large scale weather systems taken from orbital altitudes have revealed a great deal of new knowledge merely because large scale phenomena which had never been observed in their entirety were now brought within the scope of one single observation. These findings stem from a series of Tiros (Television and Infrared Observation Satellite) satellites launched at the rate of about two per year since April 1960. Tiros satellites were primarily intended to serve the operational needs of the meteorologist in the detection and tracking of storms, frontal systems and similar phenomena by means of the cloud patterns associated with these weather features. Spaceborne observations of weather have also contributed to

fundamental meteorological research. Nimbus I, the first of NASA's second generation meteorological satellites, has further advanced the potential application of such observations to meteorological research and to other fields of geophysics. The Nimbus I system proved to be an excellent tool for the remote observation of meteorological and geophysical parameters for several reasons: A sun-synchronous, nearly polar orbit, a fully earth oriented, amply powered spacecraft, a set of improved and directly transmitting television cameras and a newly developed high resolution infrared radiometer (Reference 1).

## THE NIMBUS I SYSTEM

Nimbus I was launched into a nearly polar orbit on 28 August 1964 from Vandenberg Air Force Base, California. Because of a launch vehicle malfunction, an elliptic orbit (perigee 423 kilometers and apogee 933 kilometers) instead of the planned circular orbit at 900 kilometers, was achieved. As planned, the orbital plane was inclined to the equator by 98.7 degrees which caused the orbit to precess around the center of the earth in synchronism with the revolution of the earth around the sun. As a consequence the relative orientation between the orbital plane and the sun remained essentially constant during the life of the spacecraft. Since at launch the orbit was chosen so that the earth-sun line lay in the orbital plane, the satellite passed over most areas of the world twice every 24 hours, near local noon and near local midnight. Two stations in the United States, one in North Carolina, the other in Alaska, were used to command the spacecraft and to read out the stored telemetry and sensory data. Of the 14 to 15 orbits in a 24-hour period, eleven were expected to pass within acquisition range of one of the two stations. The eccentricity of the orbit, however, reduced the acquisition capability to fewer than ten orbits per day. Nevertheless, day and night photographs were obtained over 50 to 75 percent of the world on a daily basis.

The entire Nimbus system, including a complex array of about ten spacecraft subsystems (attitude control, power supplies, telemetry) as well as data transmission and handling facilities on the ground, had been designed to demonstrate the capability of delivering the complete information sensed by the spacecraft into the hands of the meteorological analyst in a format suited for immediate application. For a period of about four weeks this experiment functioned perfectly. The three-axis, active control system kept the spacecraft axis (sensor axis) oriented toward the center of the earth at all times, generally within better than one degree in all three axes; the solar cell power supply continually delivered an average power of about 300 watts to the spacecraft; and the spacecraft data storage and transmission system processed in excess of 50 million items of information (data words) per orbit. Pictorial presentations of the observations (Figure 1) made either during daytime with television cameras or during the night with a High Resolution Infrared Radiometer (HRIR) were generally available at the NASA Nimbus Control Center in Greenbelt, Maryland, within less than 30 minutes after the command for playback of the data was given to the spacecraft. Within these 30 minutes the information recorded in the spacecraft during any previous orbit (nominally 100 minutes of observation) were transmitted to the command station (in Alaska for example), recorded there, then transmitted further via communication circuits to Greenbelt, Maryland, where appropriate geographic referencing (latitudinal and longitudinal grids) as applied

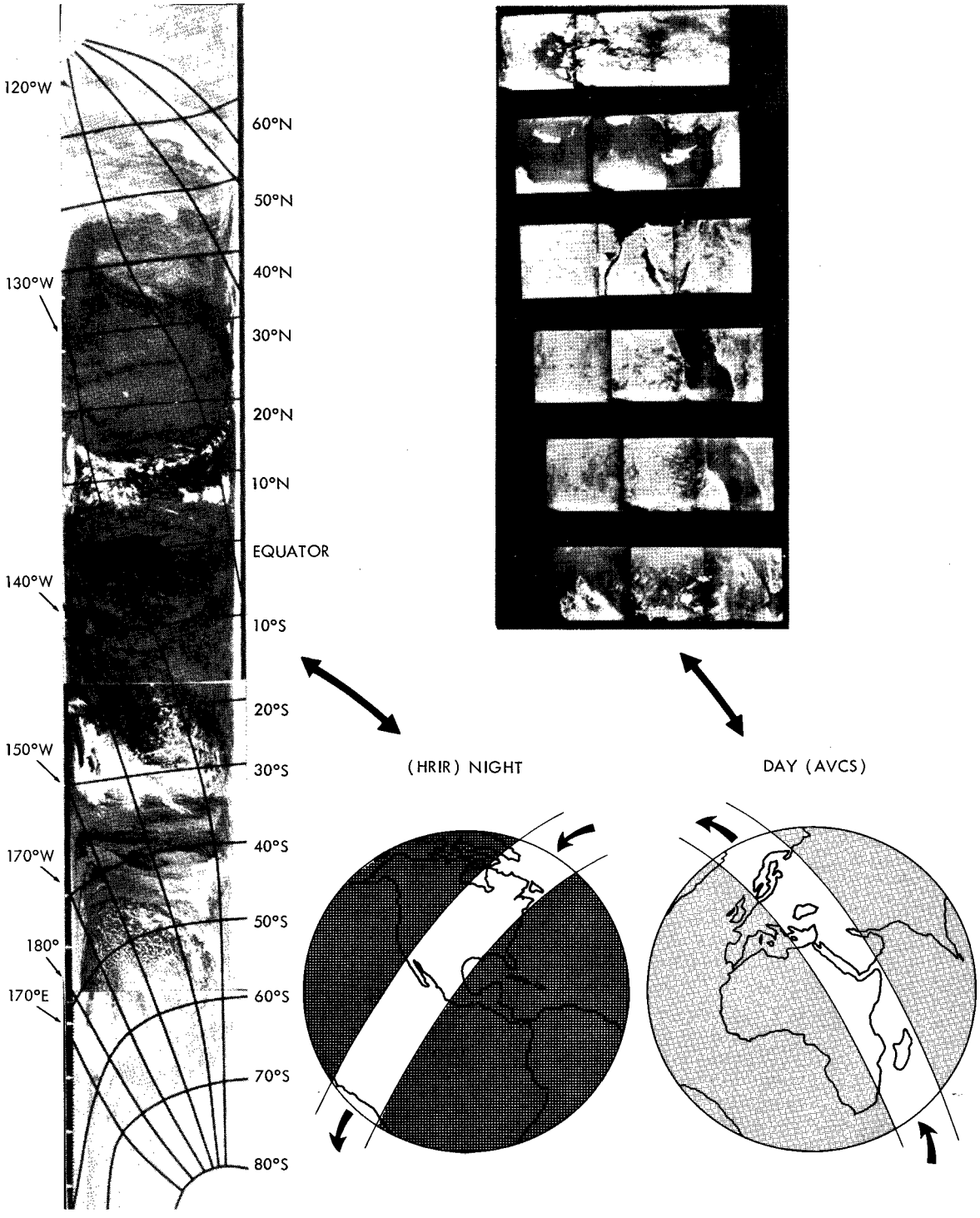


Figure 1—Extract of AVCS picture coverage during a noon time orbit of Nimbus I over the Near East on 16 September 1964 and HRIR coverage from North to South Poles across North America and the Pacific Ocean during midnight orbit, also on 16 September 1964.

automatically after which the data were transcribed onto 70 mm photographic film resulting in the strips shown in Figure 1. These strips permit a detailed analysis of weather and surface phenomena along the entire globe circling path of the satellite within less than two hours after the observations were taken. For operational meteorological applications an Automatic Picture Transmission (APT) system transmitted television observations instantly to about 50 simple and inexpensive ground stations located all over the globe. These ground stations were operated by the United States Weather Bureau, the meteorological services of the United States Armed Forces, foreign weather services, and, in some cases, by educational institutions.

## NIMBUS SENSORS

In the past, television cameras had proved to be the most effective instruments for observations of meteorological features from satellites. Nimbus I carried two types of cameras: A set of three very high resolution cameras each with a field of view of about 35 degrees and one camera with lesser resolution but equipped with a photosensitive surface which retained a latent image sufficiently long so that images could be transmitted directly via the APT system without intermediate storage on magnetic tape. The resolution obtained with this camera permitted the recognition of cloud and terrain features of less than four kilometers in diameter. The three high resolution television cameras formed the Advanced Vidicon Camera System (AVCS) and yielded considerably greater detail in their pictures. Objects of linear dimensions of less than one-half kilometer could be resolved. This resolution was adequate to observe practically all objects of meteorological significance. The Advanced Vidicon cameras were arranged side by side such that they covered a strip approximately 2000 kilometers wide along the satellite track (Figure 1).

In contrast to the cameras which formed television images of reflected solar radiation during daytime, the High Resolution Infrared Radiometer (HRIR) provided pictorial presentations of emitted, telluric, infrared radiation at night with high quantitative accuracy (Reference 2). Radiation was sensed in the narrow spectral window between 3.4 and 4.2 microns. A rotating mirror scanned the earth from horizon to horizon perpendicularly to the orbital path. Due to the satellite motion each successive scan line was advanced by approximately 9 kilometers which is comparable to the linear resolution of the sensor near apogee. Because of the elliptical orbit the resolution near perigee was about 4 kilometers. An entire nighttime half of the orbit was covered by about 2300 contiguous scans (Figure 1). The HRIR has been outstandingly successful not only in providing continuous nighttime cloud cover with a quality comparable to Tiros television pictures, but also in resolving equivalent blackbody temperatures of radiating surfaces at night within about ± 1K. The HRIR was also capable of imaging cloud patterns during daylight, but the temperature resolution was lost as, in that case, the instrument responded primarily to reflected solar radiation which masked the telluric emission.

## MAPPING BLACKBODY TEMPERATURES WITH HIGH RESOLUTION RADIOMETRY

The principle of mapping cloud and terrain features by means of infrared radiation is quite simple. All objects emit electromagnetic radiation, the spectral distribution and intensity of which

are unique functions of the object's temperature (T) and its surface configuration. For blackbodies the intensity is a function of temperature $T_{BB}$ only. This fact is expressed mathematically by Planck's law,

$$I_{BB} = \int_{\lambda_1}^{\lambda_2} \frac{C_1}{\lambda^5} \left( \exp \frac{C_2}{\lambda T} - 1 \right)^{-1} d\lambda = \int_{\lambda_1}^{\lambda_2} B(\lambda, T_{BB}) d\lambda \ , \qquad (1)$$

where $C_1$ and $C_2$ are constants and $I_{BB}$ is the intensity of the radiation emitted per unit area by the blackbody surface within the wavelength interval $\lambda_2 - \lambda_1$. The Nimbus HRIR was built to make accurate measurements of $I_{BB}$ from which surface blackbody temperatures could be inferred. To this end $\lambda_1$ and $\lambda_2$ were selected to correspond to wavelengths of 3.4 and 4.2 microns respectively. The atmosphere is quite transparent in this spectral range. Thus, in the absence of clouds, radiation emitted by the earth's land or water surfaces reaches the satellite with only minor interference by the clear atmosphere. This interference can be corrected for according to computations made by Kunde (Reference 3). If hot (300°K) blackbody surfaces are seen through a tropical (warm and moist) atmosphere, the $T_{BB}$ values derived from the radiation measurements must be corrected by +2 to +4 degrees K. For a dry atmosphere the correction is somewhat less and for cold surfaces (<280°K) no correction is necessary. In the presence of clouds the satellite receives radiation from the uppermost surface of the cloud. When we derive blackbody surface temperatures $T_{BB}$ from the measured values of $I_{BB}$ (Equation 1 ) we assume that the radiation is emitted isotropically and that the instantaneous field of view of the radiometer is filled by a surface of uniform temperature. The assumption of isotropy is not rigidly valid but must be used for lack of better knowledge of the directional variation of $I_{BB}$. The assumption of uniformity restricts the interpretation of the Nimbus I surface temperature measurements to objects which are homogeneous over a distance greater than about 6 kilometers. This is quite adequate for cloud formations associated with large scale meteorological phenomena (fronts, storms, fog layers) and for many terrestrial features (deserts, ice caps, lakes).

## Blackbody Temperatures and Surface Temperatures

Equation 1 applies only to blackbodies. Many surfaces such as water, clouds and heavily vegetated areas are sufficiently black in this spectral region that temperatures $T_{BB}$ derived from Equation 1 are generally within 2°K of the actual surface temperatures T. An error of 2°K is commensurate with the error inherent in the measurement of $I_{BB}$.

Some other surfaces, however, cannot be assumed as black. Laboratory measurements show that at wavelengths of about 4 microns, certain minerals and soils may absorb only a fraction $\epsilon$ of the radiation incident upon their surfaces. Kirchoff's law states that in this case the blackbody emission given by Equation 1 must be multiplied by the same fraction $\epsilon$ to obtain the radiant emittance $I_G$ from a non-black (grey) body,

$$I_G = \int_{\lambda_1}^{\lambda_2} \epsilon(\lambda) B(\lambda, T) \, d\lambda \ . \qquad (2)$$

The fraction $\epsilon$ is the emissivity of the surface. Defining an average emissivity $\bar{\epsilon}$ within the wavelength 3.4 to 4.2 microns, we may rewrite Equation 2

$$I_G = \bar{\epsilon} \int_{\lambda_1}^{\lambda_2} B(\lambda, T)\, d\lambda = \bar{\epsilon}\, I_{BB} \quad . \tag{3}$$

Using the appropriate values for $C_1$ and $C_2$ and for $\lambda_1$ and $\lambda_2$ in Equation 1, we find that at a blackbody temperature of 290°K, which is typical for the earth's surface seen by Nimbus at low latitudes, the value of $I_{BB}$ is about $1.4 \times 10^{-1}$ watts/m$^2$. A reduction of this value by 10 percent corresponds to a $T_{BB}$ value of 288.2°K. This means that a surface of 290°K with an average emissivity of 0.9 emits radiation of the same intensity as a blackbody surface of about 288.2°K. Since the minimum temperature change discernible with the HRIR is about 1° to 2°K, the knowledge of $\bar{\epsilon}$ in the derivation of T from $I_G$ is important only if the emissivity is considerably smaller than 0.9.

Surface emissivities can actually be derived from HRIR daytime observations of reflected solar radiation. In this case the measured radiation intensities are not only due to surface temperatures but also due to the ability of the surfaces to reflect sunlight. The radiation intensity $I_D$ sensed by the radiometer during daytime is the sum of the emitted grey body radiation $I_G$ and the reflected solar radiation $rI_s$. The reflectivity r of practically all terrestrial surface is given as: $1 - \epsilon$. Thus, if we define $\bar{r}$ as the average reflectivity in the 3.4 to 4.2 micron range, we may write,

$$I_D = I_G + \bar{r} I_s = \bar{\epsilon} I_{BB} + (1 - \bar{\epsilon})\, I_s \quad . \tag{4}$$

$I_s$ is computed from the solar constant on the basis of purely geometrical considerations. A measurement of $I_D = I_S = 4.17$ watts/m$^2$ would result if the surface were a perfect, 100 percent effective, diffuse reflector for solar radiation at vertical incidence. For a reflectivity $\bar{r} = 0.3$, an emissivity $\bar{\epsilon} = 0.7$ and a surface temperature T = 290°K $I_{BB} = 0.11$ watts/m$^2$ and $\bar{r} I_s = 1.25$ watts/m$^2$. Hence, if the surface emissivity is smaller than 0.7, $I_{BB}$ may be neglected and Equation 4 reduces to

$$I_D = I_s - \bar{\epsilon} I_s \quad . \tag{5}$$

If the surface temperature is less than 290°K, Equation 5 is valid even for emissivities greater than 0.7. In this case the emissivity can be derived from daytime HRIR measurements without any knowledge of surface temperatures. For $\bar{\epsilon} > 0.7$ the emissivity can still be measured very accurately provided that the surface temperatures are known. For example if $\bar{\epsilon} = 0.99$ and T = 290°K $I_D = 0.18$ watts/m$^2$; if $\bar{\epsilon} = 1.00$ (blackbody) $I_D = 0.14$ watts/m$^2$. The difference of 0.04 watts/m$^2$ is due to the term $\bar{r} I_s$ in Equation 3 and is equivalent to a blackbody temperature change of about 2°K which is just at the sensitivity threshold of the HRIR. In sunlight emissivities of 0.99 can

therefore easily be discerned from blackbodies and the HRIR, which was in operation during daytime for several orbits of Nimbus I, provides a very accurate method to measure large scale surface emissivities at 4 microns.

Preliminary evaluations of these daytime observations indicate that emisivities for most large scale surfaces (oceans, clouds, snow and vegetated regions) are greater than 0.9. Thus, HRIR measurements permit the world wide mapping of actual temperatures of most surfaces during nighttime and the mapping of emissivities of non-blackbody surfaces during daytime. Global measurements of earth surface temperatures (as opposed to air temperatures measured near the ground) are of considerable value in meteorological research since these temperatures can be used as initial values in the numerical analysis and prediction of weather. At polar latitudes HRIR surface temperature maps relate to the morphology of ice formations. Such maps are both of practical application to navigation and of fundamental interest to glaciologists. Over oceans, surface temperature differences may indicate the location of areas such as currents and fronts. This suggests the potential use of Nimbus HRIR observations in oceanographic research. Soil moisture content can be derived at least qualitatively from the Nimbus HRIR observations since appreciably higher soil temperatures are measured in moist areas. Aircraft observations of emitted infrared radiation over regions of volcanic activity in Hawaii (Reference 4) have shown that underground lava beds can be detected with this technique; therefore, the Nimbus HRIR data were also investigated for this purpose. No definite identification of active volcanic areas could be made, however, because the spatial resolution of the HRIR is apparently too coarse. Global mapping of emissivity with such coarse resolution is, nevertheless, of geological interest. Maps of emissivity obtained by the satellite might establish a relationship between the small scale emission properties of various minerals and soil constituents measured on samples in the laboratory and the large scale properties of the same constituents in their natural state where they are blended with impurities, vary in grain sizes and morphology. The satellite observations can be considered very useful in determing whether the distribution of mineral and similar deposits can be mapped by measurement of emitted radiation with low spectral and spatial resolution. Any findings in this area may have considerable impact on the expectations for similar measurements of lunar and planetary surfaces.

## Cloud Heights

When the HRIR views a cloud covered region and a uniform cloud fills the instantaneous field of view of the radiometer, the average blackbody temperature of the cloud top surface can be derived by means of Equation 1. It is well known that in the troposphere the temperature generally decreases rapidly with altitude. It is also well known that clouds generally do not penetrate to altitudes above the troposphere where temperature increases with height. Thus, blackbody cloud top temperatures can be directly related to height (Figure 2). The deviation of cloud heights from satellite-borne radiometric measurements has been demonstrated previously with Tiros observations (References 5 and 6) but the better spatial resolution of the Nimbus radiometer permits for the first time a detailed pictorial presentation of the vertical structure of cloud tops on a large scale. Figure 3a shows a typical example of such cloud structure over the North Pacific near

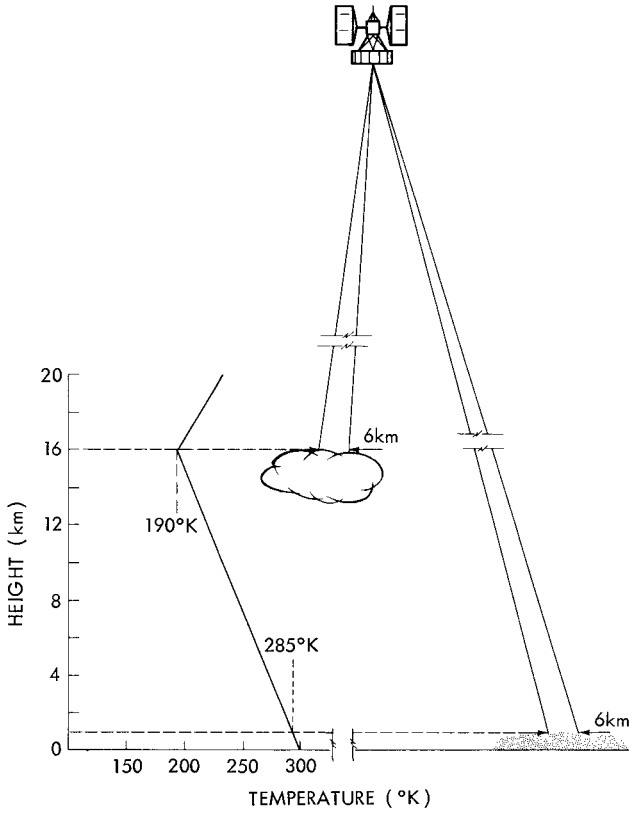


Figure 2—Typical temperature profile at tropical latitudes illustrating concept of determination of cloud top heights from satellite measurements of cloud top temperatures.

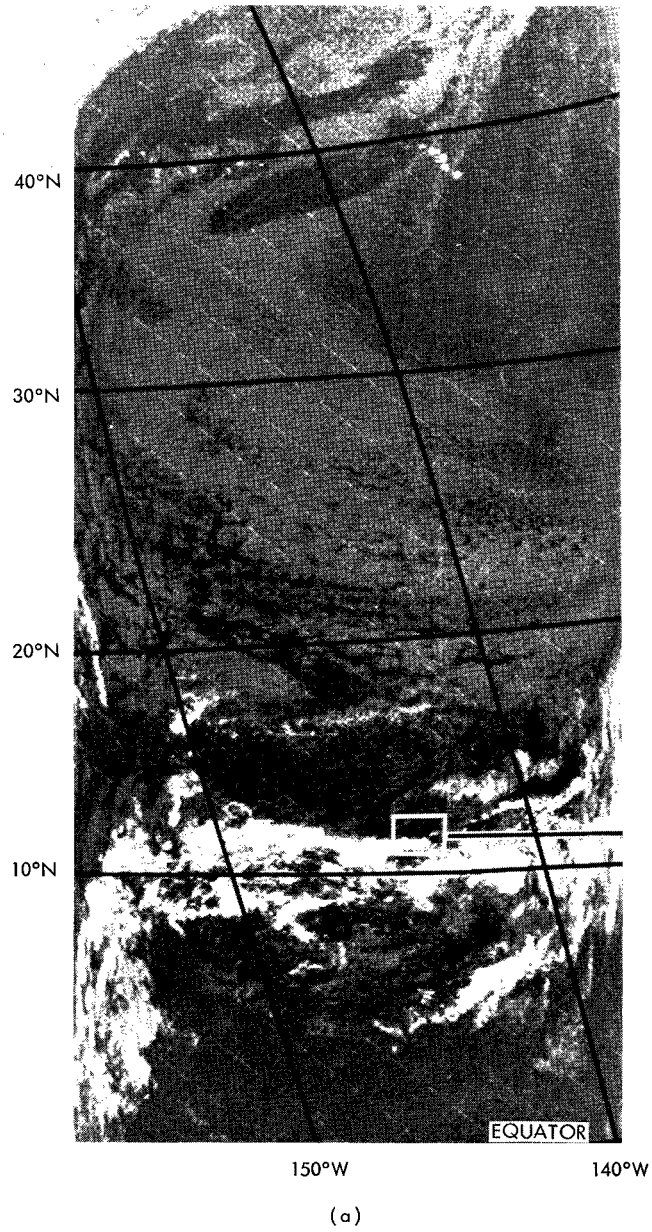


(a)

Figure 3a—Pictorial presentation of cloud and water temperatures over the North Pacific measured by the HRIR at midnight on 20 September 1964. (Dark shades are warm, white shades are cold.)

midnight on 20 September 1964. In this photographic strip as in all HRIR presentations high clouds (cold temperatures) are presented as light shades of gray, while low clouds or clear areas (warm temperatures) appear dark. It is immediately apparent that the broken cloud band near the equator consists of the highest clouds in this picture; clouds in the broad band near 50 degrees N are somewhat lower although still much higher than the large grey mass of clouds covering the North Pacific from 25 to 45 degrees N. Only a few large, very dark regions indicating clear skies can be seen near 40 degrees N and 140 degrees W. The pictorial presentation of these temperature contrasts permits an instantaneous assessment of the gross features of the meteorological situation. The narrow band of very high clouds near the equator marks the Intertropical Convergence Zone; the broad band near 50 degrees N corresponds to an intense

cold front and low lying fog and stratus clouds stretching south of the front, indicated by the dark grey area. Of particular interest is the string of small, very bright (cold) spots near 137 degrees W and 38 to 40 degrees N. These indicate isolated, very high altitude cumulus clouds relating to thunderstorm activity. Normally, the meteorologist would never expect thunderstorm activity under the prevailing situation, especially not near midnight. However, the isolated, very high clouds definitely suggest such activity and, in this case, the validity of this interpretation was confirmed by a report from a single ship which happened to be in that area and reported towering cumuli and lightning.

A much more quantitative picture results from plotting the numerical temperatures automatically derived by digital computers from the radiation intensities. Extracts of such automatic, numeric presentations are shown in Figure 3b. The very highest cloud in the Intertropical Convergence Zone (11.5-12 degrees N and 145-146 degrees W) towers to about 16 kilometers, an altitude derived on the basis of Figure 2 from the extremely low temperature of 190°K near the center of the cloud top (Figure 3b). On this basis the fog near 40 degrees N (Figure 3a) gives a surface temperature of 285°K which means it reaches only to about 1 kilometer above sea level; the dark area in the same region corresponds to a temperature of about 293°K. The sea surface temperature measured by ships in this region was identical to that value which proves that the area was free of clouds. The accuracy of the HRIR cloud height measurements is vividly demonstrated in Figure 4a where the original analog record of one single scan across the center of Hurricane Gladys near midnight on 17 September 1964 over the Atlantic is reproduced. This scan covers a strip of 5 kilometers width across the storm; the observed radiation intensities,

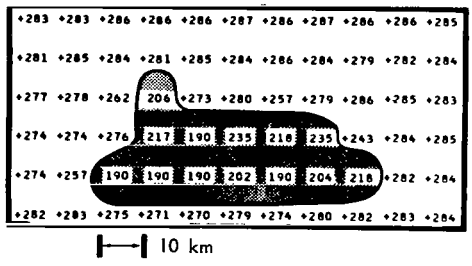


(b)

Figure 3b—Automatically produced digital map of cloud surface temperatures for a small portion of Figure 3a.

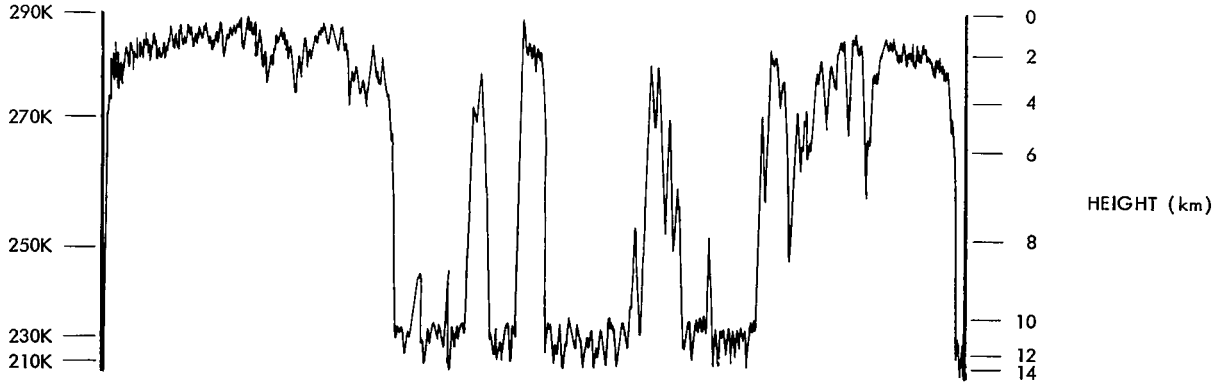


(a)

Figure 4a—Single HRIR scan, from horizon to horizon, across Hurricane Gladys at the location indicated in Figure 4b.

expressed in degrees K, are measured along the ordinate. The blackbody temperatures were converted to height on the basis of actual temperature soundings performed by balloons in the vicinity of the storm. The corresponding heights are shown along the right hand ordinate. The scan indicates temperatures near 300°K outside the storm and near 290°K in the center of the eye. The temperature of 300°K corresponds to the sea surface temperature over the clear skies outside the storm and 290°K corresponds to a height of 2 kilometers over the eye of the hurricane. Over the center of the spiral bands temperatures drop to 200°K corresponding to heights of 14 kilometers. Lower clouds and partially clear skies are scanned between the spiral bands. The photographic presentation of the storm in Figure 4b is composed of a total of about 200 such scans. Detailed analysis of these highly quantitative observations of vertical cloud structure in many cases permit a much better exploration of dynamics of the atmosphere than ordinary cloud photography.

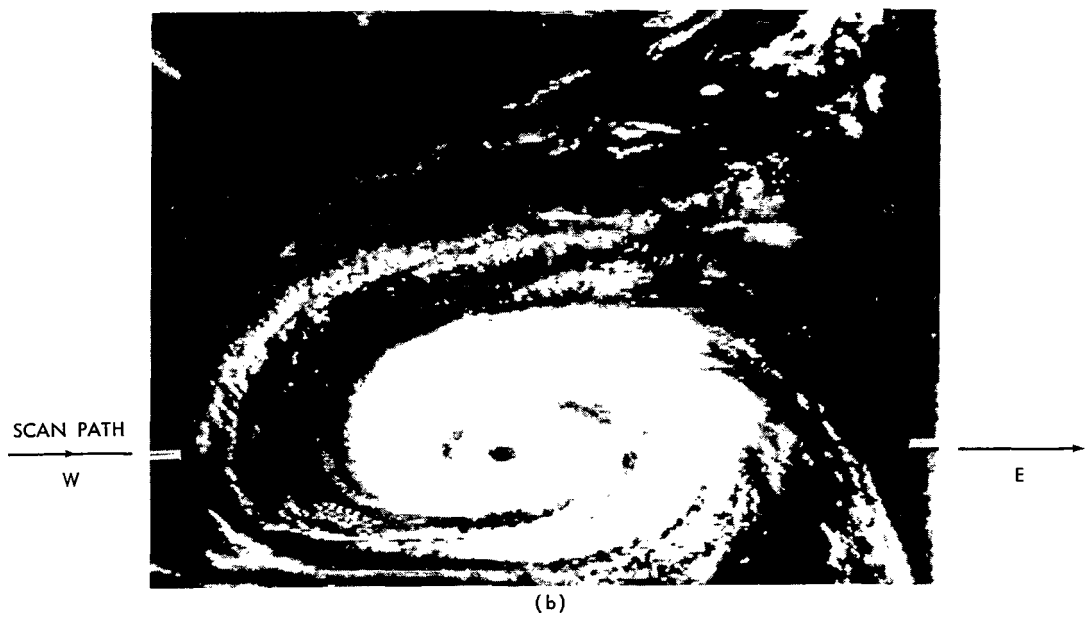


Figure 4b—HRIR observation of Hurricane Gladys over the Atlantic near midnight on 17 September 1964. (Dark shades are warm, white shades are cold.)

## Sea Surface Temperatures

Since the blackbody assumption for water surfaces is quite valid in the 3.4 to 4.2 micron wavelength range, $T_{BB}$ values derived from the radiation intensities relate directly to water surface temperatures. In cloudless regions the HRIR, therefore, can be used to map globally the surface temperatures of various bodies of water. Figure 5 shows an HRIR picture of the southwestern United States at midnight on 30 August 1964. The darkest region in the right center corresponds to a temperature of 301°K for the water surface in the Northern Gulf of California. Applying Kunde's corrections for atmospheric absorption (Reference 3), we obtain a temperature of 303°K for the

waters of the Gulf of California which is considerably warmer than the Pacific Ocean off the shore of California. There temperatures range from 293°K near the coast to about 280°K at a distance of about 200 kilometers off shore. The low off shore temperatures indicate the presence of fog or dense haze, while the temperature of 293°K measured just west of Los Angeles is in good agreement with the temperature of 292°K measured from shipboard by the U. S. Coast Guard. Even small water features such as lakes can be clearly identified and their surface temperatures can be determined. The four black (warm) dots in the upper left corner of Figure 5 are mountain lakes in the Sierra Nevada. The southwestern most lake is Lake Tahoe; its water surface temperature was measured by the HRIR as 283°K. But, for a small body of water such as this there is a question whether the field of view of the radiometer was fully covered by the lake. The actual water temperature therefore may be several degrees higher.

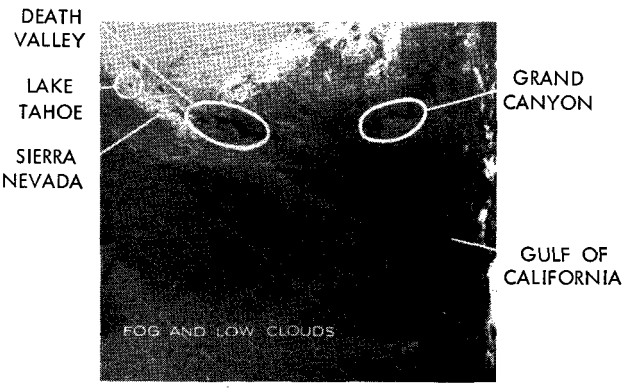


Figure 5—HRIR Ocean and terrain temperatures over the southwestern United States near midnight on 1 September 1964. (Dark shades are warm, white shades are cold.)

The ability of the HRIR to map sea surface temperatures suggests that the course of various ocean currents such as the Gulf Stream, for example, could be detected by the satellite. Unfortunately, during the life time of Nimbus I clouds obscured most areas of interest. There is, however, the possibility that certain cloud formations themselves may be related to ocean temperatures. A suggestion of this can be found in a number of cases for which Figures 6a and 6b are typical. Very long and narrow, clear streaks of open

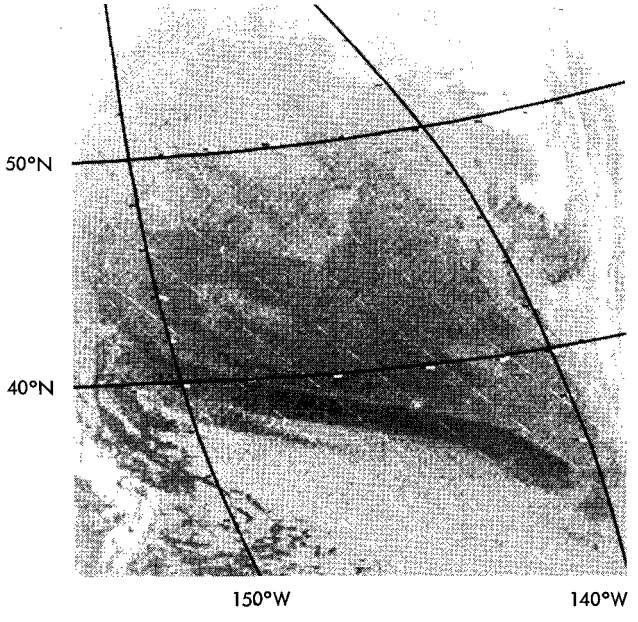


Figure 6a—HRIR cloud and water temperatures over the North Pacific near midnight on 30 August 1964. Clear streak of open water can be seen in the center. (Dark shades are warm, white shades are cold.)

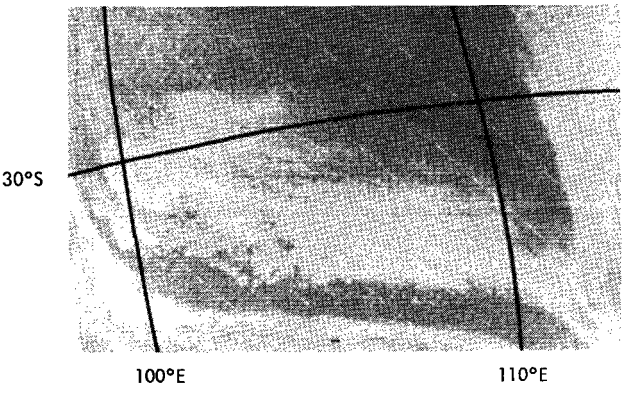


Figure 6b—HRIR cloud and water temperatures over the Indian Ocean near midnight on 9 September 1964. Clear streak of open water can be seen in the center. (Dark shades are warm, white shades are cold.)

water lie between extensive low altitude stratus cloud decks over the North Pacific in Figure 6a and over the eastern Indian Ocean in Figure 6b. Here the streaks are at least 2000 kilometers long and about 200 kilometers wide. Although the phenomenon is apparently atmospheric it is conceivable that the cloud formations and the peculiar clearings may be influenced by ocean surface temperature differences.

Another example of satellite observed variations in sea temperatures can be found in Figure 7 where sea surface temperatures over the Mediterranean are found to range from 297°K off the coast of Africa to 290°K near Corsica. Temperatures of the Adriatic and Tyrrhenian Seas are 294°K.

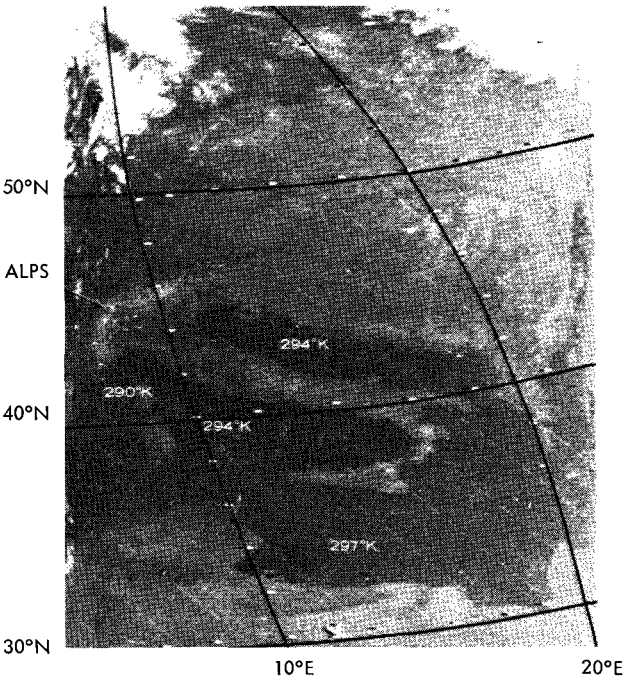


Figure 7—Temperatures over Europe observed by HRIR near midnight on 14 September 1964. (Dark shades are warm, white shades are cold.)

## Ice Formations

Nimbus I was the first weather satellite to provide continuous observations of the polar regions. A great deal of detail in the structure of the inland ice over Antarctica, Greenland, and other areas was observed with the AVCS. High resolution television observations also provided information on the morphology of floating shelf ice, icebergs and similar phenomena (Reference 7). Figure 8 is a typical example of an AVCS picture showing the extent of ice cover and the structure of snow covered mountain ranges over northwestern Greenland. Details in the mountain ranges can be observed because of the pronounced shadows produced by the low elevation of the sun which generally prevails at these high latitudes.

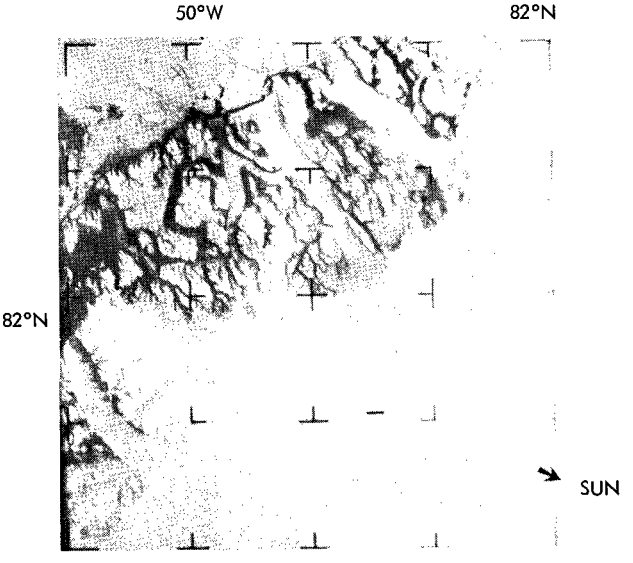


Figure 8—AVCS picture of northwestern Greenland near noon on 3 September 1964.

Figure 9 is a HRIR presentation of temperatures of Antarctic ice and water surfaces on 29 August 1964. The entire Atlantic sector of the continent is shown to be cloud free and the surface temperatures over the interior ice cap near the South Pole were determined numerically as 210-215°K. These extremely low temperatures were observed consistently during the lifetime of Nimbus from late August to late September. Near the edge of the continent surface temperatures increase markedly to about 240°K. The edge of the continent stands out sharply in the infrared picture because a band of apparently open water about 100 kilometers wide in spots stretches along the coast of Queen Maud Land. Maximum temperatures of these spots are about 256°K. This indicates that the full instantaneous field of the radiometer was not viewing an entirely open area of water but that this band probably consists of strongly broken up ice. A wide shelf of floating ice stretches northward into the Wedell Sea and the Atlantic Ocean. The Wedell Sea ice can be easily distinguished from the inland ice because its surface temperature of 244°K is about 12°K higher. Very narrow but distinct lines of warmer temperatures are found crisscrossing the shelf. These lines obviously are due to cracks in the ice and in some cases they are over 200 kilometers long. The ice shelf ranges up to 57 degrees where it is bounded by open water of temperatures of about 275°K.

Figure 10a is an HRIR picture of the Ross Ice Shelf in the Pacific Sector of Antarctica. Although these observations were made four days after those shown in Figure 9, the temperatures are nearly the same over the interior ice. Surface temperatures of the Ross Ice Shelf range from 225°K near 85 degrees S to 245°K near 70 degrees S. The latter value compares well with the temperatures of 244°K measured four days earlier over the Wedell Sea (Figure 9). In Figure 10a a number of very isolated high temperature spots can be seen along the coast of Victoria Land. The most pronounced one near 76 degrees S and 165 degrees W has a temperature of 260°K. Since this spot is located near Mt. Erebus it was originally suspected that these isolated warm regions might be related to volcanic activity. However, as the same regions were observed in subsequent HRIR pictures, it became evident that some of the spots became enlarged and formed small bands along the edge of the continent. Finally

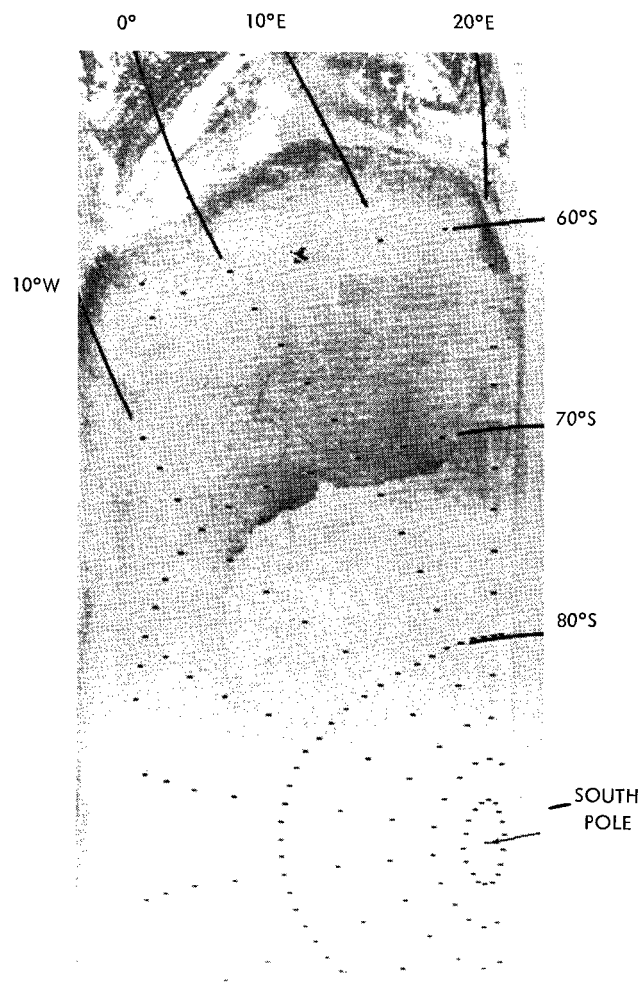


Figure 9—Temperatures over Antarctica observed by HRIR near midnight on 29 August 1964. (Dark shades are warm, white shades are cold.)

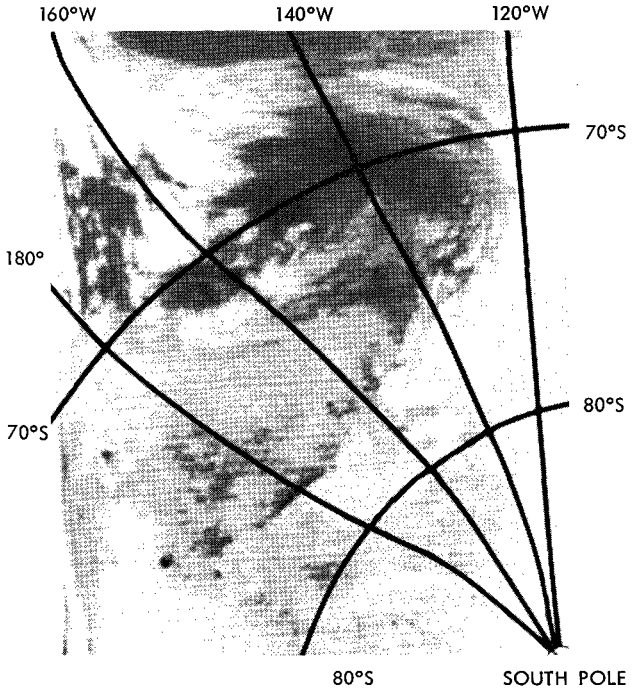


(a)

Figure 10a—Temperatures over Antarctica observed by HRIR near midnight on 1 September 1964. (Dark shades are warm, white shades are cold.)

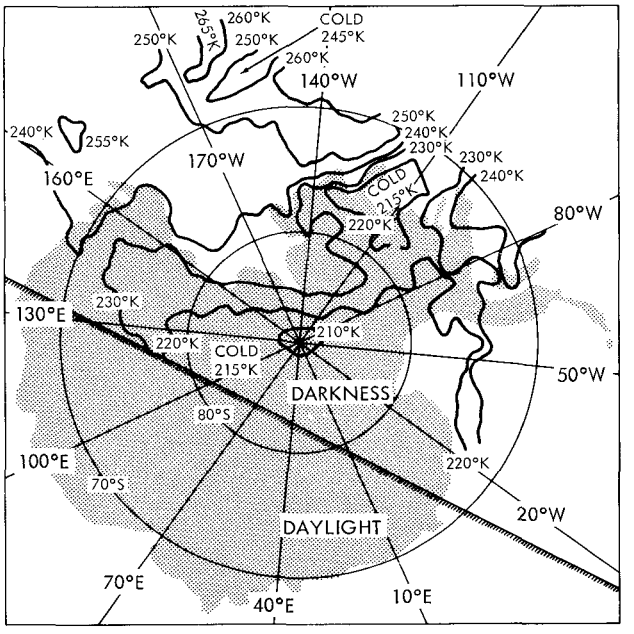


(b)

Figure 10b—Digital map of temperature contours over Antarctica for the data presented pictorially in Figure 10a.

on 21 September 1964 the spot near Mt. Erebus had enlarged to such an extent that it filled the entire field of view of the HRIR (Figure 11a) and the measured temperature was approximately 270°K. The fact that this is conspicuously close to the temperature of freezing water and that the same spot was photographed 12 hours later in sunlight with the AVCS (Figure 11b) leads to the definite conclusion that the spots indeed are open water. Note the identical shape of the open area in Figures 11a and 11b, despite the difference of one order of magnitude in the resolution capabilities of the AVCS and HRIR. Figure 10b is a temperature contour map of the Pacific Sector of Antarctica derived from the automatically plotted digital data for the picture shown in Figure 10a. The very low temperatures (215°K) over the high plateau surrounding the South Pole are obvious. The warm tongue reaching toward the pole near 180 degrees longitude coincides with the Ross Sea where the shelf ice is at a much warmer temperature than the higher and thicker inland ice. The high clouds seen in Figure 10a to the east of the Ross Ice Shelf show a temperature of about 215°K which corresponds to a cloud top altitude equal to that of the interior plateau, namely about 3000 meters. The 260°K line indicates pockets of broken ice and open water which are found in the Pacific Ocean Sector.

An HRIR picture of the Greenland ice cap is shown in Figure 12. Over clear areas the coldest region of the ice mass shows surface temperatures of about 230°K. Cloud bands can be seen extending over the southwest and eastern portion of the subcontinent. Clouds in this case appear

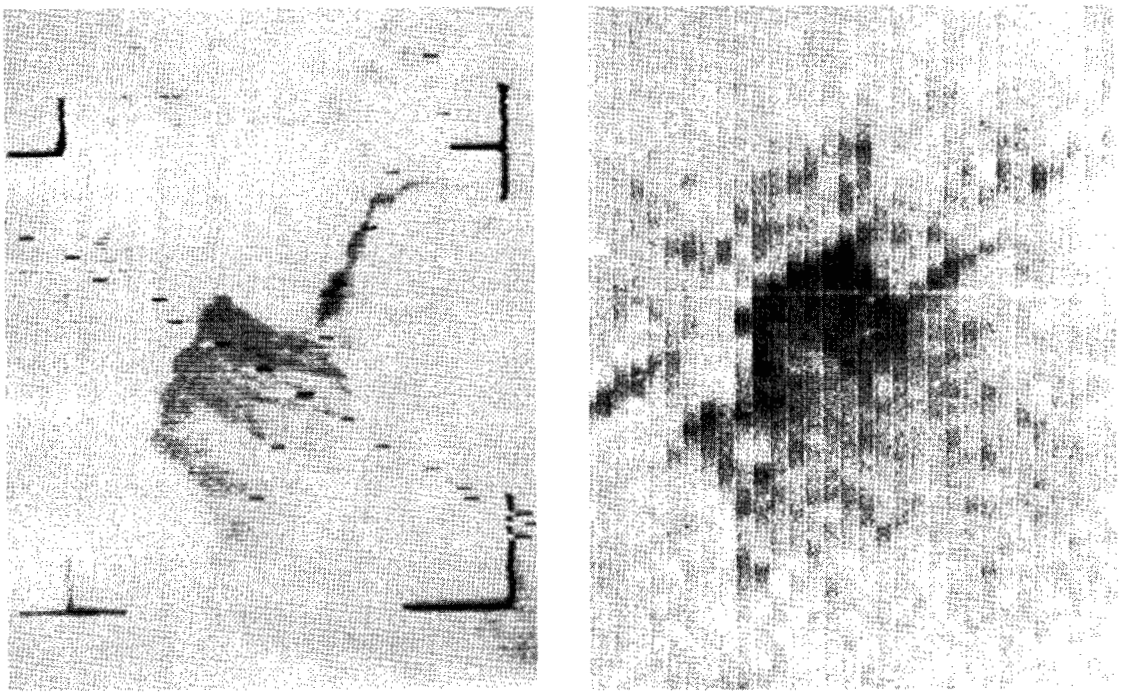

Figure 11—Comparison of warm spot observed by HRIR (a) and AVCS (b) over Antarctica on 21 September 1964.

darker (warmer) than the underlying ice. The measured cloud temperatures are about 20°K warmer than the ice surface temperature. This is plausible in view of the temperature inversions which are known to exist over the ice covered polar regions. The inversion means that over a portion of the lower atmosphere, temperatures increase rather than decrease with height, thus deviating from the typical profile shown in Figure 2. The darkest portions of the region between Greenland and the large cloud mass to the south indicate clear skies over the waters of Baffin Bay and the Davis Straits. Water surface temperatures of above 280°K were derived from the digital analysis of the data over this area.

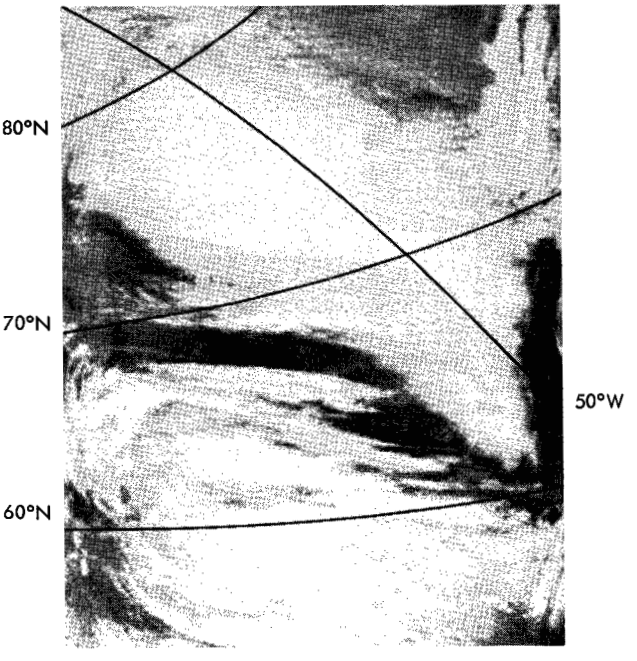


Figure 12—Temperatures over Greenland observed by HRIR near midnight on 16 September 1964. (Dark shades are warm, white shades are cold.)

## Terrain Features and Soil Moisture

Land surfaces are considerably more complex than sea or cloud surfaces. Therefore,

under certain conditions, the temperatures derived from radiation intensities measured over land surfaces depend to a large extent not only on terrain heights but also on such parameters as heat capacity, conductivity and moisture content. First, a distinction must be made whether the variations in radiation intensity are due to actual ground temperature, or due to variations in emissivity. In the radiation observations with Nimbus I most variations may be ascribed to actual surface temperatures. No cases have been found where variations in surface emissivities could be clearly identified in the HRIR measurements. Indeed, we believe from this experience with Nimbus that effective detection of surface features by means of emissivity measurements from spacecrafts will only be possible if the spatial and spectral resolutions of radiometric sensors are improved by several orders of magnitude over the capability of the Nimbus I instruments. On the other hand, a number of the topographic and geological features mentioned above may be inferred from the measurements of relatively broadband thermal emission performed with the Nimbus I HRIR. For example, the dark streaks in the upper portion of Figure 5 showing the Southwestern United States correspond to blackbody temperatures of about 290°K while the lighter grey in the surrounding regions corresponds to about 275°K. The warm streaks were identified as Death Valley (left) and the Grand Canyon (right). Thus the temperature differences seen by the satellite readily correspond to differences in terrain height. Furthermore, a more quantitative interpretation of the temperatures over Death Valley reveals that the temperature difference of about 15°K measured by the satellite corresponds to an altitude difference of about 1800 meters between the valley floor and the surrounding highlands. The measured temperature decrease with altitude is therefore about 8.3°K/kilometer which is in very good agreement with the expected temperature decrease in the free atmosphere (atmospheric lapse rate). This equilibrium between the soil and atmospheric temperatures leads to the conclusion that the heat capacity of the ground in this area must be generally very large since only such a large heat capacity will prevent the surface at night from cooling more rapidly by radiation than the overlying atmosphere.

An example where other considerations are involved, in addition to topographic height changes, may be seen in Figure 13. Figure 13 shows a very large portion of western South America as seen by the HRIR on 14 September 1964 when much of the region was essentially free of clouds except for the Intertropical Convergence Zone north of 10 degrees S, an extensive low altitude layer of stratus clouds along the entire west coast, a high altitude cloud deck off southern Chile, and some smaller clouds along the eastern horizon. The broad, white (cold) band through the center of the picture corresponds to the cold, high altitude mountain ranges of the Andes. Average blackbody temperatures of 255°K are measured over the highest elevations between 28 and 32 degrees S. To the northeast there is a remarkably rapid transition from the cold highland with average blackbody temperatures of 270°K to the very warm Amazonas Basin with blackbody temperatures of 290°K. The warm waters of Lake Poopo (19 degrees S) and Lake Titicaca (16 degrees S) are clearly evident in the generally cold highlands. In the plateaus to the east of the mountains (30-35 degrees S) and in northern Chile (24 degrees S) remarkably fine structure in the temperature patterns may be observed. The crescent shaped figure near 23 degrees S corresponds to the Salar de Atacama, a salt flat in northern Chile. The discrete band of warm temperatures (273°K) surrounding the crescent stands out clearly while the center is quite cold (263°K). The topographic map (Figure 14) shows that the entire Salar covers a region of fairly uniform altitude of about 2300 meters. Thus

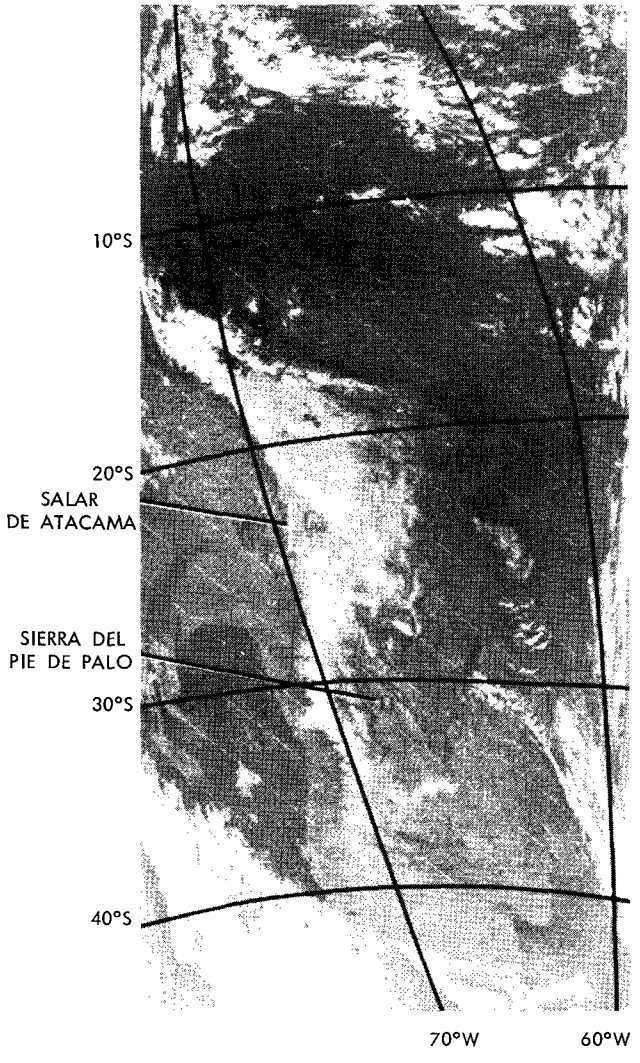


Figure 13—Temperature over South America observed by HRIR near midnight on 13 September 1964. (Dark shades are warm, white shades are cold.)

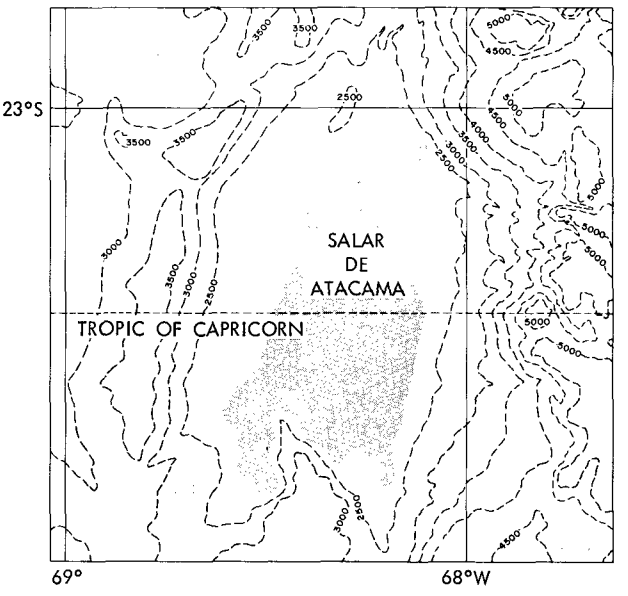


Figure 14—Topographic map of Salar de Atacama in northern Chile.

on the basis of terrain height there is no reason to assume the existence of a temperature difference between the center and the rim. Laboratory measurements by Hovis (Reference 8) have shown that of many common minerals tested in this spectral region pure rock salt has the lowest average emissivity. Hovis' measurements give a value of less than 0.5 for $\bar{\epsilon}$. Therefore, a blackbody temperature of less than 263°K would be measured over pure salt if the actual surface temperature were 273°K, while the periphery of the Salar rock formations at the same altitude and temperature would be detected essentially as blackbodies and thus produce a $T_{BB}$ measurement which is very close to the actual temperature. The difference of 10°K between the cold center and the warm band in Figure 13 could thus be explained. There is still a question, however, if the emissivities measured for pure salts in the laboratory are applicable to naturally impure salt deposits such as this Salar. A more probable interpretation is that the emissivity of the natural salt over the Salar is much greater than 0.5 but that the heat capacity of the salt is considerably less than that of the surrounding rock formations at the same altitude level. This fact combined with the very high reflectivity of sunlight and the very low heat conductivity of the relatively fine grained salt deposits prevent the storage of large amounts of solar heat over the Salar itself and, after sunset, cause it to cool very rapidly by radiation resulting in a

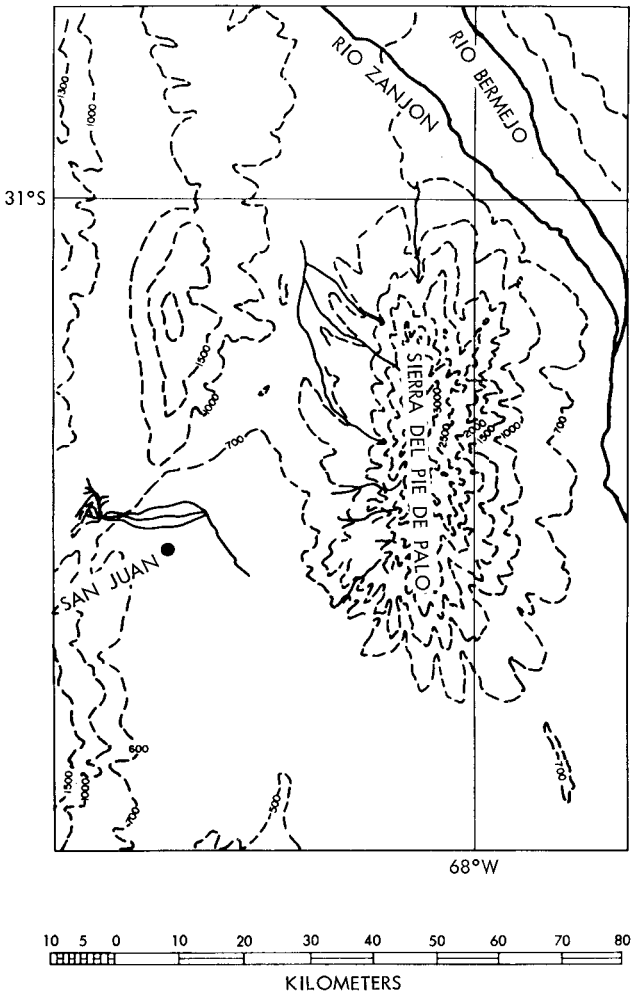


Figure 15—Topographic map of Pie de Palo mountains in western Argentina.

very low temperature (263°K) at midnight. The rocks along the periphery, however, remain warmer throughout the night (273°K) because of their larger heat capacity and greater conductivity.

A similar case may be observed in Figure 13 near 32 degrees S and 68 degrees W over western Argentina. Here, again, a nearly circular dark band of about 5 kilometers in width and about 40-50 kilometers in diameter indicates the existence of a high temperature zone along this peculiarly shaped band. The cold temperatures (white spot) in the center of the band can easily be explained by topography. The center of the band corresponds to the Pie de Palo mountain shown topographically in Figure 15. The lowest temperature measured in the center of the band is 268°K and corresponds to the highest elevation of about 3000 meters (Figure 15). The temperature along the band is about 280°K which is about 7°K warmer than the temperature of 274°K of the surrounding desert. Since the band around the mountain is certainly not at a lower altitude than the surrounding desert plateau (Figure 15), the explanation of the warmer temperatures must again be found in the difference in heat storage between the desert sand and the rocks of the Pie de Palo mountains. A visual survey by the author* revealed that the contrast between the precambrian rock formations of the Pie de Palo mountains and the alluvial sand deposits of the surrounding desert is indeed very striking and extends around the mountains approximately along the 1000 meter contour line (Figure 15). The dark band seen by the satellite parallels approximately this 1000 meter contour line. Furthermore, the temperature difference of 12°K between the warm band at 1000 meters and the mountain top rising rapidly to 3000 meters yields an approximate lapse rate of 6°K/kilometers which corresponds much better to the expected adiabatic lapse rate than the temperature difference of 6°K between the desert plateau at about 800 meters and the mountain top. That latter difference would yield a rather unrealistic lapse rate of 3°K/kilometers. Thus, the temperature over the desert is considerably lower because of the small heat capacity and conductivity of the ground causing a temperature inversion in the air over the

*This survey was made possible by the staff of the University of San Juan, Argentina, especially Professor C. V. Cesco who provided valuable background material for this investigation.

desert, while the solid rocks again remain considerably warmer resulting in the adiabatically decreasing temperature from the periphery to the center of the mountain.

HRIR pictures over the deserts of North Africa and the Near East exhibit similar fine structure in the emitted radiation with inferred temperature variations of 10 to 15°K. Again, we conclude that these gradients are due to variations in the thermal properties of the soil rather than due to emissivity variations.

In this fashion the satellite HRIR observations on a small scale permit the mapping of geological features which can be distinguished by their thermal properties. On a larger scale these patterns of heat capacity assume meteorological significance since storage of heat in the ground is an important consideration in the numerical description of atmospheric processes.

Moisture content of the soil is also evident in the HRIR observations. It has been very surprising that many rivers of widths of less than 1 kilometer stand out prominently in the radiation pictures although the linear resolution of the HRIR is generally not better than 5 kilometers. The prominence of the rivers is apparently due to the fact that the heat capacity of the ground along these rivers is altered probably by moisture in the ground and that this moisture retains solar heat absorbed during daytime much longer than the adjacent drier regions. Several rivers are noticeable to the east of the Andes in Figure 13. Two rivers are particularly prominent by their confluence which is located just to the east of the conspicuous warm band around the Pie de Palo mountains discussed above. These rivers can be identified as the Rio Zanjon and Rio Bermejo in Northwestern Argentina. Interestingly, dispite their prominence in the radiation pictures these rivers are only less than a few hundred meters wide and except for occasional spring flooding they carry practically no water. Also, the rivers do not form any deep canyons or other depressions in this area so that their warmer temperatures cannot be explained by height differences. In the course of time, however, their courses have meandered over widths of several kilometers over the desert plateau. These meanderings have apparently taken place during the flood stages and have altered the terrain to such an extent to create a sufficient contrast in the thermal properties between the desert and the river beds that the nighttime temperature differences could be detected by the satellite radiometer. Of course, such contrasts can only be created where the surrounding terrain is very dry and of very small heat capacity. For example, only vague indications can be found in Figure 13 of the Amazonas River which is much wider than the Bermejo and Zanjon rivers that stand out so clearly. In the Amazonas Basin the entire region possesses such a large heat capacity due to its moisture and heavy vegetation that a uniform and high temperature is maintained throughout the night. Because of this fact the boundaries between water and land which include the outlines of continents cannot be distinguished in the HRIR observations in tropical regions.

An example of very close equilibrium between soil and air temperatures can be found over the Siberian Tundra as shown in Figure 16. In this Figure a band of clouds, manifesting a cold front, crosses western Siberia near 60 degrees N. Cloudless skies prevail both to the north and south which is indicated by the clearly visible lakes and rivers on both sides of the front. Blackbody temperatures, however, are markedly different on the two sides. To the south the front, temperatures range from 277°K to about 280°K while to the northwest they are about 287°K. Analysis of

surface air data provided by the Hydrometeorological Service of the U. S. S. R. shows that surface air temperatures in the southern region were about 279°K while in the northwest they ranged from 283° to 288°K. This equivalence with the satellite measured soil temperatures suggests a complete equilibrium between air and soil temperatures over this region. Other HRIR Nimbus observations have been obtained over this same area during September 1964 but the temperature contrast was apparent only for this case. This leads to the rather surprising conclusion that the soil temperatures in this case were governed by the temperatures of the overlying air masses.

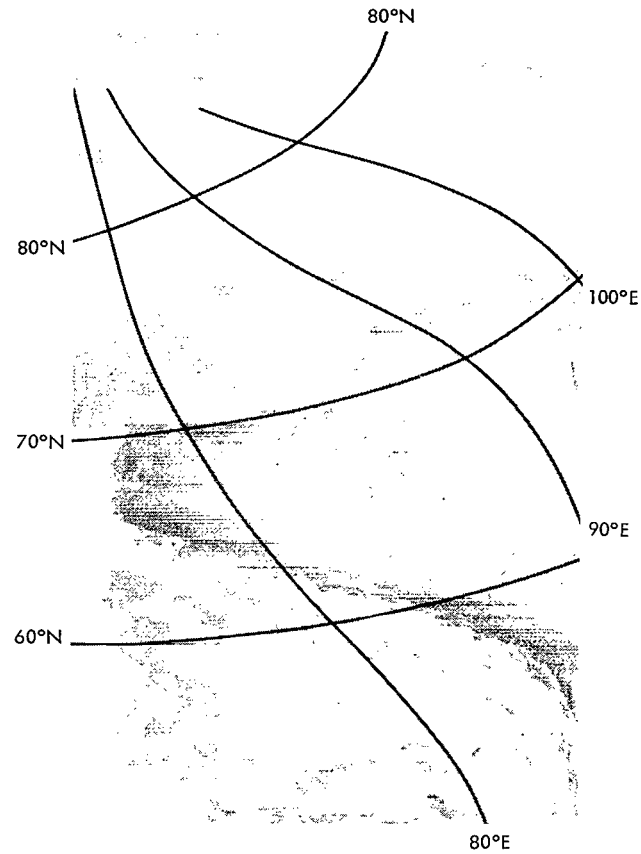


Figure 16—Temperature over Siberia observed by HRIR near midnight on 5 September 1964. (Dark shades are warm, white shades are cold.)

## CONCLUDING REMARKS

A variety of different geophysical and atmospheric facts can be inferred from the observation of temperature variations over the earth's terrain. Over heavily vegetated regions of the tropics the ground temperature can be measured and because of the larger heat capacity of this type of terrain its effect on air temperatures is similar to that over oceans. The ground acts as a reservoir which heats or cools the air moving over it depending on its temperature. At higher altitudes, especially over dry sandy terrain, the heat capacity of the ground temperature is so small that near midnight when solar radiation is absent, the satellite measured ground temperature is much less than the air temperature demonstrating temperature inversions. Over more solid rock surfaces the satellite measured ground temperatures are more equal to the air temperatures. Contrasts in the thermal properties of the surfaces usually exhibit a very pronounced fine structure in the satellite observations. In many cases these contrasts can be interpreted, qualitatively at least, as a measure of moisture content of the ground, changes in the vegetation or in the geological formation along the ground.

## REFERENCES


1. Nordberg, W., and Press, H., "The NIMBUS I Meteorological Satellite," *Bull. Amer. Meteor. Soc.* 45(11):684-687, November 1964.

2. Goldberg, I. L., Foshee, L., Nordberg, W., and Catoe, C. E., "NIMBUS High Resolution Infrared Measurements," in: *"Proceedings of the Third Symposium on Remote Sensing of Environment,"* Ann Arbor: University of Michigan, October 14, 15, 16, 1964.

3. Kunde, V. G., "Meteorological and Geophysical Observations with the NIMBUS I Satellite," NASA SP, 1965.

4. Fischer, W., et al. "Infrared Surveys of Hawaiian Volcanoes," *Science*, 146(3645):733-742, November 6, 1964.

5. Bandeen, W. R., Kunde, V. G., Nordberg, W., and Thompson, H. P., "TIROS III Meteorological Satellite Radiations Observations of a Tropical Hurricane," *Tellus*, 16(4):481-502, April 1964.

6. Allison, L. J., Gray, T. I., Jr., and Warnecke, G., "A Quasi-Global Presentation of TIROS III Radiation Data," NASA SP-53, 1964.

7. Popham, R., and Samuelson, R. E., "Meteorological and Geophysical Observations with the NIMBUS I Satellite," NASA SP, 1965.

8. Hovis, W., "Spectral Reflectivity of Common Minerals," *J. Appl. Opt.* (to be published).

9. "NIMBUS I High Resolution Radiation Data Catalog and Users Manual," 1: Greenbelt, Maryland: Goddard Space Flight Center, 1965.

# CONJUGATE INTERSECTS TO SELECTED GEOPHYSICAL STATIONS

by
J. G. Roederer*
W. N. Hess
E. G. Stassinopoulos
*Goddard Space Flight Center*

Geomagnetic field lines are traced into space for more than 500 geophysical stations, using the 48-term Jensen and Cain field expansion for 1960. Total field intensity, magnetic dip, declination, and L-values are computed at each station, and at points 300 and 400 km vertically above the station. Coordinates and B values of the conjugate intersects and of the equatorial (minimum B) points are determined for each field line, as well as the total arc length of the line between origin and conjugate intersect.

A general discussion of the resulting tables is given.

Finally, a series of maps showing constant B and L contours at various levels between surface and 3,000 km are reproduced.

## INTRODUCTION

In the past few years, the study of propagation of charged particles, electromagnetic radiation and magnetohydrodynamic waves along geomagnetic field lines has become a powerful tool in the search for a better knowledge of the structure of the earth's magnetosphere.

The determination of the exact shape of a line of force, its change with local time during geophysical perturbations, and the answer to the question of return to earth of high latitude field lines, are of crucial importance to the problem of the interaction of the solar wind with the earth's magnetic field. The process of propagation of magnetohydrodynamic and very low frequency electromagnetic waves along field lines gives information on the electron and ion densities encountered; the study of precipitation of energetic particles down the field lines into the atmosphere hopefully will lead to a better understanding of the injection and acceleration mechanisms in the magnetosphere.

Many of these investigations are based on ground measurements. Hundreds of IQSY and ex-IGY stations gather information which is being used or which could be used for these studies. These

*National Academy of Sciences - National Research Council, Senior Post Doctoral Research Associate, on leave from Facultad de Ciencias Exactas y Naturales and Centro Nacional de Radiacion Cosmica, Buenos Aires, Argentina.

measurements are particularly valuable, if carried out simultaneously at both "ends" of the same field line. It is, therefore, very useful to know with maximum possible precision, the geometry of the field line which "goes through" each station, and which intersects the ionosphere at several given vertical altitudes for a given field expansion during normal, quiet geomagnetic conditions.

There are many useful parameters related to this "field line geometry." For this preliminary edition, we have selected the following:

1. Geographic coordinates of the station (or the vertical point at high altitude), henceforth called the origin of the field line;
2. Total field intensity at origin;
3. The magnetic dip at origin;
4. The magnetic declination at origin;
5. L-value corresponding to the origin (and within about 1%, to the whole line);
6. Geographic coordinates of the conjugate intersect, i.e. the intersection of the field line with the earth's surface (or a fixed level at the same altitude as the origin), at the other side;
7. Total field intensity at the conjugate intersect;
8. Geographic coordinates of the equatorial point of the field line (defined as the point where the field intensity attains its minimum value on that line);
9. Total field intensity at the equatorial point of the field line;
10. Length of the field line between origin and conjugate intersect.

These quantities, which are printed out in the above order in Appendix B, Tables 1, 2, and 3, by no means represent all useful field magnitudes. However, for reasons of space and time, other important quantities are not reproduced here.

Stations included in our tables were selected from IQSY lists, as well as extracted more or less at random from old IGY tables. This selection does not pretend to be complete; we apologize for omissions and possible errors in name-spelling, coordinates, etc.

A careful analysis of the geographic location of conjugate areas was made. It was found that about 380 stations have their conjugates over sea, 140 stations have conjugate intersects over land, in which 16 of them are over Antarctica, and only 22 pairs of stations are nearly self-conjugate, either deliberately established as such or by chance. We present a list of these self-conjugate pairs, and give a survey of the geographic location of all other conjugate intersects which fall over land, indicating country, and whenever possible, the nearest town to the intersect.

Finally, for the sake of completeness, we present a series of maps with constant B and L contours, for altitudes between sea level and 3,000 km.

## FIELD LINE PARAMETERS

### Selection of Stations

All Stations were selected from lists published in IQSY Notes No. 4 1963 and No. 11 1965, as well as extracted more or less at random from the IGY Annals. Some stations of this latter group may be at present out of operation.

Whenever a group of stations appeared lumped together in the same geographical area, only one or two of them were picked out (generally the station bearing the name of the nearest greater city, for example: Of the pair of stations Godley Head and Christchurch, only the latter was kept). For practical reasons, stations are given in our lists in alphabetical order, according to the first two letters.

### Coordinates

All positions are given in *geographic coordinates*. Latitudes and longitudes are in degrees and *decimal* fractions; negative latitudes are south, negative longitudes are west, and altitudes and arc lengths are given in kilometers.

Information on altitude over sea level was not available for many stations. In case of doubt, sea level was adopted. A test has shown that a change of a few thousand meters in station altitude does not alter appreciably the values listed in our tables, except for stations at very low geomagnetic latitudes.

All calculations were performed for field lines passing through the stations, and through points 300 and 400 km vertically above each. These two levels, which represent typical heights of the F2 layer in its diurnal variation, were believed to be of interest to ionospheric researchers. They may serve to obtain interpolated values for field line parameters of lines of force passing through other heights than the ones selected here.

### Field Parameters

The *geomagnetic field* used in these calculations is the 48 term expansion by Jensen and Cain (Reference 1). A more recent field expansion by Cain et al., (Reference 2), which takes into account the oblateness of the earth and updates the field to 1965, was applied to several stations for comparison. Differences were very small; conjugate points fell within 20-30 km of the positions given in our tables. For the actual computation of the field, McIlwain's subroutine MAGNET was used.* Values of the field are given in gauss in which the error is expected to be of the order of $2 \times 10^{-3}$ gauss.

*MAGNET is part of INVAR (see footnote page 38).

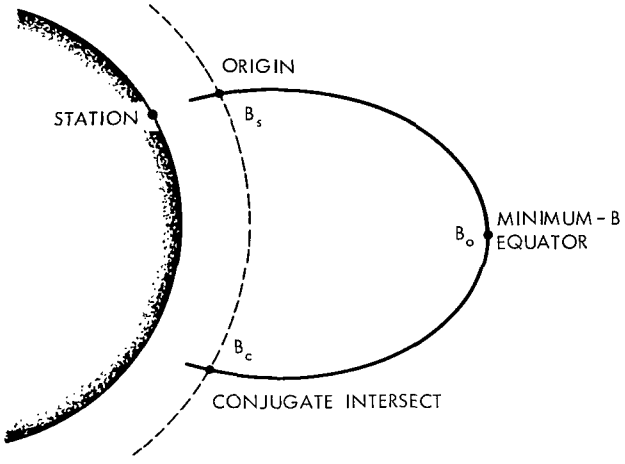


Figure 1—The conjugate intersect with a constant level of the same heights as origin.

The *conjugate intersect* is defined as the intersection of the field line emerging from the origin (surface, 300 km or 400 km above s.l.), with a constant level of the same height as the origin (Figure 1).

The *minimum-B equator* is defined as the point of minimum total field intensity on a given line of force. The locus of all these points is, of course, *not* coincident with the magnetic dip equator. The altitude of the minimum-B equator is very nearly equal to the *maximum* altitude of the field line except for low L lines ($L < 1.2$). Their latitudes, however, may differ appreciably. This was tested in separate runs for all stations. The longitude of the minimum-B equator is the parameter "par excellence" to label a given field line on a L shell, in a nearly invariant way (Reference 4).

For very low geomagnetic latitudes, it sometimes happens that there is no minimum-B value between origin and conjugate intersect. This means that the minimum-B equator of that particular field line lies *below* the origin, or below the conjugate intersect (Figure 2). This may even occur in the case of surface to surface tracing; it is an indication that in the region considered, there is a difference between the *magnetic* and the *minimum-B* or *invariant,* equator. When the field line is very short, the absence of a minimum-B may be just an error fluctuation in B.

Finally, the *L-parameter,* (Reference 3) given in earth radii, is computed through McIlwain's INVAR subroutine.*

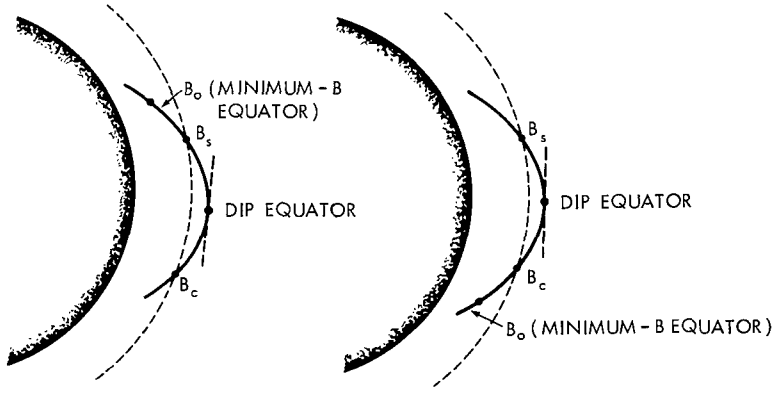


Figure 2—Relation between dip equator and minimum-B equator.

*INVAR is a computer code written by C. E. McIlwain, which has been widely distributed.

If L is high, for example, above 8 earth radii, the field line expansion used in MAGNET is no longer valid, because external sources, as determined by the interaction of the solar wind with the earth's magnetosphere, can then no longer be neglected. This is the reason why field lines were traced only when $L \leq 12$. In general, above $L = 8$, this parameter merely has to be taken as a quantity related to the "invariant" latitude defined by $\cos^2 \Lambda = 1/L$.

It is well known (References 3 and 5) that L is constant for a given magnetic shell only within about 1%. Azimuthal asymmetry of the real geomagnetic field actually splits particle shells according to their equatorial pitch angles (or mirror point field intensities) at a given field line. The INVAR-computed L-values fluctuate on a given "L-shell," and even along a given field line. A good measure of this fluctuation is the quantity $(L-L_o)/L_o$, where $L_o = (M_o/B_o)^{1/3}$ ($M = 0.3117$, $B_o$ = minimum field intensity on the given field line). A test made with our results has shown that the longitude dependence of $(L-L_o)/L_o$ is in excellent agreement with McIlwain's results (Figure 3 in Reference 3). A significant difference, however, arises in the region of longitudes between 5 and 35 degrees east, for L values in the interval 1.6 to 2.6. There we find computed L values 2 to 4% higher than the "azimuthally symmetric" value $L_o$. For many purposes, it may be a sufficient approximation to use $L_o$ for the L value of a station, or of a point in space. The elimination of the subroutine INVAR from the program would then save considerable computer time.

In order to make our tables useful to cosmic ray physicists, we may point out the results of Smart and Shea (Reference 6) who found an excellent correlation between L and the effective geomagnetic cosmic ray cutoff rigidity $P_c$. We have reanalyzed this correlation using the computed surface L values given in Table 2, and concluded that the effective cutoff rigidity can be found for each station by the expression

$$P_c = 15.60\, L^{-2}\ (\mathrm{GV}) \qquad (1)$$

which is valid for $L \gtrsim 1.2$. For equatorial regions this correlation breaks down.

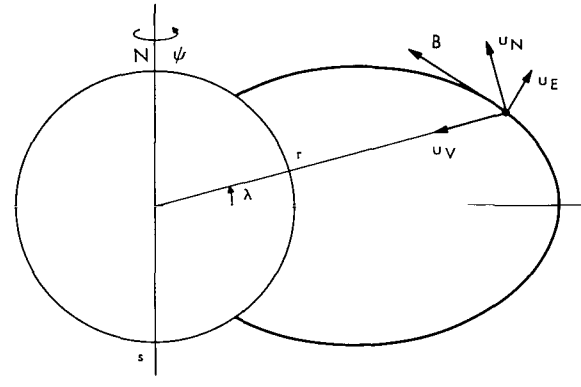

Figure 3—Coordinate system and unit vectors.

## METHOD

### Coordinate System

Figure 3 illustrates the system used. The field components along the unit vectors $u_V$, $u_N$ and $u_E$ are:

$B_V$ (vertical downward) ,

$B_N$ (horizontal north) ,

and

$$B_E \text{ (horizontal east)} .$$

The equations defining an infinitesimal portion of a line of force are then,

$$\frac{\delta S}{B} = -\frac{\delta r}{B_V} = \frac{r\delta\lambda}{B_N} = \frac{r\cos\lambda\delta\phi}{B_E} \quad . \tag{2}$$

$\delta S$ is the element of arc, with components $-\delta r$, $r\delta\lambda$ and $r\cos\lambda\delta\phi$ along the unit vectors. The coordinates of a generic point of a field line originating at $r_s$, $\lambda_s$ and $\phi_s$ are then given by

$$r_n = r_s + \sigma \sum_{i=1}^{n} \frac{B_{Vi}}{B_i} \delta S_i \quad , \tag{3a}$$

$$\lambda_n = \lambda_s - \sigma \sum_{i=1}^{n} \frac{1}{r_i} \frac{B_{Ni}}{B_i} \delta S_i \quad , \tag{3b}$$

and

$$\phi_n = \phi_s - \sigma \sum_{i=1}^{n} \frac{1}{r_i \cos\lambda_i} \frac{B_{Ei}}{B_i} \delta S_i \quad , \tag{3c}$$

where the sign factor $\sigma$ is $\pm 1$ according to whether one proceeds tracing in the opposite/same direction of the field vector. Notice that if the origin is in the magnetic Northern hemisphere ($B_V > 0$), we have to set $\sigma > 0$ in order to follow the line to the conjugate intersect* (direction opposite to $\vec{B}$).

The total arc length between origin and a generic point is

$$s_n = \sum_{i=1}^{n} \delta S_i \quad . \tag{4}$$

## COMPUTER PROGRAM

### Procedure

The flow diagram is shown in Figure 4. The altitude level of the origin is determined by an input parameter which permits one of three internally programmed choices (station altitude, 300

*In our field computations using subroutine MAGNET, we obtain the west component of the field $B_W = -B_E$. For this reason we had to reverse the sign in Equation 3c. (See listing, Appendix A).

and 400 km). Control parameters are initialized and the station is entered. The L value is computed with McIlwain's INVAR subroutine. The L value is then tested; if L > 12, no tracing is attempted. Before the program returns to read in the next station, it computes the total field, the magnetic dip and the declination at the origin. Then, if L $\leq$ 12, the code proceeds to trace the field line. The "Adams Four Point Integration Formula" (Reference 7) for numerical solutions of differential equations is used in this procedure repeatedly at equidistant intervals. The accuracy of this fit depends on the integration step size (element of arc length). To increase efficiency and to save computer time, the constant step size D for a given field line was fixed as a linear function of L in which

$$D = 50\,L - 30 \text{ (km)} \quad . \qquad (5)$$

Exhaustive testing with several step sizes for fixed L values has shown that Equation 5 is satisfactory with respect to both accuracy and machine time.

Initial conditions for the integration of the dependent variables H (altitude), DLAT and DLON are given, and the total field and its components are computed. The dip and the declination are calculated only once, on the first passage through the integration loop. A suitable control causes this part of the program to be bypassed thereafter.

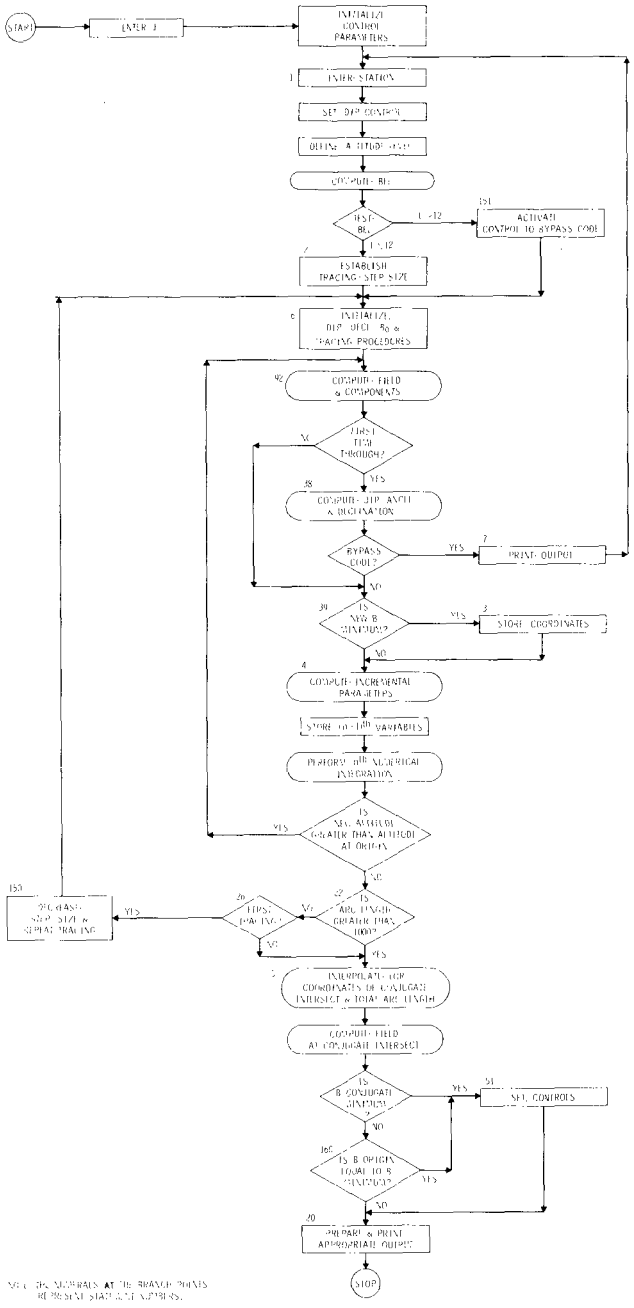


Figure 4—Flow diagram of computer program for determining conjugate intersects.

## Usage and Comments

The computer code is a FORTRAN II monitor controlled program written for the IBM 7090-7094, Standard or Moonlight system (Appendix A, Tables 1 and 2).

Execution time varies from fractions of a second for low latitude stations (small L-values) to several seconds for stations at high latitudes (large L-values). For the 511 stations considered in this work, the average time was approximately 2 seconds per station.

The choice of altitude levels presently contained in the code has previously been explained. Should other considerations prevail or different use be made of the routine, new values can easily be substituted in statements number 58 and 59.

An effort has been made to keep the code flexible for diverse usage. Additional quantities connected with a field line, such as

1. maximum altitude attained above the earth's surface,
2. geographic coordinates of the intersect with the geographic equator,
3. conjugate mirror-points,
4. curvature at the equator, and
5. field components at origin and conjugate intersect

may become readily available through minor modifications.

The field computing part of the program has been kept separate in the form of a subroutine. This is practical and advisable, as experience has shown. Since there exist several models describing the geomagnetic field in terms of a varying number of expansion coefficients and since periodic recomputations of these coefficients are necessary due to a gradually better knowledge of the field and its secular changes, this arrangement is most convenient for interchanging or updating the various models.

Two cases may arise which receive special treatment in the routine,

1. The origin may have an L-value greater than 12, and
2. No minimum-B equator may lie between the origin and the conjugate intersect.

In both, the code will indicate their occurrence by printing relevant comments in place of the regular output. In the tracing process, the location of the minimum-B equator is approximated on the field line with an error proportional to plus or minus one integration step, while there are no limitations with respect to the number of stations or the height of the origin. The restriction $L \leq 12$ imposed on the shell parameter is due to physical (see Field Parameters in the section titled FIELD LINE PARAMETERS) and practical considerations only (to save computer time) and is entirely independent of the code itself. Lines with L-values greater than 100 have been traced repeatedly without any difficulty.

In the loop, the following sequence of operations is performed: (a) the total field intensity is tested at every step, and the coordinates and field intensity of the minimum-B point are stored; (b) the altitude, latitude and longitude increment parameters are evaluated; (c) the (n-1)th dependent and independent variables are stored; (d) and the nth numerical integration is performed.

The integration is terminated whenever the altitude $H_n$ is less than or equal to the altitude of the origin $H_s$. The total arc length is then tested; if $S \leq 1000$ km, the step size is decreased by a factor of 4, and the tracing is repeated for that given field line. This is done in order to obtain a

better fit and to reduce the error in the location of the conjugate intersect, for low latitude stations. If S > 1000, or after a second tracing, the coordinates of the conjugate intersect are obtained by interpolation, and the field intensity is computed at that point.

Finally, a test is made to determine whether the minimum-B equator lies between the origin and the conjugate intersect. The results are printed, and the next station is read into the computer.

## RESULTS

Table B1 (Appendix B) gives the results of our computations for surface-to-surface tracing for 511 geophysical stations. In column 1, the names of the stations are listed. Columns 2 and 3 give the geographical coordinates of the origin; column 4, the total field in gauss; columns 5 and 6, magnetic dip and declination in degrees respectively; and column 7, the L value. Columns 8 and 9 give the coordinates of the conjugate intersect, column 10, the total field at the intersect. Columns 11 and 12 show the coordinates of the equatorial (minimum B) point of the corresponding field line, column 14, the field intensity there, and column 13, the altitude of this point over sea level (almost coincident with the maximum altitude over sea level of that line, except for low L values). Column 15, finally, gives the total arc length of the field line, between origin and conjugate intersect. All distances are in kilometers.

Appendix B, Tables 2 and 3 reproduce the values corresponding to field lines originating 300 and 400 km above each station and intersecting the same altitude as the origin, at the conjugate point. A detailed inspection of the conjugate areas has revealed several features. First of all, as expected, the great majority of the stations have conjugate areas over the sea. There are, nevertheless, 22 pairs of stations which are very nearly conjugate to each other and they are listed in Appendix C, Table 1. For additional information, the mean L value is given, as well as the percentage difference in L. With a few exceptions, this difference is not much greater than the intrinsic fluctuation of L. Another important parameter necessary to judge the "degree of conjugacy" of two stations, is given by the difference of longitudes of the equatorial points of the field lines passing through both stations. This is indicated in the last column of Table 1. Inspecting this table, one recognizes well-known conjugate pairs, in addition to others. Notice in particular, the European-African group of conjugate pairs.

Appendix C, Table 2 lists stations with conjugate areas in the Antarctica. Those already listed in Table 1 are not shown here.

Finally, in Table 3 we give some information about the conjugate area for those stations whose conjugate intersects fall over land, but where there is no other station near by, belonging to our list. In this table, we list the name of the station in alphabetical order, the L value, the name of the city or of the region in the conjugate area, and the country in question.

## B AND L CONTOURS

The last collection of figures represent constant B and L contours for different altitudes. They were obtained in the following way: For a given altitude level, a latitude-longitude grid is

generated with constant intervals of five degrees for the first and of ten degrees for the latter. At those grid points, the magnetic parameters B and L are computed and stored.

The desired constant B or L contours are then obtained by a linear interpolation, which is performed separately for both. The resulting positions are then plotted by computer and the curves are drawn manually.

## ACKNOWLEDGMENT

We are grateful to Dr. J. C. Cain for many useful discussions and for his advice.

REFERENCES

1. Jensen, D. C., and Cain, J. C., "An Interim Geomagnetic Field," *J. Geophys. Res.* 67(9):3568-3569, August 1962 (Abstract).

2. Cain, J. C., Hendricks, S., Daniels, W. E., and Jensen, D. C., "Computation of the Main Geomagnetic Field from Spherical Harmonic Expansions," GSFC Document X-611-64-316, 1964.

3. McIlwain, C. E., "Coordinates for Mapping the Distribution of Magnetically Trapped Particles," *J. Geophys. Res.* 66(11):3681-3691, November 1961.

4. Roederer, J. G., and Welch, J. A., "Calculations of Longitude Dependence of Geomagnetically Trapped Electron Fluxes, Part I, The General Fokker-Planck Equation for Electron Diffusion," GSFC Document X-640-65-149, 1965.

5. Stone, E. C., "The Physical Significance and Application of L, $B_0$, and $R_0$ to Geomagnetically Trapped Particles," *J. Geophys. Res.* 68(14):4157-4166, July 1963.

6. Smart, D. F., and Shea, M. A., "A Study of the Effectiveness of the McIlwain Coordinates in Computing Cosmic Ray Vertical Cutoff Rigidities," *Trans. Am. Geophys. Union,* 46(1):63, March 1965 (Abstract).

7. Slayton, G. R., "Automatic Integration of Differential Equations," IBM, SHARE Distribution, Number 413, 1958.

Appendix A

## Fortran II Monitor Controlled Program

Table A1 Arguments and Parameters.
Table A2 FORTRAN Listing.

Table A1

Arguments and Parameters.

| | |
|---|---|
| Input: | |
| J | fixed point parameter controlling starting altitude; for J = 1, 2, 3 altitude is fixed in the code to station height, 300, 400 km, respectively. |
| BLAT | geographic latitude of station. |
| BLON | geographic longitude of station. |
| BH | height of station above sea level. |
| NAME | designation of station. |
| Internal: | |
| RAD | conversion factor, radians to degrees. |
| N | fixed point parameter counting lines per output page. |
| LP | fixed point parameter numbering tracings per line. |
| ITEST | fixed point parameter controlling dip angle and declination bypass. |
| D | constant incremental change of independent variable (stepsize of integration along field line). |
| S | independent variable: total arc-length. |
| H | dependent variable: height above sea level. |
| DLAT | dependent variable: geographic latitude. |
| DLON | dependent variable: geographic longitude. |
| SGN | sign of vertical field component. |
| DECL | magnetic declination at origin. |
| HM | altitude above sea level of point of minimum B on field line. |
| B | field strength at generic point. |
| BN | North component of field vector at generic point. |
| BW | West component of field vector at generic point.* |
| BV | vertical component of field vector at generic point. |
| FAC | factor for increment parameters DDLAT and DDLON. |
| DH | altitude increment parameter. |
| DDLAT | latitude increment parameter. |
| DDLON | longitude increment parameter. |
| CBN | same as BN at conjugate intersect. |
| CBW | same as BW at conjugate intersect. |
| CBV | same as BV at conjugate intersect. |
| SP | (n-1)th reference arclength for conjugate intersect approximation. |
| DLATP | (n-1)th reference latitude for conjugate intersect approximation. |
| DLONP | (n-1)th reference longitude for conjugate intersect approximation. |
| HP | (n-1)th reference altitude for conjugate intersect approximation. |
| C2 | ratio of B(min) minus B(orig) to B(orig). |
| Output: | |
| BB | field strength at origin. |
| DIP | dip-angle at origin. |
| IDECL | see DECL |
| BEL | magnetic shell parameter L of field line through origin. |
| CLAT | geographic latitude of conjugate intersect. |
| CLON | geographic longitude of conjugate intersect. |
| CB | field strength at conjugate intersect. |
| DLATM | geographic latitude of minimum B point on field line. |
| DLONM | geographic longitude of minimum B point on field line. |
| IHM | see HM |
| BX | minimum field strength on field line. |
| DS | total arclength between origin and conjugate intersect. |

*All arguments are in floating point form, except where otherwise indicated.

## Table A2

## FORTRAN Listing.

```
*      CARDS COLUMN
*      LIST 8
*      LABEL
CLOF1A
C      MODIFIED LOF TRACER, VERSION NO. 3 FOR ALL STARTING ALTITUDES
C      FIELD COMPUTATION BY MCILWAINS MAGNET
C      PARAMETER  J  HAS FOLLOWING VALUES AND MEANING =
C         J=1  LOF TRACING FROM SURFACE TO SURFACE
C         J=2  LOF TRACING 300 KM ABOVE STATION TO 300 KM CONJ.INTERSECT
C         J=3  LOF TRACING 400 KM ABOVE STATION TO 400 KM CONJ.INTERSECT
       DIMENSION NAME(3)
       READ INPUT TAPE 2,1004,J
 1004  FORMAT(I3)
            RAD=57.2957795
       K = 1
       N = 0
   1   READ INPUT TAPE 2,1005,BLAT,BLON,BH,NAME
 1005  FORMAT(2F11.2,F8.2,3A6)
       ITEST = 1
       LP = 1
       IF(J - 2)57,58,59
   58  BH  = 300.
       GO TO 57
   59  BH  = 400.
   57  CALL INVAR(BLAT,BLON,BH ,0.01,BB,BEL)
       IF(BEL - 12.)2,2,151
  151  SENSE LIGHT 4
       GO TO 6
    2  D = 50.*BEL - 30.
    6  DLAT = BLAT
       DLON = BLON
       H = BH
   91  S=0.0
       SENSE LIGHT 1
       BX = 5.
   92  CALL FIELD(DLAT,DLON,H,BN,BW,BV,B)
       GO TO (38,39),ITEST
   38  DIP = ATANF(BV/SQRTF(BN**2 + BW**2))*RAD
       SGN = SIGNF(1.,BV)
       DECL =(ATANF(-BW/BN))*RAD
       IDECL = DECL + .5
   37  ITEST = 2
       IF(SENSE LIGHT 4) 7,39
    7  IF(N)9,9,10
    9  WRITE OUTPUT TAPE 3,73
       WRITE OUTPUT TAPE 3,74
   10  WRITE OUTPUT TAPE 3,77,NAME,BLAT,BLON,SP,DIP,IDECL,BEL
   77  FORMAT(1X3A6,F8.2,F9.2,F7.3,F6.1,I6,F7.2,4X55H** N O   C O M P U T
     1 A T I O N S   P E R F O R M E D **)
       N = N + 1
       GO TO 1
   39  IF(B - BX)3,4,4
    3  DLATM=DLAT
       DLONM=DLON
       HM = H
       BX=B
    4  DH = (BV/B)*SGN
       FAC=SIGNF(RAD/(B*(H+6371.2)),SGN)
       DDLAT=-BN*FAC
       DDLON= BW*FAC/COSF(DLAT/RAD)
       SP = S
```

```
      HP = H
      DLATP = DLAT
      DLONP = DLON
      S=INDVF(S,D)
      H=DPNVF(H,DH)
      DLAT=DPNVF(DLAT,DDLAT)
      DLON=DPNVF(DLON,DDLON)
      IF(H - BH)22,22,92
   22 IF(S - 1000.)26,26,5
   26 GO TO (150,5),LP
  150 D = D/4.
      LP = 2
      GO TO 6
    5 DLAT = DLATP + (DLAT - DLATP)*(BH    - HP)/(H - HP)
      DLON = DLONP + (DLON - DLONP)*(BH    - HP)/(H - HP)
      DS = SP + (S - SP)*(BH    - HP)/(H - HP)
      H = BH
      CLAT = DLAT
      CLON = DLON
      CALL FIELD(CLAT,CLON,H,CBN,CBW,CBV,CB)
      IHM = HM + .5
      IF (CB - BX)51,51,160
  160 C2 = BX/BB - 1.
   52 IF(ABSF(C2) - 1.E-5)51,51,20
   51 SENSE LIGHT 2
      SENSE LIGHT 3
   20 IF(ABSF(CLON) - 180.)88,88,87
   87 IF(CLON)82,88,83
   82 CLON = CLON + 360.
      GO TO 88
   83 CLON = CLON - 360.
   88 IF(SENSE LIGHT 3)46,45
   45 IF(ABSF(DLONM) - 180.)46,46,84
   84 IF(DLONM)85,46,86
   85 DLONM = DLONM + 360.
      GO TO 46
   86 DLONM = DLONM - 360.
   46 IF(N)30,30,21
   30 WRITE OUTPUT TAPE 3,73
   73 FORMAT(131H1     STATIONS        **       O      R      I      G      I
     1    N     ** CONJUGATE  INTERS. **  MINIMUM-B   E Q U A T O R  ** AR
     2C          //)
      WRITE OUTPUT TAPE 3,74
   74 FORMAT(22X4HLAT.,5X5HLONG.,4X1HB,4X3HDIP,3X5HDECL.,3X1HL,5X4HLAT.,
     13X5HLONG.,4X1HB,5X4HLAT.,4X5HLONG.,4X4HALT.,4X1HB,6X2HKM///)
   21 IF(SENSE LIGHT 2)23,31
   23 WRITE OUTPUT TAPE 3,78,NAME,BLAT,BLON,BB,DIP,IDECL,BLL,CLAT,CLON,C
     1B,DS
   78 FORMAT(1X3A6,F8.2,F9.2,F7.3,F6.1,I6,F7.2,F7.1,F8.1,F7.3,4X28HNO MI
     1NIMUM B BETWEEN INTERS.,F8.0)
      GO TO 90
   31 WRITE OUTPUT TAPE 3,75,NAME,BLAT,BLON,BB,DIP,IDECL,BLL,CLAT,CLON,C
     1B,DLATM,DLONM,IHM,BX,DS
   75 FORMAT(1X3A6,F8.2,F9.2,F7.3,F6.1,I6,F7.2,F7.1,F8.1,F7.3,F8.2,F9.2,
     1I7,F7.3,F9.0)
   90 N = N + 1
      IF(N - 45)32,33,33
   33 N = 0
      WRITE OUTPUT TAPE 3,76,K
   76 FORMAT(////60X5HPAGE I4)


      K = K + 1
   32 GO TO 1
      END
```

Appendix B

## Field Line Parameters for Selected Geophysical Stations

Table B1 Tracing from Surface to Surface.
Table B2 Tracing 300 km Above Stations.
Table B3 Tracing 400 km Above Stations.

Table B1

Tracing from Surface to Surface.

Table B1

Tracings from Surface to Surface.

| STATIONS | ** C | R | I | G | I | N | ** CONJUGATE | INTERS. | ** MINIMUM-B | E Q U A T O R | ** ARC | | |
|---|---|---|---|---|---|---|---|---|---|---|---|---|---|
| | LAT. | LONG. | B | DIP | DECL. | L | LAT. | LONG. | B | LAT. | LONG. | ALT. | B | KM |
| ABASHIRI | 43.97 | 140.33 | 0.506 | 58.4 | -8 | 1.50 | -26.5 | 137.8 | 0.557 | 9.17 | 140.61 | 3571 | 0.092 | 13461 |
| ABISKO | 68.35 | 18.82 | 0.515 | 77.3 | 2 | 5.69 | -59.5 | 64.0 | 0.482 | 3.46 | 33.52 | 29669 | 0.002 | 86886 |
| ABERYSTWYTH | 52.40 | -4.07 | 0.477 | 68.0 | -9 | 2.57 | -47.4 | 24.8 | 0.321 | 0.40 | 7.34 | 9456 | 0.019 | 30770 |
| ACCRA | 5.63 | -0.20 | 0.311 | -7.4 | -11 | 1.00 | 11.8 | -1.5 | 0.323 | 6.95 | -0.49 | 15 | 0.311 | 710 |
| ADEN | 12.77 | 44.97 | 0.369 | 9.7 | 1 | 0.96 | 4.7 | 44.9 | 0.351 | 6.78 | 44.89 | 30 | 0.348 | 906 |
| ADDIS ABABA | 9.03 | 38.77 | 0.353 | -1.4 | 1 | 0.96 | 10.2 | 38.8 | 0.355 | NO MINIMUM B BETWEEN | | INTERS. | | 129 |
| ADELAIDE | -34.95 | 138.53 | 0.606 | -67.3 | 7 | 2.03 | 53.2 | 143.3 | 0.542 | 9.52 | 142.68 | 6945 | 0.037 | 22995 |
| ADAK | 51.90 | -176.65 | 0.486 | 63.4 | 9 | 2.11 | -38.9 | 164.8 | 0.587 | 6.03 | 174.60 | 7253 | 0.034 | 24137 |
| AGINCOURT | 43.80 | -79.30 | 0.585 | 74.3 | -7 | 3.33 | -69.8 | -99.9 | 0.547 | -12.38 | -79.11 | 14726 | 0.008 | 45473 |
| AHMEDABAD | 23.02 | 72.60 | 0.447 | 32.1 | -1 | 1.00 | -5.3 | 74.6 | 0.404 | 7.81 | 73.34 | 499 | 0.303 | 3521 |
| AIRE-SUR-ADOUR | 43.70 | -0.30 | 0.452 | 60.1 | -6 | 1.75 | -32.1 | 17.3 | 0.314 | 2.66 | 7.23 | 4447 | 0.059 | 16188 |
| AKROTIRI | 34.58 | 32.95 | 0.447 | 49.0 | 3 | 1.25 | -16.1 | 35.6 | 0.345 | 6.91 | 33.34 | 1720 | 0.156 | 7764 |
| AKLAVIK | 68.23 | -135.00 | 0.587 | 81.3 | 40 | 9.05 | -62.8 | 167.8 | 0.661 | 1.29 | -162.72 | 51758 | 0.000 | 147107 |
| AKITA | 39.73 | 140.13 | 0.483 | 53.7 | -7 | 1.35 | -22.7 | 138.1 | 0.531 | 9.03 | 140.45 | 2586 | 0.128 | 10596 |
| ALMERIA | 36.85 | -2.47 | 0.426 | 52.4 | -7 | 1.41 | -22.9 | 11.0 | 0.320 | 3.63 | 3.74 | 2494 | 0.108 | 10326 |
| ALDAN | 58.60 | 125.50 | 0.591 | 74.6 | -12 | 2.61 | -39.4 | 124.8 | 0.629 | 10.24 | 125.99 | 10707 | 0.017 | 33282 |
| ALERT | 82.55 | -63.58 | 0.560 | 85.9 | -86 | 246.02 | ** N O | C O M P U T A T I O N S | | P E R F O R M E D ** | | | | |
| ALMA-ATA | 43.20 | 76.92 | 0.558 | 62.8 | 3 | 1.53 | -25.7 | 82.7 | 0.486 | 8.35 | 77.75 | 3809 | 0.085 | 13834 |
| ALBUQUERQUE | 35.08 | -106.62 | 0.536 | 62.8 | 13 | 1.89 | -49.1 | -128.5 | 0.517 | -7.94 | -114.50 | 5762 | 0.045 | 20036 |
| ALMIRANTE BROWN | -64.88 | -62.87 | 0.436 | -57.8 | 17 | 2.31 | 35.9 | -65.5 | 0.534 | -12.97 | -59.60 | 8083 | 0.025 | 27181 |
| ANCON | -11.77 | -77.15 | 0.286 | 0.5 | 6 | 1.03 | -12.3 | -77.2 | 0.285 | NO MINIMUM B BETWEEN | | INTERS. | | 57 |
| ANCHORAGE | 61.17 | -149.98 | 0.558 | 74.1 | 27 | 4.12 | -53.6 | 172.2 | 0.634 | 2.95 | -168.74 | 20139 | 0.004 | 59846 |
| ANTOFAGASTA | -23.65 | -70.42 | 0.263 | -18.4 | 5 | 1.08 | -3.1 | -69.7 | 0.313 | -16.64 | -69.91 | 176 | 0.248 | 2373 |
| APIA | -13.80 | -171.77 | 0.398 | -28.8 | 12 | 1.05 | 15.2 | -166.1 | 0.342 | 2.47 | -168.55 | 456 | 0.273 | 3606 |
| APATITY | 67.55 | 33.33 | 0.525 | 77.6 | 12 | 5.02 | -55.7 | 69.4 | 0.488 | 5.22 | 43.60 | 25502 | 0.002 | 75121 |
| ARKHANGELSK | 64.58 | 40.50 | 0.531 | 76.7 | 15 | 4.07 | -51.7 | 69.1 | 0.473 | 5.95 | 47.44 | 19450 | 0.005 | 58219 |
| ARCETRI | 43.75 | 11.25 | 0.457 | 59.6 | -2 | 1.66 | -29.0 | 24.3 | 0.324 | 4.33 | 16.30 | 4042 | 0.068 | 14897 |
| AREQUIPA | -16.35 | -71.57 | 0.270 | -6.2 | 4 | 1.05 | -9.8 | -71.2 | 0.286 | NO MINIMUM B BETWEEN | | INTERS. | | 729 |
| ARGENTINE ISLAND | -65.25 | -64.27 | 0.441 | -58.2 | 18 | 2.35 | 36.3 | -66.0 | 0.536 | -13.17 | -60.30 | 8312 | 0.024 | 27818 |
| ARMIDALE | -30.30 | 151.40 | 0.565 | -60.9 | 11 | 1.65 | 46.9 | 159.5 | 0.474 | 8.24 | 156.83 | 4392 | 0.071 | 15974 |
| ASSWAN | 23.97 | 32.78 | 0.398 | 30.7 | 2 | 1.04 | -3.7 | 33.1 | 0.342 | 8.14 | 32.71 | 466 | 0.272 | 3413 |
| ASO | 32.88 | 131.02 | 0.470 | 46.7 | -5 | 1.17 | -16.5 | 130.3 | 0.493 | 8.72 | 131.52 | 1505 | 0.195 | 7224 |
| ASHKABAD | 37.93 | 55.10 | 0.502 | 56.3 | 5 | 1.37 | -22.0 | 59.7 | 0.385 | 6.68 | 55.42 | 2573 | 0.121 | 10349 |
| ATHENS | 37.97 | 23.72 | 0.448 | 52.8 | 1 | 1.36 | -19.7 | 29.3 | 0.340 | 6.36 | 25.48 | 2316 | 0.122 | 9636 |
| BAJA | 46.18 | 19.00 | 0.471 | 62.2 | 1 | 1.79 | -31.5 | 31.5 | 0.327 | 4.53 | 23.15 | 4791 | 0.056 | 17070 |
| BAGHDAD | 33.35 | 44.38 | 0.462 | 49.0 | 4 | 1.23 | -16.4 | 46.4 | 0.353 | 6.54 | 44.30 | 1649 | 0.165 | 7538 |
| BANGKOK | 13.75 | 100.55 | 0.417 | 9.9 | 1 | 0.92 | 5.4 | 100.4 | 0.411 | 9.06 | 100.49 | 40 | 0.401 | 932 |
| BAR I | 69.58 | -140.18 | 0.583 | 81.3 | 38 | 9.21 | -62.0 | 163.8 | 0.663 | 2.52 | -168.72 | 52826 | 0.000 | 150008 |
| BALBOA | 8.95 | -79.57 | 0.387 | 37.3 | 4 | 1.17 | -32.7 | -85.2 | 0.313 | -13.60 | -81.42 | 912 | 0.194 | 5542 |
| BAIE ST. PAUL | 47.43 | -70.50 | 0.579 | 75.8 | -19 | 4.03 | -75.5 | -79.2 | 0.539 | -12.46 | -64.90 | 19044 | 0.005 | 57701 |
| BARTER ISLAND | 70.13 | -143.67 | 0.581 | 81.1 | 37 | 9.05 | -61.4 | 161.9 | 0.664 | 3.18 | -172.15 | 51803 | 0.000 | 147162 |
| BAKER LAKE | 64.30 | -96.08 | 0.608 | 86.3 | 4 | 15.00 | ** N O | C O M P U T A T I O N S | | P E R F O R M E D ** | | | | |
| BATTLE CREEK | 42.27 | -85.17 | 0.586 | 73.1 | -0 | 3.01 | -65.9 | -109.6 | 0.551 | -11.79 | -87.99 | 12776 | 0.011 | 39911 |
| BANARAS | 25.33 | 83.02 | 0.467 | 35.3 | -0 | 1.02 | -6.2 | 84.7 | 0.429 | 8.64 | 83.62 | 629 | 0.293 | 4015 |
| BANGUI | 4.60 | 18.58 | 0.332 | -16.1 | -5 | 0.99 | 17.7 | 17.5 | 0.355 | 9.56 | 18.11 | 98 | 0.319 | 1500 |

Table B1

Tracings from Surface to Surface.

| STATIONS | ** GEOGRAPHIC | | | | | | ** CONJUGATE | | | ** MINIMUM-B EQUATOR | | | | ** ARC |
|---|---|---|---|---|---|---|---|---|---|---|---|---|---|---|
| | LAT. | LONG. | B | DIP | DECL. | L | LAT. | LONG. | B | LAT. | LONG. | ALT. | B | KM |
| BASE RCI BAUDOUIN | -70.43 | 23.32 | 0.457 | -65.0 | -32 | 5.21 | 59.5 | -31.7 | 0.516 | -5.35 | -11.56 | 26283 | 0.002 | 78127 |
| BANGUIC | 16.42 | 120.58 | 0.409 | 19.0 | 0 | 0.95 | -0.8 | 120.1 | 0.411 | 7.93 | 120.45 | 165 | 0.364 | 1986 |
| BELEM | -1.00 | -49.00 | 0.298 | 15.9 | -14 | 1.09 | -17.2 | -44.6 | 0.247 | -13.69 | -45.60 | 90 | 0.244 | 1913 |
| BELSK | 51.84 | 20.80 | 0.487 | 67.3 | 2 | 2.24 | -39.7 | 38.8 | 0.334 | 4.00 | 26.23 | 7527 | 0.029 | 25000 |
| BETTLES | 66.90 | -151.84 | 0.570 | 77.8 | 29 | 5.98 | -57.1 | 164.2 | 0.654 | 3.62 | -174.69 | 32092 | 0.001 | 92780 |
| BEDFORD | 42.48 | -71.28 | 0.569 | 72.8 | -14 | 3.11 | -70.8 | -79.3 | 0.511 | -12.90 | -66.99 | 13244 | 0.010 | 41532 |
| BERMUDA | 32.37 | -64.67 | 0.516 | 64.4 | -13 | 2.04 | -61.3 | -60.9 | 0.404 | -13.43 | -59.01 | 6303 | 0.036 | 22148 |
| BEOGRAD | 44.80 | 20.52 | 0.468 | 60.8 | 1 | 1.69 | -29.4 | 31.4 | 0.329 | 4.96 | 24.05 | 4253 | 0.065 | 15473 |
| BIRD | 56.50 | 94.20 | 0.605 | 75.7 | 2 | 2.48 | -38.0 | 101.1 | 0.585 | 9.80 | 95.52 | 9907 | 0.020 | 30963 |
| BISMARK | 46.82 | -100.77 | 0.599 | 74.6 | 12 | 3.38 | -62.6 | -135.3 | 0.592 | -8.95 | -110.21 | 15304 | 0.008 | 46711 |
| BJORNOYA | 74.52 | 19.02 | 0.527 | 80.1 | 1 | 9.55 | -63.7 | 77.3 | 0.546 | 4.23 | 40.59 | 54426 | 0.000 | 155251 |
| BORCK | 58.03 | 38.33 | 0.521 | 72.9 | 11 | 2.86 | -45.2 | 59.3 | 0.410 | 5.62 | 42.80 | 11716 | 0.013 | 36681 |
| BOLOGNA | 44.50 | 11.35 | 0.459 | 60.4 | -2 | 1.71 | -30.1 | 25.0 | 0.323 | 4.19 | 16.57 | 4307 | 0.063 | 15683 |
| BOULDER | 40.03 | -105.30 | 0.566 | 67.9 | 14 | 2.32 | -54.4 | -131.9 | 0.552 | -7.99 | -114.16 | 8516 | 0.024 | 27777 |
| BOMBAY | 19.00 | 72.83 | 0.427 | 23.7 | -1 | 0.96 | -1.2 | 74.3 | 0.396 | 7.84 | 73.45 | 247 | 0.345 | 2383 |
| BOGOTA | 4.63 | -74.08 | 0.359 | 31.8 | 1 | 1.13 | -30.5 | -77.2 | 0.285 | -15.23 | -74.97 | 605 | 0.213 | 4414 |
| BRISBANE | -27.53 | 152.92 | 0.546 | -57.6 | 10 | 1.51 | 43.7 | 160.5 | 0.454 | 8.32 | 157.96 | 3487 | 0.093 | 13394 |
| BUDAPEST | 46.68 | 21.27 | 0.475 | 62.7 | 2 | 1.81 | -32.1 | 33.6 | 0.328 | 4.79 | 25.11 | 4964 | 0.053 | 17559 |
| BUENOS AIRES | -34.52 | -58.50 | 0.255 | -32.1 | 0 | 1.20 | 7.2 | -62.1 | 0.364 | -16.28 | -59.45 | 819 | 0.183 | 5412 |
| BUNIA | 1.53 | 30.18 | 0.340 | -22.1 | -1 | 1.00 | 19.7 | 30.0 | 0.375 | 8.70 | 29.98 | 192 | 0.311 | 2114 |
| BYRD STATION | -79.98 | -120.02 | 0.605 | -74.8 | 70 | 7.25 | 55.7 | -78.9 | 0.601 | -12.02 | -77.34 | 39758 | 0.001 | 114912 |
| CAPRI | 40.57 | 14.33 | 0.448 | 55.9 | -1 | 1.48 | -23.9 | 24.0 | 0.332 | 5.20 | 18.07 | 3004 | 0.094 | 11772 |
| CASTEL TESINO | 46.05 | 11.65 | 0.464 | 62.0 | -1 | 1.81 | -32.4 | 26.5 | 0.321 | 3.88 | 17.23 | 4899 | 0.054 | 17430 |
| CATANIA | 37.50 | 15.07 | 0.437 | 51.9 | -1 | 1.35 | -19.5 | 22.7 | 0.336 | 6.05 | 18.09 | 2250 | 0.123 | 9462 |
| CAPE CHELYUSKIN | 77.72 | 104.28 | 0.578 | 86.2 | 17 | 9.36 | -56.4 | 113.3 | 0.646 | 10.83 | 104.41 | 53708 | 0.000 | 152202 |
| CAPE ZHELANIA | 76.90 | 68.60 | 0.562 | 83.9 | 29 | 9.33 | -58.0 | 98.4 | 0.607 | 9.65 | 77.70 | 53367 | 0.000 | 151583 |
| CAPE SCHMIDT | 68.87 | -179.48 | 0.560 | 77.1 | 10 | 5.16 | -52.7 | 150.9 | 0.657 | 7.15 | 164.48 | 26858 | 0.002 | 78214 |
| CAMBRIDGE UK | 52.22 | 0.10 | 0.476 | 67.7 | -7 | 2.49 | -45.4 | 26.7 | 0.320 | 1.09 | 10.43 | 8908 | 0.021 | 29160 |
| CARIBOU | 46.87 | -68.02 | 0.573 | 75.1 | -21 | 3.85 | -75.3 | -70.8 | 0.525 | -12.21 | -61.19 | 17919 | 0.005 | 54631 |
| CALCUTTA | 22.93 | 88.52 | 0.455 | 30.0 | -0 | 0.98 | -3.3 | 89.4 | 0.427 | 9.05 | 88.87 | 425 | 0.327 | 3204 |
| CAPE HALLETT | -72.32 | 178.22 | 0.660 | -83.6 | -87 | 16.06 | ** NO COMPUTATIONS PERFORMED ** | | | | | | | |
| CAMPBELL ISLAND | -52.55 | 169.15 | 0.635 | -76.0 | 27 | 4.02 | 61.7 | -154.9 | 0.553 | 3.48 | -173.05 | 19492 | 0.005 | 58042 |
| CANBERRA | -35.32 | 149.00 | 0.596 | -66.2 | 11 | 1.99 | 52.5 | 158.5 | 0.507 | 8.50 | 155.25 | 6593 | 0.040 | 22151 |
| CAPETOWN | -34.15 | 18.32 | 0.312 | -65.8 | -27 | 1.83 | 45.0 | -0.6 | 0.456 | 2.25 | 7.43 | 4970 | 0.052 | 17738 |
| CAMDEN | -34.08 | 150.68 | 0.587 | -64.8 | 12 | 1.89 | 51.0 | 160.2 | 0.496 | 8.26 | 156.90 | 5907 | 0.047 | 20246 |
| CAPE CANAVERAL | 28.40 | -80.60 | 0.517 | 61.4 | 0 | 1.77 | -53.9 | -93.5 | 0.442 | -13.05 | -82.23 | 4812 | 0.055 | 17556 |
| CAPE JONES | 54.50 | -79.50 | 0.602 | 80.9 | -18 | 6.58 | -78.8 | -117.7 | 0.602 | -12.04 | -78.49 | 35450 | 0.001 | 102970 |
| CEBU | 10.33 | 123.90 | 0.392 | 6.2 | 1 | 0.93 | 4.7 | 123.8 | 0.394 | 7.82 | 123.85 | 17 | 0.388 | 625 |
| CHAMICAL | -30.33 | -66.33 | 0.260 | -27.3 | 5 | 1.14 | 2.7 | -66.6 | 0.342 | -16.79 | -65.83 | 495 | 0.213 | 4049 |
| CHURCHILL | 58.77 | -94.17 | 0.613 | 83.5 | 3 | 8.63 | -74.4 | -152.6 | 0.638 | -9.64 | -103.74 | 48685 | 0.000 | 139215 |
| CHAMBON-LA-FORET | 48.02 | 2.27 | 0.466 | 64.1 | -5 | 2.07 | -38.0 | 22.9 | 0.312 | 1.98 | 10.59 | 6201 | 0.038 | 21324 |
| CHICAGO | 41.83 | -87.67 | 0.585 | 72.5 | 2 | 2.90 | -64.3 | -113.1 | 0.552 | -11.56 | -91.62 | 12122 | 0.012 | 38040 |
| CHARLOTTESVILLE | 38.03 | -78.22 | 0.564 | 70.1 | -5 | 2.54 | -64.7 | -93.7 | 0.506 | -12.98 | -78.06 | 9694 | 0.019 | 31436 |
| CHITA | 52.05 | 113.48 | 0.595 | 70.9 | -7 | 2.00 | -33.5 | 115.4 | 0.597 | 10.03 | 114.70 | 6916 | 0.038 | 22646 |
| CHITTAGONG | 22.35 | 91.82 | 0.453 | 28.7 | -0 | 0.97 | -2.7 | 92.4 | 0.428 | 9.09 | 92.04 | 384 | 0.336 | 3029 |

## Table B1

### Tracings from Surface to Surface.

| STATIONS | ** C | R | I | G | I | N | ** CONJUGATE | INTERS. ** | MINIMUM-B | E Q U A T O R | ** ARC | | |
|---|---|---|---|---|---|---|---|---|---|---|---|---|---|
| | LAT. | LONG. | B | DIP | DECL. | L | LAT. | LONG. | B | LAT. | LONG. | ALT. | B | KM |
| CHRISTCHURCH | -43.57 | 172.80 | 0.594 | -68.9 | 21 | 2.41 | 53.0 | -162.4 | 0.506 | 4.19 | -174.57 | 9166 | 0.023 | 29497 |
| CHACALTAYA | -16.32 | -68.15 | 0.265 | -5.4 | 1 | 1.06 | -10.5 | -68.1 | 0.280 | NO MINIMUM B BETWEEN INTERS. | | | | 647 |
| CLIMAX | 39.37 | -106.18 | 0.561 | 67.1 | 14 | 2.24 | -53.4 | -132.1 | 0.546 | -7.73 | -115.00 | 8010 | 0.027 | 26349 |
| CLONCURRY | -20.67 | 140.50 | 0.515 | -50.8 | 6 | 1.28 | 37.5 | 142.7 | 0.463 | 8.96 | 142.83 | 2147 | 0.149 | 9310 |
| CONCORD | 43.20 | -71.53 | 0.571 | 73.3 | -14 | 3.23 | -71.5 | -80.3 | 0.516 | -12.65 | -67.25 | 13969 | 0.009 | 43546 |
| COOK | -30.63 | 130.40 | 0.587 | -63.8 | 4 | 1.74 | 48.7 | 131.8 | 0.552 | 9.53 | 132.55 | 5165 | 0.059 | 17896 |
| COLLEGE | 64.85 | -147.83 | 0.570 | 77.0 | 30 | 5.43 | -56.9 | 168.6 | 0.648 | 2.94 | -169.77 | 28588 | 0.002 | 83146 |
| CORINALDO | 43.63 | 13.00 | 0.458 | 59.4 | -1 | 1.65 | -28.5 | 25.3 | 0.326 | 4.46 | 17.68 | 3960 | 0.070 | 14644 |
| COIMBRA | 40.22 | -8.42 | 0.440 | 57.1 | -10 | 1.62 | -30.2 | 9.9 | 0.309 | 1.58 | -0.05 | 3677 | 0.073 | 13973 |
| CONCEPCION | -36.58 | -72.98 | 0.291 | -35.8 | 12 | 1.21 | 9.1 | -70.7 | 0.386 | -15.53 | -70.51 | 1042 | 0.176 | 6134 |
| CORDOBA | -31.32 | -64.22 | 0.258 | -28.3 | 4 | 1.15 | 3.6 | -65.2 | 0.346 | -16.70 | -64.04 | 557 | 0.206 | 4330 |
| COLOMBO | 6.90 | 79.87 | 0.400 | -6.5 | -3 | 0.92 | 12.2 | 79.5 | 0.407 | 8.62 | 79.76 | 15 | 0.398 | 591 |
| COCOS ISLAND | -12.20 | 96.90 | 0.470 | -45.5 | -2 | 1.11 | 31.1 | 96.0 | 0.506 | 9.08 | 96.29 | 1239 | 0.226 | 6143 |
| COPENHAGEN | 55.75 | 12.50 | 0.488 | 70.1 | -0 | 2.75 | -47.0 | 38.6 | 0.345 | 2.70 | 21.21 | 10703 | 0.016 | 34137 |
| CORAL HARBOUR | 64.20 | -83.40 | 0.600 | 85.6 | -33 | 17.14 | ** N O | C O M P U T A T I O N S | | P E R F O R M E D ** | | | | |
| CRACOW | 50.05 | 19.95 | 0.482 | 65.8 | 2 | 2.10 | -37.2 | 36.1 | 0.328 | 4.18 | 24.97 | 6546 | 0.036 | 22176 |
| CURACAO | 12.08 | -68.84 | 0.404 | 43.5 | -3 | 1.27 | -40.3 | -70.2 | 0.297 | -15.57 | -67.87 | 1402 | 0.152 | 7419 |
| CUZCO | -13.52 | -71.98 | 0.276 | -1.0 | 3 | 1.05 | -12.5 | -71.9 | 0.279 | NO MINIMUM B BETWEEN INTERS. | | | | 116 |
| DAVIS | -68.60 | 78.00 | 0.563 | -73.2 | -68 | 14.02 | ** N O | C O M P U T A T I O N S | | P E R F O R M E D ** | | | | |
| DAPANGO | 10.80 | 0.07 | 0.321 | 4.2 | -10 | 1.00 | 7.3 | 0.8 | 0.315 | NO MINIMUM B BETWEEN INTERS. | | | | 402 |
| DALLAS | 32.78 | -96.80 | 0.536 | 62.7 | 9 | 1.86 | -51.1 | -116.8 | 0.497 | -10.10 | -102.87 | 5551 | 0.047 | 19485 |
| DAKAR | 14.66 | -17.43 | 0.328 | 20.8 | -13 | 1.05 | -4.8 | -11.9 | 0.288 | 2.42 | -14.08 | 211 | 0.265 | 2363 |
| DARWIN-COONAWARRA | -12.43 | 130.90 | 0.465 | -39.2 | 3 | 1.09 | 28.4 | 131.5 | 0.443 | 8.63 | 131.84 | 975 | 0.243 | 5482 |
| DEBRECEN | 47.48 | 21.65 | 0.477 | 63.5 | 2 | 1.87 | -33.2 | 34.6 | 0.328 | 4.63 | 25.64 | 5294 | 0.049 | 18525 |
| DE BILT | 52.10 | 5.18 | 0.477 | 67.4 | -4 | 2.41 | -43.5 | 29.3 | 0.321 | 1.91 | 14.22 | 8417 | 0.024 | 27699 |
| DEEP RIVER | 46.10 | -77.50 | 0.588 | 75.8 | -11 | 3.78 | -72.5 | -98.0 | 0.555 | -12.60 | -76.09 | 17572 | 0.006 | 53437 |
| DENVER | 39.75 | -105.00 | 0.565 | 67.7 | 13 | 2.30 | -54.3 | -131.3 | 0.550 | -8.14 | -113.76 | 8378 | 0.025 | 27391 |
| DEHRA DUN | 30.33 | 78.05 | 0.493 | 44.8 | 0 | 1.11 | -12.0 | 80.9 | 0.440 | 8.20 | 78.84 | 1194 | 0.223 | 5984 |
| DELHI | 28.63 | 77.22 | 0.483 | 42.0 | -0 | 1.08 | -10.4 | 79.8 | 0.431 | 8.20 | 78.01 | 994 | 0.244 | 5319 |
| DECEPCION | -62.98 | -60.72 | 0.416 | -56.1 | 15 | 2.16 | 34.1 | -64.6 | 0.524 | -13.18 | -58.67 | 7069 | 0.031 | 24327 |
| DIXON ISLAND | 73.53 | 80.70 | 0.575 | 84.0 | 26 | 6.90 | -54.2 | 100.6 | 0.611 | 10.10 | 85.33 | 37860 | 0.001 | 108589 |
| DJIBOUTI | 11.55 | 43.15 | 0.363 | 6.2 | 1 | 0.96 | 6.4 | 43.1 | 0.352 | 7.03 | 43.08 | 7 | 0.352 | 574 |
| DJAKARTA | -6.17 | 107.00 | 0.443 | -32.9 | 2 | 1.00 | 24.1 | 107.5 | 0.459 | 8.77 | 107.35 | 552 | 0.308 | 3777 |
| DODAIRA | 36.00 | 139.20 | 0.465 | 49.4 | -6 | 1.24 | -19.3 | 137.6 | 0.508 | 8.99 | 139.53 | 1918 | 0.163 | 8581 |
| DOLGOPRUDNAYA | 55.94 | 37.52 | 0.517 | 71.4 | 10 | 2.59 | -43.0 | 56.2 | 0.392 | 5.57 | 41.40 | 10008 | 0.018 | 31884 |
| DOURBES | 50.10 | 4.60 | 0.472 | 65.8 | -4 | 2.23 | -40.6 | 26.5 | 0.315 | 2.01 | 13.07 | 7194 | 0.030 | 24184 |
| DUNSINK | 53.38 | -6.33 | 0.480 | 68.8 | -11 | 2.74 | -49.9 | 25.0 | 0.329 | -0.23 | 6.06 | 10512 | 0.016 | 33804 |
| DUSHETTI | 42.08 | 44.70 | 0.498 | 60.0 | 7 | 1.54 | -26.2 | 50.6 | 0.360 | 6.21 | 45.24 | 3505 | 0.086 | 13163 |
| DURHAM | 43.08 | -70.92 | 0.570 | 73.2 | -15 | 3.20 | -71.5 | -78.5 | 0.513 | -12.70 | -66.34 | 13808 | 0.009 | 43112 |
| DUMONT D'URVILLE | -66.67 | 140.02 | 0.671 | -89.6 | -70 | 36.22 | ** N O | C O M P U T A T I O N S | | P E R F O R M E D ** | | | | |
| DURBAN | -29.83 | 31.03 | 0.328 | -65.2 | -20 | 1.71 | 45.1 | 19.7 | 0.468 | 4.82 | 23.42 | 4358 | 0.063 | 15787 |
| EDINBURGH | 55.92 | -3.18 | 0.485 | 70.4 | -9 | 3.04 | -52.3 | 30.4 | 0.347 | 0.24 | 9.53 | 12446 | 0.011 | 39244 |
| EIGHTS | -75.23 | -77.17 | 0.534 | -67.1 | 32 | 3.91 | 47.0 | -69.9 | 0.577 | -12.48 | -64.10 | 18368 | 0.005 | 55835 |
| ELLSWORTH | -77.72 | -41.13 | 0.513 | -66.3 | 9 | 4.49 | 50.7 | -59.9 | 0.560 | -11.09 | -48.12 | 21885 | 0.003 | 65813 |
| ELISABETHVILLE | -11.63 | 27.42 | 0.342 | -47.9 | -6 | 1.17 | 31.7 | 24.5 | 0.422 | 7.50 | 25.46 | 1213 | 0.189 | 6131 |

Table B1

Tracings from Surface to Surface.

| STATIONS | ** C | R | I | G | I | N | ** CONJUGATE | INTERS. | ** MINIMUM-B | E Q U A T O R | | ** ARC |
|---|---|---|---|---|---|---|---|---|---|---|---|---|
| | LAT. | LONG. | B | DIP | DECL. | L | LAT. | LONG. | B | LAT. | LONG. | ALT. | B | KM |
| ENNADAI | 61.30 | -101.20 | 0.613 | 84.2 | 17 | 9.86 | -72.4 | -164.6 | 0.648 | -8.02 | -116.17 | 56632 | 0.000 | 161017 |
| ENUGU | 6.47 | 7.55 | 0.321 | -9.0 | -9 | 0.99 | 13.9 | 6.3 | 0.334 | 8.54 | 7.20 | 27 | 0.319 | 845 |
| ESKDALEMUIR | 55.32 | -3.20 | 0.484 | 70.0 | -9 | 2.95 | -51.4 | 29.4 | 0.341 | 0.41 | 9.22 | 11857 | 0.013 | 37578 |
| ESPERANZA | -63.38 | -56.98 | 0.413 | -56.1 | 13 | 2.20 | 34.7 | -63.2 | 0.523 | -13.08 | -56.51 | 7285 | 0.029 | 24966 |
| EUREKA | 80.00 | -85.93 | 0.571 | 87.5 | 68 | 314.75 | ** N O | C O M P U T A T I O N S | P E R F O R M E D ** | | | | | |
| FAREWELL | 62.53 | -153.90 | 0.557 | 74.5 | 25 | 4.27 | -53.4 | 168.8 | 0.638 | 3.44 | -172.77 | 21141 | 0.004 | 62592 |
| FANNING ISLAND | 3.92 | -159.38 | 0.333 | 10.7 | 10 | 0.98 | -6.2 | -161.2 | 0.351 | 0.74 | -159.94 | 46 | 0.328 | 1154 |
| FLIN FLON | 54.70 | -102.00 | 0.613 | 80.1 | 15 | 5.54 | -68.2 | -149.4 | 0.628 | -8.37 | -114.22 | 29092 | 0.002 | 84892 |
| FORT YUKON | 66.57 | -145.30 | 0.576 | 78.6 | 33 | 6.45 | -58.8 | 167.1 | 0.654 | 2.68 | -169.36 | 35108 | 0.001 | 101129 |
| FORT NORMAN | 64.90 | -125.50 | 0.596 | 81.3 | 38 | 8.23 | -64.2 | 177.1 | 0.656 | -1.47 | -150.08 | 46413 | 0.001 | 132451 |
| FORT CHIMO | 58.10 | -68.43 | 0.584 | 80.7 | -35 | 8.40 | -85.4 | -83.9 | 0.587 | -11.82 | -58.89 | 46897 | 0.001 | 134933 |
| FORT MONMOUTH | 40.25 | -74.02 | 0.566 | 71.6 | -10 | 2.81 | -68.1 | -85.5 | 0.507 | -12.85 | -71.50 | 11384 | 0.014 | 36267 |
| FORT BELVOIR | 38.73 | -77.13 | 0.565 | 70.6 | -6 | 2.62 | -65.7 | -91.8 | 0.507 | -12.83 | -76.36 | 10214 | 0.017 | 32919 |
| FORT RANDOLPH | 9.38 | -79.88 | 0.390 | 37.8 | 4 | 1.17 | -33.1 | -85.7 | 0.315 | -13.67 | -81.81 | 949 | 0.191 | 5680 |
| FORT DE FRANCE | 14.10 | -61.02 | 0.405 | 44.9 | -9 | 1.32 | -41.5 | -55.2 | 0.271 | -15.20 | -57.03 | 1573 | 0.138 | 8075 |
| FREETOWN | 8.47 | -13.22 | 0.307 | 6.0 | -14 | 1.02 | 3.2 | -11.8 | 0.297 | 3.61 | -11.90 | 5 | 0.297 | 611 |
| FROBISHER | 63.75 | -68.57 | 0.582 | 82.7 | -46 | 14.83 | ** N O | C O M P U T A T I O N S | P E R F O R M E D ** | | | | | |
| FREIBURG | 48.05 | 7.58 | 0.468 | 63.9 | -3 | 2.01 | -36.5 | 26.0 | 0.316 | 2.93 | 14.65 | 5942 | 0.041 | 20519 |
| FRONT ROYAL | 38.93 | -78.18 | 0.567 | 70.8 | -5 | 2.64 | -65.6 | -94.1 | 0.512 | -13.01 | -77.91 | 10339 | 0.017 | 33247 |
| FT. DAVIS | 30.63 | -103.95 | 0.512 | 58.7 | 11 | 1.65 | -45.7 | -122.2 | 0.483 | -8.42 | -110.58 | 4258 | 0.067 | 15760 |
| GARCHY | 47.30 | 3.07 | 0.464 | 63.4 | -5 | 1.98 | -36.6 | 22.6 | 0.313 | 2.46 | 10.93 | 5803 | 0.042 | 20149 |
| GAINESVILLE | 29.63 | -82.30 | 0.525 | 62.4 | 1 | 1.82 | -54.5 | -96.6 | 0.455 | -12.85 | -84.46 | 5192 | 0.050 | 18620 |
| GENOVA MONTE CAPEL | 44.55 | 8.95 | 0.458 | 60.5 | -3 | 1.73 | -30.7 | 23.5 | 0.321 | 3.67 | 14.72 | 4392 | 0.061 | 15957 |
| GENERAL BELGRANO | -77.97 | -38.80 | 0.513 | -66.4 | 7 | 4.59 | 51.2 | -59.3 | 0.560 | -11.03 | -47.21 | 22518 | 0.003 | 67578 |
| GENERAL SAN MARTIN | -68.13 | -67.43 | 0.469 | -60.8 | 22 | 2.65 | 39.2 | -67.2 | 0.550 | -12.81 | -61.47 | 10288 | 0.016 | 33351 |
| GHANA | 10.00 | 4.00 | 0.323 | 0.6 | -9 | 0.99 | 9.5 | 4.1 | 0.322 | NO MINIMUM B BETWEEN INTERS. | | | | 57 |
| GIFU | 35.58 | 137.08 | 0.469 | 49.3 | -6 | 1.23 | -18.9 | 135.8 | 0.507 | 9.07 | 137.52 | 1864 | 0.167 | 8397 |
| GILGIT | 35.94 | 74.30 | 0.521 | 53.7 | 1 | 1.26 | -18.4 | 78.5 | 0.450 | 7.98 | 75.11 | 2103 | 0.152 | 8830 |
| GOUGH ISLAND | -40.35 | -9.89 | 0.279 | -57.5 | -27 | 1.70 | 34.7 | -34.5 | 0.445 | -5.31 | -23.04 | 4000 | 0.064 | 15275 |
| GODHAVN | 69.23 | -53.52 | 0.557 | 81.6 | -52 | 20.97 | ** N O | C O M P U T A T I O N S | P E R F O R M E D ** | | | | | |
| GOOSE BAY | 53.32 | -60.38 | 0.565 | 76.9 | -31 | 5.33 | -80.2 | -39.9 | 0.532 | -11.05 | -48.01 | 27230 | 0.002 | 80636 |
| GOTTINGEN | 51.53 | 9.93 | 0.478 | 66.9 | -2 | 2.30 | -41.3 | 31.4 | 0.322 | 2.77 | 17.61 | 7754 | 0.027 | 25749 |
| GRYTVIKEN | -54.27 | -36.50 | 0.318 | -50.9 | -5 | 1.82 | 30.4 | -54.0 | 0.479 | -11.64 | -44.90 | 4717 | 0.053 | 17651 |
| GRAZ | 47.07 | 15.47 | 0.470 | 63.0 | -0 | 1.86 | -33.3 | 29.9 | 0.323 | 4.08 | 20.54 | 5227 | 0.049 | 18369 |
| GROCKA | 44.63 | 20.77 | 0.468 | 60.6 | 1 | 1.68 | -29.1 | 31.5 | 0.330 | 4.94 | 24.23 | 4190 | 0.066 | 15286 |
| GRAND BAHAMA | 26.67 | -78.37 | 0.506 | 59.9 | -0 | 1.69 | -53.0 | -89.3 | 0.423 | -13.32 | -79.32 | 4309 | 0.062 | 16140 |
| GRAHAMSTOWN | -33.28 | 26.48 | 0.320 | -66.3 | -24 | 1.84 | 46.5 | 10.9 | 0.465 | 3.79 | 16.77 | 5113 | 0.051 | 18062 |
| GREAT WHALE RIVER | 55.27 | -77.78 | 0.600 | 81.1 | -21 | 6.99 | -80.1 | -115.6 | 0.601 | -11.99 | -75.48 | 38020 | 0.001 | 110131 |
| GULMARG | 34.05 | 74.40 | 0.511 | 51.0 | 1 | 1.21 | -16.4 | 78.2 | 0.444 | 7.86 | 75.22 | 1767 | 0.174 | 7809 |
| GUANTANAMO BAY | 19.90 | -75.15 | 0.461 | 52.9 | -0 | 1.44 | -47.0 | -82.1 | 0.365 | -14.19 | -75.55 | 2640 | 0.102 | 11249 |
| GUAM | 13.45 | 144.75 | 0.364 | 11.9 | 1 | 0.96 | 1.8 | 144.3 | 0.379 | 8.83 | 144.60 | 66 | 0.353 | 1313 |
| GUAYAQUIL | -2.17 | -79.88 | 0.323 | 17.9 | 5 | 1.05 | -20.5 | -82.3 | 0.284 | -13.90 | -81.20 | 155 | 0.267 | 2131 |
| HAMMAGHIR | 30.10 | 0. | 0.397 | 42.4 | -7 | 1.19 | -13.3 | 8.8 | 0.322 | 5.63 | 4.26 | 1210 | 0.179 | 6218 |
| HACHIJOJIMA | 33.13 | 139.80 | 0.447 | 45.6 | -5 | 1.18 | -16.7 | 138.4 | 0.489 | 8.86 | 140.03 | 1492 | 0.192 | 7257 |
| HALLETT | -72.32 | 170.22 | 0.664 | -84.9 | -77 | 21.59 | ** N O | C O M P U T A T I O N S | P E R F O R M E D ** | | | | | |
| HARTLAND | 51.00 | -4.48 | 0.473 | 66.9 | -9 | 2.43 | -45.3 | 22.7 | 0.315 | 0.51 | 6.48 | 8488 | 0.023 | 28003 |

## Table B1

### Tracings from Surface to Surface.

| STATIONS | ** C | R | I | G | I | N | ** CONJUGATE | INTERS. ** | MINIMUM-B | E Q U A T O R | ** ARC | | |
|---|---|---|---|---|---|---|---|---|---|---|---|---|---|
| | LAT. | LONG. | B | DIP | DECL. | L | LAT. | LONG. | B | LAT. | LONG. | ALT. | B | KM |
| HARVSTVA | 60.22 | 10.25 | 0.496 | 72.9 | -2 | 3.52 | -53.6 | 44.5 | 0.386 | 2.00 | 21.71 | 15632 | 0.007 | 48035 |
| HAMBURG | 53.63 | 10.00 | 0.482 | 68.5 | -2 | 2.52 | -44.5 | 34.1 | 0.330 | 2.39 | 18.47 | 9176 | 0.020 | 29826 |
| HALLE | 51.48 | 11.93 | 0.479 | 66.9 | -1 | 2.28 | -40.8 | 32.5 | 0.323 | 2.96 | 19.15 | 7624 | 0.028 | 25357 |
| HALIFAX | 44.60 | -63.60 | 0.557 | 72.8 | -22 | 3.33 | -72.9 | -56.5 | 0.489 | -12.04 | -55.07 | 14506 | 0.008 | 45219 |
| HANOVER USA | 43.70 | -72.30 | 0.574 | 73.8 | -14 | 3.31 | -71.8 | -82.6 | 0.523 | -12.84 | -68.35 | 14534 | 0.008 | 45105 |
| HABANA | 23.15 | -82.35 | 0.484 | 55.5 | 3 | 1.51 | -47.4 | -93.9 | 0.406 | -12.82 | -84.74 | 3186 | 0.088 | 12780 |
| HALLEY BAY | -75.52 | -26.60 | 0.486 | -64.6 | -1 | 4.17 | 50.5 | -55.0 | 0.548 | -10.62 | -41.38 | 19810 | 0.004 | 60117 |
| HAIFA | 32.83 | 35.10 | 0.443 | 46.7 | 4 | 1.21 | -14.3 | 37.0 | 0.346 | 6.91 | 35.23 | 1462 | 0.174 | 6941 |
| HAMILTON MASS. | 42.02 | -72.17 | 0.569 | 72.6 | -13 | 3.05 | -70.2 | -81.5 | 0.511 | -12.67 | -68.42 | 12857 | 0.011 | 40427 |
| HERSTMONCEUX | 50.90 | 0.33 | 0.473 | 66.6 | -7 | 2.35 | -43.3 | 25.1 | 0.315 | 1.51 | 10.06 | 7990 | 0.026 | 26518 |
| HEISS | 80.20 | 57.48 | 0.554 | 84.1 | 25 | 13.32 | ** N O | C O M P U T A T I O N S | | P E R F O R M E D | ** | | | |
| HEALY | 63.55 | -119.00 | 0.602 | 82.1 | 37 | 8.64 | -66.1 | -178.4 | 0.655 | -3.16 | -142.01 | 49022 | 0.000 | 139719 |
| HEL | 54.60 | 18.80 | 0.491 | 69.4 | 2 | 2.54 | -44.0 | 40.9 | 0.344 | 3.38 | 25.64 | 9439 | 0.020 | 30487 |
| HELWAN | 29.87 | 31.33 | 0.423 | 41.3 | 2 | 1.14 | -10.2 | 32.7 | 0.344 | 7.55 | 31.53 | 1024 | 0.209 | 5486 |
| HERMANUS | -34.42 | 19.22 | 0.312 | -66.0 | -26 | 1.84 | 45.4 | 0.4 | 0.458 | 2.44 | 8.27 | 5082 | 0.050 | 18058 |
| HIRAISO | 36.37 | 140.62 | 0.463 | 49.6 | -6 | 1.25 | -19.6 | 138.8 | 0.509 | 8.92 | 140.86 | 1969 | 0.160 | 8750 |
| HIGHCLIFF | -45.68 | 170.58 | 0.608 | -71.1 | 22 | 2.74 | 55.9 | -162.4 | 0.520 | 4.28 | -175.79 | 11262 | 0.015 | 35306 |
| HONOLULU | 21.30 | -158.10 | 0.363 | 39.1 | 11 | 1.14 | -20.9 | -166.7 | 0.430 | 1.51 | -161.94 | 1018 | 0.213 | 5787 |
| HOBART | -42.92 | 147.17 | 0.632 | -73.0 | 13 | 2.85 | 60.7 | 161.0 | 0.541 | 8.35 | 155.18 | 12117 | 0.014 | 37472 |
| HOLLANDIA | -2.50 | 140.52 | 0.400 | -20.7 | 3 | 0.98 | 17.9 | 141.2 | 0.377 | 8.75 | 141.05 | 215 | 0.333 | 2373 |
| HURBANOVO | 47.90 | 18.20 | 0.475 | 63.8 | 1 | 1.92 | -34.2 | 32.6 | 0.325 | 4.17 | 22.96 | 5534 | 0.046 | 19250 |
| HUMAIN | 50.20 | 5.35 | 0.472 | 65.9 | -4 | 2.23 | -40.5 | 27.1 | 0.316 | 2.14 | 13.67 | 7207 | 0.030 | 24214 |
| HUANCAYO | -12.05 | -75.33 | 0.283 | 0.7 | 5 | 1.04 | -12.8 | -75.4 | 0.282 | NO MINIMUM B BETWEEN | | INTERS. | | 79 |
| HYDERABAD | 17.42 | 78.45 | 0.424 | 19.1 | -1 | 0.94 | 1.4 | 79.5 | 0.402 | 8.46 | 78.93 | 153 | 0.369 | 1846 |
| IBADAN | 7.37 | 3.97 | 0.318 | -5.5 | -10 | 1.00 | 11.9 | 3.1 | 0.326 | 7.89 | 3.87 | 5 | 0.318 | 515 |
| I. CROZET | -46.50 | 52.00 | 0.384 | -64.8 | -40 | 2.88 | 57.8 | 28.6 | 0.507 | 4.31 | 34.69 | 11752 | 0.013 | 36916 |
| IL GORTIN | 36.22 | 14.30 | 0.431 | 50.2 | -1 | 1.31 | -17.8 | 21.5 | 0.336 | 6.24 | 17.24 | 1992 | 0.135 | 8663 |
| INUVIK | 68.20 | -133.70 | 0.588 | 81.5 | 40 | 9.29 | -63.2 | 168.2 | 0.661 | 1.04 | -161.55 | 53249 | 0.000 | 151229 |
| INVERCARGILL | -46.42 | 168.32 | 0.614 | -71.9 | 22 | 2.87 | 57.3 | -164.5 | 0.524 | 4.78 | -177.99 | 12139 | 0.013 | 37724 |
| INVERNESS | 57.45 | -4.25 | 0.488 | 71.4 | -10 | 3.32 | -54.9 | 32.4 | 0.362 | -0.16 | 9.50 | 14279 | 0.009 | 44418 |
| IQUITOS | -3.67 | -73.33 | 0.313 | 17.4 | 2 | 1.07 | -22.0 | -74.7 | 0.271 | -15.83 | -74.05 | 142 | 0.258 | 2107 |
| IRKUTSK | 52.27 | 104.30 | 0.602 | 71.8 | -3 | 2.04 | -33.7 | 108.0 | 0.587 | 9.77 | 105.51 | 7167 | 0.036 | 23303 |
| ISLA DE PASCUA | -27.17 | -109.43 | 0.353 | -36.7 | 14 | 1.14 | 13.1 | -102.1 | 0.393 | -8.20 | -105.40 | 875 | 0.211 | 5349 |
| ISFJORD | 78.07 | 13.63 | 0.534 | 81.5 | -4 | 14.50 | ** N O | C O M P U T A T I O N S | | P E R F O R M E D | ** | | | |
| ITHACA | 42.45 | -76.52 | 0.577 | 73.3 | -9 | 3.12 | -69.5 | -92.6 | 0.530 | -12.66 | -75.00 | 13367 | 0.010 | 41749 |
| IVALO | 68.60 | 27.48 | 0.521 | 77.8 | 8 | 5.54 | -57.8 | 68.3 | 0.491 | 4.49 | 40.02 | 28755 | 0.002 | 84222 |
| JICAMARCA | -11.95 | -76.87 | 0.286 | 0.3 | 6 | 1.03 | -12.2 | -76.9 | 0.285 | NO MINIMUM B BETWEEN | | INTERS. | | 29 |
| JODRELL BANK | 53.23 | -2.30 | 0.479 | 68.5 | -8 | 2.64 | -47.9 | 26.8 | 0.326 | 0.52 | 9.03 | 9912 | 0.018 | 32052 |
| JOHANNESBURG | -26.20 | 28.03 | 0.331 | -63.5 | -17 | 1.57 | 42.5 | 18.3 | 0.458 | 5.35 | 21.68 | 3510 | 0.081 | 13270 |
| JUPITER | 27.02 | -80.12 | 0.509 | 60.1 | 0 | 1.70 | -52.6 | -92.2 | 0.430 | -13.19 | -81.67 | 4365 | 0.062 | 16272 |
| JULIANEHAAB | 60.72 | -46.03 | 0.541 | 77.3 | -37 | 7.31 | -79.0 | 18.0 | 0.523 | -8.02 | -25.60 | 39729 | 0.001 | 115387 |
| JULIUSRUH-RUGEN | 54.63 | 13.38 | 0.487 | 69.3 | -0 | 2.60 | -45.2 | 37.5 | 0.338 | 2.78 | 21.45 | 9730 | 0.018 | 31369 |
| JUNGFRAUJOCH | 46.55 | 7.98 | 0.463 | 62.5 | -3 | 1.87 | -34.0 | 24.7 | 0.317 | 3.23 | 14.51 | 5240 | 0.049 | 18455 |
| KANOYA | 31.42 | 130.89 | 0.462 | 44.7 | -4 | 1.14 | -15.2 | 130.2 | 0.484 | 8.78 | 131.33 | 1317 | 0.211 | 6620 |
| KARACHI | 24.85 | 67.02 | 0.452 | 36.4 | -0 | 1.04 | -8.1 | 69.3 | 0.396 | 7.09 | 67.73 | 680 | 0.272 | 4238 |

Table B1

Tracings from Surface to Surface.

| STATIONS | ** C | R | I | G | I | N | ** CONJUGATE | INTERS. | ** MINIMUM-B | E Q U A T O R | | ** ARC |
|---|---|---|---|---|---|---|---|---|---|---|---|---|
| | LAT. | LONG. | B | DIP | DECL. | L | LAT. | LONG. | B | LAT. | LONG. | ALT. | B | KM |
| KAZACHIE | 70.70 | 136.40 | 0.584 | 81.2 | -11 | 5.20 | -50.3 | 129.0 | 0.660 | 10.52 | 131.91 | 27181 | 0.002 | 78882 |
| KAP TOBIN | 70.42 | -21.97 | 0.523 | 78.8 | -29 | 10.94 | -72.6 | 60.3 | 0.535 | -2.25 | 6.88 | 63028 | 0.000 | 179616 |
| KAZAN | 55.83 | 48.82 | 0.536 | 72.4 | 13 | 2.55 | -41.5 | 65.1 | 0.429 | 6.44 | 51.40 | 9862 | 0.019 | 31326 |
| KAKICKA | 36.23 | 140.18 | 0.463 | 49.5 | -6 | 1.25 | -19.5 | 138.5 | 0.509 | 9.09 | 140.46 | 1948 | 0.161 | 8684 |
| KAMPALA | 0.33 | 32.58 | 0.341 | -24.2 | -1 | 1.00 | 20.3 | 32.5 | 0.381 | 8.39 | 32.41 | 234 | 0.306 | 2346 |
| KEKAHA | 21.84 | -159.72 | 0.363 | 33.5 | 12 | 1.14 | -20.8 | -168.4 | 0.433 | 1.80 | -163.64 | 1044 | 0.211 | 5879 |
| KHARTOUM | 15.58 | 32.58 | 0.364 | 12.3 | 1 | 0.97 | 5.3 | 32.6 | 0.343 | 8.62 | 32.53 | 55 | 0.337 | 1160 |
| KHABAROVSK | 48.52 | 135.12 | 0.543 | 64.0 | -10 | 1.73 | -30.5 | 133.1 | 0.585 | 9.54 | 135.70 | 5053 | 0.060 | 17617 |
| KHARKOV | 50.00 | 36.23 | 0.504 | 66.8 | 8 | 2.02 | -35.8 | 48.8 | 0.356 | 5.42 | 38.68 | 6385 | 0.038 | 21590 |
| KIEL | 54.30 | 10.10 | 0.484 | 69.0 | -2 | 2.59 | -45.5 | 35.1 | 0.334 | 2.30 | 18.83 | 9677 | 0.019 | 31254 |
| KIRUNA | 67.83 | 20.43 | 0.515 | 77.1 | 4 | 5.43 | -58.7 | 63.6 | 0.477 | 3.48 | 34.27 | 27988 | 0.002 | 82212 |
| KING SALMON | 58.70 | -156.70 | 0.540 | 71.2 | 22 | 3.31 | -49.7 | 171.3 | 0.622 | 3.76 | -172.61 | 14956 | 0.009 | 45526 |
| KIEV | 50.45 | 30.50 | 0.496 | 66.7 | 6 | 2.07 | -36.7 | 44.5 | 0.345 | 4.98 | 33.82 | 6618 | 0.036 | 22307 |
| KINGSTON | 18.00 | -76.80 | 0.449 | 50.4 | 0 | 1.38 | -44.2 | -84.2 | 0.357 | -14.07 | -77.86 | 2236 | 0.117 | 9978 |
| KNOB LAKE | 54.80 | -66.82 | 0.580 | 78.9 | -31 | 6.35 | -82.6 | -68.9 | 0.566 | -11.60 | -57.35 | 33778 | 0.001 | 98654 |
| KOROR ISLAND | 7.16 | 123.48 | 0.392 | -0.8 | 2 | 0.93 | 7.9 | 123.5 | 0.392 | 7.75 | 123.50 | 0 | 0.392 | 83 |
| KOTZEBUE | 66.88 | -162.60 | 0.561 | 76.6 | 22 | 5.19 | -54.5 | 160.0 | 0.652 | 5.19 | 177.60 | 27084 | 0.002 | 78925 |
| KOLN | 50.93 | 6.92 | 0.475 | 66.5 | -3 | 2.28 | -41.2 | 28.8 | 0.318 | 2.43 | 15.09 | 7551 | 0.028 | 25190 |
| KOMURO | 35.98 | 139.62 | 0.464 | 49.3 | -6 | 1.24 | -19.3 | 138.0 | 0.508 | 8.96 | 139.92 | 1912 | 0.164 | 8566 |
| KOKUBUNJI | 35.70 | 139.48 | 0.462 | 49.0 | -6 | 1.23 | -19.0 | 137.9 | 0.506 | 9.02 | 139.79 | 1868 | 0.166 | 8431 |
| KODAIKANAL | 10.23 | 77.48 | 0.401 | 2.2 | -3 | 0.92 | 8.5 | 77.6 | 0.399 | NO MINIMUM B BETWEEN INTERS. | | | | 195 |
| KUHLUNGSBORN | 54.12 | 11.93 | 0.485 | 68.9 | -1 | 2.55 | -44.8 | 36.0 | 0.334 | 2.79 | 20.11 | 9425 | 0.020 | 30512 |
| KUMASI | 6.67 | -1.58 | 0.312 | -4.4 | -12 | 1.00 | 10.3 | -2.4 | 0.318 | NO MINIMUM B BETWEEN INTERS. | | | | 419 |
| KYOTO | 35.02 | 135.78 | 0.469 | 48.8 | -6 | 1.22 | -18.4 | 134.7 | 0.504 | 9.01 | 136.25 | 1785 | 0.173 | 8144 |
| L'AQUILA | 42.40 | 13.32 | 0.454 | 58.0 | -1 | 1.58 | -26.7 | 24.6 | 0.328 | 4.78 | 17.64 | 3553 | 0.079 | 13428 |
| LA MADDALENA | 41.22 | 9.40 | 0.447 | 56.8 | -3 | 1.54 | -25.6 | 21.2 | 0.327 | 4.71 | 14.21 | 3280 | 0.085 | 12628 |
| LAHORE | 31.55 | 74.33 | 0.497 | 47.2 | 0 | 1.14 | -13.8 | 77.6 | 0.435 | 7.88 | 75.15 | 1386 | 0.203 | 6614 |
| LA PLATA | -34.90 | -57.90 | 0.255 | -32.6 | 0 | 1.20 | 7.6 | -61.8 | 0.366 | -16.34 | -58.98 | 854 | 0.181 | 5556 |
| LA QUIACA | -22.10 | -65.60 | 0.255 | -15.2 | 1 | 1.08 | -5.1 | -65.9 | 0.300 | -17.51 | -65.55 | 106 | 0.249 | 1943 |
| LA PAZ | -16.48 | -68.05 | 0.265 | -5.7 | 1 | 1.06 | -10.4 | -68.0 | 0.281 | NO MINIMUM B BETWEEN INTERS. | | | | 682 |
| LAE | -6.72 | 147.00 | 0.416 | -28.3 | 5 | 1.02 | 22.3 | 148.6 | 0.375 | 8.96 | 148.20 | 439 | 0.293 | 3528 |
| LA CRAU | 43.10 | 6.00 | 0.452 | 59.0 | -4 | 1.66 | -29.2 | 20.5 | 0.321 | 3.65 | 12.01 | 3970 | 0.069 | 14722 |
| LA HAYE | 52.10 | 4.30 | 0.477 | 67.4 | -5 | 2.42 | -43.8 | 28.8 | 0.320 | 1.82 | 13.54 | 8481 | 0.023 | 27890 |
| LEEDS | 53.80 | -1.55 | 0.480 | 68.9 | -8 | 2.70 | -48.5 | 28.0 | 0.329 | 0.77 | 9.80 | 10296 | 0.016 | 33135 |
| LEICESTER | 52.62 | -1.10 | 0.477 | 68.0 | -8 | 2.55 | -46.5 | 26.6 | 0.322 | 0.76 | 9.70 | 9315 | 0.020 | 30336 |
| LERWICK | 60.13 | -1.16 | 0.493 | 73.0 | -9 | 3.78 | -57.1 | 38.6 | 0.388 | 0.24 | 13.24 | 17238 | 0.006 | 52666 |
| LENINGRAD | 59.95 | 30.70 | 0.513 | 73.5 | 9 | 3.20 | -48.6 | 56.4 | 0.408 | 4.63 | 37.28 | 13807 | 0.010 | 42650 |
| LEIDSCHENDAM | 52.08 | 4.38 | 0.477 | 67.4 | -5 | 2.41 | -43.8 | 28.8 | 0.320 | 1.82 | 13.60 | 8461 | 0.023 | 27833 |
| LEOPOLDVILLE | -4.37 | 15.25 | 0.330 | -34.8 | -9 | 1.07 | 25.1 | 11.5 | 0.379 | 8.20 | 13.34 | 531 | 0.251 | 3710 |
| LINDAU,HARZ | 51.65 | 10.13 | 0.478 | 67.0 | -2 | 2.31 | -41.5 | 31.6 | 0.322 | 2.86 | 17.79 | 7820 | 0.027 | 25933 |
| LISBOA | 38.77 | -9.13 | 0.435 | 55.6 | -10 | 1.56 | -28.4 | 8.4 | 0.309 | 1.63 | -1.00 | 3279 | 0.083 | 12783 |
| LITTLE AMERICA | -78.18 | -162.17 | 0.642 | -80.2 | -78 | 13.10 | ** N O | C O M P U T A T I O N S | | P E R F O R M E D ** | | | | |
| LOGRONO | 42.45 | -2.50 | 0.448 | 58.9 | -7 | 1.69 | -31.0 | 15.0 | 0.313 | 2.41 | 5.19 | 4102 | 0.065 | 15185 |
| LOVOZERO | 67.99 | 35.08 | 0.528 | 77.9 | 13 | 5.15 | -55.8 | 71.0 | 0.495 | 5.54 | 45.23 | 26306 | 0.002 | 77316 |
| LONGYEARBYEN | 78.22 | 15.67 | 0.534 | 81.6 | -2 | 14.42 | ** N O | C O M P U T A T I O N S | | P E R F O R M E D ** | | | | |
| LONDON | 51.53 | 0.10 | 0.475 | 67.1 | -7 | 2.41 | -44.3 | 25.8 | 0.317 | 1.13 | 10.17 | 8425 | 0.023 | 27776 |

Table B1

Tracings from Surface to Surface.

| STATIONS | ** O | R | I | G | I | N | ** CONJUGATE INTERS. ** | | | MINIMUM-B | E Q U A T O R | | | ** ARC |
|---|---|---|---|---|---|---|---|---|---|---|---|---|---|---|
| | LAT. | LONG. | B | DIP | DECL. | L | LAT. | LONG. | B | LAT. | LONG. | ALT. | B | KM |
| LOMNICKY STIT | 49.20 | 20.22 | 0.480 | 65.1 | 2 | 2.03 | -35.9 | 35.4 | 0.327 | 4.35 | 24.94 | 6112 | 0.040 | 20913 |
| LOURENCO MARQUES | -25.97 | 32.60 | 0.335 | -63.0 | -16 | 1.56 | 42.5 | 24.4 | 0.465 | 5.51 | 26.84 | 3491 | 0.082 | 13191 |
| LUND | 55.70 | 13.18 | 0.489 | 70.1 | -0 | 2.73 | -46.8 | 39.0 | 0.345 | 2.76 | 21.72 | 10614 | 0.016 | 33881 |
| LUANDA | -8.82 | 13.22 | 0.329 | -42.2 | -12 | 1.13 | 28.2 | 7.4 | 0.391 | 7.28 | 10.22 | 862 | 0.213 | 4970 |
| LULEA | 65.60 | 22.12 | 0.512 | 76.1 | 5 | 4.61 | -56.3 | 60.3 | 0.453 | 3.80 | 33.78 | 22759 | 0.003 | 67700 |
| LVOV | 49.82 | 24.02 | 0.486 | 65.8 | 3 | 2.05 | -36.4 | 38.8 | 0.333 | 4.48 | 28.23 | 6355 | 0.038 | 21596 |
| LWIRO | -2.25 | 28.80 | 0.340 | -30.7 | -2 | 1.03 | 23.4 | 28.1 | 0.388 | 8.57 | 28.28 | 397 | 0.279 | 3120 |
| LYCKSELE | 64.62 | 18.67 | 0.508 | 75.5 | 2 | 4.40 | -56.2 | 56.8 | 0.439 | 3.16 | 30.59 | 21357 | 0.004 | 63861 |
| MAKATEA | -16.20 | -148.20 | 0.373 | -26.5 | 12 | 1.04 | 11.0 | -143.3 | 0.342 | -1.68 | -145.41 | 388 | 0.275 | 3316 |
| MANILA | 14.52 | 121.00 | 0.403 | 15.1 | 0 | 0.94 | 1.0 | 120.6 | 0.405 | 7.95 | 120.88 | 101 | 0.375 | 1542 |
| MALVERN | 52.12 | -2.32 | 0.476 | 67.7 | -8 | 2.51 | -46.2 | 25.3 | 0.319 | 0.82 | 8.54 | 9066 | 0.021 | 29634 |
| MAJURO ISLAND | 7.08 | 171.13 | 0.340 | 5.5 | 10 | 0.97 | 1.7 | 170.2 | 0.353 | 6.92 | 171.10 | 2 | 0.340 | 604 |
| MADRID | 40.40 | -3.68 | 0.440 | 56.8 | -8 | 1.59 | -28.4 | 12.7 | 0.314 | 2.64 | 3.69 | 3490 | 0.078 | 13362 |
| MACAO | 22.20 | 113.55 | 0.443 | 30.1 | 0 | 0.99 | -5.3 | 112.9 | 0.436 | 8.42 | 113.41 | 445 | 0.322 | 3363 |
| MADRAS | 13.08 | 80.28 | 0.410 | 8.5 | -2 | 0.92 | 6.1 | 80.7 | 0.401 | 8.62 | 80.53 | 27 | 0.396 | 780 |
| MAWSON | -67.40 | 62.50 | 0.515 | -69.5 | -56 | 8.63 | 70.8 | -4.6 | 0.516 | 0.35 | 19.85 | 48277 | 0.000 | 138656 |
| MACQUARIE ISLAND | -54.30 | 158.60 | 0.653 | -79.1 | 26 | 5.25 | 67.3 | -164.8 | 0.561 | 5.44 | 175.72 | 27381 | 0.002 | 79731 |
| MARION ISLAND | -46.85 | 37.87 | 0.343 | -64.6 | -35 | 2.71 | 55.5 | 11.8 | 0.487 | 2.50 | 20.61 | 10553 | 0.016 | 33724 |
| MAUI,KIHEI | 20.80 | -156.50 | 0.363 | 38.8 | 11 | 1.13 | -21.0 | -164.9 | 0.427 | 1.05 | -160.31 | 995 | 0.215 | 5705 |
| MCMURDO SOUND | -77.85 | 166.62 | 0.655 | -83.3 | -36 | 34.48 | ** N O | C O M P U T A T I O N S | | P E R F O R M E D ** | | | | |
| MEANCCK | 54.62 | -113.33 | 0.603 | 77.8 | 24 | 4.66 | -62.9 | -158.0 | 0.627 | -5.57 | -128.91 | 23520 | 0.003 | 69351 |
| MEUDON | 48.80 | 2.25 | 0.468 | 64.8 | -6 | 2.17 | -39.2 | 23.7 | 0.312 | 2.06 | 10.79 | 6612 | 0.035 | 22516 |
| MEMAMBETSU | 43.92 | 144.20 | 0.495 | 57.6 | -8 | 1.50 | -26.6 | 140.9 | 0.555 | 9.18 | 144.11 | 3525 | 0.093 | 13369 |
| MEXICO EL CERRILLO | 19.32 | -99.55 | 0.439 | 46.0 | 9 | 1.27 | -35.2 | -110.4 | 0.392 | -9.10 | -103.92 | 1759 | 0.149 | 8323 |
| MELBOURNE | -37.82 | 144.32 | 0.614 | -69.2 | 10 | 2.26 | 55.8 | 153.0 | 0.533 | 8.88 | 150.25 | 8324 | 0.027 | 26916 |
| MIDWAY ISLAND | 6.97 | 158.22 | 0.350 | 0.4 | 6 | 0.96 | 6.6 | 158.2 | 0.351 | NO MINIMUM B BETWEEN INTERS. | | | | 41 |
| MIEDZESZYN | 52.17 | 21.20 | 0.488 | 67.6 | 3 | 2.27 | -40.1 | 39.4 | 0.335 | 4.17 | 26.63 | 7717 | 0.028 | 25538 |
| MINNEAPOLIS | 44.97 | -93.23 | 0.596 | 74.3 | 6 | 3.28 | -64.6 | -124.3 | 0.578 | -10.47 | -99.66 | 14584 | 0.009 | 44807 |
| MIRNY | -66.57 | 92.92 | 0.599 | -76.8 | -75 | 19.55 | ** N O | C O M P U T A T I O N S | | P E R F O R M E D ** | | | | |
| MINA AGUILAR | -23.10 | -65.70 | 0.255 | -16.8 | 2 | 1.08 | -4.1 | -66.0 | 0.304 | -17.44 | -65.62 | 141 | 0.246 | 2181 |
| MOULD BAY | 76.20 | -119.40 | 0.585 | 87.5 | 71 | 37.32 | ** N O | C O M P U T A T I O N S | | P E R F O R M E D ** | | | | |
| MOSHIRI | 44.37 | 142.27 | 0.503 | 58.4 | -8 | 1.52 | -26.9 | 139.3 | 0.559 | 9.25 | 142.37 | 3661 | 0.090 | 13739 |
| MOCA | 3.35 | 8.67 | 0.320 | -16.6 | -9 | 1.00 | 17.0 | 6.5 | 0.344 | 8.41 | 7.80 | 105 | 0.306 | 1581 |
| MOSCOW | 55.47 | 37.32 | 0.516 | 71.1 | 10 | 2.54 | -42.4 | 55.5 | 0.388 | 5.39 | 41.10 | 9660 | 0.019 | 30905 |
| MOUNT WASHINGTON | 44.27 | -71.30 | 0.573 | 74.0 | -15 | 3.40 | -72.5 | -80.1 | 0.522 | -12.68 | -66.72 | 15094 | 0.008 | 46685 |
| MOUNT NORIKURA | 36.12 | 137.55 | 0.470 | 49.9 | -6 | 1.24 | -19.4 | 136.2 | 0.509 | 8.93 | 137.97 | 1951 | 0.162 | 8660 |
| MONT JOLI | 48.60 | -68.20 | 0.576 | 76.1 | -22 | 4.26 | -76.9 | -72.0 | 0.537 | -12.08 | -61.09 | 20491 | 0.004 | 61775 |
| MURCHISON BAY | 80.05 | 18.30 | 0.539 | 82.5 | -1 | 17.28 | ** N O | C O M P U T A T I O N S | | P E R F O R M E D ** | | | | |
| MURMANSK | 68.97 | 33.08 | 0.527 | 78.2 | 12 | 5.56 | -57.0 | 71.6 | 0.502 | 5.20 | 44.48 | 28911 | 0.002 | 84559 |
| MUNCHEN | 48.13 | 11.70 | 0.470 | 64.0 | -1 | 1.98 | -35.6 | 28.6 | 0.319 | 3.45 | 17.88 | 5818 | 0.042 | 20124 |
| NARSSARSSUAQ | 61.18 | -45.42 | 0.541 | 77.4 | -38 | 7.50 | -78.9 | 20.5 | 0.524 | -7.80 | -24.59 | 40947 | 0.001 | 118757 |
| NARYAN MAR | 67.50 | 53.00 | 0.549 | 79.1 | 21 | 4.76 | -52.3 | 80.1 | 0.526 | 7.28 | 59.32 | 23990 | 0.003 | 70604 |
| NATAL | -5.33 | -35.12 | 0.272 | -4.4 | -18 | 1.05 | -1.3 | -36.5 | 0.283 | NO MINIMUM B BETWEEN INTERS. | | | | 476 |
| NAIROBI | -1.28 | 36.80 | 0.343 | -26.4 | -0 | 1.01 | 20.8 | 36.9 | 0.390 | 7.86 | 36.67 | 289 | 0.300 | 2623 |
| NEUSTRELITZ | 53.28 | -13.08 | 0.482 | 69.1 | -14 | 2.88 | -53.0 | 21.4 | 0.336 | -1.45 | 0.84 | 11413 | 0.013 | 36435 |

Table B1

Tracings from Surface to Surface.

| STATIONS | ** O | R | I | G | I | N | ** CONJUGATE | INTERS. | ** MINIMUM-B | E Q U A T O R | ** ARC | | |
|---|---|---|---|---|---|---|---|---|---|---|---|---|---|
| | LAT. | LONG. | B | DIP | DECL. | L | LAT. | LONG. | B | LAT. | LONG. | ALT. | B | KM |
| NIAMEY | 13.50 | 2.50 | 0.330 | 9.2 | -9 | 1.00 | 5.6 | 4.0 | 0.316 | 7.75 | 3.56 | 29 | 0.314 | 900 |
| NITSANIM | 31.73 | 34.60 | 0.437 | 44.9 | 3 | 1.18 | -12.9 | 36.2 | 0.346 | 7.17 | 34.69 | 1297 | 0.186 | 6403 |
| NIIGATA | 37.70 | 138.82 | 0.476 | 51.6 | -6 | 1.29 | -20.8 | 137.2 | 0.519 | 9.14 | 139.21 | 2208 | 0.147 | 9459 |
| NICOSIA | 35.17 | 33.28 | 0.450 | 49.9 | 4 | 1.27 | -16.9 | 36.1 | 0.345 | 6.75 | 33.70 | 1825 | 0.150 | 8098 |
| NOUVELLE AMSTERDAM | -37.84 | 77.57 | 0.486 | -67.7 | -36 | 2.32 | 54.1 | 65.5 | 0.565 | 7.72 | 66.95 | 8628 | 0.025 | 27623 |
| NOVOLAZAREVSKAYA | -70.77 | 11.85 | 0.449 | -64.0 | -25 | 4.61 | 56.3 | -37.4 | 0.519 | -6.64 | -18.81 | 22445 | 0.003 | 67498 |
| NORD | 81.60 | -16.67 | 0.544 | 83.3 | -34 | 37.39 | ** N O | C C M P U T A T I O N S | P E R F O R M E D ** | | | | | |
| NORWAY STATION | -70.50 | -2.53 | 0.439 | -62.7 | -17 | 3.93 | 52.2 | -43.5 | 0.524 | -7.90 | -27.03 | 18159 | 0.005 | 55583 |
| NORFOLK ISLAND | -29.00 | 167.60 | 0.528 | -56.4 | 14 | 1.49 | 40.8 | -179.6 | 0.422 | 6.09 | 174.51 | 3288 | 0.096 | 12894 |
| NOUMEA | -22.30 | -166.40 | 0.438 | -41.3 | 13 | 1.16 | 22.8 | -157.1 | 0.369 | 1.37 | -161.34 | 1177 | 0.200 | 6340 |
| NURMIJARVI | 60.50 | 24.65 | 0.507 | 73.5 | 6 | 3.36 | -50.4 | 53.3 | 0.402 | 4.11 | 32.72 | 14727 | 0.008 | 45308 |
| ODESSA | 46.78 | 30.88 | 0.487 | 63.4 | 5 | 1.80 | -31.7 | 41.2 | 0.339 | 5.47 | 33.25 | 4961 | 0.054 | 17497 |
| O'HIGGINS RISCPATR | -63.32 | -57.90 | 0.414 | -56.1 | 14 | 2.19 | 34.6 | -63.6 | 0.523 | -13.12 | -57.03 | 7247 | 0.029 | 24852 |
| OKINAWA | 26.50 | 128.00 | 0.442 | 37.6 | -2 | 1.06 | -10.7 | 127.4 | 0.456 | 8.38 | 128.21 | 803 | 0.264 | 4847 |
| OLENEK | 68.50 | 112.40 | 0.597 | 82.6 | -6 | 4.60 | -48.3 | 116.0 | 0.643 | 10.56 | 112.57 | 23408 | 0.003 | 68408 |
| ONAGAWA | 38.43 | 141.47 | 0.472 | 52.0 | -6 | 1.31 | -21.5 | 139.4 | 0.522 | 9.17 | 141.69 | 2323 | 0.140 | 9830 |
| OOHIRA | 35.62 | 140.50 | 0.459 | 48.7 | -5 | 1.23 | -18.9 | 138.8 | 0.505 | 8.91 | 140.74 | 1849 | 0.167 | 8383 |
| ORCADAS DEL SUR | -60.73 | -44.73 | 0.373 | -53.9 | 4 | 2.08 | 33.9 | -58.3 | 0.506 | -12.13 | -49.81 | 6433 | 0.035 | 22596 |
| OSLO KJELLER | 59.97 | 11.10 | 0.496 | 72.8 | -1 | 3.45 | -53.0 | 44.5 | 0.383 | 2.03 | 22.22 | 15216 | 0.008 | 46861 |
| OTTAWA | 45.40 | -75.75 | 0.584 | 75.2 | -12 | 3.64 | -72.5 | -93.0 | 0.545 | -12.54 | -73.43 | 16642 | 0.006 | 50892 |
| OULU | 65.00 | 25.52 | 0.514 | 76.0 | 7 | 4.37 | -55.0 | 61.0 | 0.451 | 4.01 | 35.97 | 21237 | 0.004 | 63426 |
| PALESTINE | 31.77 | -95.63 | 0.531 | 61.9 | 9 | 1.81 | -50.5 | -114.7 | 0.489 | -10.08 | -101.33 | 5223 | 0.051 | 18560 |
| PANSKA VES | 50.53 | 14.57 | 0.478 | 66.1 | -0 | 2.18 | -38.8 | 33.0 | 0.323 | 3.35 | 20.89 | 6958 | 0.032 | 23414 |
| PARIS-SACLAY | 48.12 | 2.33 | 0.466 | 64.2 | -5 | 2.08 | -38.1 | 23.0 | 0.312 | 2.28 | 10.61 | 6251 | 0.038 | 21462 |
| PARIS-BAGNEUX | 48.80 | 2.32 | 0.468 | 64.8 | -5 | 2.16 | -39.2 | 23.8 | 0.312 | 1.85 | 10.89 | 6606 | 0.035 | 22503 |
| PANAGURITSCH | 42.52 | 24.18 | 0.465 | 58.4 | 2 | 1.56 | -25.9 | 32.4 | 0.335 | 5.74 | 26.62 | 3488 | 0.082 | 13178 |
| PARAMARIBO | 5.82 | -55.22 | 0.343 | 31.1 | -11 | 1.18 | -29.0 | -48.2 | 0.240 | -15.28 | -51.01 | 568 | 0.199 | 4409 |
| PETROPAVLOVSK-ON-K | 52.98 | 158.65 | 0.509 | 64.4 | -4 | 2.02 | -35.7 | 149.0 | 0.598 | 8.60 | 155.34 | 6815 | 0.038 | 22771 |
| PEARCE | -31.67 | 115.97 | 0.589 | -66.4 | -2 | 1.86 | 50.0 | 114.4 | 0.589 | 9.74 | 115.58 | 5970 | 0.048 | 20000 |
| PIC DU MIDI | 42.93 | 0.25 | 0.449 | 59.2 | -6 | 1.69 | -30.7 | 17.0 | 0.315 | 2.88 | 7.45 | 4145 | 0.065 | 15280 |
| PILAR | -31.67 | -63.88 | 0.258 | -28.7 | 4 | 1.15 | 4.0 | -65.0 | 0.348 | -16.77 | -63.74 | 580 | 0.204 | 4434 |
| PIWNICE -TORUN | 50.52 | 14.57 | 0.478 | 66.1 | -0 | 2.18 | -38.7 | 33.0 | 0.323 | 3.34 | 20.88 | 6950 | 0.033 | 23393 |
| PLAISANCE | -20.43 | 57.67 | 0.378 | -54.3 | -15 | 1.32 | 36.4 | 53.8 | 0.493 | 6.56 | 54.01 | 2261 | 0.134 | 9414 |
| POSADAS | -27.42 | -56.10 | 0.243 | -24.2 | -4 | 1.13 | 1.3 | -59.7 | 0.326 | -16.91 | -57.24 | 355 | 0.218 | 3466 |
| PONZA | 40.92 | 12.95 | 0.448 | 56.3 | -1 | 1.51 | -24.6 | 23.3 | 0.330 | 4.93 | 17.03 | 3121 | 0.091 | 12135 |
| PONTA DELGADO | 37.77 | -25.65 | 0.443 | 57.5 | -16 | 1.73 | -37.2 | -1.7 | 0.288 | -2.78 | -14.51 | 4148 | 0.062 | 15591 |
| POTCHEFSTROOM | -26.68 | 27.08 | 0.330 | -63.8 | -18 | 1.58 | 42.7 | 16.7 | 0.457 | 5.03 | 20.44 | 3598 | 0.078 | 13541 |
| POINT BARROW | 71.33 | -156.77 | 0.573 | 80.3 | 29 | 8.08 | -58.9 | 156.1 | 0.664 | 5.12 | 177.00 | 45608 | 0.001 | 129999 |
| POTSDAM | 52.38 | 13.07 | 0.482 | 67.6 | -0 | 2.35 | -41.9 | 34.3 | 0.327 | 2.92 | 20.36 | 8140 | 0.025 | 26831 |
| POITIERS | 46.57 | 0.35 | 0.461 | 62.8 | -6 | 1.95 | -36.3 | 20.3 | 0.311 | 2.22 | 8.59 | 5613 | 0.044 | 19616 |
| PORT ARTHUR | 30.00 | -94.00 | 0.522 | 60.4 | 8 | 1.72 | -49.4 | -111.7 | 0.474 | -10.50 | -99.22 | 4664 | 0.059 | 16974 |
| POONA | 18.05 | 73.12 | 0.423 | 21.6 | -1 | 0.96 | -0.2 | 74.4 | 0.395 | 7.78 | 73.71 | 200 | 0.353 | 2130 |
| PORO POINT | 16.62 | 120.28 | 0.410 | 19.4 | 0 | 0.95 | -1.0 | 119.8 | 0.412 | 7.98 | 120.15 | 172 | 0.363 | 2031 |
| PORT AUX FRANCAIS | -49.35 | 70.27 | 0.472 | -68.0 | -48 | 3.68 | 63.0 | 45.5 | 0.537 | 6.45 | 50.86 | 17008 | 0.006 | 51349 |
| PORT STANLEY | -51.70 | -57.85 | 0.328 | -47.0 | 8 | 1.58 | 23.2 | -63.0 | 0.464 | -14.15 | -58.23 | 3278 | 0.080 | 13379 |

Table B1

Tracings from Surface to Surface.

| STATIONS | ** O R I G I N ** | | | | | | ** CONJUGATE | | INTERS. ** MINIMUM-B | E Q U A T O R ** | | | ARC |
|---|---|---|---|---|---|---|---|---|---|---|---|---|---|
| | LAT. | LONG. | B | DIP | DECL. | L | LAT. | LONG. | B | LAT. | LONG. | ALT. | B | KM |
| PORT MORESBY | -9.20 | 147.15 | 0.431 | -32.6 | 6 | 1.05 | 24.9 | 149.1 | 0.383 | 8.98 | 148.64 | 620 | 0.270 | 4289 |
| PROVIDENIE BAY | 64.38 | 186.60 | 0.547 | 73.8 | 13 | 3.96 | -50.1 | 157.8 | 0.642 | 6.27 | 171.83 | 19162 | 0.005 | 57048 |
| PRAHA | 50.07 | 14.43 | 0.477 | 65.7 | -0 | 2.14 | -38.1 | 32.4 | 0.323 | 3.67 | 20.58 | 6711 | 0.034 | 22696 |
| PRUHONICE | 49.98 | 14.55 | 0.477 | 65.6 | -0 | 2.13 | -37.9 | 32.4 | 0.323 | 3.62 | 20.66 | 6658 | 0.035 | 22542 |
| PRETORIA | -26.80 | 28.20 | 0.330 | -63.9 | -18 | 1.59 | 42.9 | 18.1 | 0.459 | 5.24 | 21.62 | 3637 | 0.078 | 13652 |
| PRINCE ALBERT | 53.20 | -105.70 | 0.609 | 78.4 | 18 | 4.73 | -65.4 | -149.8 | 0.623 | -7.53 | -118.66 | 23943 | 0.003 | 70594 |
| PULLMANN | 46.72 | -117.17 | 0.576 | 71.0 | 20 | 2.81 | -55.1 | -149.9 | 0.588 | -5.11 | -129.79 | 11732 | 0.014 | 36684 |
| PUNTA ARENAS | -53.15 | -70.90 | 0.368 | -49.8 | 18 | 1.62 | 24.2 | -68.9 | 0.481 | -14.47 | -66.39 | 3676 | 0.072 | 14475 |
| PYONGYANG | 39.07 | 125.78 | 0.519 | 55.5 | -6 | 1.33 | -21.9 | 125.4 | 0.533 | 9.14 | 126.59 | 2567 | 0.132 | 10402 |
| QUETTA | 30.18 | 66.95 | 0.482 | 45.6 | 1 | 1.13 | -13.4 | 70.2 | 0.409 | 7.18 | 67.68 | 1254 | 0.210 | 6217 |
| QUEEN MAUD LAND | -70.50 | -1.00 | 0.439 | -62.9 | -18 | 3.99 | 52.6 | -42.9 | 0.523 | -7.80 | -26.14 | 18521 | 0.005 | 56591 |
| QUENTONCITY | 19.00 | 121.00 | 0.418 | 24.3 | -0 | 0.97 | -3.3 | 120.5 | 0.421 | 8.11 | 120.90 | 280 | 0.343 | 2634 |
| QUEBEC | 46.92 | -71.08 | 0.579 | 75.6 | -18 | 3.92 | -75.0 | -80.8 | 0.538 | -12.61 | -65.90 | 18374 | 0.005 | 55825 |
| QUILON | 8.50 | 76.00 | 0.397 | -1.7 | -3 | 0.92 | 9.9 | 75.9 | 0.399 | NO MINIMUM B BETWEEN INTERS. | | | | 155 |
| RABAT | 34.02 | -6.85 | 0.414 | 49.3 | -9 | 1.34 | -20.9 | 6.5 | 0.315 | 3.16 | -0.43 | 2043 | 0.126 | 8968 |
| RAMEY AFB | 18.50 | -67.20 | 0.444 | 51.4 | -6 | 1.43 | -47.3 | -67.3 | 0.323 | -15.01 | -64.84 | 2393 | 0.107 | 10634 |
| RAROTONGA | -21.20 | -159.75 | 0.419 | -37.9 | 13 | 1.13 | 19.4 | -151.6 | 0.363 | 0.23 | -155.25 | 930 | 0.220 | 5479 |
| RESOLUTE | 74.68 | -94.92 | 0.586 | 89.1 | 87 | 101.72 | ** N O C O M P U T A T I O N S P E R F O R M E D ** | | | | | | | |
| REYKJAVIK | 64.18 | -21.70 | 0.512 | 76.0 | -25 | 6.27 | -69.3 | 39.9 | 0.474 | -2.90 | 0.33 | 33140 | 0.001 | 97038 |
| REGENSBERG | 47.48 | 8.45 | 0.467 | 63.4 | -3 | 1.94 | -35.3 | 25.9 | 0.317 | 3.08 | 15.16 | 5632 | 0.044 | 19610 |
| RIO DE JANEIRO | -22.90 | -43.22 | 0.241 | -25.2 | -15 | 1.13 | 4.1 | -50.4 | 0.324 | -13.62 | -45.88 | 337 | 0.219 | 3330 |
| RIO GALLEGOS | -51.63 | -69.22 | 0.354 | -48.3 | 16 | 1.56 | 22.7 | -68.1 | 0.471 | -14.38 | -65.53 | 3283 | 0.081 | 13316 |
| ROYAL ROADS | 48.50 | -123.50 | 0.570 | 70.9 | 23 | 2.86 | -53.9 | -156.9 | 0.594 | -3.44 | -137.30 | 12068 | 0.013 | 37600 |
| ROMA | 41.88 | 12.50 | 0.451 | 57.4 | -1 | 1.56 | -26.0 | 23.7 | 0.328 | 4.86 | 16.85 | 3410 | 0.082 | 13001 |
| ROSTOV/DON | 47.23 | 39.65 | 0.503 | 64.7 | 8 | 1.82 | -32.2 | 49.4 | 0.357 | 6.04 | 41.16 | 5182 | 0.052 | 18088 |
| SANTA CRUZ | -17.80 | -63.17 | 0.257 | -7.9 | -1 | 1.07 | -9.2 | -63.6 | 0.281 | NO MINIMUM B BETWEEN INTERS. | | | | 968 |
| SAN FERNANDO | 36.47 | -6.20 | 0.425 | 52.4 | -9 | 1.43 | -23.9 | 8.5 | 0.315 | 2.96 | 0.67 | 2547 | 0.106 | 10521 |
| SANTA CRUZ | 28.33 | -16.25 | 0.391 | 43.5 | -12 | 1.25 | -18.6 | -2.9 | 0.300 | 1.72 | -9.55 | 1416 | 0.157 | 7039 |
| SANTIAGO | -33.57 | -70.72 | 0.276 | -32.0 | 9 | 1.17 | 6.0 | -69.4 | 0.365 | -16.08 | -69.12 | 753 | 0.195 | 5075 |
| SALEKHARD | 66.58 | 66.67 | 0.568 | 80.1 | 22 | 4.39 | -49.7 | 87.4 | 0.554 | 8.71 | 70.72 | 21788 | 0.004 | 64285 |
| SASKATOON | 52.13 | -106.67 | 0.606 | 77.4 | 19 | 4.35 | -64.1 | -148.8 | 0.618 | -7.19 | -119.48 | 21501 | 0.004 | 63827 |
| SAPPORO | 43.02 | 121.35 | 0.550 | 60.8 | -7 | 1.47 | -25.4 | 121.5 | 0.556 | 9.33 | 122.33 | 3517 | 0.096 | 13116 |
| SACRAMENTO PEAK | 32.72 | -105.75 | 0.523 | 60.6 | 12 | 1.75 | -47.1 | -125.6 | 0.499 | -8.13 | -113.00 | 4876 | 0.057 | 17525 |
| SAN JUAN | 18.43 | -66.00 | 0.441 | 51.2 | -7 | 1.43 | -47.2 | -64.8 | 0.317 | -14.90 | -63.19 | 2366 | 0.107 | 10565 |
| SAN JULIAN | -49.32 | -67.78 | 0.336 | -46.1 | 14 | 1.49 | 20.4 | -67.4 | 0.456 | -14.90 | -64.90 | 2769 | 0.095 | 11788 |
| SAO PAULO | -23.55 | -46.63 | 0.240 | -23.6 | -13 | 1.12 | 2.4 | -52.7 | 0.320 | -14.83 | -48.80 | 297 | 0.222 | 3158 |
| SAO JOSE DOS CAMPO | -23.00 | -46.00 | 0.241 | -23.3 | -13 | 1.12 | 2.4 | -52.1 | 0.319 | -14.53 | -48.18 | 285 | 0.223 | 3085 |
| SALISBURY RHOD-NYA | -17.83 | 31.00 | 0.342 | -55.8 | -9 | 1.31 | 36.4 | 26.8 | 0.446 | 6.61 | 27.93 | 2011 | 0.137 | 8688 |
| SCHWARZENBURG | 46.83 | 7.33 | 0.464 | 62.8 | -3 | 1.90 | -34.6 | 24.6 | 0.316 | 3.20 | 14.07 | 5383 | 0.047 | 18886 |
| SCOTT BASE | -77.85 | 166.75 | 0.655 | -83.3 | -36 | 34.27 | ** N O C O M P U T A T I O N S P E R F O R M E D ** | | | | | | | |
| SENDAI | 38.10 | 140.55 | 0.473 | 51.7 | -6 | 1.30 | -21.2 | 138.6 | 0.521 | 9.03 | 140.83 | 2269 | 0.143 | 9657 |
| SEOUL | 37.58 | 127.05 | 0.508 | 53.5 | -6 | 1.28 | -20.6 | 126.6 | 0.524 | 8.96 | 127.79 | 2272 | 0.146 | 9537 |
| SEATTLE | 47.75 | -122.42 | 0.569 | 70.6 | 22 | 2.80 | -53.7 | -155.2 | 0.591 | -3.87 | -135.86 | 11620 | 0.014 | 36361 |
| SEMIPALATINSK | 50.40 | 80.25 | 0.583 | 70.3 | 6 | 1.95 | -32.8 | 88.0 | 0.524 | 8.71 | 81.28 | 6508 | 0.041 | 21499 |
| SEAGROVE | -37.08 | 174.78 | 0.559 | -63.1 | 18 | 1.84 | 46.1 | -166.0 | 0.464 | 4.41 | -175.28 | 5513 | 0.051 | 19284 |

Table B1

Tracings from Surface to Surface.

| STATIONS | ** O | R | I | G | I | N | ** CONJUGATE INTERS. ** | | MINIMUM-B | E Q U A T O R | | ** ARC | |
|---|---|---|---|---|---|---|---|---|---|---|---|---|---|
| | LAT. | LONG. | B | DIP | DECL. | L | LAT. | LONG. | B | LAT. | LONG. | ALT. | B | KM |
| SHEPHERD BAY | 68.75 | -93.75 | 0.599 | 88.1 | -18 | 29.31 | ** N O | C O M P U T A T I O N S | | P E R F O R M E D ** | | | | |
| SHIRAZ | 29.63 | 52.52 | 0.459 | 44.5 | 3 | 1.15 | -13.5 | 54.4 | 0.364 | 6.50 | 52.58 | 1198 | 0.204 | 6075 |
| SHACKLETON | -77.98 | -37.17 | 0.512 | -66.4 | 6 | 4.61 | 51.4 | -58.9 | 0.559 | -10.96 | -46.55 | 22675 | 0.003 | 68021 |
| SHEFFIELD | 53.43 | 1.35 | 0.479 | 68.5 | -6 | 2.61 | -46.9 | 29.0 | 0.326 | 1.33 | 11.82 | 9702 | 0.018 | 31412 |
| SIMOSATO | 33.58 | 135.94 | 0.461 | 46.9 | -5 | 1.18 | -17.1 | 134.9 | 0.494 | 8.94 | 136.36 | 1574 | 0.188 | 7486 |
| SIDMOUTH | 50.68 | 3.22 | 0.473 | 66.3 | -5 | 2.29 | -41.9 | 26.4 | 0.316 | 1.95 | 12.18 | 7634 | 0.028 | 25465 |
| SITKA | 57.05 | -135.33 | 0.572 | 74.3 | 29 | 3.91 | -55.6 | -175.2 | 0.625 | -0.35 | -153.53 | 18773 | 0.005 | 56124 |
| SIMFEROPOL | 44.83 | 34.07 | 0.487 | 61.8 | 6 | 1.68 | -29.2 | 42.3 | 0.342 | 5.70 | 35.69 | 4256 | 0.067 | 15419 |
| SINGAPORE | 1.32 | 103.82 | 0.417 | -18.4 | 2 | 0.94 | 17.2 | 104.1 | 0.427 | 8.79 | 104.00 | 147 | 0.378 | 1827 |
| SLOUGH | 51.48 | -0.57 | 0.475 | 67.1 | -7 | 2.42 | -44.5 | 25.4 | 0.317 | 1.04 | 9.64 | 8449 | 0.023 | 27851 |
| SODANKYLA | 67.37 | 26.65 | 0.519 | 77.2 | 8 | 5.09 | -56.9 | 65.7 | 0.477 | 4.44 | 38.43 | 25897 | 0.002 | 76324 |
| SOUTH POLE | -90.00 | 0. | 0.599 | -75.1 | -27 | 13.52 | ** N O | C O M P U T A T I O N S | | P E R F O R M E D ** | | | | |
| SREDNIKAN | 62.43 | 152.32 | 0.558 | 73.3 | -8 | 3.09 | -43.8 | 141.3 | 0.641 | 8.98 | 147.92 | 13723 | 0.011 | 41839 |
| ST. STEPHEN | 67.20 | -45.20 | 0.545 | 79.8 | -44 | 13.13 | ** N O | C O M P U T A T I O N S | | P E R F O R M E D ** | | | | |
| STELLENBOSCH | -33.94 | 18.85 | 0.312 | -65.9 | -26 | 1.82 | 45.0 | 0.3 | 0.457 | 2.41 | 8.10 | 4949 | 0.052 | 17668 |
| STOCKHOLM | 59.30 | 18.10 | 0.499 | 72.5 | 2 | 3.22 | -50.4 | 47.4 | 0.381 | 3.00 | 27.14 | 13785 | 0.010 | 42761 |
| STONYHURST | 53.51 | -2.47 | 0.479 | 68.7 | -8 | 2.68 | -48.4 | 27.1 | 0.327 | 0.60 | 9.00 | 10158 | 0.017 | 32753 |
| ST. LAWRENCE | 50.58 | 1.23 | 0.472 | 66.3 | -6 | 2.31 | -42.4 | 25.2 | 0.314 | 1.39 | 10.68 | 7714 | 0.027 | 25721 |
| STANLEY | -51.70 | -57.85 | 0.328 | -47.0 | 8 | 1.58 | 23.2 | -63.0 | 0.464 | -14.15 | -58.23 | 3278 | 0.080 | 13379 |
| ST. SANTIN-DE-MAUR | 44.60 | 20.20 | 0.467 | 60.6 | 1 | 1.68 | -29.1 | 31.0 | 0.329 | 4.89 | 23.75 | 4185 | 0.066 | 15274 |
| ST. MICHEL | 43.92 | 5.72 | 0.454 | 59.9 | -4 | 1.71 | -30.5 | 21.0 | 0.319 | 3.49 | 11.99 | 4270 | 0.063 | 15615 |
| STANFORD | 37.43 | -122.17 | 0.518 | 61.8 | 17 | 1.84 | -45.1 | -144.5 | 0.530 | -4.48 | -131.62 | 5515 | 0.049 | 19303 |
| ST. JOHNS | 47.52 | -52.78 | 0.536 | 72.0 | -27 | 3.47 | -71.6 | -24.8 | 0.450 | -10.03 | -39.50 | 15244 | 0.007 | 47421 |
| SUKKERTOPPEN | 65.42 | -52.90 | 0.556 | 80.3 | -46 | 13.06 | ** N O | C O M P U T A T I O N S | | P E R F O R M E D ** | | | | |
| SULPHUR MOUNTAIN | 51.10 | -115.60 | 0.592 | 74.7 | 23 | 3.62 | -59.3 | -154.3 | 0.610 | -5.24 | -129.89 | 16904 | 0.006 | 51027 |
| SURLARI | 44.68 | 26.25 | 0.475 | 61.0 | 3 | 1.68 | -28.9 | 35.7 | 0.334 | 5.26 | 28.84 | 4180 | 0.067 | 15232 |
| SVERDLOVSK | 56.73 | 61.07 | 0.559 | 74.1 | 14 | 2.62 | -41.0 | 75.7 | 0.482 | 7.67 | 63.01 | 10480 | 0.017 | 32884 |
| SWANSEA | 51.63 | -4.00 | 0.475 | 67.4 | -9 | 2.48 | -46.1 | 23.8 | 0.317 | 0.47 | 7.10 | 8880 | 0.021 | 29122 |
| SWAKTHMORE | 39.90 | -75.35 | 0.567 | 71.4 | -8 | 2.77 | -67.4 | -88.4 | 0.509 | -12.89 | -73.55 | 11117 | 0.014 | 35488 |
| SYDNEY | -33.60 | 151.10 | 0.584 | -64.3 | 12 | 1.85 | 50.4 | 160.6 | 0.492 | 8.42 | 157.30 | 5672 | 0.050 | 19592 |
| SYKTYVKAR | 61.70 | 50.80 | 0.544 | 76.1 | 17 | 3.39 | -47.3 | 72.4 | 0.477 | 6.63 | 54.95 | 15251 | 0.008 | 46375 |
| SYOWA BASE | -69.00 | 39.60 | 0.471 | -66.3 | -42 | 6.16 | 64.0 | -21.2 | 0.511 | -3.14 | 0.65 | 32380 | 0.001 | 94935 |
| TAMALE | 9.42 | -0.89 | 0.317 | 1.5 | -11 | 1.00 | 8.2 | -0.6 | 0.315 | NO MINIMUM B BETWEEN INTERS. | | | | 143 |
| TASHKENT | 41.42 | 69.20 | 0.540 | 60.8 | 4 | 1.47 | -24.6 | 75.1 | 0.452 | 7.70 | 69.94 | 3370 | 0.096 | 12609 |
| TAMANRASSET | 22.80 | 5.52 | 0.365 | 28.2 | -6 | 1.05 | -3.1 | 9.8 | 0.322 | 7.79 | 7.75 | 402 | 0.263 | 3184 |
| TAIPEI | 25.03 | 121.52 | 0.447 | 35.5 | -1 | 1.03 | -9.0 | 120.9 | 0.450 | 8.40 | 121.58 | 678 | 0.284 | 4341 |
| TALARA | -4.57 | -81.25 | 0.312 | 12.7 | 6 | 1.04 | -17.4 | -83.0 | 0.285 | -13.39 | -82.36 | 70 | 0.279 | 1463 |
| TANANARIVE | -18.92 | 47.55 | 0.354 | -53.7 | -10 | 1.30 | 35.6 | 44.7 | 0.473 | 6.42 | 44.77 | 2030 | 0.142 | 8730 |
| TAHITI | -17.48 | -149.48 | 0.381 | -29.1 | 12 | 1.06 | 12.6 | -143.9 | 0.347 | -1.46 | -146.34 | 482 | 0.264 | 3741 |
| TBILISI | 41.72 | 44.82 | 0.497 | 59.7 | 6 | 1.52 | -25.8 | 50.5 | 0.360 | 6.34 | 45.31 | 3408 | 0.088 | 12874 |
| TENIENTE MATIENZO | -64.97 | -60.05 | 0.431 | -57.5 | 16 | 2.32 | 36.1 | -64.5 | 0.532 | -12.82 | -58.02 | 8122 | 0.024 | 27309 |
| TEHRAN | 35.68 | 51.42 | 0.486 | 53.1 | 5 | 1.30 | -19.6 | 54.8 | 0.369 | 6.44 | 51.56 | 2109 | 0.141 | 8960 |
| TENERIFE | 28.00 | -17.00 | 0.389 | 43.3 | -12 | 1.25 | -18.7 | -3.6 | 0.298 | 1.41 | -10.22 | 1394 | 0.158 | 6977 |
| TEOLOYUCAN | 19.75 | -99.18 | 0.443 | 46.7 | 9 | 1.28 | -35.8 | -110.3 | 0.396 | -9.09 | -103.59 | 1839 | 0.144 | 8580 |
| THULE | 76.55 | -68.83 | 0.568 | 85.4 | -78 | 220.13 | ** N O | C O M P U T A T I O N S | | P E R F O R M E D ** | | | | |
| THE PAS | 53.80 | -101.30 | 0.612 | 79.6 | 14 | 5.24 | -67.9 | -147.1 | 0.625 | -8.34 | -112.87 | 27154 | 0.002 | 79540 |

Table B1

Tracings from Surface to Surface.

| STATIONS | ** C | R | I | G | I | N | ** CONJUGATE | INTERS. ** | MINIMUM-B | E Q U A T O R | ** ARC | | |
|---|---|---|---|---|---|---|---|---|---|---|---|---|---|
| | LAT. | LONG. | B | DIP | DECL. | L | LAT. | LONG. | B | LAT. | LONG. | ALT. | B | KM |
| TIHANY | 46.89 | 17.89 | 0.472 | 62.8 | 0 | 1.84 | -32.7 | 31.4 | 0.325 | 4.26 | 22.45 | 5100 | 0.051 | 17982 |
| TIXIE BAY | 71.55 | 128.90 | 0.588 | 82.6 | -11 | 5.55 | -50.9 | 124.9 | 0.658 | 10.53 | 125.57 | 29436 | 0.002 | 85087 |
| TIRUCHIRAPALLI | 10.83 | 78.83 | 0.403 | 3.3 | -2 | 0.92 | 8.1 | 79.0 | 0.400 | 8.54 | 78.98 | 2 | 0.400 | 302 |
| TORINO | 45.20 | 7.65 | 0.459 | 61.2 | -3 | 1.78 | -32.0 | 23.3 | 0.319 | 3.63 | 13.83 | 4687 | 0.056 | 16832 |
| TOTTORI | 35.53 | 134.22 | 0.477 | 49.7 | -6 | 1.23 | -18.9 | 133.2 | 0.508 | 8.97 | 134.76 | 1875 | 0.168 | 8405 |
| TORUN | 53.08 | 18.55 | 0.487 | 68.2 | 2 | 2.38 | -41.8 | 38.8 | 0.336 | 3.52 | 24.88 | 8376 | 0.024 | 27456 |
| TOMSK | 56.47 | 84.93 | 0.597 | 75.5 | 7 | 2.51 | -38.5 | 94.0 | 0.562 | 9.30 | 86.30 | 10034 | 0.019 | 31366 |
| TORRE CHIARUCCIA | 42.03 | 11.83 | 0.451 | 57.6 | -1 | 1.57 | -26.4 | 23.3 | 0.328 | 4.57 | 16.38 | 3467 | 0.081 | 13181 |
| TORTOSA | 40.82 | 0.50 | 0.442 | 56.9 | -6 | 1.57 | -27.5 | 15.5 | 0.319 | 3.33 | 7.09 | 3438 | 0.080 | 13170 |
| TOLEDO | 39.88 | -4.05 | 0.438 | 56.2 | -8 | 1.56 | -27.8 | 12.1 | 0.315 | 2.75 | 3.25 | 3352 | 0.082 | 12949 |
| TOYOKAWA | 35.83 | 137.37 | 0.469 | 49.5 | -6 | 1.24 | -19.1 | 136.0 | 0.508 | 8.99 | 137.80 | 1902 | 0.165 | 8516 |
| TONANZINTLA | 19.03 | -98.30 | 0.440 | 45.9 | 9 | 1.27 | -35.3 | -109.1 | 0.390 | -9.39 | -102.59 | 1745 | 0.149 | 8285 |
| TOWNSVILLE | -19.10 | 146.50 | 0.498 | -48.0 | 7 | 1.24 | 35.5 | 149.8 | 0.432 | 8.92 | 149.23 | 1803 | 0.167 | 8316 |
| TRUJILLO | -8.10 | -79.03 | 0.298 | 6.8 | 6 | 1.03 | -15.0 | -79.9 | 0.283 | -14.25 | -79.77 | 9 | 0.283 | 776 |
| TROMSO | 69.67 | 18.95 | 0.517 | 77.9 | 2 | 6.29 | -60.5 | 66.7 | 0.496 | 3.47 | 34.84 | 33505 | 0.001 | 97492 |
| TRELEW | -43.20 | -65.30 | 0.297 | -40.6 | 10 | 1.33 | 14.6 | -66.2 | 0.417 | -15.43 | -63.95 | 1739 | 0.133 | 8576 |
| TRIVANDRUM | 8.42 | 76.95 | 0.398 | -2.1 | -3 | 0.92 | 10.2 | 76.8 | 0.400 | NO MINIMUM B BETWEEN | | INTERS. | | 194 |
| TRINIDAD | 10.60 | -61.20 | 0.383 | 40.4 | -8 | 1.26 | -37.8 | -56.3 | 0.260 | -15.68 | -57.82 | 1147 | 0.162 | 6617 |
| TSCHOIBALSAN | 48.07 | 114.50 | 0.583 | 66.9 | -6 | 1.73 | -29.9 | 115.9 | 0.580 | 9.75 | 115.64 | 5181 | 0.059 | 17783 |
| TSUMEB | -19.23 | 17.72 | 0.332 | -57.2 | -16 | 1.34 | 36.5 | 8.5 | 0.428 | 5.62 | 12.50 | 2138 | 0.126 | 9146 |
| TUBINGEN | 48.53 | 9.07 | 0.470 | 64.3 | -2 | 2.04 | -36.8 | 27.4 | 0.317 | 2.93 | 15.97 | 6113 | 0.039 | 21008 |
| TUCSON | 32.23 | -110.95 | 0.510 | 58.9 | 13 | 1.67 | -44.5 | -130.0 | 0.496 | -6.76 | -118.38 | 4369 | 0.066 | 16061 |
| TUCSON | 32.23 | -110.95 | 0.510 | 58.9 | 13 | 1.67 | -44.5 | -130.0 | 0.496 | -6.76 | -118.38 | 4369 | 0.066 | 16061 |
| TUCUMAN | -26.90 | -65.40 | 0.255 | -22.5 | 3 | 1.11 | -0.5 | -65.9 | 0.323 | -17.06 | -65.23 | 299 | 0.230 | 3122 |
| UJI | 34.90 | 135.78 | 0.469 | 48.6 | -6 | 1.21 | -18.3 | 134.7 | 0.503 | 8.94 | 136.25 | 1767 | 0.174 | 8087 |
| ULAN BATOR | 47.78 | 106.75 | 0.589 | 67.3 | -3 | 1.72 | -29.5 | 109.2 | 0.571 | 9.68 | 107.82 | 5146 | 0.059 | 17636 |
| UNALASKA | 53.88 | -166.53 | 0.505 | 66.1 | 15 | 2.42 | -43.1 | 169.7 | 0.598 | 4.97 | -178.15 | 9264 | 0.022 | 29762 |
| UNIVERSITY PARK | 40.80 | -77.77 | 0.574 | 72.2 | -7 | 2.88 | -67.5 | -94.3 | 0.523 | -12.75 | -77.09 | 11840 | 0.013 | 37456 |
| UPPSALA | 59.80 | 17.60 | 0.499 | 72.8 | 2 | 3.32 | -51.1 | 47.9 | 0.386 | 3.10 | 26.98 | 14395 | 0.009 | 44474 |
| USHUAIA | -54.80 | -68.30 | 0.373 | -50.6 | 17 | 1.69 | 25.7 | -67.7 | 0.488 | -14.26 | -64.44 | 4075 | 0.064 | 15668 |
| UTSJOKI | 69.75 | 27.03 | 0.523 | 78.3 | 8 | 6.04 | -58.8 | 70.2 | 0.503 | 4.78 | 40.63 | 32002 | 0.001 | 93208 |
| VALENTIA | 51.94 | -10.25 | 0.478 | 68.0 | -12 | 2.64 | -49.5 | 21.0 | 0.322 | -0.82 | 2.48 | 9848 | 0.018 | 31959 |
| VERKHOYANSK | 67.60 | 133.40 | 0.587 | 79.7 | -13 | 4.22 | -47.5 | 128.4 | 0.654 | 10.38 | 130.86 | 20955 | 0.004 | 61677 |
| VAL D'OR | 48.00 | -77.80 | 0.593 | 77.0 | -12 | 4.22 | -74.1 | -100.9 | 0.566 | -12.46 | -76.34 | 20382 | 0.004 | 61242 |
| VICTORIA | 48.40 | -123.40 | 0.570 | 70.9 | 23 | 2.85 | -53.8 | -156.7 | 0.593 | -3.49 | -137.15 | 11998 | 0.013 | 37408 |
| VLADIVOSTOK | 43.78 | 132.03 | 0.528 | 59.8 | -9 | 1.50 | -26.2 | 130.9 | 0.560 | 9.26 | 132.85 | 3610 | 0.092 | 13489 |
| VOSTOK | -76.48 | 106.50 | 0.627 | -79.5 | 72 | 103.75 | ** N O | C O M P U T A T I O N S | | P E R F O R M E D ** | | | | |
| WATHEROO | -30.32 | 115.88 | 0.582 | -65.1 | -2 | 1.76 | 48.6 | 114.5 | 0.584 | 9.80 | 115.62 | 5368 | 0.056 | 18311 |
| WAKKANAI | 45.40 | 141.68 | 0.510 | 59.6 | -9 | 1.56 | -27.8 | 138.7 | 0.565 | 9.22 | 141.80 | 3956 | 0.082 | 14577 |
| WASHINGTON | 38.73 | -77.13 | 0.565 | 70.6 | -6 | 2.62 | -65.7 | -91.8 | 0.507 | -12.83 | -76.37 | 10217 | 0.017 | 32926 |
| WALTAIR | 17.57 | 83.30 | 0.427 | 18.6 | -1 | 0.94 | 2.0 | 84.1 | 0.408 | 8.87 | 83.67 | 146 | 0.375 | 1796 |
| WELLEN | 66.17 | -169.84 | 0.555 | 75.4 | 16 | 4.59 | -52.3 | 157.7 | 0.649 | 6.06 | 173.13 | 23209 | 0.003 | 68215 |
| WESTFORD | 42.58 | -71.42 | 0.569 | 72.9 | -14 | 3.13 | -70.9 | -79.7 | 0.512 | -12.87 | -67.19 | 13348 | 0.010 | 41819 |
| WEISSENAU | 47.80 | 9.50 | 0.468 | 63.7 | -2 | 1.97 | -35.6 | 26.9 | 0.318 | 3.32 | 16.04 | 5742 | 0.043 | 19918 |
| WELLINGTON | -41.28 | 174.77 | 0.580 | -66.7 | 20 | 2.15 | 50.1 | -162.4 | 0.491 | 4.18 | -173.52 | 7520 | 0.032 | 24919 |

Table B1

Tracings from Surface to Surface.

| STATIONS | ** C | R | I | G | I | N | ** CONJUGATE | INTERS. | ** MINIMUM-B | E Q U A T O R | | | ** ARC |
|---|---|---|---|---|---|---|---|---|---|---|---|---|---|
| | LAT. | LONG. | B | DIP | DECL. | L | LAT. | LONG. | B | LAT. | LONG. | ALT. | B | KM |
| WHITE SANDS | 32.40 | -106.87 | 0.519 | 60.0 | 12 | 1.72 | -46.3 | -126.4 | 0.497 | -7.81 | -114.12 | 4684 | 0.060 | 16973 |
| WINGST | 53.75 | 9.07 | 0.482 | 68.6 | -2 | 2.54 | -45.0 | 33.7 | 0.330 | 2.33 | 17.80 | 9327 | 0.020 | 30263 |
| WITTEVEEN | 52.82 | 6.67 | 0.479 | 68.0 | -4 | 2.46 | -44.2 | 31.1 | 0.324 | 2.05 | 15.62 | 8812 | 0.022 | 28817 |
| WIESE ISLAND | 79.83 | 76.98 | 0.564 | 85.2 | 32 | 12.00 | ** N O | C O M P U T A T I O N S | P E R F O R M E D ** | | | | | |
| WINNIPEG | 49.90 | -97.40 | 0.608 | 77.5 | 10 | 4.22 | -66.8 | -136.3 | 0.606 | -9.62 | -106.33 | 20587 | 0.004 | 61410 |
| WIEN KOBENZL | 48.27 | 16.32 | 0.474 | 64.1 | 0 | 1.97 | -35.0 | 31.7 | 0.323 | 4.15 | 21.53 | 5748 | 0.043 | 19882 |
| WILKES | -66.20 | 110.35 | 0.640 | -81.8 | -83 | 35.17 | ** N O | C O M P U T A T I O N S | P E R F O R M E D ** | | | | | |
| WOOMERA | -30.70 | 136.80 | 0.584 | -63.2 | 6 | 1.73 | 48.6 | 139.8 | 0.531 | 9.28 | 139.99 | 5026 | 0.061 | 17587 |
| WROCLAW | 51.10 | 17.08 | 0.482 | 66.6 | 1 | 2.20 | -39.2 | 35.3 | 0.327 | 3.73 | 23.02 | 7199 | 0.031 | 24086 |
| WRANGEL ISLAND | 71.00 | -178.50 | 0.566 | 78.8 | 12 | 6.15 | -54.6 | 149.1 | 0.662 | 7.21 | 163.20 | 33192 | 0.001 | 95667 |
| YAKUTSK | 62.05 | 129.67 | 0.589 | 76.4 | -13 | 3.07 | -42.5 | 127.3 | 0.641 | 10.32 | 129.23 | 13667 | 0.011 | 41512 |
| YAMAGAWA | 31.20 | 130.65 | 0.461 | 44.4 | -4 | 1.13 | -15.0 | 130.0 | 0.483 | 8.65 | 131.07 | 1291 | 0.213 | 6533 |
| YELLOWKNIFE | 62.40 | -114.40 | 0.606 | 82.3 | 33 | 8.38 | -67.2 | -173.4 | 0.652 | -4.59 | -135.26 | 47291 | 0.001 | 135001 |
| YUZHNO-SAKHALINSK | 46.95 | 142.72 | 0.515 | 61.0 | -9 | 1.63 | -29.3 | 139.3 | 0.573 | 9.30 | 142.67 | 4421 | 0.071 | 15910 |
| ZARIA | 11.15 | 7.65 | 0.328 | 1.9 | -8 | 0.99 | 9.6 | 7.9 | 0.326 | NO MINIMUM B BETWEEN INTERS. | | | | 178 |
| ZUGSPITZE | 47.42 | 10.98 | 0.467 | 63.3 | -1 | 1.92 | -34.7 | 27.4 | 0.319 | 3.36 | 17.12 | 5516 | 0.046 | 19245 |

Table B2.

Tracing 300 km Above Stations.

Table B2

Tracings 300 km Above Stations.

| STATIONS | ** | O | R | I | G | I | N | ** CONJUGATE | INTERS. | ** MINIMUM-B | E Q U A T O R | ** ARC | | |
|---|---|---|---|---|---|---|---|---|---|---|---|---|---|---|
| | | LAT. | LONG. | B | DIP | DECL. | L | LAT. | LONG. | B | LAT. | LONG. | ALT. | B | KM |
| ABASHIRI | | 43.97 | 140.33 | 0.437 | 58.3 | -7 | 1.57 | -26.3 | 137.5 | 0.479 | 9.31 | 140.28 | 4009 | 0.081 | 14011 |
| ABISKO | | 68.35 | 18.82 | 0.457 | 77.2 | 0 | 5.95 | -59.4 | 63.5 | 0.425 | 3.59 | 34.06 | 31311 | 0.001 | 90799 |
| ABERYSTWYTH | | 52.40 | -4.07 | 0.420 | 67.7 | -9 | 2.70 | -48.0 | 25.0 | 0.295 | 0.14 | 7.55 | 10317 | 0.016 | 32573 |
| ACCRA | | 5.63 | -0.20 | 0.267 | -6.0 | -11 | 1.06 | 10.8 | -1.3 | 0.275 | 6.35 | -0.36 | 308 | 0.267 | 611 |
| ADEN | | 12.77 | 44.97 | 0.315 | 9.8 | 1 | 1.02 | 4.4 | 45.0 | 0.300 | 6.76 | 44.96 | 334 | 0.298 | 978 |
| ADDIS ABABA | | 9.03 | 38.77 | 0.302 | -0.8 | 0 | 1.01 | 9.7 | 38.8 | 0.303 | NO MINIMUM B BETWEEN INTERS. | | | | 76 |
| ADELAIDE | | -34.95 | 138.53 | 0.522 | -67.1 | 7 | 2.13 | 53.3 | 143.8 | 0.469 | 9.32 | 142.64 | 7562 | 0.032 | 24064 |
| ADAK | | 51.90 | -176.65 | 0.427 | 63.9 | 10 | 2.21 | -39.0 | 164.7 | 0.509 | 6.13 | 174.52 | 7946 | 0.029 | 25409 |
| AGINCOURT | | 43.80 | -79.30 | 0.503 | 74.0 | -6 | 3.46 | -69.6 | -98.8 | 0.469 | -12.28 | -79.25 | 15553 | 0.007 | 47139 |
| AHMEDABAD | | 23.02 | 72.60 | 0.381 | 31.9 | -0 | 1.06 | -5.5 | 74.6 | 0.347 | 7.80 | 73.32 | 821 | 0.260 | 3702 |
| AIRE-SUR-ADOUR | | 43.70 | -0.30 | 0.395 | 59.8 | -7 | 1.84 | -33.3 | 17.8 | 0.278 | 2.27 | 7.46 | 5045 | 0.051 | 17284 |
| AKROTIRI | | 34.58 | 32.95 | 0.385 | 48.7 | 3 | 1.32 | -16.9 | 36.3 | 0.299 | 6.56 | 33.69 | 2121 | 0.134 | 8258 |
| AKLAVIK | | 68.23 | -135.00 | 0.512 | 81.2 | 37 | 9.46 | -62.9 | 167.9 | 0.572 | 0.98 | -162.58 | 54361 | 0.000 | 153685 |
| AKITA | | 39.73 | 140.13 | 0.418 | 53.7 | -5 | 1.41 | -22.5 | 137.9 | 0.456 | 9.25 | 140.17 | 2985 | 0.112 | 11027 |
| ALMERIA | | 36.85 | -2.47 | 0.371 | 52.3 | -8 | 1.50 | -24.3 | 11.4 | 0.278 | 3.09 | 3.95 | 2988 | 0.092 | 11119 |
| ALDAN | | 58.60 | 125.50 | 0.509 | 74.0 | -10 | 2.70 | -39.2 | 124.5 | 0.541 | 10.08 | 125.63 | 11286 | 0.016 | 34261 |
| ALERT | | 82.55 | -63.58 | 0.495 | 86.3 | -85 | 248.58 | ** N O | C O M P U T A T I O N S | | P E R F O R M E D ** | | | | |
| ALMA-ATA | | 43.20 | 76.92 | 0.477 | 62.2 | 3 | 1.60 | -25.7 | 82.7 | 0.420 | 8.37 | 77.87 | 4219 | 0.075 | 14339 |
| ALBUQUERQUE | | 35.08 | -106.62 | 0.462 | 62.9 | 12 | 1.98 | -49.3 | -128.3 | 0.447 | -7.83 | -114.38 | 6377 | 0.039 | 21100 |
| ALMIRANTE BROWN | | -64.88 | -62.87 | 0.382 | -59.0 | 16 | 2.46 | 36.4 | -65.6 | 0.462 | -12.84 | -59.98 | 9009 | 0.021 | 29107 |
| ANCON | | -11.77 | -77.15 | 0.250 | 1.0 | 5 | 1.08 | -12.8 | -77.2 | 0.248 | NO MINIMUM B BETWEEN INTERS. | | | | 116 |
| ANCHORAGE | | 61.17 | -149.98 | 0.487 | 74.3 | 25 | 4.33 | -53.7 | 172.2 | 0.550 | 2.78 | -168.66 | 21492 | 0.004 | 62960 |
| ANTOFAGASTA | | -23.65 | -70.42 | 0.233 | -18.4 | 5 | 1.13 | -3.2 | -69.8 | 0.271 | -16.28 | -69.96 | 488 | 0.218 | 2473 |
| APIA | | -13.80 | -171.77 | 0.344 | -29.2 | 12 | 1.10 | 16.0 | -166.0 | 0.300 | 2.58 | -168.51 | 802 | 0.235 | 3892 |
| APATITY | | 67.55 | 33.33 | 0.465 | 77.4 | 9 | 5.22 | -55.6 | 69.0 | 0.430 | 5.29 | 44.21 | 26758 | 0.002 | 77966 |
| ARKHANGELSK | | 64.58 | 40.50 | 0.467 | 76.4 | 11 | 4.22 | -51.5 | 68.8 | 0.418 | 5.89 | 48.05 | 20412 | 0.004 | 60255 |
| ARCETRI | | 43.75 | 11.25 | 0.398 | 59.3 | -2 | 1.76 | -30.2 | 24.9 | 0.286 | 3.85 | 16.63 | 4596 | 0.058 | 15867 |
| AREQUIPA | | -16.35 | -71.57 | 0.237 | -6.0 | 3 | 1.10 | -10.0 | -71.3 | 0.249 | -16.14 | -71.56 | 303 | 0.237 | 740 |
| ARGENTINE ISLAND | | -65.25 | -64.27 | 0.386 | -59.4 | 17 | 2.50 | 36.8 | -66.2 | 0.464 | -13.06 | -60.70 | 9252 | 0.020 | 29785 |
| ARMIDALE | | -30.30 | 151.40 | 0.487 | -60.8 | 11 | 1.73 | 46.8 | 159.8 | 0.415 | 8.24 | 156.79 | 4906 | 0.061 | 16740 |
| ASSWAN | | 23.97 | 32.78 | 0.341 | 30.9 | 1 | 1.10 | -4.6 | 33.5 | 0.293 | 7.64 | 32.93 | 806 | 0.231 | 3690 |
| ASO | | 32.88 | 131.02 | 0.404 | 46.4 | -4 | 1.22 | -16.1 | 130.2 | 0.423 | 8.92 | 131.35 | 1849 | 0.170 | 7481 |
| ASHKABAD | | 37.93 | 55.10 | 0.430 | 55.6 | 4 | 1.43 | -22.1 | 59.9 | 0.339 | 6.64 | 55.66 | 2955 | 0.106 | 10769 |
| ATHENS | | 37.97 | 23.72 | 0.387 | 52.5 | 1 | 1.44 | -20.8 | 30.0 | 0.295 | 6.06 | 25.81 | 2765 | 0.104 | 10285 |
| BAJA | | 46.18 | 19.00 | 0.410 | 61.8 | 0 | 1.88 | -32.4 | 32.2 | 0.292 | 4.31 | 23.52 | 5360 | 0.048 | 18069 |
| BAGHDAD | | 33.35 | 44.38 | 0.396 | 48.6 | 4 | 1.29 | -16.8 | 47.0 | 0.308 | 6.53 | 44.60 | 2020 | 0.143 | 7925 |
| BANGKOK | | 13.75 | 100.55 | 0.357 | 10.0 | 0 | 0.97 | 5.2 | 100.5 | 0.352 | 9.05 | 100.52 | 343 | 0.343 | 1001 |
| BAR I | | 69.58 | -140.18 | 0.509 | 81.2 | 36 | 9.63 | -62.1 | 163.9 | 0.574 | 2.26 | -168.63 | 55536 | 0.000 | 156878 |
| BALBOA | | 8.95 | -79.57 | 0.334 | 37.4 | 3 | 1.22 | -33.2 | -84.9 | 0.276 | -13.61 | -81.26 | 1274 | 0.168 | 5872 |
| BAIE ST. PAUL | | 47.43 | -70.50 | 0.500 | 75.5 | -17 | 4.18 | -75.2 | -78.3 | 0.463 | -12.21 | -65.29 | 20030 | 0.004 | 59801 |
| BARTER ISLAND | | 70.13 | -143.67 | 0.507 | 81.0 | 35 | 9.47 | -61.5 | 162.0 | 0.574 | 2.93 | -172.10 | 54500 | 0.000 | 153994 |
| BAKER LAKE | | 64.30 | -96.08 | 0.528 | 85.6 | 6 | 15.35 | ** N O | C O M P U T A T I O N S | | P E R F O R M E D ** | | | | |
| BATTLE CREEK | | 42.27 | -85.17 | 0.503 | 72.7 | -0 | 3.13 | -65.8 | -108.7 | 0.473 | -11.77 | -88.01 | 13563 | 0.010 | 41469 |
| BANARAS | | 25.33 | 83.02 | 0.398 | 35.1 | -0 | 1.07 | -6.5 | 84.7 | 0.368 | 8.70 | 83.62 | 962 | 0.251 | 4243 |
| BANGUI | | 4.60 | 18.58 | 0.283 | -14.4 | -5 | 1.04 | 16.6 | 17.5 | 0.301 | 8.86 | 18.15 | 381 | 0.274 | 1434 |

Table B2

Tracings 300 km Above Stations.

| STATIONS | ** | O | R | I | G | I | N | ** CONJUGATE | INTERS. | ** MINIMUM-B | E Q U A T O R | | ** ARC |
|---|---|---|---|---|---|---|---|---|---|---|---|---|---|
| | | LAT. | LONG. | B | DIP | DECL. | L | LAT. | LONG. | B | LAT. | LONG. | ALT. | B | KM |
| BASE ROI BAUDOUIN | | -70.43 | 23.32 | 0.404 | -66.3 | -33 | 5.57 | 59.8 | -31.5 | 0.455 | -5.53 | -11.43 | 28636 | 0.002 | 84016 |
| BANGUIO | | 16.42 | 120.58 | 0.352 | 18.5 | 0 | 1.00 | -0.4 | 120.2 | 0.353 | 8.19 | 120.47 | 463 | 0.315 | 2021 |
| BELEM | | -1.00 | -49.00 | 0.259 | 16.3 | -13 | 1.14 | -17.9 | -44.7 | 0.217 | -13.50 | -45.86 | 416 | 0.213 | 2092 |
| BELSK | | 51.84 | 20.80 | 0.427 | 66.9 | 1 | 2.34 | -40.2 | 39.3 | 0.304 | 4.06 | 26.61 | 8203 | 0.025 | 26280 |
| BETTLES | | 66.90 | -151.84 | 0.498 | 77.9 | 28 | 6.28 | -57.3 | 164.2 | 0.566 | 3.66 | -174.64 | 34007 | 0.001 | 97449 |
| BEDFORD | | 42.48 | -71.28 | 0.490 | 72.5 | -13 | 3.24 | -70.5 | -78.5 | 0.440 | -12.82 | -67.28 | 14034 | 0.009 | 43083 |
| BERMUDA | | 32.37 | -64.67 | 0.445 | 64.1 | -12 | 2.13 | -60.8 | -60.8 | 0.352 | -13.34 | -59.30 | 6861 | 0.032 | 23035 |
| BEOGRAD | | 44.80 | 20.52 | 0.408 | 60.4 | 0 | 1.78 | -30.3 | 32.1 | 0.293 | 4.60 | 24.44 | 4794 | 0.056 | 16396 |
| BIRD | | 56.50 | 94.20 | 0.519 | 74.8 | 2 | 2.56 | -37.9 | 101.0 | 0.504 | 9.90 | 95.59 | 10404 | 0.018 | 31724 |
| BISMARK | | 46.82 | -100.77 | 0.515 | 74.3 | 12 | 3.53 | -62.7 | -134.8 | 0.510 | -8.91 | -110.07 | 16235 | 0.007 | 48673 |
| BJORNOYA | | 74.52 | 19.02 | 0.469 | 80.2 | -0 | 9.97 | -63.5 | 76.8 | 0.476 | 4.54 | 41.23 | 57148 | 0.000 | 162139 |
| BOROK | | 58.03 | 38.33 | 0.457 | 72.4 | 9 | 2.97 | -45.2 | 59.3 | 0.368 | 5.35 | 43.36 | 12445 | 0.012 | 38085 |
| BOLOGNA | | 44.50 | 11.35 | 0.401 | 60.1 | -2 | 1.80 | -31.2 | 25.6 | 0.286 | 3.78 | 16.90 | 4874 | 0.054 | 16687 |
| BOULDER | | 40.03 | -105.30 | 0.487 | 67.8 | 13 | 2.43 | -54.6 | -131.7 | 0.476 | -8.28 | -114.09 | 9236 | 0.021 | 29144 |
| BOMBAY | | 19.00 | 72.83 | 0.364 | 23.6 | -1 | 1.02 | -1.4 | 74.2 | 0.339 | 7.83 | 73.43 | 559 | 0.295 | 2515 |
| BOGOTA | | 4.63 | -74.08 | 0.310 | 31.9 | 1 | 1.19 | -30.8 | -76.9 | 0.252 | -15.09 | -74.83 | 943 | 0.186 | 4653 |
| BRISBANE | | -27.53 | 152.92 | 0.470 | -57.6 | 10 | 1.58 | 43.7 | 160.7 | 0.398 | 8.17 | 157.91 | 3963 | 0.080 | 14048 |
| BUDAPEST | | 46.68 | 21.27 | 0.414 | 62.3 | 1 | 1.90 | -32.9 | 34.3 | 0.294 | 4.64 | 25.49 | 5533 | 0.046 | 18556 |
| BUENOS AIRES | | -34.52 | -58.50 | 0.230 | -32.8 | 0 | 1.25 | 7.4 | -62.0 | 0.314 | -15.83 | -59.48 | 1177 | 0.160 | 5706 |
| BUNIA | | 1.53 | 30.18 | 0.290 | -20.6 | -2 | 1.05 | 18.9 | 29.7 | 0.319 | 8.37 | 29.91 | 478 | 0.269 | 2102 |
| BYRD STATION | | -79.98 | -120.02 | 0.521 | -75.1 | 68 | 7.68 | 56.0 | -79.2 | 0.521 | -12.07 | -78.24 | 42515 | 0.001 | 121915 |
| CAPRI | | 40.57 | 14.33 | 0.389 | 55.6 | -1 | 1.57 | -25.1 | 24.6 | 0.289 | 4.77 | 18.39 | 3503 | 0.080 | 12580 |
| CASTEL TESINO | | 46.05 | 11.65 | 0.405 | 61.6 | -2 | 1.91 | -33.5 | 27.2 | 0.286 | 3.64 | 17.54 | 5494 | 0.046 | 18508 |
| CATANIA | | 37.50 | 15.07 | 0.379 | 51.8 | -1 | 1.43 | -20.7 | 23.3 | 0.291 | 5.71 | 18.36 | 2712 | 0.104 | 10152 |
| CAPE CHELYUSKIN | | 77.72 | 104.28 | 0.507 | 85.5 | 12 | 9.52 | -56.3 | 112.9 | 0.558 | 10.99 | 104.54 | 54689 | 0.000 | 154303 |
| CAPE ZHELANIA | | 76.90 | 68.60 | 0.495 | 83.7 | 22 | 9.53 | -57.9 | 98.0 | 0.526 | 9.45 | 78.31 | 54643 | 0.000 | 154490 |
| CAPE SCHMIDT | | 68.87 | -179.48 | 0.491 | 77.2 | 11 | 5.40 | -52.8 | 150.7 | 0.569 | 7.17 | 164.20 | 28427 | 0.002 | 81924 |
| CAMBRIDGE UK | | 52.22 | 0.10 | 0.419 | 67.4 | -7 | 2.61 | -46.1 | 27.0 | 0.294 | 0.87 | 10.67 | 9728 | 0.018 | 30850 |
| CARIBOU | | 46.87 | -68.02 | 0.495 | 74.8 | -19 | 4.01 | -74.9 | -70.2 | 0.452 | -12.37 | -61.60 | 18888 | 0.005 | 56682 |
| CALCUTTA | | 22.93 | 88.52 | 0.388 | 30.0 | -0 | 1.03 | -3.6 | 89.5 | 0.366 | 9.01 | 88.89 | 751 | 0.279 | 3400 |
| CAPE HALLETT | | -72.32 | 178.22 | 0.569 | -83.6 | -88 | 16.57 | ** N O | C O M P U T A T I O N S | | P E R F O R M E D ** | | | | |
| CAMPBELL ISLAND | | -52.55 | 169.15 | 0.550 | -76.1 | 27 | 4.20 | 61.7 | -155.2 | 0.483 | 3.62 | -173.12 | 20618 | 0.004 | 60528 |
| CANBERRA | | -35.32 | 149.00 | 0.514 | -66.1 | 11 | 2.08 | 52.5 | 158.8 | 0.442 | 8.57 | 155.22 | 7197 | 0.035 | 23177 |
| CAPETOWN | | -34.15 | 18.32 | 0.278 | -64.2 | -25 | 1.88 | 44.3 | -0.3 | 0.397 | 1.94 | 7.70 | 5265 | 0.048 | 17939 |
| CAMDEN | | -34.08 | 150.68 | 0.506 | -64.7 | 11 | 1.98 | 50.9 | 160.6 | 0.433 | 8.39 | 156.88 | 6483 | 0.041 | 21194 |
| CAPE CANAVERAL | | 28.40 | -80.60 | 0.444 | 61.2 | 0 | 1.85 | -53.9 | -92.7 | 0.383 | -12.93 | -82.14 | 5329 | 0.048 | 18344 |
| CAPE JONES | | 54.50 | -79.50 | 0.520 | 80.5 | -15 | 6.80 | -78.7 | -116.0 | 0.516 | -11.97 | -78.82 | 36816 | 0.001 | 106130 |
| CEBU | | 10.33 | 123.90 | 0.338 | 5.6 | 1 | 0.98 | 5.3 | 123.8 | 0.339 | 8.08 | 123.85 | 314 | 0.335 | 591 |
| CHAMICAL | | -30.33 | -66.33 | 0.233 | -27.7 | 4 | 1.19 | 2.8 | -66.7 | 0.296 | -16.19 | -65.92 | 831 | 0.187 | 4255 |
| CHURCHILL | | 58.77 | -94.17 | 0.530 | 83.0 | 4 | 8.89 | -74.5 | -151.6 | 0.548 | -9.91 | -103.82 | 50305 | 0.000 | 143085 |
| CHAMBON-LA-FORET | | 48.02 | 2.27 | 0.408 | 63.8 | -6 | 2.15 | -39.0 | 23.4 | 0.282 | 1.84 | 10.82 | 6883 | 0.032 | 22644 |
| CHICAGO | | 41.83 | -87.67 | 0.503 | 72.2 | 2 | 3.03 | -64.3 | -112.3 | 0.475 | -11.60 | -91.59 | 12900 | 0.011 | 39574 |
| CHARLOTTESVILLE | | 38.03 | -78.22 | 0.485 | 69.7 | -4 | 2.65 | -64.5 | -92.7 | 0.435 | -12.73 | -78.13 | 10366 | 0.016 | 32665 |
| CHITA | | 52.05 | 113.48 | 0.509 | 70.1 | -6 | 2.08 | -33.3 | 115.3 | 0.513 | 9.88 | 114.52 | 7382 | 0.034 | 23307 |
| CHITTAGONG | | 22.35 | 91.82 | 0.386 | 28.7 | -0 | 1.03 | -3.0 | 92.5 | 0.366 | 9.07 | 92.08 | 708 | 0.286 | 3215 |

Table B2

Tracings 300 km Above Stations.

| STATIONS | ** | O | R | I | G | I | N | ** CONJUGATE | INTERS. ** | MINIMUM-B | E Q U A T O R | ** ARC | | |
|---|---|---|---|---|---|---|---|---|---|---|---|---|---|---|
| | | LAT. | LONG. | B | DIP | DECL. | L | LAT. | LONG. | B | LAT. | LONG. | ALT. | B | KM |
| CHRISTCHURCH | | -43.57 | 172.80 | 0.515 | -68.9 | 20 | 2.52 | 52.9 | -162.5 | 0.443 | 4.33 | -174.60 | 9893 | 0.020 | 30870 |
| CHACALTAYA | | -16.32 | -68.15 | 0.234 | -5.3 | 1 | 1.10 | -10.6 | -68.1 | 0.245 | NO MINIMUM B BETWEEN INTERS. | | | | 666 |
| CLIMAX | | 39.37 | -106.18 | 0.483 | 67.1 | 13 | 2.35 | -53.6 | -131.9 | 0.473 | -8.04 | -114.94 | 8704 | 0.024 | 27649 |
| CLONCURRY | | -20.67 | 140.50 | 0.444 | -50.9 | 6 | 1.35 | 37.7 | 143.0 | 0.402 | 9.17 | 142.86 | 2567 | 0.128 | 9805 |
| CONCORD | | 43.20 | -71.53 | 0.492 | 73.0 | -13 | 3.36 | -71.1 | -79.4 | 0.444 | -12.54 | -67.55 | 14781 | 0.008 | 45162 |
| COOK | | -30.63 | 130.40 | 0.505 | -63.7 | 3 | 1.83 | 48.9 | 132.1 | 0.474 | 9.61 | 132.53 | 5713 | 0.051 | 18774 |
| COLLEGE | | 64.85 | -147.83 | 0.498 | 77.1 | 28 | 5.71 | -57.0 | 168.6 | 0.562 | 2.90 | -169.67 | 30334 | 0.002 | 87350 |
| CORINALDO | | 43.63 | 13.00 | 0.399 | 59.1 | -2 | 1.74 | -29.7 | 26.0 | 0.287 | 4.26 | 17.98 | 4509 | 0.060 | 15592 |
| COIMBRA | | 40.22 | -8.42 | 0.384 | 57.0 | -10 | 1.72 | -31.6 | 10.3 | 0.272 | 1.01 | 0.13 | 4245 | 0.062 | 14988 |
| CONCEPCION | | -36.58 | -72.98 | 0.259 | -36.4 | 11 | 1.27 | 9.2 | -70.9 | 0.333 | -15.38 | -70.72 | 1404 | 0.153 | 6449 |
| CORDOBA | | -31.32 | -64.22 | 0.231 | -28.8 | 3 | 1.20 | 3.7 | -65.3 | 0.299 | -16.31 | -64.11 | 896 | 0.181 | 4557 |
| COLOMBO | | 6.90 | 79.87 | 0.341 | -6.0 | -3 | 0.97 | 11.9 | 79.6 | 0.347 | 8.49 | 79.77 | 313 | 0.340 | 580 |
| COCOS ISLAND | | -12.20 | 96.90 | 0.403 | -44.8 | -2 | 1.16 | 31.0 | 95.8 | 0.430 | 9.09 | 96.20 | 1572 | 0.196 | 6377 |
| COPENHAGEN | | 55.75 | 12.50 | 0.430 | 69.7 | -1 | 2.88 | -47.3 | 38.9 | 0.316 | 2.46 | 21.61 | 11552 | 0.013 | 35894 |
| CORAL HARBOUR | | 64.20 | -83.40 | 0.522 | 85.2 | -25 | 17.52 | ** NO | C O M P U T A T I O N S | | P E R F O R M E D | ** | | | |
| CRACOW | | 50.05 | 19.95 | 0.422 | 65.4 | 1 | 2.17 | -37.8 | 36.7 | 0.298 | 4.02 | 25.37 | 7184 | 0.031 | 23361 |
| CURACAO | | 12.08 | -68.84 | 0.347 | 43.3 | -3 | 1.33 | -40.1 | -69.9 | 0.264 | -15.34 | -67.85 | 1766 | 0.133 | 7733 |
| CUZCO | | -13.52 | -71.98 | 0.242 | -0.8 | 3 | 1.09 | -12.7 | -71.9 | 0.243 | NO MINIMUM B BETWEEN INTERS. | | | | 94 |
| DAVIS | | -68.60 | 78.00 | 0.491 | -74.3 | -68 | 15.24 | ** NO | C O M P U T A T I O N S | | P E R F O R M E D | ** | | | |
| DAPANGO | | 10.80 | 0.07 | 0.276 | 5.4 | -10 | 1.05 | 6.1 | 1.0 | 0.269 | 6.64 | 0.92 | 305 | 0.269 | 555 |
| DALLAS | | 32.78 | -96.80 | 0.461 | 62.8 | 9 | 1.96 | -51.3 | -116.4 | 0.430 | -10.01 | -102.73 | 6145 | 0.041 | 20497 |
| DAKAR | | 14.66 | -17.43 | 0.285 | 21.8 | -13 | 1.11 | -6.2 | -11.5 | 0.248 | 1.72 | -13.90 | 549 | 0.225 | 2656 |
| DARWIN-COONAWARRA | | -12.43 | 130.90 | 0.401 | -39.6 | 3 | 1.14 | 28.8 | 131.7 | 0.383 | 8.82 | 131.85 | 1344 | 0.208 | 5819 |
| DEBRECEN | | 47.48 | 21.65 | 0.416 | 63.1 | 1 | 1.96 | -34.0 | 35.3 | 0.295 | 4.62 | 26.01 | 5876 | 0.042 | 19554 |
| DE BILT | | 52.10 | 5.18 | 0.419 | 67.1 | -5 | 2.52 | -44.2 | 29.7 | 0.294 | 1.78 | 14.50 | 9195 | 0.020 | 29273 |
| DEEP RIVER | | 46.10 | -77.50 | 0.507 | 75.4 | -9 | 3.92 | -72.3 | -96.8 | 0.477 | -12.40 | -76.30 | 18481 | 0.005 | 55331 |
| DENVER | | 39.75 | -105.00 | 0.486 | 67.7 | 13 | 2.41 | -54.5 | -131.1 | 0.475 | -8.11 | -113.63 | 9089 | 0.022 | 28734 |
| DEHRA DUN | | 30.33 | 78.05 | 0.420 | 44.5 | 0 | 1.17 | -12.2 | 80.8 | 0.378 | 8.31 | 78.84 | 1542 | 0.192 | 6276 |
| DELHI | | 28.63 | 77.22 | 0.411 | 41.7 | -0 | 1.13 | -10.6 | 79.8 | 0.370 | 8.09 | 78.01 | 1335 | 0.210 | 5585 |
| DECEPCION | | -62.98 | -60.72 | 0.366 | -57.4 | 14 | 2.29 | 34.6 | -64.7 | 0.453 | -13.02 | -59.00 | 7921 | 0.026 | 26048 |
| DIXON ISLAND | | 73.53 | 80.70 | 0.503 | 83.5 | 19 | 7.03 | -54.1 | 100.3 | 0.529 | 10.20 | 85.74 | 38727 | 0.001 | 110374 |
| DJIBOUTI | | 11.55 | 43.15 | 0.311 | 6.5 | 1 | 1.01 | 6.1 | 43.1 | 0.301 | 6.97 | 43.14 | 310 | 0.300 | 639 |
| DJAKARTA | | -6.17 | 107.00 | 0.381 | -32.7 | 1 | 1.05 | 24.2 | 107.3 | 0.392 | 8.75 | 107.23 | 877 | 0.265 | 3963 |
| DODAIRA | | 36.00 | 139.20 | 0.402 | 49.3 | -4 | 1.30 | -19.0 | 137.4 | 0.436 | 9.11 | 139.29 | 2288 | 0.143 | 8922 |
| DOLGOPRUDNAYA | | 55.94 | 37.52 | 0.452 | 71.0 | 8 | 2.70 | -43.0 | 56.4 | 0.353 | 5.58 | 41.90 | 10687 | 0.016 | 33149 |
| DOURBES | | 50.10 | 4.60 | 0.414 | 65.5 | -5 | 2.31 | -41.4 | 27.0 | 0.287 | 2.06 | 13.30 | 7918 | 0.026 | 25611 |
| DUNSINK | | 53.38 | -6.33 | 0.423 | 68.6 | -11 | 2.88 | -50.4 | 25.1 | 0.302 | -0.13 | 6.17 | 11436 | 0.013 | 35772 |
| DUSHETTI | | 42.08 | 44.70 | 0.429 | 59.5 | 5 | 1.61 | -26.5 | 51.2 | 0.321 | 6.42 | 45.59 | 3941 | 0.075 | 13752 |
| DURHAM | | 43.08 | -70.92 | 0.491 | 72.9 | -13 | 3.33 | -71.1 | -77.7 | 0.442 | -12.60 | -66.65 | 14617 | 0.008 | 44719 |
| DUMONT D'URVILLE | | -66.67 | 140.02 | 0.580 | -89.6 | -58 | 35.99 | ** NO | C O M P U T A T I O N S | | P E R F O R M E D | ** | | | |
| DURBAN | | -29.83 | 31.03 | 0.292 | -63.4 | -19 | 1.75 | 44.4 | 19.4 | 0.405 | 4.86 | 23.41 | 4657 | 0.058 | 15991 |
| EDINBURGH | | 55.92 | -3.18 | 0.428 | 70.2 | -10 | 3.19 | -52.6 | 30.5 | 0.317 | 0.01 | 9.76 | 13456 | 0.010 | 41443 |
| EIGHTS | | -75.23 | -77.17 | 0.462 | -67.8 | 31 | 4.17 | 47.4 | -70.1 | 0.500 | -12.30 | -64.74 | 19998 | 0.004 | 59720 |
| ELLSWORTH | | -77.72 | -41.13 | 0.446 | -67.2 | 8 | 4.81 | 51.2 | -59.9 | 0.488 | -11.07 | -48.59 | 23935 | 0.003 | 70860 |
| ELISABETHVILLE | | -11.63 | 27.42 | 0.294 | -45.9 | -7 | 1.22 | 30.8 | 24.2 | 0.360 | 7.26 | 25.34 | 1485 | 0.169 | 6192 |

Table B2

Tracings 300 km Above Stations.

| STATIONS | ** D | R | I | G | I | N | ** CONJUGATE | INTERS. | ** MINIMUM-B | EQUATOR | | ** ARC |
|---|---|---|---|---|---|---|---|---|---|---|---|---|
| | LAT. | LONG. | B | DIP | DECL. | L | LAT. | LONG. | B | LAT. | LONG. | ALT. | B | KM |
| ENNADAI | 61.30 | -101.20 | 0.530 | 83.6 | 16 | 10.16 | -72.5 | -163.8 | 0.558 | -7.86 | -116.05 | 58505 | 0.000 | 165589 |
| ENUGU | 6.47 | 7.55 | 0.275 | -7.5 | -9 | 1.04 | 12.8 | 6.5 | 0.284 | 7.96 | 7.29 | 318 | 0.274 | 751 |
| ESKDALEMUIR | 55.32 | -3.20 | 0.427 | 69.8 | -10 | 3.10 | -51.8 | 29.6 | 0.313 | 0.17 | 9.44 | 12837 | 0.011 | 39696 |
| ESPERANZA | -63.38 | -56.98 | 0.363 | -57.4 | 12 | 2.33 | 35.2 | -63.2 | 0.453 | -12.95 | -56.79 | 8158 | 0.024 | 26744 |
| EUREKA | 80.00 | -85.93 | 0.503 | 88.0 | 73 | 317.06 | ** NO | COMPUTATIONS | PERFORMED ** | | | | | |
| FAREWELL | 62.53 | -153.90 | 0.487 | 74.6 | 24 | 4.49 | -53.6 | 168.8 | 0.553 | 3.30 | -172.74 | 22554 | 0.003 | 65870 |
| FANNING ISLAND | 3.92 | -159.38 | 0.289 | 9.8 | 10 | 1.03 | -5.5 | -161.1 | 0.302 | 0.86 | -159.93 | 342 | 0.285 | 1121 |
| FLIN FLON | 54.70 | -102.00 | 0.528 | 79.6 | 15 | 5.75 | -68.2 | -148.8 | 0.541 | -8.44 | -114.10 | 30402 | 0.002 | 87906 |
| FORT YUKON | 66.57 | -145.30 | 0.503 | 78.6 | 31 | 6.77 | -58.9 | 167.2 | 0.567 | 2.74 | -169.23 | 37132 | 0.001 | 106103 |
| FORT NORMAN | 64.90 | -125.50 | 0.518 | 81.1 | 35 | 8.58 | -64.4 | 177.4 | 0.567 | -1.42 | -149.79 | 48635 | 0.000 | 137980 |
| FORT CHIMO | 58.10 | -68.43 | 0.508 | 80.5 | -31 | 8.71 | -85.1 | -81.5 | 0.505 | -11.68 | -59.54 | 48857 | 0.000 | 139727 |
| FORT MONMOUTH | 40.25 | -74.02 | 0.488 | 71.2 | -9 | 2.93 | -67.8 | -84.6 | 0.436 | -12.85 | -71.70 | 12106 | 0.012 | 37634 |
| FORT BELVOIR | 38.73 | -77.13 | 0.486 | 70.3 | -5 | 2.73 | -65.5 | -90.8 | 0.437 | -12.89 | -76.47 | 10901 | 0.015 | 34188 |
| FORT RANDOLPH | 9.38 | -79.88 | 0.336 | 38.0 | 3 | 1.23 | -33.5 | -85.4 | 0.278 | -13.69 | -81.64 | 1314 | 0.165 | 6017 |
| FORT DE FRANCE | 14.10 | -61.02 | 0.349 | 44.8 | -9 | 1.38 | -41.2 | -55.5 | 0.244 | -14.80 | -57.26 | 1948 | 0.122 | 8417 |
| FREETOWN | 8.47 | -13.22 | 0.266 | 7.2 | -14 | 1.07 | 2.0 | -11.5 | 0.254 | 3.04 | -11.76 | 314 | 0.254 | 789 |
| FROBISHER | 63.75 | -68.57 | 0.508 | 82.7 | -40 | 15.36 | ** NO | COMPUTATIONS | PERFORMED ** | | | | | |
| FREIBURG | 48.05 | 7.58 | 0.409 | 63.6 | -4 | 2.10 | -37.4 | 26.6 | 0.285 | 2.77 | 14.93 | 6596 | 0.035 | 21762 |
| FRONT ROYAL | 38.93 | -78.18 | 0.488 | 70.4 | -5 | 2.75 | -65.4 | -93.1 | 0.440 | -12.72 | -77.99 | 11032 | 0.015 | 34533 |
| FT. DAVIS | 30.63 | -103.95 | 0.441 | 59.0 | 11 | 1.74 | -46.0 | -122.1 | 0.419 | -8.49 | -110.50 | 4808 | 0.058 | 16641 |
| GARCHY | 47.30 | 3.07 | 0.406 | 63.1 | -6 | 2.08 | -37.6 | 23.1 | 0.282 | 2.05 | 11.21 | 6461 | 0.036 | 21410 |
| GAINESVILLE | 29.63 | -82.30 | 0.450 | 62.2 | 1 | 1.91 | -54.5 | -95.9 | 0.394 | -12.70 | -84.36 | 5728 | 0.043 | 19465 |
| GENOVA MONTE CAPEL | 44.55 | 8.95 | 0.400 | 60.2 | -3 | 1.82 | -31.9 | 24.1 | 0.284 | 3.56 | 14.98 | 4971 | 0.052 | 16990 |
| GENERAL BELGRAND | -77.97 | -38.80 | 0.446 | -67.4 | 6 | 4.92 | 51.6 | -59.3 | 0.488 | -11.05 | -47.66 | 24625 | 0.003 | 72785 |
| GENERAL SAN MARTIN | -68.13 | -67.43 | 0.409 | -61.9 | 21 | 2.82 | 39.7 | -67.4 | 0.476 | -12.79 | -61.94 | 11367 | 0.014 | 35706 |
| GHANA | 10.00 | 4.00 | 0.277 | 1.9 | -9 | 1.04 | 8.4 | 4.3 | 0.275 | NO MINIMUM B BETWEEN INTERS. | | | | 193 |
| GIFU | 35.58 | 137.08 | 0.405 | 49.1 | -5 | 1.29 | -18.6 | 135.6 | 0.435 | 9.16 | 137.28 | 2229 | 0.146 | 8722 |
| GILGIT | 35.94 | 74.30 | 0.445 | 53.2 | 1 | 1.32 | -18.5 | 78.4 | 0.389 | 7.90 | 75.17 | 2471 | 0.133 | 9202 |
| GOUGH ISLAND | -40.35 | -9.89 | 0.252 | -56.9 | -25 | 1.76 | 34.2 | -33.6 | 0.385 | -5.32 | -22.55 | 4370 | 0.058 | 15663 |
| GODHAVN | 69.23 | -53.52 | 0.491 | 81.9 | -48 | 22.19 | ** NO | COMPUTATIONS | PERFORMED ** | | | | | |
| GOOSE BAY | 53.32 | -60.38 | 0.492 | 76.8 | -28 | 5.56 | -79.8 | -40.3 | 0.459 | -11.09 | -48.61 | 28682 | 0.002 | 84020 |
| GOTTINGEN | 51.53 | 9.93 | 0.419 | 66.6 | -3 | 2.40 | -42.0 | 31.9 | 0.294 | 2.46 | 17.97 | 8483 | 0.023 | 27189 |
| GRYTVIKEN | -54.27 | -36.50 | 0.287 | -52.3 | -5 | 1.91 | 50.8 | -53.6 | 0.414 | -11.47 | -44.74 | 5337 | 0.045 | 18731 |
| GRAZ | 47.07 | 15.47 | 0.411 | 62.6 | -0 | 1.96 | -34.3 | 30.6 | 0.290 | 3.96 | 20.88 | 5826 | 0.042 | 19454 |
| GROCKA | 44.63 | 20.77 | 0.407 | 60.3 | 0 | 1.77 | -30.0 | 32.2 | 0.293 | 4.86 | 24.58 | 4730 | 0.057 | 16199 |
| GRAND BAHAMA | 26.67 | -78.37 | 0.434 | 59.7 | -0 | 1.77 | -52.9 | -88.5 | 0.367 | -13.23 | -79.25 | 4801 | 0.055 | 16853 |
| GRAHAMSTOWN | -33.28 | 26.48 | 0.286 | -64.6 | -23 | 1.89 | 45.8 | 10.9 | 0.404 | 3.44 | 16.93 | 5416 | 0.047 | 18288 |
| GREAT WHALE RIVER | 55.27 | -77.78 | 0.519 | 80.7 | -18 | 7.22 | -80.0 | -113.6 | 0.516 | -11.89 | -75.87 | 39468 | 0.001 | 113517 |
| GULMARG | 34.05 | 74.40 | 0.436 | 50.5 | 1 | 1.27 | -16.5 | 78.1 | 0.383 | 7.91 | 75.26 | 2128 | 0.151 | 8152 |
| GUANTANAMO BAY | 19.90 | -75.15 | 0.396 | 52.8 | -0 | 1.51 | -46.9 | -81.4 | 0.319 | -13.98 | -75.46 | 3062 | 0.089 | 11753 |
| GUAM | 13.45 | 144.75 | 0.316 | 11.7 | 2 | 1.01 | 2.1 | 144.2 | 0.328 | 8.82 | 144.58 | 366 | 0.307 | 1339 |
| GUAYAQUIL | -2.17 | -79.88 | 0.280 | 18.4 | 5 | 1.10 | -21.2 | -82.2 | 0.249 | -13.79 | -81.07 | 477 | 0.232 | 2310 |
| HAMMAGHIR | 30.10 | 0. | 0.344 | 42.6 | -7 | 1.27 | -14.6 | 9.1 | 0.277 | 4.97 | 4.45 | 1621 | 0.151 | 6751 |
| HACHIJOJIMA | 33.13 | 139.80 | 0.387 | 45.5 | -4 | 1.23 | -16.4 | 138.2 | 0.420 | 8.92 | 139.82 | 1846 | 0.168 | 7543 |
| HALLETT | -72.32 | 170.22 | 0.573 | -84.8 | -78 | 22.17 | ** NO | COMPUTATIONS | PERFORMED ** | | | | | |
| HARTLAND | 51.00 | -4.48 | 0.416 | 66.6 | -9 | 2.54 | -46.1 | 23.0 | 0.289 | 0.30 | 6.66 | 9302 | 0.020 | 29680 |

Table B2

Tracings 300 km Above Stations.

| STATIONS | ** | O | R | I | G | I | N | ** CONJUGATE | INTERS. | ** MINIMUM-B | E Q U A T O R | | | ** ARC |
|---|---|---|---|---|---|---|---|---|---|---|---|---|---|---|
| | | LAT. | LONG. | B | DIP | DECL. | L | LAT. | LONG. | B | LAT. | LONG. | ALT. | B | KM |
| HARVSTVA | | 60.22 | 10.25 | 0.438 | 72.7 | -3 | 3.69 | -53.6 | 44.5 | 0.349 | 1.89 | 22.10 | 16722 | 0.006 | 50439 |
| HAMBURG | | 53.63 | 10.00 | 0.424 | 68.2 | -3 | 2.63 | -45.1 | 34.5 | 0.303 | 2.51 | 18.77 | 9972 | 0.018 | 31436 |
| HALLE | | 51.48 | 11.93 | 0.420 | 66.5 | -2 | 2.37 | -41.5 | 33.0 | 0.295 | 3.00 | 19.46 | 8341 | 0.024 | 26759 |
| HALIFAX | | 44.60 | -63.60 | 0.482 | 72.6 | -20 | 3.47 | -72.4 | -56.4 | 0.422 | -12.29 | -55.50 | 15391 | 0.007 | 47031 |
| HANNOVER USA | | 43.70 | -72.30 | 0.495 | 73.4 | -13 | 3.44 | -71.4 | -81.7 | 0.450 | -12.71 | -68.64 | 15362 | 0.007 | 46767 |
| HABANA | | 23.15 | -82.35 | 0.415 | 55.5 | 2 | 1.59 | -47.6 | -93.2 | 0.353 | -12.93 | -84.61 | 3649 | 0.076 | 13414 |
| HALLEY BAY | | -75.52 | -26.60 | 0.424 | -65.7 | -2 | 4.47 | 50.9 | -54.9 | 0.478 | -10.63 | -41.68 | 21702 | 0.003 | 64729 |
| HAIFA | | 32.83 | 35.10 | 0.381 | 46.5 | 3 | 1.27 | -15.1 | 37.6 | 0.300 | 6.76 | 35.55 | 1848 | 0.149 | 7380 |
| HAMILTON MASS. | | 42.02 | -72.17 | 0.490 | 72.3 | -12 | 3.17 | -69.9 | -80.6 | 0.440 | -12.60 | -68.68 | 13630 | 0.010 | 41935 |
| HERSTMONCEUX | | 50.90 | 0.33 | 0.416 | 66.3 | -7 | 2.45 | -44.1 | 25.5 | 0.289 | 1.14 | 10.33 | 8763 | 0.022 | 28086 |
| HEISS | | 80.20 | 57.48 | 0.490 | 84.1 | 19 | 13.64 | ** N O | C O M P U T A T I O N S | | P E R F O R M E D ** | | | | |
| HEALY | | 63.85 | -119.00 | 0.522 | 81.8 | 33 | 8.98 | -66.2 | -178.0 | 0.566 | -3.08 | -141.72 | 51178 | 0.000 | 145071 |
| HEL | | 54.60 | 18.80 | 0.431 | 69.0 | 1 | 2.66 | -44.3 | 41.3 | 0.315 | 3.46 | 26.03 | 10204 | 0.017 | 32004 |
| HELWAN | | 29.87 | 31.33 | 0.364 | 41.3 | 2 | 1.20 | -11.1 | 33.3 | 0.296 | 7.30 | 31.81 | 1397 | 0.178 | 5883 |
| HERMANUS | | -34.42 | 19.22 | 0.279 | -64.4 | -25 | 1.89 | 44.7 | 0.7 | 0.398 | 2.10 | 8.54 | 5381 | 0.046 | 18269 |
| HIRAISO | | 36.37 | 140.62 | 0.401 | 49.6 | -4 | 1.31 | -19.4 | 138.6 | 0.438 | 9.05 | 140.62 | 2344 | 0.139 | 9105 |
| HIGHCLIFF | | -45.88 | 170.58 | 0.527 | -71.1 | 22 | 2.86 | 55.8 | -162.6 | 0.455 | 4.32 | -175.86 | 12074 | 0.013 | 36915 |
| HONOLULU | | 21.30 | -158.10 | 0.318 | 38.7 | 11 | 1.19 | -20.4 | -166.6 | 0.369 | 1.58 | -161.96 | 1336 | 0.188 | 5961 |
| HOBART | | -42.92 | 147.17 | 0.546 | -72.9 | 13 | 2.98 | 60.6 | 161.4 | 0.472 | 8.38 | 155.12 | 12928 | 0.012 | 39083 |
| HOLLANDIA | | -2.50 | 140.52 | 0.346 | -21.1 | 4 | 1.03 | 18.2 | 141.3 | 0.328 | 8.74 | 141.08 | 535 | 0.287 | 2532 |
| HURBANOVO | | 47.90 | 18.20 | 0.415 | 63.4 | 0 | 2.01 | -35.0 | 33.3 | 0.293 | 4.13 | 23.32 | 6138 | 0.040 | 20344 |
| HUMAIN | | 50.20 | 5.35 | 0.415 | 65.5 | -5 | 2.31 | -41.3 | 27.6 | 0.288 | 2.18 | 13.91 | 7929 | 0.026 | 25636 |
| HUANCAYO | | -12.05 | -75.33 | 0.248 | 1.1 | 4 | 1.08 | -13.1 | -75.4 | 0.246 | NO MINIMUM B BETWEEN INTERS. | | | | 128 |
| HYDERABAD | | 17.42 | 78.45 | 0.361 | 19.2 | -1 | 1.00 | 1.1 | 79.4 | 0.344 | 8.41 | 78.92 | 464 | 0.314 | 1970 |
| IBADAN | | 7.37 | 3.97 | 0.273 | -4.0 | -10 | 1.05 | 10.8 | 3.3 | 0.278 | NO MINIMUM B BETWEEN INTERS. | | | | 407 |
| I. CROZET | | -46.50 | 52.00 | 0.347 | -65.6 | -38 | 2.99 | 57.8 | 28.5 | 0.446 | 4.51 | 35.07 | 12490 | 0.012 | 38340 |
| IL QORTIN | | 36.22 | 14.30 | 0.373 | 50.1 | -2 | 1.39 | -19.1 | 22.1 | 0.290 | 5.84 | 17.50 | 2441 | 0.114 | 9314 |
| INUVIK | | 68.20 | -133.70 | 0.513 | 81.4 | 37 | 9.70 | -63.3 | 168.4 | 0.572 | 0.77 | -161.40 | 55888 | 0.000 | 157906 |
| INVERCARGILL | | -46.42 | 168.32 | 0.532 | -71.9 | 22 | 3.00 | 57.2 | -164.7 | 0.459 | 4.76 | -178.07 | 12984 | 0.012 | 39424 |
| INVERNESS | | 57.45 | -4.25 | 0.432 | 71.2 | -11 | 3.49 | -55.1 | 32.4 | 0.330 | -0.33 | 9.71 | 15389 | 0.007 | 46887 |
| IQUITOS | | -3.67 | -73.33 | 0.271 | 17.6 | 2 | 1.11 | -22.3 | -74.6 | 0.238 | -15.64 | -73.94 | 457 | 0.225 | 2242 |
| IRKUTSK | | 52.27 | 104.30 | 0.514 | 71.0 | -2 | 2.12 | -33.6 | 107.9 | 0.505 | 9.95 | 105.44 | 7628 | 0.032 | 23959 |
| ISLA DE PASCUA | | -27.17 | -109.43 | 0.307 | -36.3 | 14 | 1.18 | 12.4 | -102.2 | 0.337 | -8.33 | -105.42 | 1188 | 0.186 | 5487 |
| ISFJORD | | 78.07 | 13.63 | 0.474 | 81.7 | -6 | 15.17 | ** N O | C O M P U T A T I O N S | | P E R F O R M E D ** | | | | |
| ITHACA | | 42.45 | -76.52 | 0.497 | 72.9 | -8 | 3.25 | -69.2 | -91.6 | 0.455 | -12.59 | -75.18 | 14152 | 0.009 | 43293 |
| IVALO | | 68.60 | 27.48 | 0.462 | 77.7 | 6 | 5.77 | -57.7 | 67.9 | 0.433 | 4.61 | 40.62 | 30222 | 0.002 | 87647 |
| JICAMARCA | | -11.95 | -76.87 | 0.249 | 0.7 | 5 | 1.08 | -12.7 | -76.9 | 0.248 | NO MINIMUM B BETWEEN INTERS. | | | | 86 |
| JODRELL BANK | | 53.23 | -2.30 | 0.422 | 68.2 | -9 | 2.77 | -48.5 | 27.1 | 0.299 | 0.27 | 9.26 | 10789 | 0.015 | 33899 |
| JOHANNESBURG | | -26.20 | 28.03 | 0.291 | -61.6 | -17 | 1.61 | 41.7 | 18.1 | 0.396 | 4.94 | 21.70 | 3785 | 0.074 | 13408 |
| JUPITER | | 27.02 | -80.12 | 0.436 | 59.9 | 0 | 1.78 | -52.6 | -91.4 | 0.373 | -13.11 | -81.57 | 4864 | 0.054 | 17009 |
| JULIANEHAAB | | 60.72 | -46.03 | 0.476 | 77.4 | -35 | 7.69 | -78.8 | 16.5 | 0.454 | -8.38 | -26.10 | 42206 | 0.001 | 121614 |
| JULIUSRUH-RUGEN | | 54.63 | 13.38 | 0.428 | 68.9 | -1 | 2.72 | -45.6 | 37.9 | 0.310 | 2.88 | 21.78 | 10534 | 0.016 | 32999 |
| JUNGFRAUJOCH | | 46.55 | 7.98 | 0.405 | 62.2 | -3 | 1.97 | -35.1 | 25.3 | 0.284 | 3.09 | 14.78 | 5854 | 0.042 | 19592 |
| KANOYA | | 31.42 | 130.89 | 0.397 | 44.4 | -3 | 1.19 | -14.8 | 130.1 | 0.415 | 8.76 | 131.17 | 1653 | 0.184 | 6851 |
| KARACHI | | 24.85 | 67.02 | 0.385 | 36.0 | -0 | 1.09 | -8.1 | 69.3 | 0.341 | 7.27 | 67.73 | 1004 | 0.235 | 4433 |

Table B2

Tracings 300 km Above Stations.

| STATIONS | ** D | R | I | G | I | N | ** CONJUGATE INTERS. ** | | | MINIMUM-B E Q U A T O R | | | | ** ARC |
|---|---|---|---|---|---|---|---|---|---|---|---|---|---|---|
| | LAT. | LONG. | B | DIP | DECL. | L | LAT. | LONG. | B | LAT. | LONG. | ALT. | B | KM |
| KAZACHIE | 70.70 | 136.40 | 0.509 | 80.8 | -8 | 5.35 | -50.2 | 128.6 | 0.569 | 10.51 | 131.51 | 28170 | 0.002 | 81003 |
| KAP TOBIN | 70.42 | -21.97 | 0.465 | 79.0 | -28 | 11.62 | -72.5 | 59.3 | 0.466 | -2.03 | 6.88 | 67347 | 0.000 | 190926 |
| KAZAN | 55.83 | 48.82 | 0.467 | 71.8 | 10 | 2.64 | -41.5 | 65.1 | 0.382 | 6.38 | 51.90 | 10474 | 0.017 | 32400 |
| KAKIOKA | 36.23 | 140.18 | 0.401 | 49.5 | -4 | 1.31 | -19.3 | 138.2 | 0.437 | 8.98 | 140.20 | 2322 | 0.141 | 9035 |
| KAMPALA | 0.33 | 32.58 | 0.291 | -22.8 | -1 | 1.06 | 19.6 | 32.2 | 0.324 | 8.12 | 32.32 | 522 | 0.264 | 2354 |
| KEKAHA | 21.84 | -159.72 | 0.319 | 39.0 | 12 | 1.19 | -20.4 | -168.3 | 0.371 | 1.87 | -163.65 | 1362 | 0.186 | 6053 |
| KHARTOUM | 15.58 | 32.58 | 0.311 | 12.9 | 0 | 1.03 | 4.5 | 32.7 | 0.292 | 8.15 | 32.63 | 367 | 0.286 | 1312 |
| KHABAROVSK | 48.52 | 135.12 | 0.467 | 63.8 | -8 | 1.80 | -30.3 | 132.8 | 0.503 | 9.58 | 135.33 | 5528 | 0.053 | 18281 |
| KHARKOV | 50.00 | 36.23 | 0.439 | 66.3 | 6 | 2.11 | -36.1 | 49.3 | 0.322 | 5.54 | 39.12 | 6949 | 0.034 | 22546 |
| KIEL | 54.30 | 10.10 | 0.426 | 68.7 | -3 | 2.71 | -46.0 | 35.5 | 0.306 | 2.40 | 19.13 | 10495 | 0.016 | 32922 |
| KIRUNA | 67.83 | 20.43 | 0.457 | 77.0 | 2 | 5.67 | -58.6 | 63.2 | 0.421 | 3.59 | 34.81 | 29532 | 0.002 | 85852 |
| KING SALMON | 58.70 | -156.70 | 0.472 | 71.5 | 21 | 3.48 | -49.8 | 171.4 | 0.540 | 3.49 | -172.60 | 16060 | 0.007 | 47948 |
| KIEV | 50.45 | 30.50 | 0.433 | 66.3 | 5 | 2.16 | -37.1 | 45.0 | 0.313 | 4.84 | 34.28 | 7215 | 0.031 | 23363 |
| KINGSTON | 18.00 | -76.80 | 0.386 | 50.3 | 0 | 1.44 | -44.3 | -83.6 | 0.313 | -13.95 | -77.73 | 2646 | 0.102 | 10452 |
| KNOB LAKE | 54.80 | -66.82 | 0.504 | 78.8 | -27 | 6.59 | -82.2 | -67.9 | 0.487 | -11.56 | -57.93 | 35327 | 0.001 | 102314 |
| KOROR ISLAND | 7.16 | 123.48 | 0.338 | -1.4 | 1 | 0.97 | 8.4 | 123.5 | 0.338 | 7.96 | 123.50 | 301 | 0.338 | 150 |
| KOTZEBUE | 66.88 | -162.60 | 0.491 | 76.7 | 21 | 5.46 | -54.6 | 159.9 | 0.565 | 5.20 | 177.53 | 28770 | 0.002 | 82959 |
| KOLN | 50.93 | 6.92 | 0.417 | 66.1 | -4 | 2.37 | -42.0 | 29.3 | 0.291 | 2.26 | 15.39 | 8282 | 0.024 | 26639 |
| KOMURO | 35.98 | 139.62 | 0.401 | 49.2 | -4 | 1.30 | -19.0 | 137.8 | 0.436 | 9.07 | 139.68 | 2282 | 0.143 | 8909 |
| KOKUBUNJI | 35.70 | 139.48 | 0.400 | 48.9 | -4 | 1.29 | -18.8 | 137.7 | 0.434 | 9.12 | 139.55 | 2236 | 0.145 | 8767 |
| KODAIKANAL | 10.23 | 77.48 | 0.342 | 2.5 | -2 | 0.97 | 8.2 | 77.6 | 0.340 | NO MINIMUM B BETWEEN INTERS. | | | | 238 |
| KUHLUNGSBORN | 54.12 | 11.93 | 0.426 | 68.6 | -2 | 2.67 | -45.2 | 36.3 | 0.306 | 2.54 | 20.49 | 10220 | 0.017 | 32126 |
| KUMASI | 6.67 | -1.58 | 0.268 | -3.0 | -11 | 1.05 | 9.2 | -2.1 | 0.272 | NO MINIMUM B BETWEEN INTERS. | | | | 307 |
| KYOTO | 35.02 | 135.78 | 0.405 | 48.6 | -4 | 1.27 | -18.1 | 134.5 | 0.432 | 9.09 | 136.03 | 2145 | 0.151 | 8453 |
| L'AQUILA | 42.40 | 13.32 | 0.395 | 57.8 | -2 | 1.67 | -27.8 | 25.2 | 0.288 | 4.47 | 17.95 | 4082 | 0.067 | 14318 |
| LA MADDALENA | 41.22 | 9.40 | 0.389 | 56.5 | -3 | 1.62 | -26.9 | 21.8 | 0.286 | 4.33 | 14.49 | 3802 | 0.073 | 13503 |
| LAHORE | 31.55 | 74.33 | 0.424 | 46.7 | 0 | 1.20 | -13.9 | 77.6 | 0.374 | 7.85 | 75.17 | 1736 | 0.176 | 6918 |
| LA PLATA | -34.90 | -57.90 | 0.230 | -33.3 | 0 | 1.26 | 7.8 | -61.7 | 0.316 | -15.89 | -59.01 | 1215 | 0.158 | 5858 |
| LA QUIACA | -22.10 | -65.60 | 0.227 | -15.3 | 1 | 1.12 | -5.1 | -65.9 | 0.261 | -16.85 | -65.58 | 417 | 0.220 | 2033 |
| LA PAZ | -16.48 | -68.05 | 0.233 | -5.6 | 1 | 1.10 | -10.5 | -68.0 | 0.245 | NO MINIMUM B BETWEEN INTERS. | | | | 702 |
| LAE | -6.72 | 147.00 | 0.359 | -28.5 | 5 | 1.07 | 22.5 | 148.7 | 0.328 | 8.89 | 148.23 | 770 | 0.253 | 3729 |
| LA CRAU | 43.10 | 6.00 | 0.394 | 58.8 | -4 | 1.75 | -30.4 | 21.1 | 0.283 | 3.43 | 12.25 | 4534 | 0.059 | 15715 |
| LA HAYE | 52.10 | 4.30 | 0.419 | 67.1 | -5 | 2.53 | -44.5 | 29.2 | 0.294 | 1.68 | 13.82 | 9265 | 0.020 | 29482 |
| LEEDS | 53.80 | -1.55 | 0.423 | 68.6 | -8 | 2.84 | -49.1 | 28.2 | 0.302 | 0.53 | 10.04 | 11190 | 0.014 | 35024 |
| LEICESTER | 52.62 | -1.10 | 0.420 | 67.7 | -8 | 2.68 | -47.2 | 26.9 | 0.296 | 0.88 | 9.86 | 10161 | 0.017 | 32092 |
| LERWICK | 60.13 | -1.18 | 0.437 | 72.8 | -9 | 3.97 | -57.2 | 38.5 | 0.351 | 0.15 | 13.49 | 18486 | 0.005 | 55507 |
| LENINGRAD | 59.95 | 30.70 | 0.451 | 73.1 | 6 | 3.33 | -48.6 | 56.4 | 0.366 | 4.82 | 37.78 | 14666 | 0.009 | 44407 |
| LEIDSCHENDAM | 52.08 | 4.38 | 0.419 | 67.1 | -5 | 2.53 | -44.4 | 29.3 | 0.294 | 1.68 | 13.87 | 9244 | 0.020 | 29421 |
| LEOPOLDVILLE | -4.37 | 15.25 | 0.281 | -32.8 | -9 | 1.12 | 24.1 | 11.5 | 0.323 | 7.65 | 13.40 | 802 | 0.221 | 3703 |
| LINDAU,HARZ | 51.65 | 10.13 | 0.420 | 66.6 | -3 | 2.41 | -42.2 | 32.1 | 0.295 | 2.52 | 18.16 | 8550 | 0.023 | 27380 |
| LISBOA | 38.77 | -9.13 | 0.379 | 55.5 | -10 | 1.65 | -29.9 | 8.8 | 0.271 | 1.27 | -0.87 | 3827 | 0.070 | 13734 |
| LITTLE AMERICA | -78.18 | -162.17 | 0.553 | -80.3 | -79 | 13.73 | ** N O C O M P U T A T I O N S P E R F O R M E D ** | | | | | | | |
| LOGRONO | 42.45 | -2.50 | 0.391 | 58.7 | -8 | 1.79 | -32.3 | 15.5 | 0.277 | 1.93 | 5.41 | 4686 | 0.055 | 16242 |
| LOVOZERO | 67.99 | 35.08 | 0.467 | 77.8 | 10 | 5.34 | -55.6 | 70.6 | 0.436 | 5.62 | 45.86 | 27564 | 0.002 | 80168 |
| LONGYEARBYEN | 78.22 | 15.67 | 0.475 | 81.8 | -5 | 15.07 | ** N O C O M P U T A T I O N S P E R F O R M E D ** | | | | | | | |
| LONDON | 51.53 | 0.10 | 0.417 | 66.8 | -7 | 2.53 | -45.1 | 26.2 | 0.291 | 0.98 | 10.40 | 9222 | 0.020 | 29403 |

Table B2

Tracings 300 km Above Stations.

| STATIONS | ** D | R | I | G | I | N | ** CONJUGATE | INTERS. ** | MINIMUM-B | E Q U A T O R | ** ARC | | |
|---|---|---|---|---|---|---|---|---|---|---|---|---|---|
| | LAT. | LONG. | B | DIP | DECL. | L | LAT. | LONG. | B | LAT. | LONG. | ALT. | B | KM |
| LOMNICKY STIT | 49.20 | 20.22 | 0.420 | 64.7 | 1 | 2.10 | -36.6 | 36.0 | 0.297 | 4.06 | 25.35 | 6728 | 0.035 | 22041 |
| LOURENCO MARQUES | -25.97 | 32.60 | 0.295 | -61.2 | -16 | 1.61 | 41.8 | 24.1 | 0.402 | 5.39 | 26.78 | 3781 | 0.075 | 13366 |
| LUND | 55.70 | 13.18 | 0.430 | 69.7 | -1 | 2.86 | -47.1 | 39.2 | 0.316 | 2.52 | 22.12 | 11457 | 0.014 | 35617 |
| LUANDA | -8.82 | 13.22 | 0.281 | -40.1 | -12 | 1.18 | 27.2 | 7.5 | 0.333 | 6.75 | 10.31 | 1127 | 0.189 | 4983 |
| LULEA | 65.60 | 22.12 | 0.454 | 75.9 | 3 | 4.81 | -56.2 | 60.0 | 0.402 | 3.84 | 34.32 | 24056 | 0.003 | 70661 |
| LVOV | 49.82 | 24.02 | 0.425 | 65.3 | 2 | 2.13 | -37.0 | 39.4 | 0.302 | 4.33 | 28.65 | 6970 | 0.033 | 22712 |
| LWIRO | -2.25 | 28.80 | 0.290 | -29.0 | -3 | 1.08 | 22.6 | 27.8 | 0.330 | 8.23 | 28.18 | 678 | 0.243 | 3133 |
| LYCKSELE | 64.62 | 18.67 | 0.450 | 75.3 | 1 | 4.60 | -56.1 | 56.5 | 0.391 | 3.13 | 31.10 | 22633 | 0.003 | 66766 |
| MAKATEA | -16.20 | -148.20 | 0.323 | -26.8 | 12 | 1.10 | 11.3 | -143.1 | 0.300 | -1.54 | -145.33 | 718 | 0.238 | 3529 |
| MANILA | 14.52 | 121.00 | 0.347 | 14.5 | 0 | 0.99 | 1.4 | 120.7 | 0.348 | 8.18 | 120.90 | 398 | 0.324 | 1557 |
| MALVERN | 52.12 | -2.32 | 0.419 | 67.4 | -9 | 2.64 | -46.9 | 25.6 | 0.294 | 0.59 | 8.75 | 9902 | 0.018 | 31368 |
| MAJURO ISLAND | 7.08 | 171.13 | 0.296 | 4.8 | 9 | 1.02 | 2.4 | 170.3 | 0.304 | 6.90 | 171.10 | 302 | 0.296 | 556 |
| MADRID | 40.40 | -3.68 | 0.384 | 56.6 | -8 | 1.68 | -29.8 | 13.2 | 0.276 | 2.03 | 3.92 | 4041 | 0.066 | 14328 |
| MACAO | 22.20 | 113.55 | 0.379 | 29.7 | -0 | 1.04 | -5.1 | 113.1 | 0.374 | 8.52 | 113.46 | 754 | 0.278 | 3482 |
| MADRAS | 13.08 | 80.28 | 0.350 | 8.8 | -2 | 0.97 | 5.8 | 80.7 | 0.342 | 8.47 | 80.53 | 331 | 0.338 | 857 |
| MAWSON | -67.40 | 62.50 | 0.453 | -70.8 | -56 | 9.31 | 71.0 | -4.7 | 0.460 | 0.58 | 20.48 | 52670 | 0.000 | 150163 |
| MACQUARIE ISLAND | -54.30 | 158.60 | 0.565 | -79.1 | 26 | 5.46 | 67.2 | -164.9 | 0.491 | 5.44 | 175.61 | 28742 | 0.002 | 82870 |
| MARION ISLAND | -46.85 | 37.87 | 0.313 | -65.0 | -33 | 2.81 | 55.3 | 11.9 | 0.429 | 2.35 | 20.94 | 11176 | 0.014 | 34840 |
| MAUI,KIHEI | 20.80 | -156.50 | 0.318 | 38.3 | 11 | 1.18 | -20.5 | -164.9 | 0.367 | 1.32 | -160.30 | 1313 | 0.189 | 5879 |
| MCMURDO SOUND | -77.85 | 166.62 | 0.565 | -83.4 | -38 | 35.82 | ** N O | C O M P U T A T I O N S | | P E R F O R M E D ** | | | | |
| MEANOOK | 54.62 | -113.33 | 0.521 | 77.5 | 23 | 4.86 | -63.0 | -157.6 | 0.541 | -5.71 | -128.71 | 24778 | 0.003 | 72220 |
| MEUDON | 48.80 | 2.25 | 0.410 | 64.5 | -6 | 2.22 | -40.2 | 24.2 | 0.283 | 1.72 | 11.06 | 7312 | 0.030 | 23890 |
| MEMAMBETSU | 43.92 | 144.20 | 0.429 | 57.7 | -6 | 1.57 | -26.4 | 140.6 | 0.477 | 9.07 | 143.76 | 3972 | 0.081 | 13941 |
| MEXICO EL CERRILLO | 19.32 | -99.55 | 0.380 | 46.5 | 9 | 1.34 | -35.8 | -110.5 | 0.344 | -9.21 | -103.86 | 2189 | 0.127 | 8862 |
| MELBOURNE | -37.82 | 144.32 | 0.530 | -69.0 | 10 | 2.36 | 55.8 | 153.4 | 0.463 | 8.84 | 150.21 | 8994 | 0.024 | 28131 |
| MIDWAY ISLAND | 6.97 | 158.22 | 0.305 | 0.1 | 6 | 1.01 | 6.8 | 158.2 | 0.305 | NO MINIMUM B BETWEEN INTERS. | | | | 20 |
| MIEDZESZYN | 52.17 | 21.20 | 0.428 | 67.2 | 1 | 2.37 | -40.6 | 40.0 | 0.306 | 3.88 | 27.08 | 8397 | 0.024 | 26834 |
| MINNEAPOLIS | 44.97 | -93.23 | 0.512 | 74.0 | 6 | 3.42 | -64.7 | -123.6 | 0.497 | -10.42 | -99.59 | 15459 | 0.008 | 46612 |
| MIRNY | -66.57 | 92.92 | 0.521 | -77.7 | -74 | 20.94 | ** N O | C O M P U T A T I O N S | | P E R F O R M E D ** | | | | |
| MINA AGUILAR | -23.10 | -65.70 | 0.227 | -16.9 | 1 | 1.13 | -4.1 | -66.0 | 0.264 | -16.74 | -65.65 | 453 | 0.217 | 2282 |
| MOULD BAY | 76.20 | -119.40 | 0.513 | 87.3 | 62 | 38.84 | ** N O | C O M P U T A T I O N S | | P E R F O R M E D ** | | | | |
| MOSHIRI | 44.37 | 142.27 | 0.435 | 58.5 | -6 | 1.59 | -26.8 | 139.0 | 0.480 | 9.14 | 142.01 | 4107 | 0.078 | 14313 |
| MOCA | 3.35 | 8.67 | 0.274 | -14.9 | -9 | 1.06 | 15.9 | 6.6 | 0.292 | 7.87 | 7.89 | 390 | 0.265 | 1515 |
| MOSCOW | 55.47 | 37.32 | 0.451 | 70.6 | 8 | 2.64 | -42.5 | 55.7 | 0.350 | 5.39 | 41.60 | 10328 | 0.017 | 32142 |
| MOUNT WASHINGTON | 44.27 | -71.30 | 0.495 | 73.7 | -14 | 3.54 | -72.1 | -79.2 | 0.449 | -12.53 | -67.03 | 15939 | 0.007 | 48397 |
| MOUNT NORIKURA | 36.12 | 137.55 | 0.406 | 49.7 | -5 | 1.30 | -19.1 | 136.0 | 0.438 | 9.04 | 137.73 | 2316 | 0.141 | 8995 |
| MONT JOLI | 48.60 | -68.20 | 0.499 | 75.8 | -20 | 4.43 | -76.5 | -71.2 | 0.462 | -12.19 | -61.53 | 21548 | 0.004 | 64071 |
| MURCHISON BAY | 80.05 | 18.30 | 0.479 | 82.7 | -4 | 18.01 | ** N O | C O M P U T A T I O N S | | P E R F O R M E D ** | | | | |
| MURMANSK | 68.97 | 33.08 | 0.466 | 78.1 | 9 | 5.77 | -56.8 | 71.2 | 0.441 | 5.32 | 45.10 | 30292 | 0.002 | 87750 |
| MUNCHEN | 48.13 | 11.70 | 0.411 | 63.6 | -2 | 2.07 | -36.6 | 29.2 | 0.288 | 3.25 | 18.20 | 6453 | 0.036 | 21312 |
| NARSSARSSUAQ | 61.18 | -45.42 | 0.476 | 77.5 | -35 | 7.90 | -78.7 | 18.9 | 0.455 | -8.16 | -25.09 | 43514 | 0.001 | 125231 |
| NARYAN MAR | 67.50 | 53.00 | 0.483 | 78.8 | 16 | 4.90 | -52.2 | 79.8 | 0.460 | 7.29 | 59.93 | 24936 | 0.003 | 72596 |
| NATAL | -5.33 | -35.12 | 0.236 | -3.0 | -17 | 1.10 | -2.5 | -36.1 | 0.243 | NO MINIMUM B BETWEEN INTERS. | | | | 350 |
| NAIROBI | -1.28 | 36.80 | 0.293 | -25.1 | -1 | 1.06 | 20.2 | 36.6 | 0.331 | 7.64 | 36.55 | 580 | 0.259 | 2662 |
| NEUSTRELITZ | 53.28 | -13.08 | 0.425 | 69.0 | -14 | 3.04 | -53.4 | 21.4 | 0.308 | -1.73 | 0.93 | 12404 | 0.011 | 38588 |

Table B2

Tracings 300 km Above Stations.

| STATIONS | ** D | R | I | G | I | N | ** CONJUGATE | INTERS. | ** MINIMUM-B | L Q U A T O R | ** ARC | | |
|---|---|---|---|---|---|---|---|---|---|---|---|---|---|
| | LAT. | LONG. | B | DIP | DECL. | L | LAT. | LONG. | B | LAT. | LONG. | ALT. | B | KM |
| NIAMEY | 13.50 | 2.50 | 0.284 | 10.3 | -9 | 1.05 | 4.5 | 4.2 | 0.270 | 7.26 | 3.65 | 343 | 0.267 | 1081 |
| NITSANIM | 31.73 | 34.60 | 0.376 | 44.7 | 3 | 1.24 | -13.7 | 36.8 | 0.299 | 6.98 | 34.99 | 1677 | 0.159 | 6821 |
| NIIGATA | 37.70 | 138.82 | 0.411 | 51.5 | -5 | 1.35 | -20.6 | 136.9 | 0.446 | 9.05 | 138.94 | 2590 | 0.128 | 9837 |
| NICOSIA | 35.17 | 33.28 | 0.388 | 49.6 | 3 | 1.34 | -17.6 | 36.8 | 0.300 | 6.66 | 34.03 | 2232 | 0.129 | 8604 |
| NOUVELLE AMSTERDAM | -37.84 | 77.57 | 0.425 | -67.7 | -33 | 2.41 | 54.2 | 55.6 | 0.489 | 7.98 | 67.36 | 9198 | 0.022 | 28582 |
| NOVOLAZAREVSKAYA | -70.77 | 11.85 | 0.396 | -65.4 | -26 | 4.92 | 56.6 | -37.2 | 0.457 | -6.77 | -18.75 | 24461 | 0.003 | 72456 |
| NORD | 81.60 | -16.67 | 0.483 | 83.7 | -35 | 39.86 | ** N O | C O M P U T A T I O N S | P E R F O R M E D ** | | | | | |
| NORWAY STATION | -70.50 | -2.53 | 0.387 | -64.0 | -18 | 4.19 | 52.5 | -43.2 | 0.459 | -7.94 | -27.03 | 19826 | 0.004 | 59574 |
| NORFOLK ISLAND | -29.00 | 167.60 | 0.456 | -56.4 | 14 | 1.57 | 40.8 | -179.7 | 0.374 | 6.17 | 174.47 | 3763 | 0.083 | 13550 |
| NOUMEA | -22.30 | -166.40 | 0.378 | -41.5 | 14 | 1.22 | 23.2 | -156.9 | 0.326 | 1.53 | -161.27 | 1558 | 0.172 | 6735 |
| NURMIJARVI | 60.50 | 24.65 | 0.447 | 73.2 | 4 | 3.50 | -50.4 | 93.3 | 0.362 | 3.97 | 33.24 | 15668 | 0.007 | 47295 |
| ODESSA | 46.78 | 30.88 | 0.424 | 63.0 | 4 | 1.88 | -32.3 | 41.9 | 0.305 | 5.41 | 33.67 | 5496 | 0.047 | 18385 |
| O'HIGGINS RISUPATR | -63.32 | -57.90 | 0.364 | -57.4 | 12 | 2.33 | 35.1 | -63.6 | 0.453 | -12.98 | -57.33 | 8116 | 0.025 | 26620 |
| OKINAWA | 26.50 | 128.00 | 0.379 | 37.2 | -2 | 1.10 | -10.3 | 127.4 | 0.391 | 8.52 | 128.13 | 1120 | 0.230 | 4999 |
| OLENEK | 68.50 | 112.40 | 0.518 | 81.7 | -4 | 4.71 | -48.1 | 115.7 | 0.554 | 10.80 | 112.42 | 24096 | 0.003 | 69702 |
| ONAGAWA | 38.43 | 141.47 | 0.409 | 52.0 | -5 | 1.37 | -21.3 | 139.1 | 0.449 | 9.12 | 141.41 | 2715 | 0.122 | 10236 |
| OOHIRA | 35.62 | 140.50 | 0.397 | 48.7 | -4 | 1.29 | -18.7 | 138.6 | 0.434 | 9.02 | 140.50 | 2219 | 0.146 | 8721 |
| ORCADAS DEL SUR | -60.73 | -44.73 | 0.331 | -55.4 | 3 | 2.20 | 34.3 | -58.1 | 0.439 | -12.34 | -49.84 | 7226 | 0.029 | 24162 |
| OSLO KJELLER | 59.97 | 11.10 | 0.438 | 72.5 | -2 | 3.62 | -53.1 | 44.5 | 0.347 | 2.27 | 22.55 | 16283 | 0.007 | 49195 |
| OTTAWA | 45.40 | -75.75 | 0.503 | 74.8 | -11 | 3.78 | -72.2 | -91.9 | 0.469 | -12.36 | -73.68 | 17527 | 0.006 | 52715 |
| OULU | 65.00 | 25.52 | 0.455 | 75.8 | 5 | 4.55 | -54.9 | 60.8 | 0.400 | 4.02 | 36.52 | 22432 | 0.003 | 66103 |
| PALESTINE | 31.77 | -95.63 | 0.457 | 62.0 | 8 | 1.90 | -50.8 | -114.4 | 0.423 | -10.33 | -101.23 | 5802 | 0.044 | 19529 |
| PANSKA VES | 50.53 | 14.57 | 0.419 | 65.7 | -1 | 2.26 | -39.5 | 33.6 | 0.295 | 3.30 | 21.23 | 7636 | 0.028 | 24709 |
| PARIS-SACLAY | 48.12 | 2.33 | 0.408 | 63.9 | -6 | 2.16 | -39.1 | 23.5 | 0.282 | 1.87 | 10.89 | 6933 | 0.032 | 22787 |
| PARIS-BAGNEUX | 48.80 | 2.32 | 0.410 | 64.5 | -6 | 2.22 | -40.2 | 24.2 | 0.284 | 1.73 | 11.12 | 7307 | 0.030 | 23875 |
| PANAGURITSCH | 42.52 | 24.18 | 0.404 | 58.1 | 1 | 1.64 | -26.9 | 33.2 | 0.295 | 5.50 | 26.99 | 3987 | 0.071 | 13975 |
| PARAMARIBO | 5.82 | -55.22 | 0.297 | 31.2 | -11 | 1.23 | -29.3 | -48.6 | 0.216 | -15.02 | -51.30 | 910 | 0.174 | 4655 |
| PETROPAVLOVSK-ON-K | 52.98 | 158.65 | 0.445 | 64.7 | -3 | 2.12 | -35.7 | 148.7 | 0.516 | 8.63 | 154.98 | 7443 | 0.033 | 23863 |
| PEARCE | -31.67 | 115.97 | 0.506 | -66.2 | -2 | 1.94 | 50.3 | 114.5 | 0.504 | 9.76 | 115.54 | 6520 | 0.042 | 20896 |
| PIC DU MIDI | 42.93 | 0.25 | 0.392 | 59.0 | -7 | 1.79 | -32.0 | 17.5 | 0.279 | 2.43 | 7.68 | 4721 | 0.055 | 16319 |
| PILAR | -31.67 | -63.88 | 0.232 | -29.2 | 3 | 1.20 | 4.1 | -65.1 | 0.301 | -16.15 | -63.82 | 923 | 0.179 | 4667 |
| PIWNICE -TORUN | 50.52 | 14.57 | 0.419 | 65.7 | -1 | 2.25 | -39.5 | 33.6 | 0.294 | 3.30 | 21.23 | 7628 | 0.028 | 24687 |
| PLAISANCE | -20.43 | 57.67 | 0.331 | -53.4 | -14 | 1.38 | 36.3 | 53.5 | 0.422 | 6.55 | 53.99 | 2612 | 0.118 | 9739 |
| POSADAS | -27.42 | -56.10 | 0.218 | -24.4 | -4 | 1.18 | 1.4 | -59.5 | 0.282 | -16.23 | -57.27 | 684 | 0.192 | 3634 |
| PONZA | 40.92 | 12.95 | 0.390 | 56.1 | -2 | 1.59 | -25.8 | 23.9 | 0.288 | 4.79 | 17.30 | 3631 | 0.077 | 12967 |
| PONTA DELGADO | 37.77 | -25.65 | 0.387 | 57.6 | -16 | 1.83 | -38.7 | -1.8 | 0.258 | -3.04 | -14.61 | 4761 | 0.053 | 16721 |
| POTCHEFSTROOM | -26.68 | 27.08 | 0.290 | -61.9 | -17 | 1.63 | 41.9 | 16.5 | 0.395 | 4.89 | 20.44 | 3873 | 0.072 | 13676 |
| POINT BARROW | 71.33 | -156.77 | 0.502 | 80.3 | 28 | 8.46 | -59.0 | 156.1 | 0.575 | 5.23 | 176.97 | 48060 | 0.001 | 5082 |
| POTSDAM | 52.38 | 13.07 | 0.423 | 67.2 | -1 | 2.45 | -42.5 | 34.8 | 0.299 | 2.75 | 20.73 | 8874 | 0.022 | 28280 |
| POITIERS | 46.57 | 0.35 | 0.404 | 62.6 | -7 | 2.05 | -37.5 | 20.8 | 0.280 | 1.84 | 8.84 | 6268 | 0.037 | 20871 |
| PORT ARTHUR | 30.00 | -94.00 | 0.448 | 60.5 | 7 | 1.81 | -49.7 | -111.3 | 0.411 | -10.50 | -99.09 | 5219 | 0.051 | 17871 |
| POONA | 18.05 | 73.12 | 0.360 | 21.5 | -1 | 1.01 | -0.4 | 74.4 | 0.338 | 7.82 | 73.68 | 511 | 0.302 | 2252 |
| PORO POINT | 16.62 | 120.28 | 0.352 | 18.9 | 0 | 1.00 | -0.5 | 119.9 | 0.354 | 8.22 | 120.17 | 471 | 0.314 | 2069 |
| PORT AUX FRANCAIS | -49.35 | 70.27 | 0.418 | -69.0 | -46 | 3.84 | 63.2 | 45.6 | 0.472 | 6.28 | 51.59 | 18056 | 0.006 | 53630 |
| PORT STANLEY | -51.70 | -57.85 | 0.294 | -48.5 | -7 | 1.66 | 23.6 | -63.0 | 0.402 | -14.11 | -58.36 | 3830 | 0.068 | 14261 |

Table B2

Tracings 300 km Above Stations.

| STATIONS | ** O | R | I | G | I | N | ** CONJUGATE | INTERS. ** | MINIMUM-B | E Q U A T O R | ** ARC | | |
|---|---|---|---|---|---|---|---|---|---|---|---|---|---|
| | LAT. | LONG. | B | DIP | DECL. | L | LAT. | LONG. | B | LAT. | LONG. | ALT. | B | KM |
| PORT MORESBY | -9.20 | 147.15 | 0.372 | -32.9 | 6 | 1.10 | 25.1 | 149.3 | 0.335 | 8.96 | 148.66 | 961 | 0.233 | 4527 |
| PROVIDENIE BAY | 64.38 | 186.60 | 0.479 | 74.0 | 13 | 4.16 | -50.2 | 157.7 | 0.557 | 6.16 | 171.64 | 20458 | 0.004 | 60001 |
| PRAHA | 50.07 | 14.43 | 0.418 | 65.3 | -1 | 2.21 | -38.8 | 33.0 | 0.293 | 3.47 | 20.95 | 7377 | 0.030 | 23964 |
| PRUHONICE | 49.98 | 14.55 | 0.418 | 65.2 | -1 | 2.20 | -38.7 | 33.0 | 0.293 | 3.45 | 21.02 | 7322 | 0.030 | 23803 |
| PRETORIA | -26.80 | 28.20 | 0.291 | -61.9 | -17 | 1.63 | 42.1 | 17.9 | 0.397 | 4.82 | 21.65 | 3914 | 0.071 | 13797 |
| PRINCE ALBERT | 53.20 | -105.70 | 0.525 | 78.0 | 17 | 4.92 | -65.4 | -149.3 | 0.537 | -7.66 | -118.52 | 25152 | 0.003 | 73329 |
| PULLMANN | 46.72 | -117.17 | 0.496 | 71.0 | 19 | 2.95 | -55.2 | -149.7 | 0.508 | -5.22 | -129.65 | 12589 | 0.012 | 38433 |
| PUNTA ARENAS | -53.15 | -70.90 | 0.326 | -51.0 | 16 | 1.71 | 24.6 | -69.1 | 0.416 | -14.05 | -66.75 | 4248 | 0.062 | 15404 |
| PYONGYANG | 39.07 | 125.78 | 0.445 | 55.1 | -5 | 1.39 | -21.6 | 125.3 | 0.457 | 9.26 | 126.39 | 2942 | 0.116 | 10769 |
| QUETTA | 30.18 | 66.95 | 0.411 | 45.0 | 1 | 1.19 | -13.5 | 70.2 | 0.353 | 7.20 | 67.71 | 1595 | 0.182 | 6488 |
| QUEEN MAUD LAND | -70.50 | -1.00 | 0.388 | -64.1 | -19 | 4.25 | 52.9 | -42.6 | 0.459 | -7.85 | -26.14 | 20214 | 0.004 | 60656 |
| QUENTONCITY | 19.00 | 121.00 | 0.359 | 23.8 | 0 | 1.01 | -2.9 | 120.5 | 0.361 | 8.24 | 120.91 | 580 | 0.298 | 2697 |
| QUEBEC | 46.92 | -71.08 | 0.500 | 75.3 | -16 | 4.07 | -74.6 | -79.8 | 0.463 | -12.37 | -66.27 | 19334 | 0.005 | 57853 |
| QUILON | 8.50 | 76.00 | 0.339 | -1.4 | -3 | 0.97 | 9.6 | 75.9 | 0.340 | NO MINIMUM B BETWEEN | | INTERS. | | 133 |
| RABAT | 34.02 | -6.85 | 0.360 | 49.4 | -9 | 1.42 | -22.3 | 6.9 | 0.273 | 2.81 | -0.31 | 2516 | 0.107 | 9687 |
| RAMEY AFB | 18.50 | -67.20 | 0.381 | 51.1 | -6 | 1.49 | -46.9 | -67.0 | 0.286 | -14.67 | -64.92 | 2795 | 0.094 | 11063 |
| RAROTONGA | -21.20 | -159.75 | 0.363 | -38.2 | 13 | 1.18 | 19.8 | -151.4 | 0.320 | 0.15 | -155.21 | 1296 | 0.189 | 5820 |
| RESOLUTE | 74.68 | -94.92 | 0.514 | 89.2 | -47 | 97.70 | ** N O | C O M P U T A T I O N S | | P E R F O R M E D ** | | | | |
| REYKJAVIK | 64.18 | -21.70 | 0.454 | 76.1 | -24 | 6.63 | -69.2 | 39.2 | 0.417 | -3.24 | 0.34 | 35437 | 0.001 | 102769 |
| REGENSBERG | 47.48 | 8.45 | 0.408 | 63.1 | -3 | 2.04 | -36.4 | 26.5 | 0.285 | 3.06 | 15.42 | 6271 | 0.038 | 20807 |
| RIO DE JANEIRO | -22.90 | -43.22 | 0.215 | -24.6 | -14 | 1.17 | 3.7 | -49.9 | 0.279 | -13.38 | -45.78 | 644 | 0.194 | 3416 |
| RIO GALLEGOS | -51.63 | -69.22 | 0.314 | -49.5 | 15 | 1.65 | 23.1 | -68.3 | 0.407 | -14.25 | -65.85 | 3825 | 0.069 | 14167 |
| ROYAL ROADS | 48.50 | -123.50 | 0.492 | 70.9 | 22 | 3.00 | -54.0 | -156.7 | 0.514 | -3.53 | -137.13 | 12948 | 0.011 | 39411 |
| ROMA | 41.88 | 12.50 | 0.393 | 57.2 | -2 | 1.64 | -27.2 | 24.3 | 0.288 | 4.53 | 17.15 | 3933 | 0.070 | 13877 |
| ROSTOV/DON | 47.23 | 39.65 | 0.437 | 64.1 | 6 | 1.90 | -32.6 | 49.9 | 0.321 | 5.99 | 41.60 | 5690 | 0.046 | 18890 |
| SANTA CRUZ | -17.80 | -63.17 | 0.227 | -7.9 | -1 | 1.11 | -9.2 | -63.6 | 0.245 | -17.14 | -63.19 | 310 | 0.227 | 1011 |
| SAN FERNANDO | 36.47 | -6.20 | 0.369 | 52.4 | -9 | 1.51 | -25.3 | 8.9 | 0.274 | 2.45 | 0.84 | 3048 | 0.089 | 11334 |
| SANTA CRUZ | 28.33 | -16.25 | 0.340 | 43.8 | -12 | 1.33 | -20.1 | -2.6 | 0.260 | 1.13 | -9.43 | 1853 | 0.132 | 7650 |
| SANTIAGO | -33.57 | -70.72 | 0.247 | -32.5 | 9 | 1.22 | 6.1 | -69.6 | 0.315 | -15.80 | -69.27 | 1099 | 0.171 | 5332 |
| SALEKHARD | 66.58 | 66.67 | 0.497 | 79.6 | 17 | 4.51 | -49.5 | 87.1 | 0.482 | 8.64 | 71.24 | 22546 | 0.003 | 65760 |
| SASKATOON | 52.13 | -106.67 | 0.522 | 77.1 | 18 | 4.53 | -64.2 | -148.3 | 0.533 | -7.37 | -119.34 | 22648 | 0.003 | 66388 |
| SAPPORO | 43.02 | 121.35 | 0.470 | 60.3 | -6 | 1.54 | -25.1 | 121.4 | 0.477 | 9.35 | 122.13 | 3915 | 0.085 | 13563 |
| SACRAMENTO PEAK | 32.72 | -105.75 | 0.450 | 60.8 | 12 | 1.84 | -47.4 | -125.5 | 0.433 | -8.12 | -112.91 | 5454 | 0.049 | 18483 |
| SAN JUAN | 18.43 | -66.00 | 0.379 | 50.9 | -6 | 1.49 | -46.8 | -64.6 | 0.281 | -14.81 | -63.29 | 2765 | 0.094 | 10989 |
| SAN JULIAN | -49.32 | -67.78 | 0.299 | -47.4 | 13 | 1.56 | 20.8 | -67.6 | 0.394 | -14.47 | -65.19 | 3276 | 0.081 | 12531 |
| SAO PAULO | -23.55 | -46.63 | 0.214 | -23.3 | -12 | 1.17 | 2.1 | -52.4 | 0.275 | -14.40 | -48.75 | 610 | 0.196 | 3258 |
| SAO JOSE DOS CAMPO | -23.00 | -46.00 | 0.214 | -22.9 | -12 | 1.17 | 2.1 | -51.8 | 0.274 | -14.34 | -48.09 | 593 | 0.197 | 3176 |
| SALISBURY RHOD-NYA | -17.83 | 31.00 | 0.296 | -53.9 | -9 | 1.36 | 35.7 | 26.3 | 0.382 | 6.48 | 27.79 | 2289 | 0.124 | 8799 |
| SCHWARZENBURG | 46.83 | 7.33 | 0.406 | 62.5 | -4 | 2.00 | -35.7 | 25.2 | 0.284 | 2.76 | 14.39 | 6010 | 0.040 | 20060 |
| SCOTT BASE | -77.85 | 166.75 | 0.565 | -83.3 | -38 | 35.64 | ** N O | C O M P U T A T I O N S | | P E R F O R M E D ** | | | | |
| SENDAI | 38.10 | 140.55 | 0.409 | 51.7 | -5 | 1.36 | -21.0 | 138.4 | 0.447 | 9.21 | 140.56 | 2656 | 0.125 | 10051 |
| SEOUL | 37.58 | 127.05 | 0.435 | 53.1 | -5 | 1.34 | -20.3 | 126.4 | 0.449 | 9.04 | 127.59 | 2638 | 0.128 | 9875 |
| SEATTLE | 47.75 | -122.42 | 0.492 | 70.6 | 21 | 2.93 | -53.8 | -155.0 | 0.511 | -3.96 | -135.70 | 12481 | 0.012 | 38116 |
| SEMIPALATINSK | 50.40 | 80.25 | 0.500 | 69.5 | 5 | 2.03 | -32.7 | 87.9 | 0.454 | 8.85 | 81.45 | 6967 | 0.037 | 22151 |
| SEAGROVE | -37.08 | 174.78 | 0.484 | -63.0 | 17 | 1.93 | 46.1 | -166.1 | 0.408 | 4.52 | -175.31 | 6088 | 0.044 | 20228 |

Table B2

Tracings 300 km Above Stations.

| STATIONS | ** | O | R | I | G | I | N | ** CONJUGATE | INTERS. | ** MINIMUM-B | E Q U A T O R | | ** ARC |
|---|---|---|---|---|---|---|---|---|---|---|---|---|---|
| | | LAT. | LONG. | B | DIP | DECL. | L | LAT. | LONG. | B | LAT. | LONG. | ALT. | B | KM |
| SHEPHERD BAY | | 68.75 | -93.75 | 0.522 | 87.5 | -8 | 29.69 | ** N O | C O M P U T A T I O N S | P E R F O R M E D ** | | | | | |
| SHIRAZ | | 29.63 | 52.52 | 0.392 | 44.0 | 2 | 1.20 | -13.6 | 54.7 | 0.317 | 6.44 | 52.78 | 1538 | 0.177 | 6350 |
| SHACKLETON | | -77.98 | -37.17 | 0.445 | -67.3 | 5 | 4.95 | 51.8 | -58.9 | 0.487 | -10.98 | -47.00 | 24799 | 0.003 | 73274 |
| SHEFFIELD | | 53.43 | 1.35 | 0.422 | 68.2 | -7 | 2.74 | -47.5 | 29.3 | 0.300 | 1.09 | 12.09 | 10556 | 0.016 | 33191 |
| SIMOSATO | | 33.58 | 135.94 | 0.397 | 46.7 | -4 | 1.24 | -16.8 | 134.7 | 0.424 | 8.98 | 136.15 | 1926 | 0.164 | 7768 |
| SIDMOUTH | | 50.68 | 3.22 | 0.415 | 66.0 | -6 | 2.39 | -42.7 | 26.9 | 0.289 | 1.75 | 12.44 | 8382 | 0.024 | 26961 |
| SITKA | | 57.05 | -135.33 | 0.497 | 74.3 | 27 | 4.10 | -55.7 | -175.0 | 0.542 | -0.23 | -153.29 | 19993 | 0.004 | 58876 |
| SIMFEROPOL | | 44.83 | 34.07 | 0.423 | 61.3 | 4 | 1.76 | -29.7 | 43.0 | 0.306 | 5.78 | 36.09 | 4754 | 0.058 | 16198 |
| SINGAPORE | | 1.32 | 103.82 | 0.357 | -18.2 | 1 | 0.99 | 17.2 | 104.0 | 0.365 | 8.86 | 103.93 | 452 | 0.325 | 1904 |
| SLOUGH | | 51.48 | -0.57 | 0.417 | 66.8 | -8 | 2.53 | -45.3 | 25.7 | 0.291 | 0.88 | 9.86 | 9249 | 0.020 | 29488 |
| SODANKYLA | | 67.37 | 26.65 | 0.460 | 77.0 | 5 | 5.31 | -56.8 | 65.3 | 0.422 | 4.51 | 39.01 | 27263 | 0.002 | 79473 |
| SOUTH POLE | | -90.00 | 0. | 0.518 | -75.7 | -28 | 15.25 | ** N O | C O M P U T A T I O N S | P E R F O R M E D ** | | | | | |
| SREDNIKAN | | 62.43 | 152.32 | 0.486 | 73.3 | -6 | 3.23 | -43.7 | 141.0 | 0.553 | 9.04 | 147.46 | 14575 | 0.009 | 43565 |
| ST. STEPHEN | | 67.20 | -45.20 | 0.481 | 80.0 | -41 | 13.90 | ** N O | C O M P U T A T I O N S | P E R F O R M E D ** | | | | | |
| STELLENBOSCH | | -33.94 | 18.85 | 0.279 | -64.2 | -25 | 1.87 | 44.3 | 0.6 | 0.397 | 2.10 | 8.36 | 5243 | 0.048 | 17866 |
| STOCKHOLM | | 59.30 | 18.10 | 0.440 | 72.2 | 0 | 3.37 | -50.5 | 47.5 | 0.345 | 3.21 | 27.54 | 14737 | 0.008 | 44781 |
| STONYHURST | | 53.51 | -2.47 | 0.422 | 68.4 | -9 | 2.82 | -49.0 | 27.4 | 0.301 | 0.35 | 9.22 | 11049 | 0.014 | 34634 |
| ST. LAWRENCE | | 50.58 | 1.23 | 0.415 | 66.0 | -7 | 2.41 | -43.3 | 25.6 | 0.288 | 1.48 | 10.87 | 8474 | 0.023 | 27246 |
| STANLEY | | -51.70 | -57.85 | 0.294 | -48.5 | 7 | 1.66 | 23.6 | -63.0 | 0.402 | -14.11 | -58.36 | 3830 | 0.068 | 14261 |
| ST. SANTIN-DE-MAUR | | 44.60 | 20.20 | 0.407 | 60.2 | 0 | 1.77 | -30.1 | 31.8 | 0.292 | 4.81 | 24.10 | 4726 | 0.057 | 16191 |
| ST. MICHEL | | 43.92 | 5.72 | 0.397 | 59.7 | -4 | 1.80 | -31.7 | 21.6 | 0.282 | 3.05 | 12.28 | 4847 | 0.054 | 16652 |
| STANFORD | | 37.43 | -122.17 | 0.448 | 61.9 | 16 | 1.94 | -45.3 | -144.5 | 0.459 | -4.36 | -131.53 | 6107 | 0.042 | 20300 |
| ST. JOHNS | | 47.52 | -52.78 | 0.467 | 71.9 | -25 | 3.63 | -71.3 | -25.6 | 0.393 | -10.28 | -40.00 | 16287 | 0.007 | 49673 |
| SUKKERTOPPEN | | 65.42 | -52.90 | 0.489 | 80.5 | -42 | 13.76 | ** N O | C O M P U T A T I O N S | P E R F O R M E D ** | | | | | |
| SULPHUR MOUNTAIN | | 51.10 | -115.60 | 0.511 | 74.6 | 21 | 3.79 | -59.4 | -154.0 | 0.528 | -5.14 | -129.66 | 17943 | 0.006 | 53289 |
| SURLARI | | 44.68 | 26.25 | 0.413 | 60.6 | 2 | 1.76 | -29.7 | 36.4 | 0.297 | 5.23 | 29.22 | 4702 | 0.058 | 16090 |
| SVERDLOVSK | | 56.73 | 61.07 | 0.486 | 73.5 | 11 | 2.71 | -40.9 | 75.6 | 0.423 | 7.60 | 63.45 | 11051 | 0.016 | 33846 |
| SWANSEA | | 51.63 | -4.00 | 0.418 | 67.1 | -9 | 2.61 | -46.9 | 24.1 | 0.292 | 0.23 | 7.29 | 9712 | 0.018 | 30848 |
| SWAKTHMORE | | 39.90 | -75.35 | 0.488 | 71.1 | -8 | 2.88 | -67.1 | -87.5 | 0.438 | -12.92 | -73.72 | 11830 | 0.013 | 36831 |
| SYDNEY | | -33.60 | 151.10 | 0.504 | -64.2 | 11 | 1.94 | 50.3 | 160.9 | 0.430 | 8.27 | 157.24 | 6239 | 0.044 | 20512 |
| SYKTYVKAR | | 61.70 | 50.80 | 0.476 | 75.7 | 13 | 3.51 | -47.1 | 72.2 | 0.421 | 6.81 | 55.48 | 15997 | 0.007 | 47816 |
| SYOWA BASE | | -69.03 | 39.60 | 0.416 | -67.7 | -43 | 6.61 | 64.3 | -21.1 | 0.453 | -2.95 | 0.87 | 35296 | 0.001 | 102370 |
| TAMALE | | 9.42 | -0.89 | 0.273 | 2.7 | -11 | 1.05 | 7.0 | -0.4 | 0.269 | NO MINIMUM B BETWEEN INTERS. | | | | 283 |
| TASHKENT | | 41.42 | 69.20 | 0.462 | 60.2 | 3 | 1.54 | -24.6 | 75.1 | 0.392 | 7.69 | 70.09 | 3768 | 0.084 | 13079 |
| TAMANRASSET | | 22.80 | 5.52 | 0.315 | 28.8 | -6 | 1.11 | -4.3 | 10.1 | 0.275 | 7.20 | 7.89 | 754 | 0.222 | 3513 |
| TAIPEI | | 25.03 | 121.52 | 0.383 | 35.1 | -1 | 1.08 | -8.6 | 121.0 | 0.386 | 8.51 | 121.56 | 990 | 0.247 | 4476 |
| TALARA | | -4.57 | -81.25 | 0.271 | 13.3 | 6 | 1.09 | -18.1 | -83.0 | 0.250 | -13.55 | -82.30 | 384 | 0.242 | 1617 |
| TANANARIVE | | -18.92 | 47.55 | 0.310 | -52.5 | -10 | 1.35 | 35.3 | 44.3 | 0.404 | 6.38 | 44.63 | 2356 | 0.126 | 8980 |
| TAHITI | | -17.48 | -149.48 | 0.330 | -29.4 | 12 | 1.11 | 13.0 | -143.7 | 0.304 | -1.47 | -146.28 | 818 | 0.228 | 3976 |
| TBILISI | | 41.72 | 44.82 | 0.428 | 59.1 | 5 | 1.59 | -26.1 | 51.1 | 0.320 | 6.25 | 45.68 | 3838 | 0.077 | 13451 |
| TENIENTE MATIENZO | | -64.97 | -60.05 | 0.378 | -58.8 | 15 | 2.47 | 36.7 | -64.5 | 0.461 | -12.72 | -58.37 | 9055 | 0.020 | 29258 |
| TEHRAN | | 35.68 | 51.42 | 0.416 | 52.5 | 4 | 1.36 | -19.8 | 55.2 | 0.325 | 6.56 | 51.81 | 2482 | 0.123 | 9350 |
| TENERIFE | | 28.00 | -17.00 | 0.339 | 43.6 | -12 | 1.32 | -20.1 | -3.3 | 0.259 | 0.83 | -10.10 | 1830 | 0.133 | 7586 |
| TEOLOYUCAN | | 19.75 | -99.18 | 0.383 | 47.1 | 9 | 1.35 | -36.4 | -110.4 | 0.347 | -9.21 | -103.53 | 2276 | 0.124 | 9137 |
| THULE | | 76.55 | -68.83 | 0.500 | 85.9 | -72 | 190.56 | ** N O | C O M P U T A T I O N S | P E R F O R M E D ** | | | | | |
| THE PAS | | 53.80 | -101.30 | 0.527 | 79.2 | 14 | 5.44 | -67.9 | -146.4 | 0.538 | -8.43 | -112.76 | 28410 | 0.002 | 82404 |

Table B2

Tracings 300 km Above Stations.

| STATIONS | ** D | R | I | G | I | N | ** CONJUGATE | INTERS. | ** MINIMUM-B | E Q U A T O R | | ** ARC | |
|---|---|---|---|---|---|---|---|---|---|---|---|---|---|
| | LAT. | LONG. | B | DIP | DECL. | L | LAT. | LONG. | B | LAT. | LONG. | ALT. | B | KM |
| TIHANY | 46.89 | 17.89 | 0.412 | 62.5 | 0 | 1.93 | -33.6 | 32.1 | 0.291 | 4.12 | 22.80 | 5685 | 0.044 | 19028 |
| TIXIE BAY | 71.55 | 128.90 | 0.512 | 81.9 | -8 | 5.70 | -50.8 | 124.5 | 0.567 | 10.51 | 125.25 | 30360 | 0.002 | 87033 |
| TIRUCHIRAPALLI | 10.83 | 78.83 | 0.344 | 3.7 | -2 | 0.97 | 7.8 | 79.0 | 0.341 | 8.45 | 78.98 | 304 | 0.341 | 353 |
| TORINO | 45.20 | 7.65 | 0.401 | 60.9 | -4 | 1.88 | -33.1 | 23.9 | 0.284 | 3.29 | 14.12 | 5281 | 0.048 | 17913 |
| TOTTORI | 35.53 | 134.22 | 0.410 | 49.5 | -5 | 1.29 | -18.6 | 133.0 | 0.436 | 9.03 | 134.54 | 2236 | 0.147 | 8719 |
| TORUN | 53.08 | 18.55 | 0.428 | 67.9 | 0 | 2.48 | -42.3 | 39.2 | 0.307 | 3.58 | 25.26 | 9097 | 0.021 | 28859 |
| TOMSK | 56.47 | 84.93 | 0.513 | 74.7 | 6 | 2.59 | -38.4 | 93.9 | 0.485 | 9.43 | 86.48 | 10540 | 0.018 | 32151 |
| TORRE CHIARUCCIA | 42.03 | 11.83 | 0.393 | 57.4 | -2 | 1.65 | -27.6 | 24.0 | 0.287 | 4.23 | 16.68 | 3994 | 0.069 | 14069 |
| TORTOSA | 40.82 | 0.50 | 0.385 | 56.7 | -7 | 1.66 | -28.8 | 16.0 | 0.279 | 2.98 | 7.29 | 3982 | 0.068 | 14110 |
| TOLEDO | 39.88 | -4.05 | 0.382 | 56.1 | -8 | 1.65 | -29.2 | 12.6 | 0.276 | 2.09 | 3.48 | 3895 | 0.069 | 13893 |
| TOYOKAWA | 35.83 | 137.37 | 0.405 | 49.4 | -5 | 1.29 | -18.9 | 135.8 | 0.436 | 9.08 | 137.56 | 2269 | 0.144 | 8847 |
| TONANZINTLA | 19.03 | -98.30 | 0.380 | 46.4 | 9 | 1.34 | -35.9 | -109.1 | 0.342 | -9.52 | -102.53 | 2177 | 0.128 | 8828 |
| TOWNSVILLE | -19.10 | 146.50 | 0.429 | -48.1 | 7 | 1.30 | 35.6 | 150.1 | 0.377 | 8.87 | 149.24 | 2203 | 0.144 | 8748 |
| TRUJILLO | -8.10 | -79.03 | 0.260 | 7.4 | 5 | 1.08 | -15.6 | -79.9 | 0.247 | -14.23 | -79.70 | 317 | 0.246 | 881 |
| TROMSO | 69.67 | 18.95 | 0.460 | 77.9 | 0 | 6.57 | -60.4 | 66.2 | 0.436 | 3.64 | 35.39 | 35316 | 0.001 | 101869 |
| TRELEW | -43.20 | -65.30 | 0.267 | -41.7 | 9 | 1.40 | 14.9 | -66.3 | 0.361 | -15.05 | -64.14 | 2167 | 0.115 | 9089 |
| TRIVANDRUM | 8.42 | 76.95 | 0.340 | -1.8 | -3 | 0.97 | 9.9 | 76.9 | 0.341 | NO MINIMUM B BETWEEN INTERS. | | | | 171 |
| TRINIDAD | 10.60 | -61.20 | 0.330 | 40.2 | -8 | 1.31 | -37.6 | -56.5 | 0.235 | -15.27 | -58.02 | 1504 | 0.142 | 6901 |
| TSCHOIBALSAN | 48.07 | 114.50 | 0.498 | 66.3 | -5 | 1.80 | -29.6 | 115.7 | 0.497 | 9.71 | 115.47 | 5614 | 0.052 | 18343 |
| TSUMEB | -19.23 | 17.72 | 0.286 | -55.0 | -15 | 1.39 | 35.6 | 8.5 | 0.368 | 5.20 | 12.60 | 2394 | 0.115 | 9200 |
| TUBINGEN | 48.53 | 9.07 | 0.411 | 64.0 | -3 | 2.12 | -37.8 | 28.0 | 0.287 | 2.72 | 16.28 | 6771 | 0.034 | 22260 |
| TUCSON | 32.23 | -110.95 | 0.440 | 59.1 | 13 | 1.75 | -44.8 | -130.0 | 0.430 | -7.08 | -118.39 | 4922 | 0.057 | 16948 |
| TUCSON | 32.23 | -110.95 | 0.440 | 59.1 | 13 | 1.75 | -44.8 | -130.0 | 0.430 | -7.08 | -118.39 | 4922 | 0.057 | 16948 |
| TUCUMAN | -26.90 | -65.40 | 0.228 | -22.8 | 2 | 1.16 | -0.5 | -65.9 | 0.280 | -16.61 | -65.28 | 622 | 0.202 | 3276 |
| UJI | 34.90 | 135.78 | 0.404 | 48.5 | -4 | 1.27 | -18.0 | 134.5 | 0.432 | 9.01 | 136.02 | 2127 | 0.152 | 8394 |
| ULAN BATUR | 47.78 | 106.75 | 0.502 | 66.6 | -3 | 1.79 | -29.3 | 109.1 | 0.490 | 9.62 | 107.75 | 5575 | 0.053 | 18189 |
| UNALASKA | 53.88 | -166.53 | 0.443 | 66.6 | 15 | 2.54 | -43.2 | 169.7 | 0.518 | 4.85 | -178.18 | 10069 | 0.019 | 31345 |
| UNIVERSITY PARK | 40.80 | -77.77 | 0.493 | 71.8 | -6 | 3.00 | -67.3 | -93.4 | 0.450 | -12.74 | -77.22 | 12579 | 0.011 | 38872 |
| UPPSALA | 59.80 | 17.60 | 0.441 | 72.5 | 0 | 3.47 | -51.2 | 47.9 | 0.349 | 2.95 | 27.44 | 15375 | 0.008 | 46575 |
| USHUAIA | -54.80 | -68.30 | 0.330 | -51.9 | 15 | 1.78 | 26.2 | -67.9 | 0.422 | -13.87 | -64.78 | 4683 | 0.055 | 16701 |
| UTSJOKI | 69.75 | 27.03 | 0.464 | 78.2 | 5 | 6.29 | -58.7 | 69.7 | 0.442 | 4.53 | 41.31 | 33603 | 0.001 | 97005 |
| VALENTIA | 51.94 | -10.25 | 0.420 | 67.8 | -12 | 2.77 | -50.1 | 21.1 | 0.296 | -0.76 | 2.54 | 10751 | 0.015 | 33869 |
| VERKHOYANSK | 67.60 | 133.40 | 0.510 | 79.1 | -10 | 4.35 | -47.4 | 128.0 | 0.564 | 10.26 | 130.45 | 21796 | 0.004 | 63387 |
| VAL D'OR | 48.00 | -77.80 | 0.511 | 76.6 | -10 | 4.38 | -73.9 | -99.6 | 0.486 | -12.18 | -76.59 | 21371 | 0.004 | 63356 |
| VICTORIA | 48.40 | -123.40 | 0.492 | 70.9 | 22 | 2.99 | -54.0 | -156.5 | 0.513 | -3.58 | -136.99 | 12876 | 0.011 | 39210 |
| VLADIVOSTOK | 43.78 | 132.03 | 0.454 | 59.5 | -7 | 1.56 | -26.0 | 130.7 | 0.480 | 9.34 | 132.54 | 4029 | 0.081 | 13989 |
| VOSTOK | -76.48 | 106.50 | 0.542 | -80.1 | 71 | 121.37 | ** N O | C O M P U T A T I O N S | | P E R F O R M E D ** | | | | |
| WATHEROO | -30.32 | 115.88 | 0.500 | -64.8 | -2 | 1.85 | 48.8 | 114.6 | 0.500 | 9.90 | 115.57 | 5098 | 0.049 | 19146 |
| WAKKANAI | 45.40 | 141.68 | 0.441 | 59.6 | -7 | 1.63 | -27.7 | 138.4 | 0.486 | 9.15 | 141.44 | 4412 | 0.072 | 15180 |
| WASHINGTON | 38.73 | -77.13 | 0.486 | 70.3 | -5 | 2.73 | -65.5 | -90.8 | 0.437 | -12.89 | -76.48 | 10903 | 0.015 | 34195 |
| WALTAIR | 17.57 | 83.30 | 0.364 | 18.8 | -1 | 0.99 | 1.6 | 84.1 | 0.349 | 8.81 | 83.67 | 458 | 0.319 | 1928 |
| WELLEN | 66.17 | -169.84 | 0.486 | 75.6 | 16 | 4.82 | -52.4 | 197.6 | 0.562 | 6.03 | 172.97 | 24699 | 0.003 | 71706 |
| WESTFORD | 42.58 | -71.42 | 0.491 | 72.6 | -13 | 3.26 | -70.5 | -78.9 | 0.441 | -12.78 | -67.47 | 14141 | 0.009 | 43379 |
| WEISSENAU | 47.80 | 9.50 | 0.409 | 63.3 | -3 | 2.06 | -36.6 | 27.5 | 0.286 | 2.94 | 16.38 | 6380 | 0.037 | 21119 |
| WELLINGTON | -41.28 | 174.77 | 0.503 | -66.7 | 19 | 2.26 | 50.1 | -162.5 | 0.431 | 4.10 | -173.58 | 8181 | 0.028 | 26103 |

Table B2

Tracings 300 km Above Stations.

| STATIONS | ** | O | R | I | G | I | N | ** CONJUGATE | INTERS. | ** MINIMUM-B | E Q U A T O R | | | ** ARC |
|---|---|---|---|---|---|---|---|---|---|---|---|---|---|---|
| | | LAT. | LONG. | B | DIP | DECL. | L | LAT. | LONG. | B | LAT. | LONG. | ALT. | B | KM |
| WHITE SANDS | | 32.40 | -1·6.87 | 0.447 | 60.2 | 12 | 1.81 | -46.6 | -126.3 | 0.431 | -7.82 | -114.04 | 5253 | 0.052 | 17907 |
| WINGST | | 53.75 | 9.07 | 0.424 | 68.3 | -3 | 2.66 | -45.5 | 34.1 | 0.303 | 2.10 | 18.15 | 10131 | 0.017 | 31903 |
| WITTEVEEN | | 52.82 | 6.67 | 0.421 | 67.6 | -4 | 2.58 | -44.8 | 31.5 | 0.298 | 1.85 | 15.94 | 9603 | 0.019 | 30424 |
| WIESE ISLAND | | 79.83 | 76.98 | 0.497 | 85.1 | 24 | 12.22 | ** N O | C O M P U | T A T I O N S | P E R F O R M E D ** | | | | |
| WINNIPEG | | 49.90 | -97.40 | 0.523 | 77.1 | 9 | 4.38 | -56.9 | -135.6 | 0.522 | -9.40 | -106.21 | 21647 | 0.004 | 53732 |
| WIEN KOBENZL | | 48.27 | 16.32 | 0.414 | 63.7 | -0 | 2.05 | -35.9 | 32.4 | 0.292 | 3.74 | 21.93 | 6364 | 0.037 | 21019 |
| WILKES | | -66.20 | 110.35 | 0.554 | -82.3 | -81 | 36.40 | ** N O | C O M P U | T A T I O N S | P E R F O R M E D ** | | | | |
| WOOMERA | | -30.70 | 136.80 | 0.503 | -63.1 | 6 | 1.81 | 48.8 | 140.3 | 0.458 | 9.33 | 139.98 | 5569 | 0.052 | 18447 |
| WROCLAW | | 51.10 | 17.08 | 0.422 | 66.2 | 0 | 2.29 | -39.8 | 35.9 | 0.298 | 3.42 | 23.43 | 7875 | 0.027 | 25378 |
| WRANGEL ISLAND | | 71.00 | -178.50 | 0.496 | 78.8 | 13 | 6.43 | -54.7 | 148.9 | 0.573 | 7.31 | 162.93 | 34992 | 0.001 | 130020 |
| YAKUTSK | | 62.05 | 129.67 | 0.509 | 75.9 | -11 | 3.18 | -42.4 | 127.0 | 0.551 | 10.33 | 128.83 | 14333 | 0.010 | 42733 |
| YAMAGAWA | | 31.20 | 130.65 | 0.397 | 44.1 | -3 | 1.19 | -14.6 | 129.9 | 0.414 | 8.82 | 130.92 | 1626 | 0.186 | 6760 |
| YELLOWKNIFE | | 62.40 | -114.40 | 0.525 | 82.0 | 30 | 8.69 | -67.3 | -113.0 | 0.563 | -4.52 | -135.00 | 49281 | 0.000 | 139893 |
| YUZHNO-SAKHALINSK | | 46.95 | 142.72 | 0.446 | 61.0 | -7 | 1.71 | -29.1 | 139.0 | 0.493 | 9.30 | 142.29 | 4898 | 0.063 | 16574 |
| ZARIA | | 11.15 | 7.65 | 0.282 | 3.2 | -8 | 1.04 | 8.4 | 8.1 | 0.277 | NO MINIMUM B BETWEEN INTERS. | | | | 322 |
| ZUGSPITZE | | 47.42 | 10.98 | 0.409 | 63.0 | -2 | 2.02 | -35.7 | 28.0 | 0.287 | 3.31 | 17.41 | 6136 | 0.039 | 20393 |

Table B3

Tracing 400 km Above Stations.

Table B3

Tracings 400 km Above Stations.

| STATIONS | ** O R I G I N ** | | | | | | ** CONJUGATE INTERS. ** | | | MINIMUM-B E Q U A T O R ** | | | | ARC |
|---|---|---|---|---|---|---|---|---|---|---|---|---|---|---|
| | LAT. | LONG. | B | DIP | DECL. | L | LAT. | LONG. | B | LAT. | LONG. | ALT. | B | KM |
| ABASHIRI | 43.97 | 140.33 | 0.417 | 58.3 | -6 | 1.59 | -26.3 | 137.4 | 0.456 | 9.21 | 140.17 | 4154 | 0.077 | 14193. |
| ABISKO | 68.35 | 18.82 | 0.440 | 77.2 | 0 | 6.03 | -59.3 | 63.4 | 0.408 | 3.50 | 34.25 | 31863 | 0.001 | 92115. |
| ABERYSTWYTH | 52.40 | -4.07 | 0.403 | 67.6 | -10 | 2.75 | -48.2 | 25.1 | 0.287 | 0.29 | 7.57 | 10609 | 0.016 | 33181. |
| ACCRA | 5.63 | -0.20 | 0.255 | -5.5 | -11 | 1.07 | 10.4 | -1.2 | 0.262 | 6.12 | -0.31 | 405 | 0.254 | 576. |
| ADEN | 12.77 | 44.97 | 0.300 | 9.8 | 0 | 1.03 | 4.4 | 45.0 | 0.286 | 6.79 | 44.99 | 436 | 0.283 | 1003. |
| ADDIS ABABA | 9.03 | 38.77 | 0.287 | -0.6 | 0 | 1.03 | 9.5 | 38.8 | 0.288 | NO MINIMUM B BETWEEN INTERS. | | | | 59. |
| ADELAIDE | -34.95 | 138.53 | 0.497 | -67.1 | 7 | 2.16 | 53.3 | 144.0 | 0.448 | 9.33 | 142.63 | 7767 | 0.031 | 24420. |
| ADAK | 51.90 | -176.65 | 0.410 | 64.0 | 10 | 2.25 | -39.0 | 164.7 | 0.485 | 6.18 | 174.50 | 8175 | 0.028 | 25829. |
| AGINCOURT | 43.80 | -79.30 | 0.480 | 73.8 | -6 | 3.50 | -69.5 | -98.5 | 0.447 | -12.47 | -79.30 | 15831 | 0.007 | 47700. |
| AHMEDABAD | 23.02 | 72.60 | 0.362 | 31.8 | -0 | 1.08 | -5.5 | 74.6 | 0.330 | 7.80 | 73.31 | 928 | 0.248 | 3763. |
| AIRE-SUR-ADOUR | 43.70 | -0.30 | 0.378 | 59.8 | -7 | 1.88 | -33.7 | 18.0 | 0.268 | 2.20 | 7.52 | 5247 | 0.048 | 17653. |
| AKROTIRI | 34.58 | 32.95 | 0.367 | 48.7 | 2 | 1.34 | -17.1 | 36.5 | 0.286 | 6.59 | 33.78 | 2256 | 0.127 | 8423. |
| AKLAVIK | 68.23 | -135.00 | 0.490 | 81.2 | 36 | 9.60 | -63.0 | 168.0 | 0.546 | 0.88 | -162.55 | 55231 | 0.000 | 155885. |
| AKITA | 39.73 | 140.13 | 0.399 | 53.7 | -5 | 1.43 | -22.4 | 137.8 | 0.435 | 9.12 | 140.07 | 3118 | 0.107 | 11171. |
| ALMERIA | 36.85 | -2.47 | 0.354 | 52.3 | -8 | 1.53 | -24.7 | 11.5 | 0.266 | 2.87 | 4.02 | 3153 | 0.087 | 11386. |
| ALDAN | 58.60 | 125.50 | 0.485 | 73.8 | -9 | 2.73 | -39.2 | 124.4 | 0.515 | 10.16 | 125.52 | 11481 | 0.015 | 34592. |
| ALERT | 82.55 | -63.58 | 0.476 | 86.4 | -84 | 252.38 | ** N O C O M P U T A T I O N S P E R F O R M E D ** | | | | | | | |
| ALMA-ATA | 43.20 | 76.92 | 0.453 | 62.0 | 3 | 1.62 | -25.7 | 82.7 | 0.401 | 8.24 | 77.92 | 4356 | 0.072 | 14508. |
| ALBUQUERQUE | 35.08 | -106.62 | 0.440 | 63.0 | 12 | 2.02 | -49.4 | -128.3 | 0.427 | -7.86 | -114.35 | 6580 | 0.037 | 21450. |
| ALMIRANTE BROWN | -64.88 | -62.87 | 0.366 | -59.4 | 16 | 2.51 | 36.6 | -65.7 | 0.441 | -12.95 | -60.08 | 9313 | 0.019 | 29741. |
| ANCON | -11.77 | -77.15 | 0.239 | 1.1 | 5 | 1.10 | -12.9 | -77.3 | 0.237 | NO MINIMUM B BETWEEN INTERS. | | | | 134. |
| ANCHORAGE | 61.17 | -149.98 | 0.466 | 74.3 | 25 | 4.40 | -53.8 | 172.3 | 0.525 | 2.61 | -168.66 | 21941 | 0.004 | 63991. |
| ANTOFAGASTA | -23.65 | -70.42 | 0.224 | -18.4 | 5 | 1.14 | -3.2 | -69.8 | 0.259 | -16.17 | -69.97 | 592 | 0.209 | 2508. |
| APIA | -13.80 | -171.77 | 0.328 | -29.4 | 12 | 1.12 | 16.2 | -165.9 | 0.288 | 2.70 | -168.49 | 917 | 0.223 | 3985. |
| APATITY | 67.55 | 33.33 | 0.446 | 77.4 | 8 | 5.28 | -55.5 | 68.9 | 0.413 | 5.19 | 44.42 | 27181 | 0.002 | 78926. |
| ARKHANGELSK | 64.58 | 40.50 | 0.448 | 76.3 | 10 | 4.27 | -51.5 | 68.7 | 0.402 | 5.75 | 48.26 | 20736 | 0.004 | 60947. |
| ARCETRI | 43.75 | 11.25 | 0.381 | 59.2 | -2 | 1.79 | -30.5 | 25.1 | 0.275 | 3.75 | 16.73 | 4783 | 0.055 | 16193. |
| AREQUIPA | -16.35 | -71.57 | 0.227 | -5.9 | 3 | 1.11 | -10.1 | -71.3 | 0.238 | -16.08 | -71.55 | 403 | 0.227 | 744. |
| ARGENTINE ISLAND | -65.25 | -64.27 | 0.370 | -59.8 | 17 | 2.55 | 36.9 | -66.2 | 0.443 | -12.82 | -60.83 | 9562 | 0.019 | 30432. |
| ARMIDALE | -30.30 | 151.40 | 0.464 | -60.8 | 10 | 1.76 | 46.8 | 159.9 | 0.397 | 8.30 | 156.79 | 5077 | 0.059 | 16996. |
| ASSWAN | 23.97 | 32.78 | 0.325 | 30.9 | 1 | 1.12 | -4.8 | 33.7 | 0.279 | 7.66 | 32.99 | 921 | 0.219 | 3784. |
| ASO | 32.88 | 131.02 | 0.385 | 46.3 | -3 | 1.24 | -16.0 | 130.1 | 0.402 | 8.97 | 131.29 | 1963 | 0.163 | 7567. |
| ASHKABAD | 37.93 | 55.10 | 0.410 | 55.4 | 4 | 1.45 | -22.1 | 60.0 | 0.325 | 6.75 | 55.73 | 3084 | 0.101 | 10911. |
| ATHENS | 37.97 | 23.72 | 0.370 | 52.5 | 0 | 1.46 | -21.1 | 30.2 | 0.282 | 5.86 | 25.93 | 2915 | 0.099 | 10503. |
| BAJA | 46.18 | 19.00 | 0.393 | 61.7 | 0 | 1.91 | -32.7 | 32.5 | 0.282 | 4.28 | 23.63 | 5552 | 0.046 | 18405. |
| BAGHDAD | 33.35 | 44.38 | 0.377 | 48.4 | 3 | 1.31 | -16.9 | 47.1 | 0.295 | 6.58 | 44.69 | 2145 | 0.136 | 8054. |
| BANGKOK | 13.75 | 100.55 | 0.339 | 10.1 | 0 | 0.98 | 5.2 | 100.5 | 0.335 | 9.08 | 100.53 | 445 | 0.326 | 1022. |
| BAR I | 69.58 | -140.18 | 0.487 | 81.2 | 35 | 9.78 | -62.2 | 164.0 | 0.548 | 2.17 | -168.61 | 56439 | 0.000 | 159170. |
| BALBOA | 8.95 | -79.57 | 0.318 | 37.5 | 3 | 1.24 | -33.3 | -84.8 | 0.265 | -13.72 | -81.22 | 1393 | 0.160 | 5978. |
| BAIE ST. PAUL | 47.43 | -70.50 | 0.477 | 75.4 | -16 | 4.23 | -75.1 | -78.0 | 0.442 | -12.37 | -65.40 | 20362 | 0.004 | 60509. |
| BARTER ISLAND | 70.13 | -143.67 | 0.486 | 81.0 | 34 | 9.61 | -61.5 | 162.0 | 0.548 | 2.84 | -172.09 | 55397 | 0.000 | 156270. |
| BAKER LAKE | 64.30 | -96.08 | 0.504 | 85.4 | 6 | 15.47 | ** N O C O M P U T A T I O N S P E R F O R M E D ** | | | | | | | |
| BATTLE CREEK | 42.27 | -85.17 | 0.479 | 72.6 | -0 | 3.18 | -65.8 | -108.4 | 0.451 | -12.00 | -88.03 | 13826 | 0.009 | 41990. |
| BANARAS | 25.33 | 83.02 | 0.378 | 35.1 | -0 | 1.09 | -6.6 | 84.7 | 0.350 | 8.68 | 83.62 | 1072 | 0.239 | 4317. |
| BANGUI | 4.60 | 18.58 | 0.269 | -13.9 | -5 | 1.06 | 16.3 | 17.5 | 0.286 | 8.77 | 18.15 | 478 | 0.262 | 1411. |

Table B3

Tracings 400 km Above Stations.

| STATIONS | ** O | R | I | G | I | N | ** CONJUGATE | INTERS. | ** MINIMUM-B | E Q U A T O R | | ** ARC | | |
|---|---|---|---|---|---|---|---|---|---|---|---|---|---|---|
| | LAT. | LONG. | B | DIP | DECL. | L | LAT. | LONG. | B | LAT. | LONG. | ALT. | B | KM |
| BASE ROI BAUDOUIN | -70.43 | 23.32 | 0.388 | -66.7 | -33 | 5.70 | 59.8 | -31.4 | 0.437 | -5.47 | -11.41 | 29419 | 0.002 | 85971. |
| BANGUIO | 16.42 | 120.58 | 0.335 | 18.4 | 0 | 1.01 | -0.2 | 120.2 | 0.337 | 8.32 | 120.48 | 563 | 0.300 | 2034. |
| BELEM | -1.00 | -49.00 | 0.247 | 16.5 | -13 | 1.16 | -18.1 | -44.7 | 0.209 | -13.48 | -45.92 | 523 | 0.203 | 2149. |
| BELSK | 51.84 | 20.80 | 0.409 | 66.8 | 1 | 2.37 | -40.4 | 39.5 | 0.295 | 3.83 | 26.77 | 8429 | 0.024 | 26712. |
| BETTLES | 66.90 | -151.84 | 0.477 | 77.9 | 27 | 6.37 | -57.3 | 164.2 | 0.541 | 3.55 | -174.65 | 34641 | 0.001 | 98996. |
| BEDFORD | 42.48 | -71.28 | 0.467 | 72.4 | -12 | 3.28 | -70.3 | -78.2 | 0.419 | -12.65 | -67.37 | 14299 | 0.009 | 43605. |
| BERMUDA | 32.37 | -64.67 | 0.424 | 64.1 | -12 | 2.16 | -60.7 | -60.8 | 0.337 | -13.28 | -59.39 | 7047 | 0.031 | 23333. |
| BEOGRAD | 44.80 | 20.52 | 0.390 | 60.3 | 0 | 1.81 | -30.6 | 32.4 | 0.282 | 4.53 | 24.56 | 4976 | 0.053 | 16705. |
| BIRD | 56.50 | 94.20 | 0.494 | 74.6 | 1 | 2.59 | -37.8 | 100.9 | 0.480 | 9.63 | 95.63 | 10572 | 0.018 | 31986. |
| BISMARK | 46.82 | -100.77 | 0.490 | 74.2 | 12 | 3.58 | -62.7 | -134.6 | 0.486 | -9.11 | -110.07 | 16546 | 0.007 | 49328. |
| BJORNOYA | 74.52 | 19.02 | 0.451 | 80.2 | -1 | 10.11 | -63.5 | 76.6 | 0.456 | 4.51 | 41.45 | 58055 | 0.000 | 164435. |
| BOROK | 58.03 | 38.33 | 0.437 | 72.3 | 8 | 3.01 | -45.2 | 59.3 | 0.355 | 5.51 | 43.50 | 12693 | 0.012 | 38561. |
| BOLOGNA | 44.50 | 11.35 | 0.383 | 60.0 | -2 | 1.83 | -31.6 | 25.8 | 0.275 | 3.69 | 16.99 | 5065 | 0.051 | 17025. |
| BOULDER | 40.03 | -105.30 | 0.464 | 67.8 | 13 | 2.47 | -54.6 | -131.6 | 0.454 | -8.24 | -114.04 | 9474 | 0.020 | 29596. |
| BOMBAY | 19.00 | 72.83 | 0.346 | 23.5 | -1 | 1.03 | -1.4 | 74.2 | 0.323 | 7.71 | 73.43 | 663 | 0.280 | 2559. |
| BOGOTA | 4.63 | -74.08 | 0.295 | 31.9 | 1 | 1.20 | -30.8 | -76.8 | 0.243 | -14.92 | -74.78 | 1056 | 0.178 | 4730. |
| BRISBANE | -27.53 | 152.92 | 0.448 | -57.6 | 10 | 1.61 | 43.7 | 160.8 | 0.381 | 8.26 | 157.92 | 4121 | 0.076 | 14266. |
| BUDAPEST | 46.68 | 21.27 | 0.396 | 62.2 | 1 | 1.93 | -33.1 | 34.5 | 0.284 | 4.63 | 25.61 | 5724 | 0.044 | 18891. |
| BUENOS AIRES | -34.52 | -58.50 | 0.222 | -33.1 | 0 | 1.27 | 7.4 | -62.0 | 0.300 | -15.61 | -59.50 | 1297 | 0.154 | 5804. |
| BUNIA | 1.53 | 30.18 | 0.276 | -20.2 | -2 | 1.07 | 18.6 | 29.7 | 0.302 | 8.15 | 29.89 | 573 | 0.257 | 2098. |
| BYRD STATION | -79.98 | -120.02 | 0.497 | -75.2 | 68 | 7.82 | 56.1 | -79.3 | 0.497 | -11.95 | -78.51 | 43432 | 0.001 | 124242. |
| CAPRI | 40.57 | 14.33 | 0.372 | 55.6 | -1 | 1.60 | -25.4 | 24.8 | 0.277 | 4.88 | 18.45 | 3673 | 0.076 | 12851. |
| CASTEL TESINO | 46.05 | 11.65 | 0.388 | 61.5 | -2 | 1.94 | -33.8 | 27.4 | 0.276 | 3.58 | 17.64 | 5694 | 0.044 | 18871. |
| CATANIA | 37.50 | 15.07 | 0.362 | 51.7 | -1 | 1.46 | -21.1 | 23.5 | 0.278 | 5.49 | 18.47 | 2866 | 0.099 | 10383. |
| CAPE CHELYUSKIN | 77.72 | 104.28 | 0.485 | 85.3 | 11 | 9.57 | -56.3 | 112.8 | 0.532 | 10.91 | 104.58 | 55047 | 0.000 | 155094. |
| CAPE ZHELANIA | 76.90 | 68.60 | 0.475 | 83.7 | 20 | 9.60 | -57.8 | 97.8 | 0.502 | 9.40 | 78.50 | 55088 | 0.000 | 155517. |
| CAPE SCHMIDT | 68.87 | -179.48 | 0.470 | 77.2 | 11 | 5.48 | -52.8 | 150.7 | 0.543 | 7.06 | 164.09 | 28946 | 0.002 | 83150. |
| CAMBRIDGE UK | 52.22 | 0.10 | 0.402 | 67.3 | -8 | 2.65 | -46.3 | 27.1 | 0.285 | 1.01 | 10.71 | 10006 | 0.017 | 31420. |
| CARIBOU | 46.87 | -68.02 | 0.473 | 74.7 | -18 | 4.06 | -74.7 | -70.0 | 0.431 | -12.15 | -61.73 | 19214 | 0.005 | 57373. |
| CALCUTTA | 22.93 | 88.52 | 0.369 | 30.0 | -0 | 1.05 | -3.7 | 89.5 | 0.348 | 9.00 | 88.90 | 860 | 0.266 | 3464. |
| CAPE HALLETT | -72.32 | 178.22 | 0.543 | -83.5 | -88 | 16.72 | ** N O | C O M P U T A T I O N S | | P E R F O R M E D ** | | | | |
| CAMPBELL ISLAND | -52.55 | 169.15 | 0.525 | -76.1 | 27 | 4.25 | 61.6 | -155.3 | 0.462 | 3.76 | -173.12 | 20991 | 0.004 | 61350. |
| CANBERRA | -35.32 | 149.00 | 0.490 | -66.1 | 11 | 2.12 | 52.5 | 159.0 | 0.423 | 8.57 | 155.21 | 7398 | 0.033 | 23519. |
| CAPETOWN | -34.15 | 18.32 | 0.268 | -63.7 | -24 | 1.89 | 44.0 | -0.2 | 0.379 | 1.90 | 7.78 | 5368 | 0.046 | 18017. |
| CAMDEN | -34.08 | 150.68 | 0.483 | -64.6 | 11 | 2.01 | 50.9 | 160.7 | 0.415 | 8.40 | 156.86 | 6675 | 0.039 | 21510. |
| CAPE CANAVERAL | 28.40 | -80.60 | 0.423 | 61.1 | 0 | 1.88 | -53.9 | -92.5 | 0.366 | -12.96 | -82.12 | 5500 | 0.046 | 18605. |
| CAPE JONES | 54.50 | -79.50 | 0.497 | 80.3 | -14 | 6.87 | -78.7 | -115.5 | 0.492 | -12.08 | -78.93 | 37281 | 0.001 | 107213. |
| CEBU | 10.33 | 123.90 | 0.322 | 5.4 | 1 | 0.99 | 5.4 | 123.8 | 0.323 | 8.14 | 123.86 | 414 | 0.320 | 582. |
| CHAMICAL | -30.33 | -66.33 | 0.225 | -27.8 | 4 | 1.20 | 2.8 | -66.7 | 0.282 | -16.24 | -65.94 | 940 | 0.179 | 4324. |
| CHURCHILL | 58.77 | -94.17 | 0.506 | 82.8 | 4 | 8.97 | -74.5 | -151.3 | 0.522 | -9.58 | -103.80 | 50865 | 0.000 | 144432. |
| CHAMBON-LA-FORET | 48.02 | 2.27 | 0.391 | 63.7 | -6 | 2.18 | -39.3 | 23.5 | 0.273 | 1.90 | 10.87 | 7113 | 0.031 | 23088. |
| CHICAGO | 41.83 | -87.67 | 0.479 | 72.1 | 2 | 3.07 | -64.3 | -112.0 | 0.452 | -11.47 | -91.57 | 13160 | 0.011 | 40086. |
| CHARLOTTESVILLE | 38.03 | -78.22 | 0.462 | 69.6 | -4 | 2.68 | -64.4 | -92.4 | 0.415 | -12.63 | -78.15 | 10591 | 0.016 | 33077. |
| CHITA | 52.05 | 113.48 | 0.484 | 69.9 | -5 | 2.10 | -33.2 | 115.2 | 0.488 | 9.86 | 114.46 | 7539 | 0.033 | 23531. |
| CHITTAGONG | 22.35 | 91.82 | 0.367 | 28.7 | -0 | 1.04 | -3.1 | 92.5 | 0.349 | 9.08 | 92.08 | 815 | 0.272 | 3275. |

Table B3

Tracings 400 km Above Stations.

| STATIONS | ** | O | R | I | G | I | N | ** CONJUGATE | INTERS. | ** MINIMUM-B | E Q U A T O R | ** ARC | | |
|---|---|---|---|---|---|---|---|---|---|---|---|---|---|---|
| | | LAT. | LONG. | B | DIP | DECL. | L | LAT. | LONG. | B | LAT. | LONG. | ALT. | B | KM |
| CHRISTCHURCH | | -43.57 | 172.80 | 0.492 | -68.9 | 20 | 2.56 | 52.9 | -162.6 | 0.425 | 4.24 | -174.63 | 10135 | 0.019 | 31326. |
| CHACALTAYA | | -16.32 | -68.15 | 0.224 | -5.3 | 1 | 1.12 | -10.6 | -68.1 | 0.234 | NO MINIMUM B BETWEEN INTERS. | | | | 673. |
| CLIMAX | | 39.37 | -106.18 | 0.460 | 67.1 | 13 | 2.38 | -53.6 | -131.8 | 0.451 | -8.02 | -114.89 | 8936 | 0.022 | 28084. |
| CLONCURRY | | -20.67 | 140.50 | 0.423 | -50.9 | 6 | 1.37 | 37.7 | 143.1 | 0.384 | 9.11 | 142.86 | 2707 | 0.122 | 9969. |
| CONCORD | | 43.20 | -71.53 | 0.470 | 72.9 | -12 | 3.40 | -71.0 | -79.2 | 0.424 | -12.74 | -67.64 | 15054 | 0.008 | 45707. |
| COOK | | -30.63 | 130.40 | 0.481 | -63.6 | 3 | 1.86 | 49.0 | 132.2 | 0.452 | 9.70 | 132.53 | 5895 | 0.048 | 19065. |
| COLLEGE | | 64.85 | -147.83 | 0.476 | 77.1 | 28 | 5.80 | -57.0 | 168.6 | 0.536 | 2.77 | -169.67 | 30914 | 0.002 | 88743. |
| CORINALDO | | 43.63 | 13.00 | 0.381 | 59.0 | -2 | 1.77 | -30.0 | 26.2 | 0.276 | 4.16 | 18.08 | 4693 | 0.057 | 15910. |
| COIMBRA | | 40.22 | -8.42 | 0.367 | 57.0 | -10 | 1.75 | -32.0 | 10.4 | 0.261 | 0.88 | 0.18 | 4437 | 0.059 | 15329. |
| CONCEPCION | | -36.58 | -72.98 | 0.249 | -36.6 | 11 | 1.28 | 9.2 | -71.0 | 0.317 | -15.36 | -70.79 | 1524 | 0.147 | 6554. |
| CORDOBA | | -31.32 | -64.22 | 0.223 | -29.0 | 3 | 1.22 | 3.8 | -65.3 | 0.286 | -16.12 | -64.14 | 1010 | 0.173 | 4633. |
| COLOMBO | | 6.90 | 79.87 | 0.325 | -5.9 | -3 | 0.99 | 11.8 | 79.6 | 0.329 | 8.45 | 79.77 | 413 | 0.323 | 578. |
| COCOS ISLAND | | -12.20 | 96.90 | 0.383 | -44.7 | -2 | 1.18 | 31.0 | 95.8 | 0.408 | 9.08 | 96.17 | 1683 | 0.187 | 6457. |
| COPENHAGEN | | 55.75 | 12.50 | 0.413 | 69.7 | -2 | 2.92 | -47.4 | 39.0 | 0.307 | 2.63 | 21.69 | 11840 | 0.013 | 36488. |
| CORAL HARBOUR | | 64.20 | -83.40 | 0.499 | 85.1 | -23 | 17.68 | ** N O | C O M P U T A T I O N S | | P E R F O R M E D ** | | | | |
| CRACOW | | 50.05 | 19.95 | 0.404 | 65.3 | 0 | 2.21 | -38.0 | 36.9 | 0.289 | 4.08 | 25.48 | 7400 | 0.030 | 23760. |
| CURACAO | | 12.08 | -68.84 | 0.331 | 43.2 | -3 | 1.35 | -40.0 | -69.8 | 0.254 | -15.13 | -67.84 | 1888 | 0.128 | 7838. |
| CUZCO | | -13.52 | -71.98 | 0.232 | -0.7 | 3 | 1.11 | -12.8 | -71.9 | 0.233 | NO MINIMUM B BETWEEN INTERS. | | | | 89. |
| DAVIS | | -68.60 | 78.00 | 0.470 | -74.6 | -67 | 15.64 | ** N O | C O M P U T A T I O N S | | P E R F O R M E D ** | | | | |
| DAPANGO | | 10.80 | 0.07 | 0.263 | 5.7 | -10 | 1.07 | 5.8 | 1.1 | 0.256 | 6.45 | 0.96 | 407 | 0.256 | 608. |
| DALLAS | | 32.78 | -96.80 | 0.439 | 62.8 | 8 | 1.99 | -51.4 | -116.3 | 0.411 | -10.05 | -102.70 | 6342 | 0.039 | 20830. |
| DAKAR | | 14.66 | -17.43 | 0.272 | 22.1 | -13 | 1.13 | -6.6 | -11.4 | 0.237 | 1.44 | -13.83 | 662 | 0.213 | 2756. |
| DARWIN-COONAWARRA | | -12.43 | 130.90 | 0.382 | -39.7 | 3 | 1.16 | 28.9 | 131.7 | 0.366 | 8.83 | 131.85 | 1466 | 0.198 | 5930. |
| DEBRECEN | | 47.48 | 21.65 | 0.398 | 63.0 | 1 | 1.99 | -34.2 | 35.5 | 0.285 | 4.32 | 26.17 | 6070 | 0.040 | 19900. |
| DE BILT | | 52.10 | 5.18 | 0.402 | 67.0 | -5 | 2.56 | -44.4 | 29.9 | 0.286 | 1.92 | 14.56 | 9458 | 0.019 | 29804. |
| DEEP RIVER | | 46.10 | -77.50 | 0.483 | 75.3 | -9 | 3.97 | -72.2 | -96.5 | 0.454 | -12.58 | -76.38 | 18787 | 0.005 | 55971. |
| DENVER | | 39.75 | -105.00 | 0.463 | 67.6 | 13 | 2.45 | -54.5 | -131.0 | 0.453 | -8.07 | -113.58 | 9326 | 0.021 | 29181. |
| DEHRA DUN | | 30.33 | 78.05 | 0.399 | 44.4 | 0 | 1.19 | -12.3 | 80.8 | 0.360 | 8.28 | 78.85 | 1658 | 0.183 | 6372. |
| DELHI | | 28.63 | 77.22 | 0.391 | 41.6 | -0 | 1.15 | -10.6 | 79.8 | 0.353 | 8.06 | 78.01 | 1448 | 0.200 | 5673. |
| DECEPCION | | -62.98 | -60.72 | 0.351 | -57.7 | 14 | 2.34 | 34.7 | -64.7 | 0.433 | -13.10 | -59.09 | 8201 | 0.024 | 26613. |
| DIXON ISLAND | | 73.53 | 80.70 | 0.482 | 83.3 | 17 | 7.08 | -54.0 | 100.2 | 0.505 | 10.11 | 85.87 | 39036 | 0.001 | 111023. |
| DJIBOUTI | | 11.55 | 43.15 | 0.295 | 6.5 | 0 | 1.03 | 6.0 | 43.2 | 0.286 | 6.89 | 43.16 | 410 | 0.285 | 661. |
| DJAKARTA | | -6.17 | 107.00 | 0.362 | -32.7 | 1 | 1.07 | 24.2 | 107.2 | 0.373 | 8.74 | 107.19 | 985 | 0.252 | 4025. |
| DODAIRA | | 36.00 | 139.20 | 0.383 | 49.3 | -4 | 1.32 | -19.0 | 137.3 | 0.415 | 9.19 | 139.22 | 2411 | 0.136 | 9035. |
| DOLGOPRUDNAYA | | 55.94 | 37.52 | 0.433 | 70.8 | 7 | 2.73 | -43.0 | 56.4 | 0.341 | 5.37 | 42.09 | 10915 | 0.015 | 33578. |
| DOURBES | | 50.10 | 4.60 | 0.397 | 65.4 | -5 | 2.35 | -41.7 | 27.2 | 0.279 | 1.84 | 13.41 | 8160 | 0.025 | 26092. |
| DUNSINK | | 53.38 | -6.33 | 0.406 | 68.5 | -11 | 2.93 | -50.6 | 25.2 | 0.293 | -0.34 | 6.25 | 11747 | 0.013 | 36436. |
| DUSHETTI | | 42.08 | 44.70 | 0.409 | 59.3 | 5 | 1.63 | -26.6 | 51.3 | 0.309 | 6.34 | 45.72 | 4086 | 0.072 | 13949. |
| DURHAM | | 43.08 | -70.92 | 0.468 | 72.8 | -13 | 3.37 | -71.0 | -77.5 | 0.421 | -12.80 | -66.74 | 14888 | 0.008 | 45260. |
| DUMONT D'URVILLE | | -66.67 | 140.02 | 0.553 | -89.6 | -28 | 36.13 | ** N O | C O M P U T A T I O N S | | P E R F O R M E D ** | | | | |
| DURBAN | | -29.83 | 31.03 | 0.281 | -62.9 | -19 | 1.77 | 44.2 | 19.4 | 0.387 | 4.55 | 23.45 | 4758 | 0.056 | 16068. |
| EDINBURGH | | 55.92 | -3.18 | 0.411 | 70.1 | -10 | 3.24 | -52.8 | 30.5 | 0.308 | 0.20 | 9.78 | 13798 | 0.009 | 42187. |
| EIGHTS | | -75.23 | -77.17 | 0.441 | -68.1 | 31 | 4.25 | 47.6 | -70.2 | 0.477 | -12.52 | -64.93 | 20537 | 0.004 | 61004. |
| ELLSWORTH | | -77.72 | -41.13 | 0.426 | -67.5 | 7 | 4.92 | 51.3 | -59.9 | 0.467 | -11.35 | -48.70 | 24615 | 0.003 | 72535. |
| ELISABETHVILLE | | -11.63 | 27.42 | 0.279 | -45.3 | -7 | 1.24 | 30.5 | 24.1 | 0.342 | 7.13 | 25.31 | 1576 | 0.162 | 6214. |

Table B3

Tracings 400 km Above Stations.

| STATIONS | ** O R I G I N ** CONJUGATE INTERS. ** MINIMUM-B E Q U A T O R ** ARC | | | | | | | | | | | | | |
|---|---|---|---|---|---|---|---|---|---|---|---|---|---|---|
| | LAT. | LONG. | B | DIP | DECL. | L | LAT. | LONG. | B | LAT. | LONG. | ALT. | B | KM |
| ENNADAI | 61.30 | -101.20 | 0.506 | 83.5 | 16 | 10.26 | -72.5 | -163.6 | 0.532 | -7.94 | -116.04 | 59154 | 0.000 | 167181. |
| ENUGU | 6.47 | 7.55 | 0.261 | -7.0 | -9 | 1.06 | 12.4 | 6.6 | 0.270 | 7.71 | 7.34 | 414 | 0.261 | 718. |
| ESKDALEMUIR | 55.32 | -3.20 | 0.409 | 69.7 | -10 | 3.15 | -52.0 | 29.6 | 0.304 | -0.01 | 9.54 | 13166 | 0.010 | 40412. |
| ESPERANZA | -63.38 | -56.98 | 0.349 | -57.8 | 12 | 2.38 | 35.4 | -63.3 | 0.433 | -12.71 | -56.90 | 8446 | 0.023 | 27329. |
| EUREKA | 80.00 | -85.93 | 0.483 | 88.1 | 75 | 331.26 | ** N O C O M P U T A T I O N S P E R F O R M E D ** | | | | | | | |
| FAREWELL | 62.53 | -153.90 | 0.466 | 74.7 | 24 | 4.57 | -53.6 | 168.8 | 0.528 | 3.51 | -172.68 | 23021 | 0.003 | 66954. |
| FANNING ISLAND | 3.92 | -159.38 | 0.277 | 9.6 | 10 | 1.05 | -5.2 | -161.1 | 0.288 | 0.80 | -159.95 | 442 | 0.273 | 1111. |
| FLIN FLON | 54.70 | -102.00 | 0.504 | 79.5 | 14 | 5.82 | -68.3 | -148.6 | 0.515 | -8.18 | -114.02 | 30845 | 0.002 | 88927. |
| FORT YUKON | 66.57 | -145.30 | 0.481 | 78.6 | 30 | 6.87 | -58.9 | 167.2 | 0.541 | 2.62 | -169.22 | 37804 | 0.001 | 107754. |
| FORT NORMAN | 64.90 | -125.50 | 0.495 | 81.0 | 34 | 8.69 | -64.4 | 177.5 | 0.541 | -1.52 | -149.74 | 49381 | 0.000 | 139837. |
| FORT CHIMO | 58.10 | -68.43 | 0.486 | 80.5 | -30 | 8.81 | -85.0 | -80.6 | 0.481 | -11.77 | -59.73 | 49520 | 0.000 | 141352. |
| FORT MONMOUTH | 40.25 | -74.02 | 0.465 | 71.1 | -9 | 2.97 | -67.7 | -84.3 | 0.416 | -12.71 | -71.75 | 12349 | 0.012 | 38093. |
| FORT BELVOIR | 38.73 | -77.13 | 0.463 | 70.2 | -5 | 2.77 | -65.4 | -90.6 | 0.416 | -12.78 | -76.50 | 11131 | 0.014 | 34614. |
| FORT RANDOLPH | 9.38 | -79.88 | 0.320 | 38.1 | 3 | 1.25 | -33.6 | -85.3 | 0.267 | -13.57 | -81.58 | 1435 | 0.158 | 6127. |
| FORT DE FRANCE | 14.10 | -61.02 | 0.332 | 44.7 | -9 | 1.40 | -41.1 | -55.6 | 0.236 | -14.81 | -57.31 | 2071 | 0.117 | 8532. |
| FREETOWN | 8.47 | -13.22 | 0.254 | 7.6 | -14 | 1.09 | 1.6 | -11.3 | 0.242 | 2.77 | -11.69 | 417 | 0.242 | 851. |
| FROBISHER | 63.75 | -68.57 | 0.486 | 82.7 | -39 | 15.54 | ** N O C O M P U T A T I O N S P E R F O R M E D ** | | | | | | | |
| FREIBURG | 48.05 | 7.58 | 0.392 | 63.5 | -4 | 2.13 | -37.7 | 26.7 | 0.276 | 2.52 | 15.05 | 6815 | 0.033 | 22180. |
| FRONT ROYAL | 38.93 | -78.18 | 0.465 | 70.3 | -4 | 2.79 | -65.3 | -92.8 | 0.420 | -12.61 | -78.01 | 11264 | 0.014 | 34965. |
| FT. DAVIS | 30.63 | -103.95 | 0.421 | 59.0 | 11 | 1.77 | -46.1 | -122.1 | 0.400 | -8.57 | -110.49 | 4990 | 0.055 | 16931. |
| GARCHY | 47.30 | 3.07 | 0.389 | 63.0 | -6 | 2.11 | -38.0 | 23.3 | 0.272 | 2.08 | 11.27 | 6684 | 0.034 | 21835. |
| GAINESVILLE | 29.63 | -82.30 | 0.429 | 62.1 | 1 | 1.94 | -54.5 | -95.6 | 0.376 | -12.72 | -84.33 | 5906 | 0.042 | 19745. |
| GENOVA MONTE CAPEL | 44.55 | 8.95 | 0.382 | 60.1 | -3 | 1.85 | -32.2 | 24.3 | 0.274 | 3.48 | 15.07 | 5165 | 0.050 | 17337. |
| GENERAL BELGRANO | -77.97 | -38.80 | 0.427 | -67.6 | 6 | 5.03 | 51.7 | -59.4 | 0.466 | -10.93 | -47.81 | 25326 | 0.002 | 74514. |
| GENERAL SAN MARTIN | -68.13 | -67.43 | 0.392 | -62.2 | 20 | 2.88 | 39.9 | -67.4 | 0.454 | -12.92 | -62.07 | 11722 | 0.013 | 36481. |
| GHANA | 10.00 | 4.00 | 0.264 | 2.3 | -9 | 1.06 | 8.0 | 4.4 | 0.261 | NO MINIMUM B BETWEEN INTERS. | | | | 241. |
| GIFU | 35.58 | 137.08 | 0.386 | 49.1 | -4 | 1.31 | -18.6 | 135.5 | 0.414 | 9.01 | 137.21 | 2351 | 0.140 | 8830. |
| GILGIT | 35.94 | 74.30 | 0.423 | 53.0 | 1 | 1.34 | -18.5 | 78.4 | 0.371 | 7.92 | 75.19 | 2595 | 0.127 | 9326. |
| GOUGH ISLAND | -40.35 | -9.89 | 0.243 | -56.7 | -25 | 1.78 | 34.1 | -33.3 | 0.368 | -5.35 | -22.40 | 4495 | 0.056 | 15797. |
| GODHAVN | 69.23 | -53.52 | 0.471 | 82.0 | -46 | 22.60 | ** N O C O M P U T A T I O N S P E R F O R M E D ** | | | | | | | |
| GOOSE BAY | 53.32 | -60.38 | 0.470 | 76.7 | -28 | 5.64 | -79.7 | -40.4 | 0.438 | -11.23 | -48.78 | 29168 | 0.002 | 85156. |
| GOTTINGEN | 51.53 | 9.93 | 0.402 | 66.5 | -3 | 2.43 | -42.2 | 32.0 | 0.286 | 2.59 | 18.04 | 8730 | 0.022 | 27675. |
| GRYTVIKEN | -54.27 | -36.50 | 0.277 | -52.7 | -5 | 1.95 | 30.9 | -53.5 | 0.396 | -11.54 | -44.67 | 5541 | 0.043 | 19086. |
| GRAZ | 47.07 | 15.47 | 0.393 | 62.5 | -1 | 1.99 | -34.5 | 30.8 | 0.280 | 3.95 | 20.98 | 6028 | 0.040 | 19818. |
| GROCKA | 44.63 | 20.77 | 0.390 | 60.2 | 0 | 1.80 | -30.3 | 32.4 | 0.282 | 4.79 | 24.70 | 4910 | 0.054 | 16505. |
| GRAND BAHAMA | 26.67 | -78.37 | 0.413 | 59.7 | -0 | 1.80 | -52.9 | -88.3 | 0.351 | -13.27 | -79.23 | 4964 | 0.052 | 17090. |
| GRAHAMSTOWN | -33.28 | 26.48 | 0.276 | -64.2 | -23 | 1.91 | 45.6 | 10.9 | 0.386 | 3.42 | 16.96 | 5522 | 0.045 | 18375. |
| GREAT WHALE RIVER | 55.27 | -77.78 | 0.495 | 80.6 | -17 | 7.30 | -80.0 | -113.1 | 0.491 | -11.98 | -76.00 | 39962 | 0.001 | 114678. |
| GULMARG | 34.05 | 74.40 | 0.414 | 50.3 | 1 | 1.28 | -16.6 | 78.1 | 0.365 | 7.91 | 75.27 | 2249 | 0.144 | 8265. |
| GUANTANAMO BAY | 19.90 | -75.15 | 0.377 | 52.7 | -0 | 1.53 | -46.9 | -81.2 | 0.306 | -14.06 | -75.44 | 3201 | 0.085 | 11920. |
| GUAM | 13.45 | 144.75 | 0.302 | 11.6 | 2 | 1.02 | 2.2 | 144.2 | 0.313 | 8.89 | 144.58 | 466 | 0.293 | 1348. |
| GUAYAQUIL | -2.17 | -79.88 | 0.267 | 18.5 | 5 | 1.12 | -21.3 | -82.2 | 0.239 | -13.79 | -81.04 | 584 | 0.221 | 2367. |
| HAMMAGHIR | 30.10 | 0. | 0.328 | 42.6 | -7 | 1.29 | -15.0 | 9.2 | 0.264 | 4.73 | 4.52 | 1759 | 0.143 | 6933. |
| HACHIJOJIMA | 33.13 | 139.80 | 0.369 | 45.5 | -3 | 1.25 | -16.3 | 138.1 | 0.400 | 8.99 | 139.76 | 1964 | 0.160 | 7638. |
| HALLETT | -72.32 | 170.22 | 0.546 | -84.8 | -79 | 22.37 | ** N O C O M P U T A T I O N S P E R F O R M E D ** | | | | | | | |
| HARTLAND | 51.00 | -4.48 | 0.399 | 66.6 | -10 | 2.58 | -46.3 | 23.1 | 0.281 | 0.09 | 6.75 | 9575 | 0.019 | 30245. |

Table B3

Tracings 400 km Above Stations.

| STATIONS | ** O | R | I | G | I | N | ** CONJUGATE | INTERS. ** | MINIMUM-B | E Q U A T O R | ** ARC | | |
|---|---|---|---|---|---|---|---|---|---|---|---|---|---|
| | LAT. | LONG. | B | DIP | DECL. | L | LAT. | LONG. | B | LAT. | LONG. | ALT. | B | KM |
| HARVSTVA | 60.22 | 10.25 | 0.421 | 72.6 | -3 | 3.74 | -53.6 | 44.5 | 0.337 | 2.11 | 22.18 | 17091 | 0.006 | 51252. |
| HAMBURG | 53.63 | 10.00 | 0.407 | 68.1 | -3 | 2.67 | -45.2 | 34.7 | 0.294 | 2.30 | 18.91 | 10238 | 0.017 | 31980. |
| HALLE | 51.48 | 11.93 | 0.403 | 66.4 | -2 | 2.41 | -41.7 | 33.2 | 0.287 | 2.78 | 19.60 | 8582 | 0.023 | 27232. |
| HALIFAX | 44.60 | -63.60 | 0.460 | 72.5 | -19 | 3.52 | -72.3 | -56.4 | 0.403 | -12.10 | -55.65 | 15688 | 0.007 | 47639. |
| HANNOVER USA | 43.70 | -72.30 | 0.472 | 73.3 | -12 | 3.49 | -71.3 | -81.4 | 0.429 | -12.53 | -68.72 | 15641 | 0.007 | 47327. |
| HABANA | 23.15 | -82.35 | 0.396 | 55.4 | 2 | 1.61 | -47.6 | -93.0 | 0.338 | -13.02 | -84.57 | 3802 | 0.073 | 13623. |
| HALLEY BAY | -75.52 | -26.60 | 0.406 | -66.0 | -2 | 4.57 | 51.0 | -54.8 | 0.457 | -10.51 | -41.79 | 22331 | 0.003 | 66260. |
| HAIFA | 32.83 | 35.10 | 0.363 | 46.4 | 2 | 1.29 | -15.3 | 37.8 | 0.286 | 6.78 | 35.65 | 1977 | 0.142 | 7527. |
| HAMILTON MASS. | 42.02 | -72.17 | 0.467 | 72.2 | -11 | 3.21 | -69.8 | -80.4 | 0.419 | -12.81 | -68.76 | 13889 | 0.009 | 42443. |
| HERSTMONCEUX | 50.90 | 0.33 | 0.399 | 66.2 | -7 | 2.49 | -44.3 | 25.6 | 0.280 | 0.92 | 10.43 | 9023 | 0.021 | 28615. |
| HEISS | 80.20 | 57.48 | 0.471 | 84.1 | 17 | 13.75 | ** N O | C O M P U T A T I O N S | P E R F O R M E D ** | | | | | |
| HEALY | 63.85 | -119.00 | 0.499 | 81.7 | 33 | 9.10 | -66.3 | -177.9 | 0.540 | -3.18 | -141.67 | 51907 | 0.000 | 146881. |
| HEL | 54.60 | 18.80 | 0.414 | 68.9 | 0 | 2.69 | -44.5 | 41.4 | 0.305 | 3.25 | 26.19 | 10460 | 0.016 | 32516. |
| HELWAN | 29.87 | 31.33 | 0.346 | 41.2 | 1 | 1.22 | -11.4 | 33.5 | 0.282 | 7.07 | 31.90 | 1521 | 0.169 | 6015. |
| HERMANUS | -34.42 | 19.22 | 0.269 | -63.9 | -24 | 1.91 | 44.4 | 0.8 | 0.380 | 2.08 | 8.61 | 5485 | 0.045 | 18349. |
| HIRAISO | 36.37 | 140.62 | 0.382 | 49.6 | -4 | 1.33 | -19.3 | 138.5 | 0.417 | 9.14 | 140.55 | 2468 | 0.133 | 9223. |
| HIGHCLIFF | -45.88 | 170.58 | 0.503 | -71.1 | 21 | 2.90 | 55.8 | -162.6 | 0.436 | 4.19 | -175.90 | 12344 | 0.013 | 37448. |
| HONOLULU | 21.30 | -158.10 | 0.305 | 38.5 | 11 | 1.20 | -20.3 | -166.6 | 0.351 | 1.49 | -161.99 | 1443 | 0.180 | 6021. |
| HOBART | -42.92 | 147.17 | 0.520 | -72.8 | 13 | 3.02 | 60.6 | 161.6 | 0.452 | 8.62 | 155.14 | 13198 | 0.011 | 39619. |
| HOLLANDIA | -2.50 | 140.52 | 0.330 | -21.2 | 4 | 1.05 | 18.3 | 141.3 | 0.314 | 8.81 | 141.10 | 641 | 0.274 | 2585. |
| HURBANOVO | 47.90 | 18.20 | 0.397 | 63.3 | 0 | 2.04 | -35.3 | 33.5 | 0.283 | 4.16 | 23.42 | 6341 | 0.038 | 20711. |
| HUMAIN | 50.20 | 5.35 | 0.397 | 65.5 | -5 | 2.35 | -41.6 | 27.7 | 0.279 | 1.96 | 14.03 | 8170 | 0.025 | 26115. |
| HUANCAYO | -12.05 | -75.33 | 0.237 | 1.2 | 4 | 1.10 | -13.3 | -75.4 | 0.235 | NO MINIMUM B BETWEEN INTERS. | | | | 143. |
| HYDERABAD | 17.42 | 78.45 | 0.343 | 19.2 | -1 | 1.01 | 1.0 | 79.4 | 0.327 | 8.32 | 78.92 | 568 | 0.299 | 2011. |
| IBADAN | 7.37 | 3.97 | 0.260 | -3.6 | -10 | 1.06 | 10.4 | 3.4 | 0.264 | NO MINIMUM B BETWEEN INTERS. | | | | 370. |
| I. CROZET | -46.50 | 52.00 | 0.335 | -65.8 | -38 | 3.03 | 57.7 | 28.5 | 0.427 | 4.34 | 35.23 | 12736 | 0.011 | 38817. |
| IL QORTIN | 36.22 | 14.30 | 0.356 | 50.0 | -2 | 1.41 | -19.5 | 22.3 | 0.277 | 5.60 | 17.60 | 2591 | 0.108 | 9533. |
| INUVIK | 68.20 | -133.70 | 0.490 | 81.4 | 37 | 9.84 | -63.4 | 168.4 | 0.546 | 0.67 | -161.36 | 56770 | 0.000 | 160141. |
| INVERCARGILL | -46.42 | 168.32 | 0.508 | -71.9 | 21 | 3.05 | 57.2 | -164.7 | 0.439 | 4.62 | -178.12 | 13265 | 0.011 | 39988. |
| INVERNESS | 57.45 | -4.25 | 0.414 | 71.2 | -11 | 3.55 | -55.1 | 32.4 | 0.320 | -0.13 | 9.73 | 15765 | 0.007 | 47721. |
| IQUITOS | -3.67 | -73.33 | 0.259 | 17.6 | 2 | 1.13 | -22.3 | -74.6 | 0.229 | -15.40 | -73.90 | 564 | 0.216 | 2286. |
| IRKUTSK | 52.27 | 104.30 | 0.489 | 70.8 | -2 | 2.14 | -33.5 | 107.8 | 0.481 | 9.93 | 105.43 | 7784 | 0.031 | 24181. |
| ISLA DE PASCUA | -27.17 | -109.43 | 0.294 | -36.2 | 14 | 1.20 | 12.2 | -102.2 | 0.321 | -8.48 | -105.45 | 1293 | 0.178 | 5535. |
| ISFJORD | 78.07 | 13.63 | 0.456 | 81.8 | -7 | 15.39 | ** N O | C O M P U T A T I O N S | P E R F O R M E D ** | | | | | |
| ITHACA | 42.45 | -76.52 | 0.474 | 72.8 | -8 | 3.29 | -69.2 | -91.3 | 0.434 | -12.80 | -75.24 | 14415 | 0.009 | 43813. |
| IVALO | 68.60 | 27.48 | 0.444 | 77.6 | 5 | 5.84 | -57.6 | 67.8 | 0.415 | 4.52 | 40.83 | 30714 | 0.002 | 88800. |
| JICAMARCA | -11.95 | -76.87 | 0.239 | 0.9 | 5 | 1.10 | -12.8 | -77.0 | 0.237 | NO MINIMUM B BETWEEN INTERS. | | | | 104. |
| JODRELL BANK | 53.23 | -2.30 | 0.404 | 68.2 | -9 | 2.82 | -48.7 | 27.1 | 0.291 | 0.43 | 9.29 | 11087 | 0.014 | 34522. |
| JOHANNESBURG | -26.20 | 28.03 | 0.279 | -61.0 | -16 | 1.63 | 41.5 | 18.0 | 0.377 | 4.99 | 21.68 | 3882 | 0.072 | 13462. |
| JUPITER | 27.02 | -80.12 | 0.416 | 59.8 | 0 | 1.81 | -52.6 | -91.2 | 0.357 | -13.15 | -81.55 | 5030 | 0.052 | 17253. |
| JULIANEHAAB | 60.72 | -46.03 | 0.456 | 77.5 | -34 | 7.82 | -78.7 | 16.0 | 0.434 | -8.08 | -26.32 | 43037 | 0.001 | 123697. |
| JULIUSRUH-RUGEN | 54.63 | 13.38 | 0.411 | 68.8 | -1 | 2.76 | -45.7 | 38.0 | 0.301 | 2.68 | 21.93 | 10804 | 0.015 | 33549. |
| JUNGFRAUJOCH | 46.55 | 7.98 | 0.388 | 62.1 | -4 | 2.00 | -35.4 | 25.5 | 0.274 | 3.08 | 14.86 | 6063 | 0.040 | 19979. |
| KANOYA | 31.42 | 130.89 | 0.378 | 44.3 | -3 | 1.21 | -14.7 | 130.1 | 0.395 | 8.81 | 131.12 | 1766 | 0.176 | 6928. |
| KARACHI | 24.85 | 67.02 | 0.366 | 35.8 | -0 | 1.11 | -8.2 | 69.3 | 0.325 | 7.27 | 67.73 | 1112 | 0.224 | 4498. |

Table B3

Tracings 400 km Above Stations.

| STATIONS | ** O R I G I N ** | | | | | ** CONJUGATE | | INTERS. ** MINIMUM-B | | E Q U A T O R ** | | | ARC |
|---|---|---|---|---|---|---|---|---|---|---|---|---|---|
| | LAT. | LONG. | B | DIP | DECL. | L | LAT. | LONG. | B | LAT. | LONG. | ALT. | B | KM |
| KAZACHIE | 70.70 | 136.40 | 0.487 | 80.6 | -7 | 5.41 | -50.2 | 128.5 | 0.542 | 10.38 | 131.39 | 28506 | 0.002 | 81730. |
| KAP TOBIN | 70.42 | -21.97 | 0.447 | 79.1 | -28 | 11.85 | -72.4 | 59.0 | 0.446 | -2.08 | 6.91 | 68793 | 0.000 | 194713. |
| KAZAN | 55.83 | 48.82 | 0.447 | 71.7 | 10 | 2.67 | -41.5 | 65.1 | 0.368 | 6.49 | 52.04 | 10681 | 0.016 | 32765. |
| KAKICKA | 36.23 | 140.18 | 0.383 | 49.5 | -4 | 1.32 | -19.2 | 138.2 | 0.416 | 9.06 | 140.13 | 2446 | 0.134 | 9151. |
| KAMPALA | 0.33 | 32.58 | 0.277 | -22.3 | -2 | 1.07 | 19.4 | 32.1 | 0.307 | 7.92 | 32.29 | 617 | 0.252 | 2357. |
| KEKAHA | 21.84 | -159.72 | 0.305 | 38.9 | 12 | 1.21 | -20.2 | -168.3 | 0.354 | 2.00 | -163.63 | 1469 | 0.178 | 6114. |
| KHARTOUM | 15.58 | 32.58 | 0.296 | 13.1 | 0 | 1.05 | 4.2 | 32.8 | 0.278 | 8.15 | 32.66 | 472 | 0.271 | 1363. |
| KHABAROVSK | 48.52 | 135.12 | 0.445 | 63.7 | -8 | 1.82 | -30.3 | 132.7 | 0.479 | 9.52 | 135.21 | 5686 | 0.051 | 18502. |
| KHARKOV | 50.00 | 36.23 | 0.420 | 66.1 | 6 | 2.14 | -36.2 | 49.4 | 0.312 | 5.59 | 39.26 | 7139 | 0.032 | 22869. |
| KIEL | 54.30 | 10.10 | 0.409 | 68.6 | -3 | 2.76 | -46.1 | 35.6 | 0.297 | 2.20 | 19.27 | 10769 | 0.015 | 33486. |
| KIRUNA | 67.83 | 20.43 | 0.439 | 77.0 | 1 | 5.75 | -58.5 | 63.1 | 0.404 | 3.50 | 35.00 | 30050 | 0.002 | 87078. |
| KING SALMON | 58.70 | -156.70 | 0.452 | 71.6 | 21 | 3.54 | -49.9 | 171.4 | 0.515 | 3.66 | -172.56 | 16426 | 0.007 | 48749. |
| KIEV | 50.45 | 30.50 | 0.414 | 66.1 | 4 | 2.19 | -37.3 | 45.2 | 0.303 | 4.91 | 34.41 | 7416 | 0.030 | 23719. |
| KINGSTON | 18.00 | -76.80 | 0.367 | 50.3 | 0 | 1.46 | -44.3 | -83.4 | 0.300 | -14.04 | -77.70 | 2782 | 0.098 | 10608. |
| KNOB LAKE | 54.80 | -66.82 | 0.482 | 78.7 | -26 | 6.67 | -82.1 | -67.5 | 0.464 | -11.67 | -58.10 | 35850 | 0.001 | 103550. |
| KOROR ISLAND | 7.16 | 123.48 | 0.322 | -1.6 | 1 | 0.99 | 8.6 | 123.5 | 0.322 | 8.11 | 123.50 | 401 | 0.322 | 171. |
| KOTZEBUE | 66.88 | -162.60 | 0.470 | 76.7 | 21 | 5.49 | -54.6 | 159.9 | 0.539 | 4.95 | 177.46 | 29327 | 0.002 | 84292. |
| KOLN | 50.93 | 6.92 | 0.400 | 66.0 | -4 | 2.41 | -42.2 | 29.5 | 0.282 | 2.04 | 15.52 | 8527 | 0.023 | 27127. |
| KOMURO | 35.98 | 139.62 | 0.383 | 49.2 | -4 | 1.32 | -19.0 | 137.7 | 0.415 | 9.16 | 139.61 | 2406 | 0.137 | 9023. |
| KOKUBUNJI | 35.70 | 139.48 | 0.382 | 48.9 | -4 | 1.31 | -18.7 | 137.6 | 0.414 | 8.97 | 139.47 | 2360 | 0.139 | 8879. |
| KODAIKANAL | 10.23 | 77.48 | 0.325 | 2.6 | -2 | 0.99 | 8.1 | 77.6 | 0.323 | 8.22 | 77.61 | 401 | 0.323 | 252. |
| KUHLUNGSBORN | 54.12 | 11.93 | 0.409 | 68.5 | -2 | 2.71 | -45.4 | 36.5 | 0.298 | 2.69 | 20.57 | 10490 | 0.016 | 32671. |
| KUMASI | 6.67 | -1.58 | 0.255 | -2.6 | -11 | 1.07 | 8.9 | -2.1 | 0.258 | NO MINIMUM B BETWEEN INTERS. | | | | 268. |
| KYOTO | 35.02 | 135.78 | 0.386 | 48.5 | -4 | 1.29 | -18.0 | 134.4 | 0.412 | 9.16 | 135.96 | 2265 | 0.145 | 8556. |
| L'AQUILA | 42.40 | 13.32 | 0.378 | 57.7 | -2 | 1.70 | -28.2 | 25.4 | 0.276 | 4.34 | 18.05 | 4259 | 0.064 | 14617. |
| LA MADDALENA | 41.22 | 9.40 | 0.372 | 56.5 | -3 | 1.65 | -27.3 | 22.0 | 0.274 | 4.17 | 14.58 | 3977 | 0.069 | 13797. |
| LAHORE | 31.55 | 74.33 | 0.403 | 46.6 | 0 | 1.22 | -14.0 | 77.6 | 0.357 | 7.83 | 75.18 | 1853 | 0.168 | 7018. |
| LA PLATA | -34.90 | -57.90 | 0.222 | -33.5 | 0 | 1.28 | 7.9 | -61.6 | 0.302 | -15.67 | -59.02 | 1336 | 0.151 | 5959. |
| LA QUIACA | -22.10 | -65.60 | 0.218 | -15.3 | 1 | 1.14 | -5.1 | -65.9 | 0.249 | -16.77 | -65.59 | 520 | 0.211 | 2064. |
| LA PAZ | -16.48 | -68.05 | 0.224 | -5.6 | 1 | 1.12 | -10.5 | -68.0 | 0.235 | NO MINIMUM B BETWEEN INTERS. | | | | 710. |
| LAE | -6.72 | 147.00 | 0.343 | -28.6 | 5 | 1.09 | 22.6 | 148.8 | 0.314 | 9.01 | 148.24 | 880 | 0.242 | 3796. |
| LA GRAU | 43.10 | 6.00 | 0.377 | 58.7 | -5 | 1.78 | -30.8 | 21.3 | 0.272 | 3.32 | 12.33 | 4723 | 0.056 | 16049. |
| LA HAYE | 52.10 | 4.30 | 0.402 | 67.0 | -5 | 2.57 | -44.7 | 29.4 | 0.285 | 1.47 | 13.94 | 9528 | 0.019 | 30018. |
| LEEDS | 53.80 | -1.55 | 0.406 | 68.5 | -9 | 2.88 | -49.2 | 28.3 | 0.294 | 0.34 | 10.14 | 11491 | 0.013 | 35662. |
| LEICESTER | 52.62 | -1.10 | 0.403 | 67.6 | -8 | 2.72 | -47.4 | 27.0 | 0.287 | 0.68 | 9.96 | 10445 | 0.016 | 32684. |
| LERWICK | 60.13 | -1.18 | 0.420 | 72.7 | -10 | 4.04 | -57.2 | 38.5 | 0.339 | 0.40 | 13.52 | 18908 | 0.005 | 56467. |
| LENINGRAD | 59.95 | 30.70 | 0.433 | 73.0 | 6 | 3.38 | -48.6 | 56.4 | 0.354 | 4.65 | 37.97 | 14955 | 0.008 | 45002. |
| LEIDSCHENDAM | 52.08 | 4.38 | 0.402 | 67.0 | -5 | 2.56 | -44.7 | 29.4 | 0.285 | 1.47 | 13.99 | 9507 | 0.019 | 29957. |
| LEOPOLDVILLE | -4.37 | 15.25 | 0.267 | -32.2 | -9 | 1.13 | 23.7 | 11.5 | 0.306 | 7.48 | 13.41 | 892 | 0.211 | 3700. |
| LINDAU,HARZ | 51.65 | 10.13 | 0.402 | 66.6 | -3 | 2.44 | -42.4 | 32.3 | 0.286 | 2.65 | 18.23 | 8798 | 0.022 | 27867. |
| LISBOA | 38.77 | -9.13 | 0.362 | 55.5 | -10 | 1.68 | -30.3 | 8.9 | 0.260 | 1.11 | -0.82 | 4011 | 0.066 | 14055. |
| LITTLE AMERICA | -78.18 | -162.17 | 0.527 | -80.3 | -80 | 13.93 | ** N O | C O M P U T A T I O N S | | P E R F O R M E D ** | | | | |
| LOGRONO | 42.45 | -2.50 | 0.374 | 58.7 | -8 | 1.82 | -32.7 | 15.6 | 0.266 | 1.83 | 5.46 | 4882 | 0.053 | 16597. |
| LOVOZERO | 67.99 | 35.08 | 0.448 | 77.7 | 9 | 5.41 | -55.6 | 70.5 | 0.418 | 5.52 | 46.07 | 27988 | 0.002 | 81132. |
| LONGYEARBYEN | 78.22 | 15.67 | 0.457 | 81.9 | -5 | 15.29 | ** N O | C O M P U T A T I O N S | | P E R F O R M E D ** | | | | |
| LONDON | 51.53 | 0.10 | 0.400 | 66.7 | -7 | 2.57 | -45.3 | 26.3 | 0.283 | 1.12 | 10.43 | 9491 | 0.019 | 29952. |

Table B3

Tracings 400 km Above Stations.

| STATIONS | ** O R I G I N ** | | | | | | ** CONJUGATE INTERS. ** | | MINIMUM-B | E Q U A T O R ** | | ARC | | |
|---|---|---|---|---|---|---|---|---|---|---|---|---|---|---|
| | LAT. | LONG. | B | DIP | DECL. | L | LAT. | LONG. | B | LAT. | LONG. | ALT. | B | KM |
| LOMNICKY STIT | 49.20 | 20.22 | 0.402 | 64.5 | 0 | 2.13 | -36.8 | 36.2 | 0.287 | 4.12 | 25.46 | 6937 | 0.033 | 22423. |
| LOURENCO MARQUES | -25.97 | 32.60 | 0.283 | -60.6 | -15 | 1.62 | 41.6 | 23.9 | 0.383 | 5.42 | 26.75 | 3881 | 0.073 | 13431. |
| LUND | 55.70 | 13.18 | 0.413 | 69.6 | -1 | 2.90 | -47.2 | 39.3 | 0.307 | 2.69 | 22.21 | 11742 | 0.013 | 36203. |
| LUANDA | -8.82 | 13.22 | 0.267 | -39.5 | -12 | 1.19 | 26.8 | 7.5 | 0.317 | 6.60 | 10.34 | 1216 | 0.182 | 4987. |
| LULEA | 65.60 | 22.12 | 0.436 | 75.9 | 2 | 4.88 | -56.2 | 59.9 | 0.387 | 3.73 | 34.51 | 24493 | 0.003 | 71660. |
| LVOV | 49.82 | 24.02 | 0.406 | 65.2 | 2 | 2.17 | -37.1 | 39.6 | 0.292 | 4.38 | 28.77 | 7177 | 0.031 | 23087. |
| LWIRO | -2.25 | 28.80 | 0.276 | -28.5 | -3 | 1.10 | 22.3 | 27.7 | 0.313 | 8.07 | 28.15 | 772 | 0.232 | 3138. |
| LYCKSELE | 64.62 | 18.67 | 0.433 | 75.3 | 0 | 4.66 | -56.1 | 56.5 | 0.377 | 3.40 | 31.21 | 23063 | 0.003 | 67747. |
| MAKATEA | -16.20 | -148.20 | 0.309 | -26.9 | 12 | 1.11 | 11.4 | -143.0 | 0.287 | -1.66 | -145.33 | 828 | 0.227 | 3598. |
| MANILA | 14.52 | 121.00 | 0.330 | 14.4 | 0 | 1.00 | 1.6 | 120.7 | 0.332 | 8.18 | 120.90 | 498 | 0.309 | 1562. |
| MALVERN | 52.12 | -2.32 | 0.402 | 67.3 | -9 | 2.68 | -47.1 | 25.7 | 0.285 | 0.38 | 8.85 | 10182 | 0.017 | 31953. |
| MAJURO ISLAND | 7.08 | 171.13 | 0.283 | 4.7 | 9 | 1.03 | 2.6 | 170.4 | 0.290 | 6.81 | 171.09 | 402 | 0.283 | 542. |
| MADRID | 40.40 | -3.68 | 0.367 | 56.6 | -8 | 1.71 | -30.2 | 13.3 | 0.265 | 1.88 | 3.98 | 4226 | 0.063 | 14654. |
| MACAO | 22.20 | 113.55 | 0.360 | 29.6 | -0 | 1.05 | -5.0 | 113.1 | 0.356 | 8.55 | 113.47 | 858 | 0.265 | 3522. |
| MADRAS | 13.08 | 80.28 | 0.332 | 8.9 | -2 | 0.99 | 5.7 | 80.7 | 0.325 | 8.50 | 80.52 | 432 | 0.321 | 882. |
| MAWSON | -67.40 | 62.50 | 0.434 | -71.2 | -56 | 9.54 | 71.1 | -4.7 | 0.442 | 0.65 | 20.68 | 54118 | 0.000 | 153955. |
| MACQUARIE ISLAND | -54.30 | 158.60 | 0.540 | -79.1 | 25 | 5.54 | 67.2 | -164.9 | 0.470 | 5.58 | 175.60 | 29192 | 0.002 | 83907. |
| MARION ISLAND | -46.85 | 37.87 | 0.303 | -65.1 | -33 | 2.84 | 55.2 | 11.9 | 0.411 | 2.53 | 21.00 | 11388 | 0.014 | 35217. |
| MAUI,KIHEI | 20.80 | -156.50 | 0.305 | 38.2 | 11 | 1.20 | -20.4 | -164.9 | 0.349 | 1.24 | -160.32 | 1420 | 0.181 | 5939. |
| MCMURDO SOUND | -77.85 | 166.62 | 0.539 | -83.4 | -39 | 36.04 | ** N O C O M P U T A T I O N S P E R F O R M E D ** | | | | | | | |
| MEANCOK | 54.62 | -113.33 | 0.496 | 77.4 | 22 | 4.92 | -63.0 | -157.5 | 0.516 | -5.47 | -128.60 | 25200 | 0.003 | 73181. |
| MEUDON | 48.80 | 2.25 | 0.393 | 64.4 | -6 | 2.25 | -40.5 | 24.4 | 0.275 | 1.81 | 11.11 | 7550 | 0.028 | 24352. |
| MEMAMBETSU | 43.92 | 144.20 | 0.410 | 57.7 | -5 | 1.59 | -26.4 | 140.5 | 0.454 | 9.24 | 143.67 | 4119 | 0.078 | 14129. |
| MEXICO EL CERRILLO | 19.32 | -99.55 | 0.362 | 46.6 | 9 | 1.36 | -35.9 | -110.5 | 0.330 | -9.36 | -103.87 | 2332 | 0.121 | 9040. |
| MELBOURNE | -37.82 | 144.32 | 0.505 | -69.0 | 10 | 2.40 | 55.8 | 153.6 | 0.443 | 8.79 | 150.19 | 9217 | 0.023 | 28536. |
| MIDWAY ISLAND | 6.97 | 158.22 | 0.292 | -0.0 | 6 | 1.02 | 7.0 | 158.2 | 0.291 | 7.01 | 158.22 | 400 | 0.291 | 5. |
| MIEDZESZYN | 52.17 | 21.20 | 0.410 | 67.1 | 1 | 2.40 | -40.7 | 40.1 | 0.297 | 3.99 | 27.19 | 8627 | 0.023 | 27271. |
| MINNEAPOLIS | 44.97 | -93.23 | 0.488 | 73.9 | 6 | 3.47 | -64.7 | -123.4 | 0.473 | -10.63 | -99.59 | 15750 | 0.007 | 47215. |
| MIRNY | -66.57 | 92.92 | 0.498 | -77.9 | -73 | 21.39 | ** N O C O M P U T A T I O N S P E R F O R M E D ** | | | | | | | |
| MINA AGUILAR | -23.10 | -65.70 | 0.218 | -17.0 | 1 | 1.15 | -4.1 | -66.1 | 0.253 | -16.64 | -65.66 | 557 | 0.208 | 2317. |
| MOULD BAY | 76.20 | -119.40 | 0.492 | 87.2 | 59 | 39.08 | ** N O C O M P U T A T I O N S P E R F O R M E D ** | | | | | | | |
| MOSHIRI | 44.37 | 142.27 | 0.415 | 58.4 | -6 | 1.61 | -26.7 | 138.9 | 0.457 | 9.32 | 141.92 | 4255 | 0.075 | 14503. |
| MOCA | 3.35 | 8.67 | 0.260 | -14.4 | -9 | 1.07 | 15.6 | 6.7 | 0.278 | 7.59 | 7.94 | 484 | 0.252 | 1492. |
| MOSCOW | 55.47 | 37.32 | 0.432 | 70.5 | 7 | 2.68 | -42.5 | 55.7 | 0.338 | 5.52 | 41.74 | 10554 | 0.016 | 32561. |
| MOUNT WASHINGTON | 44.27 | -71.30 | 0.472 | 73.6 | -13 | 3.58 | -72.0 | -78.9 | 0.428 | -12.72 | -67.13 | 16225 | 0.007 | 48978. |
| MOUNT NORIKURA | 36.12 | 137.55 | 0.387 | 49.7 | -4 | 1.32 | -19.1 | 135.9 | 0.417 | 9.12 | 137.66 | 2439 | 0.135 | 9107. |
| MONT JOLI | 48.60 | -68.20 | 0.476 | 75.7 | -19 | 4.48 | -76.3 | -71.0 | 0.440 | -12.35 | -61.66 | 21903 | 0.003 | 64845. |
| MURCHISON BAY | 80.05 | 18.30 | 0.461 | 82.8 | -5 | 18.27 | ** N O C O M P U T A T I O N S P E R F O R M E D ** | | | | | | | |
| MURMANSK | 68.97 | 33.08 | 0.448 | 78.1 | 8 | 5.84 | -56.8 | 71.1 | 0.423 | 5.23 | 45.32 | 30757 | 0.002 | 88826. |
| MUNCHEN | 48.13 | 11.70 | 0.394 | 63.5 | -2 | 2.10 | -36.8 | 29.4 | 0.278 | 3.29 | 18.29 | 6668 | 0.035 | 21713. |
| NARSSARSSUAQ | 61.18 | -45.42 | 0.456 | 77.6 | -34 | 8.03 | -78.7 | 18.5 | 0.435 | -7.86 | -25.30 | 44373 | 0.001 | 127397. |
| NARYAN MAR | 67.50 | 53.00 | 0.463 | 78.7 | 15 | 4.95 | -52.1 | 79.7 | 0.441 | 7.53 | 60.09 | 25258 | 0.003 | 73278. |
| NATAL | -5.33 | -35.12 | 0.226 | -2.6 | -17 | 1.12 | -2.8 | -35.9 | 0.231 | NO MINIMUM B BETWEEN INTERS. | | | | 309. |
| NAIROBI | -1.28 | 36.80 | 0.279 | -24.8 | -1 | 1.08 | 20.1 | 36.5 | 0.314 | 7.46 | 36.52 | 676 | 0.247 | 2675. |
| NEUSTRELITZ | 53.28 | -13.08 | 0.408 | 68.9 | -14 | 3.09 | -53.6 | 21.4 | 0.299 | -1.57 | 0.91 | 12739 | 0.011 | 39314. |

Table B3

Tracings 400 km Above Stations.

| STATIONS | ** O R I G I N ** | | | | | | ** CONJUGATE INTERS. ** | | | MINIMUM-B E Q U A T O R ** | | | | ARC |
|---|---|---|---|---|---|---|---|---|---|---|---|---|---|---|
| | LAT. | LONG. | B | DIP | DECL. | L | LAT. | LONG. | B | LAT. | LONG. | ALT. | B | KM |
| NIAMEY | 13.50 | 2.50 | 0.270 | 10.7 | -9 | 1.07 | 4.1 | 4.3 | 0.257 | 6.91 | 3.72 | 446 | 0.253 | 1145. |
| NITSANIM | 31.73 | 34.60 | 0.358 | 44.7 | 2 | 1.27 | -13.9 | 37.0 | 0.285 | 6.76 | 35.10 | 1802 | 0.152 | 6960. |
| NIIGATA | 37.70 | 138.82 | 0.392 | 51.5 | -5 | 1.36 | -20.5 | 136.9 | 0.424 | 9.15 | 138.87 | 2717 | 0.123 | 9962. |
| NICOSIA | 35.17 | 33.28 | 0.370 | 49.5 | 2 | 1.36 | -17.9 | 37.0 | 0.287 | 6.45 | 34.15 | 2366 | 0.122 | 8773. |
| NOUVELLE AMSTERDAM | -37.84 | 77.57 | 0.408 | -67.7 | -32 | 2.44 | 54.2 | 65.6 | 0.466 | 7.93 | 67.49 | 9390 | 0.021 | 28908. |
| NOVOLAZAREVSKAYA | -70.77 | 11.85 | 0.381 | -65.8 | -27 | 5.03 | 56.7 | -37.1 | 0.438 | -6.69 | -18.76 | 25132 | 0.002 | 74103. |
| NORD | 81.60 | -16.67 | 0.464 | 83.8 | -35 | 40.66 | ** N O | C O M P U T A T I O N S | | P E R F O R M E D ** | | | | |
| NORWAY STATION | -70.50 | -2.53 | 0.372 | -64.4 | -18 | 4.28 | 52.6 | -43.2 | 0.440 | -8.22 | -26.99 | 20378 | 0.004 | 60898. |
| NORFOLK ISLAND | -29.00 | 167.60 | 0.435 | -56.4 | 14 | 1.59 | 40.9 | -179.7 | 0.359 | 6.25 | 174.46 | 3921 | 0.080 | 13768. |
| NOUMEA | -22.30 | -166.40 | 0.361 | -41.6 | 14 | 1.24 | 23.4 | -156.9 | 0.313 | 1.46 | -161.27 | 1685 | 0.164 | 6865. |
| NURMIJARVI | 60.50 | 24.65 | 0.429 | 73.1 | 3 | 3.55 | -50.4 | 53.3 | 0.349 | 3.81 | 33.42 | 15984 | 0.007 | 47967. |
| ODESSA | 46.78 | 30.88 | 0.405 | 62.8 | 4 | 1.91 | -32.5 | 42.1 | 0.294 | 5.39 | 33.80 | 5675 | 0.045 | 18683. |
| O'HIGGINS RISOPATR | -63.32 | -57.90 | 0.350 | -57.8 | 12 | 2.37 | 35.3 | -63.6 | 0.433 | -12.74 | -57.43 | 8403 | 0.023 | 27200. |
| OKINAWA | 26.50 | 128.00 | 0.361 | 37.0 | -2 | 1.12 | -10.1 | 127.4 | 0.372 | 8.56 | 128.10 | 1225 | 0.220 | 5050. |
| OLENEK | 68.50 | 112.40 | 0.495 | 81.5 | -4 | 4.75 | -48.1 | 115.6 | 0.528 | 10.63 | 112.38 | 24336 | 0.003 | 70165. |
| ONAGAWA | 38.43 | 141.47 | 0.390 | 52.0 | -5 | 1.39 | -21.3 | 139.0 | 0.427 | 9.23 | 141.33 | 2844 | 0.117 | 10370. |
| OOHIRA | 35.62 | 140.50 | 0.379 | 48.6 | -4 | 1.31 | -18.7 | 138.5 | 0.413 | 9.10 | 140.43 | 2342 | 0.139 | 8833. |
| ORCADAS DEL SUR | -60.73 | -44.73 | 0.319 | -55.8 | 3 | 2.24 | 34.5 | -58.0 | 0.419 | -12.11 | -49.89 | 7490 | 0.028 | 24676. |
| OSLO KJELLER | 59.97 | 11.10 | 0.421 | 72.4 | -3 | 3.67 | -53.1 | 44.5 | 0.336 | 2.12 | 22.70 | 16641 | 0.006 | 49984. |
| OTTAWA | 45.40 | -75.75 | 0.480 | 74.7 | -10 | 3.82 | -72.1 | -91.5 | 0.446 | -12.54 | -73.76 | 17824 | 0.005 | 53331. |
| OULU | 65.00 | 25.52 | 0.437 | 75.7 | 4 | 4.62 | -54.8 | 60.7 | 0.385 | 4.28 | 36.65 | 22835 | 0.003 | 67008. |
| PALESTINE | 31.77 | -95.63 | 0.435 | 62.0 | 8 | 1.93 | -50.8 | -114.3 | 0.404 | -10.37 | -101.20 | 5994 | 0.042 | 19848. |
| PANSKA VES | 50.53 | 14.57 | 0.402 | 65.6 | -1 | 2.29 | -39.7 | 33.8 | 0.285 | 3.40 | 21.32 | 7864 | 0.027 | 25146. |
| PARIS-SACLAY | 48.12 | 2.33 | 0.391 | 63.8 | -6 | 2.19 | -39.4 | 23.7 | 0.273 | 1.94 | 10.94 | 7164 | 0.031 | 23234. |
| PARIS-BAGNEUX | 48.80 | 2.32 | 0.393 | 64.4 | -6 | 2.25 | -40.5 | 24.4 | 0.275 | 1.82 | 11.16 | 7545 | 0.028 | 24337. |
| PANAGURITSCH | 42.52 | 24.18 | 0.386 | 58.0 | 1 | 1.67 | -27.2 | 33.4 | 0.283 | 5.38 | 27.11 | 4154 | 0.067 | 14242. |
| PARAMARIBO | 5.82 | -55.22 | 0.283 | 31.2 | -10 | 1.24 | -29.4 | -48.7 | 0.209 | -14.76 | -51.42 | 1026 | 0.167 | 4735. |
| PETROPAVLOVSK-ON-K | 52.98 | 158.65 | 0.426 | 64.8 | -2 | 2.15 | -35.7 | 148.6 | 0.492 | 8.66 | 154.87 | 7651 | 0.032 | 24223. |
| PEARCE | -31.67 | 115.97 | 0.482 | -66.1 | -2 | 1.97 | 50.3 | 114.6 | 0.479 | 9.83 | 115.54 | 6704 | 0.040 | 21195. |
| PIC DU MIDI | 42.93 | 0.25 | 0.376 | 58.9 | -7 | 1.82 | -32.4 | 17.6 | 0.268 | 2.33 | 7.75 | 4916 | 0.052 | 16672. |
| PILAR | -31.67 | -63.88 | 0.223 | -29.4 | 3 | 1.22 | 4.1 | -65.1 | 0.287 | -16.19 | -63.84 | 1035 | 0.171 | 4746. |
| PIWNICE -TORUN | 50.52 | 14.57 | 0.402 | 65.6 | -1 | 2.29 | -39.7 | 33.8 | 0.285 | 3.39 | 21.32 | 7857 | 0.027 | 25123. |
| PLAISANCE | -20.43 | 57.67 | 0.317 | -53.2 | -14 | 1.40 | 36.3 | 53.4 | 0.401 | 6.68 | 53.97 | 2730 | 0.114 | 9849. |
| POSADAS | -27.42 | -56.10 | 0.211 | -24.5 | -3 | 1.19 | 1.4 | -59.5 | 0.269 | -16.08 | -57.27 | 793 | 0.184 | 3690. |
| PONZA | 40.92 | 12.95 | 0.372 | 56.0 | -2 | 1.62 | -26.1 | 24.1 | 0.276 | 4.63 | 17.40 | 3802 | 0.073 | 13247. |
| PONTA DELGADO | 37.77 | -25.65 | 0.371 | 57.7 | -16 | 1.86 | -39.1 | -1.8 | 0.250 | -3.39 | -14.58 | 4963 | 0.050 | 17097. |
| POTCHEFSTROOM | -26.68 | 27.08 | 0.278 | -61.3 | -17 | 1.64 | 41.7 | 16.4 | 0.377 | 4.92 | 20.43 | 3969 | 0.070 | 13729. |
| POINT BARROW | 71.33 | -156.77 | 0.481 | 80.3 | 28 | 8.59 | -59.1 | 156.1 | 0.549 | 5.17 | 176.93 | 48874 | 0.000 | 138197. |
| POTSDAM | 52.38 | 13.07 | 0.405 | 67.1 | -1 | 2.49 | -42.7 | 35.0 | 0.290 | 2.88 | 20.81 | 9123 | 0.021 | 28769. |
| POITIERS | 46.57 | 0.35 | 0.387 | 62.5 | -7 | 2.08 | -37.8 | 21.0 | 0.270 | 1.54 | 8.95 | 6487 | 0.035 | 21293. |
| PORT ARTHUR | 30.00 | -94.00 | 0.427 | 60.5 | 7 | 1.84 | -49.7 | -111.2 | 0.392 | -10.56 | -99.05 | 5402 | 0.048 | 18166. |
| POONA | 18.05 | 73.12 | 0.342 | 21.4 | -1 | 1.03 | -0.4 | 74.4 | 0.322 | 7.72 | 73.68 | 614 | 0.287 | 2292. |
| PORO POINT | 16.62 | 120.28 | 0.336 | 18.8 | 0 | 1.01 | -0.4 | 119.9 | 0.337 | 8.18 | 120.17 | 570 | 0.299 | 2082. |
| PORT AUX FRANCAIS | -49.35 | 70.27 | 0.402 | -69.2 | -45 | 3.89 | 63.2 | 45.6 | 0.452 | 6.46 | 51.77 | 18405 | 0.005 | 54385. |
| PORT STANLEY | -51.70 | -57.85 | 0.283 | -48.9 | 7 | 1.69 | 23.8 | -63.0 | 0.383 | -13.83 | -58.43 | 4014 | 0.065 | 14550. |

Table B3

Tracings 400 km Above Stations.

| STATIONS | ** | O | R | I | G | I | N | ** CONJUGATE | INTERS. | ** MINIMUM-B | E Q U A T O R | | ** ARC | |
|---|---|---|---|---|---|---|---|---|---|---|---|---|---|---|
| | | LAT. | LONG. | B | DIP | DECL. | L | LAT. | LONG. | B | LAT. | LONG. | ALT. | B | KM |
| PORT MORESBY | | -9.20 | 147.15 | 0.355 | -32.9 | 6 | 1.12 | 25.1 | 149.3 | 0.321 | 8.91 | 148.67 | 1074 | 0.223 | 4606. |
| PROVIDENIE BAY | | 64.38 | 186.60 | 0.459 | 74.1 | 13 | 4.23 | -50.3 | 157.7 | 0.531 | 6.36 | 171.62 | 20886 | 0.004 | 60975. |
| PRAHA | | 50.07 | 14.43 | 0.400 | 65.2 | -1 | 2.25 | -39.1 | 33.2 | 0.284 | 3.20 | 21.10 | 7600 | 0.028 | 24391. |
| PRUHONICE | | 49.98 | 14.55 | 0.400 | 65.1 | -1 | 2.24 | -38.9 | 33.2 | 0.284 | 3.18 | 21.17 | 7544 | 0.029 | 24227. |
| PRETORIA | | -26.80 | 28.20 | 0.279 | -61.3 | -17 | 1.65 | 41.9 | 17.8 | 0.379 | 4.84 | 21.64 | 4011 | 0.069 | 13853. |
| PRINCE ALBERT | | 53.20 | -105.70 | 0.500 | 77.9 | 17 | 4.99 | -65.5 | -149.1 | 0.511 | -7.44 | -118.43 | 25558 | 0.002 | 74249. |
| PULLMANN | | 46.72 | -117.17 | 0.473 | 70.9 | 19 | 2.99 | -55.3 | -149.6 | 0.485 | -5.12 | -129.57 | 12874 | 0.011 | 39013. |
| PUNTA ARENAS | | -53.15 | -70.90 | 0.313 | -51.4 | 16 | 1.74 | 24.7 | -69.2 | 0.397 | -14.04 | -66.86 | 4436 | 0.059 | 15710. |
| PYONGYANG | | 39.07 | 125.78 | 0.423 | 55.0 | -5 | 1.41 | -21.6 | 125.2 | 0.435 | 9.35 | 126.33 | 3067 | 0.111 | 10891. |
| QUETTA | | 30.18 | 66.95 | 0.390 | 44.9 | 0 | 1.21 | -13.5 | 70.2 | 0.337 | 7.19 | 67.73 | 1709 | 0.174 | 6578. |
| QUEEN MAUD LAND | | -70.50 | -1.00 | 0.372 | -64.5 | -19 | 4.34 | 53.0 | -42.5 | 0.439 | -8.13 | -26.09 | 20775 | 0.004 | 62005. |
| QUENTONCITY | | 19.00 | 121.00 | 0.342 | 23.6 | 0 | 1.03 | -2.7 | 120.6 | 0.344 | 8.33 | 120.91 | 681 | 0.284 | 2719. |
| QUEBEC | | 46.92 | -71.08 | 0.477 | 75.2 | -16 | 4.12 | -74.5 | -79.6 | 0.441 | -12.54 | -66.38 | 19657 | 0.004 | 58537. |
| QUILCN | | 8.50 | 76.00 | 0.322 | -1.3 | -3 | 0.99 | 9.6 | 75.9 | 0.323 | NO MINIMUM B BETWEEN INTERS. | | | | 127. |
| RABAT | | 34.02 | -6.85 | 0.344 | 49.4 | -9 | 1.45 | -22.8 | 7.0 | 0.261 | 2.59 | -0.25 | 2674 | 0.101 | 9931. |
| RAMEY AFB | | 18.50 | -67.20 | 0.363 | 51.1 | -6 | 1.51 | -46.8 | -66.9 | 0.275 | -14.71 | -64.94 | 2928 | 0.090 | 11207. |
| RAROTONGA | | -21.20 | -159.75 | 0.346 | -38.2 | 13 | 1.20 | 20.0 | -151.4 | 0.307 | 0.29 | -155.17 | 1417 | 0.181 | 5932. |
| RESOLUTE | | 74.68 | -94.92 | 0.492 | 89.2 | -36 | 96.91 | ** N O | C O M P U T A T I O N S | | P E R F O R M E D ** | | | | |
| REYKJAVIK | | 64.18 | -21.70 | 0.436 | 76.1 | -24 | 6.75 | -69.2 | 39.0 | 0.400 | -3.35 | 0.35 | 36209 | 0.001 | 104697. |
| REGENSBERG | | 47.48 | 8.45 | 0.391 | 63.0 | -3 | 2.07 | -36.7 | 26.7 | 0.276 | 2.75 | 15.56 | 6484 | 0.036 | 21209. |
| RIO DE JANEIRO | | -22.90 | -43.22 | 0.207 | -24.4 | -14 | 1.19 | 3.6 | -49.8 | 0.265 | -13.23 | -45.76 | 747 | 0.186 | 3446. |
| RIO GALLEGOS | | -51.63 | -69.22 | 0.302 | -49.9 | 14 | 1.67 | 23.2 | -68.4 | 0.388 | -14.23 | -65.95 | 4004 | 0.066 | 14447. |
| ROYAL ROADS | | 48.50 | -123.50 | 0.470 | 70.9 | 21 | 3.05 | -54.0 | -156.7 | 0.490 | -3.77 | -137.13 | 13241 | 0.011 | 40013. |
| ROMA | | 41.88 | 12.50 | 0.375 | 57.1 | -2 | 1.67 | -27.6 | 24.5 | 0.276 | 4.38 | 17.26 | 4108 | 0.067 | 14171. |
| ROSTOV/DON | | 47.23 | 39.65 | 0.417 | 64.0 | 6 | 1.93 | -32.7 | 50.0 | 0.310 | 5.99 | 41.73 | 5861 | 0.044 | 19160. |
| SANTA CRUZ | | -17.80 | -63.17 | 0.218 | -7.9 | -1 | 1.13 | -9.2 | -63.6 | 0.234 | -17.13 | -63.19 | 410 | 0.218 | 1026. |
| SAN FERNANDO | | 36.47 | -6.20 | 0.353 | 52.4 | -9 | 1.54 | -25.7 | 9.0 | 0.262 | 2.25 | 0.90 | 3216 | 0.085 | 11609. |
| SANTA CRUZ | | 28.33 | -16.25 | 0.325 | 44.0 | -12 | 1.35 | -20.5 | -2.5 | 0.248 | 0.92 | -9.38 | 1999 | 0.125 | 7857. |
| SANTIAGO | | -33.57 | -70.72 | 0.238 | -32.6 | 8 | 1.24 | 6.1 | -69.6 | 0.301 | -15.56 | -69.32 | 1216 | 0.164 | 5418. |
| SALEKHARD | | 66.58 | 66.67 | 0.475 | 79.4 | 16 | 4.55 | -49.5 | 87.0 | 0.461 | 3.49 | 71.41 | 22806 | 0.003 | 66275. |
| SASKATOON | | 52.13 | -106.67 | 0.498 | 77.0 | 17 | 4.59 | -64.2 | -148.2 | 0.508 | -7.53 | -119.31 | 23032 | 0.003 | 67246. |
| SAPPORO | | 43.02 | 121.35 | 0.447 | 60.1 | -5 | 1.56 | -25.1 | 121.3 | 0.454 | 9.48 | 122.07 | 4048 | 0.081 | 13713. |
| SACRAMENTO PEAK | | 32.72 | -105.75 | 0.429 | 60.8 | 12 | 1.87 | -47.4 | -125.5 | 0.413 | -8.18 | -112.89 | 5645 | 0.047 | 18798. |
| SAN JUAN | | 18.43 | -66.00 | 0.361 | 50.8 | -6 | 1.51 | -46.7 | -64.5 | 0.270 | -14.56 | -63.33 | 2899 | 0.091 | 11132. |
| SAN JULIAN | | -49.32 | -67.78 | 0.288 | -47.8 | 13 | 1.59 | 20.9 | -67.7 | 0.376 | -14.45 | -65.27 | 3443 | 0.077 | 12776. |
| SAO PAULO | | -23.55 | -46.63 | 0.206 | -23.2 | -11 | 1.18 | 2.0 | -52.3 | 0.263 | -14.27 | -48.74 | 715 | 0.188 | 3293. |
| SAO JOSE DOS CAMPO | | -23.00 | -46.00 | 0.206 | -22.8 | -12 | 1.18 | 2.0 | -51.7 | 0.261 | -14.21 | -48.08 | 697 | 0.189 | 3208. |
| SALISBURY RHOD-NYA | | -17.83 | 31.00 | 0.283 | -53.3 | -10 | 1.37 | 35.4 | 26.2 | 0.363 | 6.32 | 27.75 | 2382 | 0.120 | 8839. |
| SCHWARZENBURG | | 46.83 | 7.33 | 0.389 | 62.4 | -4 | 2.03 | -36.0 | 25.4 | 0.274 | 2.77 | 14.46 | 6223 | 0.038 | 20455. |
| SCOTT BASE | | -77.85 | 166.75 | 0.539 | -83.4 | -39 | 36.13 | ** N O | C O M P U T A T I O N S | | P E R F O R M E D ** | | | | |
| SENDAI | | 38.10 | 140.55 | 0.390 | 51.7 | -5 | 1.38 | -20.9 | 138.3 | 0.426 | 9.07 | 140.47 | 2785 | 0.120 | 10182. |
| SEOUL | | 37.58 | 127.05 | 0.414 | 53.0 | -5 | 1.36 | -20.2 | 126.4 | 0.427 | 9.11 | 127.54 | 2760 | 0.123 | 9988. |
| SEATTLE | | 47.75 | -122.42 | 0.469 | 70.6 | 21 | 2.98 | -53.9 | -155.0 | 0.488 | -3.85 | -135.63 | 12767 | 0.012 | 38698. |
| SEMIPALATINSK | | 50.40 | 80.25 | 0.476 | 69.3 | 4 | 2.05 | -32.7 | 87.9 | 0.433 | 8.82 | 81.51 | 7121 | 0.035 | 22371. |
| SEAGROVE | | -37.08 | 174.78 | 0.462 | -63.0 | 17 | 1.96 | 46.1 | -166.1 | 0.392 | 4.52 | -175.32 | 6280 | 0.042 | 20542. |

Table B3

Tracings 400 km Above Stations.

| STATIONS | ** GEOG. LAT. | GEOG. LONG. | INVAR. B | INVAR. DIP | INVAR. DECL. | INVAR. L | ** CONJUGATE LAT. | CONJUGATE LONG. | CONJUGATE B | MINIMUM-B EQUATOR LAT. | MINIMUM-B EQUATOR LONG. | MINIMUM-B EQUATOR ALT. | MINIMUM-B EQUATOR B | ARC KM |
|---|---|---|---|---|---|---|---|---|---|---|---|---|---|---|
| SHEPHERD BAY | 68.75 | -93.75 | 0.499 | 87.4 | -5 | 29.92 | ** NO COMPUTATIONS PERFORMED ** | | | | | | | |
| SHIRAZ | 29.63 | 52.52 | 0.373 | 43.8 | 2 | 1.22 | -13.6 | 54.8 | 0.304 | 6.47 | 52.84 | 1652 | 0.169 | 6443. |
| SHACKLETON | -77.98 | -37.17 | 0.426 | -67.6 | 4 | 5.06 | 51.9 | -58.9 | 0.466 | -10.87 | -47.15 | 25505 | 0.002 | 75019. |
| SHEFFIELD | 53.43 | 1.35 | 0.405 | 68.1 | -7 | 2.78 | -47.6 | 29.4 | 0.291 | 0.89 | 12.20 | 10843 | 0.015 | 33792. |
| SIMOSATO | 33.58 | 135.94 | 0.379 | 46.6 | -4 | 1.26 | -16.7 | 134.6 | 0.404 | 9.04 | 136.09 | 2043 | 0.157 | 7862. |
| SIDMOUTH | 50.68 | 3.22 | 0.398 | 65.9 | -6 | 2.43 | -43.0 | 27.0 | 0.280 | 1.53 | 12.56 | 8633 | 0.023 | 27465. |
| SITKA | 57.05 | -135.33 | 0.475 | 74.3 | 27 | 4.16 | -55.8 | -175.0 | 0.517 | -0.37 | -153.25 | 20399 | 0.004 | 59790. |
| SIMFEROPOL | 44.83 | 34.07 | 0.404 | 61.2 | 4 | 1.78 | -29.9 | 43.2 | 0.295 | 5.75 | 36.22 | 4921 | 0.055 | 16459. |
| SINGAPORE | 1.32 | 103.82 | 0.340 | -18.1 | 1 | 1.00 | 17.1 | 104.0 | 0.347 | 8.90 | 103.92 | 554 | 0.309 | 1931. |
| SLOUGH | 51.48 | -0.57 | 0.400 | 66.7 | -8 | 2.57 | -45.5 | 25.8 | 0.282 | 1.02 | 9.89 | 9520 | 0.019 | 30040. |
| SODANKYLA | 67.37 | 26.65 | 0.442 | 77.0 | 4 | 5.38 | -56.7 | 65.2 | 0.405 | 4.41 | 39.21 | 27723 | 0.002 | 80535. |
| SOUTH POLE | -90.00 | 0. | 0.494 | -75.8 | -29 | 14.88 | ** NO COMPUTATIONS PERFORMED ** | | | | | | | |
| SREDNIKAN | 62.43 | 152.32 | 0.465 | 73.2 | -5 | 3.27 | -43.7 | 140.9 | 0.527 | 9.20 | 147.33 | 14858 | 0.009 | 44137. |
| ST. STEPHEN | 67.20 | -45.20 | 0.461 | 80.1 | -40 | 14.17 | ** NO COMPUTATIONS PERFORMED ** | | | | | | | |
| STELLENBOSCH | -33.94 | 18.85 | 0.269 | -63.7 | -24 | 1.89 | 44.1 | 0.7 | 0.379 | 2.08 | 8.43 | 5346 | 0.047 | 17943. |
| STOCKHOLM | 59.30 | 18.10 | 0.423 | 72.1 | 0 | 3.42 | -50.5 | 47.5 | 0.334 | 3.05 | 27.71 | 15058 | 0.008 | 45464. |
| STONYHURST | 53.51 | -2.47 | 0.405 | 68.4 | -9 | 2.86 | -49.2 | 27.4 | 0.292 | 0.51 | 9.25 | 11351 | 0.014 | 35269. |
| ST. LAWRENCE | 50.58 | 1.23 | 0.398 | 65.9 | -7 | 2.45 | -43.5 | 25.8 | 0.279 | 1.27 | 10.98 | 8729 | 0.022 | 27760. |
| STANLEY | -51.70 | -57.85 | 0.283 | -48.9 | 7 | 1.69 | 23.8 | -63.0 | 0.383 | -13.83 | -58.43 | 4014 | 0.065 | 14550. |
| ST. SANTIN-DE-MAUR | 44.60 | 20.20 | 0.389 | 60.1 | 0 | 1.80 | -30.3 | 32.0 | 0.281 | 4.74 | 24.22 | 4907 | 0.054 | 16499. |
| ST. MICHEL | 43.92 | 5.72 | 0.379 | 59.6 | -5 | 1.84 | -32.1 | 21.8 | 0.272 | 2.96 | 12.36 | 5042 | 0.051 | 17000. |
| STANFORD | 37.43 | -122.17 | 0.428 | 62.0 | 16 | 1.97 | -45.3 | -144.5 | 0.438 | -4.39 | -131.52 | 6303 | 0.040 | 20630. |
| ST. JOHNS | 47.52 | -52.78 | 0.447 | 71.9 | -24 | 3.68 | -71.2 | -25.9 | 0.376 | -10.48 | -40.14 | 16634 | 0.006 | 50425. |
| SUKKERTOPPEN | 65.42 | -52.90 | 0.469 | 80.5 | -41 | 13.98 | ** NO COMPUTATIONS PERFORMED ** | | | | | | | |
| SULPHUR MOUNTAIN | 51.10 | -115.60 | 0.487 | 74.5 | 21 | 3.84 | -59.4 | -153.9 | 0.503 | -5.36 | -129.64 | 18292 | 0.005 | 54048. |
| SØRLARI | 44.68 | 26.25 | 0.395 | 60.4 | 2 | 1.79 | -30.0 | 36.6 | 0.286 | 5.16 | 29.35 | 4877 | 0.055 | 16377. |
| SVERDLOVSK | 56.73 | 61.07 | 0.464 | 73.3 | 10 | 2.74 | -40.9 | 75.6 | 0.405 | 7.71 | 63.58 | 11245 | 0.015 | 34175. |
| SWANSEA | 51.63 | -4.00 | 0.401 | 67.0 | -9 | 2.65 | -47.1 | 24.1 | 0.283 | 0.37 | 7.31 | 9994 | 0.017 | 31430. |
| SWARTHMORE | 39.90 | -75.35 | 0.465 | 71.0 | -7 | 2.92 | -67.1 | -87.2 | 0.418 | -12.78 | -73.76 | 12069 | 0.012 | 37282. |
| SYDNEY | -33.60 | 151.10 | 0.480 | -64.1 | 11 | 1.97 | 50.3 | 161.0 | 0.412 | 8.29 | 157.23 | 6428 | 0.042 | 20819. |
| SYKTYVKAR | 61.70 | 50.80 | 0.456 | 75.5 | 12 | 3.55 | -47.1 | 72.1 | 0.404 | 7.01 | 55.62 | 16251 | 0.007 | 48308. |
| SYOWA BASE | -69.03 | 39.60 | 0.400 | -68.1 | -43 | 6.76 | 64.3 | -21.1 | 0.436 | -2.89 | 0.94 | 36261 | 0.001 | 104833. |
| TAMALE | 9.42 | -0.89 | 0.260 | 3.1 | -11 | 1.07 | 6.7 | -0.3 | 0.256 | NO MINIMUM B BETWEEN INTERS. | | | | 332. |
| TASHKENT | 41.42 | 69.20 | 0.439 | 60.0 | 3 | 1.56 | -24.6 | 75.1 | 0.375 | 7.81 | 70.13 | 3902 | 0.081 | 13236. |
| TAMANRASSET | 22.80 | 5.52 | 0.301 | 29.0 | -6 | 1.13 | -4.7 | 10.2 | 0.262 | 6.84 | 7.96 | 871 | 0.210 | 3625. |
| TAIPEI | 25.03 | 121.52 | 0.364 | 34.9 | -1 | 1.10 | -8.5 | 121.0 | 0.367 | 8.54 | 121.55 | 1094 | 0.236 | 4521. |
| TALARA | -4.57 | -81.25 | 0.259 | 13.5 | 6 | 1.10 | -18.3 | -83.0 | 0.239 | -13.51 | -82.26 | 489 | 0.232 | 1666. |
| TANANARIVE | -18.92 | 47.55 | 0.297 | -52.2 | -10 | 1.37 | 35.2 | 44.2 | 0.384 | 6.48 | 44.57 | 2466 | 0.121 | 9065. |
| TAHITI | -17.48 | -149.48 | 0.315 | -29.5 | 12 | 1.13 | 13.1 | -143.7 | 0.291 | -1.38 | -146.25 | 930 | 0.218 | 4053. |
| TBILISI | 41.72 | 44.82 | 0.408 | 58.9 | 5 | 1.62 | -26.2 | 51.2 | 0.308 | 6.45 | 45.78 | 3984 | 0.074 | 13645. |
| TENIENTE MATIENZO | -64.97 | -60.05 | 0.363 | -59.2 | 14 | 2.52 | 36.8 | -64.5 | 0.440 | -12.82 | -58.47 | 9362 | 0.019 | 29898. |
| TEHRAN | 35.68 | 51.42 | 0.396 | 52.3 | 4 | 1.38 | -19.8 | 55.3 | 0.311 | 6.65 | 51.89 | 2608 | 0.118 | 9482. |
| TENERIFE | 28.00 | -17.00 | 0.324 | 43.7 | -12 | 1.35 | -20.6 | -3.2 | 0.247 | 0.61 | -10.06 | 1975 | 0.126 | 7792. |
| TEOLOYUCAN | 19.75 | -99.18 | 0.365 | 47.3 | 9 | 1.38 | -36.5 | -110.4 | 0.332 | -9.36 | -103.53 | 2421 | 0.117 | 9319. |
| THULE | 76.55 | -68.83 | 0.480 | 86.0 | -70 | 192.86 | ** NO COMPUTATIONS PERFORMED ** | | | | | | | |
| THE PAS | 53.80 | -101.30 | 0.503 | 79.0 | 13 | 5.51 | -68.0 | -146.2 | 0.512 | -8.54 | -112.75 | 28834 | 0.002 | 83372. |

Table B3

Tracings 400 km Above Stations.

| STATIONS | ** O | R | I | G | I | N | ** CONJUGATE | INTERS. | ** MINIMUM-B | E Q U A T O R | ** ARC | | |
|---|---|---|---|---|---|---|---|---|---|---|---|---|---|
| | LAT. | LONG. | B | DIP | DECL. | L | LAT. | LONG. | B | LAT. | LONG. | ALT. | B | KM |
| TIHANY | 46.89 | 17.89 | 0.394 | 62.4 | -0 | 1.96 | -33.9 | 32.3 | 0.281 | 4.11 | 22.91 | 5883 | 0.042 | 19380. |
| TIXIE BAY | 71.55 | 128.90 | 0.490 | 81.8 | -7 | 5.75 | -50.7 | 124.4 | 0.541 | 10.77 | 125.17 | 30679 | 0.002 | 87712. |
| TIRUCHIRAPALLI | 10.83 | 78.83 | 0.327 | 3.7 | -2 | 0.99 | 7.7 | 79.0 | 0.324 | 8.38 | 78.98 | 404 | 0.324 | 369. |
| TORINO | 45.20 | 7.65 | 0.384 | 60.8 | -4 | 1.91 | -33.5 | 24.1 | 0.273 | 3.24 | 14.21 | 5481 | 0.046 | 18277. |
| TOTTORI | 35.53 | 134.22 | 0.391 | 49.4 | -4 | 1.30 | -18.5 | 133.0 | 0.415 | 9.10 | 134.47 | 2356 | 0.140 | 8824. |
| TORUN | 53.08 | 18.55 | 0.410 | 67.7 | 0 | 2.52 | -42.5 | 39.4 | 0.298 | 3.36 | 25.42 | 9339 | 0.020 | 29332. |
| TOMSK | 56.47 | 84.93 | 0.489 | 74.5 | 5 | 2.62 | -38.3 | 93.9 | 0.463 | 9.16 | 86.55 | 10711 | 0.017 | 32421. |
| TORRE CHIARUCCIA | 42.03 | 11.83 | 0.376 | 57.3 | -2 | 1.68 | -27.9 | 24.2 | 0.276 | 4.09 | 16.78 | 4171 | 0.065 | 14367. |
| TORTOSA | 40.82 | 0.50 | 0.368 | 56.6 | -7 | 1.69 | -29.2 | 16.1 | 0.268 | 2.83 | 7.36 | 4165 | 0.064 | 14427. |
| TOLEDO | 39.88 | -4.05 | 0.365 | 56.1 | -8 | 1.68 | -29.6 | 12.7 | 0.265 | 1.94 | 3.54 | 4078 | 0.065 | 14212. |
| TOYOKAWA | 35.83 | 137.37 | 0.386 | 49.4 | -4 | 1.31 | -18.8 | 135.8 | 0.415 | 9.16 | 137.49 | 2391 | 0.138 | 8957. |
| TONANZINTLA | 19.03 | -98.30 | 0.362 | 46.6 | 9 | 1.36 | -36.1 | -109.1 | 0.327 | -9.43 | -102.49 | 2321 | 0.121 | 9005. |
| TOWNSVILLE | -19.10 | 146.50 | 0.409 | -48.1 | 7 | 1.32 | 35.7 | 150.2 | 0.361 | 8.80 | 149.24 | 2337 | 0.137 | 8892. |
| TRUJILLO | -8.10 | -79.03 | 0.248 | 7.5 | 5 | 1.10 | -15.7 | -79.9 | 0.237 | -14.19 | -79.68 | 419 | 0.236 | 914. |
| TROMSO | 69.67 | 18.95 | 0.442 | 77.9 | 0 | 6.66 | -60.3 | 66.1 | 0.419 | 3.56 | 35.58 | 35923 | 0.001 | 103338. |
| TRELEW | -43.20 | -65.30 | 0.257 | -42.1 | 9 | 1.42 | 15.0 | -66.3 | 0.344 | -15.03 | -64.19 | 2307 | 0.110 | 9258. |
| TRIVANDRUM | 8.42 | 76.95 | 0.323 | -1.7 | -3 | 0.99 | 9.8 | 76.9 | 0.324 | NO MINIMUM B BETWEEN INTERS. | | | | 165. |
| TRINIDAD | 10.60 | -61.20 | 0.315 | 40.2 | -8 | 1.33 | -37.6 | -56.6 | 0.227 | -15.28 | -58.07 | 1621 | 0.136 | 6996. |
| TSCHCIBALSAN | 48.07 | 114.50 | 0.473 | 66.1 | -5 | 1.82 | -29.6 | 115.7 | 0.473 | 9.63 | 115.42 | 5759 | 0.051 | 18531. |
| TSUMEB | -19.23 | 17.72 | 0.273 | -54.4 | -15 | 1.40 | 35.3 | 8.5 | 0.350 | 5.28 | 12.59 | 2484 | 0.111 | 9223. |
| TUBINGEN | 48.53 | 9.07 | 0.394 | 63.9 | -3 | 2.16 | -38.1 | 28.1 | 0.277 | 2.83 | 16.35 | 6993 | 0.032 | 22681. |
| TUCSON | 32.23 | -110.95 | 0.420 | 59.2 | 13 | 1.78 | -44.9 | -130.0 | 0.410 | -6.87 | -118.33 | 5105 | 0.054 | 17240. |
| TUCSON | 32.23 | -110.95 | 0.420 | 59.2 | 13 | 1.78 | -44.9 | -130.0 | 0.410 | -6.87 | -118.33 | 5105 | 0.054 | 17240. |
| TUCUMAN | -26.90 | -65.40 | 0.219 | -22.9 | 2 | 1.17 | -0.5 | -66.0 | 0.267 | -16.47 | -65.29 | 729 | 0.194 | 3328. |
| UJI | 34.90 | 135.78 | 0.385 | 48.4 | -4 | 1.29 | -17.9 | 134.4 | 0.411 | 9.08 | 135.96 | 2246 | 0.146 | 8496. |
| ULAN BATOR | 47.78 | 106.75 | 0.477 | 66.4 | -3 | 1.82 | -29.3 | 109.1 | 0.466 | 9.54 | 107.73 | 5718 | 0.051 | 18375. |
| UNALASKA | 53.88 | -166.53 | 0.425 | 66.7 | 15 | 2.59 | -43.2 | 169.7 | 0.495 | 4.94 | -178.16 | 10334 | 0.018 | 31868. |
| UNIVERSITY PARK | 40.80 | -77.77 | 0.470 | 71.7 | -6 | 3.03 | -67.2 | -93.1 | 0.429 | -12.60 | -77.25 | 12826 | 0.011 | 39348. |
| UPPSALA | 59.80 | 17.60 | 0.423 | 72.4 | 0 | 3.52 | -51.2 | 48.0 | 0.338 | 3.16 | 27.54 | 15707 | 0.007 | 47286. |
| USHUAIA | -54.80 | -68.30 | 0.317 | -52.3 | 15 | 1.81 | 26.3 | -67.9 | 0.403 | -13.88 | -64.88 | 4883 | 0.052 | 17041. |
| UTSJOKI | 69.75 | 27.03 | 0.446 | 78.2 | 4 | 6.38 | -58.6 | 69.6 | 0.424 | 4.86 | 41.45 | 34141 | 0.001 | 98283. |
| VALENTIA | 51.94 | -10.25 | 0.403 | 67.7 | -13 | 2.82 | -50.3 | 21.2 | 0.288 | -0.98 | 2.60 | 11053 | 0.014 | 34513. |
| VERKHOYANSK | 67.60 | 133.40 | 0.487 | 79.0 | -9 | 4.40 | -47.3 | 127.9 | 0.537 | 10.46 | 130.33 | 22081 | 0.004 | 63971. |
| VAL D'OR | 48.00 | -77.80 | 0.487 | 76.5 | -10 | 4.43 | -73.9 | -99.2 | 0.463 | -12.32 | -76.67 | 21705 | 0.004 | 64072. |
| VICTORIA | 48.40 | -123.40 | 0.469 | 70.9 | 21 | 3.04 | -54.0 | -156.5 | 0.490 | -3.83 | -136.98 | 13167 | 0.011 | 39809. |
| VLADIVOSTOK | 43.78 | 132.03 | 0.432 | 59.4 | -7 | 1.58 | -25.9 | 130.6 | 0.457 | 9.50 | 132.45 | 4168 | 0.078 | 14155. |
| VOSTOK | -76.48 | 106.50 | 0.518 | -80.3 | 70 | 123.06 | ** N O | C O M P U T A T I O N S | | P E R F O R M E D | ** | | | |
| WATHEROO | -30.32 | 115.88 | 0.477 | -64.8 | -2 | 1.87 | 48.9 | 114.6 | 0.475 | 9.70 | 115.56 | 6075 | 0.047 | 19425. |
| WAKKANAI | 45.40 | 141.68 | 0.421 | 59.6 | -6 | 1.66 | -27.6 | 138.3 | 0.463 | 9.35 | 141.34 | 4564 | 0.069 | 15380. |
| WASHINGTON | 38.73 | -77.13 | 0.463 | 70.2 | -5 | 2.77 | -65.4 | -90.6 | 0.416 | -12.77 | -76.51 | 11133 | 0.014 | 34621. |
| WALTAIR | 17.57 | 83.30 | 0.346 | 18.8 | -1 | 1.01 | 1.5 | 84.1 | 0.332 | 8.73 | 83.67 | 562 | 0.303 | 1970. |
| WELLEN | 66.17 | -169.84 | 0.465 | 75.6 | 16 | 4.90 | -52.4 | 157.6 | 0.536 | 5.89 | 172.89 | 25192 | 0.003 | 72858. |
| WESTFORD | 42.58 | -71.42 | 0.468 | 72.5 | -12 | 3.30 | -70.4 | -78.6 | 0.420 | -12.61 | -67.56 | 14407 | 0.009 | 43904. |
| WEISSENAU | 47.80 | 9.50 | 0.392 | 63.2 | -3 | 2.09 | -36.9 | 27.7 | 0.277 | 2.99 | 16.46 | 6596 | 0.035 | 21523. |
| WELLINGTON | -41.28 | 174.77 | 0.480 | -66.7 | 19 | 2.29 | 50.1 | -162.6 | 0.413 | 4.06 | -173.61 | 8400 | 0.026 | 26496. |

Table B3

Tracings 400 km Above Stations.

| STATIONS | ** O R I G I N ** | | | | | | ** CONJUGATE INTERS. ** | | | MINIMUM-B E Q U A T O R ** | | | ARC |
|---|---|---|---|---|---|---|---|---|---|---|---|---|---|
| | LAT. | LONG. | B | DIP | DECL. | L | LAT. | LONG. | B | LAT. | LONG. | ALT. | B | KM |
| WHITE SANDS | 32.40 | -106.87 | 0.426 | 60.2 | 12 | 1.84 | -46.7 | -126.3 | 0.411 | -7.88 | -114.03 | 5441 | 0.049 | 18214. |
| WINGST | 53.75 | 9.07 | 0.407 | 68.2 | -3 | 2.70 | -45.6 | 34.3 | 0.294 | 2.24 | 18.22 | 10403 | 0.016 | 32457. |
| WITTEVEEN | 52.82 | 6.67 | 0.404 | 67.5 | -4 | 2.62 | -45.0 | 31.6 | 0.289 | 1.99 | 16.00 | 9870 | 0.018 | 30966. |
| WIESE ISLAND | 79.83 | 76.98 | 0.477 | 85.0 | 21 | 12.30 | ** N O C O M P U T A T I O N S P E R F O R M E D ** | | | | | | | |
| WINNIPEG | 49.90 | -97.40 | 0.498 | 77.0 | 9 | 4.44 | -66.9 | -135.4 | 0.497 | -9.57 | -106.21 | 22003 | 0.003 | 64512. |
| WIEN KOBENZL | 48.27 | 16.32 | 0.397 | 63.6 | -0 | 2.08 | -36.1 | 32.6 | 0.282 | 3.78 | 22.03 | 6573 | 0.036 | 21401. |
| WILKES | -66.20 | 110.35 | 0.529 | -82.5 | -81 | 36.85 | ** N O C O M P U T A T I O N S P E R F O R M E D ** | | | | | | | |
| WOOMERA | -30.70 | 136.80 | 0.479 | -63.1 | 6 | 1.84 | 48.8 | 140.4 | 0.437 | 9.41 | 139.98 | 5750 | 0.050 | 18733. |
| WROCLAW | 51.10 | 17.08 | 0.404 | 66.1 | -0 | 2.32 | -40.0 | 36.1 | 0.289 | 3.52 | 23.53 | 8104 | 0.025 | 25814. |
| WRANGEL ISLAND | 71.00 | -178.50 | 0.475 | 78.8 | 13 | 6.52 | -54.7 | 148.8 | 0.547 | 7.21 | 162.83 | 35589 | 0.001 | 101462. |
| YAKUTSK | 62.05 | 129.67 | 0.486 | 75.7 | -10 | 3.21 | -42.3 | 126.9 | 0.525 | 10.12 | 128.70 | 14557 | 0.009 | 43147. |
| YAMAGAWA | 31.20 | 130.65 | 0.378 | 44.0 | -3 | 1.20 | -14.5 | 129.8 | 0.394 | 8.87 | 130.88 | 1738 | 0.178 | 6836. |
| YELLOWKNIFE | 62.40 | -114.40 | 0.502 | 81.8 | 29 | 8.80 | -67.4 | -172.9 | 0.537 | -4.62 | -134.94 | 49956 | 0.000 | 141554. |
| YUZHNO-SAKHALINSK | 46.95 | 142.72 | 0.425 | 61.0 | -7 | 1.73 | -29.1 | 138.9 | 0.470 | 9.24 | 142.17 | 5057 | 0.060 | 16794. |
| ZARIA | 11.15 | 7.65 | 0.268 | 3.6 | -8 | 1.06 | 8.0 | 8.1 | 0.264 | NO MINIMUM B BETWEEN INTERS. | | | | 372. |
| ZUGSPITZE | 47.42 | 10.98 | 0.392 | 62.9 | -2 | 2.05 | -36.0 | 28.2 | 0.277 | 3.32 | 17.50 | 6346 | 0.037 | 20783. |

Appendix C

## Conjugates of Stations and Areas

Table C1 Conjugate Pairs of Stations.
Table C2 Stations with Conjugate Areas in the Antarctica for $L \leq 12$.
Table C3 Conjugate Areas to Geophysical Stations with $1.1 \leq L \leq 12$.

Table C1

Conjugate Pairs of Stations

Table C2

Stations with Conjugate Areas in the Antarctica, for $L \leq 12$

Table C1

Conjugate Pairs of Stations.

| North | South | Average $\overline{L}$ | $\frac{\Delta L}{\overline{L}}$ % | $\Delta\phi_0$ |
|---|---|---|---|---|
| Great Whale River | Byrd Station | 7.12 | 3.6 | 1.85° |
| Reykjavik | Syowa Base | 6.22 | 1.9 | 0.27 |
| Kotzebue | MacQuarie | 5.23 | 1.1 | 1.85 |
| Farewell | Campbell Island | 4.17 | 6.0 | 0.26 |
| Quebec | Eights Station | 3.92 | 0.2 | 1.81 |
| Lund | Marion Island | 2.73 | 0.7 | 1.15 |
| Unalaska | Christchurch | 2.41 | 0.3 | 3.57 |
| Bermuda | Decepcion | 2.10 | 5.6 | 0.36 |
| Petropavlovsk | Canberra | 2.00 | 1.6 | 0.10 |
| Castel Tesino | Grahamstown | 1.83 | 1.6 | 0.41 |
| Aire Sur L'Adour | Capetown | 1.79 | 4.5 | 0.17 |
| Tschoibalsan | Watheroo | 1.74 | 1.8 | 0.02 |
| Khabarovsk | Woomera | 1.73 | 0.1 | 4.29 |
| Beograd | Durban | 1.70 | 0.8 | 0.63 |
| Panaguritsch | Lourenço Marques | 1.58 | 0.1 | 0.21 |
| L'Aquila | Potschefstroom | 1.58 | 0.3 | 2.77 |
| Ramey AFB | San Julian | 1.46 | 3.9 | 0.07 |
| Ashkabad | Plaisance | 1.35 | 3.6 | 1.40 |
| Athens | Salisbury (Rhod.) | 1.33 | 3.9 | 2.46 |
| Sendai | Cloncurry | 1.29 | 1.2 | 2.00 |
| Baghdad | Tananarive | 1.26 | 5.0 | 0.47 |
| Honolulu | Noumea | 1.15 | 2.3 | 0.60 |

Table C2

Stations with Conjugate Areas in the Antarctica ($L \leq 12$).

| Station | L | Conjugate Area |
|---|---|---|
| Kap Tobin | 10.94 | Enderby Land |
| Barter Island | 9.05 | Ocean Station (South Pacific Ocean) |
| Fort Chimo | 8.40 | South Polar Plateau |
| Narssarssuaq | 7.50 | Queen Maud Land |
| Julianehaab | 7.31 | Queen Maud Land |
| Cape Jones | 6.58 | Near Byrd Station |
| Knob Lake | 6.35 | Edith Ronne Land |
| Goose Bay | 5.33 | Edith Ronne Land |
| Mont Joli | 4.26 | Elsworth Highland |
| Val D'Or | 4.22 | Mary Byrd Land |
| Caribou | 3.86 | Near Eights Station |
| Deep River | 3.78 | Mary Byrd Land |
| Fort Monmouth | 2.82 | Peter I Island |

Table C3

Conjugate Areas to Geophysical Stations with $1.1 \leq L \leq 12$.

Table C3

Conjugate Areas for Stations with $1.1 \leq L \leq 12$.

| Station | L | Conjugate Area | Country |
|---|---|---|---|
| Adelaide | 2.03 | Piltun (near Okha, Sakhalin) | USSR |
| Akita | 1.35 | Rockborough Downs (Queensland) | Australia |
| Akrotiri | 1.25 | Mlanje | Malawi |
| Arcetri | 1.67 | Plooysburg (near Kimberley) | RSA |
| Aso | 1.17 | Victoria River Downs (Northern Territory) | Australia |
| Bologna | 1.71 | Reebokraut (Orange Free State) | RSA |
| Buenos Aires | 1.20 | Santa Barbara (Bolivar) | Venezuela |
| Capri | 1.49 | Lutlhe (Bechuanaland) | Br. Protectorate |
| Catania | 1.36 | Massubia (Bechuanaland) | Br. Protectorate |
| Chita | 2.00 | Wonnerup (Western Australia) | Australia |
| Chamical | 1.14 | Capibara (Amazonas) | Venezuela |
| Cocos Island | 1.11 | Garme (Chamdo) | Tibet |
| Concepcion | 1.21 | San Carlos de Zulia | Venezuela |
| Cordoba | 1.15 | Piedra Lais (Amazonas) | Venezuela |
| Corinaldo | 1.65 | Boshof (Orange Free State) | RSA |
| Cook | 1.74 | Birakan (near Birobidzhan) | USSR |
| Curacao | 1.27 | San Carlos de Bariloche | Argentina |
| Dodaira | 1.24 | Near Alexandria (Northern Territory) | Australia |
| Elizabethville | 1.18 | Near Tobruk | Lybia |
| General Belgrano | 4.59 | Mecatina River (Prov. of Quebec) | Canada |
| Genova | 1.73 | Britstown | RSA |
| Gifu | 1.23 | Near Tennant Creek (Northern Territory) | Australia |
| Hachijojima | 1.18 | Near Burketown (Queensland) | Australia |
| Haifa | 1.21 | Metarica | Mozambique |
| Halley Bay | 4.17 | Williamsport (Newfoundland) | Canada |
| Helwan | 1.14 | Isoka | Zambia |
| Hermanus | 1.85 | Riberac (Near Perigueux) | France |
| Highcliff | 2.74 | Near Fort Randall (Alaska) | USA |
| Hiraiso | 1.25 | Near Camooweal (Queensland) | Australia |
| I. Crozet | 2.88 | Pskov (Novgorod) | USSR |
| Il. Qortin | 1.31 | Cubia | Angola |
| Johannesburg | 1.57 | Dubrovnik | Yugoslavia |
| Jungfraujoch | 1.87 | Humansdorp (Near Port Elizabeth) | RSA |

Table C3

Conjugate Areas for Stations with $1.1 \leq L \leq 12$.

| Station | L | Conjugate Area | Country |
|---|---|---|---|
| Kanoya | 1.14 | Auvergne (Northern Territory) | Australia |
| Kakioka, Komuro, Kokubunji | 1.25 | Near Camooweal (Queensland) | Australia |
| Kyoto | 1.22 | Tennant Creek (Northern Territory) | Australia |
| La Crau | 1.66 | Kenhardt | RSA |
| La Maddalena | 1.54 | Khokowe (Bechuanaland) | Br. Protectorate |
| La Plata | 1.20 | Near El Callao | Venezuela |
| Luanda | 1.13 | Tilmas | Algeria |
| Mawson | 8.63 | Near St. Mayen Island | Norway |
| Memambetsu | 1.50 | Great Victoria Deserts (South Australia) | Australia |
| Moshiri | 1.52 | Clifton Hills (Queensland) | Australia |
| Mount Norikura | 1.24 | Alroy Downs (Northern Territory) | Australia |
| Nicosia | 1.27 | Zambeze | Mozambique |
| Niigata | 1.29 | Austral Downs (Northern Territory) | Australia |
| Nitsanim | 1.18 | Near Vila Cabral | Mozambique |
| Nouvelle Amsterdam | 2.32 | Demyanovka (Kazakhstan) | USSR |
| Onagawa | 1.31 | Butru (Queensland) | Australia |
| Oohira | 1.23 | Near Camooweal (Queensland) | Australia |
| Paramaribo | 1.18 | Near Florianopolis | Brazil |
| Pearce | 1.86 | Ust Llya (Near Olovyannaya) | USSR |
| Pilar | 1.15 | Manarunga (Bolivar) | Venezuela |
| Ponza | 1.51 | Kukong | Bechuanaland |
| Port aux Francais | 3.68 | Vasilevo (Near Kotlas) | USSR |
| Posadas | 1.13 | Near Boa Vista (Rio Branco) | Brazil |
| Pretoria | 1.59 | Dubrovnik | Yugoslavia |
| Punta Arenas | 1.62 | Caicos Island (Bahamas) | UK |
| Pyongyang | 1.33 | Great Sandy Desert (Western Australia) | Australia |
| Roma | 1.56 | Near Vryburg | RSA |
| San Juan | 1.43 | Near Puerto Descado | Argentina |
| Santiago | 1.17 | Nueva Antioquia (Arauco) | Colombia |
| Sao Jose dos Campos Sao Paulo | 1.12 | Near Oscar | French Guiana |
| Sapporo | 1.47 | Eara Heedy (Western Australia) | Australia |

Table C3

Conjugate Areas for Stations with $1.1 \leq L \leq 12$.

| Station | L | Conjugate Area | Country |
|---|---|---|---|
| Seoul | 1.28 | Great Sandy Desert (Western Australia) | Australia |
| Simosato | 1.18 | Tanumbirini (Northern Territory) | Australia |
| Shackleton | 4.61 | St. Augustine River (Prov. of Quebec) | Canada |
| Stellenbosch | 1.82 | Saint Martial (Near Bordeaux) | France |
| Torino | 1.78 | Nelspoort (Near Beaufort West) | RSA |
| Tortosa | 1.57 | Bogenfels (Near Luderitz) | South West Africa |
| Torre Chiaruccia | 1.57 | Near Vryburg | RSA |
| Tottori | 1.23 | Tennant Creek (Northern Territory) | Australia |
| Toyokawa | 1.24 | Alexandria (Northern Territory) | Australia |
| Trinidad | 1.26 | Near Mar del Plata | Argentina |
| Tsumeb | 1.34 | Tabarka (Near Tunis) | Tunisia |
| Tucuman | 1.11 | Uaruti (Amazonas) | Brazil |
| Uji | 1.21 | Tennant Creek (Northern Territory) | Australia |
| Vladivostok | 1.50 | Great Victoria Deserts (South Australia) | Australia |
| Wakkanai | 1.56 | Eta Dunna (South Australia) | Australia |
| Yamagawa | 1.13 | Near Port Keats (Northern Territory) | Australia |
| Yuzhno-Sakhalinsk | 1.64 | Blanchewater (South Australia) | Australia |

LINES OF CONSTANT B (gauss)

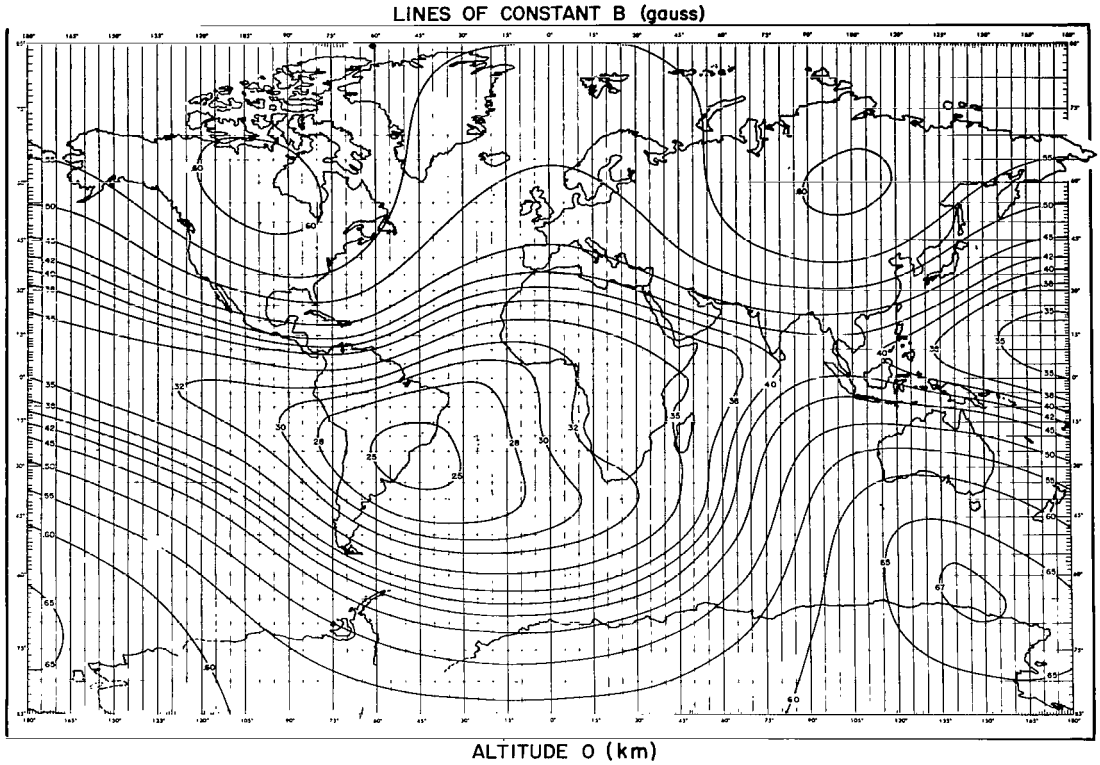

ALTITUDE 0 (km)

LINES OF CONSTANT B (gauss)

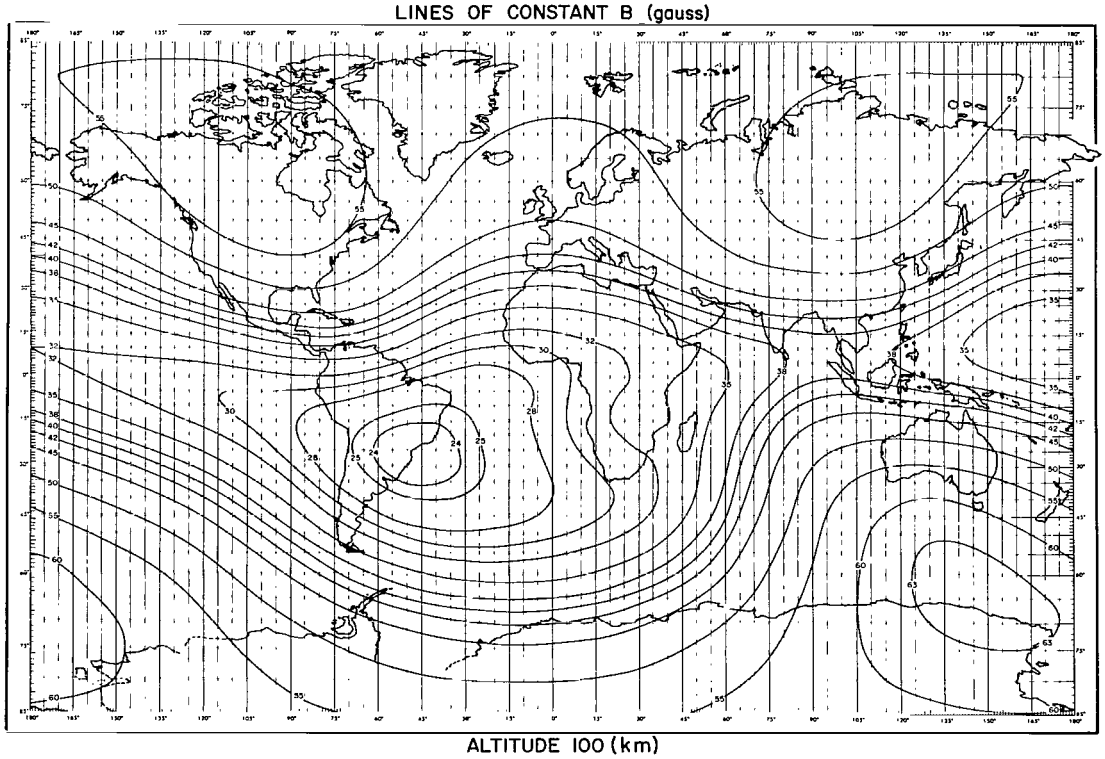

ALTITUDE 100 (km)

LINES OF CONSTANT B (gauss)

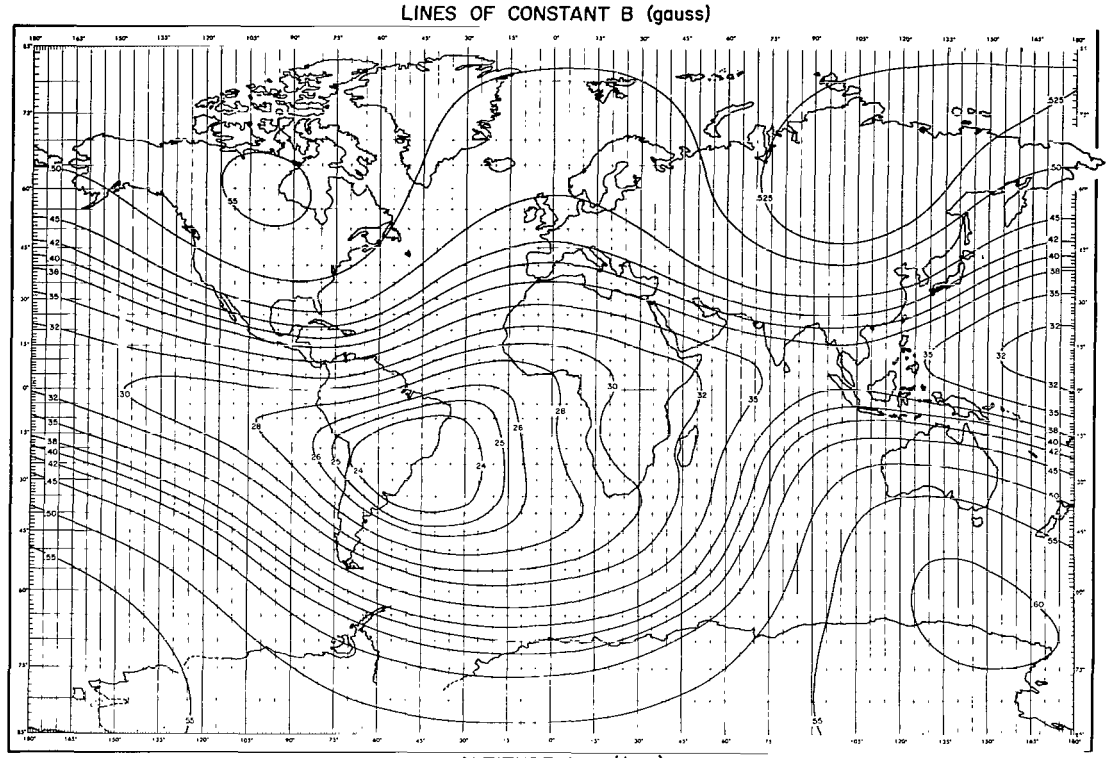

ALTITUDE 200 (km)

LINES OF CONSTANT B (gauss)

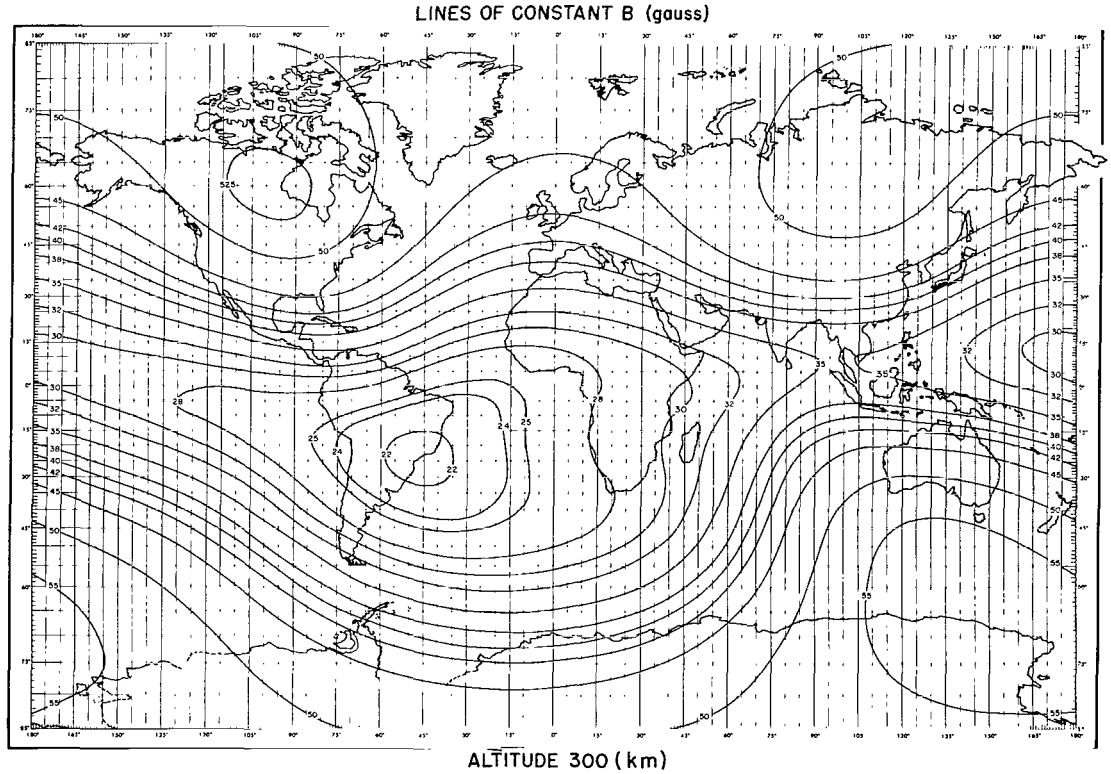

ALTITUDE 300 (km)

LINES OF CONSTANT B (gauss)

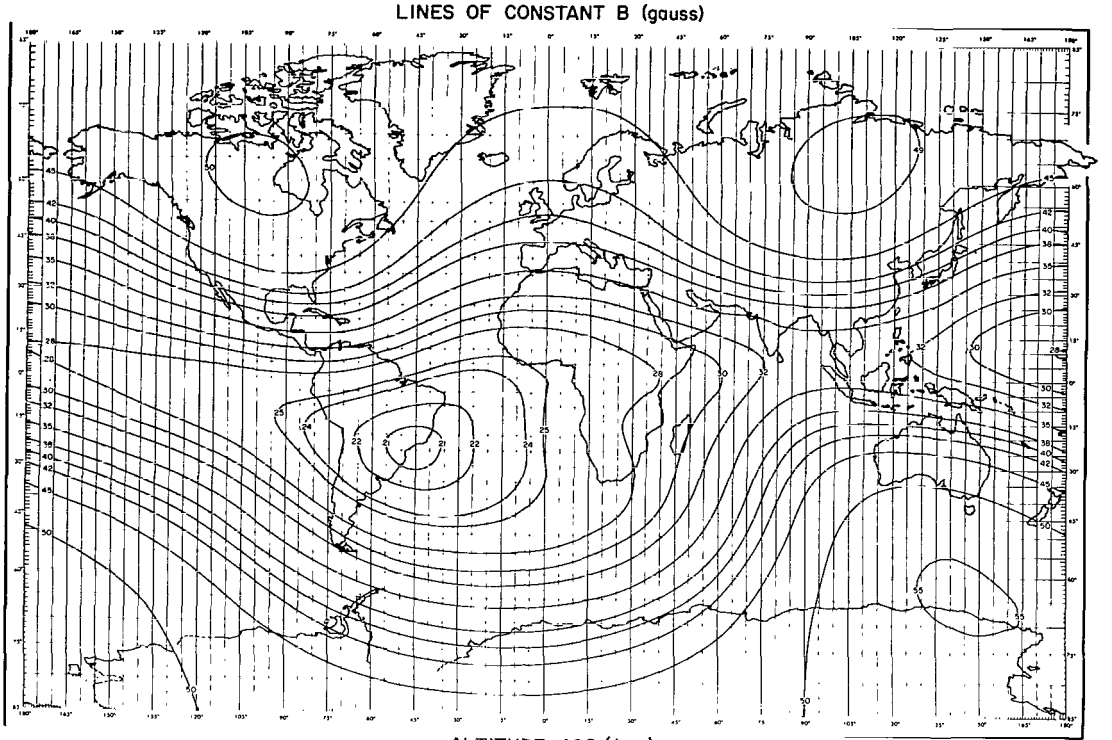

ALTITUDE 400 (km)

LINES OF CONSTANT B (gauss)

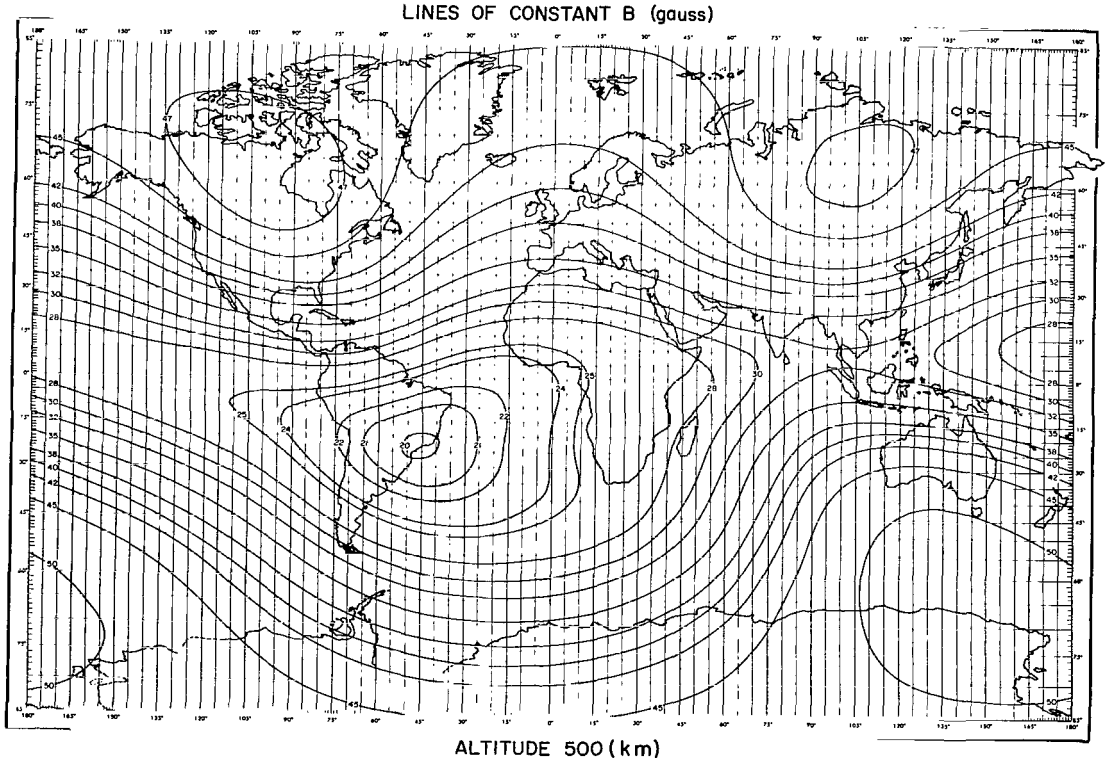

ALTITUDE 500 (km)

LINES OF CONSTANT B (gauss)

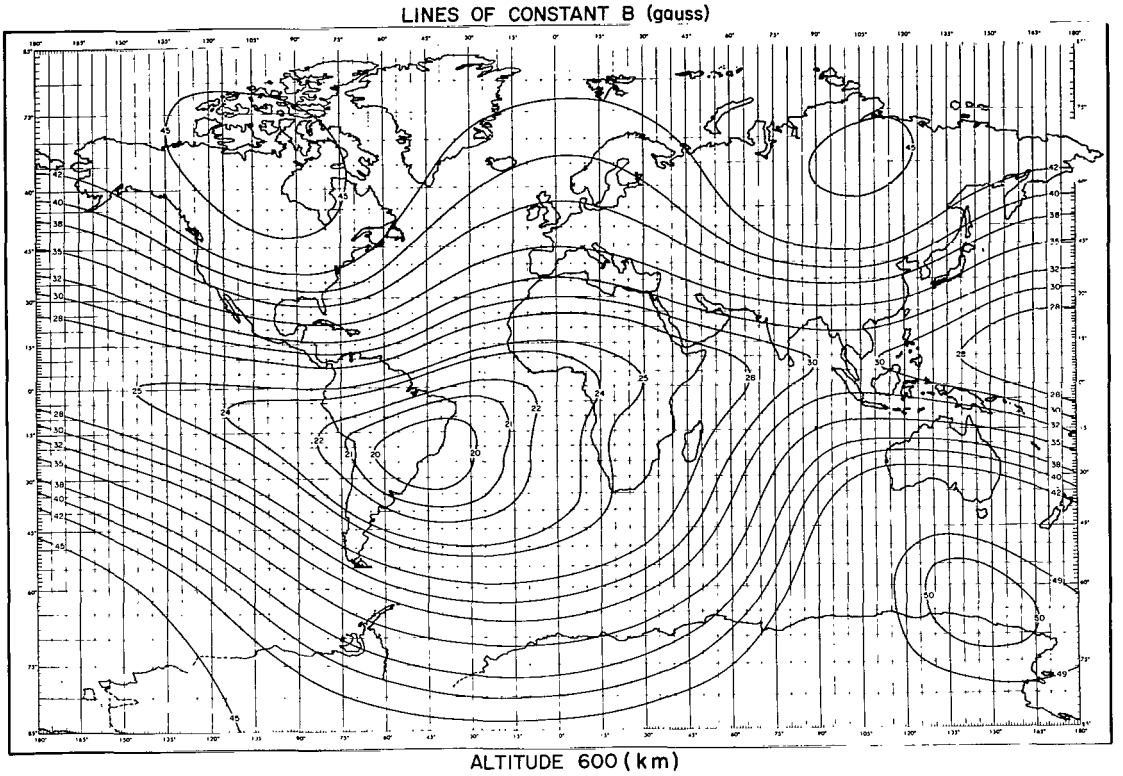

ALTITUDE 600 (km)

LINES OF CONSTANT B (gauss)

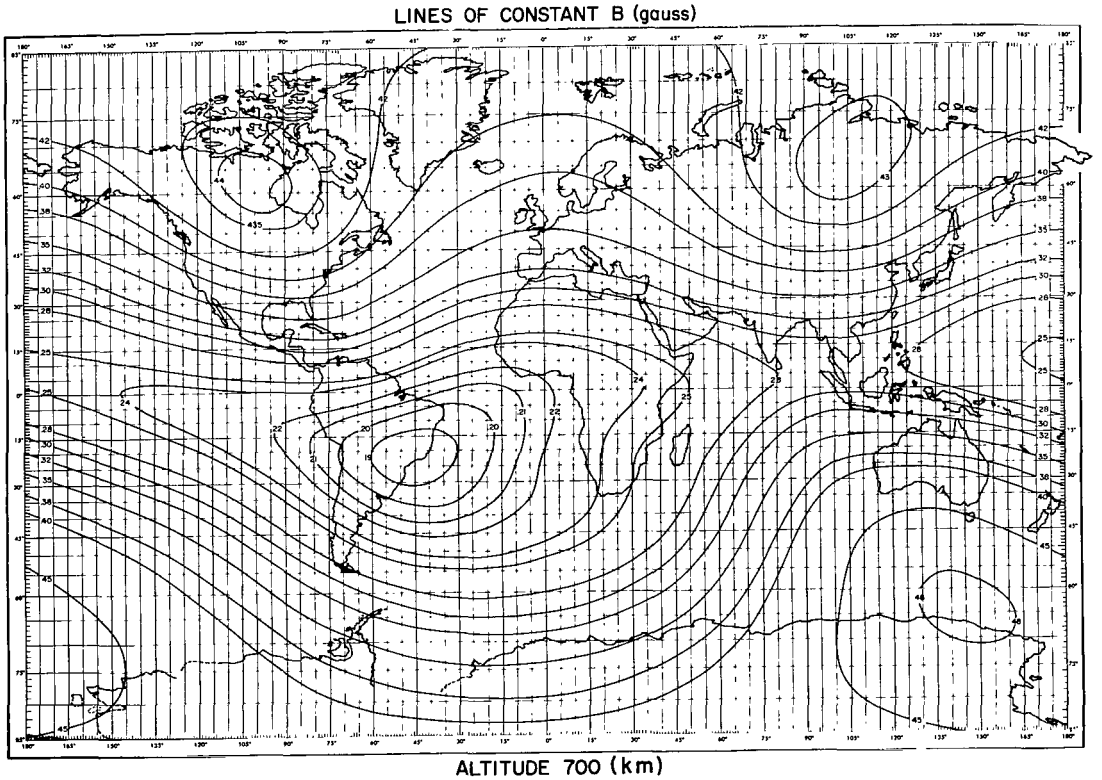

ALTITUDE 700 (km)

LINES OF CONSTANT B (gauss)

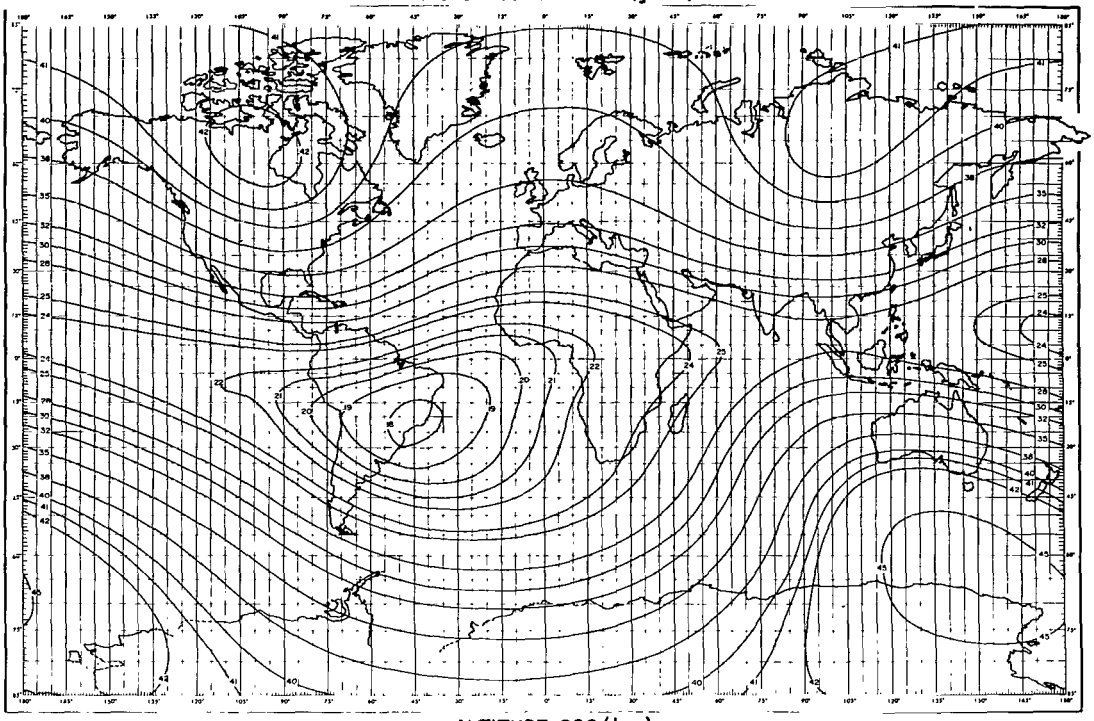

ALTITUDE 800 (km)

LINES OF CONSTANT B (gauss)

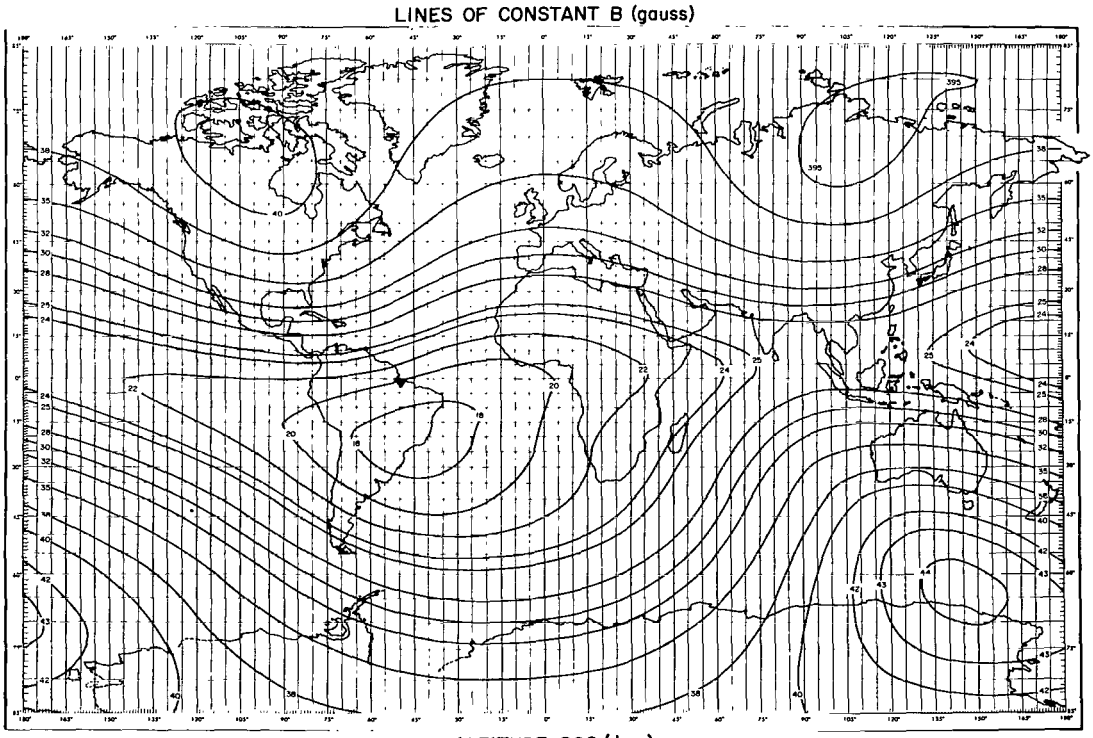

ALTITUDE 900 (km)

LINES OF CONSTANT B (gauss)

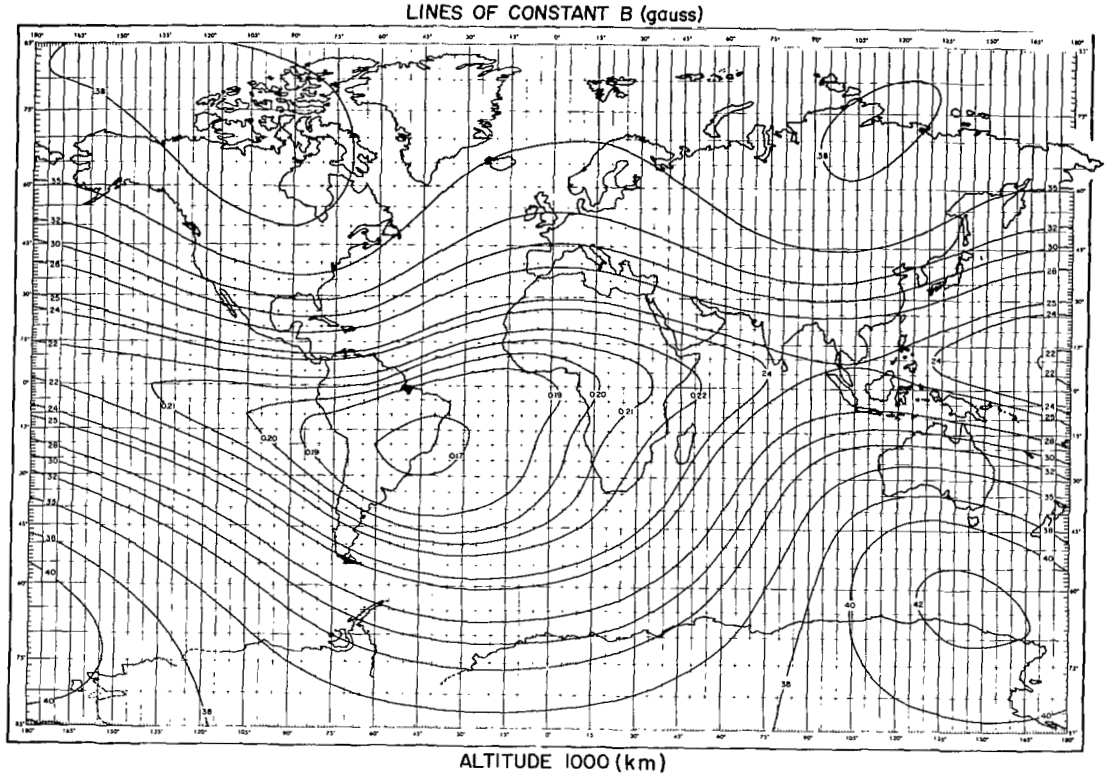

ALTITUDE 1000 (km)

LINES OF CONSTANT B (gauss)

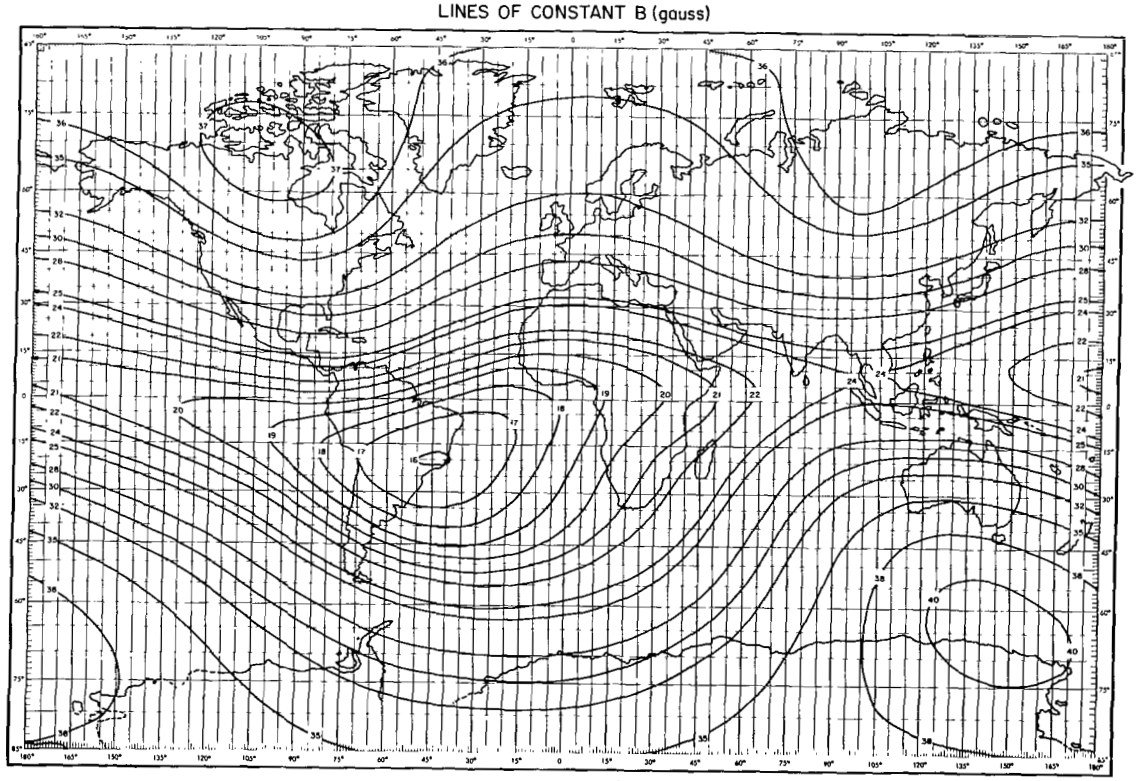

ALTITUDE 1100 (km)

LINES OF CONSTANT B (gauss)

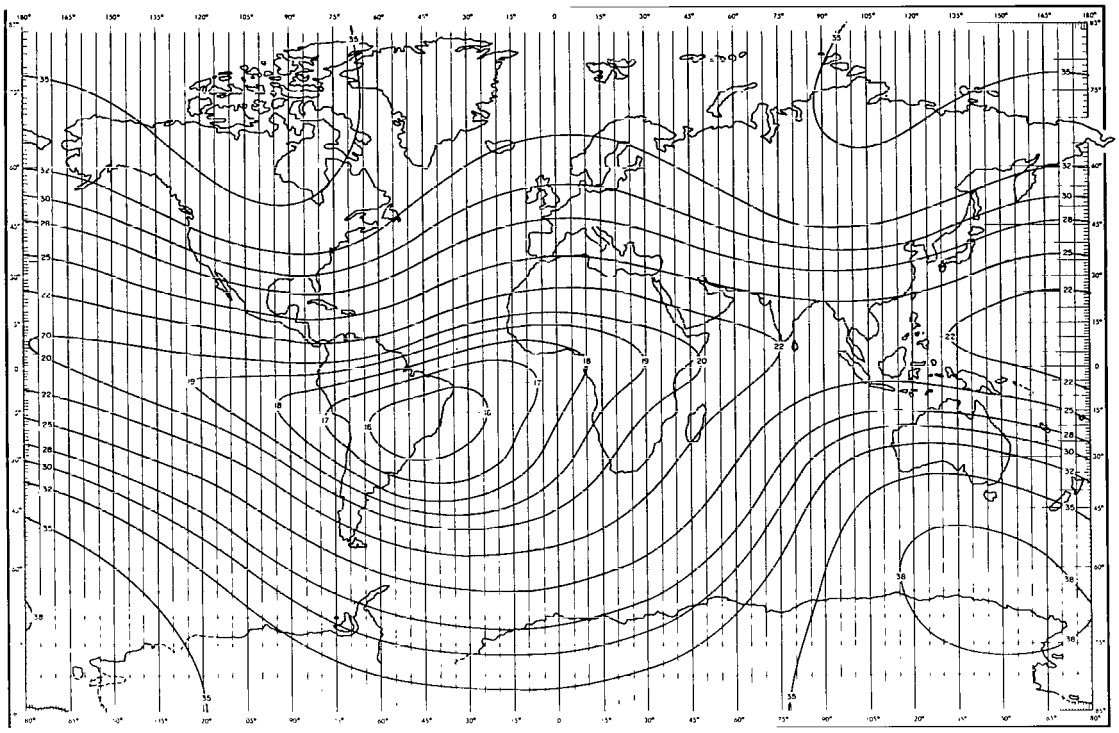

ALTITUDE 1200 (km)

LINES OF CONSTANT B (gauss)

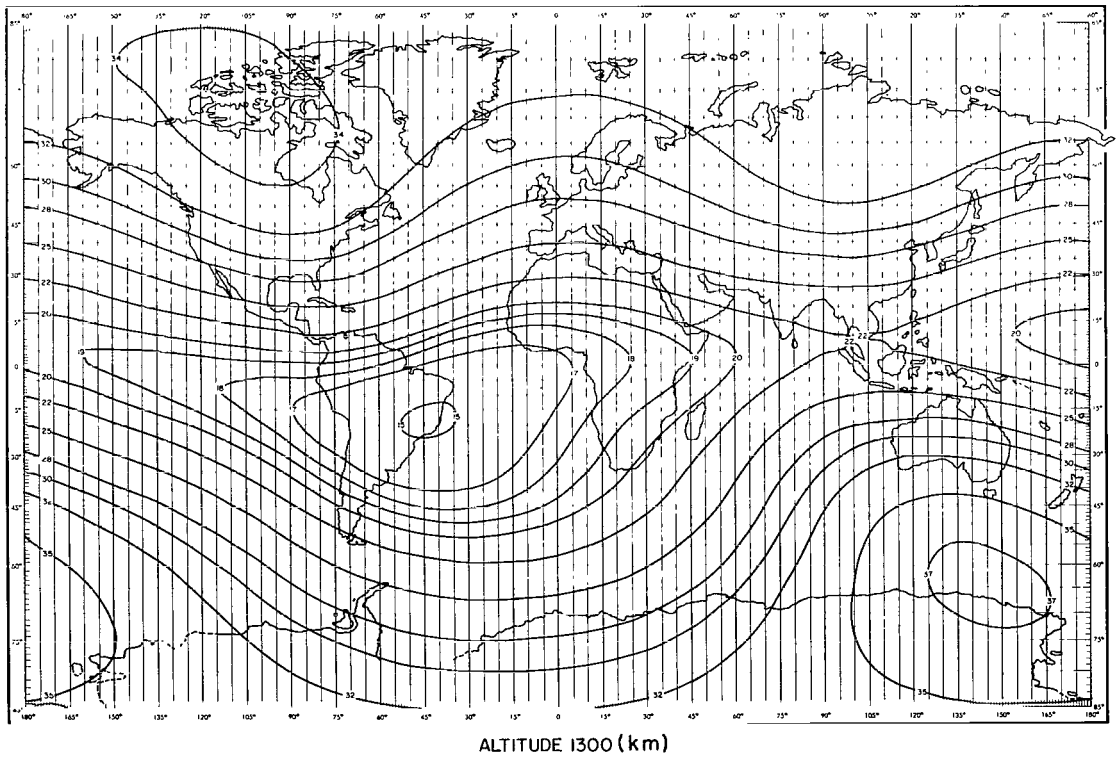

ALTITUDE 1300 (km)

LINES OF CONSTANT B (gauss)

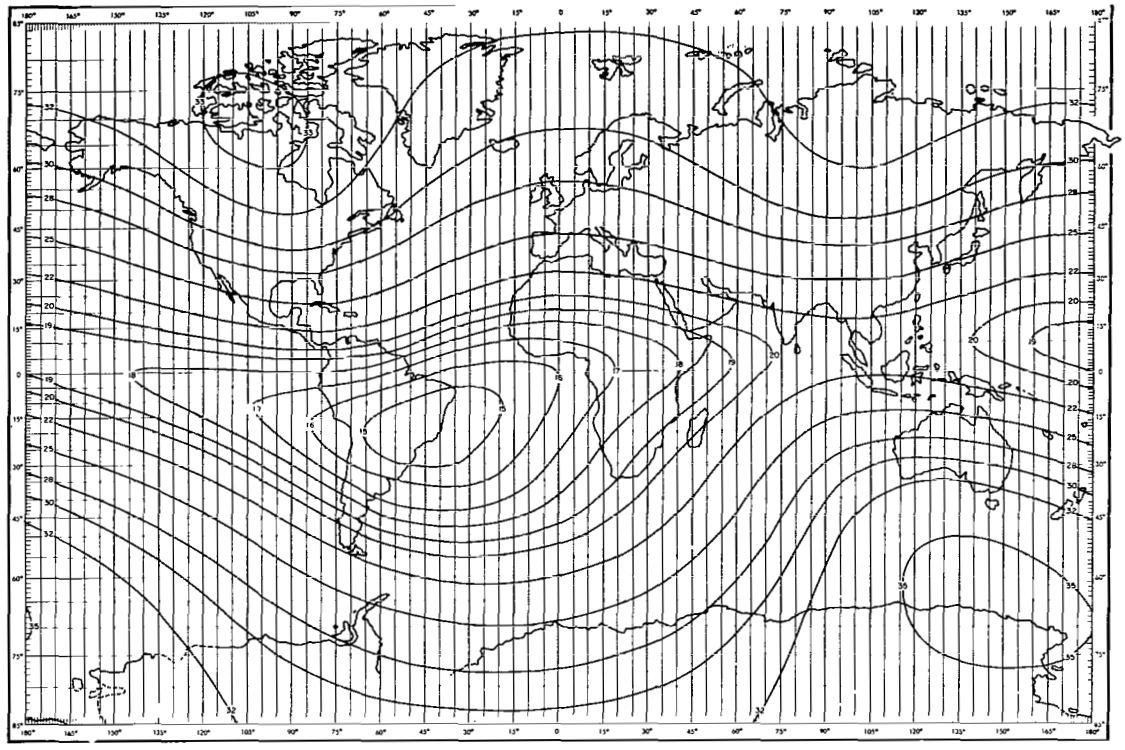

ALTITUDE 1400 (km)

LINES OF CONSTANT B (gauss)

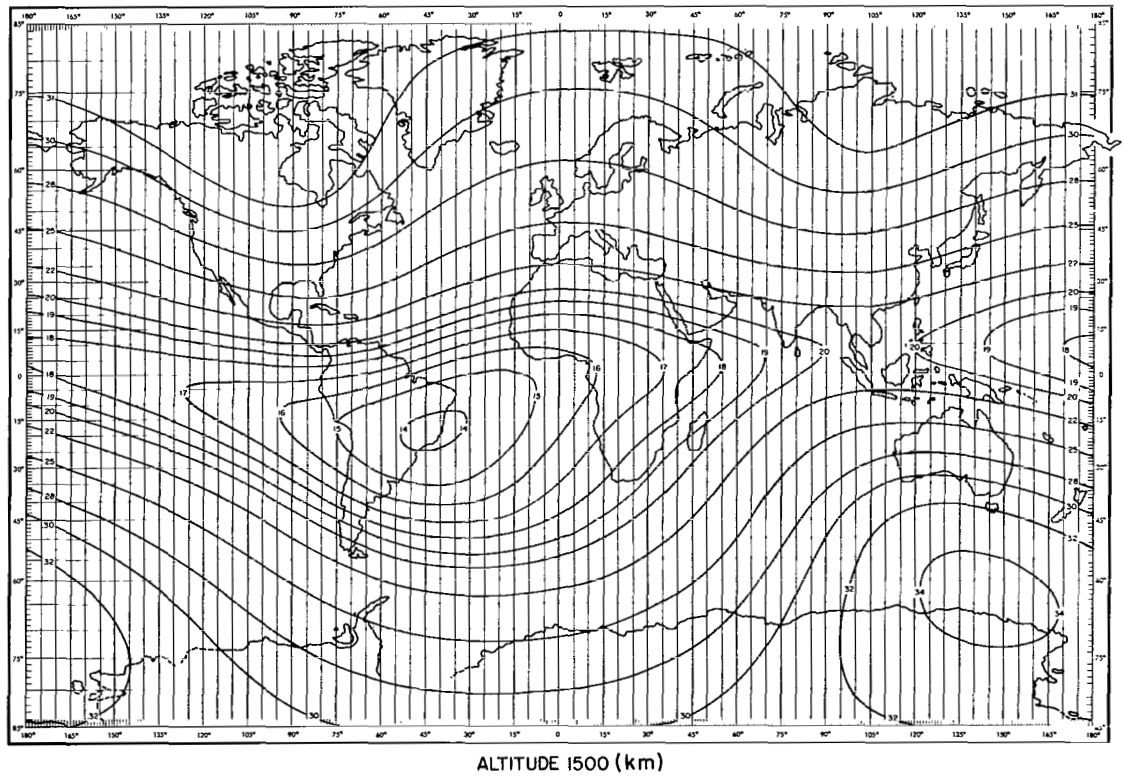

ALTITUDE 1500 (km)

LINES OF CONSTANT B (gauss)

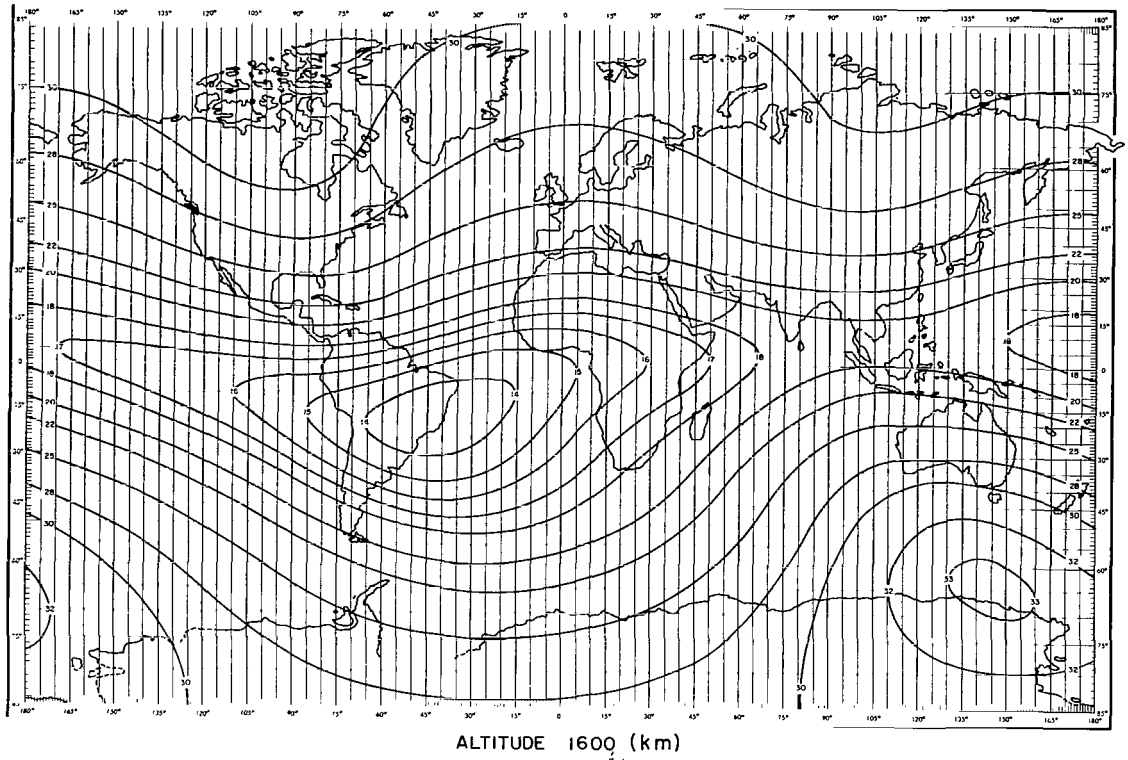

ALTITUDE 1600 (km)

LINES OF CONSTANT B (gauss)

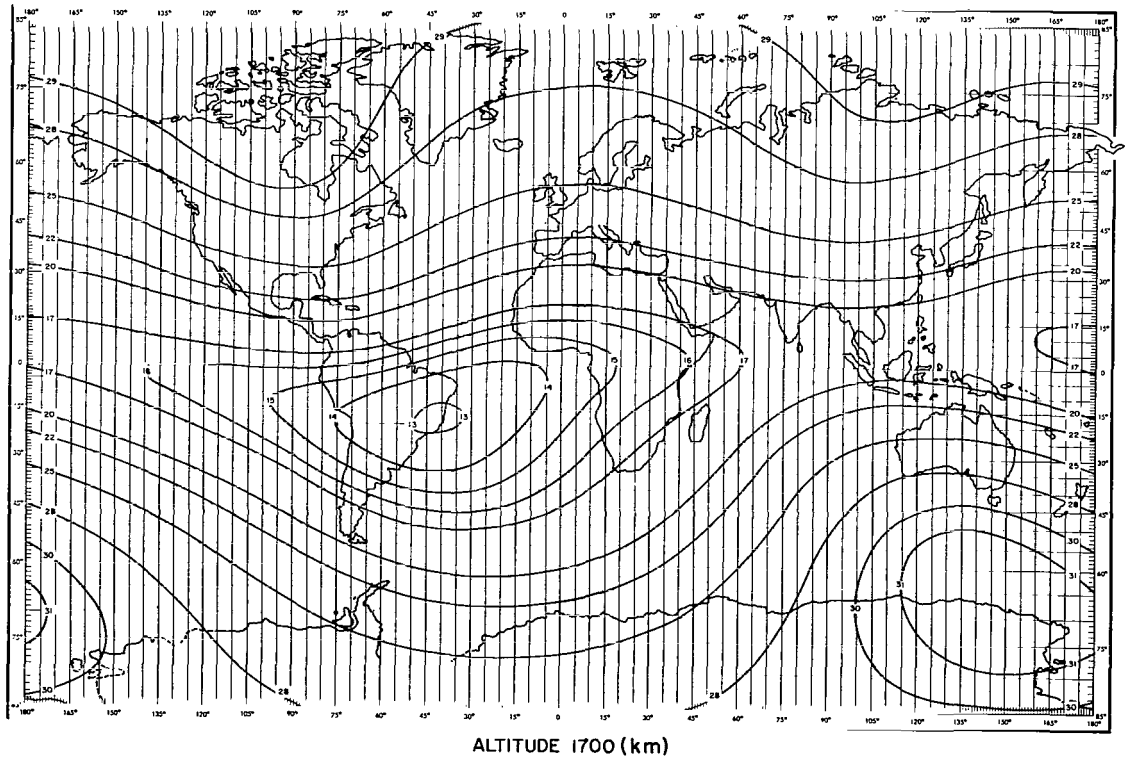

ALTITUDE 1700 (km)

LINES OF CONSTANT B (gauss)

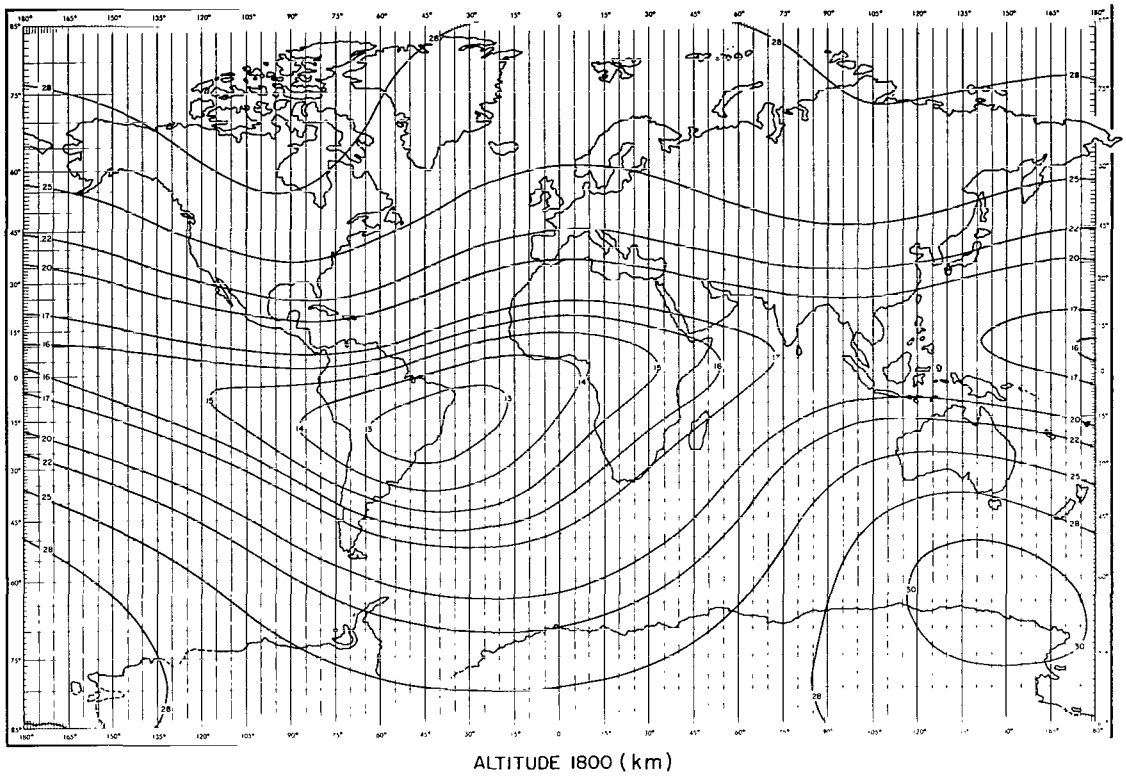

ALTITUDE 1800 (km)

LINES OF CONSTANT B (gauss)

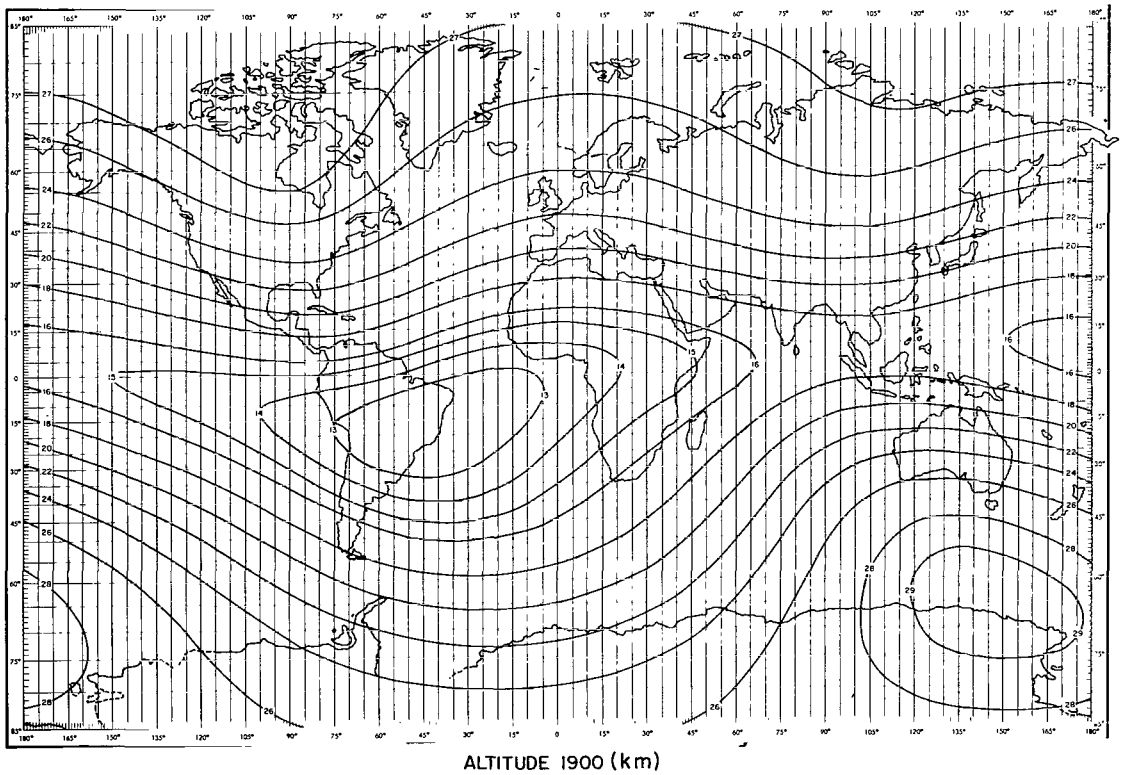

ALTITUDE 1900 (km)

LINES OF CONSTANT B (gauss)

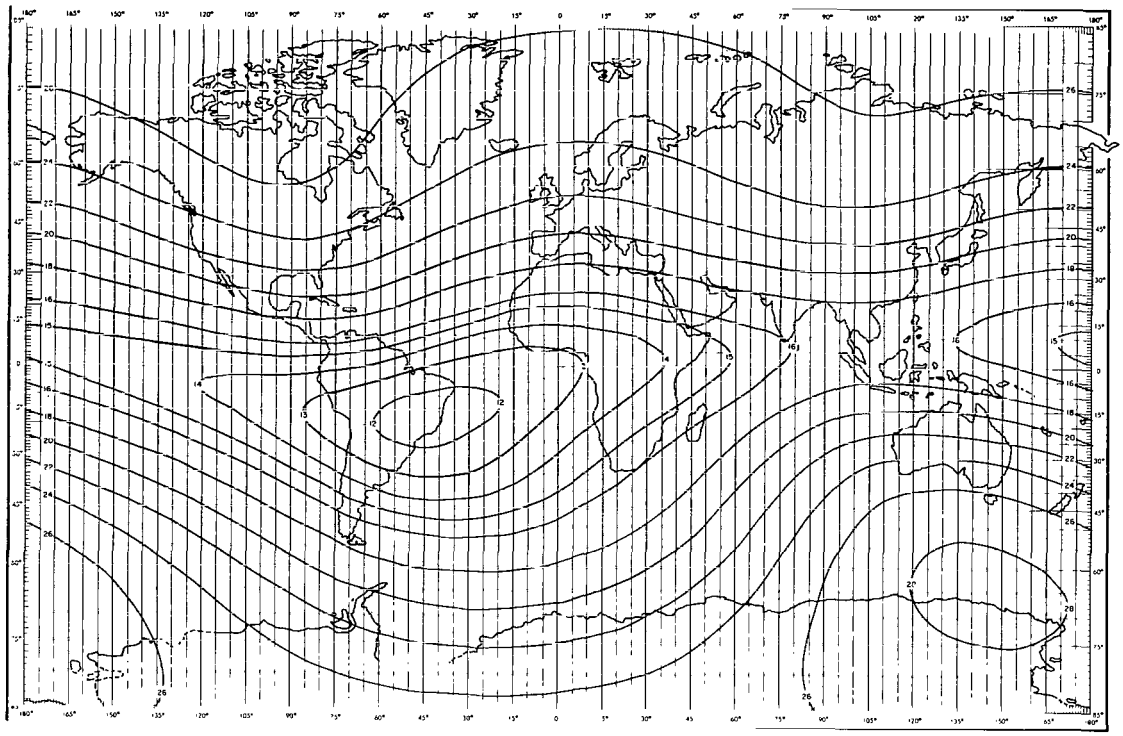

ALTITUDE 2000 (km)

LINES OF CONSTANT B (gauss)

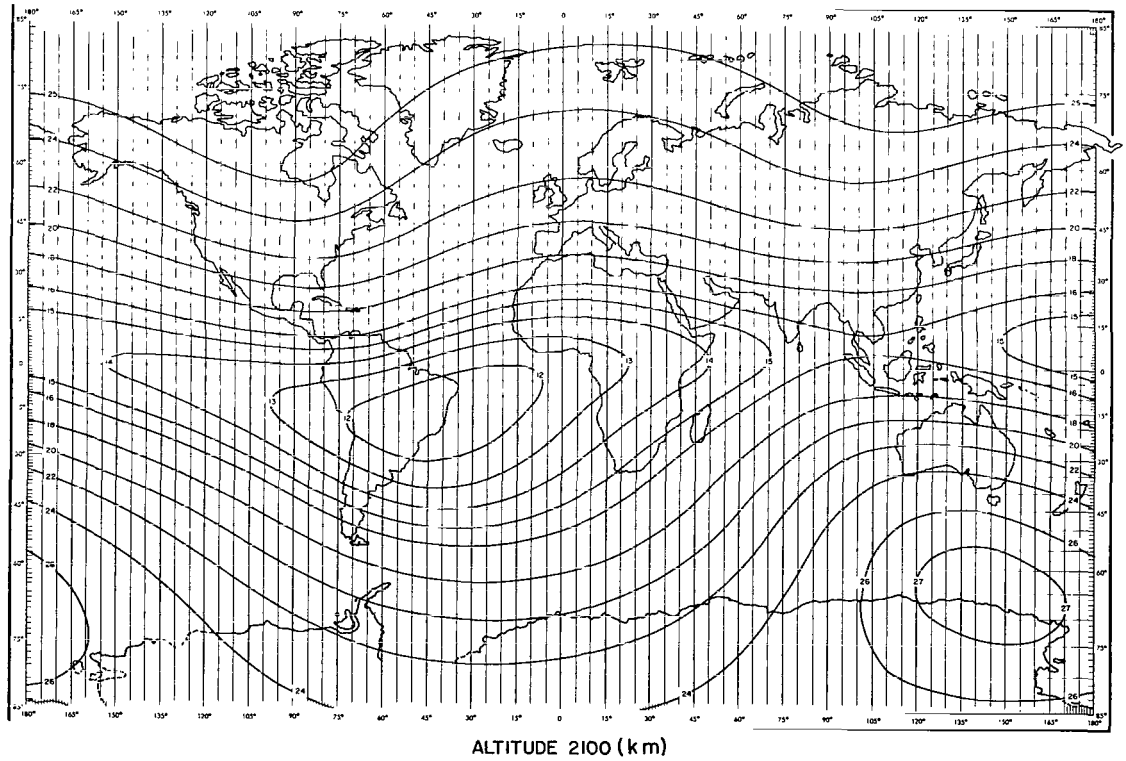

ALTITUDE 2100 (km)

LINES OF CONSTANT B (gauss)

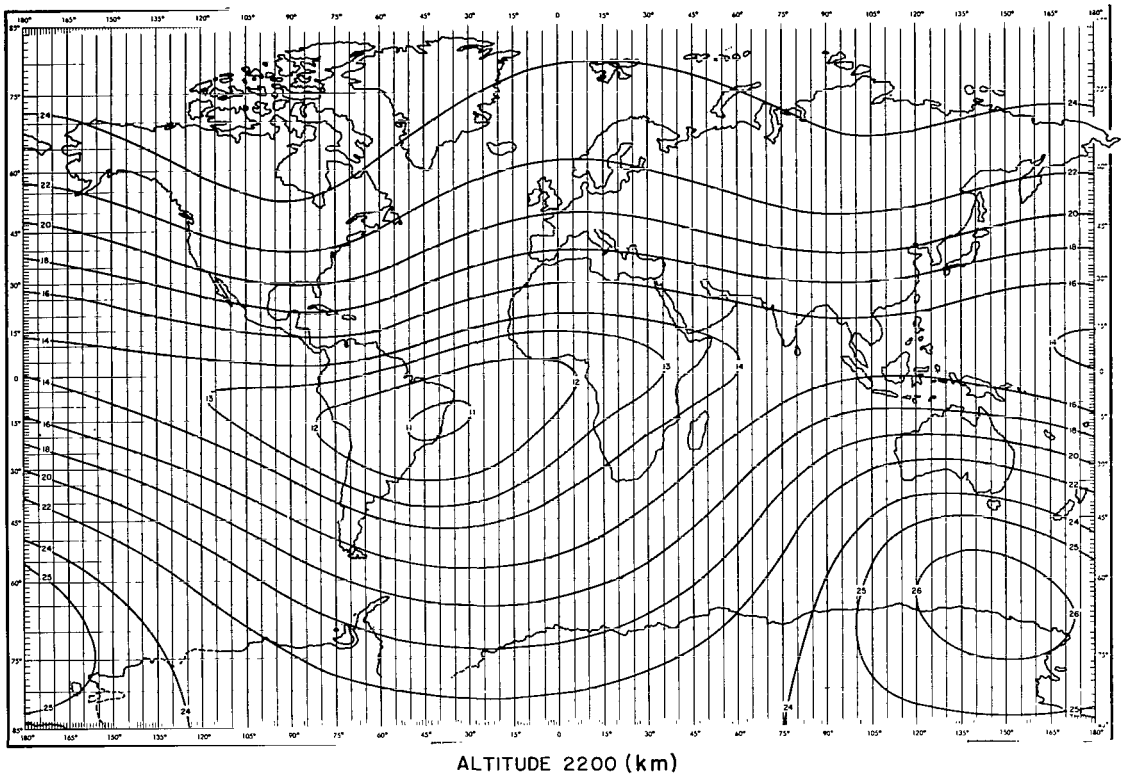

ALTITUDE 2200 (km)

LINES OF CONSTANT B (gauss)

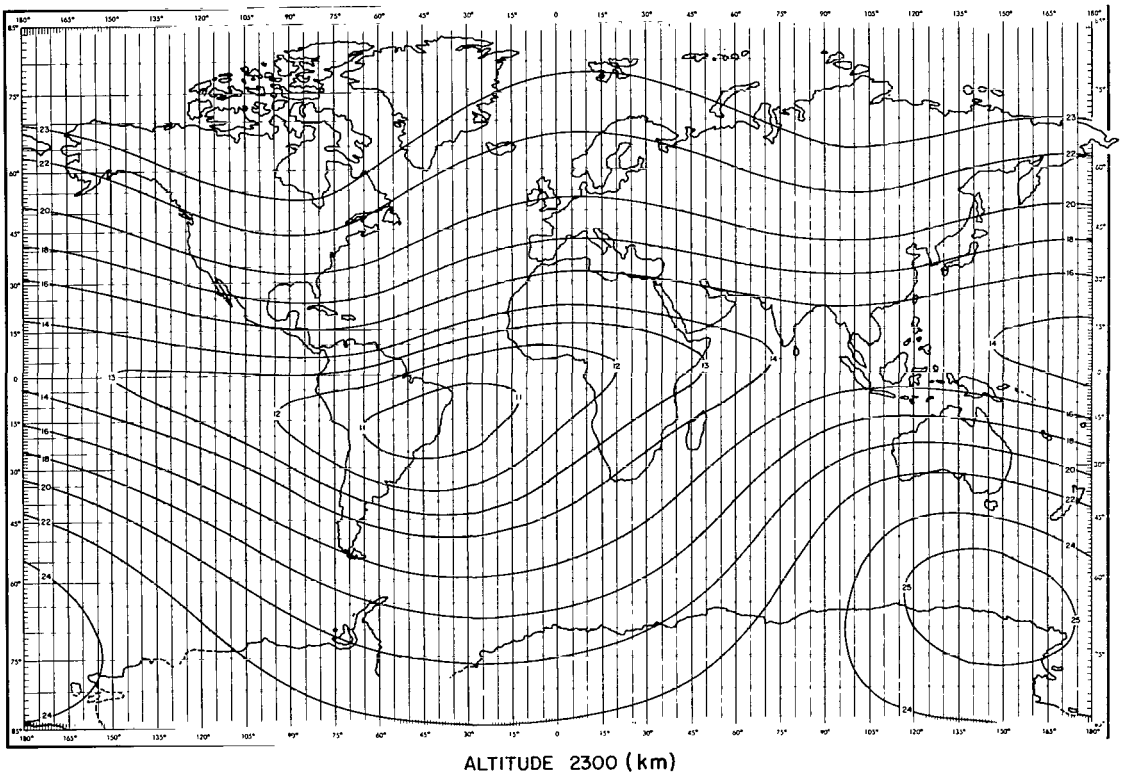

ALTITUDE 2300 (km)

LINES OF CONSTANT B (gauss)

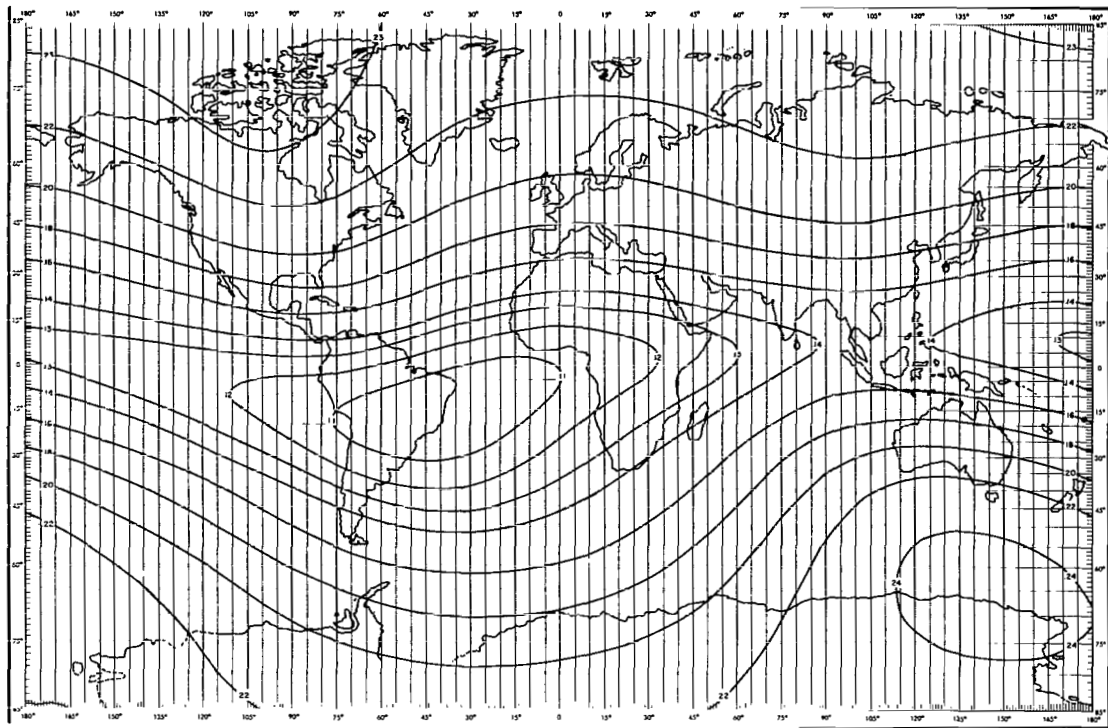

ALTITUDE 2400 (km)

LINES OF CONSTANT B(gauss)

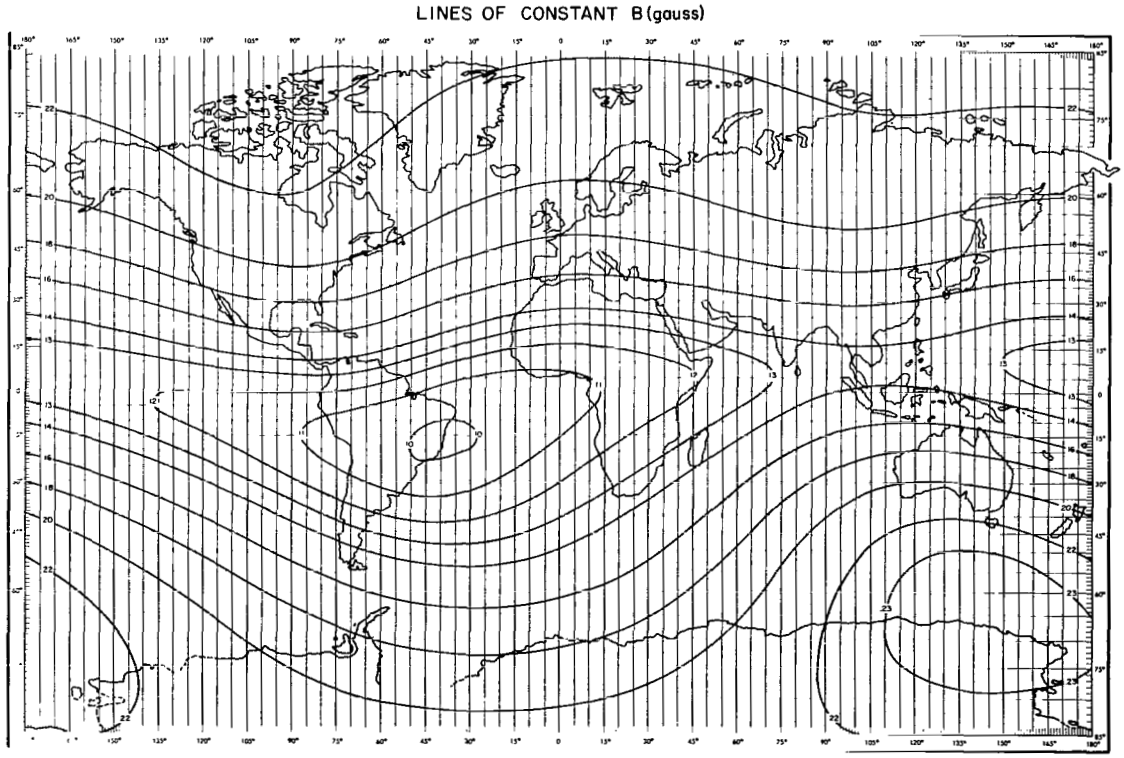

ALTITUDE 2500 (km)

LINES OF CONSTANT B (gauss)

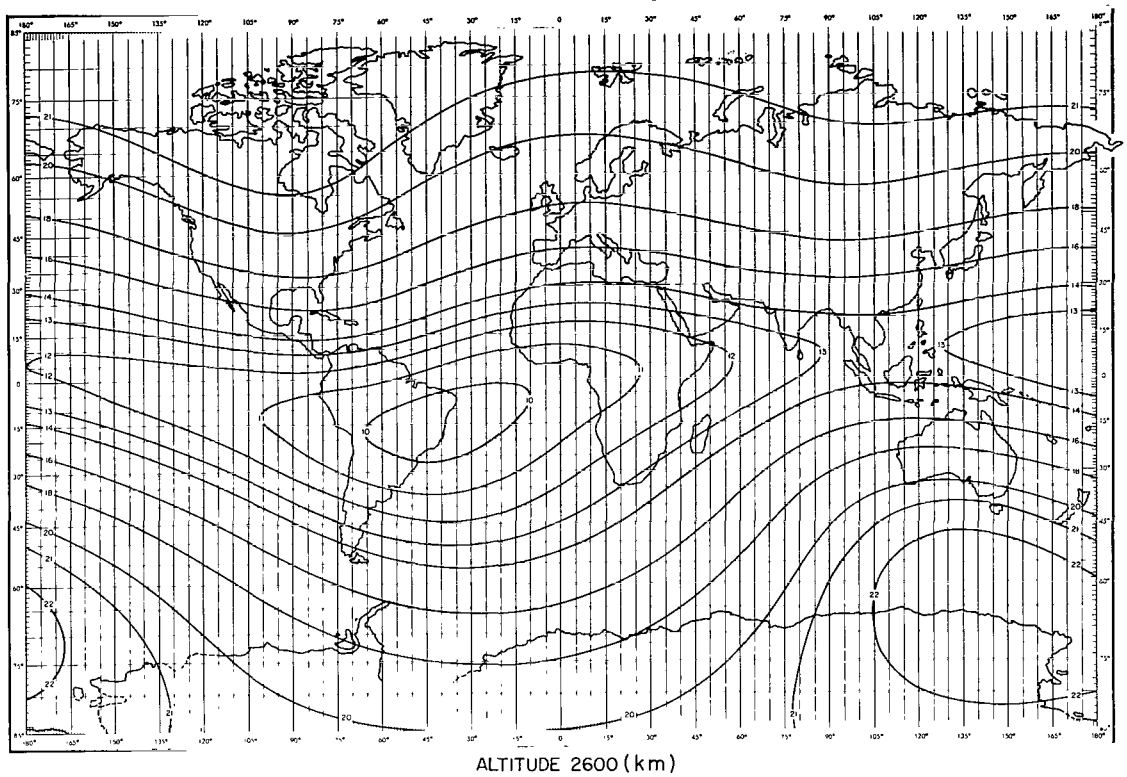

ALTITUDE 2600 (km)

LINES OF CONSTANT B (gauss)

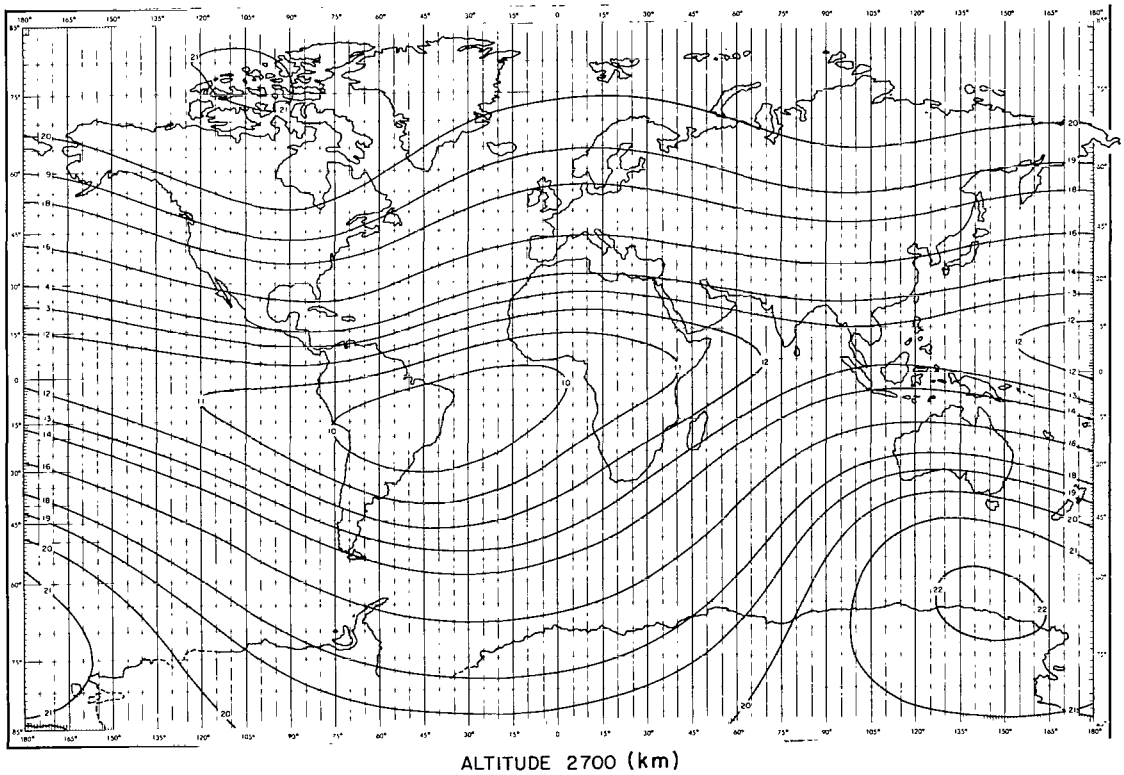

ALTITUDE 2700 (km)

LINES OF CONSTANT B (gauss)

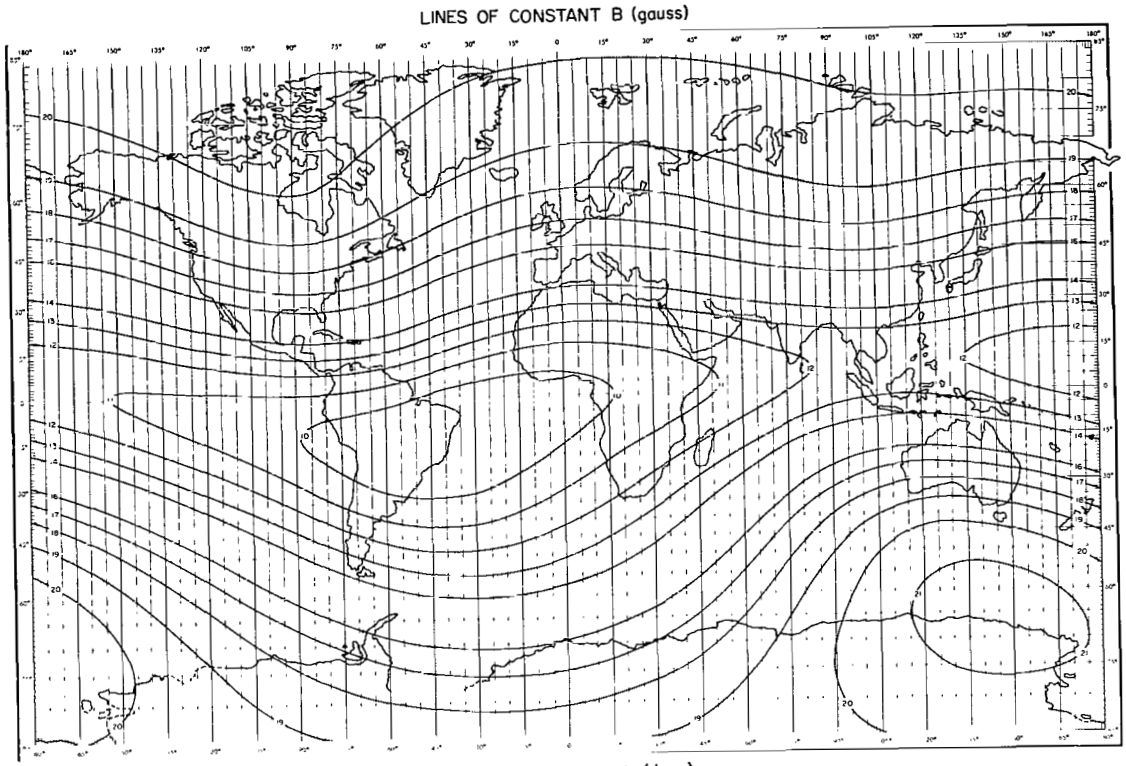

ALTITUDE 2800 (km)

LINES OF CONSTANT B (gauss)

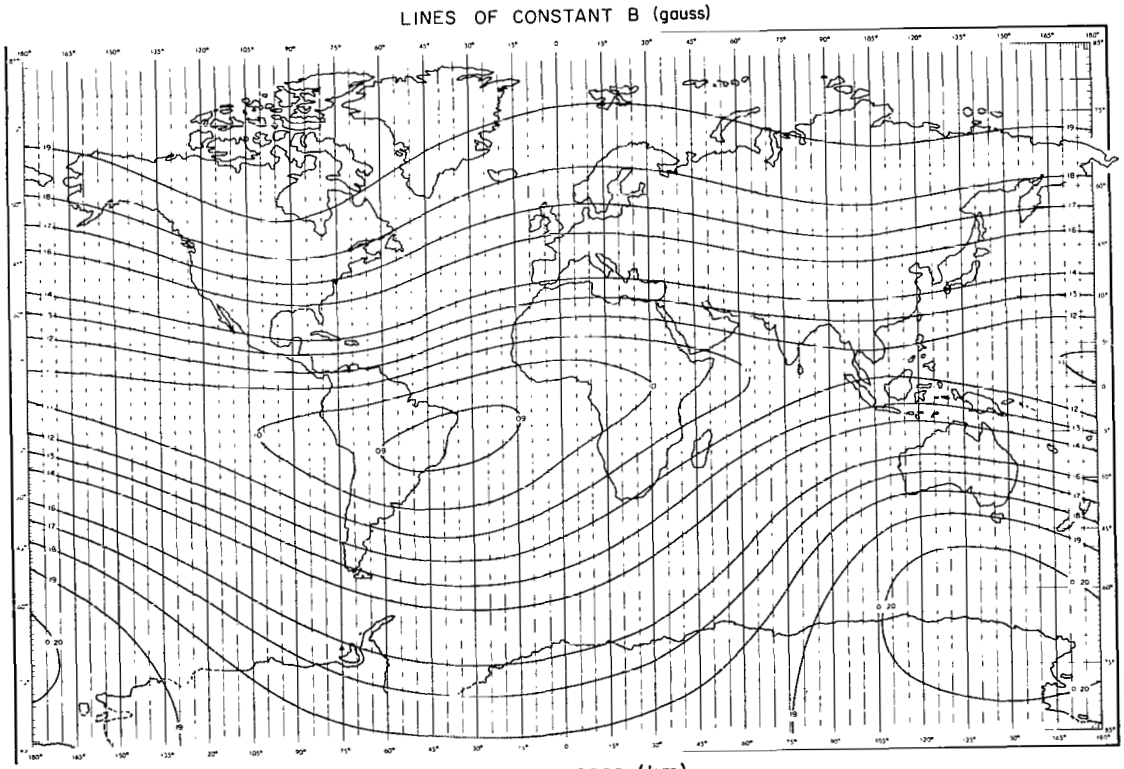

ALTITUDE 2900 (km)

LINES OF CONSTANT B (gauss)

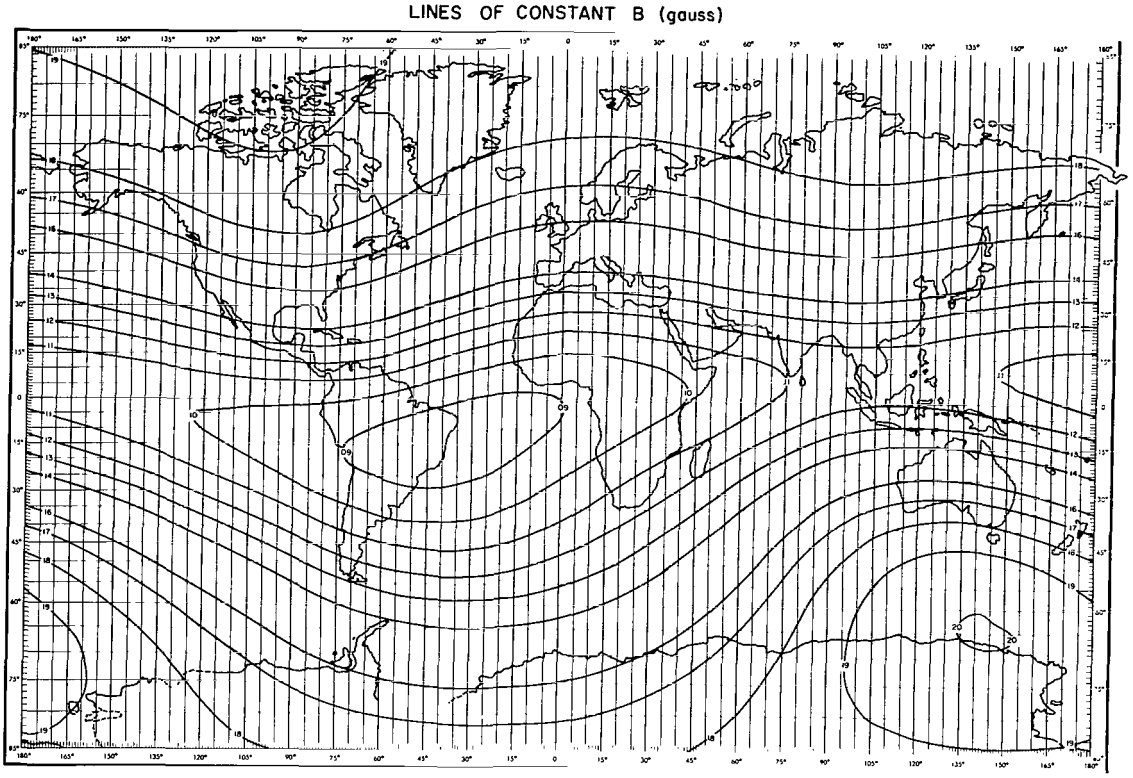

ALTITUDE 3000 (km)

LINES OF CONSTANT L (earth radii)

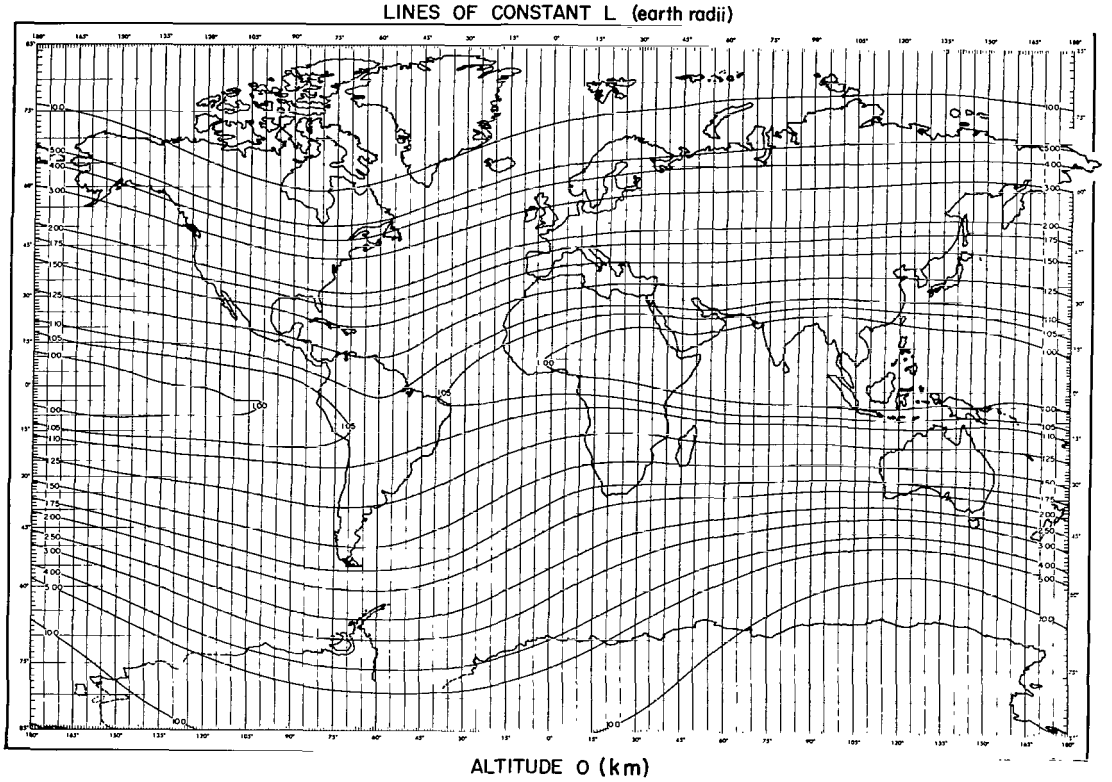

ALTITUDE 0 (km)

LINES OF CONSTANT L (earth radii)

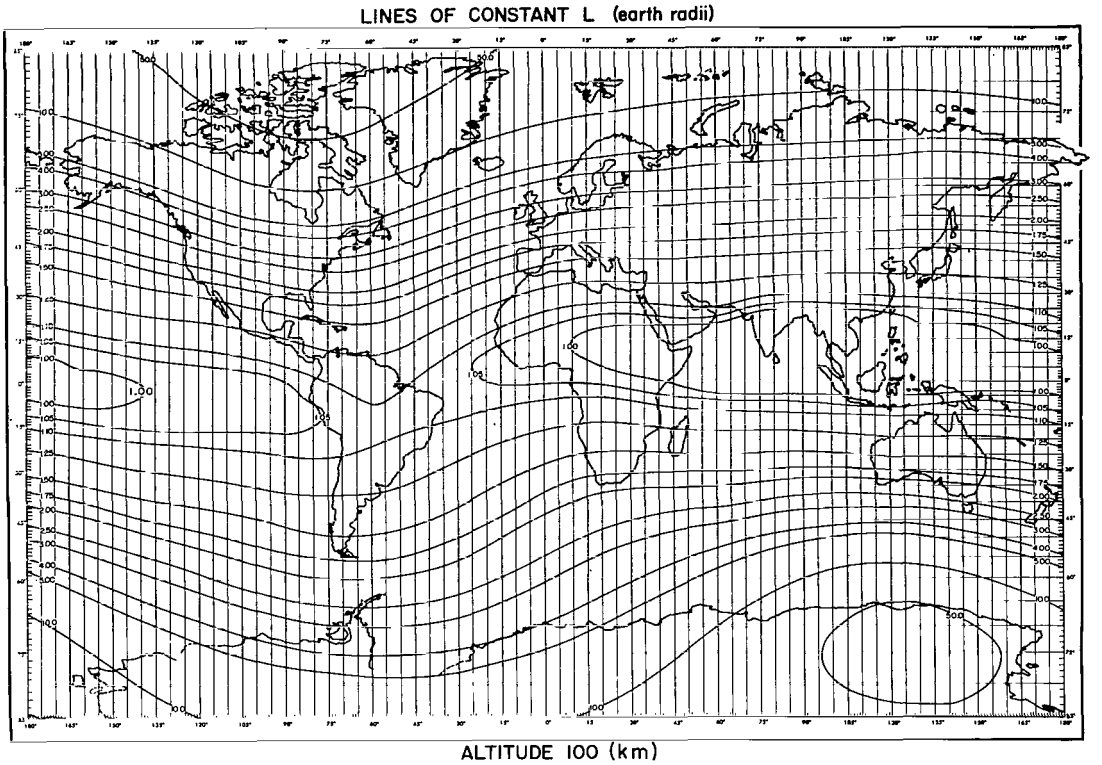

ALTITUDE 100 (km)

LINES OF CONSTANT L (earth radii)

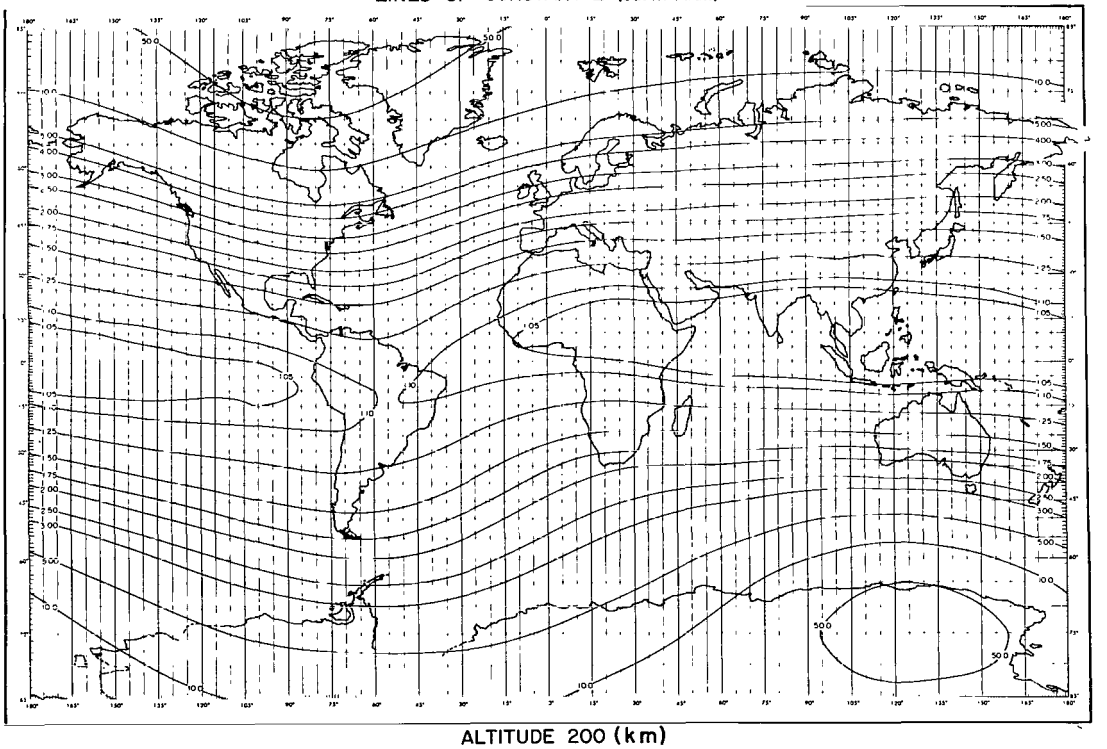

ALTITUDE 200 (km)

LINES OF CONSTANT L (earth radii)

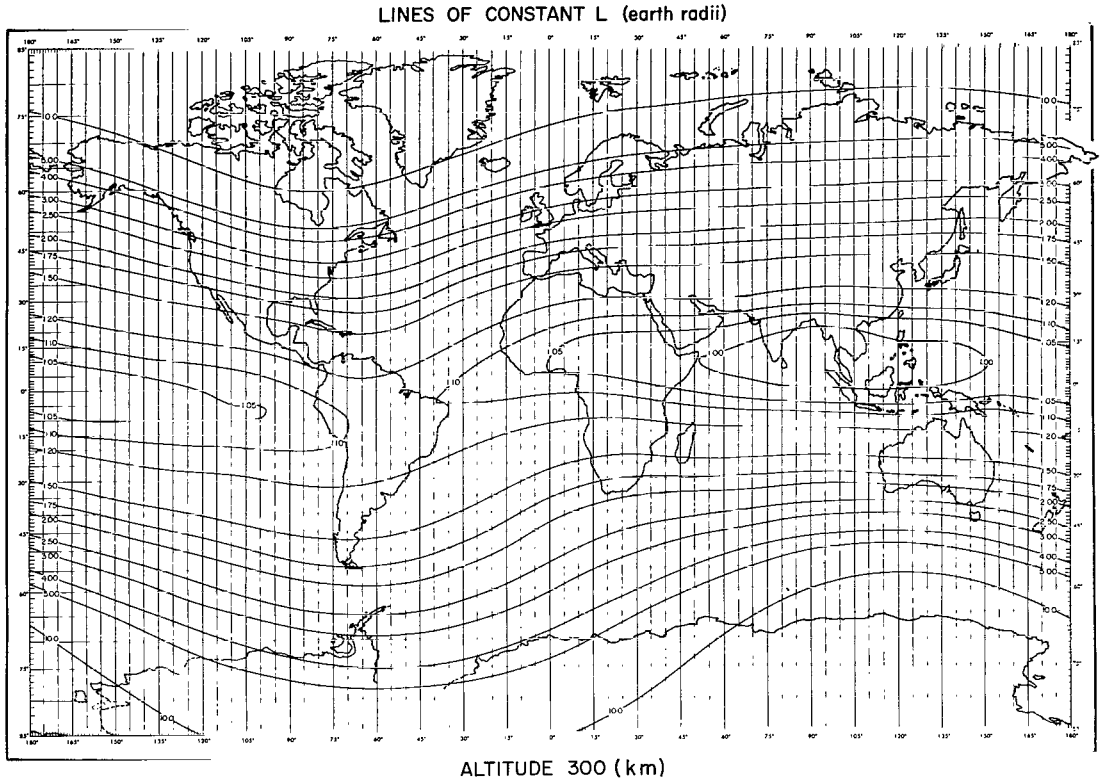

ALTITUDE 300 (km)

LINES OF CONSTANT L (earth radii)

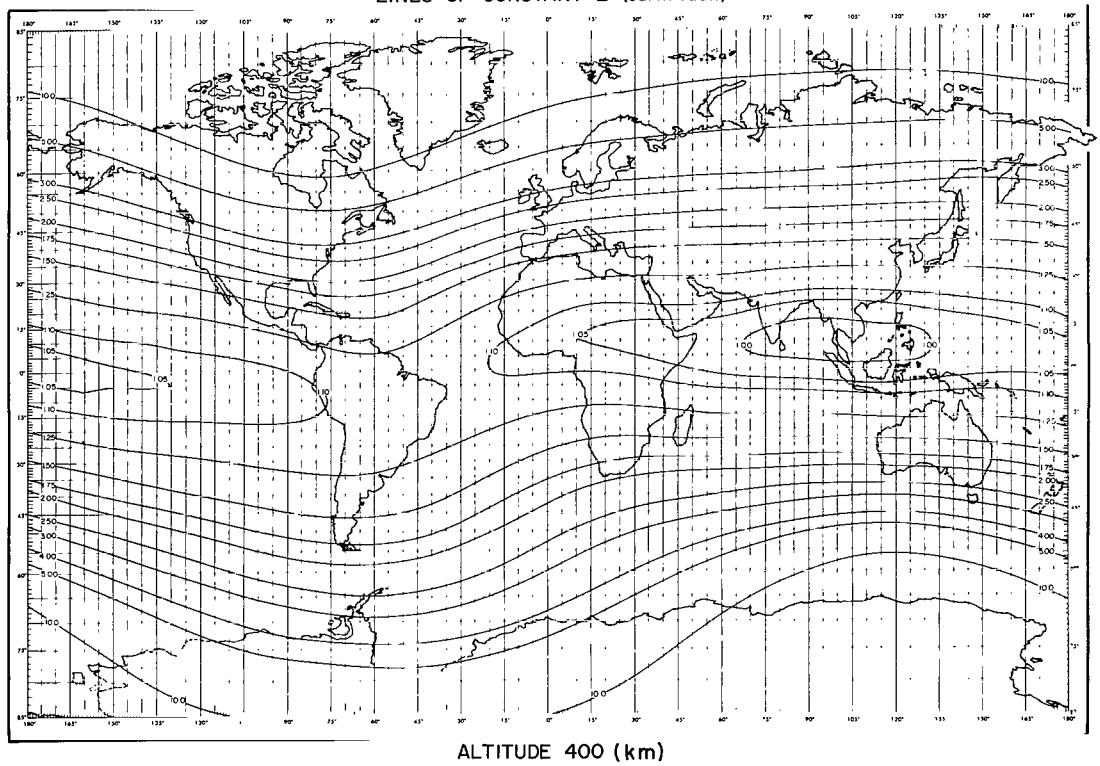

ALTITUDE 400 (km)

LINES OF CONSTANT L (earth radii)

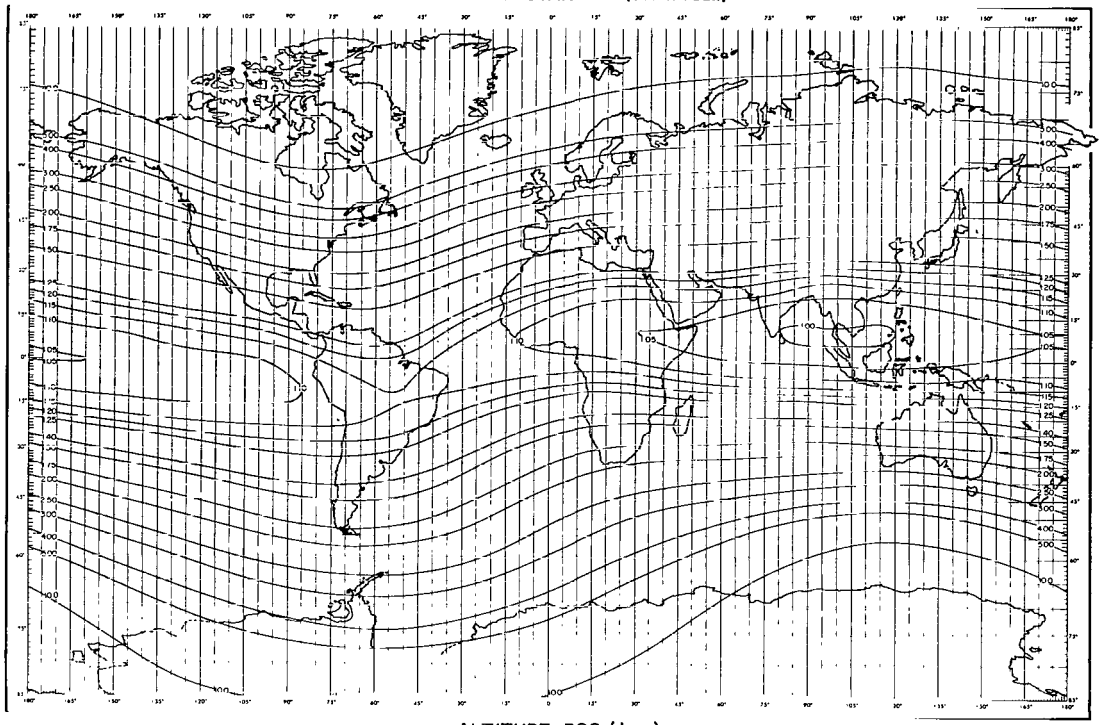

ALTITUDE 500 (km)

LINES OF CONSTANT L (earth radii)

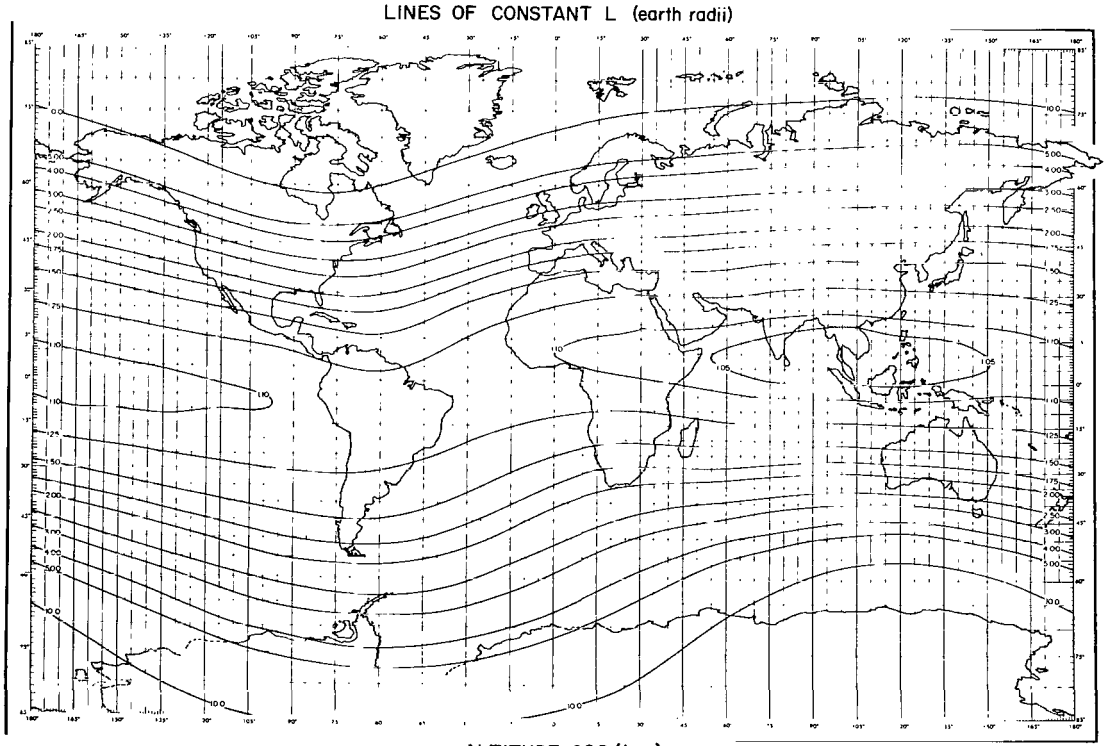

ALTITUDE 600 (km)

LINES OF CONSTANT L (earth radii)

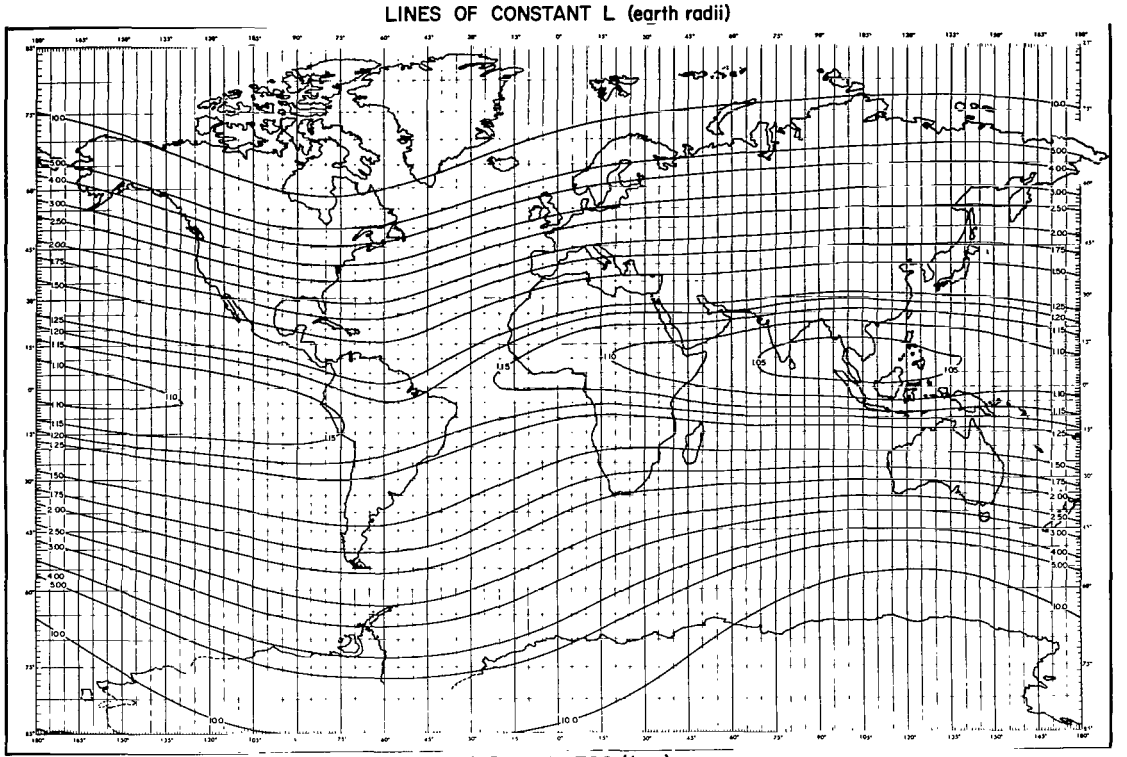

ALTITUDE 700 (km)

LINES OF CONSTANT L (earth radii)

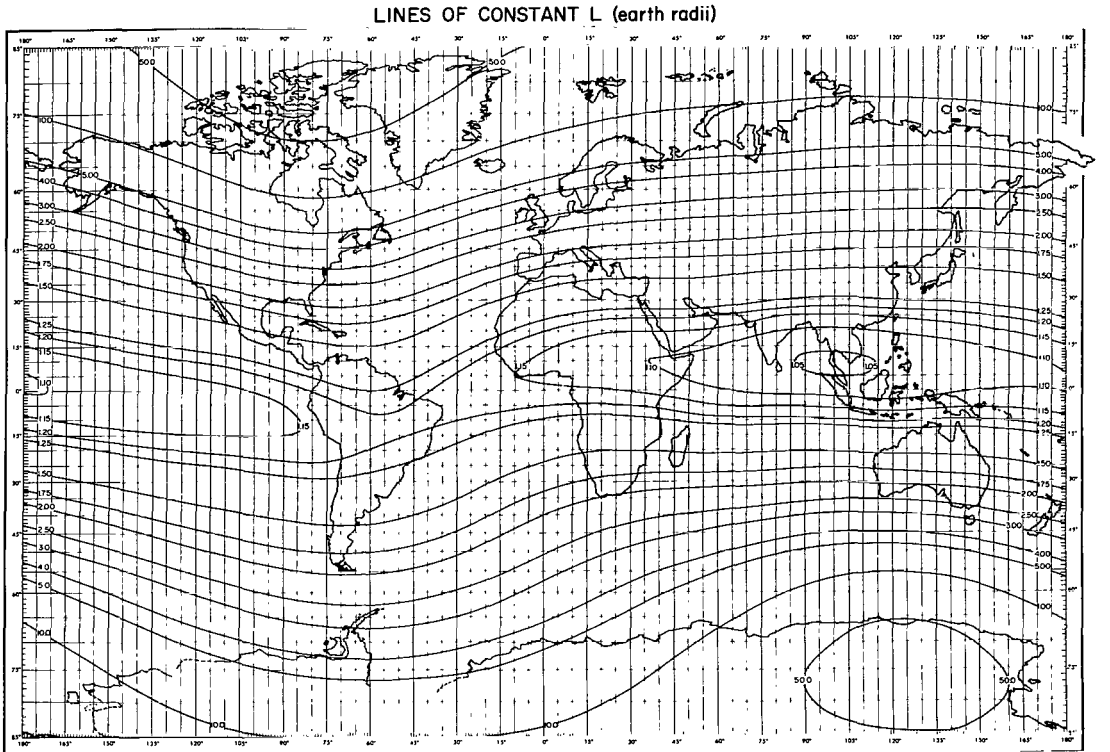

ALTITUDE 800 (km)

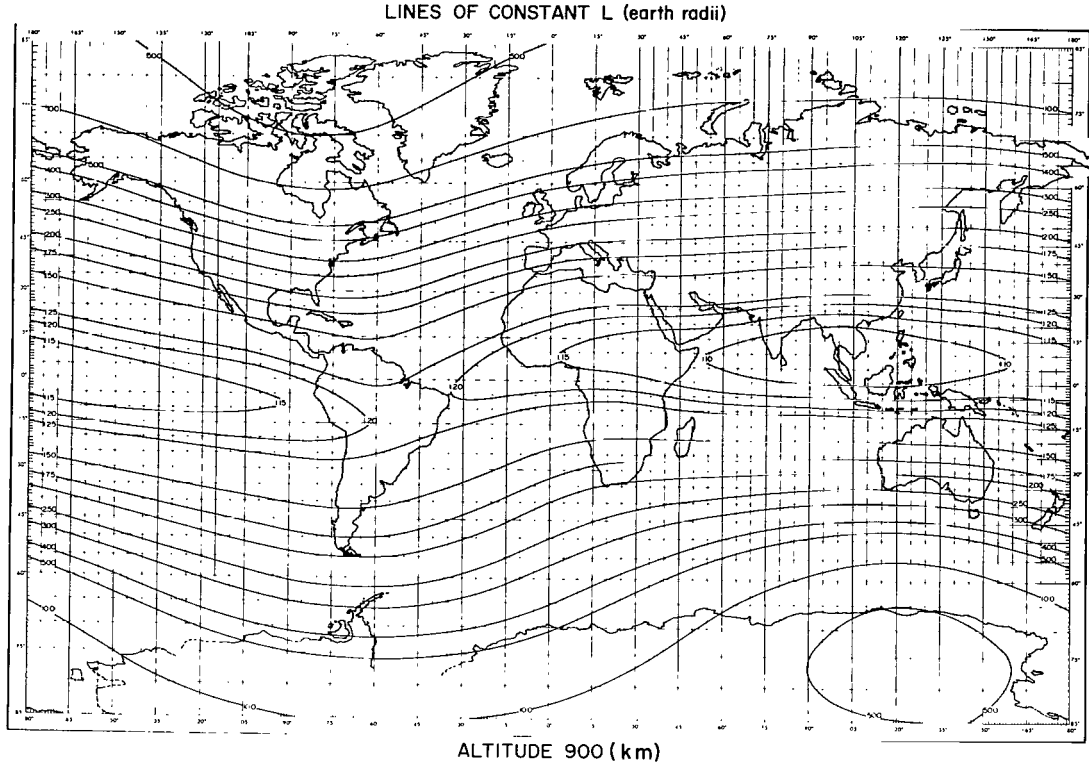


ALTITUDE 900 (km)

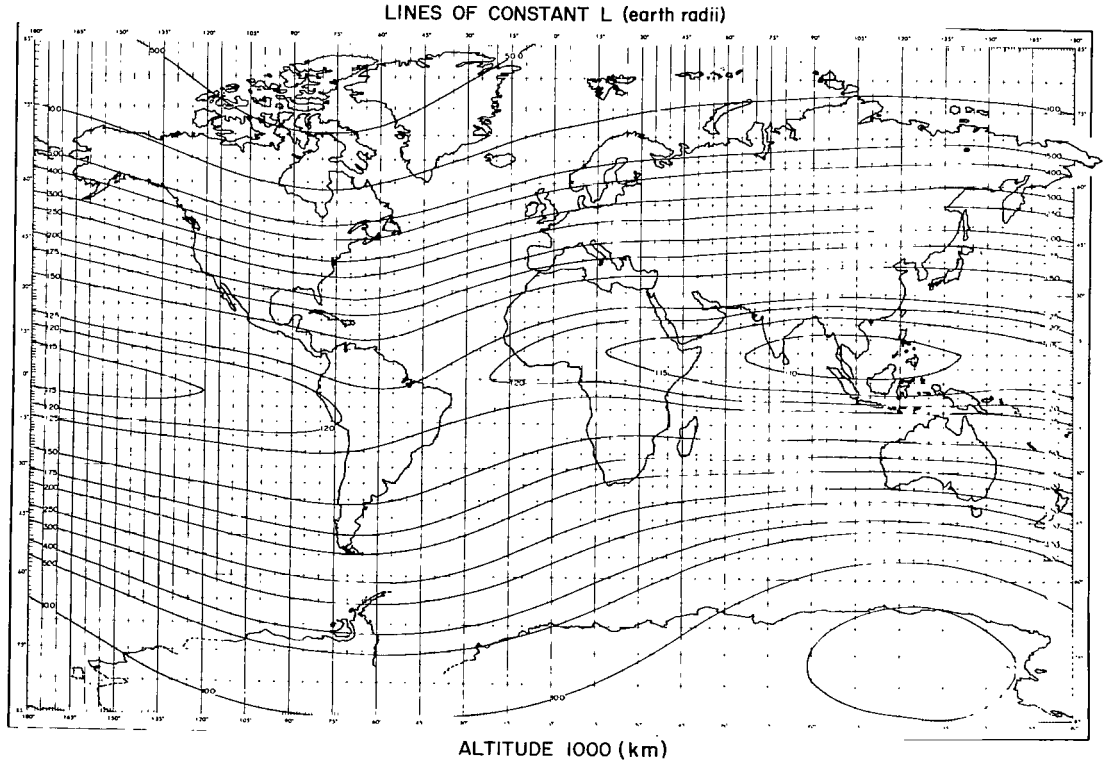


ALTITUDE 1000 (km)

LINES OF CONSTANT L (earth radii)

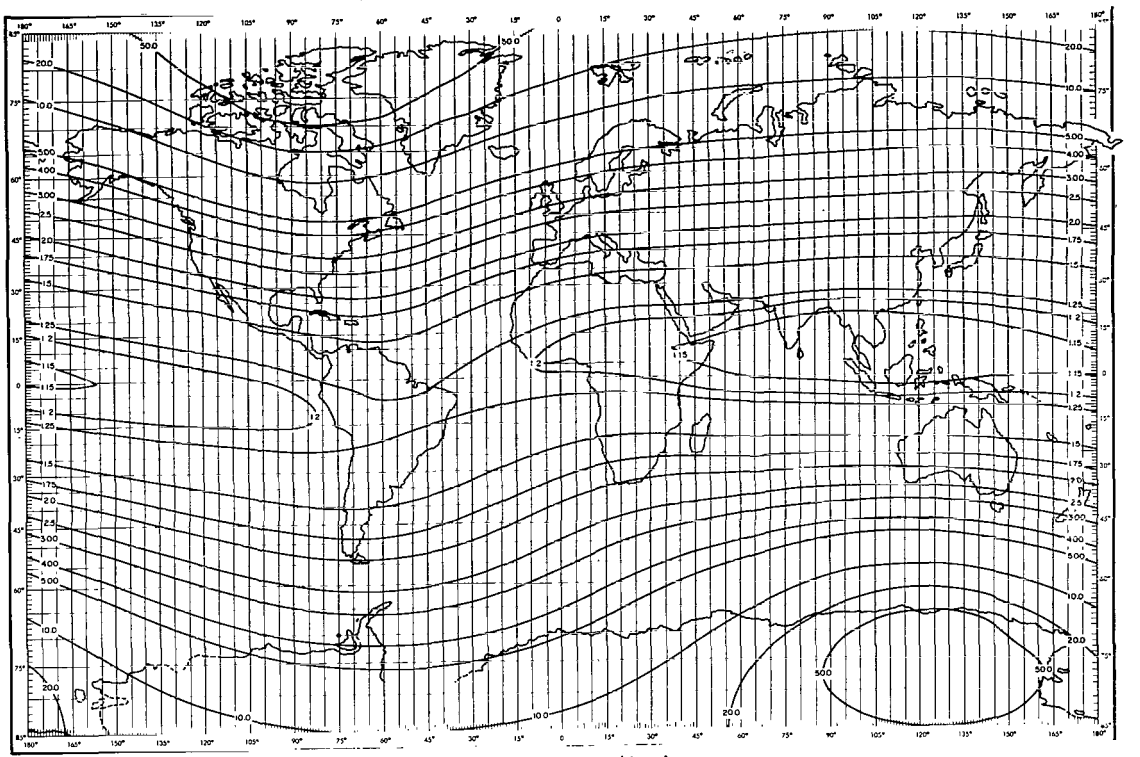

ALTITUDE 1100 (km)

LINES OF CONSTANT L (earth radii)

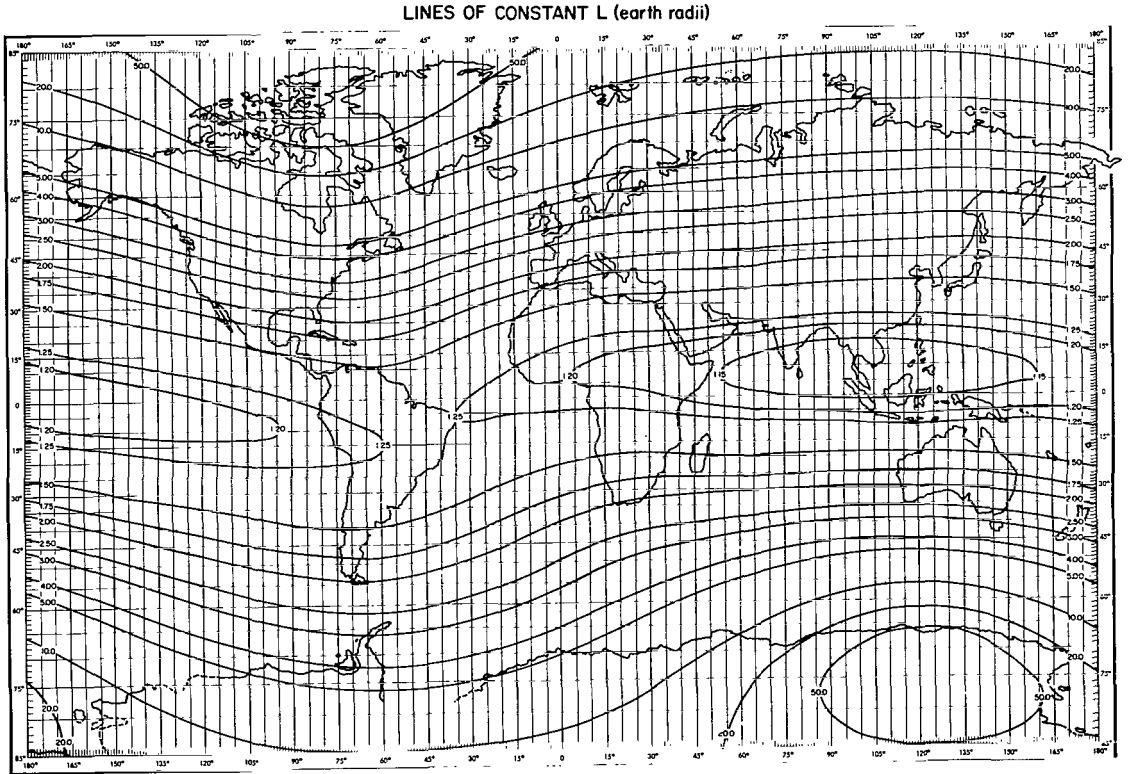

ALTITUDE 1200 (km)

LINES OF CONSTANT L (earth radii)

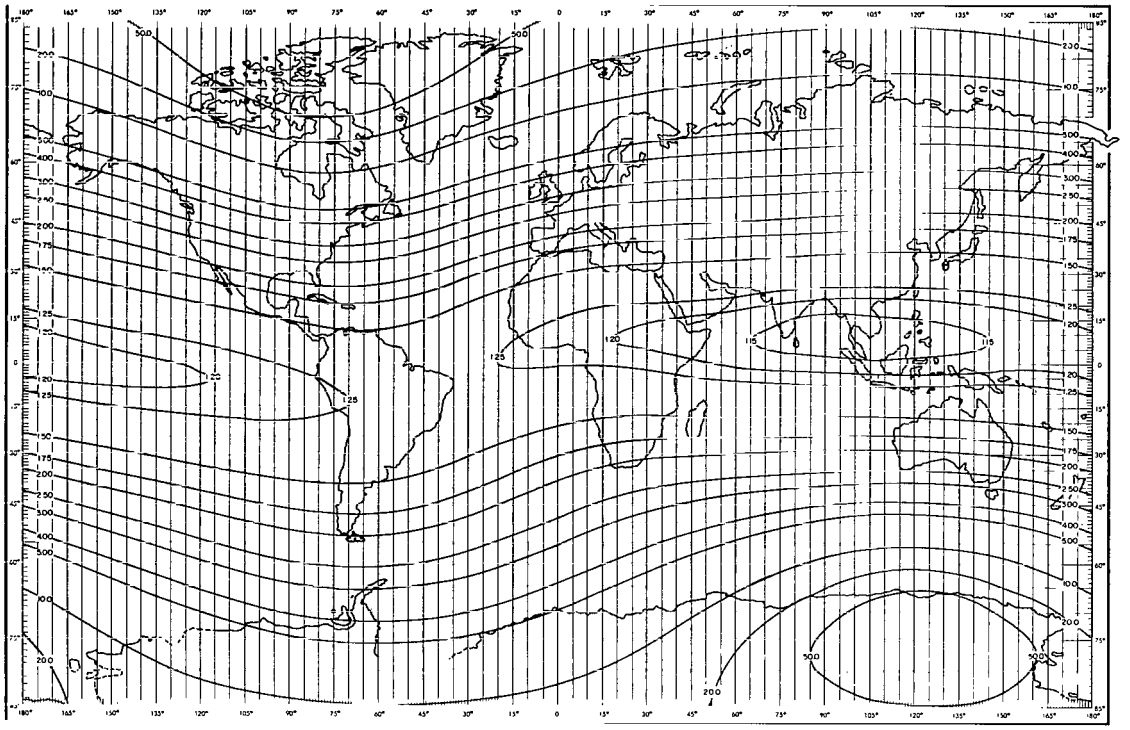

ALTITUDE 1300 (km)

LINES OF CONSTANT L (earth radii)

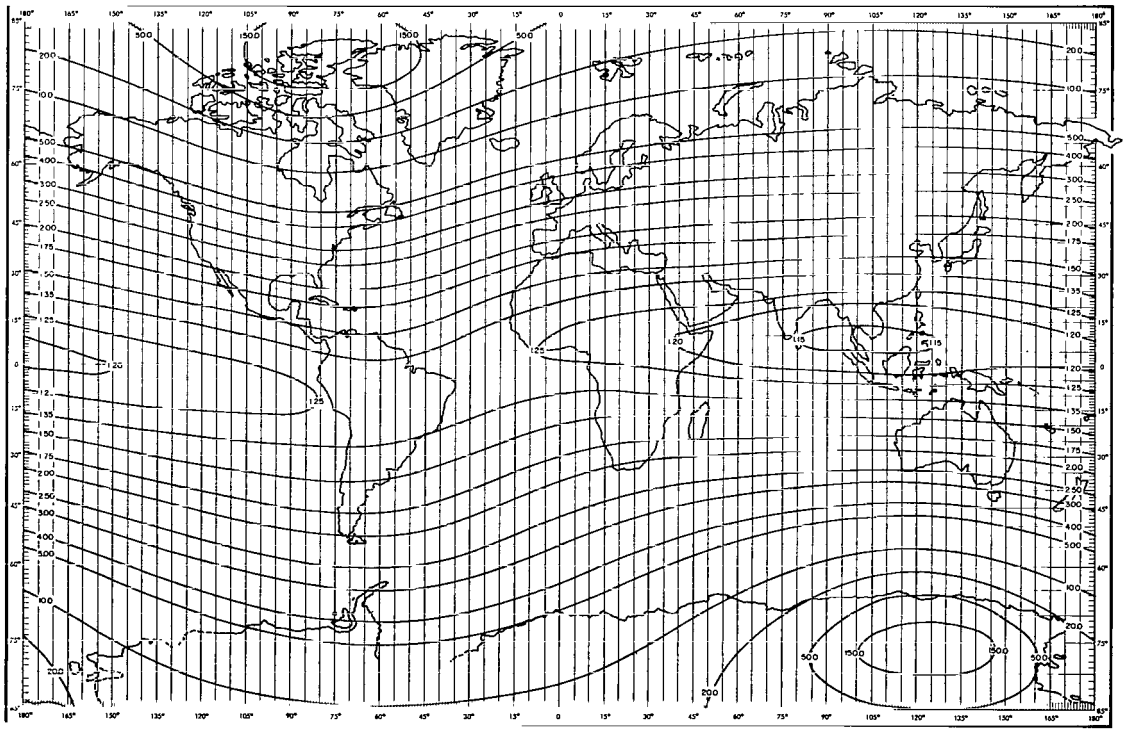

ALTITUDE 1400 (km)

LINES OF CONSTANT L (earth radii)

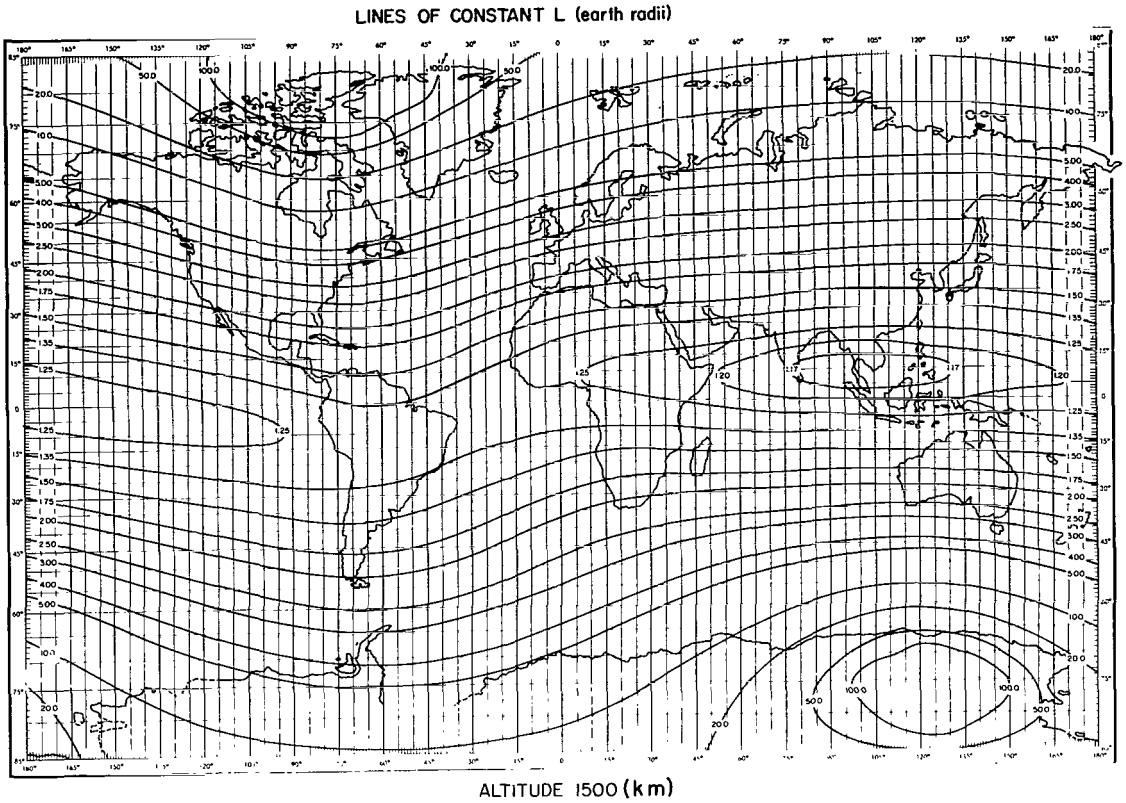

ALTITUDE 1500 (km)

LINES OF CONSTANT L (earth radii)

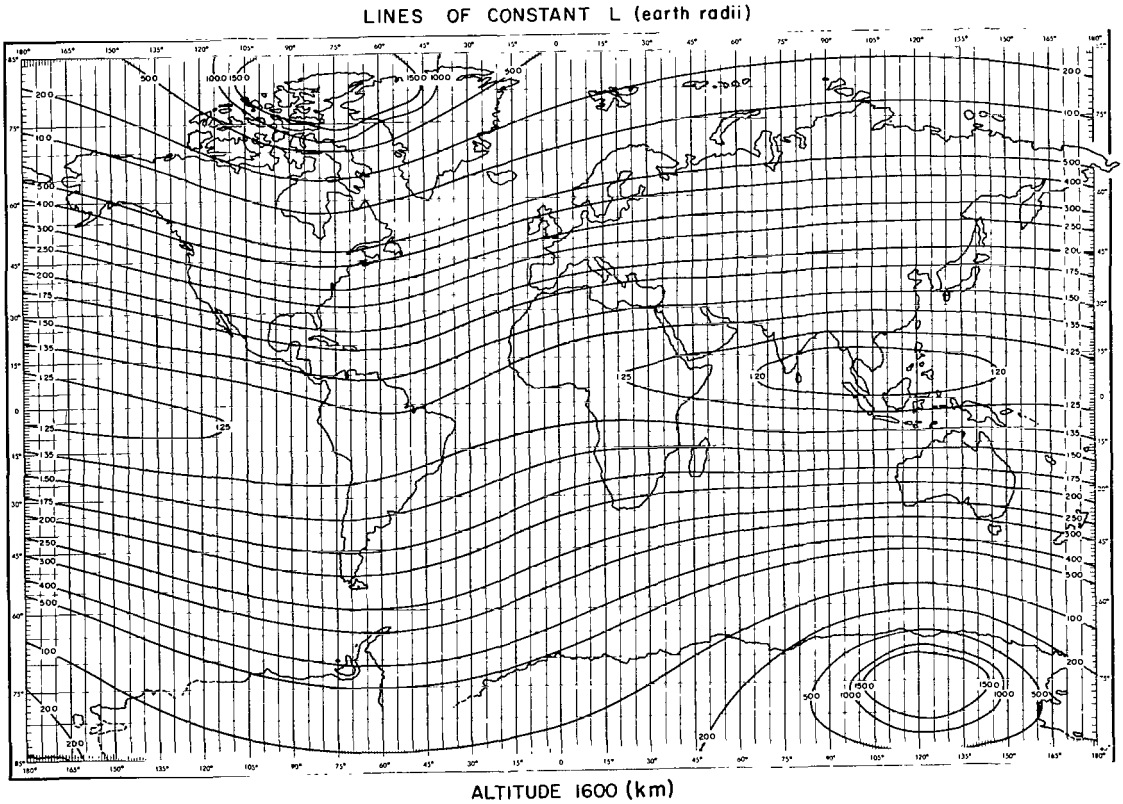

ALTITUDE 1600 (km)

LINES OF CONSTANT L (earth radii)

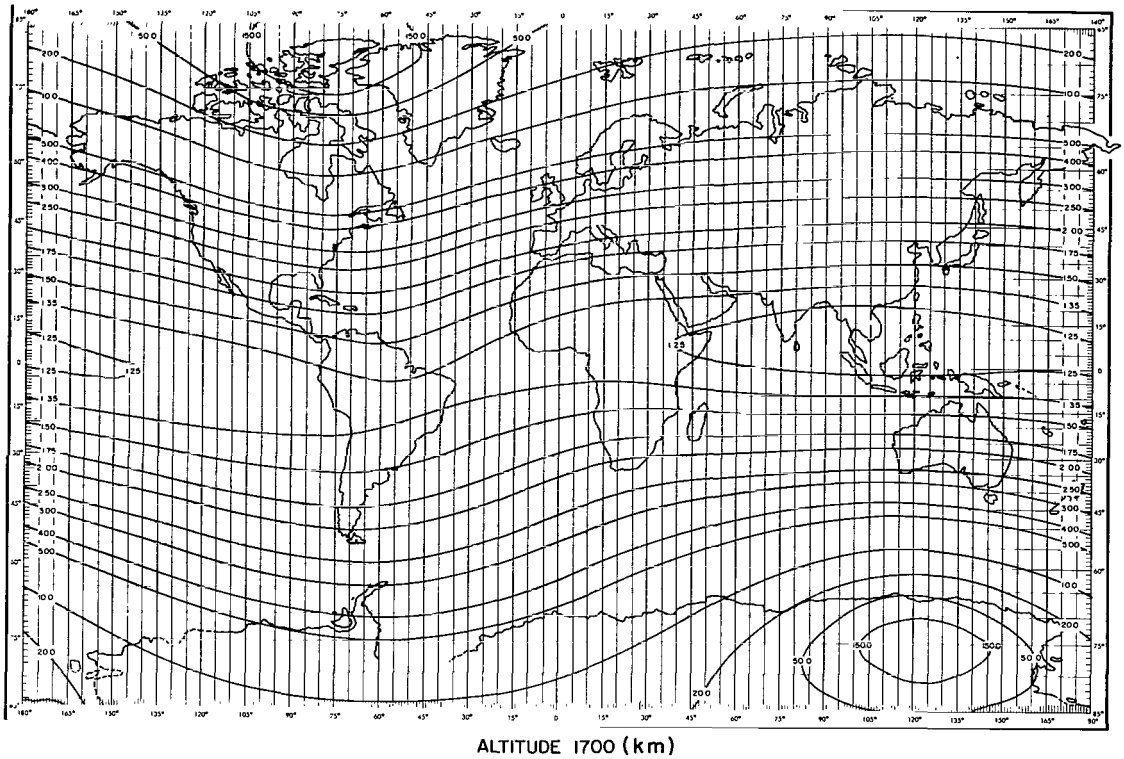

ALTITUDE 1700 (km)

LINES OF CONSTANT L (earth radii)

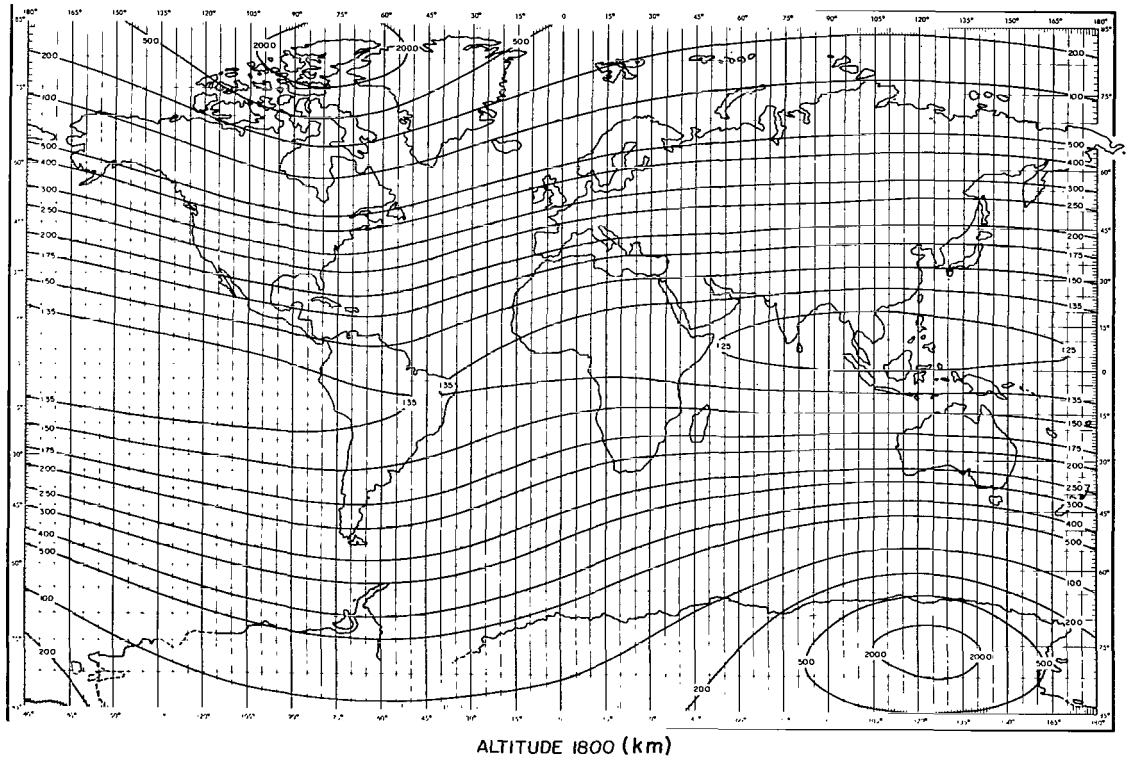

ALTITUDE 1800 (km)

LINES OF CONSTANT L (earth radii)

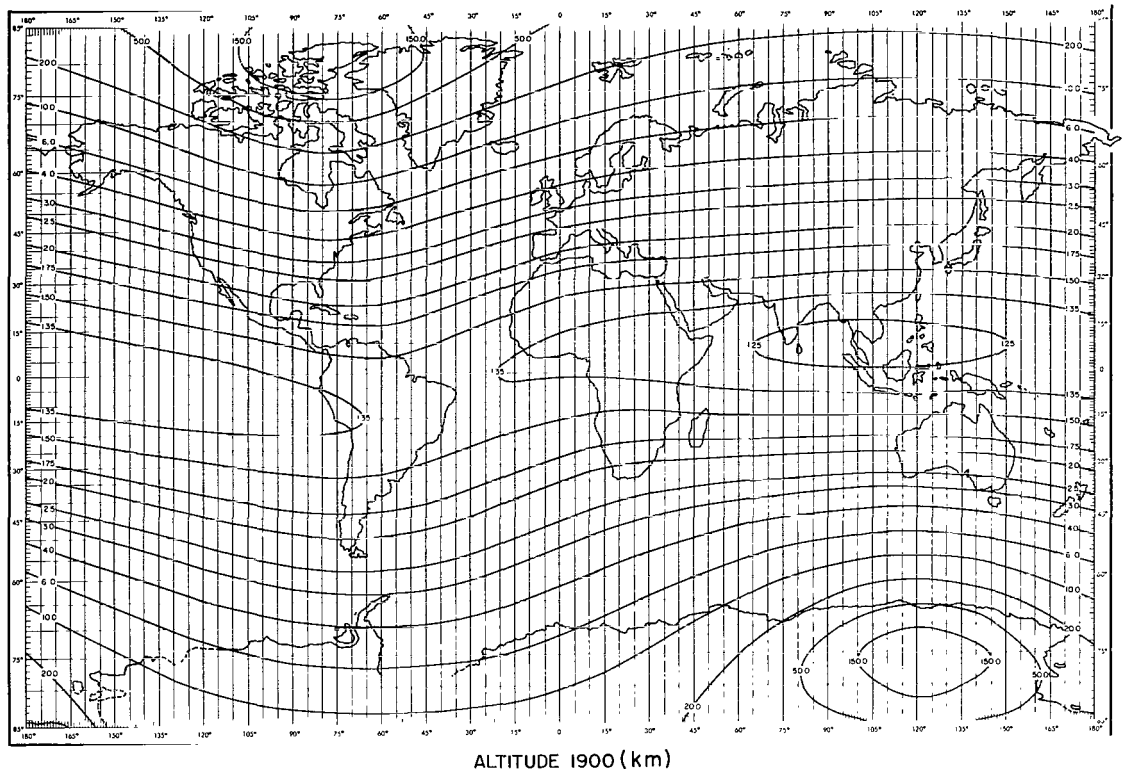

ALTITUDE 1900 (km)

LINES OF CONSTANT L (earth radii)

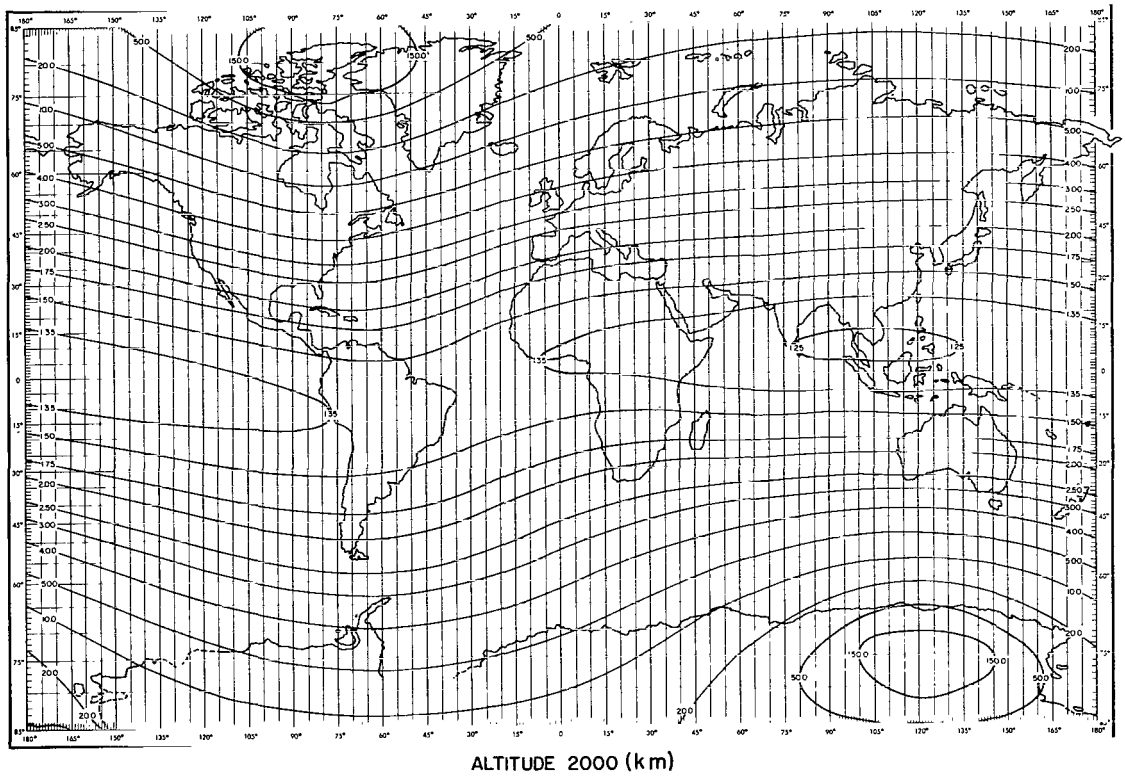

ALTITUDE 2000 (km)

LINES OF CONSTANT L (earth radii)

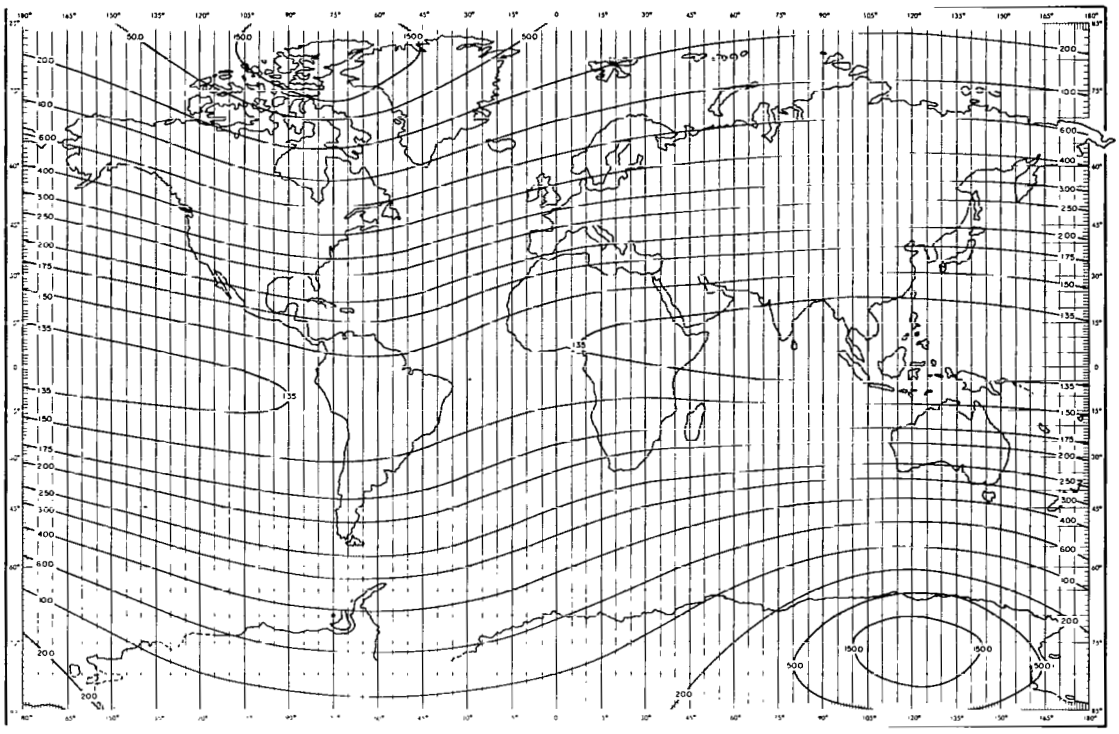

ALTITUDE 2100 (km)

LINES OF CONSTANT L (earth radii)

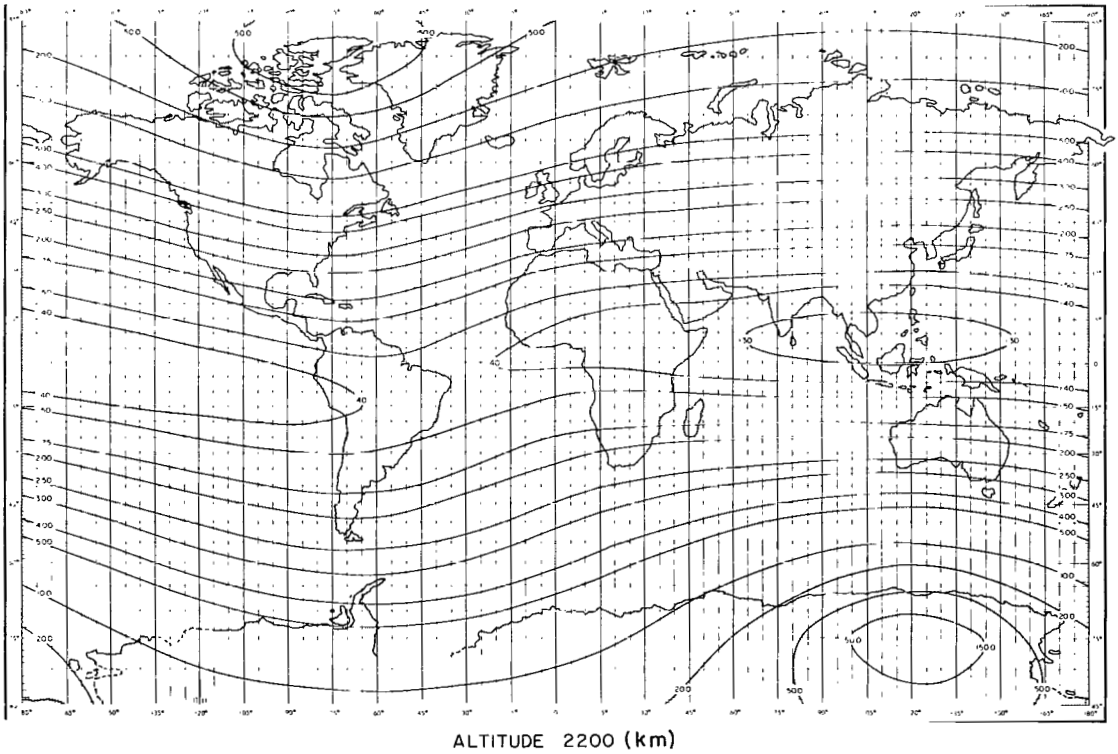

ALTITUDE 2200 (km)

LINES OF CONSTANT L (earth radii)

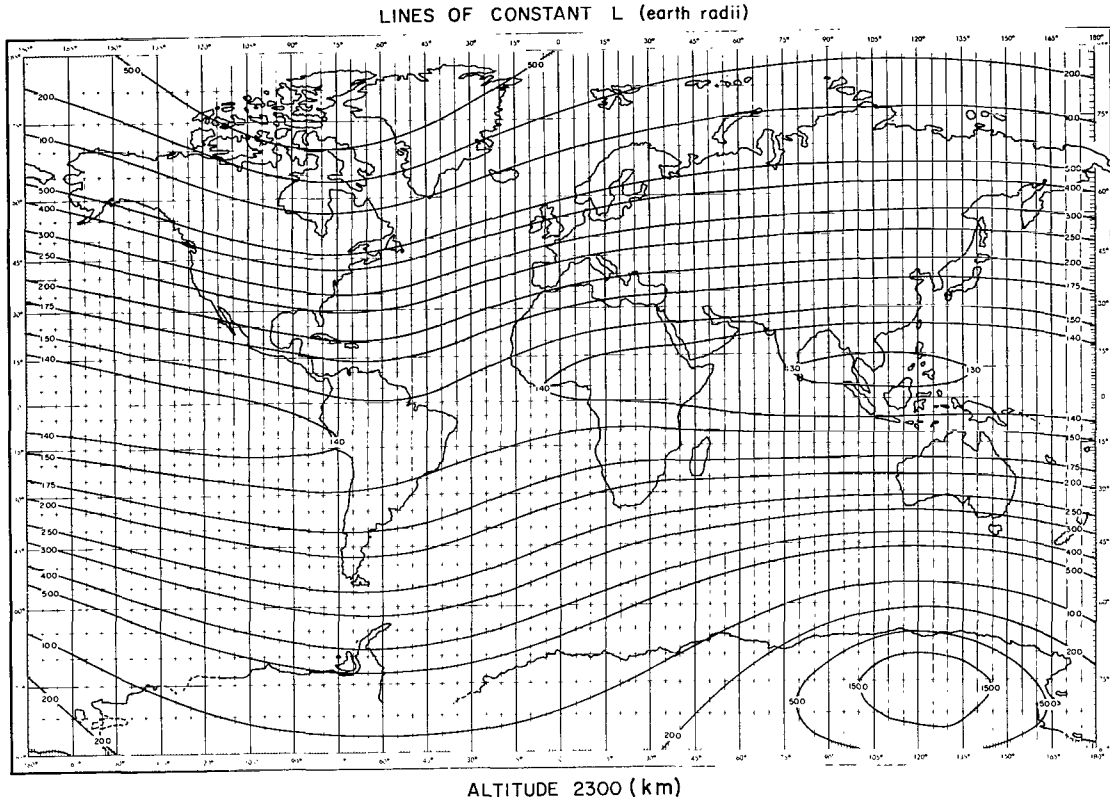

ALTITUDE 2300 (km)

LINES OF CONSTANT L (earth radii)

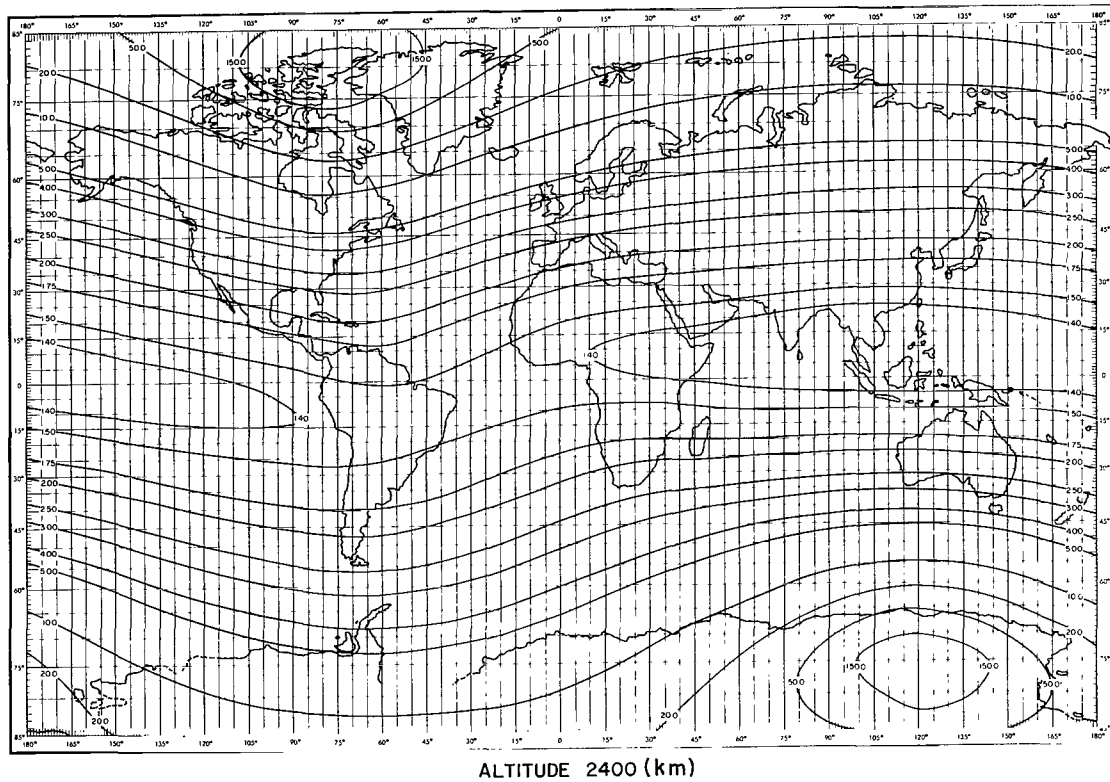

ALTITUDE 2400 (km)

LINES OF CONSTANT L (earth radii)

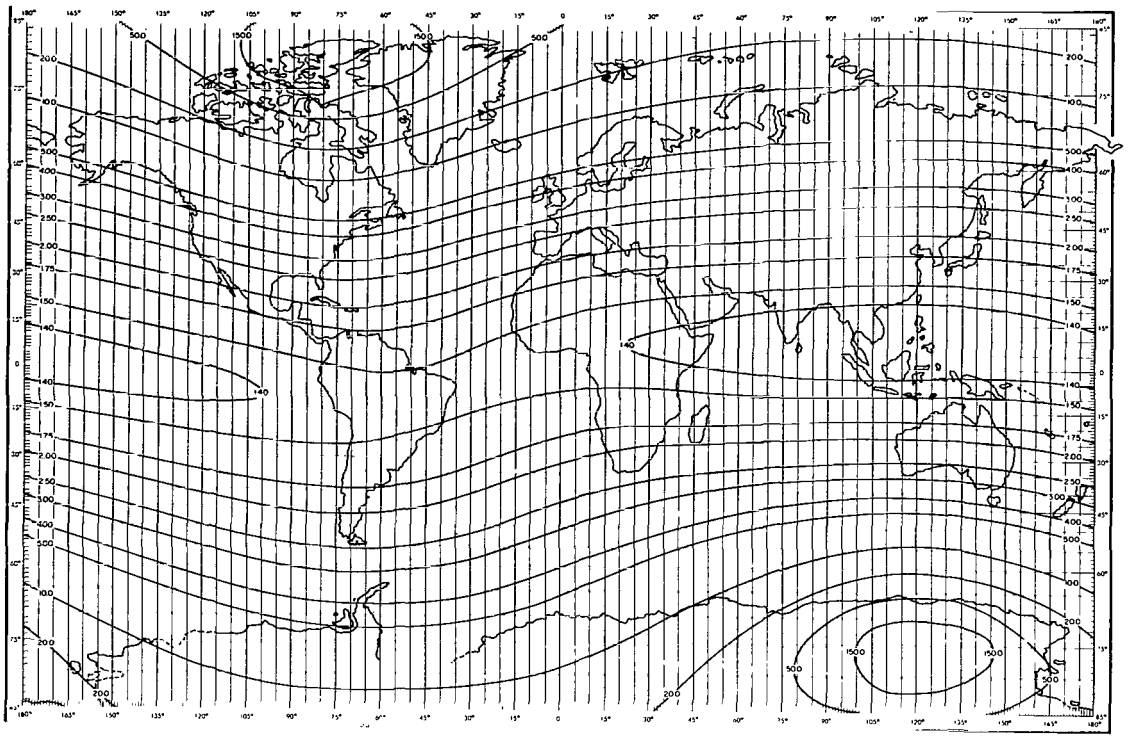

ALTITUDE 2500 (km)

LINES OF CONSTANT L (earth radii)

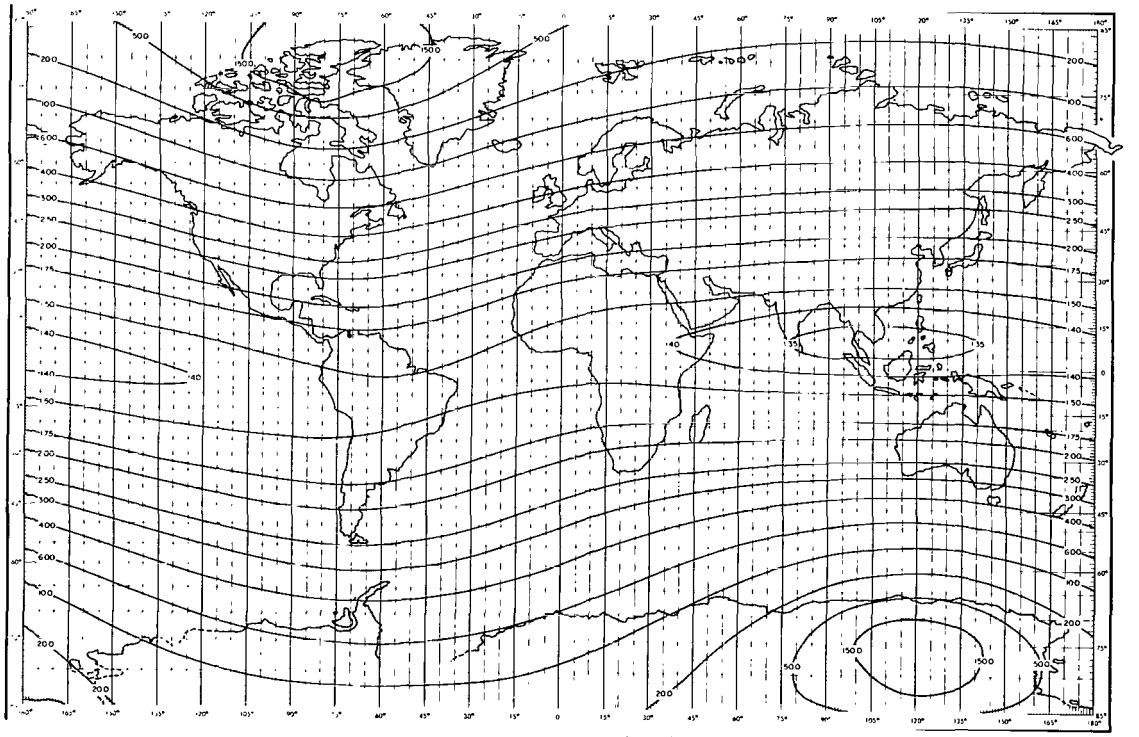

ALTITUDE 2600 (km)

LINES OF CONSTANT L (earth radii)

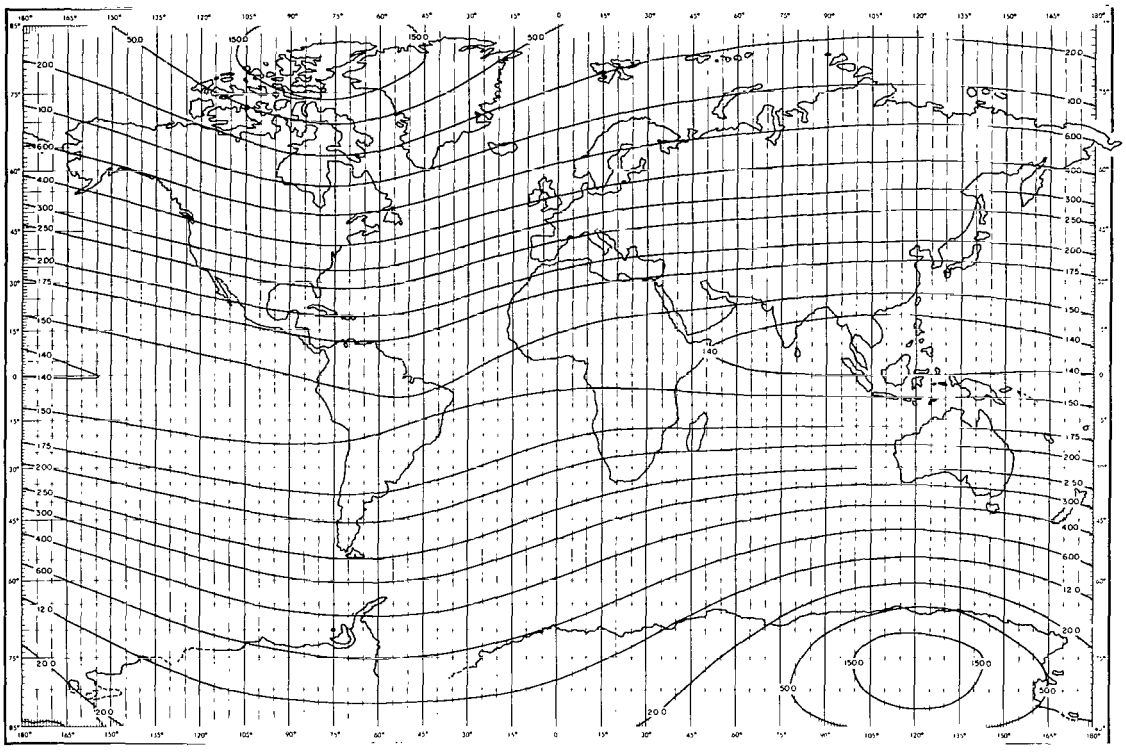

ALTITUDE 2700 (km)

LINES OF CONSTANT L (earth radii)

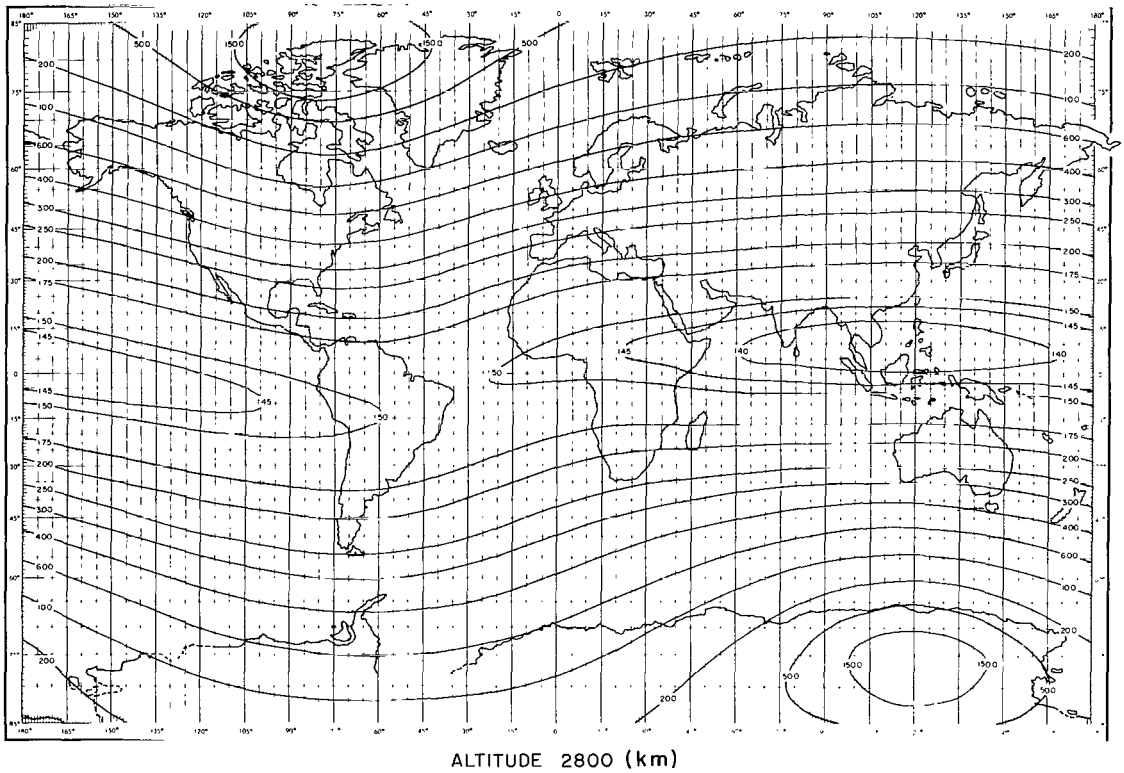

ALTITUDE 2800 (km)

LINES OF CONSTANT L (earth radii)

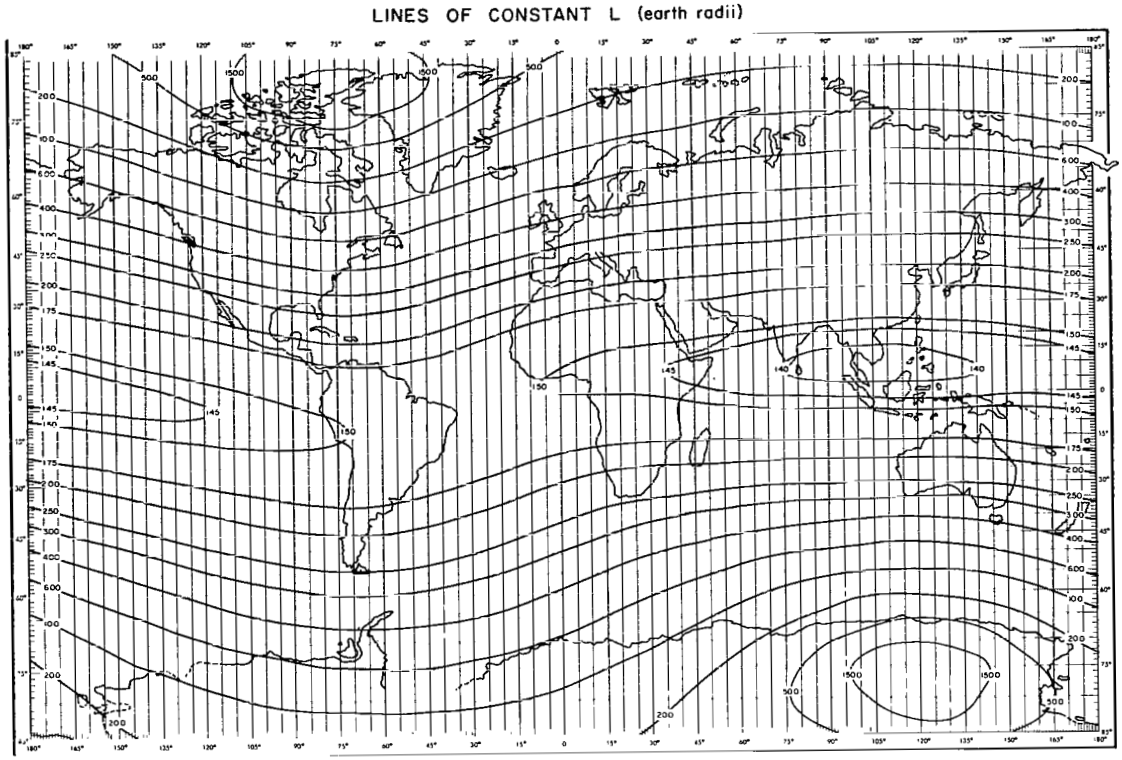

ALTITUDE 2900 (km)

LINES OF CONSTANT L (earth radii)

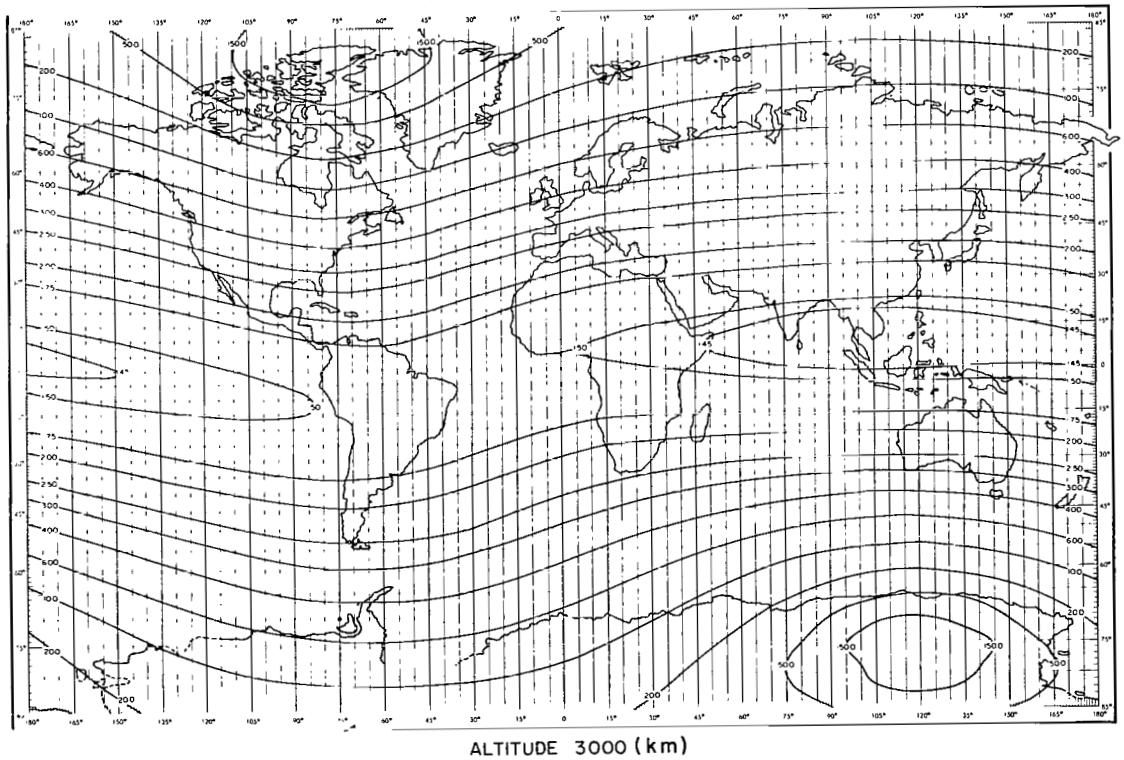

ALTITUDE 3000 (km)

# A SUMMARY OF RESULTS FROM THE IMP-I MAGNETIC FIELD EXPERIMENT

by
N. F. Ness, C. S. Scearce, and J. B. Seek
*Goddard Space Flight Center*

and

J. M. Wilcox
*Space Sciences Laboratory, University of California*

The Interplanetary Monitoring Platform (IMP-I) launched in November 1963 with an apogee of 31.7 $R_e$, has provided the first accurate measurements of the interplanetary magnetic field, the magnetosphere boundary and the collisionless magnetohydrodynamic shock wave associated with the solar wind interaction with the geomagnetic field. The shape of the magnetosphere is found to be roughly cylindrical in shape, diameter = 44 $R_e$, with a hemispherical cap with a radius of curvature of approximately 14 $R_e$. The average direction of the interplanetary field is approximately 140° east of the earth-sun line or 60° west of the sun.

The interplanetary results confirm the general Archimedean spiral structure of the interplanetary magnetic field. This is a direct result of the radial flux of ionized gas from the solar corona by super-Alfvénic magnetohydrodynamic expansion as predicted by Parker. The interaction of the super-Alfvénic plasma flow from the sun with the geomagnetic field leads to the development of a detached bow shock wave and a turbulent transition region in which tangled and rapidly fluctuating magnetic fields are observed.

The experimental detection of an extended magnetic tail on the nighttime side of the earth and an enclosed magnetically neutral sheet represents the most recent important result with respect to the earth's outer magnetic field. Significant time variations of the magnetic field in the tail are in opposition with the solar phase of the sudden geomagnetic storms. Thus the tail appears to play a dominant role in various terrestrial phenomena. The neutral sheet is populated with energetic electrons which may be the source of radiation leading to auroral displays and the Van Allen belts.

## INTRODUCTION

The Interplanetary Monitoring Platform IMP-I, the first in a series of satellites monitoring the interplanetary medium in cislunar space, was launched on 27 November 1963. It carried instruments to perform detailed measurements of magnetic fields, plasmas, energetic particles, and

solar and galactic cosmic rays. A number of publications on the initial results of the magnetic field experiment have already appeared (References 1-6). In addition, some results of other experiments carried on board the satellite have appeared in the literature (References 7-12). This paper briefly summarizes and reviews the significant results of the magnetic field experiment and presents certain new aspects of the experimental measurements and their interpretation.

The initial apogee of the satellite was on the sunlit side of the earth at an earth-sun angle of approximately 33° west of the sun at a geocentric distance of 197,616 kilometers = 31.7 earth radii and an initial perigee of 192 kilometers. The period of this highly eccentric orbit is 93.5 hours. Interpretation of the results from the IMP-I satellite was initially performed by transforming all data obtained into a solar ecliptic coordinate system. This is because the interaction of the solar wind with the geomagnetic field shows a strong day-night asymmetry with apparent cylindrical symmetry about the earth-sun line. The geocentric solar ecliptic coordinate system is defined by an X-axis directed from the earth to the sun, the Y-axis in the plane of the ecliptic, and the Z-axis pointing towards the north ecliptic pole. In this coordinate system, the apparent motion of the satellite apogee is one of westward precession of 4° per orbit as the earth moves about the sun.

Figure 1 shows the variation of the apogee of the satellite in solar ecliptic coordinates. The angle $\theta_a$ is defined as the solar ecliptic latitude and the angle $\phi_a$ as the solar ecliptic longitude of satellite apogee. The measurements of the magnetic field in space will also be presented in the solar ecliptic coordinate system with $\theta$ and $\phi$ defining the direction of the field with magnitude $\bar{F}$. The useful lifetime of the satellite extended over a period of approximately 6 months while satellite apogee varied from a solar ecliptic longitude of 335° to 155° (Figure 1). This permitted mapping of the boundary of the geomagnetic field formed by interaction with the solar wind from the subsolar point through the sunrise terminator and far into the nighttime region of the earth.

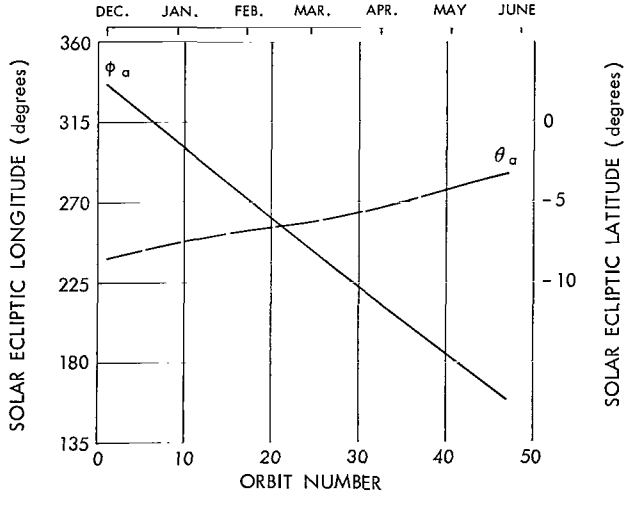


Figure 1—Variation of the apogee (31.7 $R_e$ geocentric) of the IMP-I satellite for orbits 1-47 during the time interval 27 November 1963 through 27 May 1964. The two angles $\theta_a$ and $\phi_a$ represent, respectively, the latitude and longitude of the apogee of the satellite in solar ecliptic coordinates.

Apogee was sufficiently high (Figure 2) that during the first 21 orbits direct measurements of the interplanetary medium were possible which were not affected by the earth's presence and its magnetic field in the supersonic flow of the solar wind. Following orbit 21, measurements in cislunar space were limited to that portion associated with the interaction of the solar wind with the geomagnetic field. Finally, subsequent to orbit 31, the measurements were performed while the satellite was completely enclosed within the distorted geomagnetic field.

The space surrounding the earth is divided into three characteristic physical regions (Figure 2):

1. the *interplanetary medium,*
2. the turbulent *transition region,* and
3. the *magnetosphere* or distorted geomagnetic field of the earth.

These three regions are separated from each other by two characteristic boundaries:

1. The collisionless magnetohydrodynamic *shock wave* (References 13-15)

and

2. The magnetosphere boundary or *magnetopause.*

Repeated traversals of these two boundaries by IMP-I have yielded extensive measurements defining their physical properties and have permitted the geometrical description and physical separation of cislunar space into these three characteristic regions.

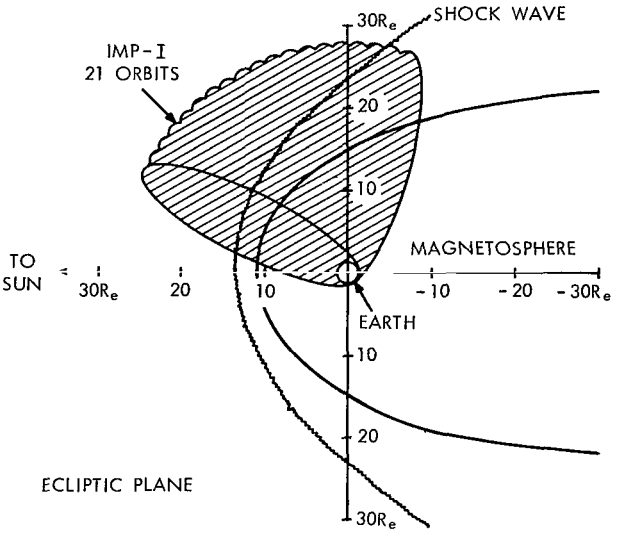


Figure 2—Simplified summary of results of mapping the terrestrial magnetosphere boundary with the interplanetary medium. Illustrated on the plane of the ecliptic are the positions of the magnetosphere boundary and the collisionless magnetohydrodynamic shock wave. The shape and position of the detached bow shock wave closely parallel that observed in supersonic gas dynamics at Mach numbers corresponding to the ratio of the solar wind velocity to the Alfvén velocity.

The *interplanetary medium* is characterized by a weak magnetic field of approximately 5.1 gammas average magnitude embedded within a radial plasma flux emitted from the surface of the sun, which is referred to as the solar wind (Reference 16). At the earth's distance of 1 Astronomical Unit (AU) the plasma shows flow velocities between 300 to 700 kilometers per second and densities between 2 to 20 protons per cubic centimeter. The direction of the magnetic field is variable but the magnitude is impressively constant over long periods of time so that $\delta F/\bar{F} < 0.1$. A general Archimedean spiral structure has been observed in the interplanetary field which can be correlated with the rotational period of the sun and hence corotates with the sun and is suggested to be of solar origin.

The *transition region* is observed to be a turbulent, thermalized, magnetized plasma with field strengths varying between 5 and 20 gammas and fluctuations over short time scales of 10 to 20 gammas. No periodic wave forms are readily discernible in the data and the fields are thus described as tangled or randomly oriented. A thermalized plasma is observed near the stagnation point of the solar wind flow in which the spectrum is considerably broadened and the density increases by a factor of approximately 8 (Reference 9). The solar wind is found to resume a supersonic flow condition around the flanks of the *magnetosphere.*

The measurements of the distorted geomagnetic field on the night side of the earth reveal the extension of the geomagnetic field far behind the earth forming a *magnetic tail.* Embedded within this magnetic tail, a magnetically neutral surface has been discovered which separates regions of oppositely directed fields over a thin planar region of space. This is referred to as a *neutral sheet* and can be correlated with increased particle fluxes illustrating a balance between field and particle pressures.

This paper presents first a summary of the results obtained while the satellite was in interplanetary space beyond the shock wave during orbits 1 through 21, representing the time interval 27 November 1963 through 17 February 1964 and corresponding approximately to three solar rotations, 1784 through 1786. In general, solar activity has remained at a low level throughout the satellite's lifetime. This paper will not discuss any storm-time variations, either of the interplanetary magnetic field or the earth's magnetic tail field. Subsequent publications will deal with these transient phenomena in as comprehensive a treatment as possible.

## INTERPLANETARY MAGNETIC FIELD RESULTS

After the early suggestions by Biermann (Reference 17) that the sun must be a continual source of a low-energy corpuscular flux or solar plasma, Parker (Reference 18) developed the theory of the solar wind, describing the expansion of solar coronal gases into interplanetary space at super-Alfvénic velocity. A particular distinguishing result of Parker's model is the twisting of solar photospheric magnetic fields into an Archimedean spiral in the ecliptic plane as a result of the uniform radial flux of coronal gases and the rotation of the sun. This is illustrated in Figure 3 for solar wind velocities as typically measured in the interplanetary medium from 300 to 900 kilometers per second (References 9 and 19). It is seen that the angle $\phi$ or $\phi'$ is approximately 135° or 315°, respectively. Thus the direction of the field is approximately 45° with respect to the earth-sun line. This is a direct result of the approximate equality of radial velocity of solar plasma with the tangential velocity of a radius vector fixed to the sun and rotating with a synodic period of 27.3 days.

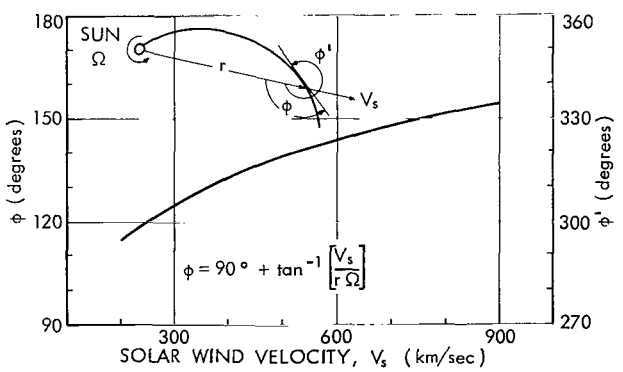


Figure 3—Theoretical direction of the interplanetary magnetic field, assumed to be of solar origin, twisted into an Archimedean spiral by the rotation of the sun and the radial efflux of highly ionized gases. The two directions $\phi$ and $\phi'$ correspond to fields directed essentially away from or towards the sun along the characteristic streaming angle. Note the relative insensitivity of the direction to changes in typical solar wind velocities from 300 to 700 km/sec.

The measurement of the magnetic field on IMP-I was performed for 4.8 seconds every 20.4 seconds repeatedly within a telemetry format for a consecutive total of 12 such data points distributed over an interval of 5.46 minutes in transmission time. These measurements yielded 12 vector samples of the interplanetary magnetic field. Individual orthogonal components of the vector field were averaged

and used to construct an average vector magnetic field for the time interval of 5.46 minutes.

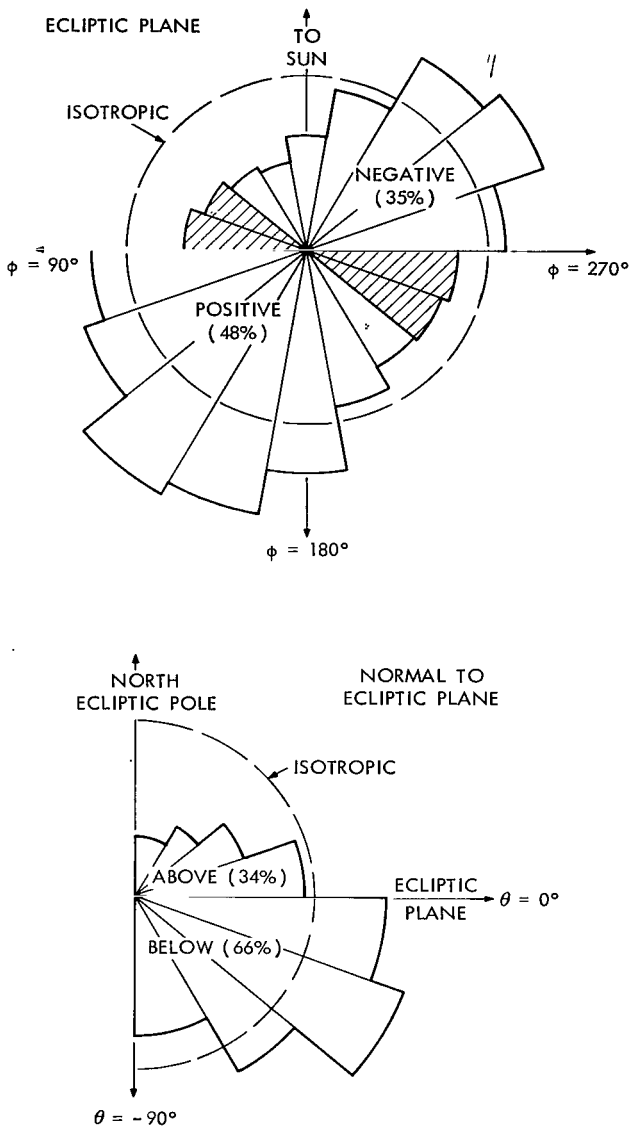


Figure 4—Statistical distribution of the direction of the 5.46-minute component-averaged interplanetary magnetic field as observed on IMP-I during solar rotations 1784-1786. The distribution in the plane of the ecliptic indicates a close correspondence with the theoretical model of a continual uniform solar coronal expansion developed by Parker. The field distribution normal to the plane of the ecliptic indicates a small but distinct southward-directed component.

The statistical distribution of the direction of the interplanetary magnetic field observed by the IMP-I satellite when beyond the shock wave is shown in Figure 4. A broad but distinct peak in the direction of the field is observed at approximately the angle predicted by Parker's uniform coronal expansion model. The top of Figure 4 shows the direction of the interplanetary field projected into the plane of the ecliptic. The bottom view of the figure shows the direction of the field as projected normal to the plane of the ecliptic and without regard to the direction of the field in the plane of the ecliptic.

The magnitude distribution of the interplanetary magnetic field is shown in Figure 5. It should be noted that extremely stringent requirements were placed upon the satellite experiment hardware to minimize their magnetic

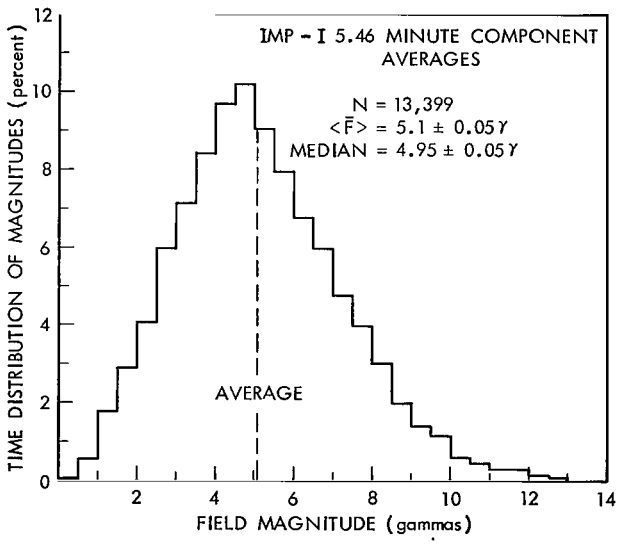


Figure 5—Statistical distribution of the interplanetary magnetic field magnitude for the same data corresponding to that shown in Figure 4. The uniformity of the distribution with an average value of 5.1 gammas is indicative of average photospheric fields of the sun of a few gauss, according to Parker's model.

properties. In addition, the satellite was constructed with long booms which supported the magnetometer sensors at remote distances. These procedures yielded measurements of fields accurate to ±1/4 gamma, the most accurate in space yet performed.

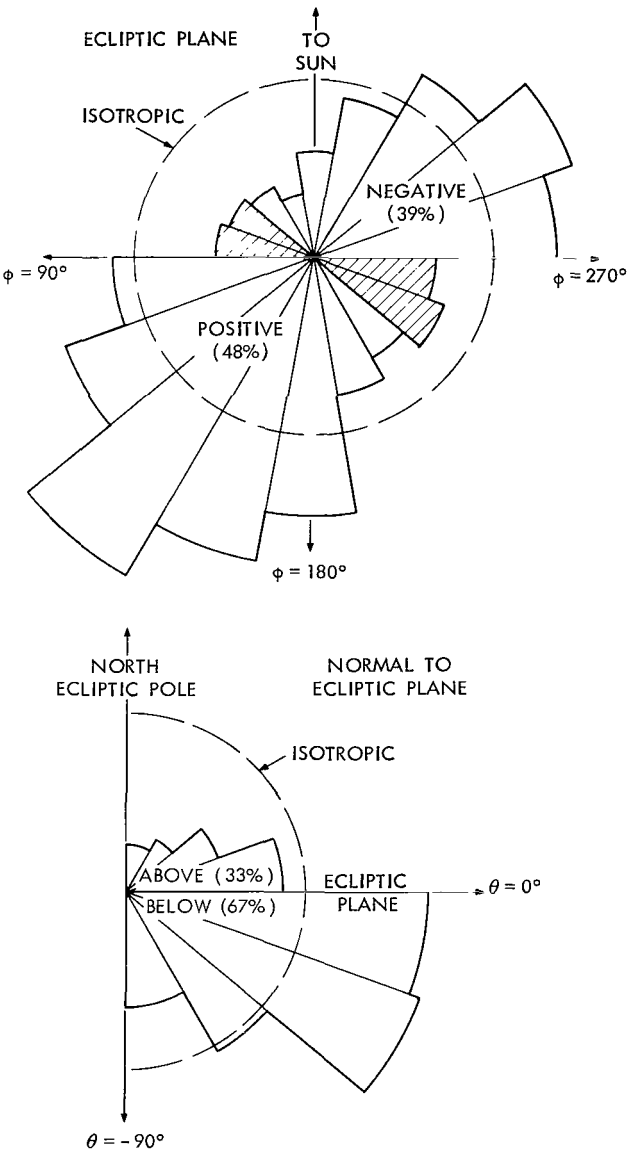


Figure 6—Statistical distribution of the direction of the 1-hour component-averaged interplanetary magnetic field as observed on IMP-I during solar rotations 1784-1786. The distribution in the plane of the ecliptic indicates a closer correspondence with the theoretical model of a continual uniform solar coronal expansion than the 5.46-minute data as shown in Figure 4.

Individual measurements averaged over 5.46 minutes have been component-averaged over a time interval of 1 hour. The statistical distribution of the direction of the interplanetary magnetic field on such a time scale is shown in Figure 6 in the same format as used in Figure 4. The average direction closely parallels that proposed by Parker, as clearly evidenced by the closer and more peaked distribution about the theoretical angles. Figure 7 shows the interplanetary magnetic field magnitude constructed from the hourly component averages. The average magnitude is seen to be 4.5 gammas, approximately 1/2 gamma less than that for the individual values. This indicates that the magnetic field fluctuates in direction and magnitude about the average spiral direction such that the average field magnitude

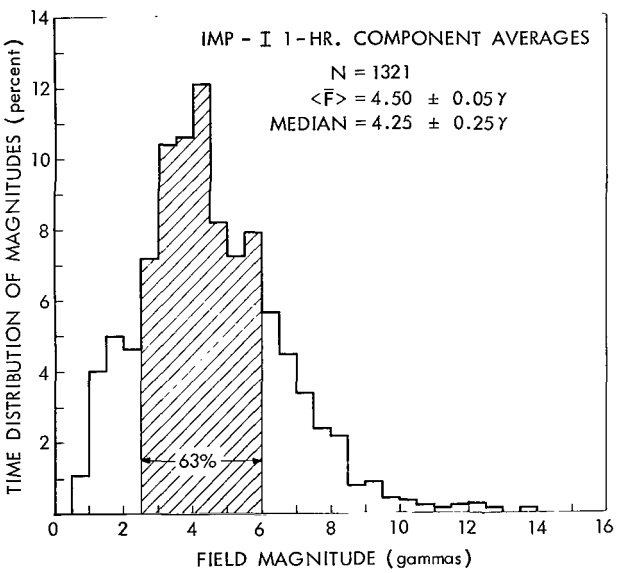


Figure 7—Statistical distribution of the interplanetary magnetic field magnitude for the same data corresponding to that shown in Figure 6. The uniformity of the distribution with an average value of 4.5 gammas is indicative of average photospheric fields of the sum of a few gauss.

decreases as averages extend over longer time intervals.

Additional statistical characteristics of the interplanetary magnetic field are presented in Figures 8, 9, and 10. These show respectively,

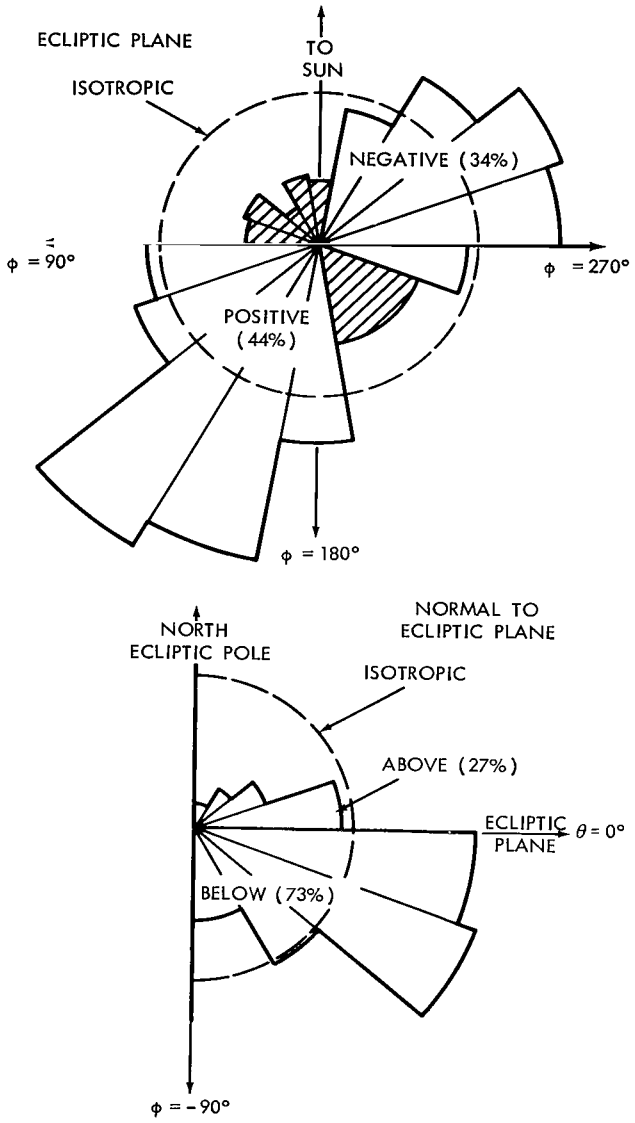


Figure 8—Statistical distribution of the direction of the 3-hour component-averaged interplanetary magnetic field as observed on IMP-I during solar rotations 1784-1786. The distribution in the plane of the ecliptic indicates a still closer correspondence with the theoretical model than shown in Figures 4 and 6 although the lack of 180° symmetry is clearly evident.

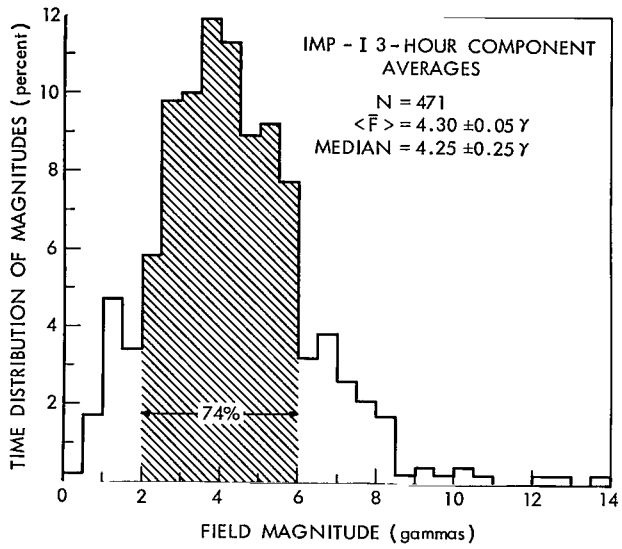


Figure 9—Statistical distribution of the interplanetary magnetic field magnitude for the same data corresponding to that shown in Figure 8. The uniformity of the distribution with an average value of 4.3 gammas is indicative of average photospheric fields of the sun a few gauss according to Parker's model.

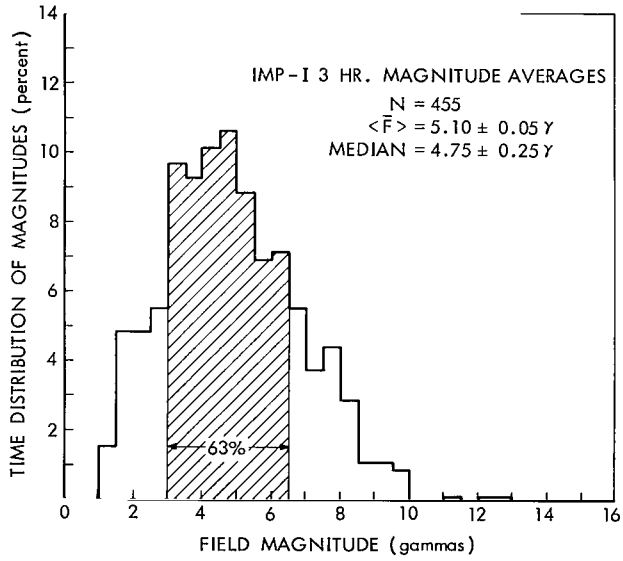


Figure 10—Statistical distribution of the averaged magnitudes of the interplanetary magnetic field over a 3-hour interval. This figure is to be distinguished from the preceding figure in which component averages were employed to construct a 3-hour magnitude average. The average value of 5.1 gammas is identical to Figure 5, as is to be expected.

the directional distribution of the 3-hour component averages of the interplanetary magnetic field, the average magnetic field magnitude over 3-hour intervals, and finally a magnitude-averaged interplanetary magnetic field over a 3-hour time interval. Figure 10 illustrates the differences of averaging the magnetic field components or magnitudes over different time intervals by comparison with Figure 9.

The description of a vector field which is time-variable in both direction and magnitude is a complex task, since simple component averages may represent an average vector field which does not correspond to one which the "real" field ever showed. Thus in the analysis of the time changes of the magnetic field direction in the following section, recourse was always made to the original 5.46-minute averages. Rather than directly averaging the components of the magnetic field separately and then constructing an average field direction, directional histograms were constructed for time intervals of 3, 6, 12, and 24 hours, yielding characteristic directions for the field.

The measurement of 5.1 gamma average magnitude field roughly in the plane of the ecliptic, but with a slight southward component of the field, and directed approximately parallel to the angle predicted by Parker for the field, dramatically confirms the uniform coronal expansion model proposed by him, at least during the years of the quiet sun. It strongly suggests the sun as the origin of the interplanetary magnetic field and indeed in the next section this argument will be developed further to illustrate the continuity of field lines from the sun out to 1 AU.

## CORRELATION WITH THE PHOTOSPHERIC MAGNETIC FIELD

As shown in Figures 4, 6, and 8 the direction of the field can be assigned as either positive or negative depending upon whether or not the field appears to be directed away from or towards the sun along the streaming angle. Using the range of $\phi$ indicated in Figure 4 as positive or negative, it is possible to assign a +1 or -1 to each 3-hour interval covered by the interplanetary data on IMP-I. This time series of alternating values shows the changes in direction of the field as measured at 1 AU by IMP-I. Construction of the autocorrelation function will reveal any basic recurrence tendencies within this time series. Figure 11 presents the normalized autocorrelation of the direction of the interplanetary magnetic field and the results show a statistically significant peak

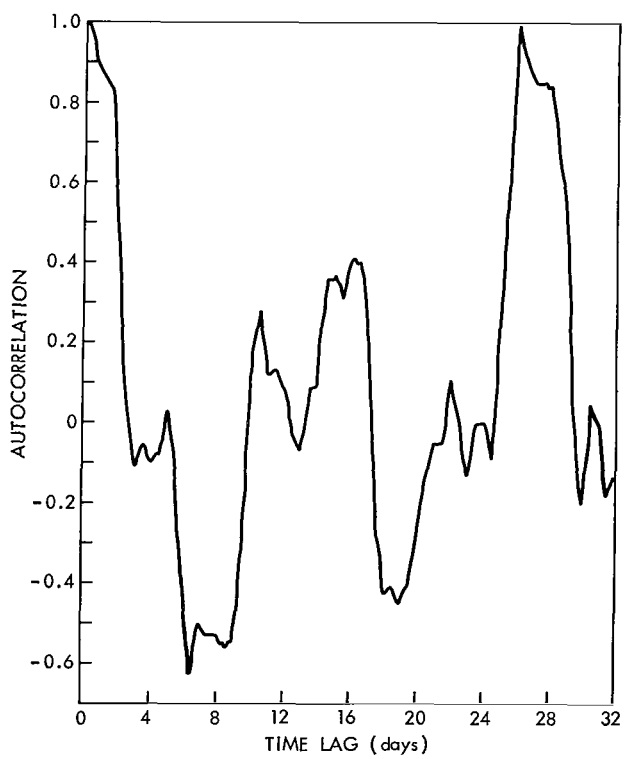


Figure 11—Autocorrelation of the direction of the interplanetary magnetic field as observed by IMP-I. The direction of the field is defined to be either positive or negative according to Figure 4. The autocorrelation of this time series yields a significant peak at approximately 27 days (see text).

at a time interval of approximately 27 days. Since this corresponds to the solar synodic rotation period, it is strongly suggestive of a direct connection of the interplanetary magnetic field with magnetic fields originating on the sun.

It is possible to directly compare the interplanetary and solar fields by utilizing data obtained with the solar magnetograph at the Mount Wilson Observatory in California (Reference 20). Figure 12 illustrates the result from the solar magnetograph during the IMP-I lifetime which presents a mapping of the photospheric magnetic field as observed at central meridian passage (CMP) on each day. The magnitude of the line-of-sight component of the photospheric magnetic field is measured by the longitudinal Zeeman effect on one of the Fe lines in the solar spectrum. Consecutive daily measurements at CMP are combined to produce a contour map which shows large areas on the surface of the sun with magnetic fields in the photosphere which are directed either out of or into the sun.

In a process similar to that for the interplanetary data, a time series was constructed for individual latitude bands 10° wide across the sun: the field direction was determined within a surface area of the solar disk corresponding to a 12-hour longitude interval (equivalent to 6.7° heliographic longitude). With a time series covering the same interval as IMP-I in interplanetary space, it is possible to construct a cross-correlation function between the directions of the interplanetary magnetic field and the photospheric magnetic field.

This result is shown in Figure 13, in which a statistically significant and coherent peak is

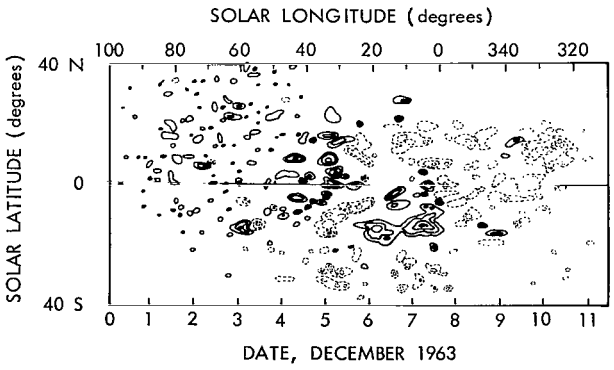


Figure 12—Representative solar magnetograph obtained from the Mount Wilson Observatory showing the magnitude and direction of the line-of-sight component of the photospheric magnetic field at CMP on date shown. The contour interval for these data are taken to be 2, 4, 8, 12, and 25 gauss. A solid line indicates field directed out of the sun while dashed lines indicate fields directed into the sun.

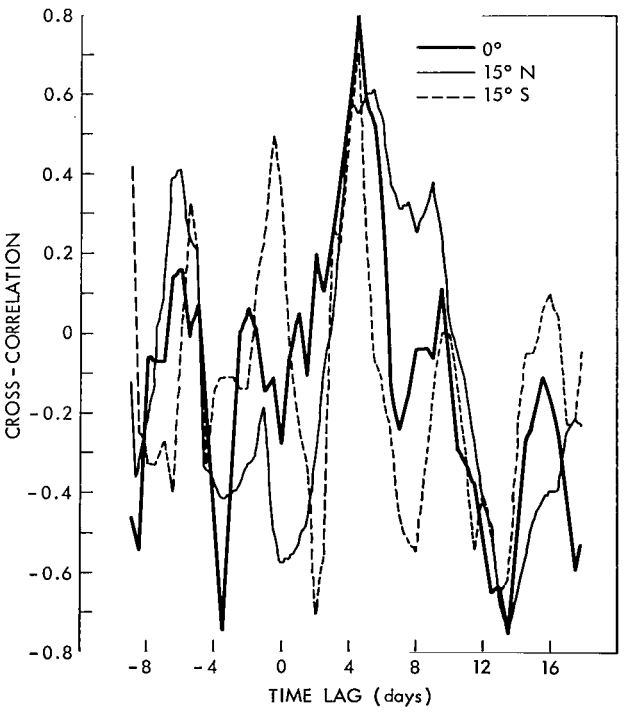


Figure 13—Cross-correlation of the IMP-I interplanetary magnetic field data and the photospheric magnetic field for three latitudes illustrating the coherent and statistically significant peak at 4.5 days. This corresponds to a transport velocity of solar lines of flux to 1 AU of approximately 385 km/sec.

shown for three separate latitude bands across the solar disk. The time lag of 4.5 days is evident, which corresponds to a transport velocity of lines of flux by the solar wind to 1 AU of approximately 385 kilometers per second. The uncertainty in the time lag corresponds to the smallest unit of time available, ±12 hours, so that the average solar wind velocity from the magnetic field measurements is inferred to be 385 ± 45 kilometers per second. The lower limit of this velocity, 340 kilometers per second, is very close to the direct measurement of the solar wind velocity by the MIT plasma probe which yielded an average of 320 kilometers per second (Reference 9).

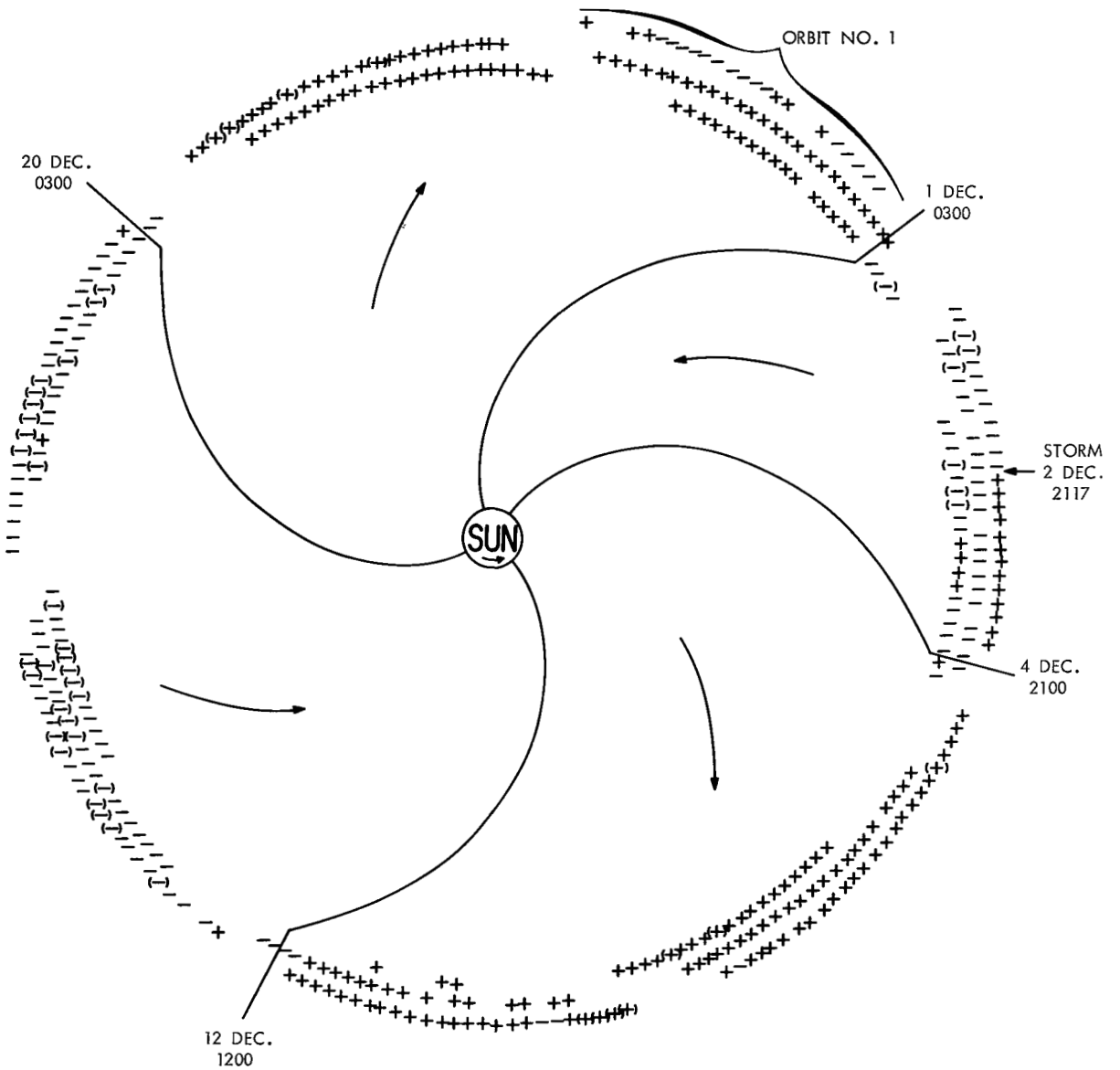


Figure 14—Superposed epoch structure of the interplanetary magnetic field direction for solar rotations 1784-1786. Immediately evident is the sectoring of the interplanetary field into four portions of which three are approximately equal in angular extent. This sector structure co-rotates with the sun and hence observable effects associated with this structure should be detectable at periodic time intervals of approximately 27 days.

In addition to investigating the solar origin of the interplanetary magnetic field by the previous method of analysis, it is also possible to superpose the time variations in magnetic field direction in a circular epoch graph as shown in Figure 14. It is seen that the direction of the interplanetary magnetic field is repetitive on a time scale of 27 days in a very dramatic fashion which reveals the existence of four distinct sectors. Within each sector the magnetic field is directed either away from or towards the sun within the entire sector. Three of the sectors have a time interval of approximately 7.6 days, while the third sector shows a time interval corresponding to 3.8 days at 1 AU.

This superposed epoch chart also illustrates the characteristic geometrical configuration of the field lines within the interplanetary medium during three solar rotations of the quiet sun. As the sun rotates, this sector structure sweeps past the earth and changes associated with spatial variations within each sector can be associated with changes on the surface of the earth in magnetic field activity and cosmic ray variations. Figure 15 gives the variation of the planetary magnetic index $K_p$ within the 2/7 sectors of the interplanetary magnetic field. It is seen that high $K_p$ follows shortly after a sector boundary passes and that low $K_p$ values are reached towards the end of each sector. There appears to be no significant difference between + and - sectors, at least at the present time.

It should be noted that there is a close correspondence of the orbital period (3.9 days) with the time scale of the sector structure (1/7 sector = 3.8 days). The analyses have been critically reviewed to verify that the sector results are not an artifact generated in the analysis.

In summary, these results show that during the three solar rotations near the minimum of the solar cycle, the photospheric field is dragged out by the solar wind to form the nearby interplanetary magnetic field and that a semipermanent sector structure exists. These conclusions are consistent with the model suggested by Ahluwalia and Dessler (Reference 21) in which the sense of the field in the sectors is related to the sense of photospheric magnetic field regions.

To interpret the solar wind interaction with the geomagnetic field, it is necessary to have average values of the interplanetary medium available from direct measurements to justify a comparison between supersonic gas dynamics

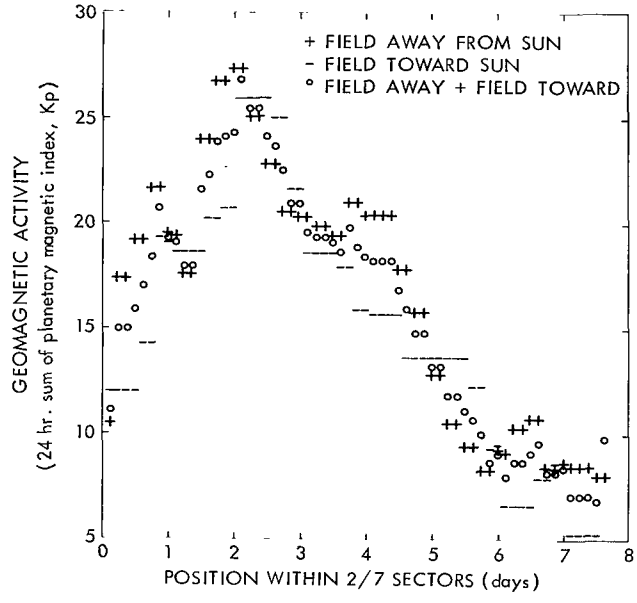


Figure 15—Characteristic variation of the $K_p$ index as observed in the combined sectors illustrated in Figure 14. The high $K_p$ index follows the change in sense of the directed flux tube from the sun and $K_p$ decreases to a minimum at the end of the sector. Implications regarding the recurrent M-region storms on the sun are discussed in the text.

and the flow of solar wind. Figure 16 summarizes the average values of pertinent physical parameters in the interplanetary medium deduced from the magnetic field experiment on IMP-I. The average magnitude of the magnetic field is 5.1 gammas and the directional changes indicate a solar wind velocity of 385 kilometers per second, which yields a proton cyclotron radius of 820 kilometers. It has been suggested by Axford (Reference 13) and Kellogg (Reference 15) that this represents the appropriate physical scale unit to utilize in considering the characteristics of the interaction of the solar plasma flow with the geomagnetic field. Since the magnetosphere as shown in Figure 2 is approximately 44 $R_e$ in diameter, clearly the plasma flow can be considered as fluid since the proton cyclotron radius is much smaller than the size of the magnetosphere.

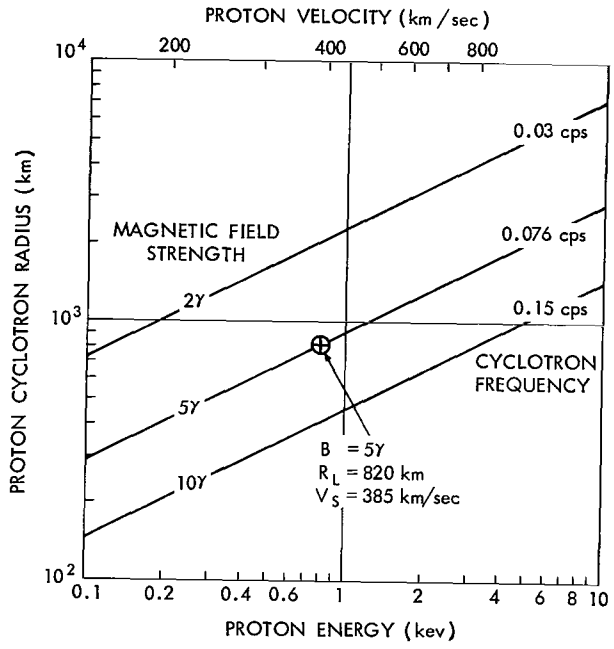


Figure 16—Representative values of the interplanetary medium during the quiet sun as observed by IMP-I. The interplanetary magnetic field magnitude and velocity, as derived from directional considerations and cross-correlation with the sun, yield a characteristic proton cyclotron radius of 820 kilometers.

## MAGNETOSPHERE AND BOUNDARY LAYER RESULTS

Magnetic field measurements by the IMP-I satellite, in comparison with plasma measurements, have shown a unique and coherent picture of the termination of the geomagnetic field and the transition to the interplanetary medium. The first traversal of the magnetosphere and shock wave boundaries by IMP-I is shown in Figure 17 for the magnetic field experiment. The magnitude, $\bar{F}$, and the two angles $\theta$ and $\phi$ describe the vector magnetic field over the 5.46-minute time interval. The root-mean-square deviation of the individual solar ecliptic components is also shown as $\delta X$, $\delta Y$, and $\delta Z$. It is seen that the transition region is one in which both the direction and magnitude of the field vary on short and long time scales. Within the interplanetary medium, magnetic field fluctuations are less than the quantization errors of the telemetry system and correspond to a few tenths of a gamma. Thus for the interplanetary medium, the characteristic fluctuations $\delta\bar{F}/\bar{F}$ are seen to be less than 0.1 while within the transition region, $\delta\bar{F}/\bar{F}$ varies generally between 0.5 and 2.

An enlarged time scale presentation of the traversal of the shock wave boundary is shown in Figure 18. Individual measurements at 20.4 second intervals are illustrated for the three orthogonal components. The motion of the satellite between successive 20.4 second samples corresponds to approximately 40 kilometers in space. The identification of the shock wave boundary as an abrupt change from a stable, weak, ordered field to a turbulent, stronger field is clear and indicated by the dashed line in the figure.

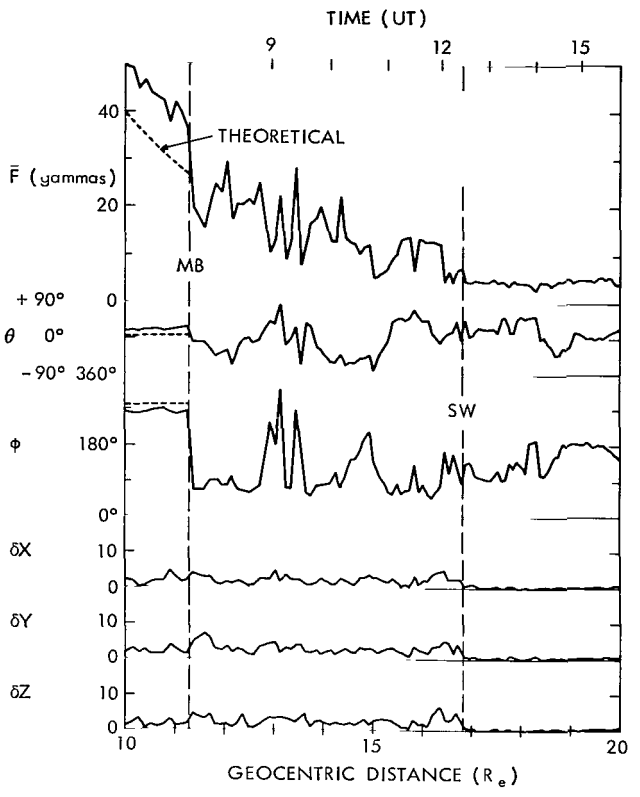


Figure 17—Observed magnetic field results on outbound orbit 1 by the IMP-I satellite, 27 November 1963. Clearly evident are the magnetosphere boundary at 11.3 $R_e$ and the collisionless shock wave at 16.8 $R_e$. For a definition of these boundaries see text.

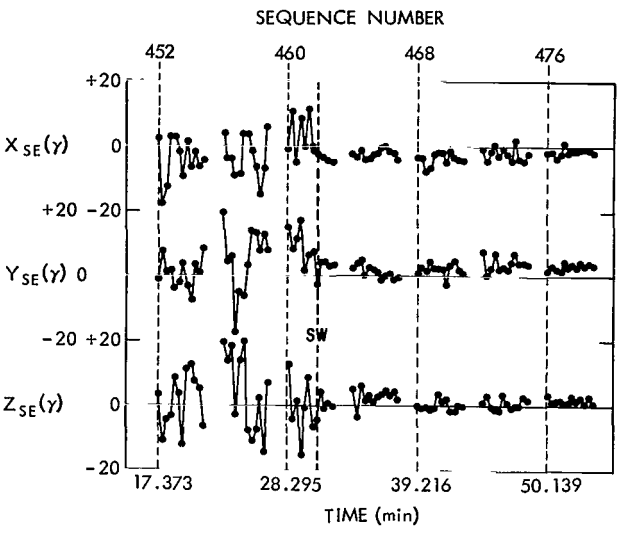


Figure 18—Detailed variation of the three orthogonal components of the magnetic field observed during the first outbound traversal of the shock wave by IMP-I. These data expand the time scale shown in Figure 17 to a distance scale corresponding to satellite motion of approximately 40 kilometers between successive sample points. The gaps in the data correspond to continuous transmission of the rubidium vapor magnetometer data in the telemetry sequence.

On an expanded scale Figure 19 shows the characteristic raw telemetry signals corresponding to individual samples of the magnetic field as sampled by the fluxgate magnetometers at time intervals of 0.160 second. The individual spin-modulated segments of the telemetry signal are presented on an enlarged scale but in time sequence. Again the identification of the boundary is evidenced as a transition from a uniform stable field to a turbulent and rapidly fluctuating magnetic field. This characteristic thinness of the shock wave boundary separating stable and turbulent fields was not anticipated and is one unique aspect of the magnetic field measurements by IMP-I.

Corresponding to the magnetic field measurements on outbound orbit 1, Figure 20 shows the pertinent plasma measurements from the MIT plasma Faraday Cup (Reference 9). The diagram shows the maximum and minimum flux values during each spin period as measured in the channel correspond to protons with energies between 220 and 660 electron volts. A measurement of the extreme fluxes during each satellite spin is an indirect measurement of the anistropy of the plasma flow. Within the transition region, which corresponds perfectly with that defined by the magnetometer measurements, the plasma flow is seen to be generally isotropic and other energy channels not shown would indicate a similar response characteristic. The MIT plasma measurements have revealed a broad region of turbulent, thermalized plasma flow immediately behind the shock wave

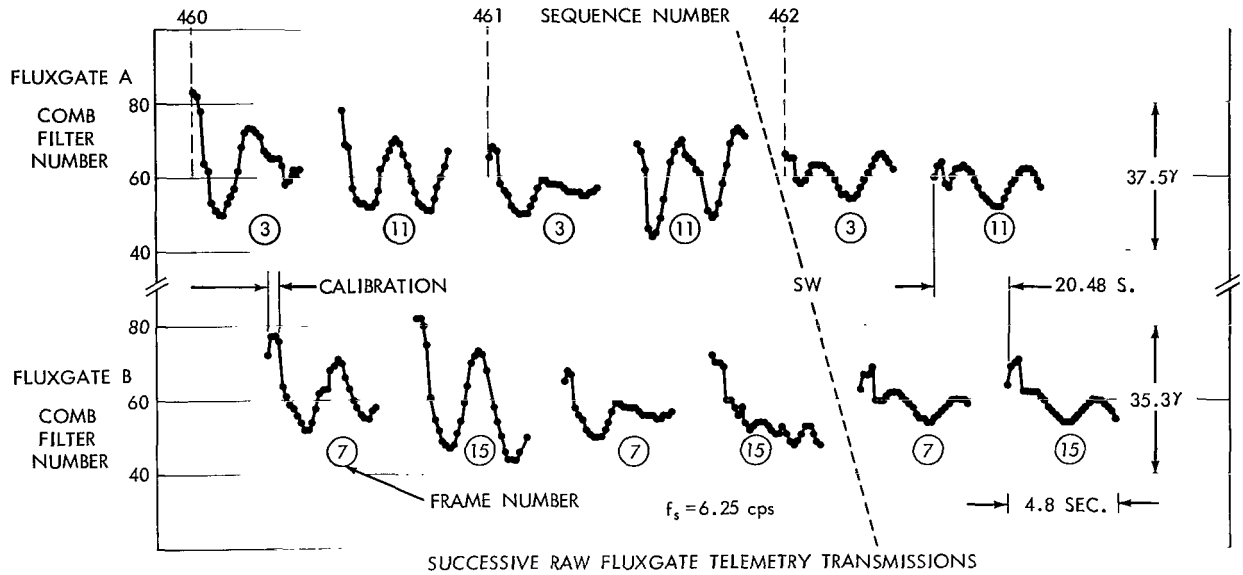


Figure 19—Fine detail of the collisionless shock wave thickness as observed on outbound orbit 1 by IMP-I. Individual spin-modulated signals observed for time intervals of 4.8 seconds are shown in time sequence. The position of the shock wave and the characteristic differences in the magnetic field modulation of the detected flux gate magnetometer signal are evident.

and enclosing the magnetosphere. The remainder of orbits 2 through 21, which permit sampling of the interplanetary medium, show excellent agreement between plasma and magnetic field measurements with respect to the positions of the characteristic shock wave and magnetosphere boundaries in cislunar space.

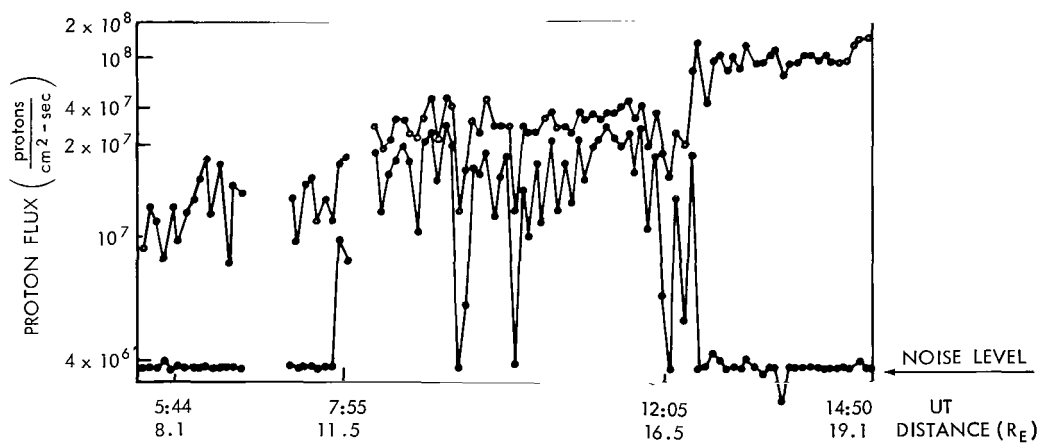


*Figure 20—Representative results from the MIT plasma probe showing measurements of* thermalized plasma by IMP-I during outbound orbit 1. The positions of the boundaries are evidenced by the distinct change to small spin modulation of the observed flux between 11.3 and 16.8 $R_e$ compared to measurements beyond these points (Reference 9).

Figure 21 presents the inbound orbit 1 magnetic field measurements illustrating the character of the magnetosphere boundary near the stagnation point. The magnetic field interior to the boundary is seen to be increased by approximately a factor of two above that theoretically predicted by extrapolation from the earth's surface using spherical harmonics. This corresponds to the compression of the geomagnetic field by an infinitely conducting plasma and the factor of two is in agreement with theoretical prediction (Reference 22). The direction of the field is seen to be only slightly distorted interior to the magnetosphere boundary. Beyond this a magnetic field turbulent both in direction and magnitude is seen, as shown previously in Figure 17.

The energetic particle results for inbound orbit 1 showing electrons with energies greater than 45 kev as detected by the geiger counter experiment of Anderson, Harris, and Paoli (Reference 7) are given in Figure 22. An intense flux of particles is observed interior to the magnetosphere boundary to the trapped particles in the outer radiation belts. The termination of the trapping region is seen to coincide with the boundary of the magnetosphere as observed first by Freeman, Van Allen, and Cahill on Explorer XII (References 23 and 24). This is a characteristic feature of orbital data obtained near the stagnation point, that is, within 45° of the earth-sun line. Magnetic fields interior to the magnetosphere boundary in this region of space are connected in a distorted but approximately continuous dipole topology which supports trapped particle motion.

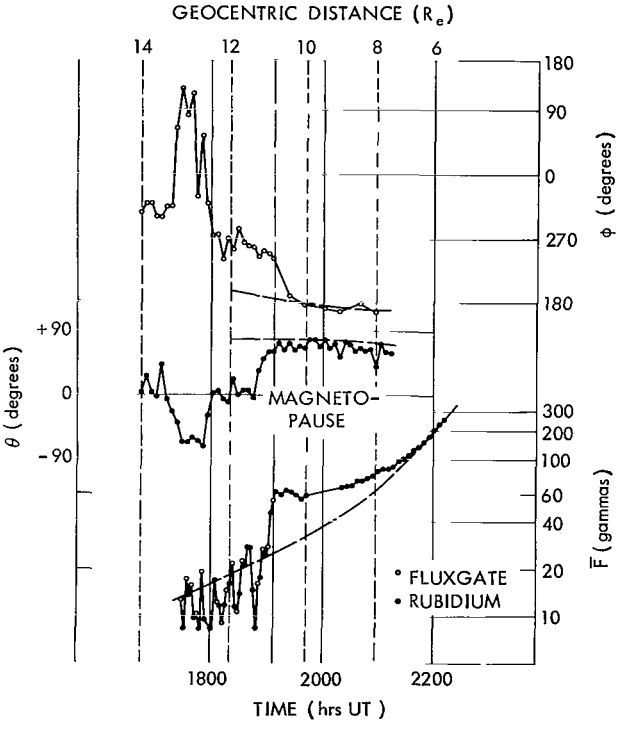


Figure 21—Magnetic field measurements on inbound orbit 1 from the IMP-I satellite on 30 November 1963. The magnetosphere boundary is observed distinctly as an abrupt magnitude and direction change at a geocentric distance of 10.8 $R_e$.

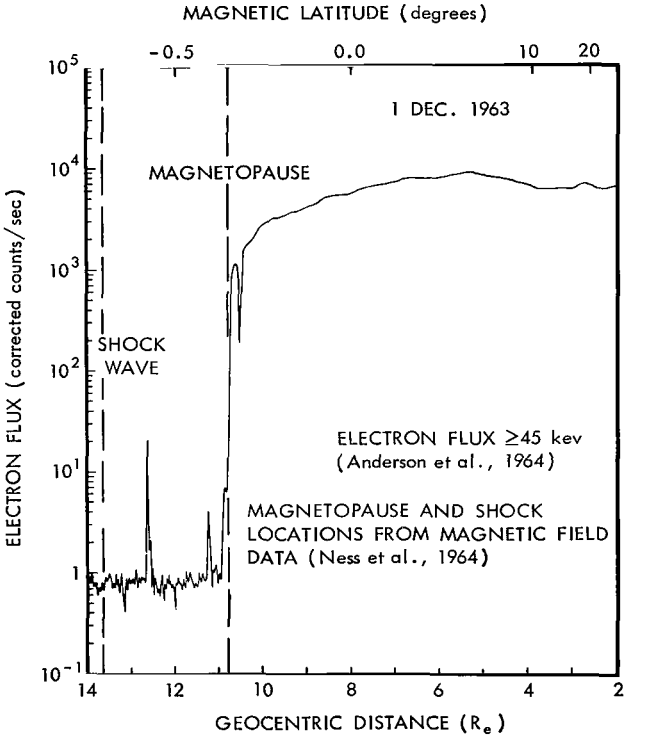


Figure 22—Measurements of flux of electrons with energy greater than 45 kev on IMP-I inbound orbit 1 showing coincidence of trapping region boundary with magnetopause at 10.8 $R_e$.

Figure 23 illustrates magnetic field measurements obtained on orbit 6 inbound previously reported by Ness, Scearce, and Seek (Reference 1). For this orbit, original determination of the boundary was based upon magnitude measurements and showed a boundary at 10.3 $R_e$. Subsequent re-evaluation of the data has indicated that the termination of the magnetosphere boundary must be determined by the topology of the field; i.e., whether or not the field is connected to the earth or to interplanetary space. On the assumption that the change in direction of the field is the pertinent parameter determining such connection, the boundary of the magnetosphere is identified at a distance of 8.1 $R_e$. That the magnetic field magnitude is continuous across the boundary is an interesting aspect which cannot be expanded upon in this brief summary of results.

Figure 24 shows the flux of electrons with energy greater than 45 kev. Again the termination of the trapping region is seen to coincide exactly with the boundary of the magnetosphere even though it has moved in to a distance of 8.1 $R_e$ in this particular orbit. No important solar event or related terrestrial event has been associated with a boundary as close in as this. The only

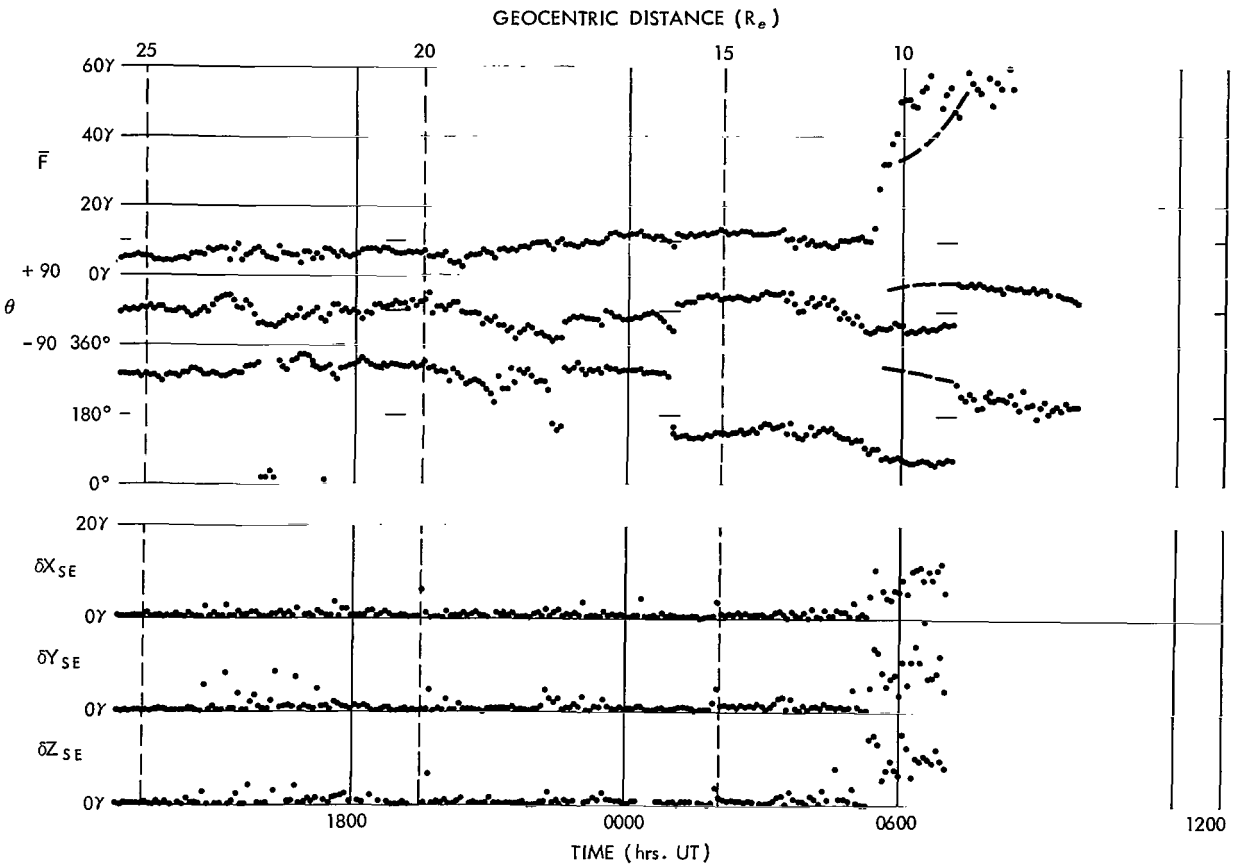


Figure 23—Magnetic field measurements on inbound orbit 6 from the IMP-I satellite on 20 December 1964 showing the interplanetary magnetic field beyond approximately 15 $R_e$ and magnetosphere boundary at 8.1 $R_e$. This is determined by the abrupt change in direction of the field which is seen to be not coincident with the magnitude change. This particular orbit shows the magnetosphere boundary in considerably closer to the earth than generally observed by IMP-I.

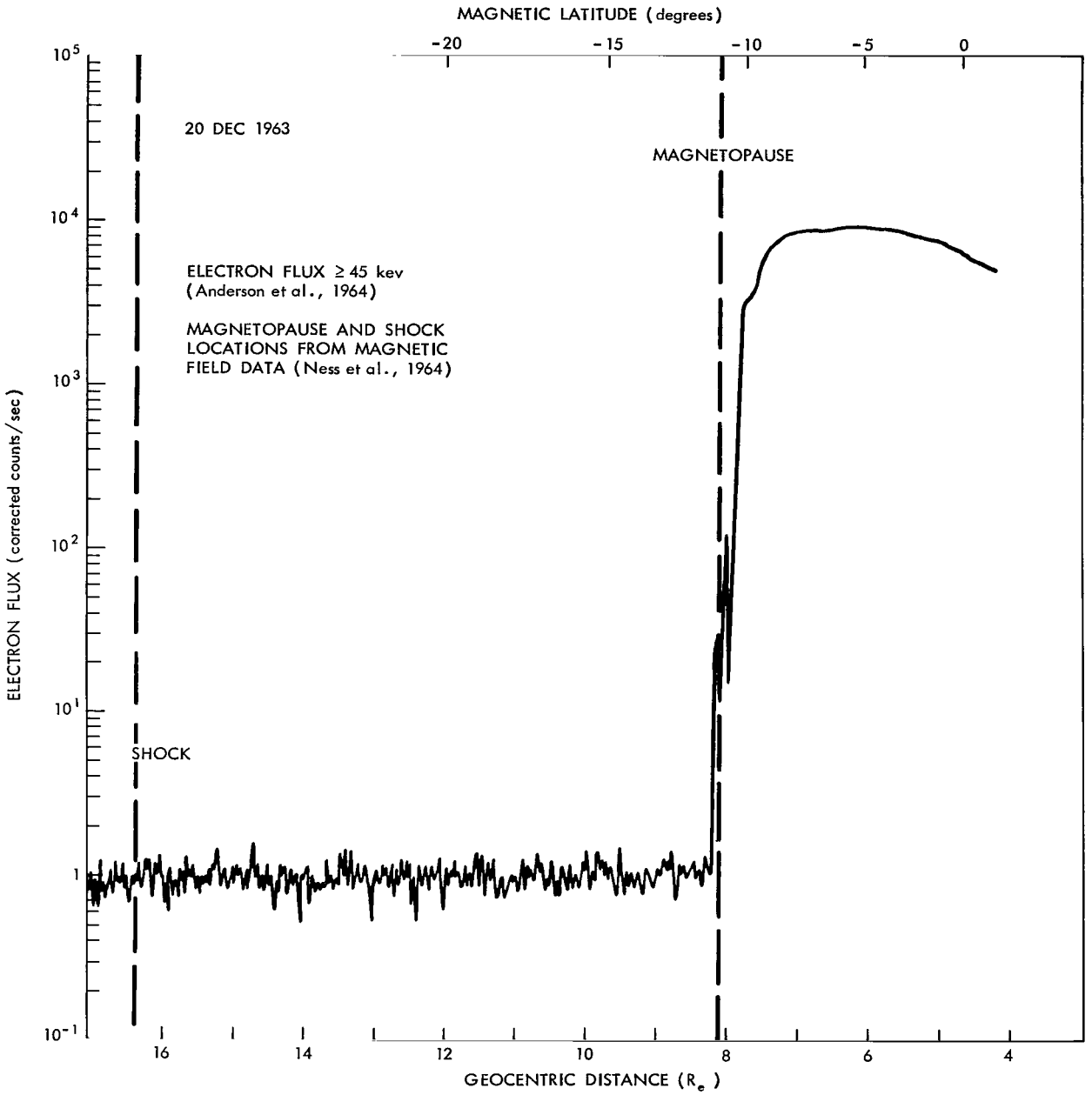


Figure 24—Measurements of the flux of electrons with energy greater than 45 kev on inbound orbit 6 by the IMP-I satellite. Coincidence of the magnetosphere boundary and the trapping region is again evidenced with small electron fluxes beyond the boundary.

other unique event associated with orbit 6 which possibly might be physically related to it is that during orbit 5, the magnetohydrodynamic wake of the moon was detected by the IMP-I satellite while in interplanetary space (Reference 3). Whether or not it is possible for the wake of the moon to disturb the characteristics in the transition region and thereby effect the position of the magnetosphere boundary is presently unknown but currently under investigation.

Continuing in orbital coverage around to the sunrise terminator, Figure 25 shows magnetic field measurements from outbound orbit 11. The boundary of the magnetosphere is discernible as an abrupt change in the direction of the field and in this case is again accompanied by a change in the magnitude of the field. Beyond this boundary the turbulent and tangled magnetic field is observed until the shock wave boundary is detected at 19.7 $R_e$.

Figure 26 shows the flux of energetic electrons greater than 45 kev energy for the same orbit. Here it is seen that the boundary of the trapping region occurs close to the earth at approximately 4 or 5 $R_e$ and hence not coincident with the boundary of the magnetosphere.

This is a characteristic feature of the results from the IMP-I satellite. The boundary of the trapping region and the magnetosphere boundary are coincident near the stagnation point but gradually separate towards the sunrise terminator to an appreciable distance on the night side of the earth. This implies that the magnetic field topology within the magnetosphere is such that durably trapped particle motions are possible for field lines which are approximately dipolar and connected from one hemisphere to the other. However, particles are not capable of stably drifting in

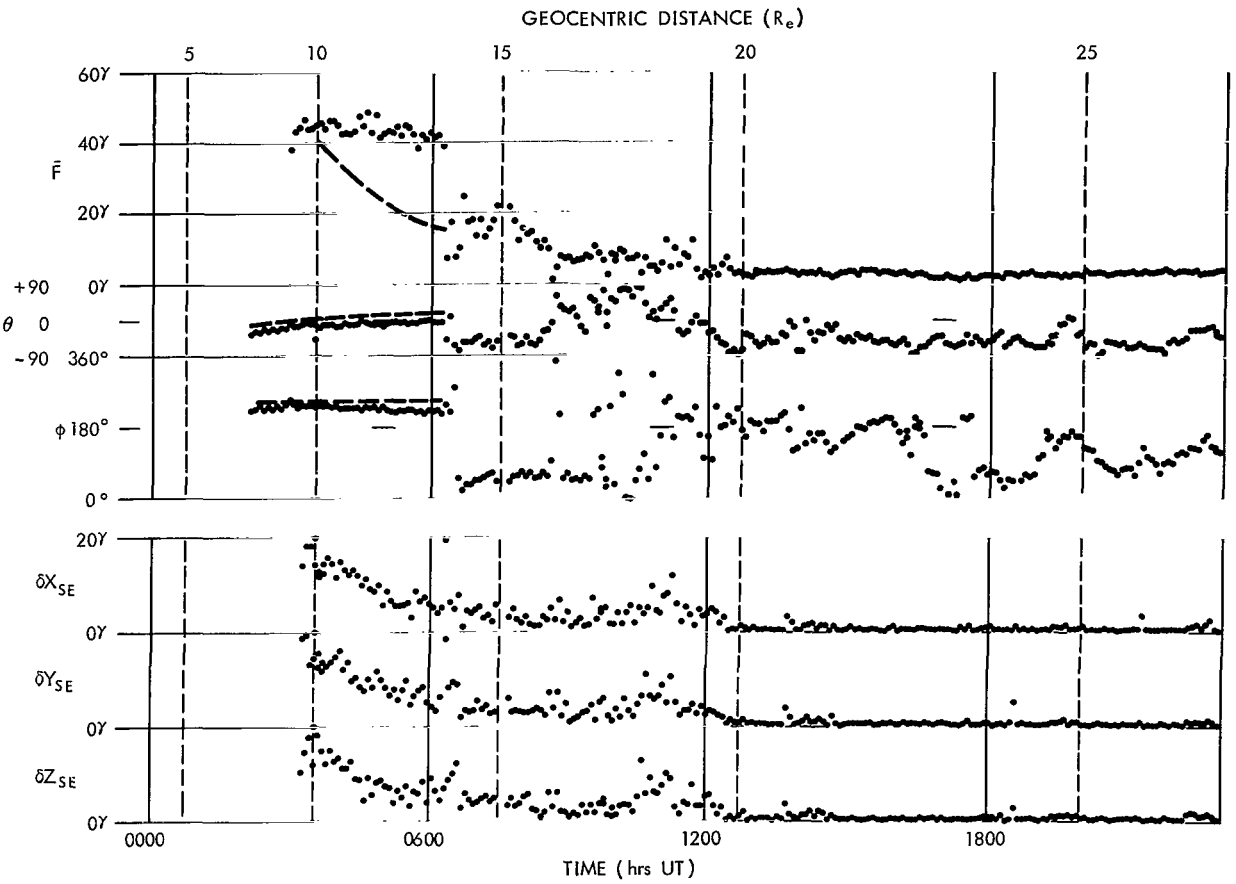


Figure 25—Magnetic field measurements on outbound orbit 11 from the IMP-I satellite on 5 January 1964. The magnetosphere boundary is observed at a distance of 13.6 $R_e$ and the shock wave at a distance of 19.7 $R_e$. The satellite at this time was approximately on the sunrise terminator position with respect to the sun-earth line.

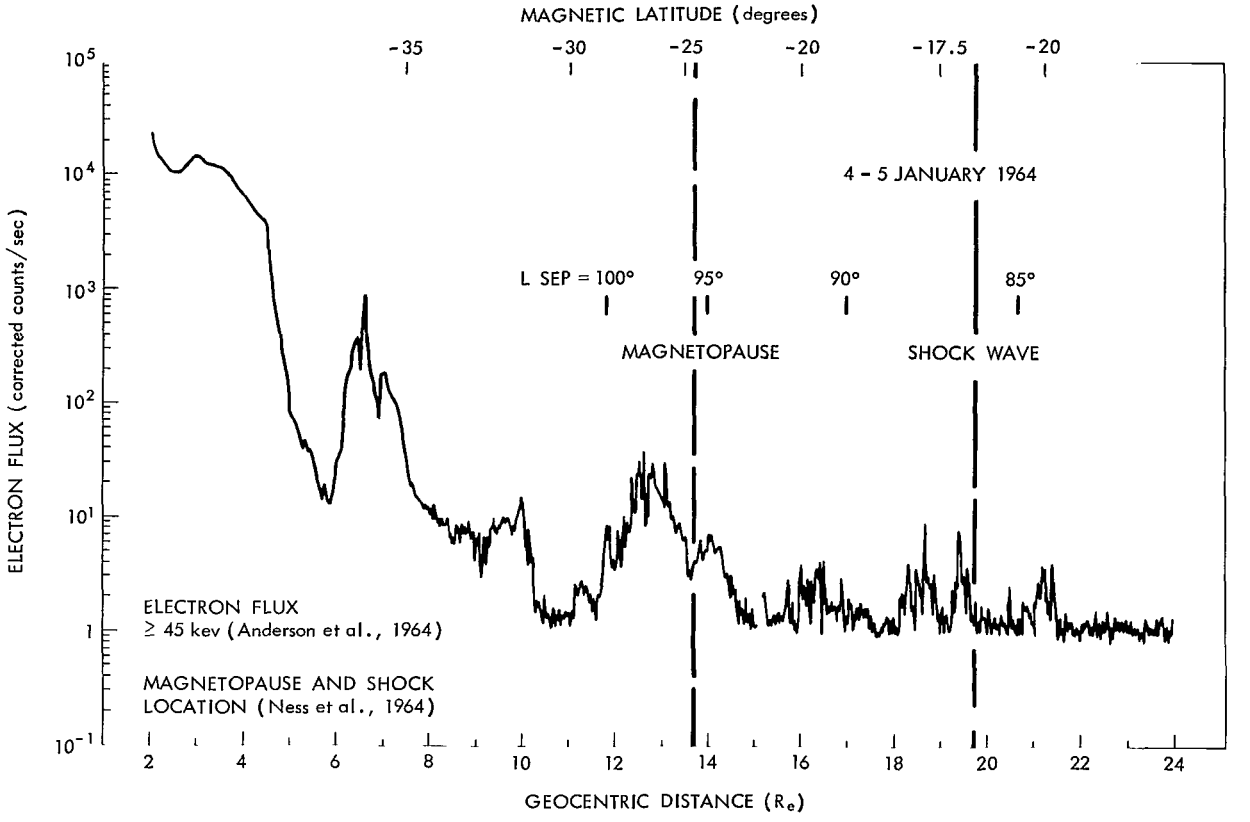


Figure 26—Outbound orbit 11 from the IMP-I satellite on 5 January 1964, showing flux of electrons with energy greater than 45 kev. The boundary of trapping is observed at approximately 5 $R_e$ while the magnetopause is not observed until 13.6 $R_e$. The gap in these positions is associated with a change in the geomagnetic field topology surrounding the earth and illustrates the strong day-night asymmetry in the characteristics of the magnetospheric cavity.

longitudes which correspond to field lines beyond approximately 8 $R_e$ on the night side of the earth. Although beyond this region of space intense transient fluxes are observed on field lines which originate at the surface of the earth, the field lines do not appear to be directly connected to the other hemisphere. Additional discussion of the field topology within the magnetosphere will be presented in the following section.

The last orbit on which interplanetary magnetic field measurements were performed was orbit 21. Outbound orbit 21 is illustrated in Figure 27 showing the magnetopause at a distance of 18.7 $R_e$. Again the magnetosphere boundary is identified by an abrupt change in the direction of the field. The magnitude of the field is many times larger than that theoretically predicted. The simple model which explains the factor of two increase in magnitude at the stagnation point is no longer applicable on the flanks of the magnetosphere.

The remainder of outbound orbit 21 is shown in Figure 28, where the transition region is seen to consist of intervals in which the field strengths are high, when compared to the interplanetary

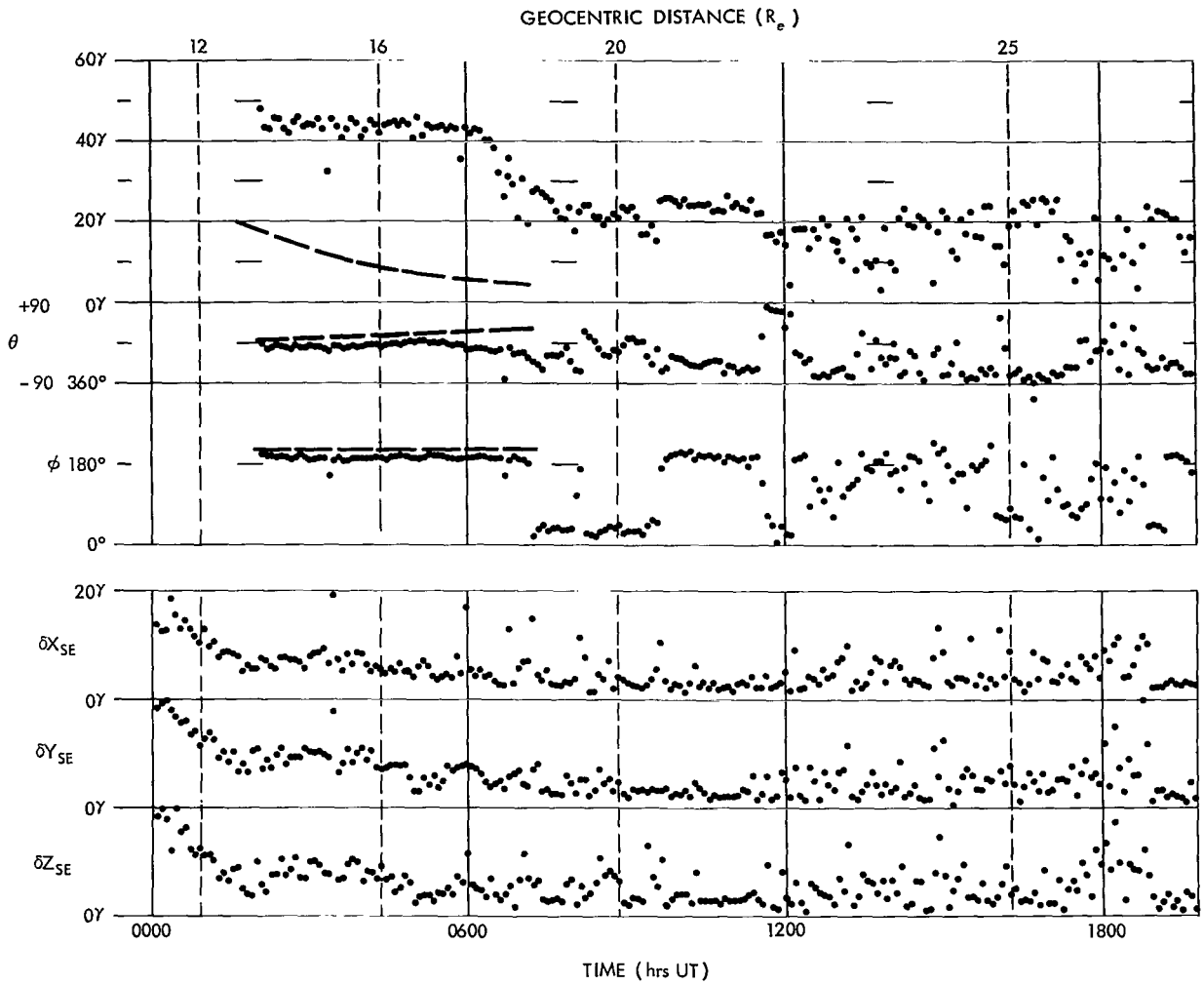


Figure 27—Magnetic field measurements on outbound orbit 21 from the IMP-I satellite on 13 February 1964. The magnetosphere boundary is not observed until a radial distance of 18.7 $R_e$ is reached. The boundary is evidenced by an abrupt directional change in the magnetic field corresponding to approximately antiparallel fields across the boundary. Characteristic disturbed fields of the turbulent transition region are observed throughout the remainder of this data sample.

region, and the directions, reasonably stable, that alternate with regions of fluctuating and weak magnetic fields. This is a feature reminiscent of the Explorer X results near the sunset terminator side of the magnetosphere (References 25 and 26). Detailed correlations of these data with the plasma measurements will be necessary to determine whether or not the boundary of the magnetosphere has been traversed more than once on this particular orbit. The motion of the boundary of the magnetosphere was first deduced in the Explorer X results in 1961 (Reference 27).

A summary of the positions of the magnetosphere boundary and the shock wave is given in Figure 29. Each dot represents either the inner-most or outer-most position of the boundary as observed on each orbit. The boundary terminations on successive orbits are connected by solid

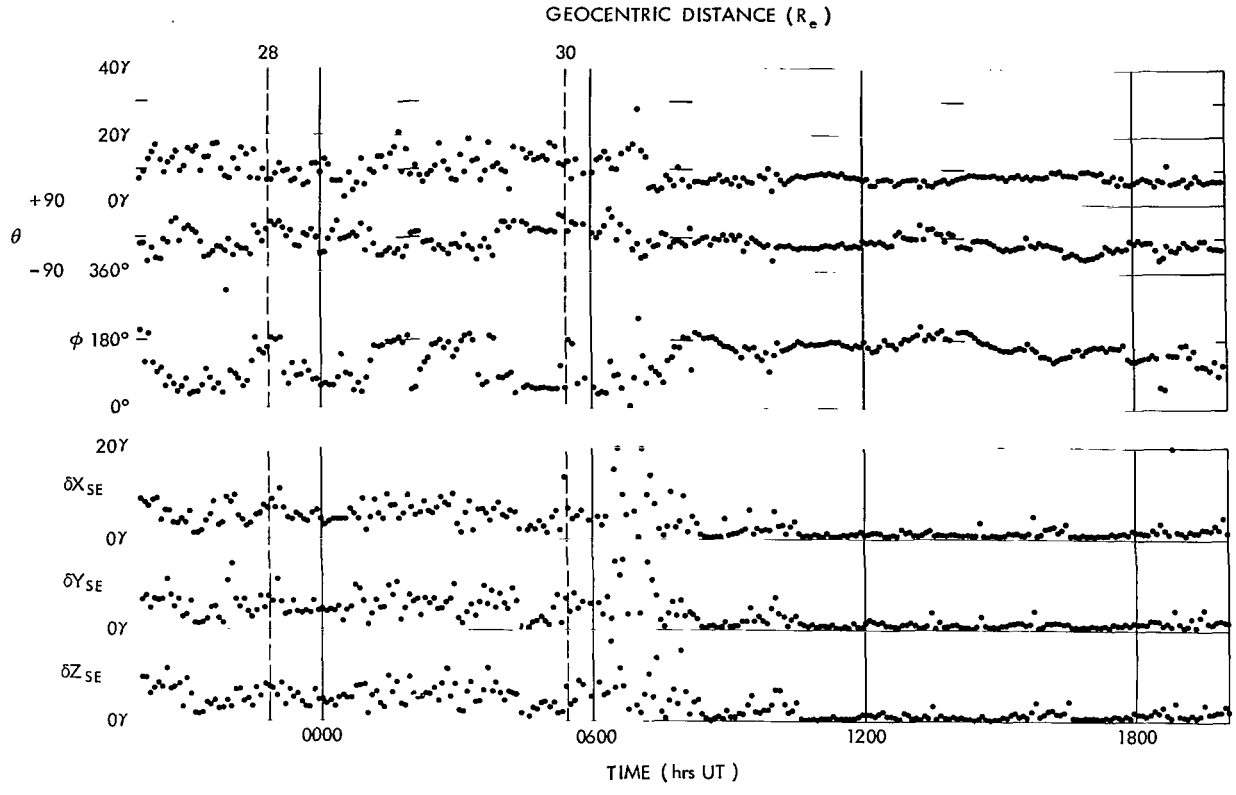


Figure 28—Continued measurements of the magnetic field on outbound orbit 21 from the IMP-I satellite on 14 February 1964. The shock wave is not observed until a distance of 30.4 $R_e$ is reached or approximately at satellite apogee. According to the magnetic field measurements this represents the last orbit on which the interplanetary medium was capable of being sampled by the IMP-I satellite.

lines if no data are missing or no boundary was ambiguously defined, and dashed if otherwise. In general it is seen that the magnetosphere is roughly hemispherical on the earth's sunlit side with a radius of 13.9 $R_e$ (Reference 4), but broadens out to approximately a diameter of 44 $R_e$ on the flanks. The shock wave boundary is separated from the magnetosphere by a distance of 3-4 $R_e$ at the stagnation point and increases to 5-7 $R_e$ on the flanks of magnetosphere.

It is possible to consider a comparison of the supersonic gas dynamic analog of the solar wind flow with the magnetosphere, as studied initially by Spreiter and Jones (Reference 28). It is important, however, in this interpretation to attempt to take into account the variable angle of attack which the earth's magnetic dipole presents to the solar wind flow. This is associated with the obliquity to the ecliptic of 23.4° and the 11.7° tilt of the dipole axis of the geomagnetic field to the spin axis of the earth. Figure 30 shows the variation in the angle of attack over the lifetime of the IMP-I satellite. This angle, $\chi_{ss}$, has been used previously in attempts to rectify the positions of the boundary to the ideal position of impact of the solar wind flux normal to the axis of the earth's magnetic dipole (Reference 1).

As the angle of attack increases it would normally be expected that the magnetosphere would increase in size, since the magnitude of field at the stagnation point increases. A first-order

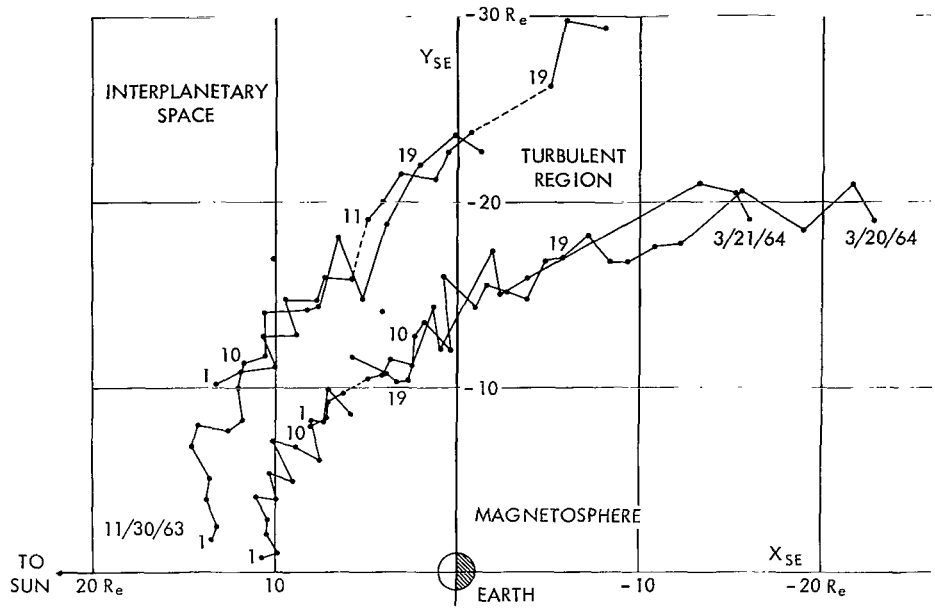


Figure 29—Summary of the magnetopause and shock wave boundary positions as observed by the IMP-I satellite. Individual observations have been rotated in a solar ecliptic meridian plane into the ecliptic plane. Successive traversals of the boundary are connected by straight lines if no gap exists in the data. Three regions of space are distinguished by these two boundaries: the *interplanetary medium*, the *turbulent transition region* and the *magnetosphere* or distorted geomagnetic field.

correction using $\chi_{ss}$ yields the rectified positions of the magnetosphere boundary and shock wave as shown in Figure 31. The inner solid line corresponds to the theoretical predictions by Spreiter and Jones (Reference 28) of the shape of the magnetosphere boundary and assuming an individual particle model with specular reflections, a gas dynamic shock analog has been used to compute the shock wave position and shape using this theoretical magnetosphere. In general, the shape comparison is excellent for the shock wave indicating substantial agreement in the physical model. This is to be expected since in any physical model of a shock wave mass, momentum, and energy must be conserved. It should be noted that the shape of the boundary on the flanks of the magnetosphere does not appear to correspond well with that predicted. The magnetosphere appears to be broader than was anticipated and indeed is suggested to have a radius of 22 $R_e$. Also, the position of the shock wave has been adjusted slightly to yield the comparison shown (Reference 1).

This section has summarized briefly the results of the mapping of the magnetosphere boundary and shock wave by the IMP-I satellite. Detailed discussions of individual experiment results can be found in the literature by other authors. The confining of the geomagnetic field permanently by a continual flux of plasma from the sun is a very new aspect in the understanding of the earth's environment in space, as compared to earlier work on a transient Chapman-Ferraro cavity as reviewed by Chapman (Reference 29). Equally important are the results obtained on the night side of the earth from IMP-I, which shall be discussed in the following section.

## TAIL OF THE MAGNETOSPHERE

Detailed measurements of the distorted geomagnetic field on the earth's night side were performed by the IMP-I satellite on orbits 31 through 47 (Reference 4). A conspicuous and dominant feature of these measurements was the direction and strength of the magnetic field when the satellite was beyond approximately 10 to 15 $R_e$ from the earth. The direction of the field was observed mainly to parallel the earth-sun line with magnitudes of 10 to 20 gammas. A representative orbit illustrates these characteristics: In Figure 32 the outbound portion of orbit 41 shows the field paralleling direction of the earth-sun line within a few degrees and with magnitudes many times larger than predicted as shown by the dashed curve. These data extend out to satellite apogee, which corresponds to approximately halfway to the moon.

The inbound portion of orbit 41 is shown in Figure 33. In this, a continuation of the characteristic direction of the field is indicated with magnitudes again between 10 and 20 gammas. However, at a distance of 16 $R_e$ the magnitude of the field is observed to decrease rapidly while its direction abruptly reverses towards the sun. This change in direction of the field is interpreted to be associated with the magnetic neutral surface in the earth's magnetic tail (Reference 30). This surface separates regions of space in which the direction of the distorted geomagnetic field is either away from or towards the sun.

That the direction of the field parallels the earth-sun line appears to be associated with the mechanism for the formation of the tail. Although this is not yet understood in detail, it is clearly associated with the interaction of the solar wind with the magnetic field of the earth.

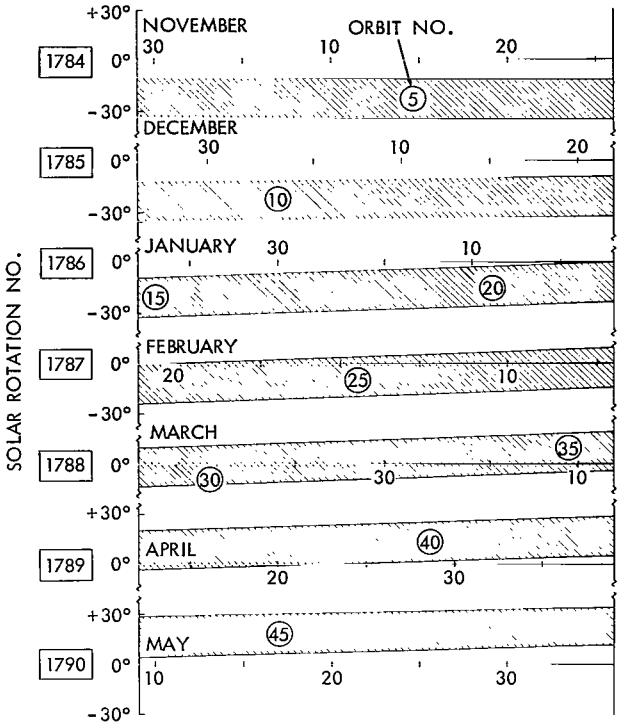


Figure 30—Variation of the geomagnetic latitude of the subsolar point during the lifetime of the IMP-I satellite. During the early portion of the satellite the "angle-of-attack" of the solar wind is seen to have been approximately -10 to -30 degrees.

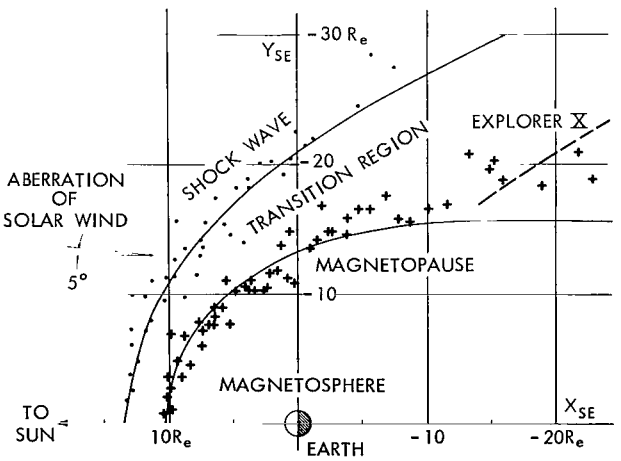


Figure 31—Comparison of the IMP-I rectified boundary crossings with the high-speed gas dynamic shock model of Spreiter and Jones (Reference 28). The standoff ratio has been adjusted to match the observed measurements. The predicted shape of the shock is seen to be rather closely matched by observations.

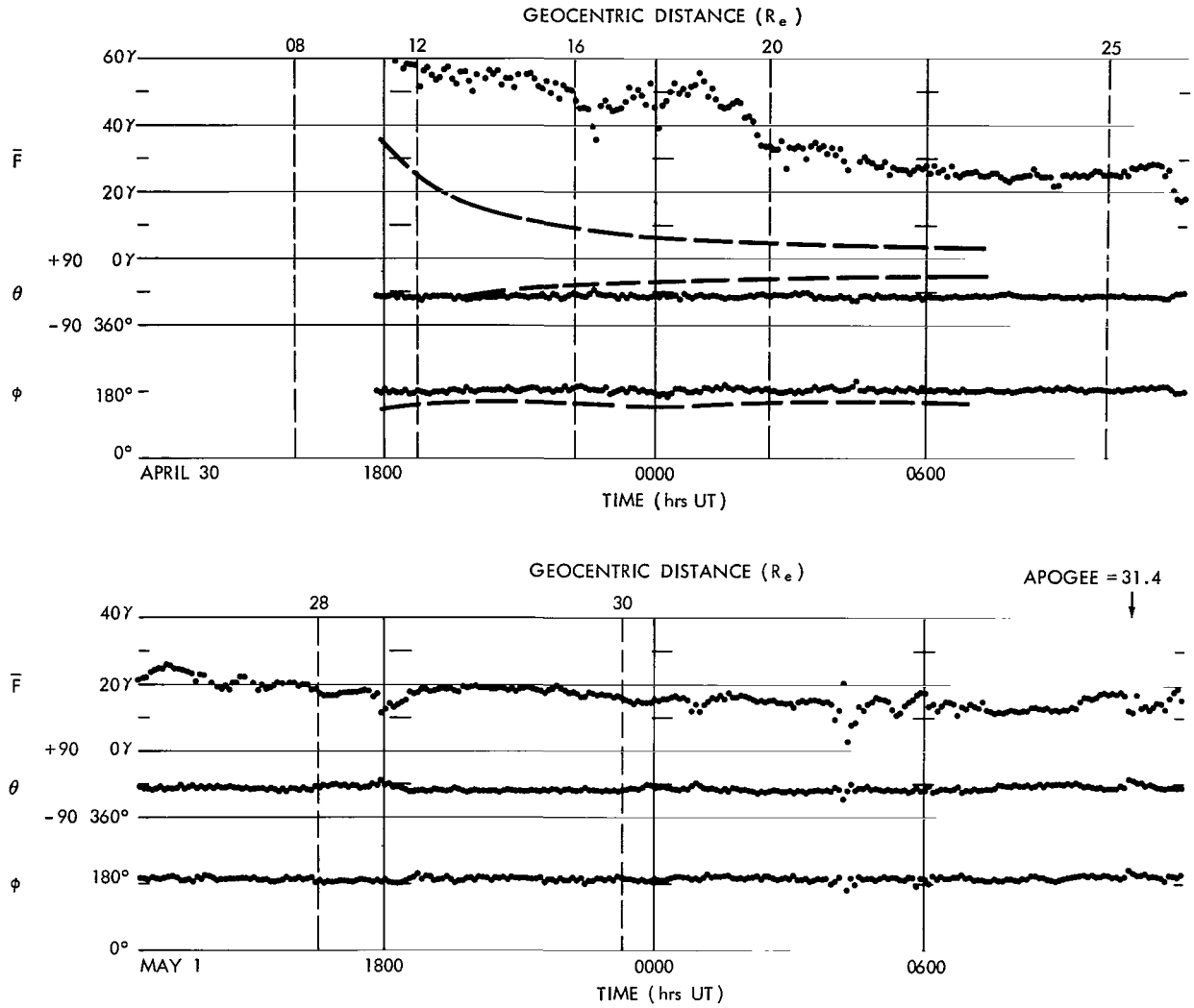


Figure 32—Magnetic field measurements of the earth's magnetic tail by IMP-I on orbit 41 outbound on 30 April, 1-2 May 1964. The apogee of this orbit was approximately at a solar ecliptic longitude of 180°. Hence these results correspond to a noon-midnight meridian plane sample. Note the steady direction of the magnetic field parallel to the earth-sun line and pointed away from the sun.

Since this parallels the earth-sun line, neglecting the 3°-5° aberration effect, then the direction of the tail and indeed the field direction within the tail can be expected to parallel the earth-sun line. The discovery of the neutral sheet in the earth's magnetic tail by IMP-I is one of the very significant results of the experiment. Theoretical treatment of the formation of a magnetic tail of the earth by Piddington (References 31 and 32) was on the basis of storm theory and more recently by Dessler and Juday (Reference 33) and Axford, Petschek and Siscoe (Reference 30) on the basis of limited satellite experimental data (References 25 and 34). This extended magnetic tail represents a change in the concept of the earth's magnetospheric cavity shape.

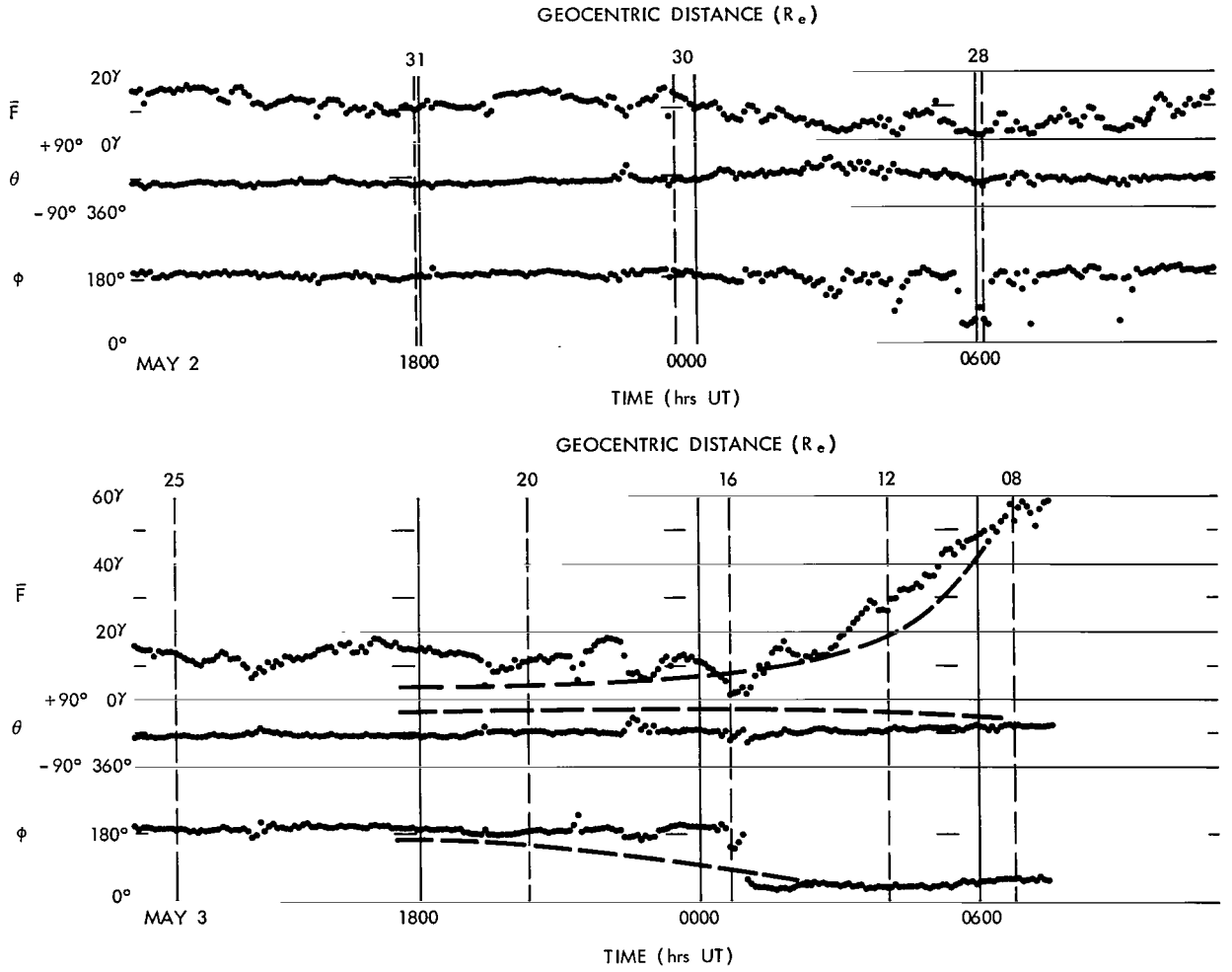


Figure 33—Magnetic field measurements of the earth's magnetic tail by IMP-I on orbit 41 inbound on 2-4 May 1964 corresponding to the remainder of the orbit shown in Figure 32. The direction of the field again closely parallels the earth-sun line with a rapid change in sense at a distance of 16 $R_e$. This is representative of the traversal of the magnetic neutral sheet in the earth's magnetic tail by IMP-I.

A summary of the hourly average components projected on the X-Y plane within the magnetosphere is shown in Figures 34 and 35. The measurements are shown for even hours only for clarity of presentation. The formation of the extended magnetic tail of the earth is dramatically evidenced in this presentation. The crosses correspond to traversal of the magnetosphere boundary by the satellite and individual orbits are distinguished by a continuous pattern of vectors which can be discerned in these figures.

Figure 34 shows the X-Y component of the magnetic field corresponding to positions of the satellite when below the plane with $Z_{se} = -2.5\ R_e$, while Figure 35 corresponds to $Z_{sat} > -2.5\ R_e$. In this figure the reversal of direction of the field across the neutral sheet is readily evidenced. In some instances the direction of the field does not change by exactly 180° and the field topology

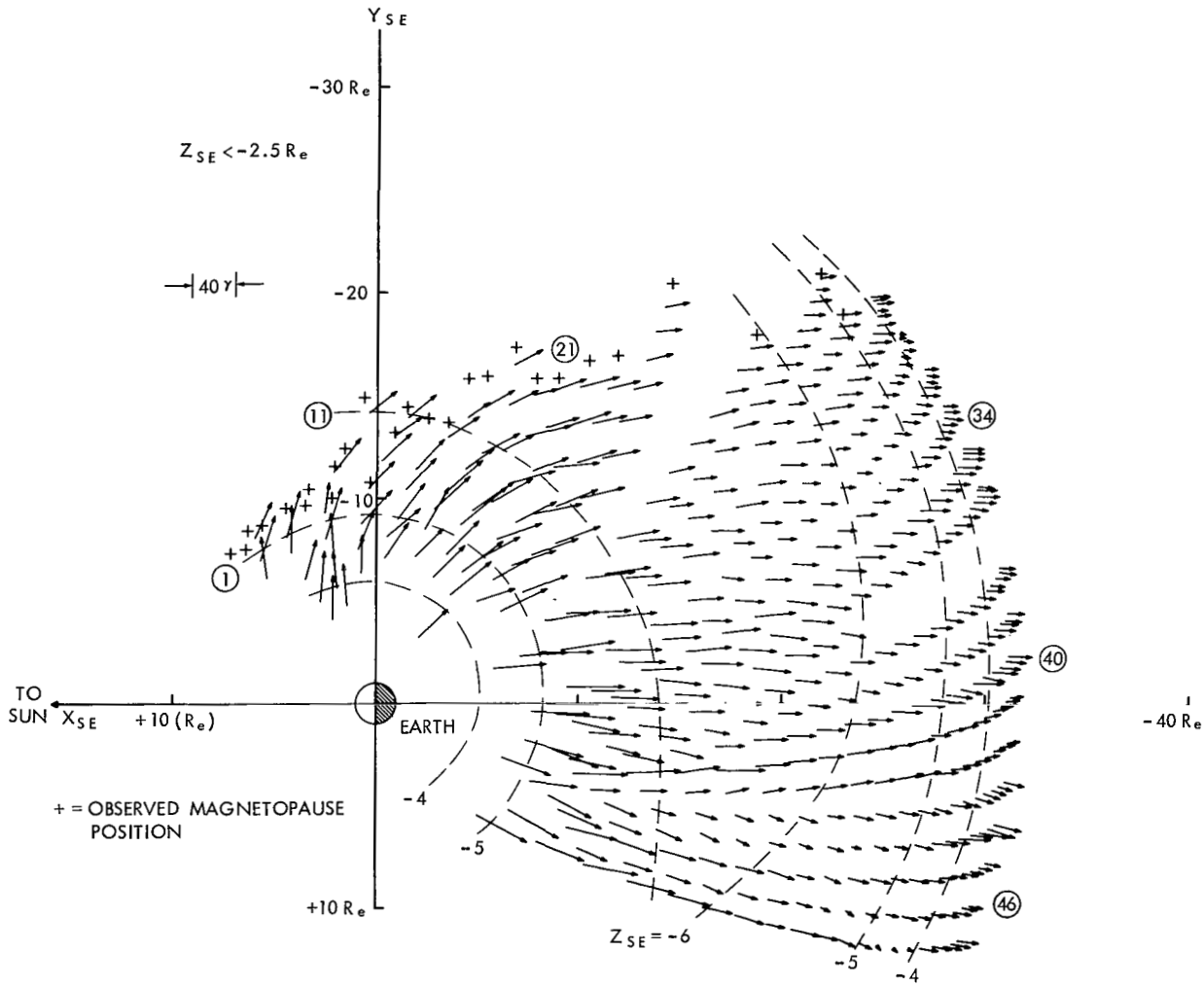


Figure 34—Summary of the X-Y hourly average component measurements by the IMP-I satellite for $Z_{sat} \leq -2.5$ $R_e$ in the earth's magnetic tail for orbits 1 through 47. Crosses indicate observed traversals of the magnetosphere boundary. Clearly evident is the distortion of the geomagnetic field forming an extended magnetic tail of the earth.

across the neutral sheet is not exactly antiparallel but rather crossed. The thickness of the neutral sheet can be inferred but not accurately determined, since it is not known if the neutral sheet is in motion at the time of traversal by the satellite. Assuming that the satellite motion is the only pertinent relative velocity, it is then possible to estimate the thickness of the neutral sheet as a fraction of an earth radius over the 14 orbits in which it has been observed. This indicates a very thin, magnetically neutral sheet (on the scale of the magnetosphere) embedded within the earth's magnetic tail.

An attempt has been made to present a three-dimensional view of the tail field in Figures 36-39, which show the hourly components projected on X-Z planes for positions of the satellite above and below the plane of the ecliptic and with the Y coordinate greater and less than -3.0 $R_e$. The

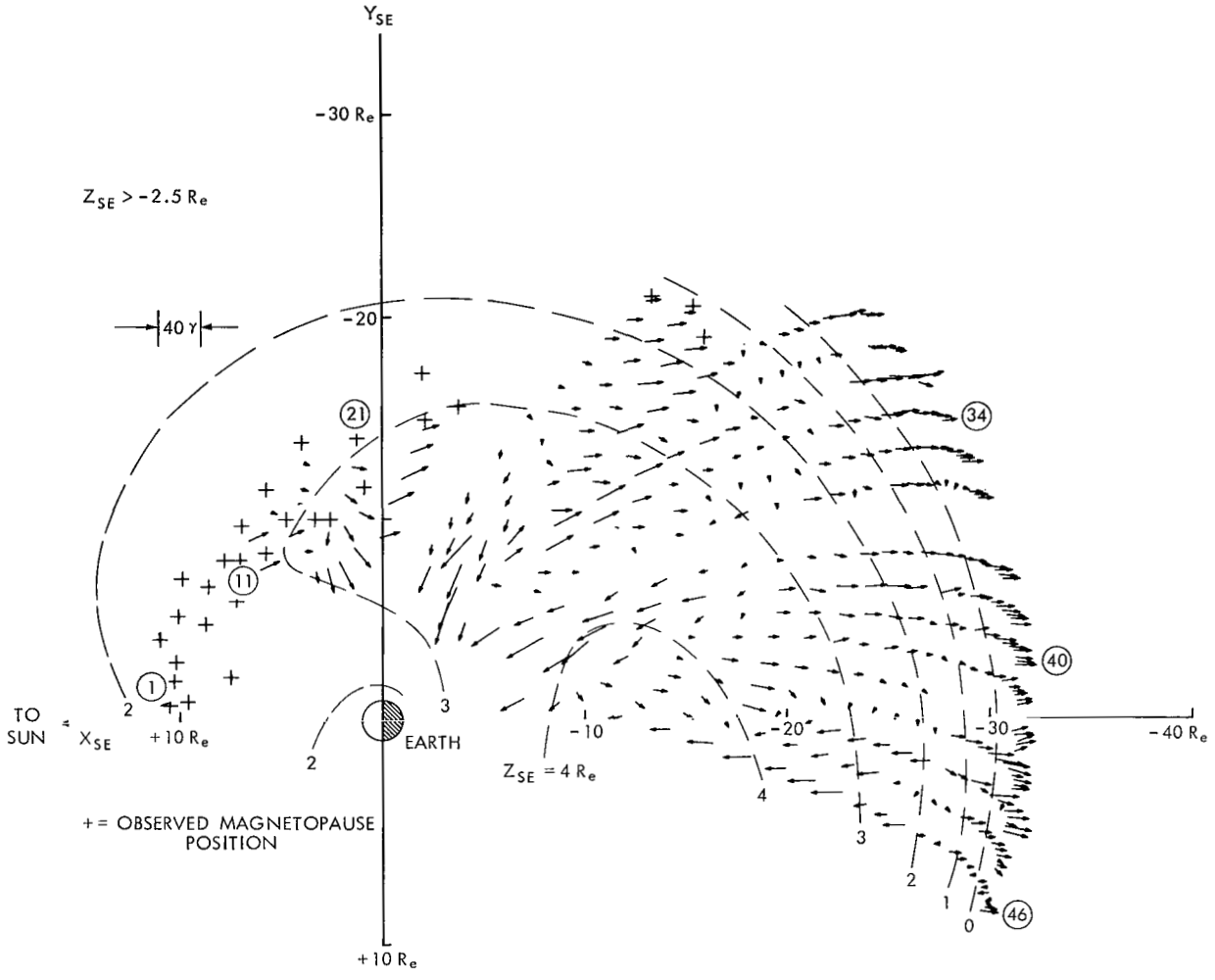


Figure 35—Summary of the X-Y hourly average component measurements by the IMP-I satellite for $Z_{SE} > -2.5$ $R_e$ in the earth's magnetic tail for orbits 1 through 47. Crosses indicate observed traversals of the magnetosphere boundary. Clearly evident is the distortion of the geomagnetic field forming an extended magnetic tail. Abrupt changes in the sense of direction of the tail field correspond to vertical traversals of the roughly horizontal neutral sheet.

projection of the vector on planes separated by intervals of 2 $R_e$ are shown offset in an isometric projection. Careful inspection of Figures 36-39 and also Figures 34 and 35 yields the details of the physical existence and directional characteristics of the magnetic tail of the earth.

The measurements of the magnetic tail extend over a time interval of approximately 4 months. Thus the earth's magnetic tail appears to be as permanent a feature of the earth's environment as was previously deduced about the confinement of the geomagnetic field by the flow of solar plasma. The original suggestion by Piddington (Reference 31) was for the temporary existence of a magnetic tail of the earth. The characteristics of the neutral sheet are an important aspect of the earth's tail and shall be discussed in the following section.

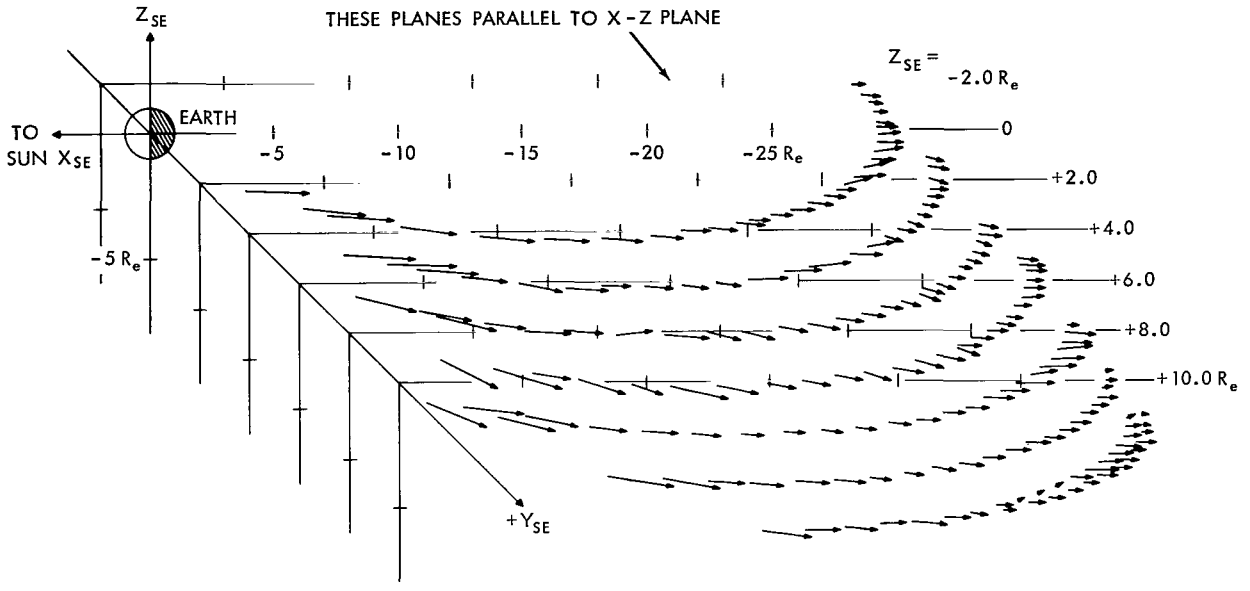


Figure 36—Summary of the X-Z hourly average component of the earth's magnetic tail field for $Y_{sat} \geq -3.0\ R_e$ and $Z_{sat} < 0$. The field is seen to be parallel to the earth-sun line when compared with Figures 34 and 35.

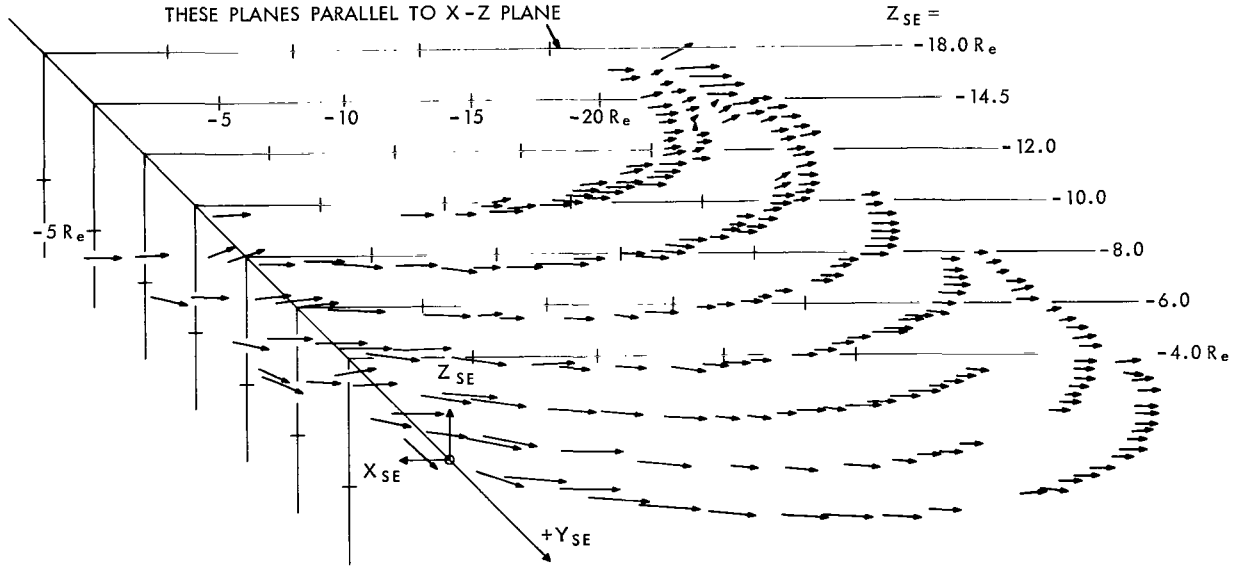


Figure 37—Summary of the X-Z hourly average component of the earth's magnetic tail field for $Y_{sat} \leq -3.0\ R_e$ and $Z_{sat} < 0$. The field is seen to be parallel to the earth-sun line when compared with Figures 34 and 35.

A schematic summary of the cislunar space environment is shown in Figure 40. This shows the projection of the interplanetary field lines on the plane of the ecliptic as well as the shock wave and magnetosphere boundary. The magnetosphere tail is shown to be filled with lines of force which originate from the southern polar cap region. An estimate of the total magnetic flux in the

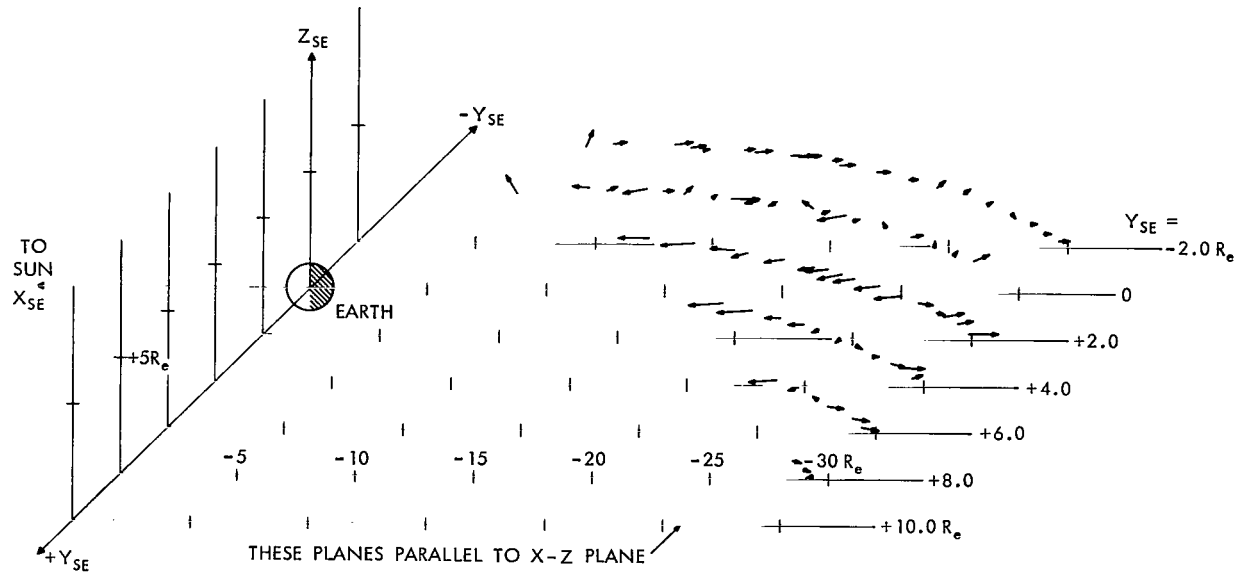


Figure 38—Summary of the X-Z hourly average component of the earth's magnetic tail field for $Y_{sat} \geq -3.0\ R_e$ and $Z_{sat} > 0$. The field is seen to be parallel to the earth-sun line when compared with Figures 34 and 35.

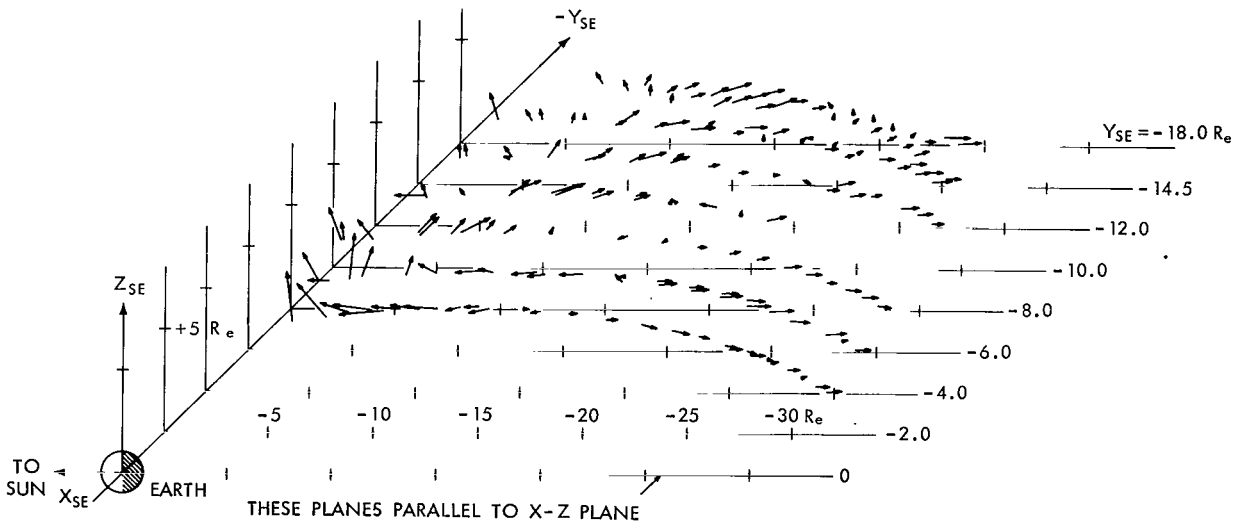


Figure 39—Summary of the X-Z hourly average component of the earth's magnetic tail field for $Y_{sat} \leq -3.0\ R_e$ and $Z_{sat} \geq 0$. The field is seen to be parallel to the earth-sun line when compared with Figures 34 and 35.

earth's magnetic tail can be obtained by integrating over an assumed cylindrical surface. Equating this total flux to that through a polar cap region of colatitude = ( should yield equivalence if the total flux in the cap is dragged behind the earth to form the earth's magnetic tail.

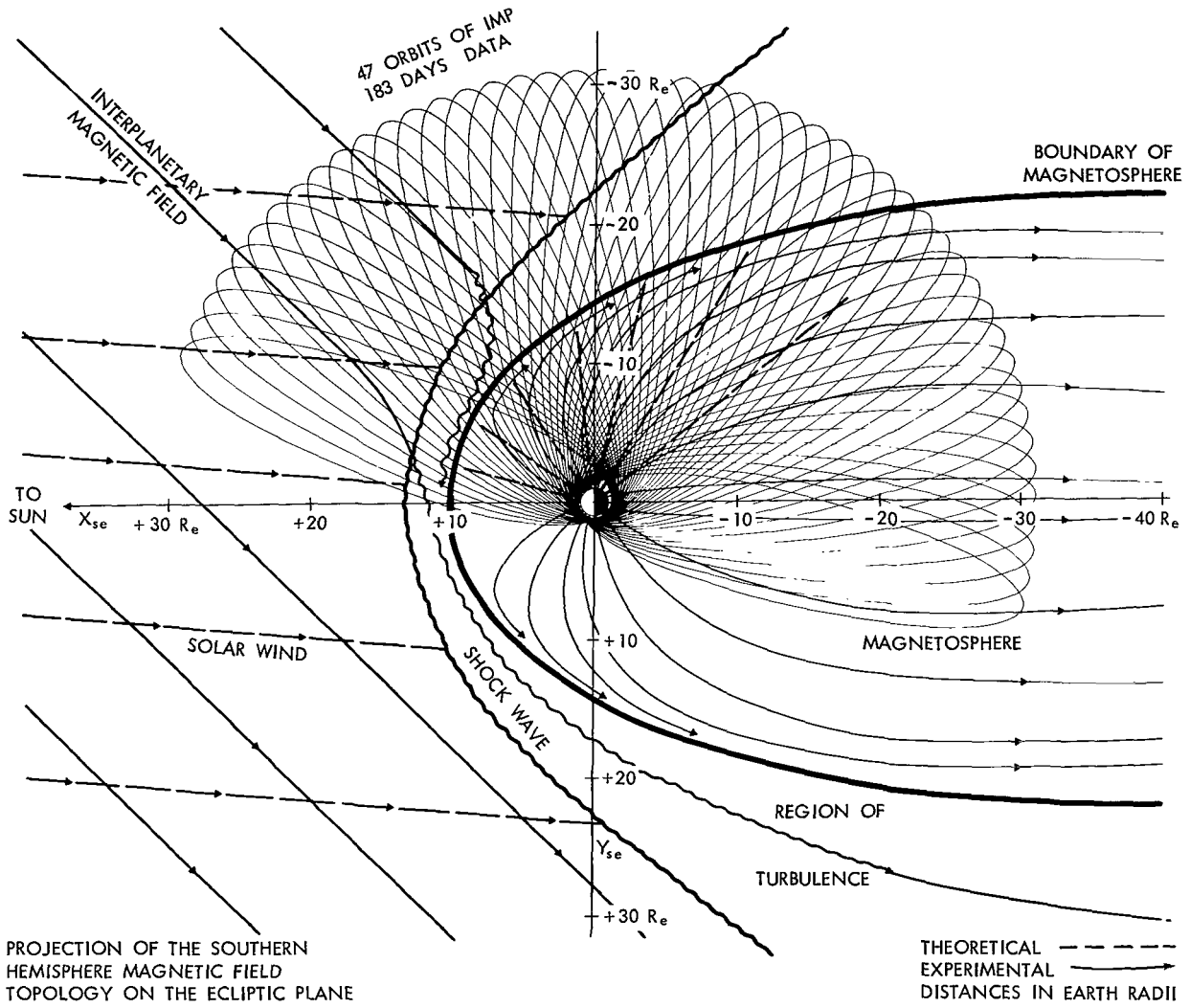


*Figure 40—Interpretation of the IMP-I magnetic field measurements of the cislunar environment. Illustrated are the directions of the interplanetary magnetic field, the positions of the magnetosphere boundary and the collisionless shock wave as observed by the magnetic field experiment. The extended magnetic tail as shown to be roughly cylindrical about the earth-sun line although IMP-I did not probe the sunset terminator portion of the boundary.*

Figure 41 illustrates this relationship and inspection of the chart shows that for observed field strengths of 20 gammas and a tail radius of 22 $R_e$, the colatitude predicted for the polar cap region is approximately 16°. This is in remarkable agreement with the positions of the auroral zones as directly measured and substantiates the general qualitative model of the earth's tail which is formed by the distortion of the geomagnetic field by the solar wind. Recent low altitude measurements of particle fluxes on the night side of the earth at high latitudes above the trapping regions support the field topology proposed (Reference 35).

## NEUTRAL SHEET CHARACTERISTICS

Observations of the magnetic neutral sheet in the earth's tail have been performed on 14 of orbits 31 through 47. These have ranged over geocentric distances of 9.9 $R_e$ to 28 $R_e$. In general, the early orbits possessed neutral sheet traversals closer to the earth than later orbits. Analyses have been performed to deduce the orientation of the neutral sheet in the earth's magnetic tail. Indeed, that the neutral surface separating fields of opposite direction is more or less a flat planar feature, as suggested by the word sheet, is one result of this particular investigation. The latitude of the positions of crossing of the neutral surface in the earth's magnetic tail has been examined in three coordinate systems:

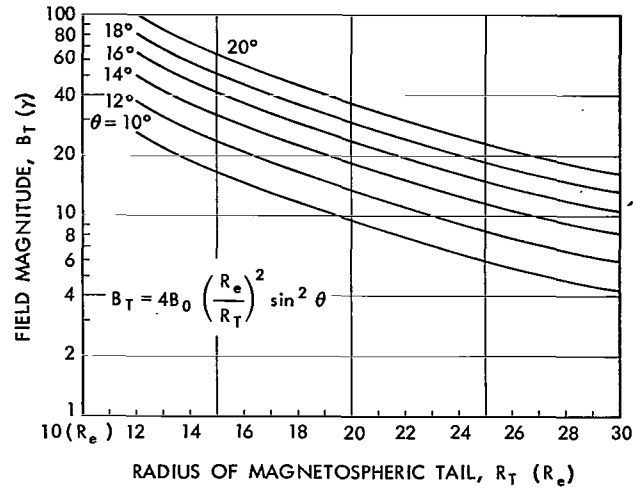


Figure 41—Chart for computing magnetic field strength in the earth's magnetic tail assuming conservation of magnetic flux from polar cap regions. The variable parameters are the radius of the magnetospheric tail, $R_T$, and the colatitude of the polar cap region, $\theta$.

1. solar ecliptic
2. geomagnetic
3. solar magnetospheric.

The last system is a recent addition to those coordinates used in interpretation of magnetospheric phenomena. It incorporates the earth-sun line as the X-axis but unlike solar ecliptic, includes a dependence upon the position of the geomagnetic axis rather than the ecliptic plane. The coordinate system is illustrated in Figure 42 showing the X-Z plane as including the magnetic axis of the earth. This implies that the Y-axis in the new coordinate system is always normal to both the earth-sun line and the earth's magnetic dipole axis.

Previous research workers in the field of magnetosphere physics have suggested that such a coordinate system might be appropriate in the analysis of magnetospheric phenomenona (Reference 33) but until these IMP-I data were available there appeared to be no appropriate need for its consideration. The variation and position of the neutral sheet in the three coordinate systems discussed has been investigated. The best fit to the equatorial plane in the three coordinate systems occurred in the solar magnetospheric coordinate system. This is shown in Figure 43 in which it is seen that the position of the neutral

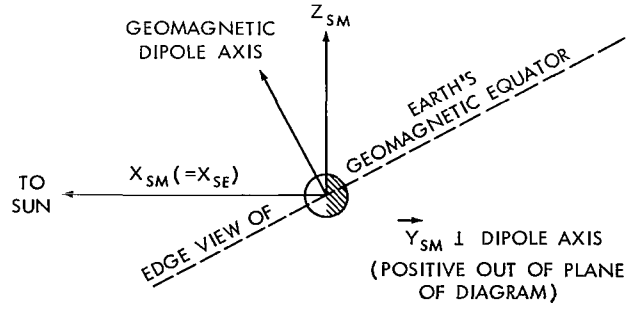


Figure 42—Definition of the solar magnetospheric coordinate system used in the interpretation of the position of the neutral sheet as observed in the magnetic tail of the earth.

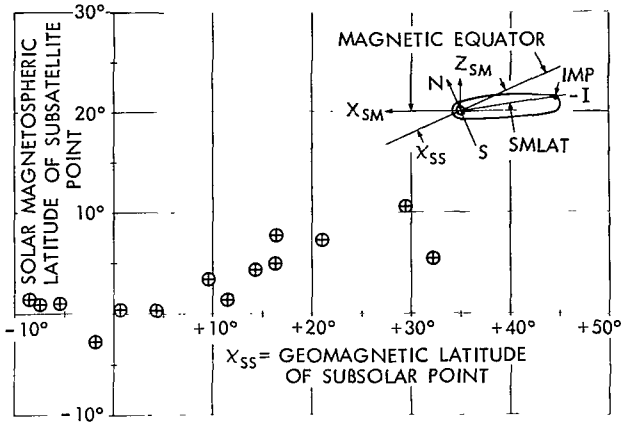


Figure 43—Position of the neutral sheet as observed by the IMP-I magnetic field experiment while in the magnetic tail of the earth. The sheet is observed to be within 5° or 10° of the solar magnetospheric equatorial plane for the 14 observed crossings.

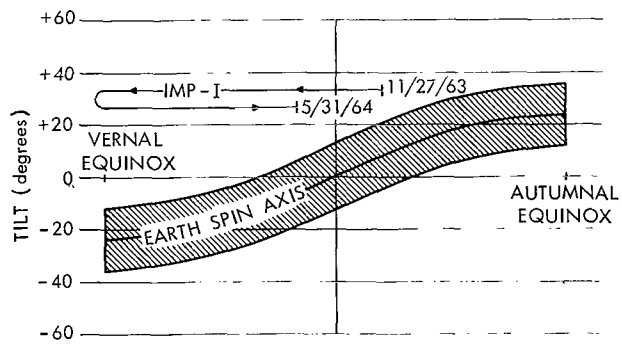


Figure 44—Illustration of the variation of the tilt of the equatorial plane of the solar magnetospheric coordinate system with respect to the ecliptic plane. Superimposed is the time interval covered by IMP-I.

surface crossing is always within 5° or 10° of the solar magnetospheric equatorial plane. Thus it is suggested by these results that the neutral sheet in the earth's magnetic tail is roughly parallel to the solar magnetospheric equatorial plane and indeed is approximately equivalent to it. The variation in the tilt of the neutral sheet to the ecliptic plane is an important parameter in comparing these results with previous and future satellite measurements. Figure 44 shows the annual variation of the tilt of the neutral sheet with respect to the ecliptic plane when viewed along the earth-sun line. The maximum inclination is ±35.4° with an annual seasonal variation.

Measurements in recent years (References 7 and 36-40) have shown enhanced particle fluxes on the night side of the earth. Some of these are probably related to the magnetic neutral sheet. Previous measurements by Frank (Reference 36) are particularly pertinent in this respect since they revealed the formation of an electron "tail" of the magnetosphere on the night side of the earth with the Explorer 14 satellite. As noted by Axford, Petschek and Siscoe (Reference 41), in order that a magnetic neutral sheet exist in the earth's magnetic tail, the sheet must be filled with an increased plasma flux which balances the opposing field configurations.

Figure 45 predicts the minimum particle flux necessary to balance a magnetic field in the earth's tail and superimposes experimental evidence of the neutral sheet. These measurements were not originally interpreted to be indicative of the neutral sheet but with the magnetic field topology of the earth's tail as measured by the IMP-I satellite, it is possible to place these measurements in a proper perspective. As noted by Van Allen (Reference 42), the measurements by Gringauz (Reference 38) do not necessarily indicate a third radiation belt. They now can be reasonably interpreted in terms of the neutral sheet in the earth's magnetic tail.

In Figure 46 correlated particle and field measurements performed on IMP-I in the earth's magnetic tail are shown. Precipitous increases in particle fluxes are observed coincident with

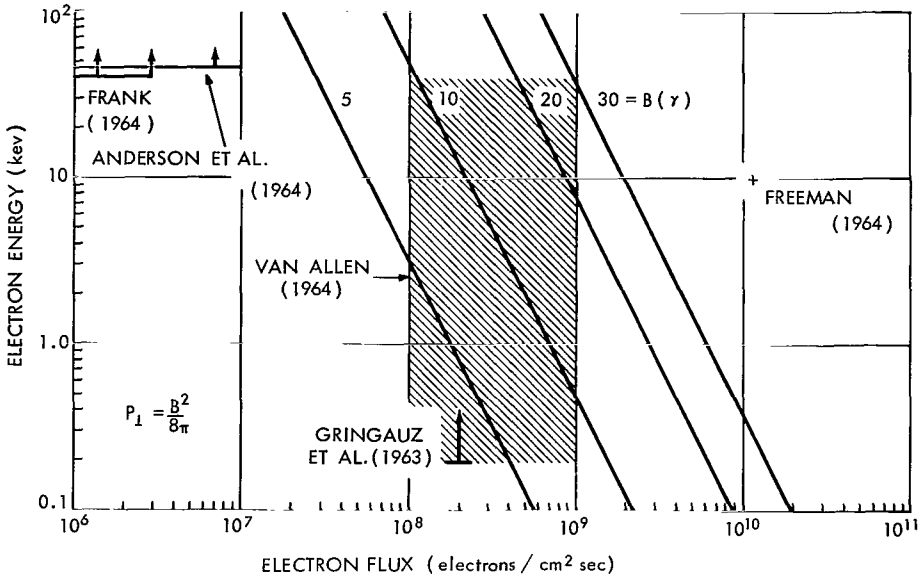


Figure 45—Assumed pressure balance between vacuum magnetic fields and non-magnetized electron plasma corresponding to idealized model of neutral sheet. Superimposed are particle and plasma observations pertinent to the interpretation of the neutral sheet in the earth's magnetic tail.

rapid decreases in magnetic field intensity. The interpretation of these time variations is that the total flux of the electrons in the earth's tail at this time is sufficiently large that the diamagnetic moment of the particles cancels the magnetic field in the earth's tail, at least locally. Thus the earth's magnetic tail may at times form a third regime in cislunar space quite unlike that of the interplanetary medium in which plasma energy completely dominates magnetic field energy or of the radiation belts in which the reverse situation is true. Rather, there is an intimate coupling of the magnetosphere plasma and field in which the $\beta$ value is close to unity.

The principal problem related to the tail is whether or not it is the source of auroral particles which are accelerated from low to high energies by a mechanism acting only in the earth's tail. Ness (Reference 4) has previously suggested that this mechanism may be related to instabilities of the neutral sheet similar to well-known sheet pinch instabilities studied in the plasma fusion program (Reference 43).

A schematic summary of the geomagnetic field topology and its interaction with the solar wind in the noon-midnight meridian plane is shown in Figure 47. A strong day-night asymmetry is indicated in the trapped radiation belts and the neutral sheet is shown as including the earth-sun line. A sample orbit of IMP is shown in the earth's tail to illustrate the region of space in which magnetic field measurements revealing the formation of this extended magnetic tail of the earth, were

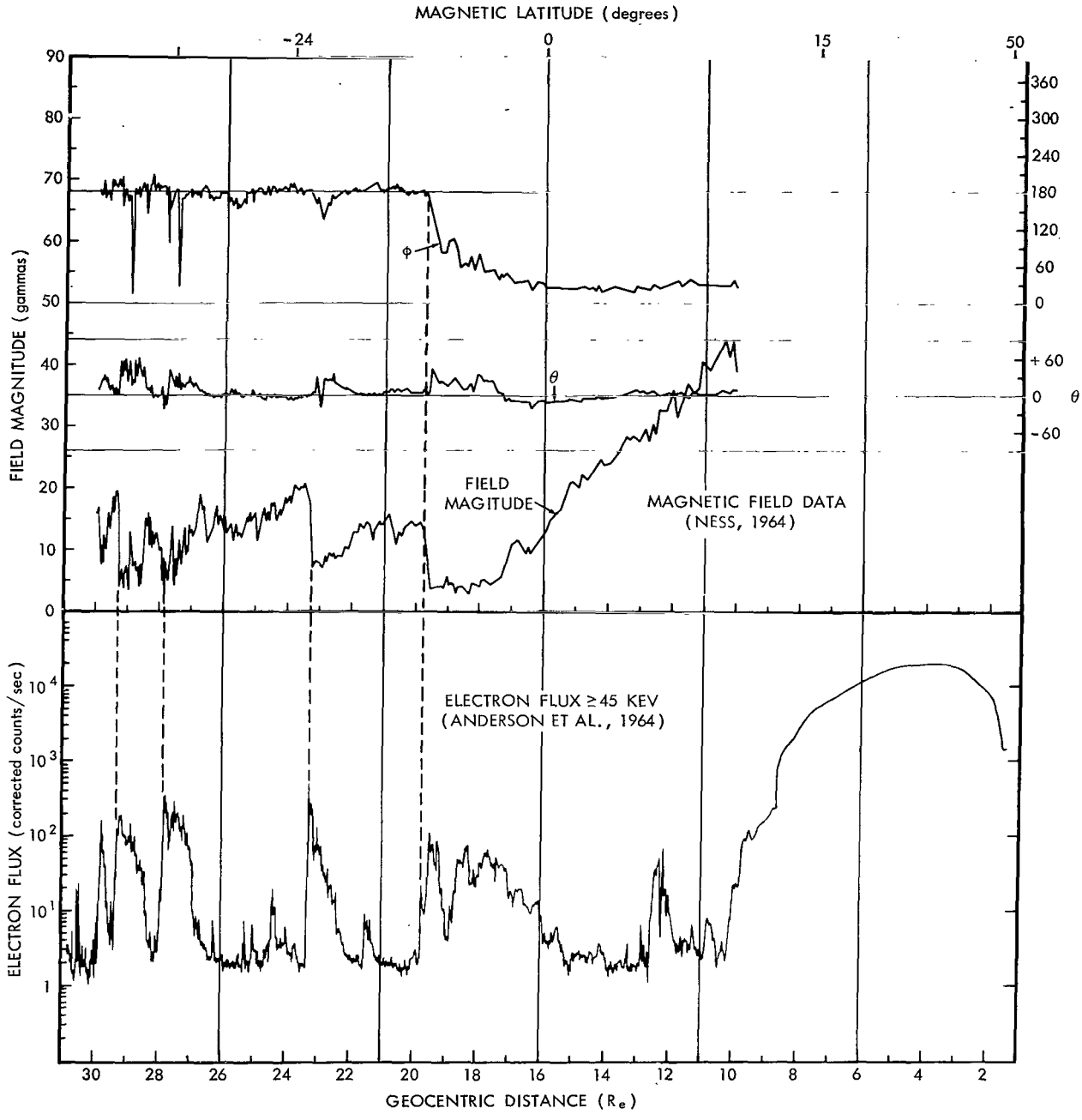


Figure 46—Correlated electron flux and magnetic field magnitude variations in the tail of the magnetosphere observed by IMP-I on orbit 40 inbound 29 April 1964. The sheet was observed during this orbit at a position of 19.8 $R_e$, coincident with an abrupt increase in the electron flux.

performed. Polar regions of the earth are as yet unmapped at great distances. The indentations shown on the boundary of the magnetosphere are associated with theoretically suggested neutral points of the earth's magnetic field in the geomagnetic cavity (Reference 22).

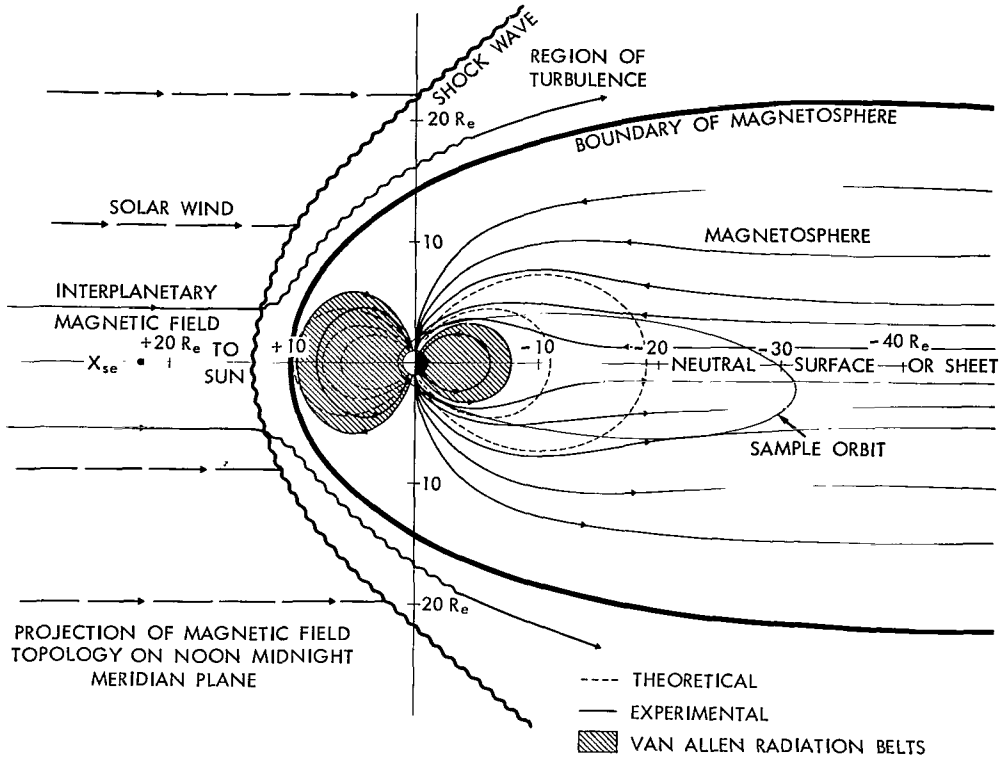


Figure 47—Summary illustration of the interpretation of the IMP-I data perpendicular to the plane of the ecliptic illustrating strong day-night asymmetry in the radiation belts and the development of the extended magnetic tail of the earth.

## SUMMARY

The continual flux of solar plasma confines the geomagnetic field to a region of space surrounding the earth but extending on the night side to a distance as yet unknown. It appears certain that the earth's magnetic tail extends beyond the orbit of the moon and thus the moon must traverse the earth's magnetic tail once every 29.5 days. The presence of the neutral sheet in the earth's magnetic tail implies an enhanced particle flux within it to balance the field pressure.

It is possible to view the earth as a magnetic comet if the earth is considered as a nucleus, the radiation belts as a coma, and the earth's magnetic tail as a cometary tail with characteristic Type-I cometary tail rays represented by the earth's neutral sheet. Certain aspects of this analog are currently being investigated and will be reported upon in future publications. At the present time investigation of the earth's magnetic tail and its association with auroral and radiation belt phenomena present distinct challenges to future space experiments and theory.

## ACKNOWLEDGMENTS

The authors gratefully acknowledge the outstanding efforts of the IMP project staff and personnel at GSFC who so ably assisted us in our efforts to achieve a "magnetically clean" satellite.

Without their support and cooperation and that of our co-experimenters this work could not have been completed. One of us (J.M.W.) thanks the Director of the Mt. Wilson Observatory for guest investigator privileges extended him.

## REFERENCES

1. Ness, N. F., Scearce, C. S., and Seek, J. B., "Initial Results of the IMP-I Magnetic Field Experiment," *J. Geophys. Res.* 69(17):3531-3569, September 1, 1964.

2. Ness, N. F. and Wilcox, J. M., "The Solar Origin of the Interplanetary Magnetic Field," *Phys. Rev. Letters* 13(15):461-464, October 12, 1964.

3. Ness, N. F., "The Magnetohydrodynamic Wake of the Moon," *J. Geophys. Res.* 70(3):517-534, February 1, 1965.

4. Ness, N. F., "The Earth's Magnetic Tail," *J. Geophys. Res.* 70(13):2989-3005, July 1, 1965

5. Ness, F. and Wilcox, J. M., "Extension of the Photospheric Magnetic Field into Interplanetary Space," Goddard Space Flight Center Document X-612-65-79, 1965, and *Astrophys. J.*, 143(1):23-31, January 1966.

6. Ness, N. F. and Wilcox, J. M., "Sector Structure of the Quiet Interplanetary Magnetic Field," *Science* 148(3677):1592-1594, June 18, 1965.

7. Anderson, K. A., Harris, H. K., and Paoli, R. J., "Energetic Electron Fluxes in and beyond the Earth's Outer Magnetosphere," *J. Geophys. Res.* 70(5):1039-1050, March 1, 1965.

8. Balasubramanyan, V. K., Ludwig, G. H., McDonald, F. B., and Palmeira, R. A. R., "Results from the IMP-I GM Counter Telescope Experiment," GSFC Document X-611-65-49, 1965.

9. Bridge, H., Egidi, A., Lazarus, A., Lyon, E., and Jacobson, L., "Preliminary Results of Plasma Measurements on IMP-A," in: *Space Research V; Proc. 5th Internat. Space Sci. Symp., Florence, Italy, May 12-15, 1964,* ed. by D. G. King-Hele, P. Muller, and G. Righini, Amsterdam: North-Holland Publishing Co.; New York: Interscience Publishers, 1965, pp. 969-978.

10. Fan, C. Y., Gloecker, G., and Simpson, J. A., "Evidence for 30 Kev Electrons Accelerated in the Shock Transition Region beyond the Earth's Magnetospheric Boundary," *Phys. Rev. Letters* 13(5):149-153, August 13, 1964.

11. McDonald, F. B. and Ludwig, G. H., "Measurement of Low-Energy Primary Cosmic-Ray Protons on IMP-I Satellite," *Phys. Rev. Letters* 13(26):783-786, December 28, 1964.

12. Serbu, G. P., "Results from the IMP-I Retarding Potential Analyser," in: *Space Research V; Proc. 5th Internat. Space Sci. Symp., Florence, Italy, May 12-15, 1964,* ed. by D. G. King-Hele, P. Muller, and G. Righini, Amsterdam: North-Holland Publishing Co.; New York: Interscience Publishers, 1965, pp. 564-574.

13. Axford, W. I., "The Interaction between the Solar Wind and the Earth's Magnetosphere," *J. Geophys. Res.* 67(10):3791-3796, September 1962.

14. Harrison, E. R., "The Earth's Distant Magnetic Field," *Geophys. J.* 6(4):479-492, June 1962.

15. Kellogg, P. J., "Flow of Plasma around the Earth," *J. Geophys. Res.*, 67(10):3805-3811, September 1962.

16. Parker, E. N., "Dynamics of the Interplanetary Gas and Magnetic Field," *Astrophys. J.* 128(3): 664-676, November 1958.

17. Biermann, L., "Kometenschweife und solare Korpuscularstrahlung," *Z. Astrophys.* 29(3):274-286, September 1951.

18. Parker, E. N., "The Hydrodynamic Theory of Solar Corpuscular Radiation and Stellar Winds," *Astrophys. J.* 132(3):821-866, November 1960.

19. Snyder, C. W. and Neugebauer, M., "Interplanetary Solar Wind Measurements by Mariner 2," in: *Space Research Science Symposium, 4th, Warsaw, Poland, June 4-10, 1963,* Amsterdam: North-Holland Publisning Co.; New York: Interscience Publishers, 1964.

20. Babcock, H. W., "The Solar Magnetograph," *Astrophys. J.* 118(3):387-396, November 1953.

21. Ahluwahlia, H. S. and Dessler, A. J., "Diurnal Variation of Cosmic Radiation Intensity Produced by a Solar Wind," *Planet. Space Sci.* 9:195-210, 1962.

22. Beard, D. B., "The Solar Wind Geomagnetic Field Boundary," *Rev. Geophys.* 2(2):335-365, May 1964.

23. Freeman, J. W., Van Allen, J. A., and Cahill, L. J., "Explorer 12 Observations of the Magnetospheric Boundary and the Associated Solar Plasma on September 13, 1961," *J. Geophys. Res.* 68(8):2121-2130, April 15, 1963.

24. Cahill, L. J. and Amazeen, P. G., "The Boundary of the Geomagnetic Field," *J. Geophys. Res.* 68(7):1835-1843, April 1, 1963.

25. Heppner, J. P., Ness, N. F., Skillman, T. L., and Scearce, C. S., "Explorer 10 Magnetic Field Measurements," *J. Geophys. Res.* 68(1):1-46, January 1, 1963.

26. Bonetti, A., Bridge, H. A., Lazarus, A. J., Rossi, B., and Scherb, F., "Explorer 10 Plasma Measurements," *J. Geophys. Res.* 68(13):4017-4064, July 1, 1963.

27. Ness, N. F., "Observations of the Geomagnetic Cavity Boundaries," *C. U. Symposium on Plasmas in Space (1963)*, Amsterdam: North-Holland Publishing Co., 1965.

28. Spreiter, J. R. and Jones, W. P., "On the Effect of a Weak Interplanetary Magnetic Field on the Interaction between the Solar Wind and the Geomagnetic Field," *J. Geophys. Res.* 68(12): 3555-3564, June 15, 1963.

29. Chapman, S., "Solar Plasma, Geomagnetism and Aurora in Geophysics," in *Geophysics: The Earth's Environment*, ed. by C. DeWitt, J. Hieblot, and A. Lebeau, 373-502, New York: Gordon and Breach, Science Publishers, 1963.

30. Axford, W. I., Petschek, H. E., and Siscoe, G. L., "The Tail of the Magnetosphere," *J. Geophys. Res.* 70(5):1231-1236, March 1, 1965.

31. Piddington, J. H., "The Transmission of Geomagnetic Disturbances Through the Atmosphere and Interplanetary Space," *Geophys. J.* 2(3):173-189, September 1959.

32. Piddington, J. H., "Geomagnetic Storm Theory," *J. Geophys. Res.* 65(11):93-106, January 1960.

33. Dessler, A. J. and Juday, R. D., "Configuration of Auroral Radiation in Space," *Planet. Space Sci.*, 13(1):63-72, January 1965.

34. Cahill, L. J., "Preliminary Results of Magnetic Field Measurements in the Tail of the Geomagnetic Cavity," *Internat. Geophys. Bull.* No. 79. 11-15 January 1964.

35. McDiarmid, I. B. and Burrows, J. R., "Electron Fluxes at 1000 Km. Associated with the Tail of the Magnetosphere," *J. Geophys. Res.*, 70, in press, 1965.

36. Frank, L. A. and Van Allen, J. A., "A Survey of Magnetospheric Boundary Phenomena," in: *Res. in Geophys.* Vol. 1, ed. by H. Odishaw, Cambridge: MIT Press, 1964, pp. 161-185.

37. Freeman, J. W., "Electron Distribution in the Outer Radiation Zone," *J. Geophys. Res.* 69(9): 1691-1723, May 1, 1964.

38. Gringauz, K. I., Kurt, V. G., Moroz, V. I., and Shklovskii, I. S., "Results of Observations of Charged Particles Observed out to 100,000 Km with the Aid of Charged-Particle Traps on Soviet Space Probes," *Astron Zh. 37(4):716-735, July-August, 1960;* translated in *Soviet Astron.-AJ*, 4(4):680-695, January-February, 1961.

39. Montgomery, M. D., Singer, S., Conner, J. P., and Stogsdill, E. E., "Spatial Distribution, Energy Spectra and Time Variations of Energetic Electrons (E > 50 Kev) at 17.7 Earth Radii," *Phys. Rev. Letters* 14(7):209-213, February 15, 1965.

40. Singer, S., Conner, J. P., Evans, W. D., Montgomery, M. D., and Stogsdill, E. E., "Plasma Observations at $10^5$ Km.," in: *Space Research V; Proc. 5th Internat. Space Sci. Symp., Florence, Italy, May 12-15, 1964,* ed. by D. G. King-Hele, P. Muller, and G. Righini, Amsterdam: North-Holland Pub. Co.; New York: Interscience Publishers, 1965, pp. 546-563.

41. Frank, L. A., "A Survey of Electrons beyond 5 Earth Radii with Explorer XIV," *J. Geophys. Res.* 79(7):1593-1626, April 1, 1965.

42. Van Allen, James A., "Remarks on Accompanying Letter by K. I. Gringauz," *J. Geophys. Res.* 69(5):1011-1013, March 1, 1964.

43. Furth, H. P., Killeen, J., and Rosenbluth, M. N., "Finite Resistivity Instabilities of a Sheet Pinch," *Phys. Fluids* 6(4):459-484, April 1963.

# SOUTHERN HEMISPHERE ANOMALIES

by
J. G. Roederer*
*Goddard Space Flight Center*

The eccentricity of the geomagnetic dipole and the presence of multipole perturbations give rise to a series of phenomena observable in the southern hemisphere which are important to the physics of the magnetosphere and ionosphere, and to the study of cosmic rays.

In the first part of this review, the morphology of the geomagnetic field peculiarities in the southern hemisphere will be analyzed. In the second part, some of the efforts on cosmic rays, geomagnetically trapped radiation and the ionosphere will be discussed.

## INTRODUCTION

Most of the peculiarities of the geophysical behavior of the southern hemisphere ultimately originate in the eccentricity and the asymmetry of the geomagnetic field, both of which lead to particularly strong effects south of the equator. The purpose of this brief review then, is first to describe the morphology of these geomagnetic peculiarities, and second to summarize some of their effects on several phenomena of ionospheric physics, trapped radiation, and cosmic rays.

## PECULIARITIES OF THE GEOMAGNETIC FIELD IN THE SOUTHERN HEMISPHERE

It is well known that the earth's magnetic field behaves like a centered dipole only in a very first approximation. An improvement in the field description is achieved if the center of the dipole is displaced about 340 km off the geographic center of the earth, into a direction 6.5 N and 162 E, i.e., roughly towards the East Asian region. This means that field lines of a given dipole shall come "closest" to the earth's surface over the east coast of South America and over the South Atlantic Ocean. As a result, there is an absolute minimum field intensity over Eastern Brazil.

Figure 1 shows iso-intensity contours of the geomagnetic field;† notice the low field intensities in the magnetic equatorial region over South America, and the higher equatorial intensities over

*National Academy of Sciences - National Research Council, Senior Post-Doctoral Research Associate, on leave from Facultad de Ciencias Exactas y Naturales and Cento Nacional de Radiacion Cosmica, Buenos Aires, Argentina.
†See pages 35 – 131.

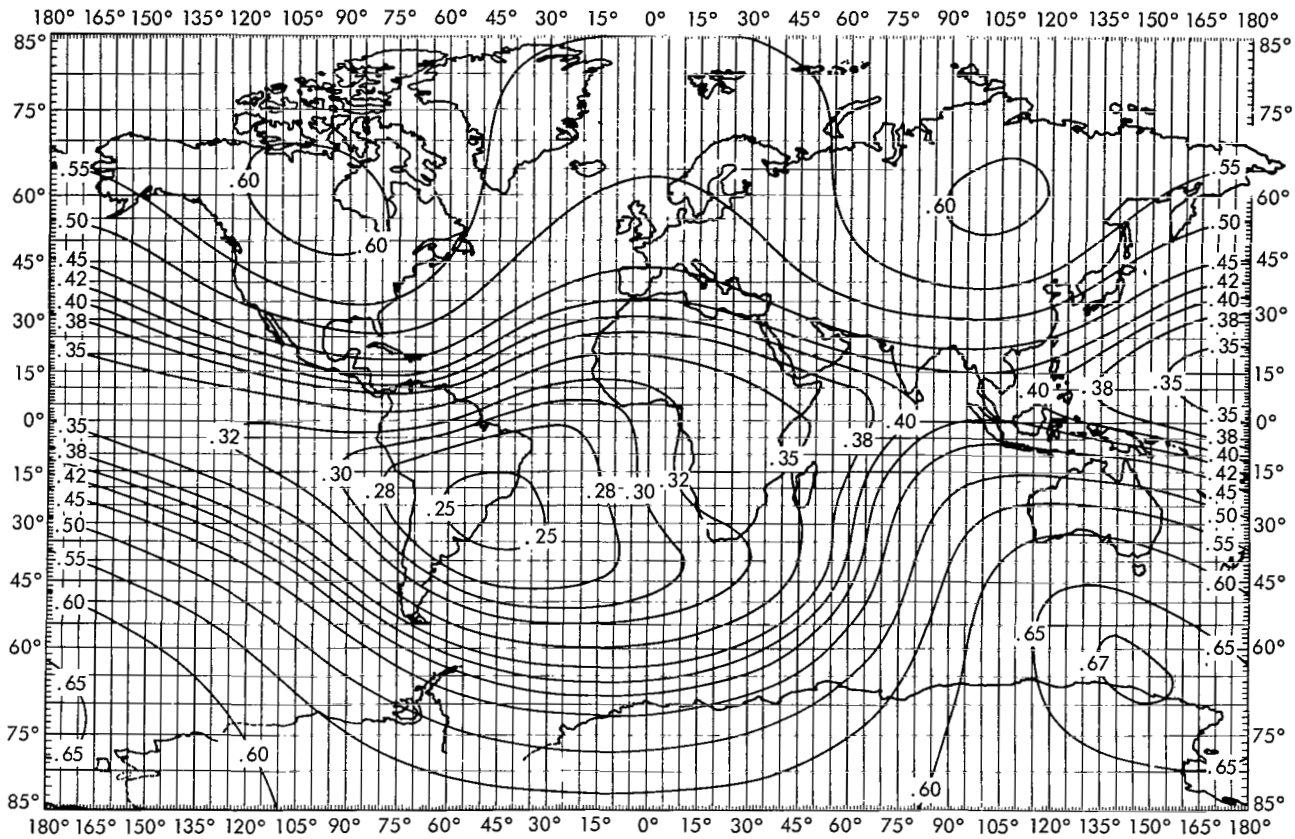


Figure 1—Contours of constant total field intensity.

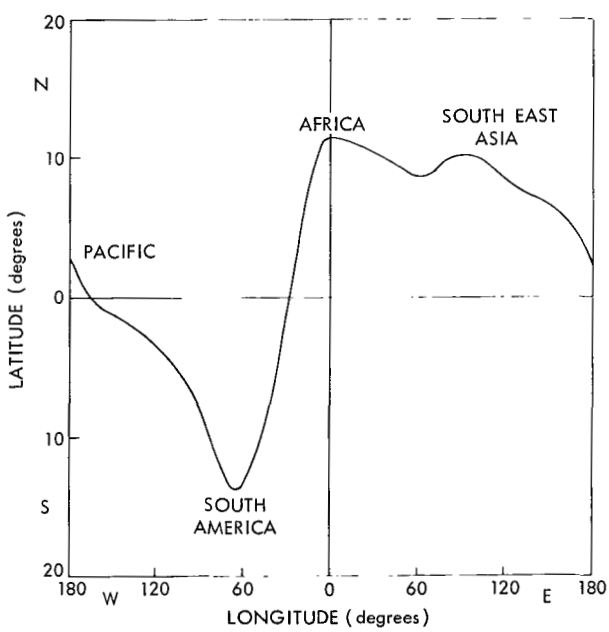


Figure 2—Geographic position of the magnetic (dip) equator.

Malaysia. Notice further the different absolute intensities at the geomagnetic poles (North Canada and Antarctica).

These differences, however, cannot be explained by merely displacing the magnetic center. Such a displacement would lead to extreme equatorial values of 0.27 and 0.34 gauss, respectively, whereas the observed extreme values are 0.24 gauss over the Brazilian east coast and 0.41 gauss over the northeast Indian Ocean. This means that higher multipoles do play a substantial role in the field asymmetry. But the net effect is still that *the geomagnetic shells come closest to the earth's surface over South America and the South Atlantic.*

The eccentricity and asymmetry of the geomagnetic field are closely associated with the facts revealed in Figure 2, and Figure 3 from

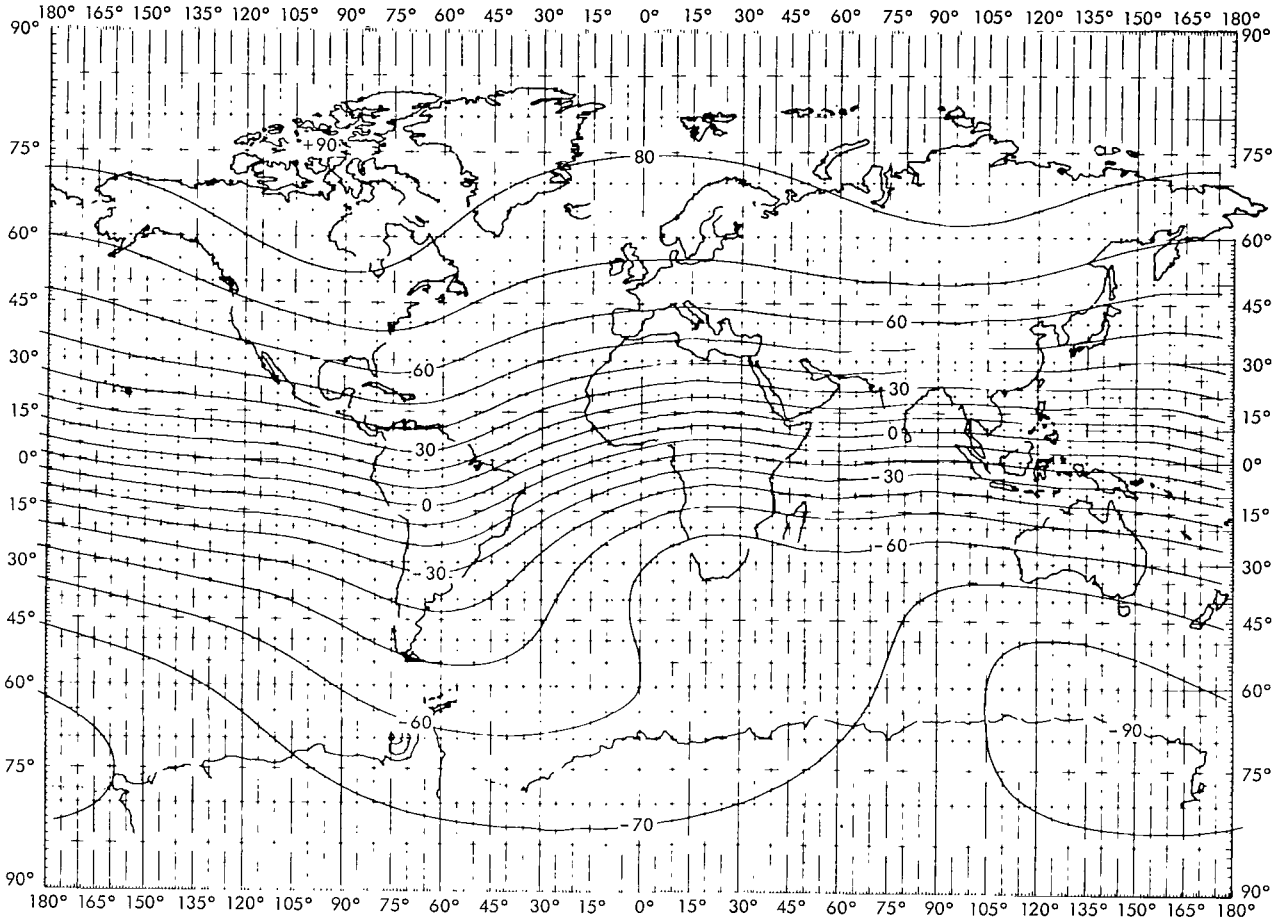


Figure 3—Contours of constant magnetic dip (from Reference 1).

(Reference 1). They are: (1) *the magnetic (dip) equator has its maximum displacement from the geographic equator over South America* and (2) *there is a displacement of low dip angles toward the antarctic geographic polar region, over South America and the Palmer Peninsula.*

These variations in the geomagnetic-geographic relationships mean, for instance, that the sun, at local noon during equinoxes, is farthest away from the magnetic equator in a region over South America. In addition, this region of maximum departure over South America is very narrow in longitude compared to the extension in longitude of the maximum departure region in the northern hemisphere over Africa and South East Asia (Figure 2).

On the other hand, Figure 3 shows that, in general, magnetic field lines are less inclined over the southern geographic polar area than in the northern counterpart. In particular, the "tongue" of low dips invading Antarctica over the Palmer Peninsula is responsible for the existence of a unique

region with unique geophysical stations and high geographic latitudes, and yet with almost mid-latitude magnetic dip angles.

Another morphological feature relevant to the different geophysical behavior of the two opposite polar regions is the fact that the *distance between the geographic South Pole and the corresponding magnetic pole is considerably greater than the distance between geographic and magnetic poles in the north.* This is clearly seen in Figure 4 (Reference 1), which shows curves of constant horizontal field intensity.

Examination of the "spread" of geomagnetic field lines, or of the magnetic flux tubes when followed from the equator to an intersection at the earth's surface, reveals *a region of maximum spread of field lines over South America and the Palmer Peninsula.* This is caused by the same multipole contribution which leads to the absolute minimum of the total field intensity over Brazil, and is responsible for the longitudinally narrow displacement of the magnetic equator from the geographic equator over South America.

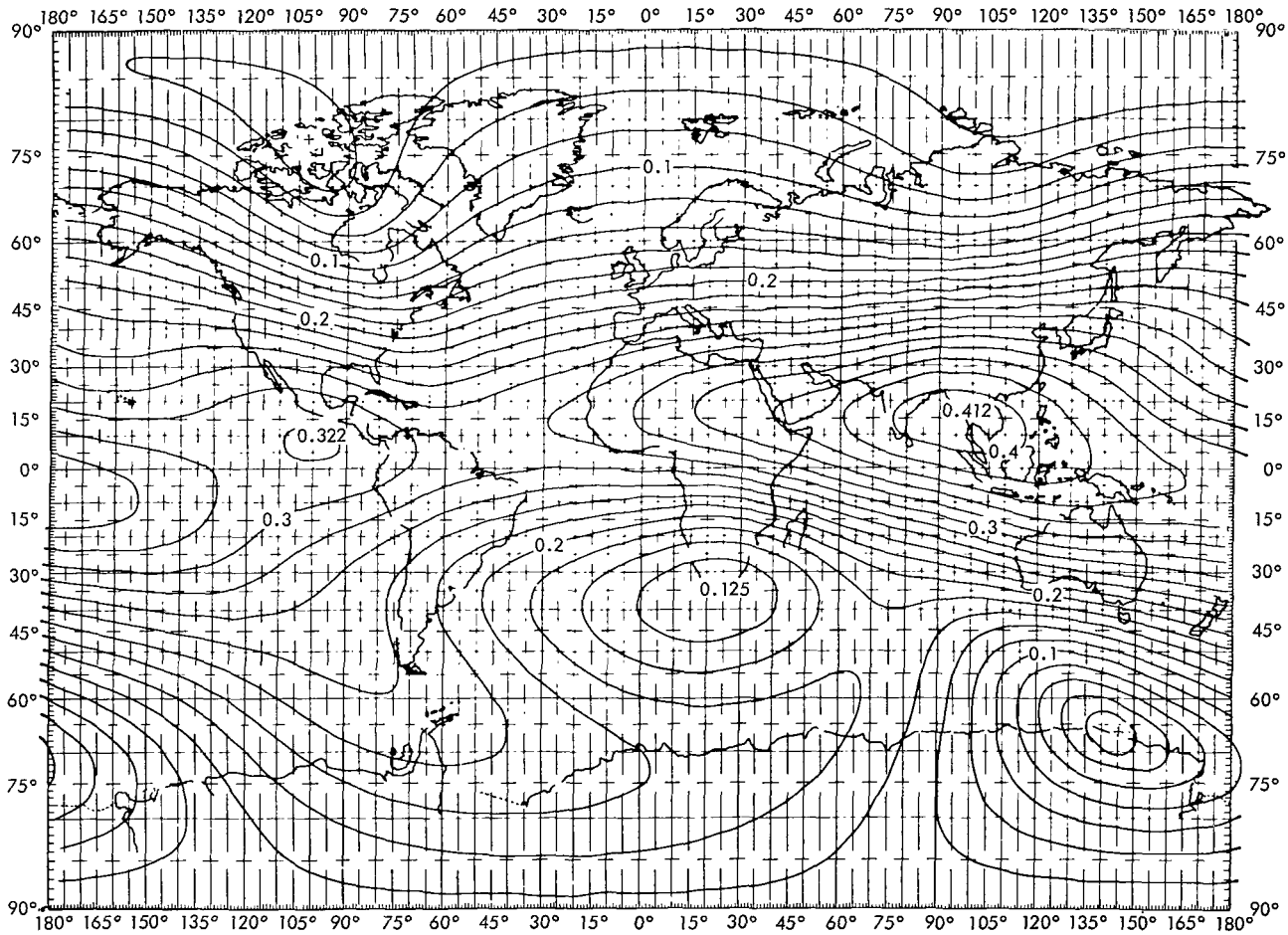


Figure 4—Contours of constant horizontal intensity (from Reference 1).

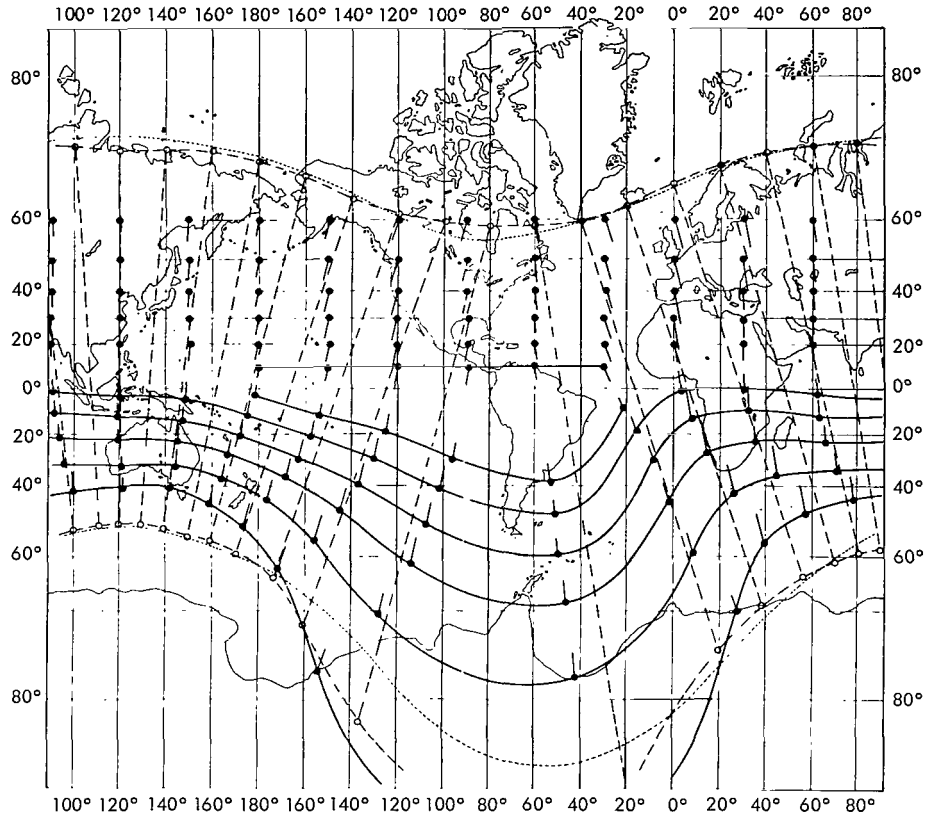


Figure 5—Conjugate intersects (dots) of geomagnetic field lines (from Reference 2).

This maximum spread can be visualized to some extent by plotting conjugate intersects for a network of field lines (Figure 5 and Reference 2), and is taken into account whenever considering phenomena of plasma flow from the equator toward the poles. It is also ultimately responsible for the average longitudinal drift velocity of geomagnetically trapped particles being greater over South America and the Atlantic Ocean.

There are two additional effects, not so well known, but which might play a role in southern hemisphere anomalies. The first of these effects is shown in Figure 6.* Here the

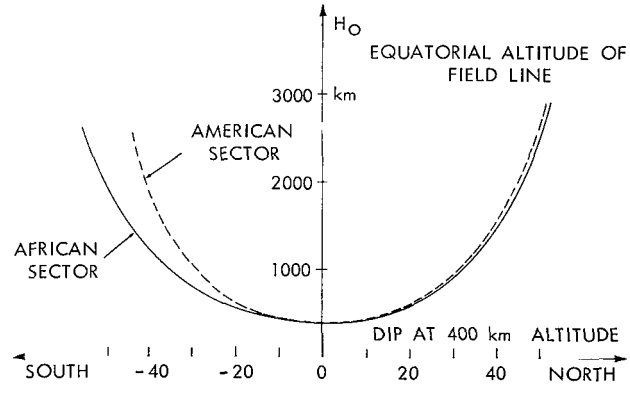


Figure 6—Equatorial altitude (in km) of a field line, as a function of its dip angle at the 400 km level, for the American (dotted curve) regions. The east Asian region curve falls very close to the American curve.

*See pages 35 – 131.

altitude in kilometers of the equatorial (minimum B) points of a field line is plotted as a function of the dip angles at the northern and southern intersections with a constant altitude surface, for the two longitudinal regions of Africa and America.* A third region in the Far East and the Pacific gives results very close to the American region. Both curves clearly show that for a given dip, field lines attain the lowest equatorial altitude when emerging from South Africa.

The second effect is concerned with the variation of McIlwain's L parameter (Reference 3) along a given field line. *Recent calculations show that the degree of violation of the invariant character of L is highest for field lines starting south of Capetown,* and for L between 1.6 and 2.6.

## GEOPHYSICAL EFFECTS OF MAGNETIC FIELD PECULIARITIES IN THE SOUTHERN HEMISPHERE

Geophysical phenomena may be classified as follows: (1) Exclusively field-controlled phenomena such as the motion of cosmic rays, solar protons and auroral particles. (2) Field-controlled phenomena influenced by the atmosphere, as in the geomagnetically trapped radiation where motion and storage is field-controlled but diffusion and loss processes are determined by the atmosphere. (3) Atmosphere-controlled phenomena influenced by the field, as in the variety of ionospheric phenomena where source, loss, and overall motion are controlled by atmosphere but the geomagnetic field determines electric currents, drifts diffusion, etc.

In discussing the groups of phenomena enumerated above, only very general remarks are made regarding quiet epochs only. Transient perturbations, as those associated with storms, are not treated.

Examples of the first group of phenomena are two "anomalies" in the equatorial values of vertical effective cut-off rigidities for cosmic ray protons; the highest absolute value of vertical cut-off rigidity ($\approx$18 GV) is over the north-east Indian Ocean, and the lowest ($\approx$13.5 GV) is over South America. In other words, the *equatorial* cosmic ray flux is highest over South America and has an absolute minimum somewhere over the north-east Indian Ocean.

Indirectly related to the tongue of low dip angles extending from South America over the Palmer Peninsula are the unusually higher cut-off rigidities of cosmic ray observatories like Ushuaia, Ellsworth, and Base General Belgrano in spite of the high geographic latitude of these stations.

An important result of detailed cosmic ray particle orbit calculations by Shea et al. (Reference 4) reveals that the structure of so-called shadow cones, i.e., the region in rigidity space where allowed and forbidden zones alternate, is widest and most complicated at points in South America and the adjacent South Atlantic Ocean. Furthermore, discrepancies among different cut-off calculations is greatest in this region (Reference 5). Particles impinging on the earth's atmosphere

*See pages 35 – 131.

over South America feel the multipole perturbations most intensively and possibly cause these anomalies.

The second group of phenomena considers the behavior of the radiation belts. If there were no interactions with the medium (the atmosphere), charged particles would remain trapped on L shells, mirroring at a constant B value. In other words, the "mirror point trajectories" of a particle would be given by a pair of constant B-L rings (intersections of constant B and constant L surfaces), one in each hemisphere. The altitude over the earth's surface of a B-L ring is not constant; the southern rings get very close to the dense layers of the atmosphere just over the east coast of South America (low L shells), or over the South Atlantic Ocean (high L values). Plots of (southern) B-L ring altitudes as a function of longitude for the L = 1.25 shell (solid curves) are displayed in Figure 7.*

The behavior of the B-L rings is responsible for two main effects. First, charged particle fluxes at a given constant altitude (such as measured by a satellite in circular orbit) will be highest

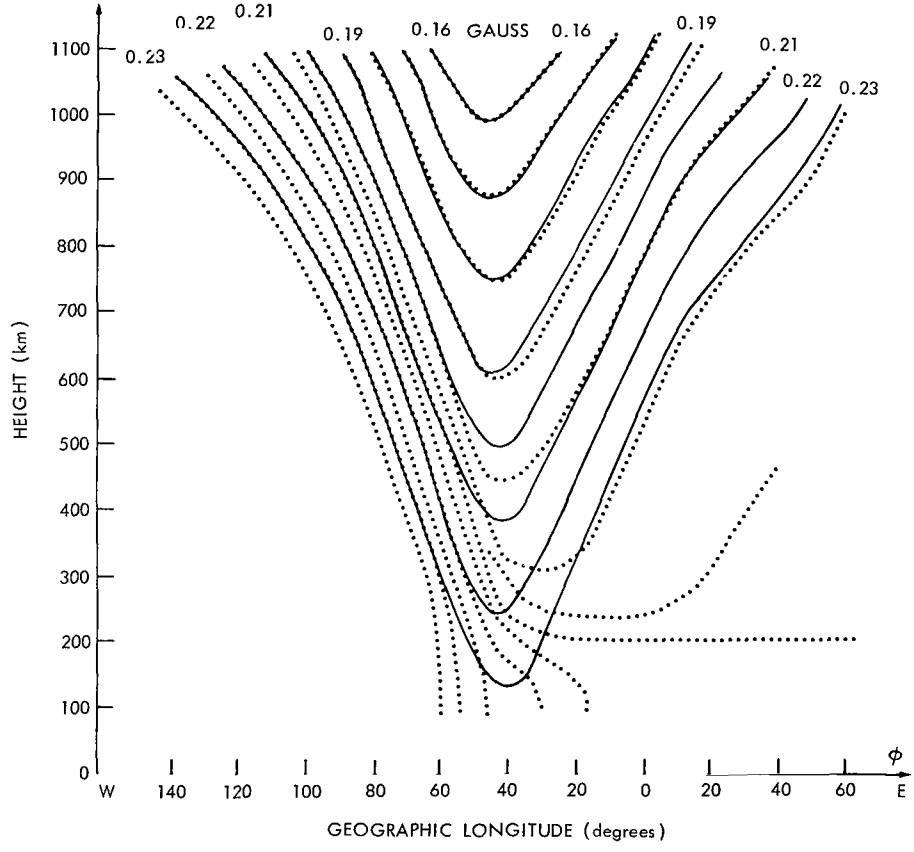


Figure 7—Altitudes in the km of constant B-L rings (solid curves), for L = 1.25. Dotted curves: Average mirror point trajectories of 300 kev electrons drifting through the anomaly, subject to Coulomb scattering.

*See pages 183 – 207.

in a region extending from the east coast of South America to the South Atlantic (References 6, 7 and 8). Second, it is here that the satellite will sample trapped radiation at the lowest B values of a given shell.* This represents the South American anomaly of the radiation belt.

Additionally, since mirror points submerge deepest into the atmosphere in the region of the South American anomaly, this is where scattering and loss processes are most intense. Particle precipitation into the atmosphere will be highest in the anomaly (References 9 through 13). A schematic drawing of average trajectories of mirror points of 300 kev electrons (dotted curves) as they drift through the anomaly are shown in Figure 7. The enhanced atmospheric scattering causes them to diffuse on the average to higher B values. A certain fraction is lost, precipitating into the lower atmosphere; others manage to "get around" the anomaly, populating the high B region of the shell (which drops below sea level in the anomaly) and surviving just one more turn around the earth.† This is the "windshield wiper effect."

The study of particle precipitation and its effects on the ionosphere in the South American anomaly is of great importance. The first evidence of electron precipitation through Bremsstrahlung X-ray measurements with balloons was found by Ghielmetti, et al. (Reference 14). Its effect on the ionosphere was discussed by De Mendonça (Reference 15), and the evidence for airglow enhancement in the South Atlantic was reported by Greenspan and Stone (Reference 16).

Finally, the effect of maximum variation of L along field lines starting out south of Capetown might be relevant to the trapped particle dynamics in the affected L region. Violation of the invariant character of L means splitting of trapped particle shells according to their mirror point field intensity (Reference 17). A scattering process, which under normal conditions merely changes the particle's pitch angle to mirror point, leaving the shell untouched, will now also change the particle's shell. This change will depend on the longitude at which scattering took place. In other words, this effect introduces a *radial* scattering coupled to each pitch angle scattering process. This might affect substantially the particle density in the corresponding L shells.

The third group of phenomena includes the study of southern hemisphere anomalies in the ionosphere. While a systematic review of this subject is not practical here, a few examples are in order.

The position of the sun in relation to the geomagnetic field and also the motion or sweep of the subsolar point through the field, as viewed from a field-invariant system, are likely to be the main factors determining the peculiar behavior of the ionosphere in some regions of the southern hemisphere.

In the case of the equatorial anomaly in $f_0$ F2 (References 18 through 22), the facts pointed out in Figure 2 must be considered. The sun, in its annual cycle, scans a different portion of the "critical" field lines (along which the enhanced ionization is found to be aligned) in this South

*The steady state distribution of trapped particles along a line of force is always such that the omnidirectional intensity decreases from the equator towards the higher B point.
†See pages 183 – 207.

American region than at any other longitude. This effect might explain some of the summer-winter differences in the equatorial anomaly at different longitudes. It should be taken into account in any detailed theoretical description of the equatorial anomaly and its diurnal variations.

The systematic differences between the position (expressed in dip angle or in magnetic latitude) of the equatorial anomaly maxima in the African and the South American zone (Reference 18) are explained by taking into consideration Figure 6. When transforming dip angle at conjugate intersects into altitude of the equatorial point of a field line by means of these curves, the conclusion is reached that the different latitudinal "positions" of northern and southern $f_0F2$ maxima in the South American and African zones, at a given local time, merely correspond to the different positions and dip angles of the conjugate intersects of field lines reaching out to the *same* geographic altitude at their equatorial point. It appears as if the relevant quantity for the position of the anomaly maxima is given by the *maximum altitude* of the critical field line for all longitudes.

Several points related to field peculiarities must be considered when studying the processes of the transportation of ionization from the equator to the poles, either along field lines or as drifts in the F region. First, the maximum displacement of low dip angles toward the antarctic geographic polar region and the maximum spread of field lines over the Palmer Peninsula are important in relation to the geographic location of the flow of plasma (Reference 23) and that of its concentration or density, respectively (Reference 24). Second, it must be taken into account that the sun, in its daily cycle, stays for a much shorter period of the day over the magnetic equatorial region in southern summer than in northern summer (Figure 2).

These effects might explain the different behavior of the universal time in control of $f_0F2$ in the Antarctic versus the Arctic regions (References 25 and 26). They also should be connected with the anomalous behavior of the diurnal variation of $f_0F2$ at several South American and Antarctic stations in the area where one has a maximum divergence of field lines (Figure 5) and where there is a maximum shift between geographic and magnetic latitudes. In this unique group of stations in southern Argentina, Malvinas Islands, Decepcion, and Palmer Peninsula, there are long periods of darkness in winter in spite of their relatively low magnetic latitude. Deeper in the Antarctic territory there are stations in this range of longitudes which, at magnetic latitudes of only 60 degrees, are in constant darkness in winter.

Finally, considering the explanation of the mentioned anomalous variations of $f_0F2$ in the southern polar region (Reference 27) in terms of Dungey's wind shear model for the creation of ionization layers (Reference 28) and the greater distance between the geographic South Pole and the corresponding magnetic pole must be taken into account (Figure 4). Since the field lines are on the average more inclined over the southern (geographic) polar region, plasma compression by wind shear should be more effective there. When the effects of electric field ($E \times (B/B^2)$) drifts are considered, the same morphological N-S pole field difference must be taken into account, in order to explain the different behavior of the winter anomaly in the north and south pole regions (Reference 27). It will probably require another solar cycle of ionospheric measurements, especially data obtained with topside sounders (Reference 29), before a clear picture is attained of the very complicated play between geomagnetically and geographically controlled processes which lead to the southern hemisphere anomalies in the ionosphere.

## REFERENCES


1. Cain, J. C., and Neilon, J. R., "Automatic Mapping of the Geomagnetic Field," *J. Geophys. Res.* 68(16):4689-4696, August 15, 1963.

2. Vestine, E. H., and Sibley, W. L., "The Geomagnetic Field in Space, Ring Currents and Auroral Isochasms," *J. Geophys. Res.* 65(7):1967-1980, July 1960.

3. McIlwain, C. E., "Coordinates for Mapping the Distribution of Magnetically Trapped Particles," *J. Geophys. Res.* 66(11):3681-3691, November 1961.

4. Shea, M. A., Smart, D. F., and McCracken, K. G., "A Study of Vertical Cut-off Rigidities Using Sixth Degree Simulations of the Geomagnetic Field," *J. Geophys. Res.* 70(17):4117-4130, September 1, 1965.

5. Kenney, J. F., Gauger, J., Smart, D. F., and Shea, M. A., "A Study of the Relative Merits of Various Cosmic-Ray Vertical Cut-off Rigidity Models," *Trans. Amer. Geophys. Union.* 46(1): 62-63, March 1965 (abstract).

6. Yoshida, S., Ludwig, G. H., and Van Allen, J. A., "Distribution of Trapped Radiation in the Geomagnetic Field," *J. Geophys. Res.* 65(3):807-813, March 1960.

7. Vernov, S. N., Gorchakov, E. V., Logachev, Yu. I., Nesterov, V. E., Pisarenko, N. F., Savenko, I. A., Chudakov, A. E., and Shavrin, P. I., "Investigations of Radiation During Flights of Satellites, Vehicles and Rockets," *J. Phys. Soc. Japan.* 17(supp. A-II):162-186, January 1962.

8. Freden, S. C., and Paulikas, G. A., "Trapped Protons at Low Altitudes in the South Atlantic Magnetic Anomoly," *J. Geophys. Res.* 69(7):1259-1269, April 1, 1964.

9. Mann, L. G., Bloom, S. D., and West, H. I., Jr., "Electron Spectrum from 90 to 1200 KeV as Observed on Discoverer Satellites 29 and 31," in: *Space Research III; Proc. 3rd Internat. Space Sci. Sympos., Washington, D. C., May 2-8, 1962,* ed. by W. Priester, Amsterdam: North-Holland Pub. Co.; New York: Interscience Publishers, Inc., 1963, pp. 447-462. Inc., 1963, pp. 447-462.

10. Freden, S. C., and Paulikas, G. A., "Precipitation of Energetic Electrons into the Atmosphere," *J. Geophys. Res.* 69(7):1239-1249, April 1, 1964.

11. Mihalov, J. D., Mozer, F. S., and White, R. S., "Artificially Injected Electrons at Low Altitudes," *J. Geophys. Res.* 69(19):4003-4013, October 1, 1964.

12. MacDonald, W. M., and Walt, M., "Diffusion of Electrons in the Van Allen Radiation Belt. Pt. 2, Particles with Mirroring Points at Low Altitudes," *J. Geophys. Res.* 67(13):5025-5033, December 1962.

13. Welch, J. A., Jr., Kaufmann, L., and Hess, W. N., "Trapped Electron Time Histories for L = 1.18 to L = 1.30," *J. Geophys. Res.* 68(3):685-700, February 1, 1963.

14. Ghielmetti, H. S., Becerra, N., Godel, A. M., Heredia, H., and Roederer, J. G., "Enhancement of the X-Ray Intensity at Balloon Altitudes in the South American Anomaly," *Phys. Rev. Letters*, 12(14):388-390, April 6, 1964.

15. De Mendonça, F., "Ionospheric Electron Content Measurements in Regions of Low Magnetic Dip Angles and Through the Brazilian Magnetic Anomaly," in: *Space Research V; Proc. 5th Internat. Space Sci. Sympos., Florence, May 12-16, 1964*, ed. by D. G. King-Hele, P. Muller, and G. Righini, Amsterdam: North-Holland Pub. Co.; New York: Interscience Publishers, 1965, pp. 687-701.

16. Greenspan, J. A., and Stone, C. A., "The Longitudinal Variation of Night Airglow Intensity in the Region of the South Magnetic Anomaly," *J. Geophys. Res.* 69(3):465-469, February 1, 1964.

17. Stone, E. C., "The Physical Significance and Application of L, $B_0$, and $R_0$ to Geomagnetically Trapped Particles," *J. Geophys. Res.* 68(14):4157-4166, July 15, 1963.

18. Croom, S., Robbins, A., and Thomas, J. O., "Two Anomalies in the Behavior of the $F_2$ Layer of the Ionosphere," *Nature*, 184(4704):2003-2004, December 26, 1959.

19. Lyon, A. J., and Thomas, L., "The $F_2$-Region Equatorial Anomaly in the African, American and East Asian Sectors during Sunspot Maximum," *J. Atoms. Terr. Phys.* 25(7):373-386, July 1963.

20. Rao, C. S. R., and Malthora, P. L., "A Study of Geomagnetic Anomaly during IGY," *J. Atmos. Terr. Phys.* 26(11):1075-1085, November 1964.

21. Bramley, E. N., and Peart, M., "Diffusion and Electromagnetic Drift in the Equatorial $F_2$ Region," *J. Geophys. Res.* 69(21):4609-4616, November 1, 1964.

22. Goldberg, R. A., "The Effect of a Variable Electron Temperature on the Equatorial Electron Density Distribution in the Upper Ionosphere," *J. Geophys. Res.* 70(3):655-665, February 1, 1965.

23. Sato, T., and Rourke, G. F., "F-Region Enhancements in the Antarctic," *J. Geophys. Res.* 69(21):4591-4607, November 1, 1964.

24. Rastogi, R. G., "Abnormal Features of the $F_2$ Region of the Ionosphere at Some Southern High Latitude Stations," *J. Geophys. Res.* 65(2):585-592, February 1960.

25. King, J. W., Eccles, D., Legg, A. J., Smith, P. A., Galindo, P. A., Kaiser, B. A., Preece, D. M., and Rice, K. C., "An Explanation of Various Ionospheric and Atmospheric Phenomena including the Anomalous Behaviour of the F-Region," Gr. Britain Dept. of Sci. Indus. Res., Radio Research Station, Report Number RRS/IM-191, December 1964.

26. Duncan, R. A., "Universal-Time Control of the Arctic and Antarctic F Region," *J. Geophys. Res.* 67(5):1823-1830, May 1962.

27. Hill, G. E., "Anomalous $f_0F2$ Variations in the Antarctic," *J. Geophys. Res.* 65(7):2011-2023, July 1960.

28. Axford, W. I., "The Formation and Vertical Movement of Dense Ionized Layers in the Ionosphere due to Neutral Wind Shears," *J. Geophys. Res.* 68(3):769-779, February 1, 1963.

29. King, J. W., "Investigations of the Upper Ionosphere Deduced from Topside Sounder Data," *Nature,* 197(4868):639-641, February 16, 1963.

# THE GENERAL FOKKER–PLANCK EQUATION FOR TRAPPED ELECTRON DIFFUSION

by
J. G. Roederer*
*Goddard Space Flight Center*
and
J. A. Welch†
*Air Force Systems Command*

SUMMARY

A general Fokker-Planck equation is deduced which describes the distribution of geomagnetically trapped electrons as a function of longitude, time, energy, and mirror point field intensity. A special variable for the longitudinal position of a particle is introduced.

The physical interpretation of this equation is analyzed for several special cases. In particular, it is found that the usual procedure of averaging over longitude in order to obtain a longitude-independent equation is not valid for the description of electrons mirroring at low altitudes. In that case, the longitude dependence cannot be averaged out and a four-dimensional equation must be used.

The coefficients representing longitudinal drift, ionization loss, and multiple, screened Coulomb scattering in the general Fokker-Planck equation are deduced. An approximation is given for a simple model of the field and the atmosphere in the South American Anomaly. Qualitative conclusions are drawn for the mirror point "flow" along lines of force, for a stationary electron distribution drifting through the Anomaly. It is concluded that the region east of the Anomaly, initially depleted by precipitation, is replenished by electrons whose mirror points were situated in a narrow "window" in B, before passing through the Anomaly. A very limited extension of the atmosphere in the region of the Anomaly is responsible for this mechanism of replenishment. A diurnal effect for the electron fluxes in the replenished region controlled by the diurnal variation of the atmosphere in the Anomaly is predicted.

## INTRODUCTION

The time has come to look with more detail into the latitude dependence of geomagnetically trapped particle fluxes from the theoretical point of view. Until recently, experimental information

*National Academy of Sciences–National Research Council, Senior Post Doctoral Research Associate, on leave from Facultad de Ciencias Exactas y Naturales and Centro Nacional de Radiacion Cosmica, Buenos Aires, Argentina.
†Major, United States Air Force.

on this subject was very scarce. It was only after the discovery of the so-called South American Anomaly (Reference 1) and the more detailed surveys with Discoverer satellites by Mann, Bloom, and West (Reference 2), that attention became increasingly focused on the experimental analysis of particle precipitation in the Anomaly and the mechanism of subsequent replenishment of the depleted shell regions. In particular, Imhof and Smith (Reference 3) Paulikas and Freden (Reference 4), and Mihalov, Mozer, and White (Reference 5) have made a careful study of artificially injected electron fluxes measured by various satellites. On the other hand, Freden and Paulikas (Reference 6) and White (Reference 7) have analyzed proton fluxes at low altitudes in the Anomaly and evidence for Bremsstrahlung X-rays from electrons precipitating into the Anomaly was recently found by Ghielmetti, Becerra, Godel, Heredia and Roederer (Reference 8). It is therefore desirable to set up a theoretical description of the longitudinal behavior of trapped particles and to test by comparison with experimental data, the various assumptions made about interaction processes governing particle diffusion.

Theoretical description of electron trapping, diffusion, and precipitation was so far done only for configurations averaged over all longitudes (References 9-13). In these papers, a time-dependent Fokker-Planck equation was set up for the electron distribution function and used to follow the evolution in time of a given, initial electron flux.

In order to study the longitude dependence of the electron distribution on a given magnetic shell, it is necessary to derive a more general diffusion equation which contains an additional variable related to longitude. In this equation the coefficients, which depend upon the atmosphere, will be a function of longitude and local time of day in the Anomaly. One important by-product of the equation derivation will be the identification of an appropriate variable by which to describe the longitudinal dependence. We will call this variable X. It will be used together with the particle energy E, the scalar magnetic field B at the mirror point, and the well-known McIlwain shell parameter L (Reference 14), to describe the space in which particle densities change with time, t.

The main purpose of this paper is to set up such a general equation, to discuss its physical meaning, to compare it with the previously used longitude-averaged equation, and to draw some general, qualitative conclusions about longitude dependence of trapped electrons. Subsequent publications will deal with atmosphere-field configurations to be used in this longitude-dependent description and the results of a numerical integration of the general equation.

Before setting up our equation, let us picture the problem in general terms. Consider the familiar B-L space in which trapped radiation fluxes are usually described (Figure 1). It can be shown that electrons whose mirror points are below 100 kilometers cannot remain trapped for more than a few bounces. Thus, it is qualitatively useful to consider the 100-kilometer level as the location of a sink. We shall return to this point in more detail later. At a given longitude the 100 kilometer level can be displayed as a locus, $B_c$ (L, X), in B-L space. Essentially no electrons will be found with mirror points above this curve, that is, for mirror point fields larger than $B_c$ (L, X). We have plotted two extreme loci of the 100 kilometer level, corresponding to a longitude (that is, a value of X) right in the "center" of the South American Anomaly and a longitude over the Pacific Ocean, respectively. From Figure 1, one can see that for particles of a given energy, the

100 kilometer curve, $B_c$ (L, X), "oscillates" with longitudinal drift frequency between these two extreme positions. As $B_c$ (L, X) lowers from its maximum or "Pacific", position, the region in B-L space between the two extreme positions, called the "shadow region" is wiped clean of particles. As $B_c$ (L, X) rises from its minimum, or "Anomaly", position, the opportunity exists for atmospheric scattering, or any other non-adiabatic process, to repopulate this shadow region. This wiping clean and repopulation has been likened to the action of a windshield wiper.

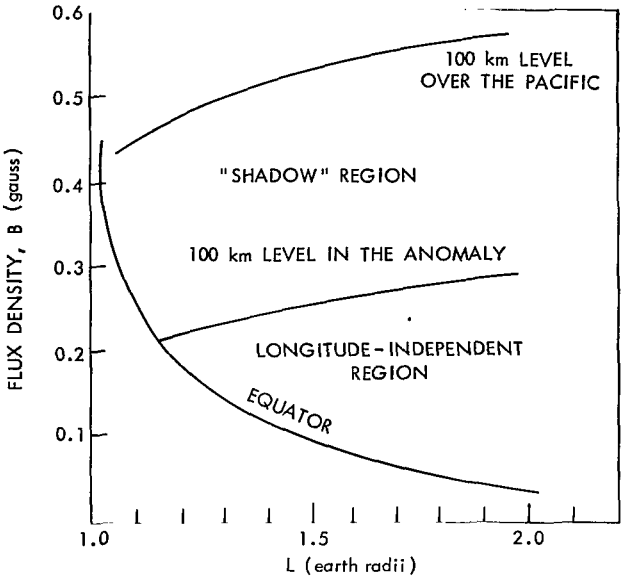


Figure 1—The "windshield wiper" effect in B-L space.

Satellite observations do, in fact, find particles in the shadow region (Reference 3). This observation means that particles have enough nonadiabatic interaction during one drift around the earth to diffuse into the wiped-out or "shadow" region. Our main goal is to study this process of fast replenishment of the shadow region in the case of electrons interacting with the atmosphere by Coulomb scattering and energy loss.

## REPRESENTATION OF THE ELECTRON DISTRIBUTION AS A FUNCTION OF LONGITUDE

We shall describe the trapped electrons by the distribution function used by Welch, Kaufmann and Hess (Reference 10). For a given L-shell, we denote by

$$\delta N = U(B, E, \phi, t)\, \delta\phi\, \delta B\, \delta E \tag{1}$$

the number of electrons contained at the time t in a tube of field lines of magnetic flux $\delta\phi$ situated at a longitude $\phi$ (for the time being, we shall use the geographic longitude of the magnetic equatorial point), with mirror points between B and $B + \delta B$, and with kinetic energies between E and $E + \delta E$. We shall neglect L-scattering; this is why we do not include explicitly L as a variable in U.

The distribution U is not directly measurable. It is, however, the physical magnitude which most appropriately describes trapped particles. Relations with experimentally accessible quantities are given in Reference 10. In particular, the number $\delta n$ of particles contained in the volume element $\delta A\, \delta s$ of a tube at a point where the field is B′ and which mirror in the interval dB at $B > B'$ (Figure 2), is given by

$$\delta n = U(B, E, \phi, t)\, dB\, \delta E\, B\, \delta A \overline{\frac{\delta s}{v_{||}(B', B, E)}}\, \tau_b(B, \overline{E, \phi}) \quad . \tag{2}$$

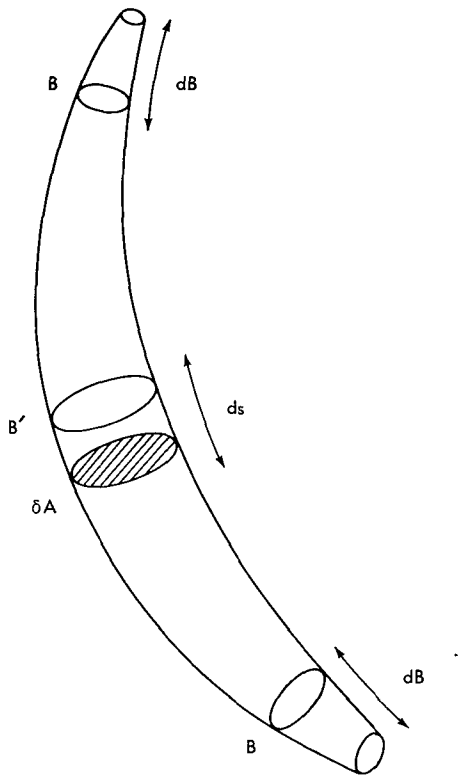


Figure 2—Volume element of $\delta A\,\delta s$ of a tube at a point where the field is B′.

The ratio in Equation 2 represents the probability of finding a particle of the population of Equation 1 in the volume element $\delta A\,\delta s$. $\tau_b\,(B, E, \phi)$ is the half-period of bouncing of these particles, i.e., the time it takes to go from one mirror point to its conjugate. In the real geomagnetic field, it depends slightly on longitude. $v_{||}\,(B', B, E) = v(E)\sqrt{1 - B'/B}$ is the particle's velocity parallel to the field line, at the point B′. For a dipole field, the total path of a particle during a bounce period is $v\tau_b \approx 2LR$ (R = radius of earth). The total particle density per unit energy at a given point B′ is therefore

$$n(B', E, \phi, t) = \frac{\delta n}{\delta A\,\delta s\,\delta E}$$

$$= \frac{B'}{v(E)} \int_{B'}^{B_c} \frac{U(B, E, \phi, t)\,dB}{\tau_b\,(B, E, \phi)\sqrt{1 - B'/B}} \approx \frac{B'}{2RL} \int_{B'}^{B_c} \frac{U dB}{\sqrt{1 - B'/B}} \quad . \quad (3)$$

The integration is performed along the field line between the B value at the given point, and some upper cut-off, $B_c$, beyond which all particles are absorbed in the atmosphere. The density (Equation 3) is related to the omnidirectional counting rate C of a spherical detector by

$$C = \int_{E_0}^{\infty} vn\,A\,dE \quad , \quad (4)$$

where A(E) is the effective cross sectional area of the counter for particles of energy E.

Let us now consider electrons of a given energy, mirroring at the same B, trapped between two neighboring shells labeled I and $I + \delta I$ (Figure 3). I is the second adiabatic invariant (Reference 14) of these particles computed for field lines belonging to the inner shell.

$$I = \int_{-s(B)}^{s(B)} \frac{v_{||}}{v}\,ds = \int_{-s(B)}^{s(B)} \sqrt{1 - \frac{B(s)}{B}}\,ds$$

$I + \delta I$ is the value of the second invariant, taken along a line of force belonging to the outer shell, between mirror points with the *same* field intensity B. $B_0$ is the field at the equatorial point of a line of force (point of minimum B on a given shell); $\phi$ is the geographic longitude of this equatorial point. We call $\vec{\nabla}_0 I = \vec{n}\,\delta I/\delta y$ the gradient of I at the equatorial point of a magnetic shell (Figures 3 and 4). Northrop and Teller (Reference 15) have shown that the equatorial drift velocity,

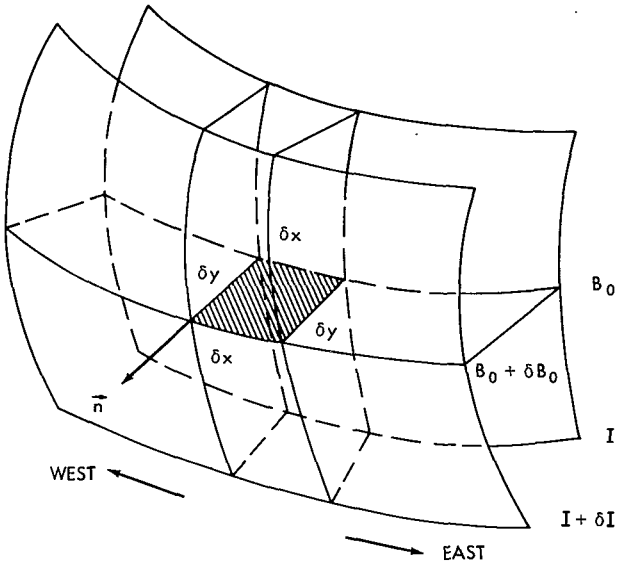


Figure 3—Shell geometry and elementary flux tube.

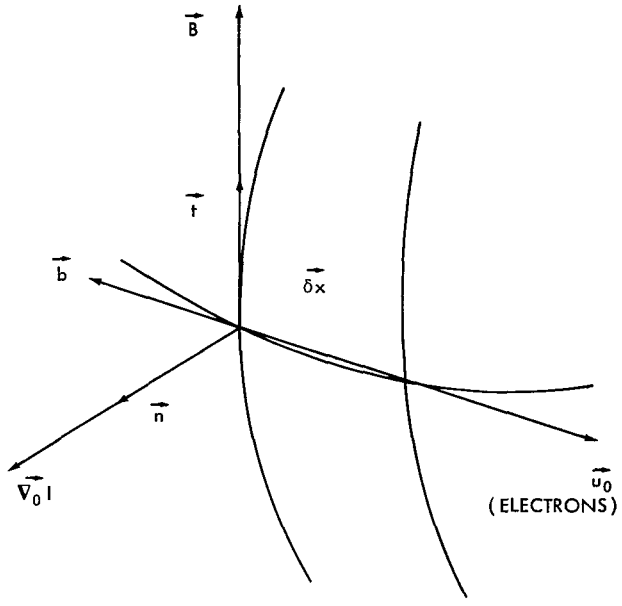


Figure 4—Unit vectors, mean equatorial drift velocity, and gradient of I.

averaged over one bounce, is given by

$$\vec{u}_0 = \frac{mv}{eB_0^2 \tau_b} \vec{\nabla}_0 I \times \vec{B} = \frac{p}{eB_0} \frac{\vec{\nabla}_0 I}{\tau_b} \vec{b} \tag{5}$$

where p is the particle's momentum, e the charge (<0 for electrons) and $\tau_b$ is the half-period of bouncing. For the different vectors, see Figure 4.

We denote with $\delta\vec{x} = u_0 \delta\vec{t}$ the distance between equatorial points of two neighboring field lines of a given shell; $\delta\vec{x}$ is then the element of arc of the shell's equatorial $B_0$-ring; $\vec{x} = \int d\vec{x}$ is the total arc length along the equator from a given initial point and can be used as a label to locate field lines on a given shell. Evidently

$$\delta\vec{x} = \frac{\partial\vec{x}}{\partial\phi} \delta\phi \tag{6}$$

and

$$\vec{x} = \int_{\phi_0}^{\phi} \frac{\partial\vec{x}}{\partial\phi} d\phi \tag{7}$$

where $\partial\vec{x}/\partial\phi$ is a field-geometric factor ($\partial\vec{x}/\partial\phi = 2\pi/360$ RL for a centered dipole), and $\phi$, the geographic longitude of the equatorial point. Let us take a tube of lines of force of equatorial cross section $\delta\vec{x}\,\delta\vec{y}$ and magnetic flux $B_0\,\delta\vec{x}\,\delta\vec{y}$ (Figure 3). By the definition of U (Equation 1), the number

of electrons in this flux tube, which mirror between B and $B + \delta B$ and with kinetic energy between E and $E + \delta E$, is given by

$$\delta N = U B_0 \, \delta\vec{x} \, \delta\vec{y} \, \delta B \, \delta E \quad . \tag{8}$$

We now want to follow the history of these particles as a function of time. Before setting up the Boltzmann-type equation governing the distribution U, we have to introduce a convenient variable for the longitude, i.e., a convenient label for the line of force of a given magnetic shell around which a particle is instantaneously spiralling. We cannot take $\phi$ or x (Equation 7) as suitable variables because U is a distribution in *flux*, not in $\phi$ or x. And in the flux expression $B_0 \, \delta x \, \delta y$ intervening in Equation 8, not only $\delta x$, but *also* $\delta y$ is a function of longitude for the general geomagnetic field.

In order to find the correct longitudinal variable, we have to transform the flux into an expression $\delta\phi = B_0 \, \delta X \, \delta Y$, in which $\delta Y$—still related to the radial increment $\delta y$—is now longitude-independent, so that it may be ignored when following the particles during their longitudinal drift. In that case, X would be the correct longitudinal variable, its differential $\delta X$ containing complete information about the longitude dependence of the flux $\delta\phi$ of a tube filled with particles as they drift around the earth.

In order to find X and Y, we just have to determine the longitude dependence of $\delta y$, the equatorial distance between two neighboring magnetic shells. Notice that this dependence is a purely geometric one, independent of the particles' dynamic variables. Let us take McIlwain's definition of L (Reference 14), which we write here:

$$\frac{R^3 L^3 B}{M} = F\left(\frac{I^3 B}{M}\right) , \tag{9}$$

(R: radius of the earth, L, dimensionless, I, in centimeters). We further consider the relation,

$$B_0 = \frac{M}{R^3 L^3} , \tag{10}$$

only valid within about a few percent, because L actually fluctuates along a line of force (References 14 and 16). Combining Equations 9 and 10, and differentiating, we have

$$\frac{\delta B_0}{B_0} = -\frac{3I^2}{R^3 L^3} F' \, \delta I \tag{11}$$

for a constant mirror field, B. F′ is the derivative of McIlwain's function with respect to its argument. Dividing by $\delta y$, we obtain, for absolute values

$$\frac{\delta I}{\delta\vec{y}} = \frac{\frac{1}{B_0}\frac{\delta B_0}{\delta\vec{y}}}{3/RL} \frac{R^2 L^2}{I^2 F'} \quad . \tag{12}$$

Notice that $1/B_0\ \delta B_0/\delta y \to 1/B_0 \nabla_0 B$ as $\delta y \to 0$, where $\nabla_0 B$ is the gradient of $|B|$ taken at the equatorial point. For a current-free magnetic field, $1/B_0 \nabla_\perp B$ is equal to the curvature of the line of force at the point where the normal gradient is taken; in our case, $1/B_0 \nabla_0 B$ is therefore the curvature at the equatorial point. We shall introduce the dimensionless number

$$\kappa_0 = \frac{\frac{1}{B_0} \nabla_0 B}{3/RL} , \tag{13}$$

which is the curvature of a line of force at the equatorial point in units of the equatorial curvature, $3/RL$ of the corresponding dipole line ($\kappa_0 = 1$ for all dipole shells). In the general case, $\kappa_0$ depends on longitude. From Equations 12 and 13, we finally have:

$$\frac{\delta I}{\delta \vec{y}} = \vec{\nabla}_0 I = \frac{\kappa_0}{\lambda(B)} , \tag{14}$$

where

$$\lambda(B) = \frac{I^2 F'}{R^2 L^2} \tag{15}$$

is a dimensionless function of the mirror point field intensity B. Notice that according to Equations 5 and 14, we have

$$u_0 = \frac{p}{eB_0} \frac{\kappa_0}{\tau_b \lambda} \tag{16}$$

and for the angular drift velocity, taking into account Equation 6,

$$\dot{\phi} = \frac{1}{\frac{\partial \vec{x}}{\partial \phi}} u_0 = \frac{1}{\frac{\partial \vec{x}}{\partial \phi}} \frac{p}{eB_0} \frac{\kappa_0}{\tau_b \lambda} . \tag{17}$$

It is important to point out that $\lambda(B)$ (Equation 15) is a "pure dipole function", even in the case of a slightly distorted dipole as the real geomagnetic field (this is not true for $\tau_b$). It is easy to verify that our function $\lambda$ is identical with $1/6E$, where E is the function calculated by Hamlin, Karplus, Vik, and Watson (formula 22 in Reference 17). All this of course is valid only within a few percent (fluctuation of L on a magnetic shell). Notice finally that $\kappa_0$ contributes to the longitude dependence of the drift velocity. However, one must not forget that $\tau_b$ also depends on longitude in the real field. According to Equation 14,

$$\delta \vec{y} = \frac{\lambda \delta I}{\kappa_0} . \tag{18}$$

In this relation, the only longitude-dependent quantity is $\kappa_0$. We then introduce the variables Y and X in the following way:

$$\delta Y = \kappa_0 \delta \vec{y} = \lambda \delta I \quad \therefore \quad Y = \lambda I \tag{19a}$$

$$\delta X = \frac{\delta \vec{x}}{\kappa_0} \quad \therefore \quad X = \int \frac{d\vec{x}}{\kappa_0} = \int \frac{1}{\kappa_0} \frac{\partial \vec{x}}{\partial \phi} \, d\phi \quad . \tag{19b}$$

X increases from west to east. Notice that labeling field lines by the coordinate X is equivalent to picking up lines of a shell with a density (number per unit equatorial ring arc length) inversely proportional to the curvature $\kappa_0$ (Equation 13). For a pure dipole field, or for the outer shells in the real field, $\kappa_0 = 1$, and X is identical with x (Equation 7). For low L-shells, $\kappa_0$ may differ from 1 as much as ±6%. With the new coordinates (Equations 19a and 19b), the flux $\delta\phi$ is

$$\delta\phi = B_0 \, \delta \vec{x} \, \delta \vec{y} = B_0 \, \delta X \, \delta Y$$

in which $\delta Y$ is now independent of longitude. Adopting X (Equation 19b) as the appropriate longitudinal variable, we can write the number of electrons in a flux tube as

$$\delta N = U(B, E, X, t) \, \delta B \, \delta E \, \delta X \cdot B_0 \, \delta Y \quad . \tag{20}$$

As $B_0 \, \delta Y$ is a constant throughout the whole forthcoming discussion, we shall drop it at once whenever we consider the number of particles in a flux tube.

Finally, it is important to remark that there is a more exact expression for the fundamental relation (Equation 14), which takes into account the fact that in the real geomagnetic field, L differs from $1/R(M/B_0)^{1/3}$ (Equation 10) by a small, longitude-dependent amount, $\Delta L = \Delta L(L, B, \phi)$ (Reference 16). This relation is given by

$$\frac{\delta I}{\delta \vec{y}} = \nabla_0 I = \frac{1}{\lambda(B)} \left[ \kappa_0 - RL \frac{\partial}{\partial \vec{y}} \left( \frac{\Delta L}{L} \right) \right] \quad .$$

However, the correction term $RL \, \partial/\partial y(\Delta L/L)$ is expected to be small as compared with $\kappa_0$, and the longitude variations of $\kappa_0$. On the other hand, the correction term implies the existence of a shell splitting as a function of the mirror point field intensity (Reference 16). But in the whole treatment which follows, this splitting is being neglected and all electrons, initially on a given line of force, are supposed to populate the same shell, regardless of their mirror points.

## DERIVATION OF THE FOKKER–PLANCK EQUATION FOR LONGITUDE DEPENDENCE

We are now in condition to set up the general equation governing the distribution of trapped electrons. These electrons will undergo displacements in B, E, and longitude, caused by three types of mutually independent interactions:

1. a change in the mirror point field B, due to the *stochastic* process of multiple Coulomb scattering in the atmosphere;

2. a change in kinetic energy, E, due to ionization slowing-down in the atmosphere, considered here as a *non*-stochastic process (i.e., neglecting straggling); and

3. a change in longitude due to interaction with the static magnetic field (longitudinal drift), again a *non*-stochastic process.

All these processes are physically independent of each other, although all intervening parameters are in general functions of the three variables B, E, and longitude.

Let us relate the distribution of electrons as it appears in Equation 20, with the distribution of electrons at a slightly earlier time, $t - \Delta t$, at a different longitudinal position. For the time being, we shall forget the non-stochastic character of E and X and treat all variables as if they were of the same stochastic nature. We write,

$$U(B, E, X, t) = \iiint U(B-\beta, E-\epsilon, X-\xi, t-\Delta t)\, \Pi(B-\beta, E-\epsilon, X-\xi, \beta, \epsilon, \xi, \Delta t)\, d\beta d\epsilon d\xi + Q(B, E, X, t)\, \Delta t. \quad (21)$$

In this relation, the distribution of electrons which at the time t are at a position X, is linked to the distribution of those electrons which at an earlier time, $t - \Delta t$, were at $X - \xi$ and which happened to scatter, slow down, and drift the right amount in the interval $\Delta t$ in order to become part of the population described by the left hand of Equation 21.

$\Pi\, d\beta\, d\epsilon\, d\xi$ is the *a priori* probability that these electrons have undergone just the right changes in mirror point field, energy, and longitudinal position, in the time interval $\Delta t$.

The source term $Q\Delta t$ represents the contribution of electrons added by injection to the original bunch of particles during $\Delta t$.

Expanding all intervening functions in Taylor series in $\beta$, $\epsilon$, $\xi$, and $\Delta t$, we obtain:

$$\frac{\partial U}{\partial t} + \frac{\partial}{\partial X}\left(U\langle\xi\rangle\right) = -\frac{\partial}{\partial E}\left(U\langle\epsilon\rangle\right) - \frac{\partial}{\partial B}\left(U\langle\beta\rangle\right) + \frac{1}{2}\frac{\partial^2}{\partial B^2}\left(U\langle\beta^2\rangle\right) +$$

$$Q + \text{higher order terms in } \xi^2,\ \epsilon^2,\ \epsilon\beta, \text{ etc.} \quad (22)$$

The brackets stand for the *average per unit time* of the enclosed variables,

$$\langle A\rangle = \frac{1}{\Delta t}\iiint A\, \Pi\, d\beta\, d\epsilon\, d\xi\ .$$

We can now reinstate the non-stochastic character to E and X by taking $\Pi$ as a delta function in energy and longitude,

$$\Pi(B, E, X, \beta, \epsilon, \xi, \Delta t) = \Pi_0 (B, E, X, \beta, \Delta T)\, \delta(\epsilon + \dot{\epsilon}\Delta t)\, \delta(\xi - \dot{\xi}\Delta t) \quad .$$

In this expression, $\dot{\epsilon}$ is the change of energy per unit time due to ionization loss. Evidently

$$\dot{\epsilon} = \frac{1}{\tau_b} \{\epsilon\} \tag{23}$$

where $\{\epsilon\}$ is the energy loss in one half-bounce (path from one mirror point to its conjugate). We have taken $\{\epsilon\}$ and $\dot{\epsilon}$ as positive quantities and evidenced the energy *decrease* by the sign in the first delta function.

As to $\dot{\xi}$, the drift velocity in the X-coordinate, we have, according to Equations 19b, 16 and 17:

$$\dot{\xi} = \dot{\xi}(B, E, X) = \frac{dX}{dt} = \frac{u_0}{\kappa_0} = \frac{1}{\kappa_0} \frac{\partial x}{\partial \phi} \dot{\phi} = \frac{p}{eB_0} \frac{1}{\tau_b \lambda} \quad . \tag{24}$$

$\Pi_0$ is the probability for a change in the mirror point field due to Coulomb scattering in the interval $\Delta t$. It is evidently given by

$$\Pi_0 (B, E, X, \beta, \Delta t) = P(B, E, X, \beta) \frac{\Delta t}{\tau_b (B, E, X)} \quad , \tag{25}$$

where P is the probability for B-scattering during one half-bounce.

In all this we have implicitly assumed that scattering and slowing down are extremely small during one half-bounce of the electron. In other words, we suppose that $P << 1$ for $\beta \neq 0$ and approximately = 1 for $\beta = 0$ (this imposes a limiting condition on the applicability of our discussions when dealing with very high atmospheric densities).

Equation 22 finally becomes, up to the second order in $\beta$:

$$\frac{\partial U}{\partial t} + \frac{\partial}{\partial X} (U\dot{\xi}) = \frac{\partial}{\partial E} (U\dot{\epsilon}) - \frac{\partial}{\partial B} \left(U\langle\beta\rangle\right) + \frac{1}{2} \frac{\partial^2}{\partial B^2} \left(U\langle\beta^2\rangle\right) + Q \quad , \tag{26}$$

where

$$\langle\beta\rangle = \frac{1}{\tau_b} \{\beta\} \qquad \{\beta\} = \int \beta P \, d\beta$$

with

$$\langle\beta^2\rangle = \frac{1}{\tau_b} \{\beta^2\} \qquad \{\beta^2\} = \int \beta^2 P \, d\beta \quad . \tag{27}$$

The angular brackets $\langle\ \rangle$ are average changes *per unit time*; the curled brackets $\{\ \}$ represent average changes *per half-bounce.*

We can rewrite the longitude-convection term as a function of ordinary geographic longitude, taking into account Equation 24,

$$\frac{\partial}{\partial X}\left(U\dot{\xi}\right) = \frac{1}{\frac{1}{\kappa_0}\frac{\partial x}{\partial \phi}}\frac{\partial}{\partial \phi}\left(U\frac{1}{\kappa_0}\frac{\partial x}{\partial \phi}\dot{\phi}\right) = \frac{\kappa_0}{\frac{\partial x}{\partial \phi}}\frac{p}{eB_0\lambda}\frac{\partial}{\partial \phi}\left(\frac{1}{\tau_b}U\right) . \tag{28}$$

Notice that in a pure, centered dipole, $\kappa_0 = 1$, $\partial x/\partial\phi$ and $\dot{\phi}$ constants and the convection term would reduce to $\dot{\phi}\,\partial U/\partial\phi$.

Equation 26 is the most general Fokker-Planck equation describing the longitude and time dependence of a trapped-particle flux which scatters and slows down in the atmosphere.

The initial condition for Equation 26 is the distribution U given at a certain longitude for a given initial time. There is a "natural" boundary condition at the magnetic equator,

$$\frac{\partial U}{\partial B} = 0 \text{ for } B = B_0 . \tag{29}$$

At the ends of lines of force in the high atmospheric density region, *there is no physical boundary condition* for U as a function of B; as particles enter higher densities, they get slowed down by ionization and *die away in energy space*. Therefore, it would be incorrect to impose a condition of the type $U = 0$ for $B \geq B_0$. Moreover, Equation 26 is not valid at all near such a fictious boundary (for derivatives and integrals could not be interchanged any more when passing from Equation 21 to Equation 22). Of course, if one is only interested in electron fluxes in B-regions which always remain high up, i.e., far away from high atmospheric densities, a boundary condition for U as a function of B may well be adopted for practical computational reasons.

## DISCUSSION OF THE GENERAL EQUATION

Let us now discuss Equation 26 from the point of view of its physical meaning. First of all, in absence of scattering, slowing down and sources, the right hand of Equation 26 is zero. We then have,

$$\frac{\partial U}{\partial t} + \frac{\partial}{\partial X}\left(U\dot{\xi}\right) = 0 . \tag{30}$$

This equation tells us that a given initial distribution of electrons injected at a time $t_0$ at a line labeled $X_0$, will proceed drifting eastwards with speed $\dot{\xi}$, always keeping the electron distribution inversely proportional to the *local* drift speed $\dot{\xi}$,

$$U\dot{\xi} = \text{constant}. \tag{31}$$

As $\dot{\xi}$ is energy-dependent, Equation 30 represents a "flight-time spectrometer effect" on the particles after injection. Notice carefully that expression 31 means constancy along the drift path of a given bunch of particles. It is *not* a constancy in time.

If we now integrate Equation 26 over one complete longitudinal cycle of X, for a *fixed* time t, the second term on the left vanishes. We obtain

$$\frac{\partial}{\partial t}\oint U\,dX = \frac{\partial}{\partial E}\oint U\dot{\epsilon}\,dX - \frac{\partial}{\partial B}\oint U\langle\beta\rangle\,dX + \frac{1}{2}\frac{\partial^2}{\partial B^2}\oint U\langle\beta^2\rangle\,dX + \bar{Q} \quad . \tag{32}$$

Dividing by $\oint dX$ and calling

$$U_{AV} = \frac{\oint U\,dX}{\oint dX} = \frac{\oint U\frac{dx}{\kappa_0}}{\oint \frac{dx}{\kappa_0}} \tag{33a}$$

$$\dot{\epsilon}_{AV} = \frac{\oint \dot{\epsilon}\,U\,dX}{\oint U\,dX} \tag{33b}$$

$$\left.\begin{aligned} \langle\beta\rangle_{AV} &= \frac{\oint \langle\beta\rangle U\,dX}{\oint U\,dX} \\ \langle\beta^2\rangle_{AV} &= \frac{\oint \langle\beta^2\rangle U\,dX}{\oint U\,dX} \end{aligned}\right\} \tag{33c}$$

we obtain the longitude-independent equation

$$\frac{\partial U_{AV}}{\partial t} = \frac{\partial}{\partial E}\left(U_{AV}\,\dot{\epsilon}_{AV}\right) - \frac{\partial}{\partial B}\left(U_{AV}\langle\beta\rangle_{AV}\right) + \frac{1}{2}\frac{\partial^2}{\partial B^2}\left(U_{AV}\langle\beta^2\rangle_{AV}\right) + \bar{Q} \quad . \tag{34}$$

This equation is formally equivalent to the time-dependent equation used by several authors (References 9-13). Notice, however, the following remarks:

1. The average distribution $U_{AV}$ is computed integrating over the new variable X, which according to Equation 33a, means that *U must be weighted at the different longitudes with the inverse of the equatorial curvature* of the field lines.

2. The "coefficients" $\dot{\epsilon}_{AV}$, $\langle\beta\rangle_{AB}$ and $\langle\beta^2\rangle_{AV}$ are not simple averages over the new coordinate, but *are weighted with the distribution U itself.* In other words, they are functionals of the unknown distribution.

All this leads us to the conclusion that *a longitude-average Fokker-Planck treatment of the problem of trapped particle diffusion is not valid* unless we restrict our description to only those particles which mirror high enough at all longitudes so that their distribution function can be expected *a priori* as very little longitude-dependent. Equation 34 is certainly meaningless as a simple differential equation for that portion of B-L space which descends below about 300 - 350 kilometers in the South American Anomaly. This is precisely the domain where the longitude-independent treatment has so far failed to give numerical results compatible with experimental measurements.

In order to "legalize" the longitude-independent description for such cases in which we know *a priori* that U will not depend strongly on X, we have to evaluate the coefficients in Equation 33 for a distribution U which has the *smallest possible longitude dependence.* This dependence is given precisely by Equation 31, i.e., for the case of *absence of interactions* with the atmosphere. Introducing Equation 31 in Equation 33, and taking into account Equation 24, we obtain "true" coefficients (independent of U):

$$\dot{\epsilon}_{AV} = \frac{\oint \dot{\epsilon}\,\frac{dX}{\dot{\xi}}}{\oint \frac{dX}{\dot{\xi}}} = \frac{\oint \dot{\epsilon}\,\frac{d\vec{x}}{u_0}}{\oint \frac{d\vec{x}}{u_0}}$$

$$\langle\beta\rangle_{AV} = \frac{\oint \langle\beta\rangle \frac{d\vec{x}}{u_0}}{\oint \frac{d\vec{x}}{u_0}} \qquad \langle\beta^2\rangle_{AV} = \frac{\oint \langle\beta^2\rangle \frac{d\vec{x}}{u_0}}{\oint \frac{d\vec{x}}{u_0}} \tag{35}$$

These expressions are formally identical with the longitude-average coefficients used by Hassitt (Reference 18), in which the atmospheric constituents (the only strongly longitude-dependent variables actually contained in $\dot{\epsilon}$, $\langle\beta\rangle$ and $\langle\beta^2\rangle$ are weighted inversely proportional to the equatorial drift velocity at each longitude.

We must, however, insist again that the use of a longitude-independent Fokker-Planck equation for the description of trapped electron diffusion is not valid at all for those high B values for which the atmospheric interactions in the region of the Anomaly will introduce a notable departure of U from the "collisionless" expression 31.

Let us now return to Equation 26, for the steady state case $\partial U/\partial t = 0$. This is very nearly true for natural radiation belt electrons during quiet solar wind conditions, and even for artificially injected fluxes, provided we are interested in the longitude dependence of the electron distribution at times after injection long compared to a typical longitudinal drift period. In that case, we can also neglect the contribution of the natural source term Q. Taking into account Equations 23, 24, and 27, we introduce the distribution function

$$W = U\dot{\xi} = U \frac{p}{eB_0} \frac{1}{\tau_b \lambda} \tag{36}$$

and the coefficients

$$\overline{\dot{\epsilon}} = \frac{1}{\dot{\xi}} \dot{\epsilon} = \lambda \frac{eB_0}{p} \{\epsilon\}$$

$$\overline{\beta} = \frac{1}{\dot{\xi}} \langle\beta\rangle = \lambda \frac{eB_0}{p} \{\beta\}$$

$$\overline{\beta^2} = \frac{1}{\dot{\xi}} \langle\beta^2\rangle = \lambda \frac{eB_0}{p} \{\beta^2\} \tag{37}$$

which now represent changes *per unit longitudinal coordinate* X. Notice that the factor

$$\lambda \frac{eB_0}{p} = \frac{1}{\tau_b \dot{\xi}} = b(B, E) \tag{38}$$

physically represents the "bounce-density," i.e. the number of half-bounces per unit longitudinal coordinate which a particle of mirror point field B and energy E makes at any position on the shell. Notice that this bounce density is independent of the longitudinal position X.

Using Equations 36 and 37, the steady state form of Equation 26 reads:

$$\frac{\partial W}{\partial X} = \frac{\partial}{\partial B} (W\overline{\beta}) + \frac{1}{2} \frac{\partial^2}{\partial B^2} (W\overline{\beta^2}) + \frac{\partial}{\partial E} (W\overline{\dot{\epsilon}}) \quad . \tag{39}$$

This is the fundamental equation which describes the longitude dependence of a stationary, source-free electron distribution, now represented by W (Equation 36). It will be the main subject for the rest of this work.

A useful concept for a qualitative analysis of Equation 39 is that of the "mirror point flow in B-X space," i.e., the mean change of the mirror point field intensity of a particle, *per unit longitudinal coordinate.* Let us consider the following relation,

$$\int_{B_0}^{B(X)} W\,dB = \text{constant}, \qquad (40)$$

where the integral is taken along a given field line between the equatorial point $B_0$ and a generic field point $B(X)$. We shall call the relation $B = B(X)$, which ensures the constancy of (Equation 40), the "characteristic trajectory of a mirror point" (see Figure 5). Notice carefully that, in general, $B = B(X)$ is *not* the real path of the mirror point of a *given* electron in B-X space. However, it does become the actual *average* path, if we neglect energy loss and also neglect the longitude dependence of $\tau_b$. In that case, Equation 40 is proportional to the number of particles mirroring between the equator and $B(X)$. But even if these conditions are not satisfied, the function $B = B(X)$ defined in Equation 40 is a useful concept.

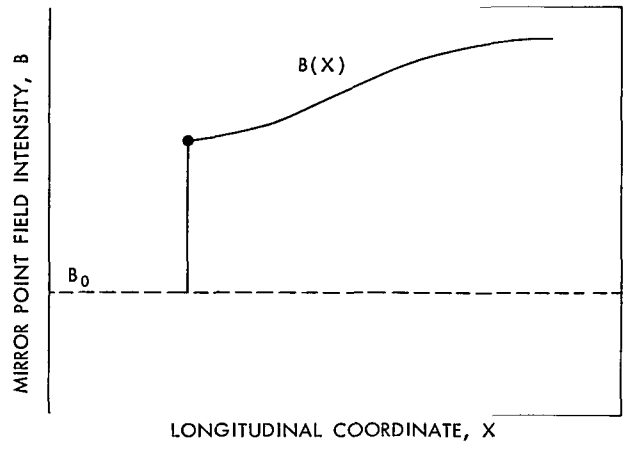


Figure 5—Characteristic trajectory of a mirror point.

In absence of all interactions, $B(X)$ = constancy, i.e., the mirror point field intensities remain unchanged. We now turn to Coulomb scattering, but still neglect energy loss. We then introduce the quantity $v_m = dB(X)/dX$ as the "mirror point flow in B-X space," obtaining, with the use of Equation 39 and 40,

$$v_m = \frac{dB(X)}{dX} = -\frac{1}{W}\int_{B_0}^{B(X)} \frac{\partial W}{\partial X}\,dB = \overline{\beta} - \frac{1}{2}\frac{\partial \overline{\beta^2}}{\partial B} - \frac{1}{2}\overline{\beta^2}\frac{\partial \ln W}{\partial B}. \qquad (41)$$

As defined in Equation 41, $v_m$ describes the average "flow" along the field lines of mirror points of electrons of a given energy as they drift in longitude. If we wish to add the energy loss mechanism, an additional term would appear in the right side of Equation 41 and particle individuality would be lost.

Notice that there are three physically quite distinct contributions to the mirror point flow. The *first* term of the right-hand of Equation 41 represents a steady increase of B, ($\beta$ is positive), i.e., a steady *lowering* of mirror point altitude. This contribution comes from the first-order "streaming" term in B (Equation 39). In absence of dispersion ($\overline{\beta^2} = 0$), $\overline{\beta}$ is the only contribution to $v_m$; in that case, $B = B(X) = \int v_m\,dX$ is just the characteristic of the corresponding first-order differential equation.

The second and third terms on the right-hand side of Equation 41 arise in the dispersion mechanism. Their presence in Equation 41 clearly shows that dispersion *also* contributes to a steady, average flow of mirror points along the lines of force. These two terms are governed by the gradients (along field lines) of the coefficient $\overline{\beta^2}$, and of W (or U), respectively. The gradient

of $\overline{\beta^2}$ is always positive, so that the *second* term in Equation 41 always represents an *upward motion* of the particle's mirror points (back-scattering from the denser atmosphere). If, on the other hand $\partial W/\partial B < 0$, the *third* term represents a *lowering* of the mirror point altitude. If $W\beta^2$ = constancy along a line of force, the contribution from the two dispersion terms is zero. The number of mirror points thrown upwards by the gradient in $\overline{\beta^2}$ exactly compensates the number of mirror points streaming downwards due to the gradient of W. The only mirror point flow which remains in this case is that of the first order term, $v_m = \overline{\beta}$.

## DETERMINATION OF THE COEFFICIENTS

In this section we shall obtain expressions for the various coefficients intervening in Equation 39. According to Equation 37, the principal quantities to be found are $\lambda$, $\{\epsilon\}$, $\{\beta\}$ and $\{\beta^2\}$.

With respect to the dimensionless function $\lambda$ defined in Equation 15, we recall that it is inversely proportional to a dipole-type function computed by Hamlin, Karplus, Vik and Watson (Reference 17). A good approximation of $\lambda$ for the interval $1/4 < B_0/B \leq 1$ is given by

$$\lambda(B) \cong 0.384 + 0.128 \exp\left(-\frac{1}{1.37}\frac{B}{B_0}\right) . \tag{42}$$

The energy loss per half-bounce $\{\epsilon\}$ is given by the integral

$$\{\epsilon\} = \int_{-s(B)}^{s(B)} \left|\frac{\partial E}{\partial s}\right| \frac{ds}{\sqrt{1 - \frac{B'(s)}{B}}} . \tag{43}$$

The origin of the field line arc length is taken at the geomagnetic equator. $ds/\sqrt{1 - B'(s)/B}$ is the element of trajectory of the electron at a point s where the field is B'. Using tables given by Berger and Seltzer (Reference 19), we obtain the following very good approximation,

$$\left|\frac{\partial E}{\partial s}\right| = 10^{-20} N_{eff.\,ion.}\, h(E)\ (\text{kev/cm}) ,$$

where

$$h(E) = \begin{cases} 2.61 + 349.0\, E^{-0.844} & \text{for } E < 470\,\text{kev} \\ 4.54 & \text{for } E \geq 470\,\text{kev} \end{cases} \tag{44}$$

and

$$N_{eff.\,ion.} = N_{oxygen} + 0.881\, N_{nitrogen} + 0.273\, N_{helium} \tag{45}$$

is the "effective" atmospheric number density for ionization loss of electrons. As for the time being we are interested in low L shells only, we did not include the contribution from atmospheric ions and electrons.

In order to evaluate $\{\beta\}$, the average change of B per half-bounce, we first have to perform the average of collisions over the isotropic azimuthal distribution of scattering angles. Following Welch, Kaufmann, and Hess (Reference 10) and slightly changing their notation, we obtain

$$\tilde{\beta} = B\left(\frac{B}{B'} - \frac{1}{2}\right) \sin^2\theta \quad . \tag{46}$$

$\tilde{\beta}$ is the change in mirror point field intensity B when the electron's pitch angle scatters an amount $\theta$ at a field position B', averaged over all possible azimuthal angles of scattering. Now we have to find the *average* of $\sin^2\theta$ at the given field point B'. This will be given by

$$\overline{\sin^2\theta} = \sum_i N_i \eta_i \quad , \tag{47}$$

where

$$\eta_i = \int_0^{\pi/2} \sin^2\theta \frac{d\sigma_i}{d\theta} \, d\theta \tag{48}$$

is the average contribution from one atom of class i. $N_i$ is the number densities of the different atmospheric constituents at the field point B'; $d\sigma_i/d\theta$ are the differential cross sections for screened Coulomb scattering for each constituent. Using Moliere's expression for $d\sigma_i/d\theta$, and following closely Welch, Kaufmann, and Hess (Reference 10), we obtain

$$\sum_i N_i \eta_i = 4 \times 10^{-22} N_{\text{eff. scatt.}} \frac{1 + 0.167 \ln \sqrt{\frac{E}{mc^2}\left(\frac{E}{mc^2} + 2\right)}}{\frac{E}{mc^2}\left(\frac{E}{mc^2} + 2\right)} \left(\text{cm}^{-1}\right) \quad , \tag{49}$$

where

$$N_{\text{eff. scatt.}} = N_{\text{oxygen}} + 0.774 N_{\text{nitrogen}} + 0.058 N_{\text{helium}} \tag{50}$$

is the effective atmospheric number density for screened Coulomb scattering of electrons. Again, the contribution of atmospheric ions and electrons is excluded.

We finally have to perform the integration along the path of a particle from one mirror point to its conjugate,

$$\{\beta\} = B \int_{-s(B)}^{s(B)} \left(\frac{B}{B'(s)} - \frac{1}{2}\right)\left(\sum_i N_i \eta_i\right) \frac{ds}{\sqrt{1 - \frac{B'(s)}{B}}} \quad . \tag{51}$$

Again following Welch, Kaufmann, and Hess (Reference 10), we obtain,

$$\tilde{\beta}^2 = 2B^2 \left(\frac{B}{B'} - 1\right) \sin^2\theta \quad . \tag{52}$$

Therefore:

$$\{\beta^2\} = 2B^2 \int_{-s(B)}^{s(B)} \left(\frac{B}{B'(s)} - 1\right)\left(\sum_i N_i \eta_i\right) \frac{ds}{\sqrt{1 - \frac{B'(s)}{B}}} \quad . \tag{53}$$

If we now call

$$S_1(B, X) = \int_{-s(B)}^{s(B)} \frac{B}{B'(s)} \frac{N_{\text{eff scatt}}(s, X)}{\sqrt{1 - B'(s)/B}} \, ds \; (\text{cm}^{-2})$$

$$S_2(B, X) = \int_{-s(B)}^{s(B)} \frac{N_{\text{eff scatt}}(s, X)}{\sqrt{1 - B'(s)/B}} \, ds \; (\text{cm}^{-2})$$

$$S_2'(B, X) = \int_{-s(B)}^{s(B)} \frac{N_{\text{eff ion}}(s, X)}{\sqrt{1 - B'(s)/B}} \, ds \; (\text{cm}^{-2}) \tag{54}$$

$$K(B, E) = 4 \times 10^{-22} B \frac{1 + 0.167 \ln \sqrt{\frac{E}{mc^2}\left(\frac{E}{mc^2} + 2\right)}}{\frac{E}{mc^2}\left(\frac{E}{mc^2} + 2\right)} \; (\text{gauss cm}^2)$$

$$C(E) = 10^{-20} h(E) \qquad \text{kev cm}^2 \quad ,$$

we can summarize expressions 51, 53 and 43 in the form

$$\{\beta\} = K\left(S_1 - \frac{1}{2} S_2\right)$$

$$\{\beta^2\} = 2BK(S_1 - S_2)$$

$$\{\epsilon\} = CS_2' \quad . \tag{55}$$

## DISCUSSION OF ELECTRON DRIFT AND SCATTERING THROUGH A MODEL FOR THE ANOMALY

Before setting up numerical integrations for low-altitude electrons, it is very helpful to discuss Equation 39 qualitatively, using a simple, approximate model of the atmosphere along field lines in the region of the South American Anomaly, where most of the scattering and energy loss occurs.

We shall restrict ourselves to the region between 250 and 750 km altitude, and to longitudes within about ±30 degrees of the center of the Anomaly (supposed at a longitude $\phi_a = 318°E$). In the present discussion we shall neglect the energy loss term and suppose $\partial x/\partial\phi$ = constancy and $\kappa_0 = 1$. These latter suppositions lead to a proportionality between X and the longitude $\phi$ of the equatorial point of a field line (Equation 19b).

Using the Harris-Priester atmosphere (Reference 20) for a low solar activity (S = 70), and Southern Hemisphere geomagnetic field B-L rings as calculated by Stassinopoulos,* we obtain a quite good fit for the effective number density (Equation 50) as a function of B and $\phi$, of the type

$$N_{eff\ scatt} = N_0 \exp\left(\frac{B - B_a}{\Delta B}\right) \exp\left(-\frac{|\phi - \phi_a|}{\Delta\phi}\right) \quad . \tag{56}$$

Due to the supposed proportionality between $\phi$ and X, it is easy to convert this expression into a function of X. All this is valid only for very low L values.

For $L = 1.25$, we have†

*13 hours* local time at the center of the Anomaly:

$$N_0 = 10^{11}\ cm^{-3}, \quad B_a = 0.243\ gauss, \quad \Delta B = 5.25 \times 10^{-3}\ gauss, \quad \Delta\phi = 4.69°$$

*Stassinopoulos, E., private communication.

†For higher L shells ($L \geq 1.8$), the approximation of Equation 56 becomes very crude. Qualitatively, as L increases, $\phi_a$ shifts to the east and $\Delta\phi$ increases considerably.

*02 hours* local time at the center:

$$N_0 = 10^{11}\ \text{cm}^{-3},\quad B_a = 0.243\ \text{gauss},\quad \Delta B = 4.23\times 10^{-3}\ \text{gauss},\quad \Delta\phi = 3.78^\circ .$$

For an expression of Equation 56, with a "scale height" $\Delta B$ very small compared to B, the main contribution to the integrals in Equation 54 comes from a region close to that mirror point which lies in the high atmospheric density end of the line of force. We can therefore approximate:

$$S_1 \cong S_2 \cong N_0 \exp\left(\frac{B - B_a}{\Delta B}\right) \exp\left(-\frac{|\phi - \phi_a|}{\Delta\phi}\right) \frac{\sqrt{\pi \frac{\Delta B}{B}}}{\frac{\partial B}{\partial s}} \tag{57}$$

and

$$S_1 - S_2 \cong S_1 \frac{\Delta B}{2B} \cdot \tag{58}$$

$\partial B/\partial s$ is the average gradient of B along the field line in the region of interest. Taking into account Equation 55, the following relation between the coefficients $\{\beta\}$ and $\{\beta^2\}$ holds

$$\{\beta^2\} = 2\Delta B\{\beta\} . \tag{59}$$

This is similar to a relation found by Walt and McDonald (Reference 12) for the coefficients of a time-dependent (but longitude-independent) Fokker-Planck equation set up in terms of mirror point altitudes, in the region of high atmospheric densities. Relation 59 is expected to hold quite generally in the region of high densities, provided one inserts for $\Delta B$ the value $\Delta B = N_{eff}/|\partial N_{eff}/\partial B|$ where the derivation is taken along a line of force.

With Equation 59 and the linear relationship between X and $\phi$, Equation 39 becomes

$$\frac{\partial W}{\partial X} = \frac{1}{\frac{\partial X}{\partial \phi}} \frac{\partial W}{\partial \phi} = -\frac{\partial}{\partial B}(W\bar{\beta}) + \Delta B \frac{\partial^2}{\partial B^2}(W\bar{\beta}) , \tag{60}$$

in which $\bar{\beta}$ is of the form

$$\bar{\beta} = K' \exp\left(\frac{B - B_a}{\Delta B}\right) \exp\left(-\frac{|\phi - \phi_a|}{\Delta\phi}\right) . \tag{61}$$

K′ is obtained from Equations 37, 54, 55 and 57, and is a slowly varying function of B (slow in comparison with $\exp(B/\Delta B)$.

The mirror point flow (Equation 41) is now

$$v_m = \overline{\beta} - \Delta B \frac{\partial \overline{\beta}}{\partial B} - \Delta B \overline{\beta} \frac{\partial \ln W}{\partial B} \quad .$$

Taking into account (Equation 61) we can approximate

$$\frac{\partial \overline{\beta}}{\partial B} \simeq \frac{\overline{\beta}}{\Delta B} \quad . \tag{62}$$

Therefore,

$$v_m \simeq - \Delta B \overline{\beta} \frac{\partial \ln W}{\partial B} \quad . \tag{63}$$

Physically, the cancellation of the first term with the second term in Equation 41 means that the *upstream* of mirror points due to diffusion from the denser atmosphere ("backscattering" at lower altitudes) exactly compensates the *downstream* due to the first order term. What is left is a mirror point streaming entirely due to diffusion and which may be upwards or downwards according to the gradient of the actual electron distribution along a line of force.

In particular, if $\partial U/\partial B = 0$ for some value $B_1$, there will be no net flow of mirror points across this B value. An initial distribution of electrons at a longitude $\phi_0$ like the one shown in Figure 6 will therefore keep the maximum at the same $B_1$ but will broaden towards both sides as the particles drift towards the east $(\phi_2 > \phi_1 > \phi_0)$ . This smearing-out will be faster at the high-B side (towards lower altitudes), for $\overline{\beta}$ is much greater there (see expression (63)). A similar result was obtained numerically by MacDonald and Walt (Reference 12).

If now W is of the form

$$W \sim \frac{1}{K' \exp\left(\frac{B - B_a}{\Delta B}\right)} \quad , \tag{64}$$

we have a solution of Equation 60, which represents a steady state in longitude. In this case, the mirror point flow (Equation 63) is approximately equal to $\overline{\beta}$,

$$v_m \simeq - \Delta B \overline{\beta} \frac{\partial \ln W}{\partial B} \simeq \overline{\beta} \quad . \tag{65}$$

It can be shown that such a steady state form (Equation 64) is attained very soon provided the gradient of W along a line of force is negative.

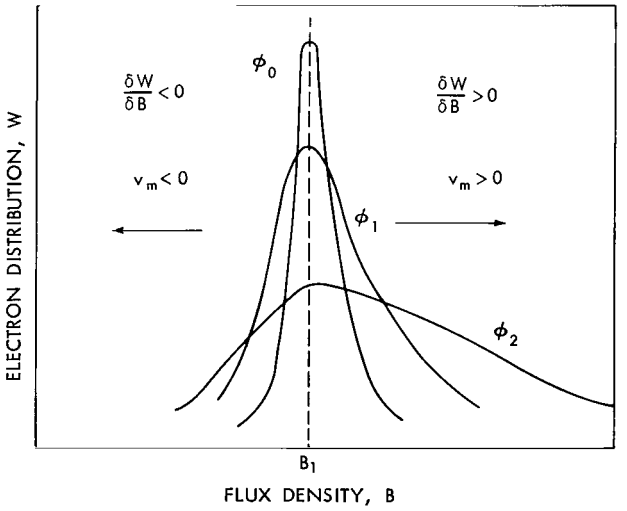


Figure 6—Qualitative description of the evolution of a mirror point distribution at very low altitudes.

It is also easy to verify that Equation 64 is an "equilibrium" configuration: Any small departure of W from Equation 64 will cause mirror point flows which will tend to correct such a departure.

For all these reasons, it is extremely instructive to inspect in detail the motion of mirror points for such a longitude-independent equilibrium state of Equation 64. Although, of course, all this is only a crude approximation, we expect all qualitative physical features to be valid also in the real case. This qualitative analysis will then help us to set up and interpret the tedious numerical calculations.

We shall analyze the characteristic trajectories of mirror points $B = B(X)$ (Equation 40) throughout the South American Anomaly described approximately by Equation 56, for an equilibrium state electron distribution (Equation 64). First of all, we will do our discussion in terms of the more familiar longitude variable $\phi$ rather than X, which anyway in our description is supposed proportional to the former. In order to obtain the characteristic trajectories in $B$-$\phi$ space, we have to integrate Equation 65, taking into account Equation 61, and the relation of Equation 19b, which now reads

$$X = \frac{2\pi}{360} RL\phi \ .$$

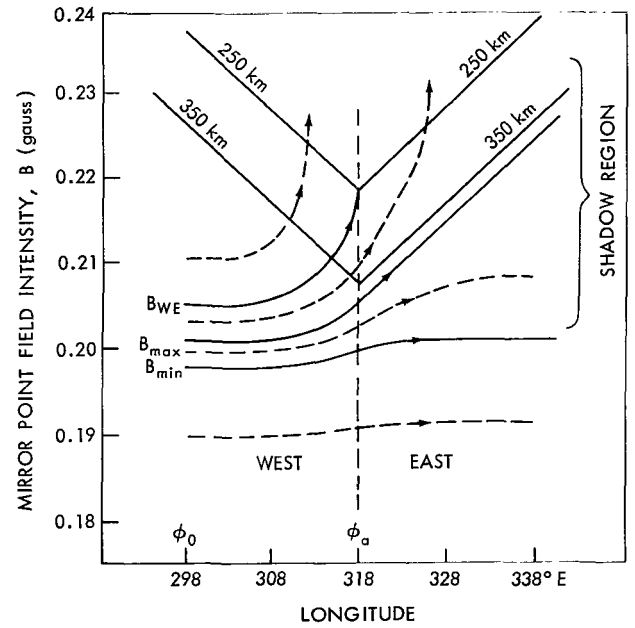


Figure 7—Characteristic mirror point trajectories in the region of the South American Anomaly (model 56) for a steady state distribution of 300 kev electrons of the form 64, and for L = 1.25 (1300 LT in the Anomaly). Electrons whose mirror points are initially (i.e., west of the Anomaly) between $B_{min}$ and $B_{max}$, populate the "shadow" region. Those between $B_{max}$ and $B_{WE}$ precipitate east of $\phi_a$; those with $B > B_{EW}$ precipitate on the west side. Constant altitude lines for h = 250 and 350 km are shown. Energy loss is neglected.

Starting from an initial longitude $\phi_0$ well west of the center of the Anomaly, and for a shell L = 1.25, we obtain characteristic mirror point trajectories for 300 kev electrons, schematically represented in Figure 7. Remember that they correspond to a distribution of the type in Equation 64. In this figure, lines of constant altitude for the approximate expression 56 are also shown. Below 250 kilometers, the $N_{eff} = N_{eff}(B, \phi)$ dependence is still nearly exponential in B and $|\phi - \phi_a|$, but with a smaller "scale height" $\Delta B$. We can safely assume for this discussion, that particles getting below this level will be removed by precipitation. Above 750 kilometers, the scattering effect is extremely small during one drift through the region of interest.

Notice in Figure 7 that there is a narrow "window," $B_{min} - B_{max}$, at the initial longitude $\phi_0$ west of the Anomaly which contains the mirror points of those electrons that populate the high B or "shadow" region east of the Anomaly. After one more turn around the earth, all these electrons are precipitated into the dense layers.

A certain portion of these $(B_{max} - B_{WE})$ will manage to get "around" the center of the Anomaly, and precipitate into its eastern side. Electrons mirroring initially at higher altitudes than those corresponding to the window, will lower slightly their mirror points during each passage through the Anomaly until they fall into the critical window. Please remember carefully that all this corresponds to an equilibrium distribution of Equation 64, neglecting energy loss and remember that the mirror point trajectories are average paths, not actual patterns for a given electron.

The most striking result of this analysis, is that *if multiple Coulomb scattering is the only process responsible for the replenishment* of the shadow region east of the Anomaly, then there is a *very limited region of the atmosphere* in the South American Anomaly (limited in both longitude and altitude) which entirely governs this replenishing process. We therefore should expect that in the real case, electron fluxes in the shadow are strongly influenced by the instantaneous atmospheric structure in this critical region.

In particular, we may expect a *diurnal variation* of electron fluxes and electron precipitation, determined by the diurnal variation of the atmosphere within about ±5° of the center of the Anomaly, between about 250-400 km altitude. We conclude that it would be unrealistic to carry out numerical calculations with a 24-hour averaged atmosphere. Rather, numerical integration should be performed for different local times at the Anomaly.

Notice finally, that according to this picture, replenishment occurs right at, or shortly "after," i.e., east of the Anomaly. Diffusion into the shadow region far east of the Anomaly is negligible, for Coulomb scattering. We may conclude our discussion by pointing out that in the picture described above, there is a steady flow of particles out of the lower B-region of a shell towards higher B values and from there into the atmosphere at the Anomaly. In an equilibrium state, this loss must be exactly balanced by a continuous injection from a source mainly effective in the lower B-region. In absence of such a source, i.e., in a nonequilibrium state, this flow and subsequent loss should determine the *lifetime* of the trapped radiation in question.

As a numerical example, we have calculated the position of the critical window in B (for the definition of $B_{min}$ and $B_{max}$ see Figure 7), for local times in the Anomaly as 1300 and 0200. The values obtained for $L = 1.25$ are shown in Table 1. Although the B values differ only very little, remember that they are in a region where the distribution U is a very steep function of B.

Table 1

Critical Field Values $B_{min}$, $B_{max}$ for 1300 and 0200 Local Time, L = 1.25.

| | Flux density, B (gauss) at 300 kev | Flux density, B (gauss) at 625 kev |
|---|---|---|
| 1300 Local Time | 0.198 min. | 0.205 min. |
| | 0.201 max. | 0.209 max. |
| 0200 Local Time | 0.207 min. | 0.213 min. |
| | 0.210 max. | 0.216 max. |

Detailed quantitative results on electron fluxes can be obtained only by numerical integration of Equation 39. In particular, the energy loss term, neglected in the above discussion, has to be taken into account; this is particularly important if we analyze the behavior of electrons which dip below about 300 kilometers altitude in the Anomaly.

## ACKNOWLEDGMENTS

We are indebted to Drs. W. N. Hess, D. Stern, J. Herring and M. Liwshitz for valuable discussions and critical remarks.

REFERENCES

1. Vernov, S. N., Gorchakov, E. V., Logachev, Yu. I., Nesterov, V. E., Pisarenko, N. F., Savenko, I. A., Chudakov, A. E., and Shavrin, P. I., "Investigations of Radiation During Flights of Satellites, Space Vehicles and Rockets," *J. Phys. Soc. Japan,* 17(supp. A-II):162-186, January 1962.

2. Mann, L. G., Bloom, S. D., and West, H. I., Jr., "Electron Spectrum 90 to 1200 KeV as Observed on Discoverer Satellites 29 and 31," in: *Space Research III, Proc. 3rd Internat. Space Sci. Sympos., Washington, D. C., May 2-8, 1962,* ed. by W. Priester, Amsterdam: North-Holland Pub. Co. and New York: Interscience Publishers, Inc., 1963, pp. 447-462.

3. Imhof, W. L., and Smith, R. V., "Longitudinal Variations of High Energy Electrons at Low Altitudes," *J. Geophys. Res.* 70(3):569-577, February 1, 1965.

4. Freden, S. C., and Paulikas, G. A., "Precipitation of Energetic Electrons into the Atmosphere," *J. Geophys. Res.* 69(7):1239-1249, April 1, 1964.

5. Mihalov, J. D., Mozer, F. S., and White, R. S., "Artificially Injected Electrons at Low Altitudes," *J. Geophys. Res.* 69(19):4003-4013, October 1, 1964.

6. Freden, S. C., and Paulikas, G. A., "Trapped Protons at Low Altitudes in the South Atlantic Magnetic Anomaly," *J. Geophys. Res.* 69(7):1259-1269, April 1, 1964.

7. White, R. S., Austin, M. M., and Dragt, A. J., "CRAND and SPAND Proton Injection," in: *Space Research V, Proc. 5th Internat. Space Sci. Sympos., Florence, May 12-15, 1964,* ed by D. G. King-Hele, P. Müller, and G. Righini, Amsterdam: North-Holland Pub. Co. and New York: Interscience Publishers, Inc., 1965, pp. 498-599.

8. Ghielmetti, H. S., Becerra, N., Godel, A. M., Heredia, H., and Roederer, J. G., "Enhancement of the X-Ray Intensity at Balloon Altitudes in the South American Anomaly," *Phys. Rev. Letters,* 12(14):388-390, April 6, 1964.

9. MacDonald, W. M., and Walt, M., "Distribution Function of Magnetically Confined Electrons in a Scattering Atmosphere," *Ann. Phys.* 15(1):44-62, July 1961.

10. Welch, J. A., Jr., Kaufmann, L., and Hess, W. N., "Trapped Electron Time Histories for L = 1.18 to L = 1.30," *J. Geophys. Res.* 68(3):685-700, February 1, 1963.

11. MacDonald, W. M., and Walt, M., "Diffusion of Electrons in the Van Allen Radiation Belt. Pt. 1, Treatment of Particles with Mirroring Points at High Altitude," *J. Geophys. Res.* 67(13):5013-5024, December 1962.

12. MacDonald, W. M., and Walt, M., "Diffusion of Electrons in the Van Allen Radiation Belt. Pt. 2, Particles with Mirroring Points at Low Altitudes," *J. Geophys. Res.* 67(13):5025-5033, December 1962.

13. Anderson, A. D., Crane, G. E., Francis, W. E., Newirk, L. L., and Walt, M., "Theoretical Investigation of Geomagnetically Trapped Electrons from High Altitude Nuclear Explosions," Final Report, Sunnyvale, California: Lockheed Missiles and Space Company Report Number 3-24-64-1; AD 612-737, DASA 148, June 1964.

14. McIlwain, C. E., "Coordinates for Mapping the Distribution of Magnetically Trapped Particles," *J. Geophys. Res.* 66(11):3681-3691, November 1961.

15. Northrop, T. G., and Teller, E., "Stability of the Adiabatic Motion of Charged Particles in the Earth's Field," *Phys. Rev.* 117(1):215-225, January 1, 1960.

16. Stone, E. C., "Physical Significance and Application of L, $B_0$, and $R_0$ to Magnetically Trapped Particles," *J. Geophys. Res.* 68(14):4157-4166, July 15, 1963.

17. Hamlin, D. A., Karplus, R., Vik, R. C., and Watson, K. M., "Mirror and Azimuthal Drift Frequencies for Geomagnetically Trapped Particles," *J. Geophys. Res.* 66(1):1-4, January 1961.

18. Hassitt, A., "The Drift of Trapped Particles," *J. Geophys. Res.* 70(3):535-540, February 1, 1965.

19. Berger, M. J., and Seltzer, S. M., "Tables of Energy Losses and Ranges of Electrons and Protons," NASA SP-3012, 1964.

20. Working Group IV of COSPAR, 1965, *CIRA 1965, COSPAR International Reference Atmosphere,* 2nd edition, Amsterdam: North Holland Pub. Co., 1965.

# THE NEUTRON FLUX IN SPACE FOLLOWING A POLAR CAP NEUTRON EVENT ON NOVEMBER 15, 1960

by
W. N. Hess
*Goddard Space Flight Center*

and

E. L. Chupp
*University of New Hampshire*

and

C. Curry
*University of California*

A neutron detector flown on an Atlas pod during the 15 November 1960 solar event measured a larger neutron flux than another detector flown on a similar vehicle during a quiet solar period. The excess neutron flux at low latitudes obtained by comparing these two measurements is about an order of magnitude higher than expected from the neutron production in the atmosphere by solar protons as deduced from Lingenfelter's calculations and Webber's model for the 15 November event. It is suggested that most of the discrepancy can be accounted for by considering neutron production by energetic solar alpha particles and lowered geomagnetic cutoffs.

## INTRODUCTION

It has been suggested (References 1 and 2) that solar protons bombarding the polar caps could produce a sufficient neutron flux in space (referred to hereafter as a Polar Cap Neutron event or PCN event) to provide at least part of the source of Van Allen belt protons. This possibility followed the discovery of an anomalous component of protons with energies $E > 50$ Mev trapped on magnetic field lines with a magnetic shell parameter $L > 1.7$. Lenchek (Reference 3) has concluded that the observed trapped proton flux is in rough agreement with his theoretical estimates of leakage neutrons from solar proton interactions in the atmosphere. He also concludes that the lifetime of the trapped protons is of the order of 100 years, a time long compared with expected neutron injection from major solar proton events. Thus the anomalous component of trapped protons may be built up by PCN events gradually to its present level by injection over several solar cycles.

More recently, Lingenfelter and Flamm (Reference 4) have calculated the neutron leakage flux from solar protons using the exponential rigidity model of Freier and Webber (Reference 5). Their calculations apply only to neutrons with energies E < 10 Mev but provide both the leakage neutron energy spectrum and angular distribution for an arbitrary solar proton event.

It is the purpose of this paper to present the results of two experiments carried out with neutron detectors on Atlas pods, one of which measured an excess neutron counting rate about four hours after the solar flare at 0207 UT on 15 November 1960. The second experiment provides control data taken one year later. The theory of Lingenfelter and Flamm (Reference 4) is then used along with the solar proton model of Freier and Webber (Reference 5) and the detector characteristics to calculate theoretically the expected excess neutron counting rate as a function of position along the trajectory of the Atlas pod. The detector was not in the sunlight at any time, so direct solar neutrons could not contribute to the excess counting rate.

## DESCRIPTION OF THE SOLAR FLARE EVENT ON 15 NOVEMBER 1960

At 0207 UT on 15 November 1960 the onset of a great solar flare was recorded in $H\alpha$. The optical flare reached a maximum about fourteen minutes later (0221 UT) and ended at 0427 UT.* As early as 0233.6 UT the onset of a cosmic ray intensity increase was recorded at the earth (Reference 6), with neutron monitors at sea level and at mountain altitudes. Direct observations of the solar flare cosmic ray flux were made (Reference 7) using balloon-borne detectors, and indirect observations were made by means of riometers. Prior to this solar flare, the interplanetary magnetic field conditions had been altered by a previous flare on 12 November. A full discussion of these two solar flare cosmic ray events has been given in literature (References 5 and 8), and it is unnecessary to review all the details of the events. For our purposes here it will be sufficient to establish as well as possible the solar cosmic ray flux time history and spectrum near the earth and the geomagnetic conditions about 0600 to 0630 UT 15 November 1960. This corresponds to the time when the Atlas neutron monitor was collecting data.

Ney and Stein (Reference 8) have considered the conditions of the geomagnetic field at the time of the 15 November flare and have concluded that the magnetic field of the earth had returned to its undisturbed condition by late 14 November following the geomagnetic disturbances produced by the solar flare on 12 November. However, following a solar flare at 0246 UT on 14 November, a sudden commencement magnetic storm occurred at 1304 UT on 15 November. The 15 November flare at 0207 produced a sudden commencement at 2200 UT on 15 November. Thus, at the time of the Atlas neutron monitor flight the evidence indicates that the geomagnetic field structure had essentially recovered from its disturbed condition produced by the 12 November flare. Hence, we will first assume that at 0600 on 15 November the normal (Reference 9) cosmic ray threshold rigidities apply.

At 0500 UT on 15 November, Winckler (Reference 7) made the earliest direct observation of the solar flare particles. On the basis of these observations and neutron monitor records, Freier

*Solar flare data from CRPL Reports, NBS, Boulder.

and Webber (Reference 5) have suggested that the spectrum may be best represented at this time by an exponential rigidity spectrum with a characteristic rigidity $P_0 = 350$ Mev. A differential power law energy spectrum with exponent $n = 3.3$ does not give as good a fit as the exponential rigidity spectrum. This spectrum gives a reasonably close fit to the data up to a rigidity of about 3 Bev. These authors have also recommended that this event be best described at all times by the differential form

$$\frac{dJ}{dP} = \left(\frac{dJ}{dP}\right)_0 e^{-P/P_0} \text{ particles/cm}^2\text{-sec-Mev-steradian},$$

where $(dJ/dP)_0$ and $P_0$ are functions of time during the event. These two parameters are simply related by the relation

$$J_0 = P_0 \left(\frac{dJ}{dP}\right)_0,$$

where $J_0$ is the total flux of charged particles with rigidity greater than $P = 0$. It has further been found that both the proton and alpha particle fluxes can be represented by this form. The ratio of $(dJ/dP)_0$ for protons to the same quantity for alpha particles is $1 \pm 0.5$ based on the data of Reference 8 from balloon flights at 1030 to 1230 UT on 15 November. Thus we also assume that the differential flux of protons and alpha particles is the same in any given rigidity interval. Freier and Webber (Reference 5) give, for the time interval covered by this event, the values of $J_0$ and $P_0$ as a function of time. For the time of interest for our analysis (0600 UT) we have chosen $J_0 = 260$ protons/cm$^2$-sec-ster and $P_0 = 355$ Mev giving a value for $(dJ/dP)_0$ of 0.73 protons/cm$^2$-sec-ster-Mev. We make the further assumption that the incoming radiation is isotropic at 0600-0630 UT.

## DESCRIPTION OF ATLAS NEUTRON EXPERIMENT

Moderated Anton $BF_3$ proportional counters were flown on an Atlas pod during the solar proton event on 15 November 1960. The general scheme was similar to that described in Reference 10, the pod being cast off from the Atlas after it was aloft. Figure 1 (solid line) shows the pod trajectory for the flight which took place at about 0600 UT, about four hours after the start of a large solar flare and during the time when considerable fluxes of polar cap protons were being detected. A 1-inch $B^{10}F_3$ counter moderated by 2 inches of epoxy was used and a similar counter but filled with $B^{11}F_3$ was flown to indicate counts not due to neutrons. The count rate ratios of the two detectors throughout the flight was consistent with that expected from the ratio of $B^{10}$ abundance in the two counters indicating that only neutrons were being detected. Individual counts from the detectors were returned to ground by FM telemetry. The count rate history for this detector is shown in Figure 2 as curve a.

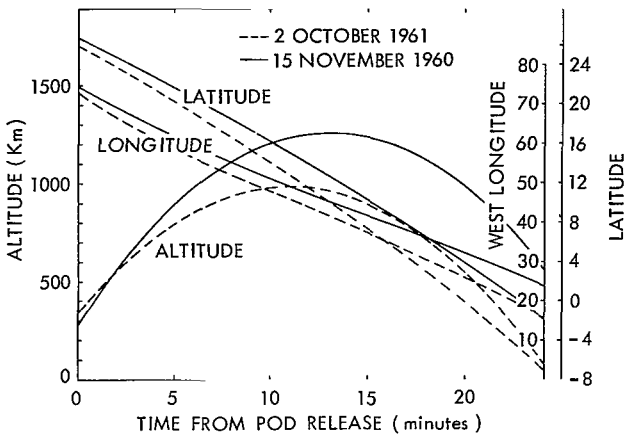


Figure 1—Trajectory of Atlas pod.

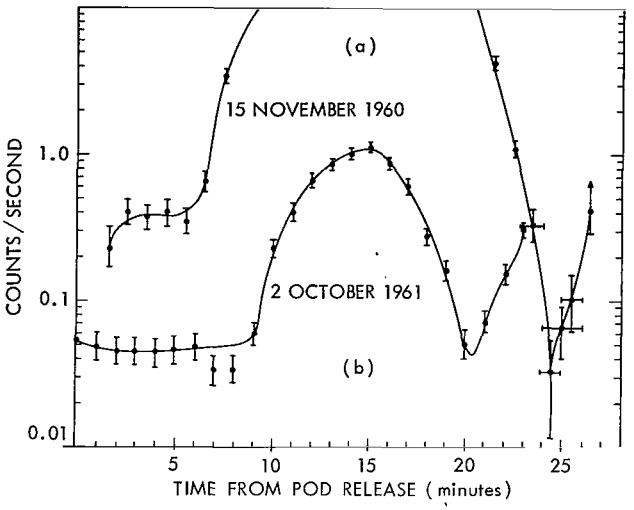


Figure 2—Comparative counting rate histories for neutron detectors on Atlas pod flights. The counting rate shown for October 2, 1961 is 1/10 the actual counting rate since the detector on this flight had an efficiency of about 10 times larger than for the other detector.

A nearly identical system of $BF^3$ counters was flown on another Atlas pod on 2 October 1961 during a relatively quiet solar period. For this flight the detector geometry was the same, but the detectors were replaced by Reuter-Stokes counters filled to a higher pressure and the detectors were moderated with polyethylene; thus the system had higher efficiency than for the flight on 15 November. The count rate history for this flight for the $B^{10} F_3$ counter is shown as curve b in Figure 2. The Atlas trajectory for this flight was slightly different than on 15 November 1960, so this data is plotted for comparison with the first flight on Figure 1 as dotted curves. The curves a and b in Figure 2 may not be compared directly except at early times because of the large difference in trajectories apparent at late times (Figure 1). At late times both detectors show an anomalous rise in counting rate after reaching a minimum following the pod's exit from the radiation belt. The minima occur at different times following release of the respective pods because of the difference of trajectories but still at nearly the same altitudes and geographic coordinates. We have no explanation for this behavior.

The pod for the second flight was quite similar in geometry to that for the first flight. It was slightly larger and heavier and the location of the components in it was not identical to the first but it was similar enough so that the vehicle produced neutron fluxes should be nearly equal. The approximate weight of the first pod was 65 pounds, and the second pod 100 pounds. An estimate based on the relative masses and distributions of components indicates that the second pod had 20 percent more locally produced neutrons which could be counted by its detector than for the first pod. Thus, the difference in counting rates for the two measurements is a lower limit. That is, any correction for differences in local neutron production would only increase the differences in counting rates between the two flights.

The efficiencies of these detectors were measured using standard neutron sources of Sb-Be, Mock Fission and Po-Be. The mean neutron energies for these sources are respectively 25 kev,

1 Mev and 4 Mev. We feel the detectors and pod trajectories for the two flights are sufficiently similar on the ascending portion of the trajectory that it is meaningful to make a direct comparison of counting rates of the two instruments in order to determine what effect the phenomena associated with the solar flare might have on the neutron flux in space. We make the following assumptions: First, that the differential albedo neutron flux due to galactic cosmic rays at both detectors is the same for corresponding detector locations; and, second, that the differential neutron flux at both detectors due to neutrons locally produced in the pods and in the detectors are the same in both cases. This, of course, assumes that the charged particle flux at the pod is always the same at corresponding locations in both cases.*

The $B^{10}$ neutron counting rate for the 15 November 1960 flight and at a particular location is then

$$C_1 = \int \Sigma_1 (E) \left[ N_f (E) + N_\ell (E) + N_g (E) \right] dE \quad ,$$

where

$\Sigma_1 (E)$ = detector efficiency versus neutron energy (counts-$cm^2$/neutron),

$N_f (E)$ = the differential neutron flux at the detector associated with the solar flare,

$N_\ell (E)$ = the differential neutron flux locally produced by the ambient charged particle radiation, and

$N_g (E)$ = the differential neutron flux produced by the galactic cosmic rays and returning to space.

In a similar manner we can write the counting rate for the detector flown on the quiet solar day 2 October 1961 as

$$C_2 = \int \Sigma_2 (E) \left[ N_\ell (E) + N_g (E) \right] dE \quad .$$

The detector efficiencies for the 1961 detector compared to the 1960 detector are very nearly in the ratio of 10 to 1 at all energies so $\Sigma_2 (E) = 10 \Sigma_1 (E)$. As can be seen in Figure 1, the trajectories are sufficiently similar at early times so that the galactic cosmic ray flux is the same for both flights, and we assume the term $\left[ N_\ell (E) + N_g (E) \right]$ is the same in both cases to ≈10 percent. This, of course, requires that the cutoff rigidities are the same for both flights. The Forbush

*A 3+ solar flare on 28 September 1961 was followed by an SC magnetic storm and associated Forbush decrease on 30 September. By the time of the pod flight on 2 October, the galactic cosmic ray intensity had nearly recovered to its pre-storm level; thus the galactic albedo neutron flux would only be expected to be a few percent lower than normal. The solar cycle variation of galactic cosmic rays also compensates for this effect.

decrease associated with the 12 November 1960 event was well over by 15 November and geomagnetic conditions were also normal during the second flight so this assumption is reasonable.

Thus the excess counting rate due to the flare is then

$$(\Delta C_f) = C_1 - \frac{C_2}{10} = \int \Sigma_1 (E)\, N_f (E)\, dE \ .$$

The integral on the right provides a means of comparing theory with experiment as will be discussed later. Figure 3 shows the experimental values of $(\Delta C_f)_{exp}$ as deduced directly from the counting rate data. The estimated absolute error in $(\Delta C_f)_{exp}$, the flare associated enhanced neutron flux is ≈30 percent and is mostly due to the detector calibration errors and counting statistics. Any errors associated with the assumptions justifying the subtraction of the two sets of data will not produce a large error in $(\Delta C_f)_{exp}$ since $C_1 \gg C_2/10$. We also are neglecting the fact that the galactic cosmic ray flux was actually somewhat higher during the second flight but correction for this effect would enhance the experimental value of $(\Delta C_f)_{exp}$. Also any correction for differences in local neutron production from galactic cosmic rays for the two detectors would increase the value of $(\Delta C_f)_{exp}$ since the pod containing the second detector was actually somewhat heavier than for the flight following the solar flare. The possibility that an excess of charged particle flux could be present at the detector during the 15 November flight can be ruled out qualitatively from the behavior of $(\Delta C_f)_{exp}$ versus latitude as shown in Figure 3. If solar protons or extra galactic cosmic rays due to lowered cutoffs were present at the detector and produced a significant flux of locally produced neutrons then $(\Delta C_f)_{exp}$ should fall off with time (i.e., as the detector progresses to more southern latitudes), but this is contrary to the behavior in Figure 3. This is expected since there would be a higher flux of such leakage charged particles at the earlier times (i.e., higher latitudes) and hence more locally produced neutrons.

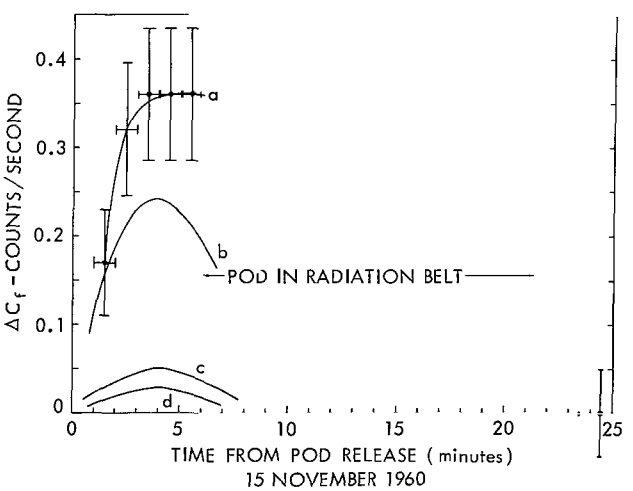


Figure 3—(a) The flare associated enhanced neutron counting rate $(\Delta C_f)_{exp}$ versus time after Atlas pod release. (b) The value of $(\Delta C_f)_{theo} \times 10$ according to Lingenfelter's theory. (c) The value of $(\Delta C_f)_{theo}$ for all cutoffs 80 percent of normal. (d) $(\Delta C_f)_{theo}$. The theoretical values are based on neutron production solely by solar protons.

Because of the anomalous behavior of the counting rate curves (Figure 2) on the descending portion of the trajectories, it is difficult to have a great deal of confidence in this part of the data. Since the minima of the counting rates occur at nearly the same location in space and are essentially the same, we take the view that both detectors are responding normally here and find the excess counting rate zero within the error of measurement as shown in Figure 3.

## ANALYSIS

The flare associated neutron flux enhancement $(\Delta C_f)_{exp}$, defined above, appears to be due to only one cause. Since solar protons were bombarding the polar cap regions at the time of the Atlas pod flight the most likely extra source of neutrons in space is from the reactions these protons make with atmospheric nuclei. During most of the time of interest during the experiment (when the detector was below the radiation belt) part of those regions of the polar atmosphere accessible to the solar protons were above the horizon for the neutron detector; thus a PCN event of sufficient magnitude could logically explain the flux enhancement. An additional source of extra neutrons is the sun itself, but the detector was never in the sunlight so this possible source may be excluded.

Generalized theoretical calculations performed by Lingenfelter and Flamm (Reference 4) give the leakage flux at the top of the atmosphere for neutrons produced by polar cap protons. These results may not be directly compared with the present experimental results since they give only the leakage flux into space from a unit area at the top of the atmosphere. The results of these calculations must be used as a source and the geometrical calculation performed to give the differential flux at the detector location which is changing with time due to the motion of the detector in latitude, longitude and altitude. It has been established above that the best description of the time variation of the flux of solar protons and alpha particles at the earth following the solar flare of 15 November 1960 is given by an exponential differential rigidity spectrum of the form

$$\frac{dJ}{dP} = \left(\frac{dJ}{dP}\right)_0 e^{-P/P_0} \quad \frac{\text{protons or alphas}}{\text{cm}^2\text{-sec-Mev-steradian}} ,$$

where $(dJ/dP)_0 = 0.73$ particles/cm$^2$-sec-Mev-steradian and $P_0 = 355$ Mev at the time of the Atlas neutron monitor flight. It is further assumed that the lowest rigidity particle reaching the earth's atmosphere at a given latitude and longitude is determined by the quiet cosmic ray vertical cutoff rigidities of Quenby and Wenk (Reference 9). Lingenfelter's model also takes the incident charged particle flux as isotropic over the upper hemisphere.

Lingenfelter's calculations give the equilibrium neutron flux in the atmosphere produced by protons with the above rigidity spectrum using the diffusion theory approximation to neutron transport theory. He gives the neutron flux as a function of atmospheric depth for energies up to 10 Mev. In addition the leakage flux from the top of the atmosphere and its angular distribution with respect to the zenith is given for eighteen energy groups. Since all of these calculations have been done for several different values of characteristic rigidity $P_0$ and cutoff rigidities, it is a simple geometrical problem to calculate the leakage flux at any point in space from a leakage flux source element at a given latitude and longitude.*

*Lingenfelter's model takes the incident charged particle flux as isotropic over the upper hemisphere. Since his leakage flux is normalized to a total of 1 proton/cm$^2$ sec incident the absolute leakage flux value for the conditions of this event is based on $2\pi \times .73 = 4.6$ $\frac{\text{protons}}{\text{cm}^2\text{sec Mev}}$ as the isotropic incident flux.

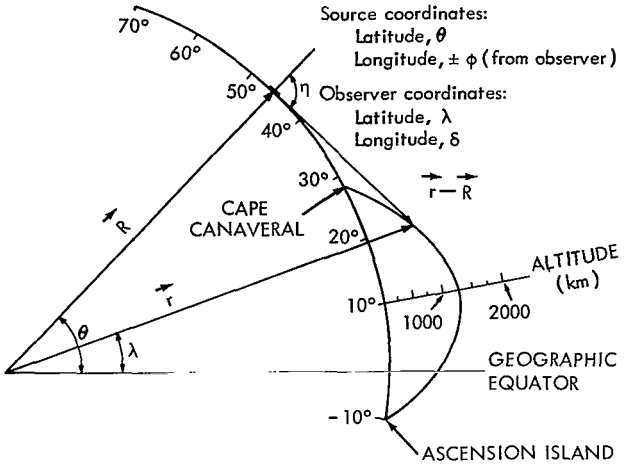


Figure 4—The coordinate system relating the observer coordinates to the source coordinate for a PCN event.

The geometry pertaining to this calculation is shown in Figure 4. It should be noted that only the source elements which are in a direct line of sight (above the horizon) from the detector at a given time give contributions to the flux at the detector. Those neutrons whose trajectories are modified by the gravitational field ($E_n < 10$ volts) do not add significantly to the detector count rate here.

Referring to Figure 4 the vector flux, or the number of neutrons traveling through a unit area normal to the direction, $\vec{\Omega}$, from a source element and into unit solid angle in the direction of the observer is

$$\vec{J}(\eta, 0, \phi, \Delta E_i) = A(\eta, \Delta E_i)\left(\frac{2\Pi J_0}{P_0}\right)\left[\frac{F(P_0 = 355, P_c)}{F(P_0 = 125, 0)}\right]\vec{\Omega}\left(\frac{\text{neutrons}}{\text{cm}^2(\text{source})\ \text{sec-steradian}}\right)$$

The term $A(\eta, \Delta E_i)$* gives the normalized vector flux for a given energy group $\Delta E_i$ and zenith angle $\eta$ from Lingenfelter's work for $P_0 = 125$ Mev and $P_c = 0$.** The normalization term $(2\Pi J_0/P_0)$ is required since Lingenfelter's theoretical calculations were normalized to unity for this quantity. The remaining term in brackets, deduced from Lingenfelter's work, is necessary to transform to our specific case of interest where $P_0 = 355$ Mev and the cutoff rigidity $P_c$ is defined by the location of a given source element. For a given energy group then the flux at a particular observer's location for all source elements above the horizon is

$$J_0(\lambda, \delta, r, \Delta E_i) = \int_{(\text{source})} \frac{J(\eta, \theta, \phi, \Delta E_i)\cos\eta\cos\theta\, d\theta\, d\phi}{|\vec{r} - \vec{R}|^2}\left(\frac{\text{neutrons}}{\text{cm}^2\text{-sec}}\right)$$

All symbols are defined in Figure 4 and $\cos\theta\, d\theta\, d\phi$ is the source element of area. The magnitudes of the position vectors $\vec{r}$ and $\vec{R}$ are expressed in earth radii. $J_0(\lambda, \delta, r, \Delta E_i)$ is properly defined as the flux through a sphere of unit cross-sectional area at the observer's location. This calculation has been performed numerically for several detector locations and all energy groups used by Lingenfelter. The integration was performed in one degree steps in latitude and longitude over all

*Our values of $A(\eta, \Delta E_i)$ are determined taking into account a correction to Lingenfelter's earlier work as noted in J. Geophys. Res., 69:4201 (1964).

**Lingenfelter (private communication) has found the dependence of the zenith angle distribution on variation of $P_0$ and $P_c$ less than 10 percent.

possible source coordinates satisfying the line of sight condition ($\eta \leq \Pi/2$). In general the counting rate produced by this differential flux is

$$(\Delta C_f)_{theo} = \sum_{i=1}^{i=18} \frac{J_0(\lambda, d, \Delta E_i)}{\Delta E_i} \times \Sigma_1(\Delta E_i) \times \Delta E_i \quad .$$

$\Sigma_1(\Delta E_i)$ is the average efficiency corresponding to the energy group $\Delta E_i$. There is not good agreement between $(\Delta C_f)_{theo}$ and $(\Delta C_f)_{exp}$; in fact, the theoretical value is more than an order of magnitude below the experimental value. Curve b, Figure 3 shows $(\Delta C_f)_{theo}$ multiplied by ten. The shape at early times follows that for $(\Delta C_f)_{exp}$ indicating that the latter is consistent with a PCN source. $(\Delta C_f)_{theo}$ shows a peak at an altitude of ≈700 kilometers, but this behavior cannot be verified in $(\Delta C_f)_{exp}$ because of the large experimental uncertainty.

## DISCUSSION OF DISCREPANCY

Arguments have been given previously which indicate that the experimental value $(\Delta C_f)_{exp}$ is a lower limit. Further, the behavior of the experimental curve (Figure 3) with latitude is not consistent with any significant local production of neutrons. It is not clear how the experimental excess counting rate can be reduced and therefore we wish to inquire how the theoretical prediction can be significantly increased.

We will consider both the possibility that the absolute leakage flux calculated by Lingenfelter and Flamm (Reference 4) is low for this event; and the effect of changes in the parameters $P_0$ and $P_c$. In regard to the first point, Freier and Webber's model (Reference 5) indicates that the ratio of alpha particles to protons at the same rigidity is $\approx 1 \pm 0.5$ for the solar flare event on 15 November 1960 and also $P_0$ is the same. Lingenfelter and Flamm, however, have only considered protons as the primary neutron producing radiation. Adequate data on neutron production by alpha particles is not available. However, a rough estimate of the extra neutron production from the alpha particles can be found from the following argument: At a cutoff rigidity of 1 Bev the differential and integral fluxes of protons and alphas is the same but the proton kinetic energy is ≈435 Mev, while the kinetic energy per nucleon for the alpha is ≈125 Mev. Now if each of the four nucleons of the alpha particle is as effective in producing neutrons in an air nucleus as a proton of the same energy, then the ratio of the neutron excitation cross section for alphas to the excitation cross section for protons is, from Figure 1 (Reference 5)

$$\frac{4\sigma\,(125\ \text{Mev/Nuc},\ \alpha)}{\sigma\,(435\ \text{Mev},\ P)} \simeq \frac{4 \times .3}{.6} \approx 2.$$

Thus it seems reasonable that the theoretical absolute neutron leakage flux should be increased by a factor of 3.

Lingenfelter's earlier work on production of neutrons by galactic cosmic rays is in reasonable agreement with experiment. He has also compared his calculations on neutron production by solar protons with neutron measurements in the atmosphere (Reference 11) following the solar proton event on 18-19 July 1961. Again the agreement is within experimental error. In both of these cases, however, the ratio of protons to alphas ($P/\alpha$) is quite high; for galactic cosmic rays at solar min $P/\alpha \approx 7.2 (> 4.5\,\text{Bev})$ and for the event on 18 July 1961 the evidence (Reference 5) indicates that $P/\alpha = 6 \pm 1$ about ten hours after the associated flare. On the other hand, in the case of the 15 November 1960 event, the evidence indicates that $P/\alpha = 1 \pm 0.5$ about eight hours after the associated flare. At the time of the measurement described here it is therefore possible that alpha particles make a comparable contribution to the excess neutron flux as do the protons, or possibly a larger contribution.

Another factor we suggest that could conceivably increase the expected theoretical flux at the detector concerns the lowered cutoff rigidity for charged particles entering the earth's atmosphere from the west. The theoretical calculations are based on vertical cutoff rigidities. For a sufficiently steep rigidity spectrum this may significantly enhance the neutron production in the atmosphere for this event.

Freier and Webber (Reference 5) indicate that a geomagnetic cutoff of 80 percent of normal can be deduced from the balloon flight data of Winckler (Reference 7) at 0500 UT, 15 November, about 45 minutes before the Atlas pod measurements. To test the effect of reduced cutoffs on the theoretical results, we have made the gross assumption that all cutoffs are lowered to 80 percent of normal and recalculated $(\Delta C_f)_{theo}$. The result is shown as curve c in Figure 3. At the peak of the theoretical curve this increases $(\Delta C_f)_{theo}$ by about a factor of two over the result found assuming all cutoffs are normal. It is possible to get a reasonably close fit to $(\Delta C_f)_{exp}$ by further adjusting $P_0$ and $P_c$ but there is no evidence to support such modifications to the model used here.

## CONCLUSIONS

In summary then we have found a disagreement by a factor of ten to fifteen between theoretical expectations and the measurement of the neutron flux in space from a PCN event following the solar flare of 15 November 1960. The experimentally observed excess neutron counting rate cannot be decreased by any reasonable argument. There is some inconsistency in the relative response of our detectors when the pods are in the trapped radiation, but we believe this can be accounted for by uncertainties in the apogees of the two pod trajectories. The low theoretical result (for the conditions of the experiment) probably should be increased for two reasons. If account is taken of the production of evaporation neutrons from the alpha particles accompanying the protons from the flare then the theoretical flux could possibly be increased by a factor of three. Further if the assumption is made that the geomagnetic cutoff is 80 percent of normal at all latitudes (as was the case at Minneapolis shortly before the experiment) then the theoretical flux can be increased by another factor of two. If these tentative conclusions stand, then the discrepancy is reduced to a factor of two to three.

This experiment has demonstrated the value of a low latitude, ballistic rocket experiment to study a PCN event and provides a basis for planning experiments to study future events. At a representative point in space during the 1960 flight the polar cap neutron flux is about 2 neutrons/$cm^2$ sec to be compared with a galactic albedo neutron flux of about 0.2 neutrons/$cm^2$ sec. Unfortunately it was not possible in this experiment to provide any data on the flux of neutrons $(E_{n-} > 70 \text{ Mev})$ which could be related to the high energy trapped protons.

## ACKNOWLEDGMENTS

The authors wish to acknowledge several conversations with Dr. R. E. Lingenfelter on theoretical questions, and discussions with Dr. J. A. Lockwood on several aspects of the solar cosmic rays on 15 November 1960. We are particularly indebted to Mr. Allen Silver for ably carrying out the numerical integrations with the Goddard Space Flight Center computer, and Mr. Donald Peters of UCLRL and Mr. Robert Henderson of UCLRL who did the electronic circuit design and mechanical design, respectively, for the pod experiment. Critical comments by Dr. C. Gilbert of UCLRL in reviewing our analysis are also deeply appreciated.

REFERENCES

1. Armstrong, A. H., Harrison, F. B., Heckman, H. H., and Rosen, L., "Charged Particles in the Inner Van Allen Radiation Belt," *J. Geophys. Res.* 66(2):351-357, February 1961.

2. Naugle, J. E., and Kniffen, D. A., "Flux and Energy Spectra of the Protons in the Inner Van Allen Belt," *Phys. Rev. Letters*, 7(1):3-6, January 1961.

3. Lenchek, A. M., "On the Anomalous Component of Low-Energy Geomagnetically Trapped Protons," *J. Geophys. Res.* 67(6):2145-2157, June 1962.

4. Lingenfelter, R. E., and Flamm, E. J., "Neutron Leakage Flux From Interactions of Solar Protons in the Atmosphere," *J. Geophys. Res.* 69(11):2199-2207, June 1964.

5. Freier, P. S., and Webber, W. R., "Exponential Rigidity Spectrums for Solar-Flare Cosmic Rays," *J. Geophys. Res.* 68(6):1605-1629, March 1963.

6. Lockwood, J. A., and Shea, M. A., "Variations of the Cosmic Radiation in November 1960," *J. Geophys. Res.* 66(10):3083-93, October 1961.

7. Winckler, J. R., "Geomagnetic and Interplanetary Effects on Cosmic Rays," *J. Phy. Soc.* Japan, 17(Suppl. A-II):337-44, January 1962.

8. Ney, E. P., and Stein, W. A., "Solar Protons, Alpha Particles, and Heavy Nuclei in November 1960," *J. Geophys. Res.* 67(6):2087-2105, June 1962.

9. Quenby, J. J., and Wenk, G. J., "Cosmic Ray Threshold Rigidities and the Earth's Magnetic Field," *Phil. Mag.* 7(81):1457-1471, September 1962.

10. Hess, W. N. and Starnes, A. J., "Measurement of the Neutron Flux in Space," *Phys. Rev. Letters* 5(2):48-50, July 15, 1960.

11. Smith, R. V., Chase, L. F., Imhof., W. L., Reagan, J. B., and Walt, M., "Radiation Measurements with Balloons," Final Report, Aeromedical Res. Lab., Holloman AFB, New Mexico, ARL-TDR-62-2, 1962.

# HEAT BUDGET OF THE SOUTHERN HEMISPHERE

by
S. I. Rasool and C. Prabhakara
*Goddard Space Flight Center*

Analysis has been carried out of radiation measurements made by the Tiros VII satellite covering a period of one full year. The annual heat budget has been computed separately for the northern and southern hemispheres. It is found that there is a northward flux of heat across the equator of $\approx 40 \times 10^{18}$ calories/day by transport of water vapor. As the two hemispheres are individually in radiative balance with space, this northward flux of heat must therefore be compensated by southward transport of heat by ocean currents and the atmosphere.

Seasonal variations in the intensity of meridional transport of heat in the southern and northern hemispheres have also been examined. It is found that in the months of December, January and February there is a large northward flux of heat at all latitudes between 20 degrees S and 90 degrees N. During the other three seasons the flux is moderate and is predominantly southward at all latitudes between 15 degrees N and 90 degrees S.

## INTRODUCTION

Earlier studies of the heat budget of the earth have been mainly confined to the northern hemisphere (References 1 and 2). The main reason for this has been the scarcity of temperature and radiation data in the southern hemisphere where 80.9 percent of the surface is covered with oceans. It has therefore been customary to estimate the heat balance of the southern hemisphere by using northern hemisphere data for corresponding latitude and season. This type of analysis is, however, likely to give misleading results because the topography of the southern hemisphere is considerably different from that of the northern hemisphere; also, the albedo, cloud cover, and water vapor amounts in the southern hemisphere, being mostly oceanic, may not necessarily be the same as in the northern hemisphere; and, because of the eccentricity of the earth's orbit around the sun and the inclination of the earth, the solar energy input in the southern hemisphere is $\approx 6$ percent higher in the local summer than in the northern hemisphere.

Since the IGY, however, a considerable amount of data have become available and the subsequent studies of the heat budget of the south polar regions made by Gabites, Rubin and Kort (References 3, 4 and 5) have indicated significant differences in the heat balance of the two poles.

Now, with the availability of data from meteorological satellites, providing uniform coverage over both hemispheres with a frequency of observations never before achieved (a million data

points per day), it has become possible to make at least preliminary estimates of the heat balance of the southern and northern hemispheres separately. It is the purpose of this paper to present some of the new results obtained on the differences in the heat balance of the two hemispheres as derived from the analysis of one full year's radiation data from Tiros VII.

## HEAT BALANCE

Solar energy, the primary source for driving the atmospheric heat engine, has a flux of $1.4\times10^6$ ergs/cm$^2$ sec or 2 calories/cm$^2$ min at the top of the earth's atmosphere. Part of this radiation is reflected back to space mainly by the clouds. The albedo of the whole globe has been estimated by various authors and the values range between 35 and 40 percent (References 6, 7 and 8). The remaining 60 to 65 percent of the solar energy is absorbed in the atmosphere and at the surface of the earth.

The earth-atmosphere system radiates back to space in the far infrared. Over long periods of time, of the order of years, the total amount of radiation thus emitted back to space equals the total incoming solar radiation. This long-period global radiative balance for the rotating earth may be expressed:

$$\frac{SC}{4}(1-A) = E_s \equiv E_r = \sigma T_e^4 , \qquad (1)$$

where $SC$ is the solar constant at the distance of the earth (2 calories/cm$^2$ min), A is the average albedo of the whole globe, $E_s$ is the effective incoming solar radiation, $E_r$ is the total outgoing radiation from the earth atmosphere system in the far infrared, $\sigma$ is the Stefan-Boltzmann constant, and $T_e$ is the effective temperature of the earth.

Over a short period of time, and for any given region of the globe, however, $E_s \neq E_r$, and the difference between the incoming and outgoing radiation $(E_s - E_r)$, known as the local radiation balance of the earth atmosphere system, is not necessarily zero and may be a finite quantity. This radiation balance, R, varies with latitude, longitude and season and is generally known to be positive near the equator and negative at the poles (References 1, 2 and 9).

The radiation imbalance ($R \neq 0$) over a given region may manifest itself in three different ways: (1) by a change in the combined heat content of the oceans or land and of the atmosphere, (2) by an increase or decrease of the latent heat, and (3) by transport of energy by ocean and air currents from or to this region. The following equation expresses the local heat balance of the earth-atmosphere system:

$$R = S + LE + T , \qquad (2)$$

where S is the storage of energy which itself has three components: $S_O$, $S_L$, $S_A$, being the storage in oceans, land and the atmosphere. Of these, the storage in the oceans is the most significant,

and can have an approximate magnitude of the radiation balance itself (References 10 and 11). $S_L$ and $S_A$ are usually 10 percent of $S_0$ (Reference 10). LE is the net latent heat available in the atmosphere, being the difference between the amount of energy spent in evaporation and that released by condensation in the atmosphere. T is the residual heat available for transport by ocean currents and by winds.

On an annual basis, within a wide latitudinal zone ($\approx 10°$), both the storage and the net latent heat terms in Equation 2 go to zero, and therefore the latitudinal variations in the annual radiation balance are an indicator of the energy transported across the latitudinal circles

In the present study we have attempted to derive, from the meteorological satellite data, the radiation balance of the earth-atmosphere system for one full year, separately for the northern and the southern hemispheres. Also, monthly and latitudinal variations in the radiation balance have been derived. These values are combined with climatological estimates of the storage of energy in oceans, land and atmosphere, and of the net latent heat available in the atmosphere. Equation 2 is then solved for T to obtain the latitudinal and monthly variations in the energy available for transport by oceans and the atmosphere.

## RADIATION MEASUREMENTS FROM TIROS SATELLITES

Apart from the now well known television cameras, most of the Tiros series of meteorological satellites were also equipped with medium resolution scanning radiometers. These radiometers have been described in considerable detail by Bandeen and Astheimer (References 12 and 13). They measure the absolute intensities of the emitted terrestrial radiation and of the solar radiation as reflected by the earth. Also, the orbital characteristics of the Tiros VII satellite have been discussed in great detail (References 14 and 15) and therefore will not be repeated here.

For the determination of the radiation balance we have used the data from Channel 2 and Channel 5 (Reference 14). Recent analyses of the radiation data obtained from Tiros VII have indicated that there has been considerable degradation in the instrumental response, thereby introducing an error in the observed radiation values (Reference 14). Because the Tiros satellites are not equipped for on-board calibration, the corrections to these degradations have to be determined indirectly. Bandeen (Reference 16) studied this problem in great detail and has introduced the correction factors for individual channels of the radiometer. These corrections are based on the assumption that the quasi-global (60 degrees N - 60 degrees S) mean value of the radiation reflected in the short wave and emitted in the long wave regions remains constant over long periods of time (several months).

## SEASONAL AND LATITUDINAL VARIATION OF HEAT BALANCE

### Incoming Solar Radiation

The incoming radiation, $E_s$, in a given 10 degree latitudinal belt for each month, is calculated from the expression:

$$E_s = E(1 - \bar{A}) \quad , \tag{3}$$

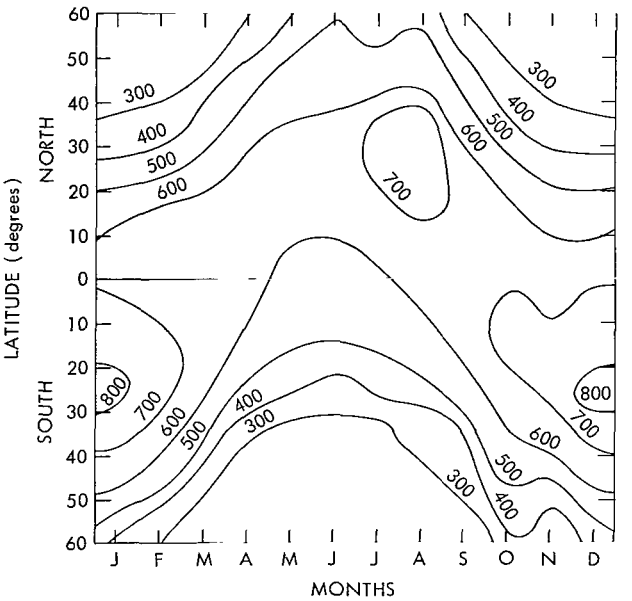


Figure 1—Latitude and time distribution of the incoming solar radiation in calories/cm² day derived from the albedo measurements made by Tiros VII.

where E is the average radiation flux incident at the top of the atmosphere for the month and $\bar{A}$ is the monthly mean albedo for the latitudinal belt. The values of $\bar{A}$ are based on the Tiros VII measurements in the Channel 5 (0.5 - 0.7$\mu$) as corrected for the degradation in the response of the radiometer (Reference 14). Figure 1 shows the distribution of the incoming solar radiation as a function of latitude and month between 60 degrees N and 60 degrees S in calories/cm² day. It is seen that the maximum radiation is received at the subtropical belts during the local summers of the two hemispheres. The values of the effective incoming radiation at 20 degrees - 30 degrees S, during summer, are ≈ 10 percent higher than those for the northern hemisphere for the corresponding season and latitude. This is both because of the larger oceanic regions in the southern hemisphere which have a relatively low albedo and because slightly more solar radiation (≈ 6 percent) is incident at the top of the atmosphere during the southern hemisphere summer. The other features of Figure 1 conform with earlier studies made using ground-based observations of the incoming radiation (Reference 10).

## Outgoing Terrestrial Radiation

The outgoing terrestrial radiation in the far infrared is the other component of the radiation balance. Tiros data has already been used by several authors to determine the latitudinal distribution of outgoing radiation for specific periods of the year (References 17, 18, 19 and 20). The values in the northern hemisphere derived from these measurements have been fairly consistent with the earlier estimates made by Houghton (Reference 1) and London (Reference 2). Now with the availability of data from Tiros VII, and applying the degradation corrections communicated by Bandeen (Reference 16), we calculate the monthly values of the total outgoing radiation for each 10 degree latitudinal belt from

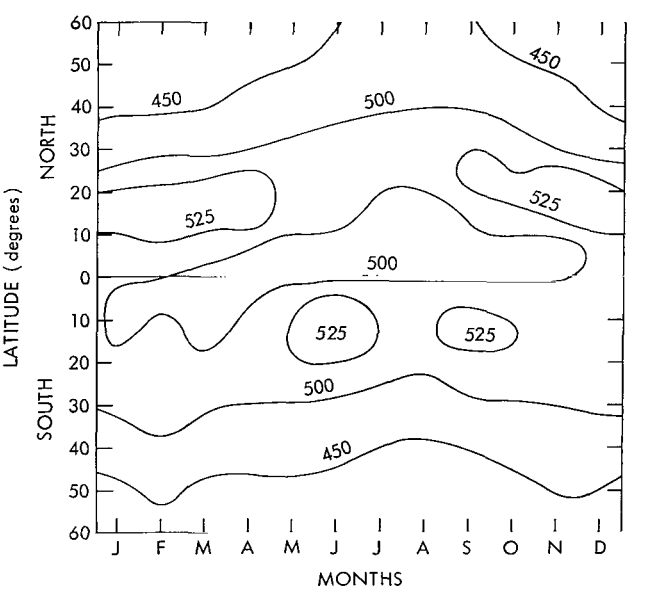


Figure 2—Latitude and time distribution of the outgoing terrestrial radiation in the far infrared in calories/cm² day derived from measurements made by Tiros VII.

June 1963 through June 1964. Figure 2 shows the latitudinal and time variations of the total outgoing radiation in calories/cm$^2$ day.

The variation in the outgoing radiation with latitude is small and the change with season is still smaller. The weak highs of outgoing radiation at the subtropical latitudinal belts in both hemispheres are to be noted. Also the latitude of the inter-tropical convergence zone (region of the equatorial minimum in the outgoing radiation) changes as expected from 5 degrees S in February to ≈10 degrees N in July and August.

## Radiation Balance of the Earth-Atmosphere System

Combining Figures 1 and 2, we now obtain the radiation balance of the earth-atmosphere system shown in Figure 3. Because the total outgoing terrestrial radiation does not vary considerably with season and with latitude between 60 degrees N and 60 degrees S, the radiation balance of the earth-atmosphere system shows a pattern similar to that of the incoming radiation (Figure 1). The main excess of incoming over outgoing radiation occurs in the latitudes 20 - 40 degrees in both the hemispheres in their respective months of summer. In the tropical latitudes between 20 degrees N and 15 degrees S, there is an excess of incoming radiation all year round.

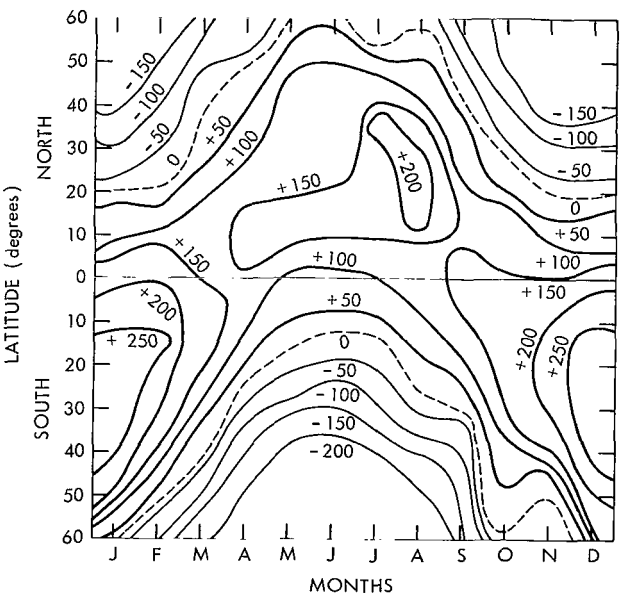


Figure 3—Radiation balance of the earth-atmosphere system in calories/cm$^2$ sec derived from Figures 1 and 2.

## Net Heat Available for Transport

The radiation balance as shown in Figure 3 gives the net amount of energy deposited by the sun in the earth-atmosphere system. As discussed earlier, a substantial part of this energy is stored in the oceans and to some extent also in the land and atmosphere. Also part of this energy is spent in evaporation of water which may later be released in the atmosphere by condensation in the form of clouds. Estimates of the magnitude of energy involved in each of these processes and its variation with time and latitude have recently been made by the authors (Reference 15) and the results are shown in Figures 4 and 5. For the source of data and the method of computation on which Figures 4 and 5 are based, the reader is referred to Reference 15. After accounting for the expenditure of heat in the above-mentioned processes, it is found that there is a finite amount of residual energy at any given time and place. This remaining part is termed as the energy available for transportation across the latitudinal circles, both by the atmosphere (sensible heat) and by the oceans.

By adding the radiation balance (Figure 3), the storages (Figure 4, land and atmosphere storages not shown), and the net latent heat, we obtain Figure 6 which shows the distribution of the

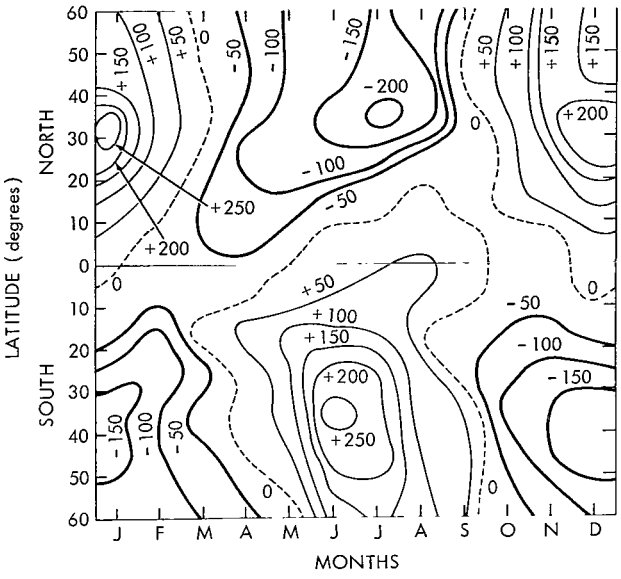


Figure 4—Latitude and time distribution of the storage of heat in the oceans in calories/cm² day; (-) heat gained, (+) heat released (Rasool and Prabhakara, Reference 15).

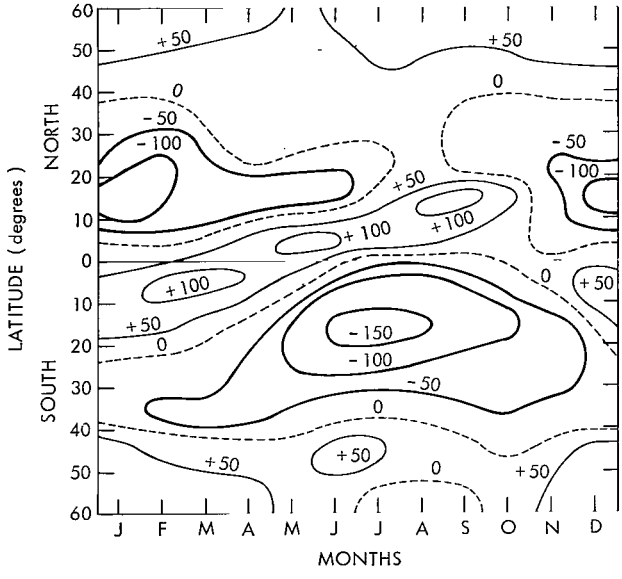


Figure 5—Latitude and time distribution of the net latent heat in the earth's atmosphere in calories/cm² day; (-) heat lost by the atmosphere by excess of evaporation over precipitation, (+) heat gained by the atmosphere by the excess of precipitation over evaporation (Rasool and Prabhakara, Reference 15).

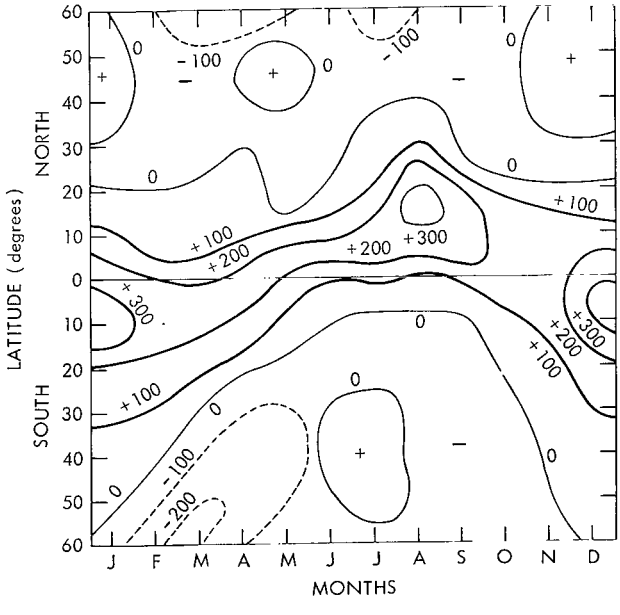


Figure 6—Latitude and time distribution of the net heat in calories/cm² day available for transport by the atmosphere and oceans across the latitude circles.

net heat available for transport. It seems difficult to comment on the accuracy of these quantitative estimates shown in Figure 6. These numbers result from differences of the three large quantities which inherently have some errors due to the various assumptions made in their evaluation. It is, nevertheless, hoped that the distribution of transportable heat shown in Figure 6 is physically meaningful and could be compared with some observed characteristics of the circulation in the atmosphere and oceans.

A large excess of heat in the equatorial latitudes almost throughout the year is indicated in Figure 6. The reason for this is the positive radiation balance (Figure 3) and positive net latent heat (Figure 5) arising from an excess of precipitation over evaporation at these latitudes. The ocean storage (Figure 4) in the equatorial regions is too small to influence the balance.

In February and March the maximum of this equatorial excess of heat occurs at 10 degrees S, while in July and August, following the thermal equator, the maximum moves to 15 degrees N.

In the subtropical and middle (20 - 40 degree) latitudes, the radiation balance (Figure 3) and net latent heat (Figure 5) appear to vary in phase with each other, being largest in summer and smallest in winter. On the other hand, the total heat storage in the oceans is equal in magnitude to the sum of radiation and the net latent heat, but has an opposite sign. Consequently, in the subtropical latitudes, there is little energy available for transport through most of the year. In the case of the northern hemisphere, Fritz (Reference 11) has already shown that between 20 - 40 degree latitudes, the atmosphere may be in radiative equilibrium throughout the year, in agreement with our results shown in Figure 6. Unlike the northern hemisphere, we find an anomalous feature of high negative values in the southern hemisphere at 40 - 50 degree latitudes in March, April and May. This is brought about by the circumstance that at these latitudes in the southern hemisphere, the ocean absorbs heat until the month of May (late fall) (Figure 4) when the radiation balance has already become highly negative. This results in a negative value for transportable heat.

## RESULTS

### Seasonal Variations in the Meridional Transport of Heat

The flux of heat transported across each latitudinal circle is derived from Figure 6 by assuming that the flux at the two poles is zero and adopting the values of heat transport given by Gabites (Reference 3) for 72 degrees S and 50 degrees S, respectively. The monthly values of the transportable heat shown in Figure 6 are averaged for three monthly periods and added algebraically for each season from 50 degrees S to 50 degrees N. The flux of heat across latitude circles is then derived and is shown in Figure 7 for the four seasons. For comparison purposes, we also give the recently published values of sensible heat transport given by Haines and Winston (Reference 21) for the 50 degrees N latitude. The actual values quoted by Haines and Winston were calculated for the atmospheric layer between 500 and 850 millibars. Winston (Reference 22) has suggested that there is a linear relation between the total atmospheric transport and the transport in this layer. The values plotted in Figure 7 are the adjusted values for the total atmosphere.

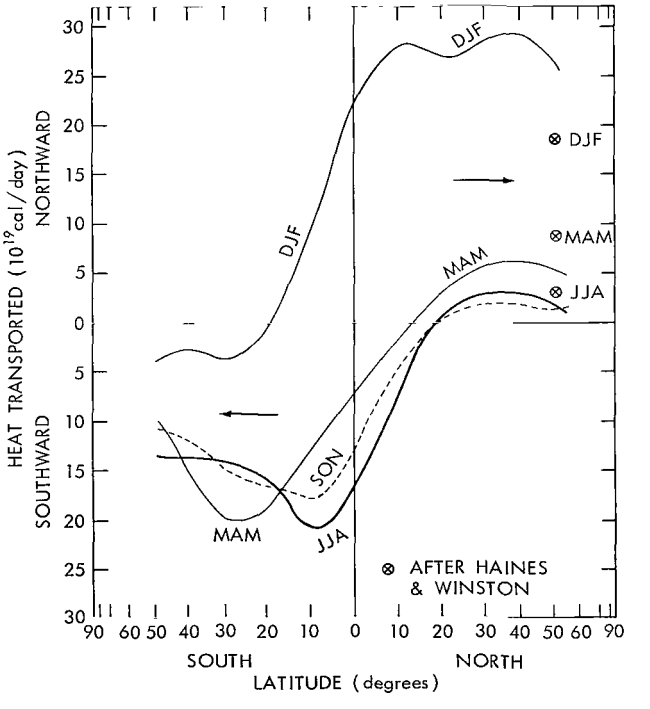


Figure 7—Three-monthly mean values of the meridional flux of heat in $10^{19}$ calories/day between 50°N and 50°S. The values are for the combined transport by ocean currents and the sensible heat in the atmosphere.

It is interesting to note that the northward transport of heat is extremely large in the months of December, January and February. For the rest of the nine months, the transport of heat is southward for all latitudes between 20 degrees N and 90 degrees S. The magnitude of the northward flux in the months of December, January and February is maximum at the latitude of 40 degrees N with a value of $\approx 30 \times 10^{19}$ calories/day. Also, there is a northward flux across the equator of $\approx 23 \times 10^{19}$ calories/day. For the remaining nine months, the southward flux maximum is fairly constant in magnitude, $\approx 20 \times 10^{19}$ calories/day, but the latitude of the maximum southward transport varies from 30 degrees S in March, April and May to 10 degrees S in June, July and August. The northward flux of sensible heat in the northern hemisphere is extremely small during these nine months.

## Annual

The mean annual transport of heat as a function of latitude is shown in Figure 8. It is noteworthy that on an annual basis the transport of heat by the atmosphere and oceans is much more intense in the southern hemisphere than in the northern hemisphere. Also, a southward flux across the equator of $4 \times 10^{19}$ calories/day is indicated. This flux of heat balances the net annual northward transport of latent heat of water vapor of $\approx 4 \times 10^{19}$ calories/day. This value is obtained by making a yearly average of the net latent heat from Figure 5 for the northern and southern hemispheres separately. There appears to be an excess of evaporation over precipitation in the southern hemisphere, implying a northward transport of water vapor.

We have plotted in Figure 9 a summary of the annual heat balance of the earth for the two hemispheres separately. These data are based on the Tiros VII measurements of outgoing and

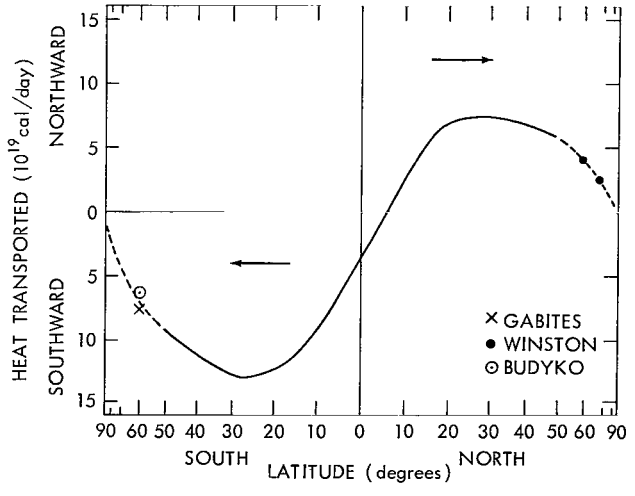


Figure 8—Mean annual poleward transport of heat as a function of latitude for the northern and southern hemispheres (in $10^{19}$ calories/day). Values for latitudes >50°N and S are taken from Gabites (Reference 3), Haines and Winston (Reference 20), and Budyko (Reference 22).

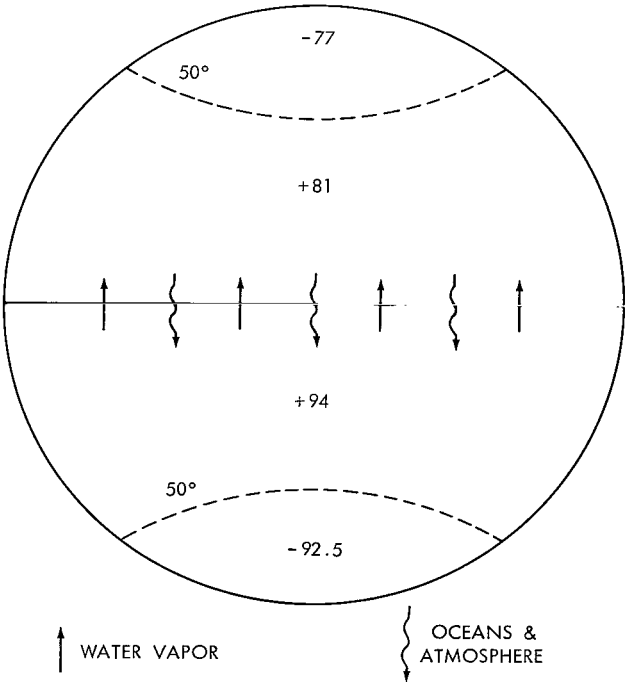


Figure 9—Heat balance of the earth in $10^{18}$ calories/day from Tiros VII. The radiation imbalance is shown. Compared to the magnitude of the total incoming and outgoing radiation on the order of $2000 \times 10^{18}$ calories/day, this imbalance is negligible.

incoming radiation for one full year, June 19, 1963 through June 7, 1964. It is assumed that on an annual basis the ocean storage and net latent heat values go to zero. The total net radiative balance of the globe between 50 degrees N and 50 degrees S is $+175 \times 10^{18}$ calories/day. In order for the whole globe to be in radiative balance with the space over one year, this amount of energy must be radiated back to space from the two polar regions (latitudes >50 degrees). Several estimates of the net radiative balance of the Arctic and Antarctic have recently become available. Independent analyses by Gabites (Reference 10) and London (Reference 2) give a concurrent value of $-55 \times 10^{18}$ calories/day for the annual radiative balance of the north polar latitudes (60 - 90 degrees N). In the case of the southern hemisphere, there is larger disagreement among the various estimates of radiative balance for latitudes >60 degrees S.

From the values given by Gabites, Rubin, and Kort (References 3, 4 and 5) we derive an average value of $-69.5 \times 10^{18}$ calories/day for the net radiative energy balance for latitudes between 60 and 90 degrees S. Combining these data for the two poles with the Tiros measured values for the area between 50 degrees N and 50 degrees S, and with Budyko and Kondratiev's estimates of the annual radiation balance of the latitude belts of 50 - 60 degrees N and S (Reference 24), we obtain the radiation balance values for the earth as shown in Figure 9.

It is encouraging to note that the combination of Tiros data which pertains to the major part of the globe ($\approx$76% of the total surface) with other reliable estimates of the radiation balance of the polar regions gives an almost zero radiation balance for the globe. The actual value derived from Figure 9 is $+5.5 \times 10^{18}$ calories/day which is a negligible amount when compared with values of the incoming and outgoing radiation which are of the order of $2000 \times 10^{18}$ calories/day. This indicates that, on an annual basis, both the hemispheres are in radiative balance, implying that the net transfer of heat across the equator is very small.

However, according to Palmén and Vuorela and Vuorela and Tuominen (References 25 and 26), the net transport of moisture across the equator in June, July and August is northward and amounts to $25.3 \times 10^{11}$ grams/second, while in December, January and February it is southward, but the flux is only $10.0 \times 10^{11}$ grams/second. If we assume that the combination of the summer and winter can give an estimate for the annual transport, we find a net northward transport in the form of latent heat of water vapor, of $73.8 \times 10^{18}$ calories/day. Our own computations of the latitudinal and monthly values of evaporation and precipitation for the two hemispheres indicate an excess of evaporation over precipitation in the southern hemisphere (0 - 50 degrees S) corresponding to a net latent heat deficit of $\approx 40 \times 10^{18}$ calories/day. This has to be compared with the estimate of Budyko who gives a net northward flux of $41 \times 10^{18}$ calories/day (Reference 23).

In order that the two hemispheres be in radiative balance, this northward flux should be compensated by a southward transport of heat by the oceans and atmosphere of $\approx 40 \times 10^{18}$ calories/day. Budyko has obtained similar results on the transport of heat across the equator. There is already a suggestion by Bryan (Reference 27) that there may be a net southward transport of heat across the equator by ocean currents, mainly in the Pacific and Indian Oceans. Our results tend to substantiate Bryan's suggestion and also indicate that this southward transport mainly takes place during the nine months of March through November (Figure 7).

It is hoped that these results on the meridional transport of heat, which are based on the actual observations of the radiative balance by meteorological satellites, can be usefully employed in the future to obtain a better understanding of the circulation of the atmosphere and oceans, particularly in the southern hemisphere.

## REFERENCES


1. Houghton, H. G., "On the Annual Heat Balance of the Northern Hemisphere," *J. Meteor.* 11(1):1-9, February 1954.

2. London, J., "A Study of the Atmospheric Heat Balance," Final Report, New York: New York University College of Engineering, AFCRC TR-57-287, AD-117 227, July 1957.

3. Gabites, J. F., "The Heat Balance of the Antarctic Through the Year," in: *Antarctic Meteorology; Proceedings of the Symposium Held in Melbourne Australia, February 1959,* New York: Pergamon Press, 1960, pp. 370-377.

4. Rubin, M. J., "Atmospheric Advection and the Antarctic Mass and Heat Budget," in: *Antarctic Research: Mathew Fontaine Maury Memorial Symposium, 10th Pacific Sci. Sympos. University of Hawaii, August 21 to September 6, 1961,* ed. by H. Wexler, M. J. Rubin, and J. E. Caskey, Jr., Washington, D. C., pp. 149-159. Also in: American Geophysical Union, National Research Council pub. 1036, 1962, and A.G.U. Mono. Number 7.

5. Kort, V. G., "On Heat Exchange of the Antarctic Waters," in: *Antarctic Research: Mathew Fontaine Maury Memorial Symposium, 10th Pacific Sci. Sympos., University of Hawaii, August 21 to September 6, 1961,* ed. by H. Wexler, M. J. Rubin, and J. E. Caskey, Jr., Washington, D. C., pp. 163-167. Also in: American Geophysical Union, National Research Council pub. 1036, 1962, and A.G.U. Mono. Number 7.

6. Danjon, A., "Nouvelles Recherches sur la Photometrie de la Lumiere Cendree et l'Albedo de la Terre," *Strasbourg Univ. Observat. Ann.* 3(3):139-180, (1936).

7. Fritz, S., "The Albedo of the Ground and Atmosphere" *Bull. Amer. Meteor. Soc.* 29(6):303-312, June 1948.

8. Angstrom, A., "Atmospheric Turbidity, Global Illumination and Planetary Albedo of the Earth," *Tellus,* 14(4):435-450, November 1962.

9. Simpson, G. C., "Distribution of Terrestrial Radiation," Roy. Meteorol. Soc. Mem. 3:53-78, April 1929.

10. Gabites, J. F., "Seasonal Variations in the Atmospheric Heat Balance," Ph.D. Thesis, Cambridge, Massachusetts: M.I.T. Press, 1950.

11. Fritz, S., "Seasonal Heat Storage in the Ocean and Heating of the Atmosphere," in: *Arch. Meteor., Geophys. Bioklimat.*, 10(4):291-300, 1958.

12. Bandeen, W. R., "Infrared and Reflected Solar Radiation Measurements from the Tiros II Meteorological Satellite," *J. Geophys. Res.* 66(10):3169-3185, October 1961

13. Astheimer, R. W., De Waard, R., and Jackson, E. A., "Infrared Radiometric Instruments on Tiros II," *Opt. Soc. Amer. J.* 51(12):1386-1393, December 1961.

14. "Tiros VII Radiation Data Catalog and Users' Manual," Goddard Space Flight Center, Greenbelt, Maryland Vol. 1, September 1964, Vol. 2, December 1964.

15. Rasool, S. I., and Prabhakara, C., "Radiation Studies from Meteorological Satellites," Geophysical Sciences Laboratory Report No. 65-1, New York: New York University, 1965.

16. Bandeen, W. R., "A Radiation Climatology in the Visible and Infrared from the Tiros Meteorological Satellites," NASA Technical Note D-2534, 1965.

17. Winston, J. S., and Krishna Rao, P., "Preliminary Study of Planetary-Scale Outgoing Longwave Radiation as Derived from Tiros II Measurements," *Month. Weath. Rev.* 90(8):307-310, January 1961.

18. Prabhakara, C., and Rasool, S. I., "Evaluation of Tiros Infrared Data," in: *Rocket and Satellite Meteorology; Proc. 1st Internat. Sympos., Washington, D. C., 1962,* ed. by H. Wexler and J. W. Caskey, Jr., Amsterdam: North-Holland Pub. Co., 1963, pp. 234-246.

19. Nordberg, W., Bandeen, W. R., Conrath, B. J., Kunde, V., and Persano, I., "Preliminary Results of Radiation Measurements from the Tiros III Meteorological Satellite," *J. Atmos. Sci.* 19(1):20-30, January 1962.

20. House, F., "The Radiation Balance of the Earth from a Satellite," Madison, Wisconsin: University of Wisconsin, Ph.D. Thesis, 1965.

21. Haines, D. A., and Winston, J. S., "Monthly Mean Values and Spatial Distribution of Meridional Transport of Sensible Heat," *Month. Weather Rev.* 91(7):319-328, July 1963.

22. Winston, J. S., "Preliminary Studies of Atmospheric Energy Parameters," Washington, D.C.: U. S. Weather Bureau, Meteorological Satellite Laboratory Report Number 3, 1961.

23. Budyko, M. I., "The Heat Balance of the Earth's Surface," Washington, D. C.: U. S. Department of Commerce, Weather Bureau, 1958; translated by Nina A. Stepanova.

24. Budyko, M. I., and Kondratiev, K. Y., "The Heat Balance of the Earth," in: *Research in Geophysics;* Vol. 2, Solid Earth and Interface Phenomena (ed. by H. Odishaw), Cambridge, Massachusetts: M.I.T. Press, 1964, pp. 529-554.

25. Palmen, E., and Vuorela, L. A., "On the Mean Meridional Circulation in the Northern Hemisphere during Winter Season," *Quart. J. Roy. Meterol. Soc.* 89(329):131-138, January 1963.

26. Vuorela, L. A., and Tuominen, I., "On the Mean Zonal and Meridional Circulations and the Flux of Moisture in the Northern Hemisphere during the Summer Season," *Pure and Applied Geophys.* 57:167-180, 1964.

27. Bryan, K., "Measurements of Meridional Heat Transport by Ocean Currents," *J. Geophys. Res.* 67(9):3403-3414, August 1962.

# SOME ENERGY IMPLICATIONS OF DIRECT MEASUREMENTS OF THERMOSPHERE STRUCTURE

by
N. W. Spencer and L. H. Brace
*Goddard Space Flight Center*

and

G. R. Carignan, D. R. Taeusch and H. Niemann
*University of Michigan*

Four rocket-borne ejectable instruments (called thermosphere probes), launched into the thermosphere above Wallops Island, have measured the concentration and temperature of molecular nitrogen and electrons under various atmospheric conditions during the period approaching solar minimum. A fixed-tuned omegatron mass spectrometer mounted within an orificed chamber was employed for the $N_2$ concentration measurements. The gas temperature was derived from the $N_2$ scale height, and in some cases measured directly by a velocity scan technique. Cylindrical and hemispherical Langmuir probes were employed for the electron temperature and density measurements. The four launchings were carried out in the afternoon, at sunset, at night, and during the July 20, 1963 solar eclipse. Calculations of energy deposition confirm earlier experimental and theoretical results which show that solar extreme ultraviolet is the major source of electron heating in the daytime F region. This is also clear from the factor of two reduction F region electron temperature during the eclipse. The heating observed in the E region can be explained only in part by solar X-rays, and appears to require an additional source such as an electric field. The gas temperatures agree well with the theoretical model temperature, but the measured $N_2$ concentrations are generally lower than model values by a factor of two. The day to night variation of the height of the thermopause, and its rapid fall and low temperature during the eclipse flight, suggests that the thermal conductivity of the thermosphere is greater than has been assumed. The flights revealed a temporal variation in $N_2$ concentration in the lower thermosphere (140 kilometers) which may be either diurnal or seasonal in nature. Assuming that these $N_2$ variations are related to temporal variations in the altitude of the effective diffusion level, this level must have been variable by about ±5 kilometers over all of the conditions existing at the times of these flights.

## INTRODUCTION

The thermosphere region of the earth's atmosphere is characterized by a mixture of gases, predominantly neutral particles, existing principally in thermal and diffusive equilibrium. A fraction of these particles, small in comparison with the neutrals but significant in terms of the

chemistry of the region, are electrons and ions resulting from the absorption of solar radiation by the parent gas. Although all the neutral species are generally believed to have the same temperature, this temperature is less than that of the electrons and, at the higher levels, less than that of the ions.

Quantitative determination of these temperatures, and of the density of the various neutral and charged species, permits a direct evaluation of the amount of energy deposited, through the ionization, and other processes, in the atmosphere. This paper briefly describes experiments and results which bear upon the question of energy deposition.

## THE EXPERIMENTS

Ideally, direct measurements of the concentration of the major gases, the electron temperature $(T_e)$ and density $(N_e)$, the ion temperature $(T_i)$, and the gas temperature $(T_g)$, are needed to permit an unambiguous computation of the energy deposited, Q. These facts are summarized in Equation 1:

$$Q = 1.34 \times 10^{-4} N_e \left[ N_e \left.\frac{dT_e}{dt}\right|_{+} + n(N_2) \left.\frac{dT_e}{dt}\right|_{N_2} + n(O) \left.\frac{dT_e}{dt}\right|_{O} + \cdots , \right] \tag{1}$$

where the cooling rates $\left.dT_e/dt\right|_{+, N_2, O, \cdots}$ are functions of $T_e$, $T_i$, $T_g$, $N_e$, as given by Dalgarno and McElroy, Reference 8.

Equation 2 employs a knowledge of the electron-to-ion and the ion-to-neutral cooling rates to permit computation of the ion temperature for use in Equation 1,

$$T_i - T_g = \frac{6 \times 10^6 N_e (T_e - T_i)}{n(O) T_e^{3/2}} \tag{2}$$

In the experiments discussed herein, it was possible to measure

$T_e$ - electron temperature,

$N_e$ - electron density,

$T_g$ - gas temperature,

and

$n(N_2)$ - concentration of molecular nitrogen.

The other values required for the computation, the concentrations of the neutrals, have been derived from model atmosphere values (Reference 1). It is important to note, however, that the measured values of the $N_2$ concentration and temperature were used to indicate selection of the proper model atmosphere, e.g., one appropriate to the conditions existing at the time of the measurement.

The electron density and temperature measurements were obtained through application of a Langmuir probe technique described in detail (Reference 2) and illustrated in Figure 1. The equipments provide a measurement system of two electrodes for immersion in the ionosphere, between which appropriate sweep voltages are applied. The resulting currents, and knowledge of the voltage difference, permit establishment of the volt-ampere relationship of the electrode system, which is determined by the electron temperature, ion density, and electron density of the region probed. Two variations of the Langmuir probe were employed for optimization of the desired measurements.

The molecular nitrogen concentration and temperature measurements were accomplished through use of a small omegatron mass spectrometer (Reference 3) fixed-tuned to mass 28, and employed in an orificed chamber as illustrated in Figure 1. Figure 2 shows that both Langmuir probes and the omegatron were housed

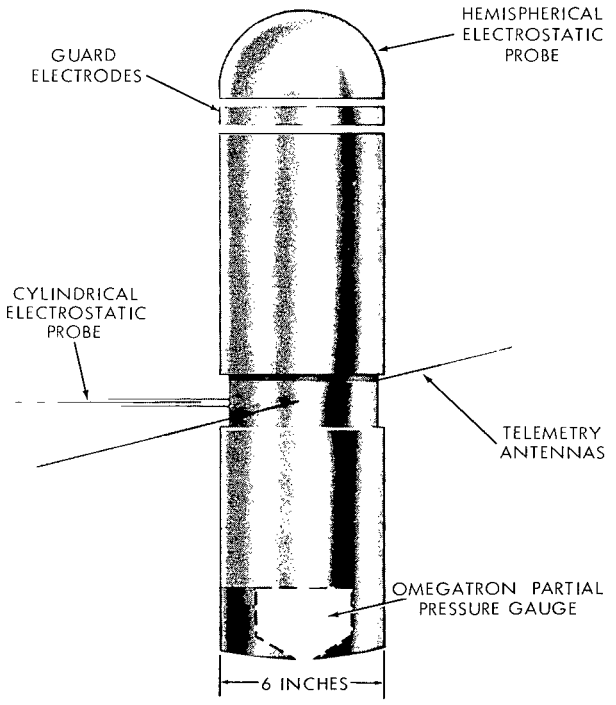


Figure 1—Thermosphere probe ejectable instrument employing an omegatron mass spectrometer for molecular nitrogen measurements and Langmuir probes for electron temperature and density measurements.

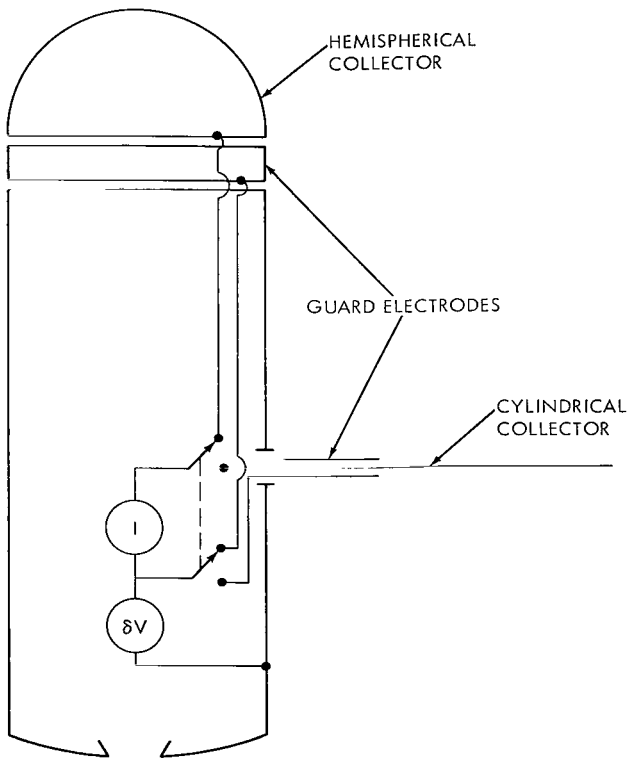


Figure 2—Electrostatic probe experimental arrangement.

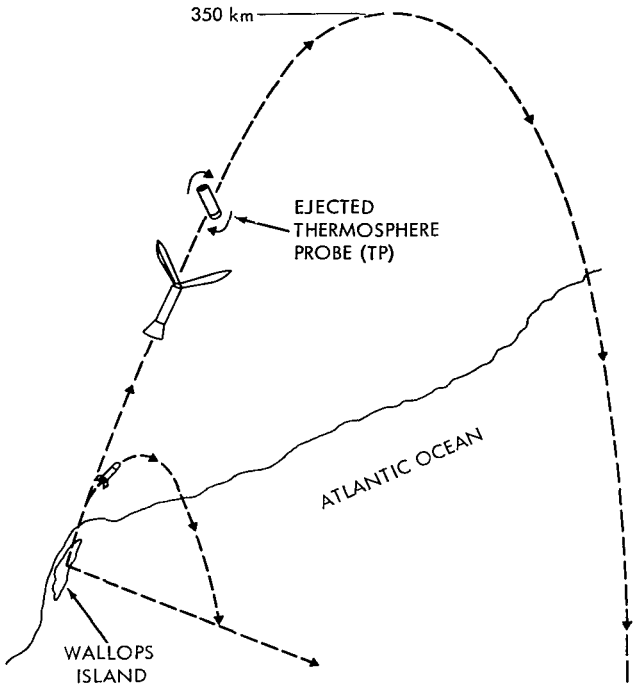


Figure 3—Typical flight geometry. At about 125 kilometers, the TP is ejected with a tumble period of 2 seconds and a separation velocity of about one meter per second. Measurements are made throughout ascent and descent.

Figure 4—A section of omegatron telemetry (labelled in terms of $N_2$ partial pressure) recorded during five consecutive tumble cycles as the TP descended through the atmosphere. The pressure variations were obtained on the second of eight linear ranges of the current detector employed by the omegatron experiment.

in a specially designed, vacuum-tight shell. The instrument, called a thermosphere probe, is ejected from the rocket nosecone into the ionosphere, and tumbled as depicted in Figure 3. The resulting $N_2$ chamber pressure variation is illustrated in Figure 4, which is a photographic reproduction of a portion of a typical telemetry record. From the maxima of such pressure variations, the ambient density is calculated with knowledge of the thermosphere probe trajectory and tumble plane orientation. Because the density of gas of a single mass is measured, the gas temperature can be readily computed from scale height considerations (Reference 2). A detailed discussion of the computational techniques employed for both the neutral particle and Langmuir probe experiment data is presented in References 2 and 4.

## RESULTS

A summary of the results obtained from several rocket experiments is presented in Figures 5 through 9 which show profiles of the various structural parameters, both measured and derived. Examination of the data reveal and confirm several interesting facts. Figure 5 shows density profiles from four flights which indicate a clearly lower density than the appropriate model values which are based on satellite drag data. This difference was also observed in direct measurements by Newton, Reference 4, and has not been explained to date. Various explanations have been suggested to explain the generally observed factor of two difference between drag derived and directly measured values; however, the explanations most commonly suggested are (a) calibration errors in the direct measurement data, and (b) incorrect drag coefficient assumption in the drag derived

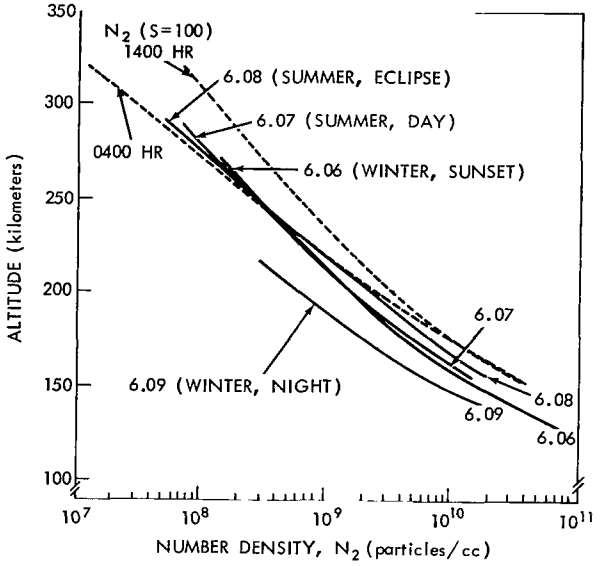


Figure 5—Composite $N_2$ concentration profiles from downlegs of all four TP flights, with extremes of diurnal variation given by Harris and Priester model.

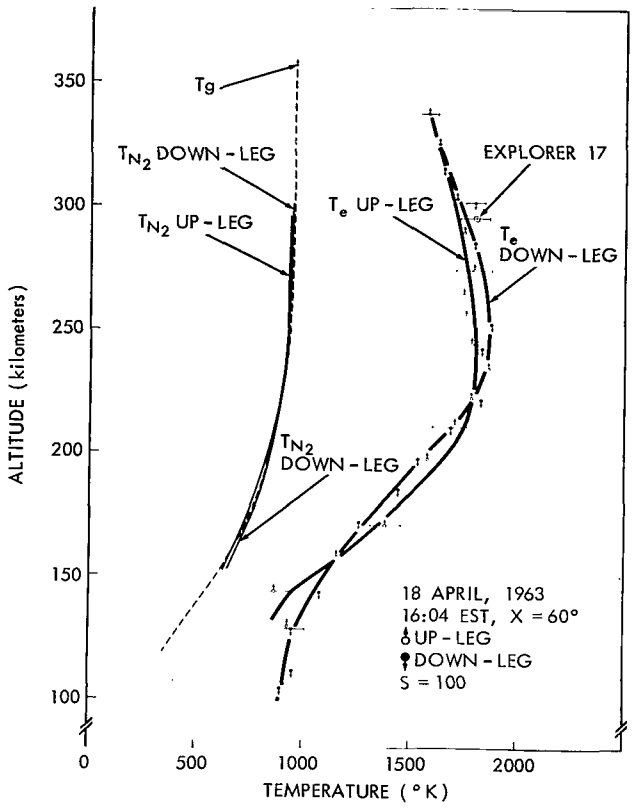


Figure 6—$T_{N_2}$ and $T_e$ measurements from NASA 6.07, with simultaneous Explorer XVII $T_e$ measurement and Harris and Priester model.

data. There appears to be ample evidence at this time to deny both possibilities.

The eclipse data (Figure 5) show a striking density decrease at the higher altitude (where eclipse totality was more nearly realized). This fact implies a very rapid decrease in the temperature at the lower altitudes during the brief (few minutes) eclipse time. This decrease seems unexpectedly rapid, although a rapid change of temperature has also been reported by Blamont (Reference 5), in reference to a measurement at Churchill.

Figure 6 presents $T_e$ and $T_{N_2}$ profiles demonstrating the elevation of electron temperature over neutral nitrogen temperature. The point labelled "Explorer 17" represents a simultaneous satellite measurement carried out very close (20 kilometers) to the rocket trajectory. Figure 7 shows composite $T_e$ profiles in comparison with day and night model gas temperatures. Clearly evident are three major points: (1) the maximum in $T_e$ increases in altitude after noon; (2) the electron temperature above 300 kilometers appears to converge upon a value of 1700°K, for daytime and non-eclipse conditions; and (3) the electron temperature during the night (or during eclipse) decreases significantly but remains higher than the gas temperature. This latter fact has been taken as evidence of nighttime energy deposition, but may, in part, reflect electron thermal conduction from much higher altitudes as proposed by Bowhill, Reference 6.

Figure 8 provides an example of an electron density measurement plotted with a simultaneously measured ionosonde electron density profile. Good agreement was obtained, and in addition,

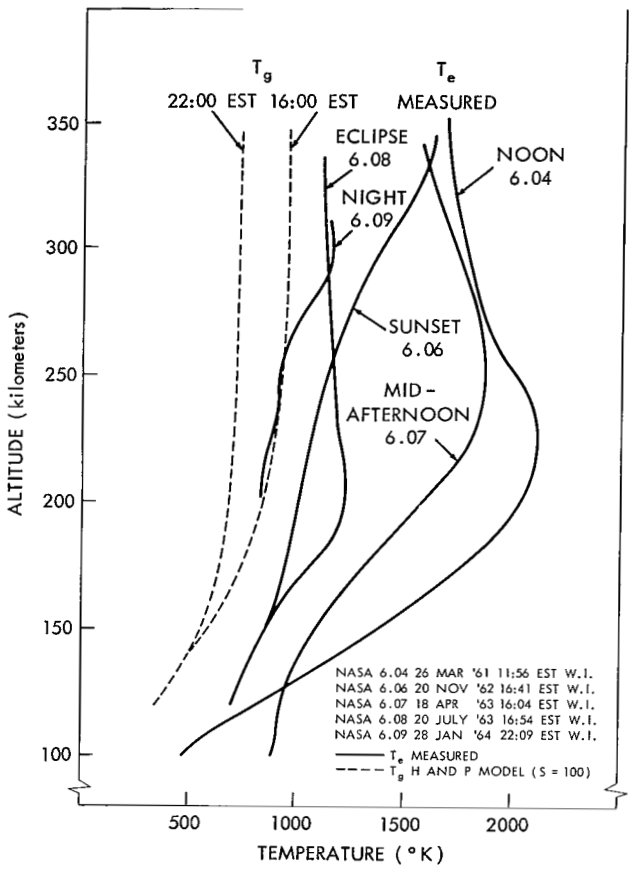


Figure 7—Composite $T_e$ profiles from downlegs of four TP and one Dumbbell flight demonstrating the variation in the altitude of the $T_e$ maximum. Model values of $T_g$ are shown for reference.

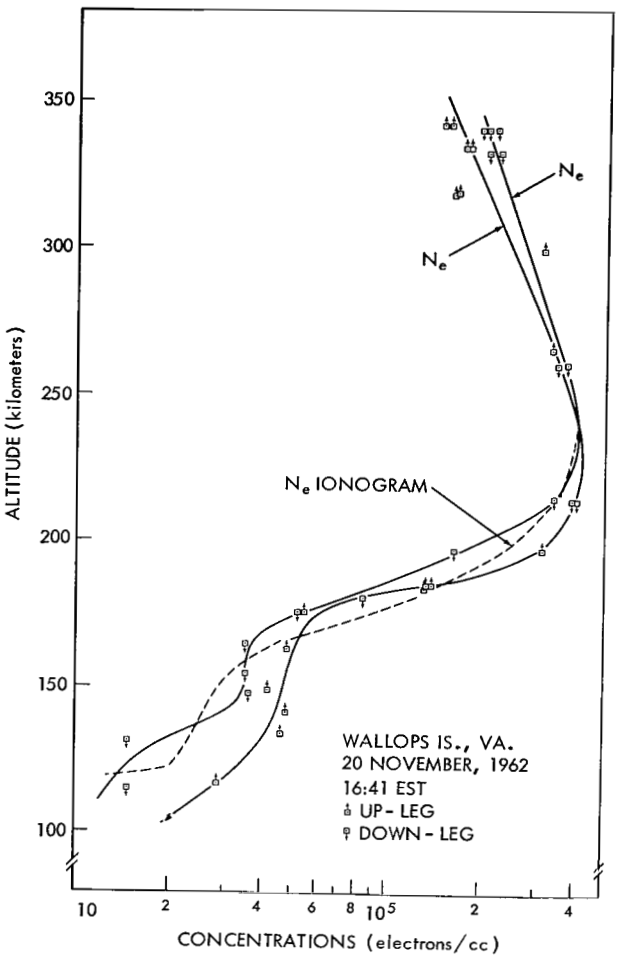


Figure 8—$N_e$ measurement from NASA 6.06 with ionosonde $N_e$ profile for time of launch.

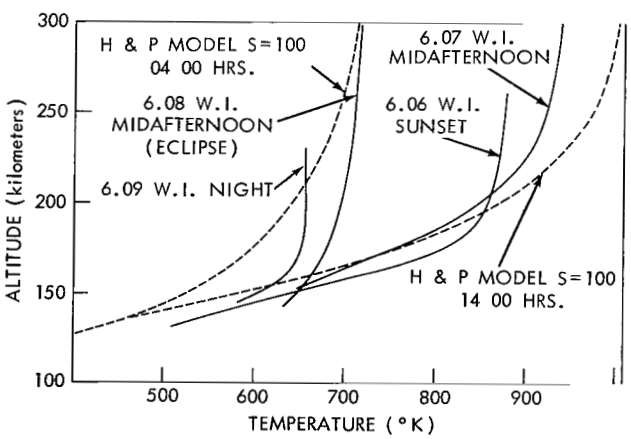


Figure 9—Composite $T_{N_2}$ profiles from downlegs of the four TP flights, with extremes of $T_g$ given by model.

topside densities for a height of 100 kilometers above the $F_2$ maximum were measured.

Figure 9 shows a summary plot of four neutral particle $(N_2)$ temperature profiles, which, at the higher altitudes, reflect the gross diurnal variation of exosphere temperature. Particularly striking is the fact that the temperature of neutrals decreased by about 200°K (6.07 curve assumed representative of a normal atmosphere) during the 85-percent eclipse. Comparison with model values of gas temperature reveals general agreement in all but the 150 to 200-kilometer region.

A word of caution is necessary with respect to the gas temperature during the eclipse. As noted above, the temperature is derived using scale height concepts which are based upon the assumption that the gas is in diffusive equilibrium. This may not be entirely appropriate during the clearly rapidly changing energy input conditions which prevailed during the eclipse. The temperature profile does, however, appear generally reasonable considering the rather unusual $N_2$ profile from which it was derived; and in the absence of a better understanding of the dynamic condition, the derived temperature profile has been accepted as essentially correct.

Figure 10 shows derived and theoretical values of the energy absorbed from solar euv and X-rays by the ionosphere electrons. Theoretical studies (Reference 7) indicate that this absorbed energy is rapidly exchanged among electrons by coulomb processes, and lost to the ions through coulomb collisions, and to neutrals by vibrational and rotational excitation of molecular nitrogen and electronic excitation of atomic oxygen. At the higher altitudes, because of the rapidly decreasing neutral density and slowly decreasing ion density, a larger share of the energy is lost to the ions gradually raising their temperature above that of the neutrals as suggested by Figure 6.

Figure 10 also shows predicted heating profiles (Reference 8) considering both solar extreme ultraviolet and X-rays for similar solar zenith angles. Comparison of the theoretical and experimental values, showing general agreement in both the magnitude and slope, confirm that solar euv is the predominant daytime source of electron heating. At the lower altitudes, the predicted energy falls rapidly, in contrast to the derived values which increase sharply. Thus, X-rays, which cannot penetrate to the E region significantly when the solar zenith angle nears 90°do not appear adequate to explain E region heating. It has been suggested, however, that E region heating of electrons may be related to electric field acceleration effects (Reference 9).

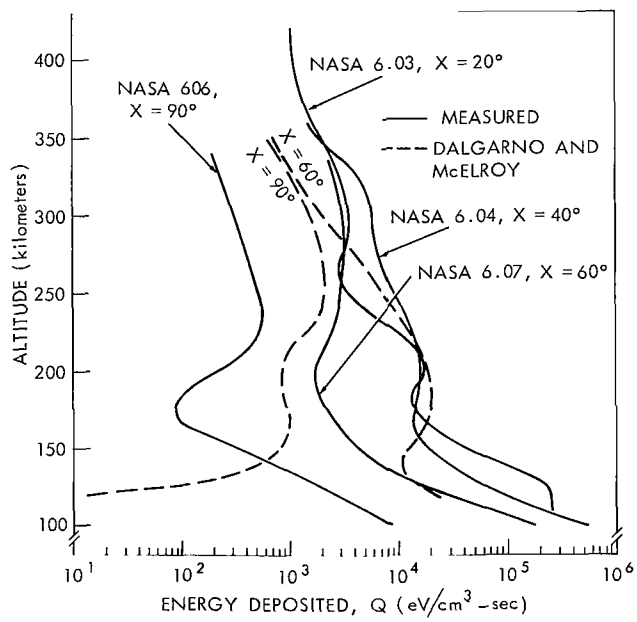


Figure 10—Comparison of experimental Q profiles with predicted profiles due to solar ultraviolet and X-ray.

## CONCLUSIONS

Measured values of electron temperature and density, molecular nitrogen temperature and density, and appropriate model values of the concentration of other neutral particle constituents have permitted the computation of energy deposited in the atmosphere due to photoionization by euv and X-rays. The results demonstrate that euv is the significant source of F region heating in the daytime, but that X-rays alone cannot explain E region heating.

Molecular nitrogen concentrations observed indicate that model values based on satellite drag studies are high by approximately a factor of two, whereas model temperature values corresponding to the times and conditions of the measurements are confirmed.

The observed decrease in electron and molecular nitrogen "scale height" temperature during a partial eclipse further supports the concept that euv is the predominant source of F region heating during the daytime.

## REFERENCES


1. Harris, I., and Priester, W., "Theoretical Models of the Solar-Cycle Variation of the Upper Atmosphere," *J. Geophys. Res.* 67(12):4585-4591, November 1962.

2. Spencer, N. W., Brace, L. H., Carignan, G. R., Taeusch, D. R., and Niemann, H., "Electron and Molecular Nitrogen Temperature and Density in the Thermosphere," *J. Geophys. Res.* 70(11):2665-2698, June 1, 1965.

3. Niemann, H., Kennedy, B. C., "Omegatron Mass Spectrometer for Partial Pressure Measurements in the Upper Atmosphere," (To be submitted to Rev. Sci. Inst.), 1965.

4. Newton, G. P., Horowitz, R., and Priester, W., "Explorer XVII Pressure Gage Data and Interpretation," to be published in *Planet. Space Sci.*, 1965.

5. Blamont, J. E., and Lory, M. L., "Sudden Heating of the Ionosphere in the Auroral Zone," *Nature*, 201(4919):593-595, February 8, 1964.

6. Geisler, J. E., and Bowhill, S. A., "An Investigation of Ionosphere-Protonosphere Coupling," Urbana, Illinois: University of Illinois Aeronomy Laboratory, Report Number 5, January 1965.

7. Dalgarno, A., McElroy, M. B., and Moffett, R. J., "Electron Temperature in the Ionosphere," *Planet. Space Sci.* 11(5):463-484, May 1963.

8. Dalgarno, A., McElroy, M. B., to be published in *Planet. Space Sci.*, 1965.

9. Megill, L. R., and Carleton, N. P., "Excitation by Local Electric Fields in the Aurora and Airglow," *J. Geophys. Res.* 69(1):101-122, January 1, 1964.

# LATITUDINAL VARIATIONS OF ELECTRON TEMPERATURE AND CONCENTRATION FROM SATELLITE PROBES

by
L. H. Brace and B. M. Reddy
*Goddard Space Flight Center*

Measurements of electron temperature $(T_e)$ and concentration $(N_e)$ have been made by the use of cylindrical electrostatic probes on the Explorer XXII (1964 64A) satellite, which was launched in October 1964. Since the satellite is an 80 degree inclination, nearly circular orbit at 1000 kilometers altitude, the latitudinal structure of the ionosphere is most easily determined. The measurements reveal a remarkable symmetry about the magnetic equator which suggests a strong degree of geomagnetic control. In the daytime a maximum of $N_e$ occurs at the equator ($\approx 3 - 4 \times 10^4$/cc), and $N_e$ decreases to a minimum at 50-60 degrees N and S magnetic latitude ($\approx 1 \times 10^4$/cc). In the daytime, $T_e$ varies somewhat inversely with $N_e$, reaching a maximum at 50-60 degrees ($\approx$3000°K), a maximum at the equator ($\approx$2400°K), and decreasing in the polar regions. At night, the equatorial maximum disappears and pronounced maxima develop at about 35-40 degrees latitude ($\approx 3 \times 10^4$/cc). A steep gradient at higher latitudes ends in a deep trough in the auroral zone ($\approx 10^3$/cc). The nighttime $T_e$ remains very low ($\approx$800°K) at low and middle latitudes but rises steeply near the auroral trough ($\approx$2500°K) and decreases at higher latitudes. The mean ion mass, inferred from the ion current measurements, suggest that $H^+$ is the dominant ion at the equator and $O^+$ predominates above 40 degrees magnetic latitude. Small scale fluctuations of the electron currents to the probes during some of the polar region measurements reveal fine irregularities in $N_e$ along the satellite path. These irregularities occur primarily in the midnight to sunrise period and have horizontal dimensions of only a few hundred meters and amplitudes of up to 30 percent. Nearly all occur poleward of the auroral zone.

## INTRODUCTION

On October 9, 1964, Explorer XXII, the ionosphere beacon satellite (References 1 and 2) was launched into an 80 degree inclination direct orbit which was nearly circular at an altitude of 1000 kilometers. The primary mission of the satellite was to permit radio propagation studies of the ionosphere on a global scale. The beacon experiment, radiating at 20, 40 and 41 megacycles, permits determination of the total electron content in the region between the satellite and an observing station on the ground. Knowledge of the electron density $(N_e)$ at the satellite is very useful in the interpretation of beacon data, and for this reason two cylindrical electrostatic probes

were employed to permit direct *in situ* measurements of the local plasma. It is the purpose of this paper to describe the probe experiment and to report some of the early results. No attempt will be made here to discuss the detailed implications of these results, since more intensive study of the data is required before this can be done.

## THE EXPERIMENT

The mounting position of the probes and the electrical system employed is shown in Figure 1. The satellite is stabilized by a passive magnetic system which causes the spin axis to remain aligned with the local geomagnetic field, somewhat like the needle of a compass. Thus, one end of the satellite always points generally northward and the other end points southward. To insure undisturbed measurements when the satellite is moving either north or south, one sensor was mounted on each end of the satellite, as shown.

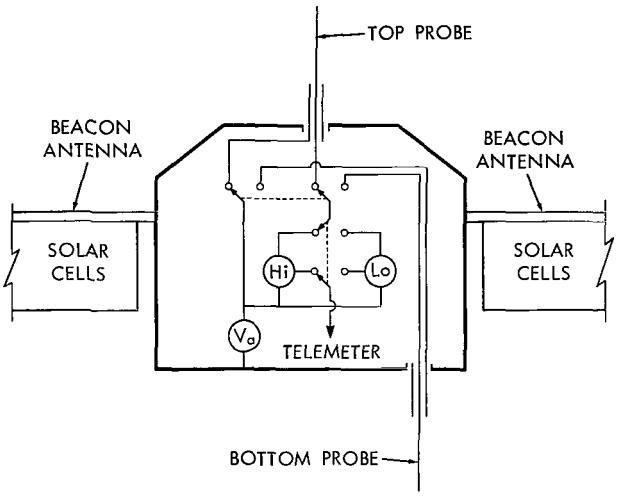


Figure 1—Block diagram of cylindrical electrostatic probe experiment on the Explorer XXII satellite. A sawtooth voltage ($V_a$) is applied to either of two collectors, and the resulting current from the plasma is measured by either of two linear response current detectors whose outputs are telemetered to Earth.

### The Experimental Arrangement

The experiment is essentially identical to that employed on the Explorer XVII satellite (Reference 3) and several rocket flights (Reference 4). In this application, a 2 cycles per second sawtooth voltage (-3 to +5 volts) is applied in series with either of two independent linear current detectors which are in turn connected alternately to each of the cylindrical probes. The sensor consists of a 5-inch guard electrode and 9-inch collector of 0.022 inches diameter. The guard prevents the collection of current in the region immediately adjacent to the spacecraft, and therefore avoids any possible related disturbance of the measurements. The collector dimensions are such that the probe operates in an orbital-motion-limited mode in which the simple Langmuir probe equations for a cylinder are applicable (Reference 5).

The net current to the collector is the sum of the ion and electron currents and in the sunlight, a small component of photoemission. When the collector is a few volts negative with respect to the plasma, the thermal electrons are entirely rejected and the probe is said to be ion saturated. The ion current to a stationary cylindrical probe is given by

$$I_i = AN_i e\left(kT_i/2\pi m_i\right)^{1/2} \cdot \frac{2}{\pi^{1/2}} \left(1 + eV/kT_i\right)^{1/2}, \quad \left(eV/kT_i > 2\right), \tag{1}$$

when

$I_i$ is the ion current,

A, the probe area,

$N_i$, the ion concentration,

e, the electron charge,

k, the Boltzmann constant,

$T_i$, the ion temperature,

$m_i$, the ion mass,

V, the potential of the probe relative to plasma.

In the ion saturation region, $eV/kT_i >> 1$, therefore Equation 1 reduces to

$$I_i = \frac{AN_i e}{\pi} (2eV/m_i)^{1/2} . \tag{2}$$

It is interesting to note that the slope of the ion saturation region depends upon $N_i/m_i^{1/2}$; i.e.,

$$dI_i/dV = \frac{Ae}{\pi} (e/2V)^{1/2} N_i/m_i^{1/2} , \tag{3}$$

when

$$\left| eV/kT_i \right| >> 1$$

so that, when the ion (or electron) concentration is known, the ion mass obtains from the slope of the ion current characteristic. It should be pointed out that the existence of a fixed component of photoemission will not affect the ion current slope.

A possible source of error in applying Equations 2 and 3 to satellite probe data is the high translational velocity of the probe with respect to the plasma. The stationary probe equations are most applicable when the ion thermal velocity is comparable to or greater than the translational velocity and this is true only for $He^+$ and $H^+$. Until further study of the effects of velocity upon ion current are carried out, the slope of $I_i$ should be regarded only as an indication of ion mass. Future use of this experiment along with high resolution ion mass spectrometers on the same spacecraft is expected to provide the best evidence for understanding the effects of velocity on the ion current slope.

At the other extreme of the applied voltage sweep, when the probe is driven positive with respect to the plasma such that it attracts electrons, it is said to be electron saturated, and the saturation equation again applies

$$I_e = \frac{AN_e e}{\pi} (2eV/m_e)^{1/2} , \tag{4}$$

when

$$\left| eV/kT_e \right| >> 1 \ .$$

Equation 4 is the primary means by which the electron concentration, $N_e$, is derived from volt-ampere characteristics. Between the ion and electron saturation regions lies the electron retardation region which is employed for the measurement of electron temperature $T_e$. In this region $I_e$ is given by

$$I_e = AN_e e\left(kT_e/2\pi m_e\right)^{1/2} \exp\left(eV/kT_e\right) \ , \tag{5}$$

when $V < 0$ and $T_e$ is given by

$$T_e = -\frac{e}{k}\frac{dV}{d\left(\ell n I_e\right)} \ . \tag{6}$$

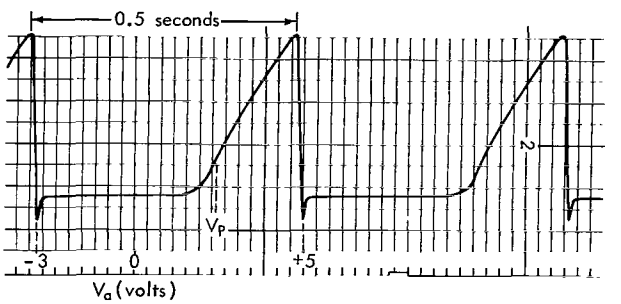


Figure 2—Photo of one second of telemetry record showing a pair of volt-ampere characteristics from which $N_e$, $T_e$ and $m_i$ are derived. The high current detector (0.3 $\mu$a full scale) was employed.

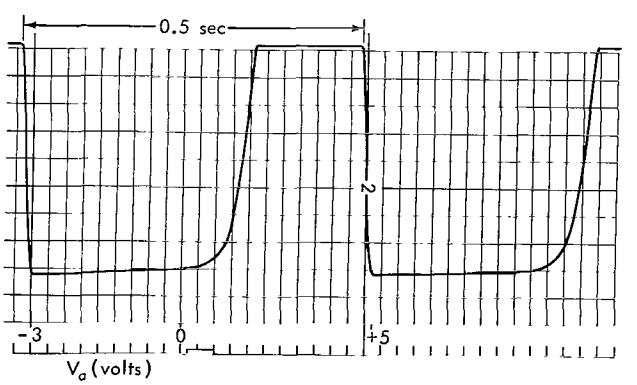


Figure 3—Photo of one second of telemetry record for the same burst of data as shown in Figure 2, but employing the low current detector (0.05 $\mu$a full scale).

A photograph of a one-second segment of telemetry record (Figure 2) shows a pair of volt-ampere curves measured at moderate temperature and concentration. The plasma potential ($V_p$), from which the probe potential is measured, is identified as the inflection point of the curve. At the far left of each curve is the ion saturation region which establishes the reference level from which $I_e$ is measured and which permits $m_i$ to be derived. Immediately to the left of $V_p$ is the exponential electron retardation region from which $T_e$ is derived. To the right is the electron saturation region which permits $N_e$ to be measured.

The average electron concentration at 1000 kilometers provides an ion current too small to be resolved with the high current detector, therefore little slope is visible to the ion saturation regions of Figure 2. Figure 3 shows a pair of curves recorded only five seconds later in the same pass and employing the low current detector. This higher sensitivity detector permits the ion slope to be measured and also provides increased resolution of the electron retardation region which is needed for $T_e$ measurements when $N_e$ is low.

The sensitivities employed permit resolution of the electron saturation region in the density range $1 \times 10^2 < N_e < 3 \times 10^4$/cc, which was expected to encompass the variations encountered in a 1000-kilometer circular polar orbit. However, $N_e$ sometimes exceeds $3 \times 10^4$/cc, and much of the electron saturation region exceeds full scale and is lost. In these cases, $N_e$ is derived using Equation 5 and the electron current at the plasma potential, which is only about 20 percent of the current at the maximum positive voltage. However, this alternate method is somewhat less accurate than the electron saturation method because of the steepness of the electron current characteristic near $V_p$ and a ±0.1-volt uncertainty in the identification of $V_p$. The resulting error in $N_e$ for such cases may be as much as 20 percent. The same uncertainty in identifying $V_p$ causes less than 5 percent error in the saturation method which is employed when $N_e < 3 \times 10^4$/cc.

### The Measurement Sequence

The entire measurement sequence in which each probe is connected alternately to each detector requires 10 seconds and is repeated twice during each operation of the experiment. To conserve power and telemetry capacity, an automatic programmer in the spacecraft energizes the experiment every three minutes continuously throughout the lifetime of the satellite. Thus, each pass of the satellite consists of several short bursts of probe data, transmitted at about 1200-kilometer intervals along the orbit. Figure 4 is a photo of a section of telemetry record showing several seconds of raw data from a single burst which helps illustrate the data sampling sequence. Each series of measurements begins with an inflight current calibration which is obtained by the substitution of appropriate resistances in place of the probes. A calibration occurs automatically every five seconds as the alternate detector is placed in the measurement circuit. Following calibration, the detector is connected first to one probe and then to the other, a transition normally accompanied by a small switching transient visible in Figure 4. In this case, the 0.3 $\mu$a detector would be employed for $N_e$ and the 0.05 $\mu$a detector would provide $T_e$ and $m_i$ measurements.

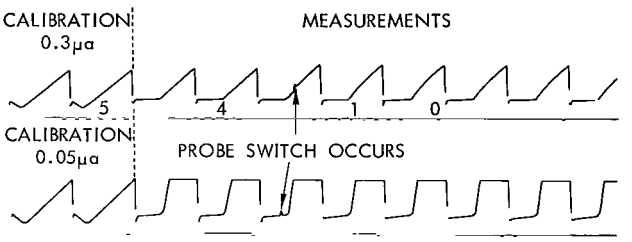


Figure 4—Photo of telemetry record showing 10 seconds of raw electrostatic probe data representing one full sampling cycle in which each probe is connected to each detector, following an inflight current calibration. The electron concentration here was approximately $1 \times 10^4$/cc.

## THE RESULTS

At the time of this writing $N_e$ and $T_e$ have been derived for about 400 passes (approximately 1600 bursts) of Explorer XXII data which have occurred between October 10, 1964 and January 7, 1965. These data represent a wide range of latitude, longitude and local time and are generally descriptive of the ionosphere at an altitude of approximately 1000 kilometers, in northern winter. Data were recorded at the following NASA STADAN stations:

Blossom Point, Maryland
Fort Myers, Florida
Newfoundland
Grand Forks, North Dakota

| | |
|---|---|
| College, Alaska | Mojave, California |
| Quito, Equador | Lima, Peru |
| Santiago, Chile | Winkfield, England |
| Johannesburg, South Africa | Woomera, Australia |

The polar orbit, and its near circularity, makes the latitudinal structure particularly evident in the resulting measurements. For this reason we have plotted the data as a function of geomagnetic latitude. The behavior of the ionosphere with respect to other variables then appears largely as differences in the latitudinal structure. To minimize the effects of local time, we have plotted only the data corresponding to the relatively stable periods following local noon and midnight.

## Actual Data Points

The $N_e$ and $T_e$ data points from all longitudes for the period 0000-0330 hours in November and December of 1964 are shown in Figures 5 and 6. The individual points from a particular pass are joined by lines to approximate the instantaneous latitudinal structure existing during the pass and

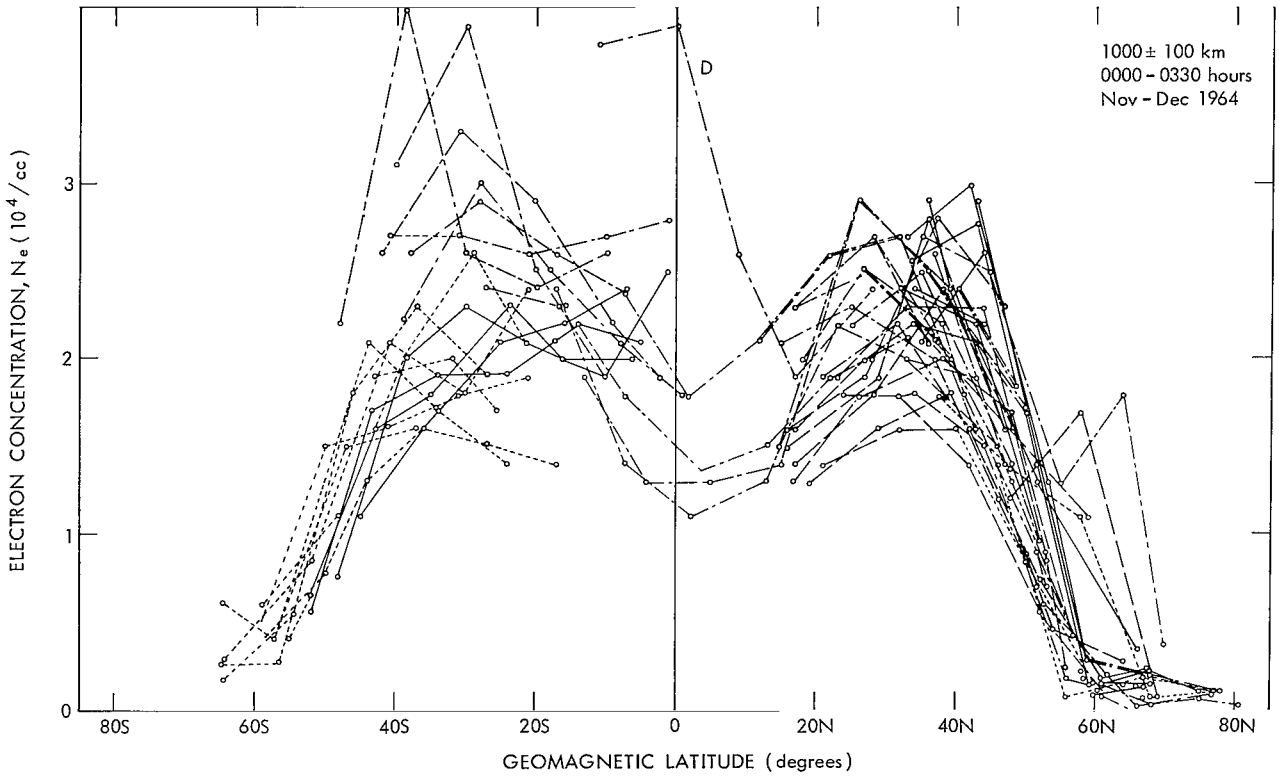


Figure 5—Raw values of $N_e$ in the post midnight period at all available longitudes. The individual points from single passes are joined by lines to approximate the instantaneous latitudinal profile they represent. The various passes, coded by longitude as discussed in the text, show strong longitudinal dependence superposed on the larger latitudinal variations in $N_e$. The pass labelled D corresponds to a magnetically disturbed day.

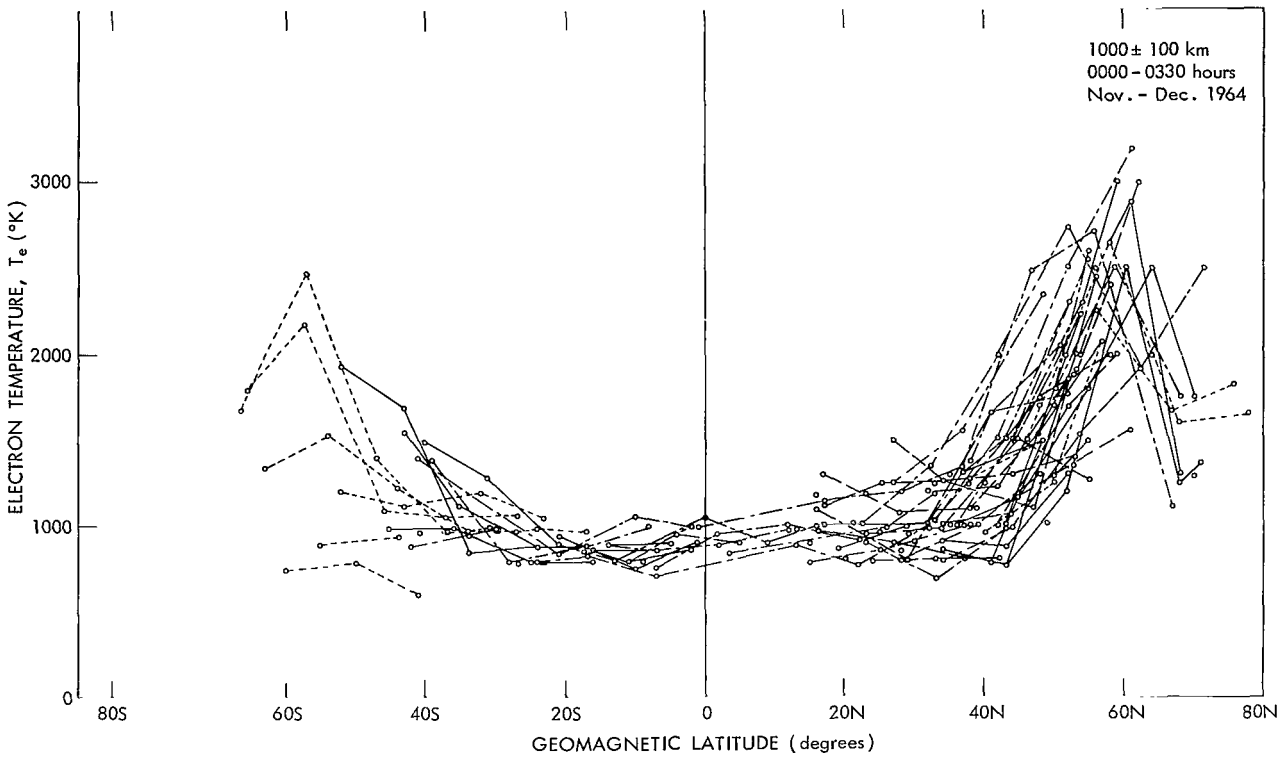


Figure 6—Raw values of $T_e$ for same nighttime passes as employed for $N_e$ data in Figure 5.

to identify the points as belonging to particular passes. The long and short dashes represent data from the stations along the 75th meridian (50-100°W), and only at these longitudes was it possible to obtain complete pole to pole coverage. The short dashed lines represent Woomera and some of the College passes (110-150°E), and the solid lines represent Johannesburg and Winkfield passes (50°E-50°W). Finally, the long dashes represent data from the western U. S. and Canada recorded at Mojave and College (100-130°W). The ionospheric $N_e$ structure in this range of longitudes was sufficiently different from that of the 75th meridian to warrant plotting it separately. It should be stressed that this particular means of sorting the data by longitude arises not so much from the characteristics of the ionosphere but more from the geographic distribution of the various STADAN stations which recorded the data. Indeed most of the spread in $N_e$ within each of the stated ranges remains longitudinal in origin. In at least one pass (labelled D), deviations have been correlated with high values of the 3-hour magnetic index $a_p$. In this case, the disturbance was associated with an enhancement of $N_e$ in the equatorial region.

## Gross Latitudinal Structure

Plots similar to Figures 5 and 6 have also been prepared for the daytime data (1200-1530 hours) in November and December of 1964. Figures 7, 8, 9 and 10 summarize the gross latitudinal structure of the ionosphere both day and night at the selected longitudes. These graphs generally outline

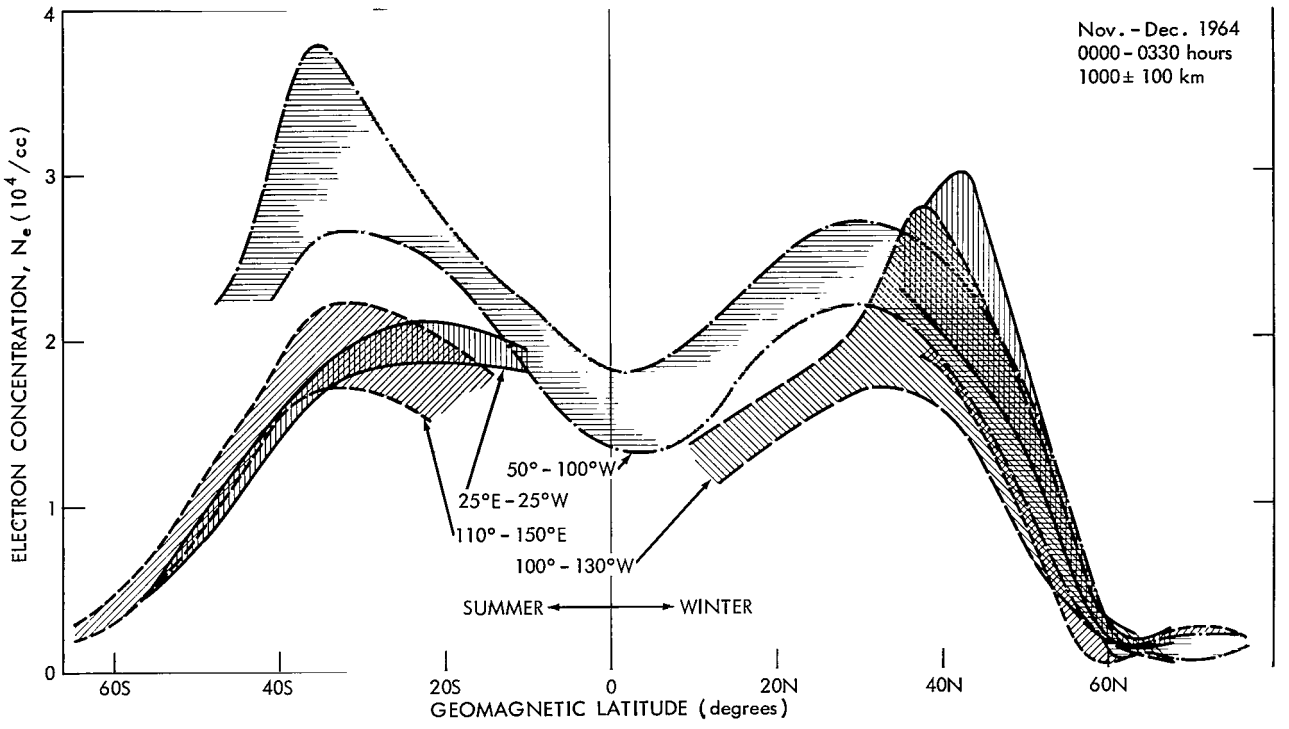


Figure 7—Gross latitudinal distribution of electrons in the nighttime ionosphere. The shaded areas represent the range of $N_e$ in the given longitude ranges.

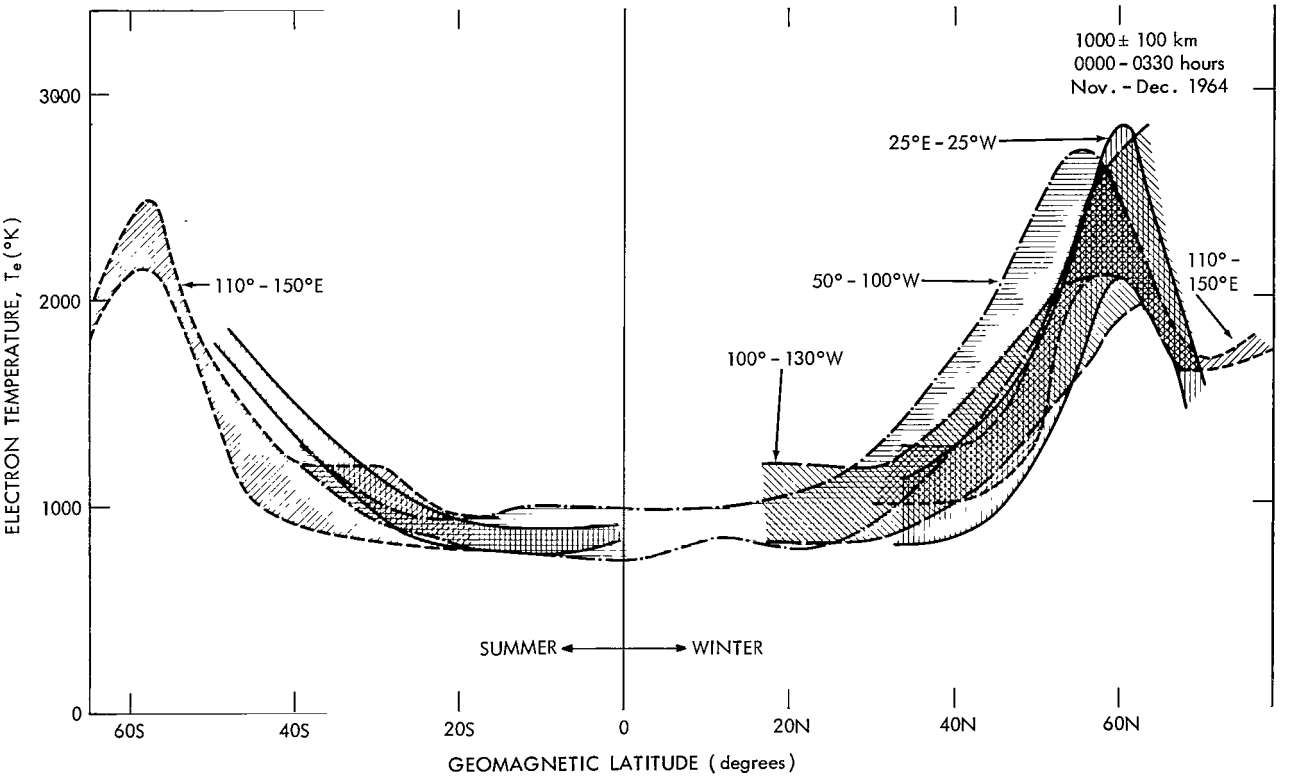


Figure 8—Gross distribution of $T_e$ in the nighttime ionosphere.

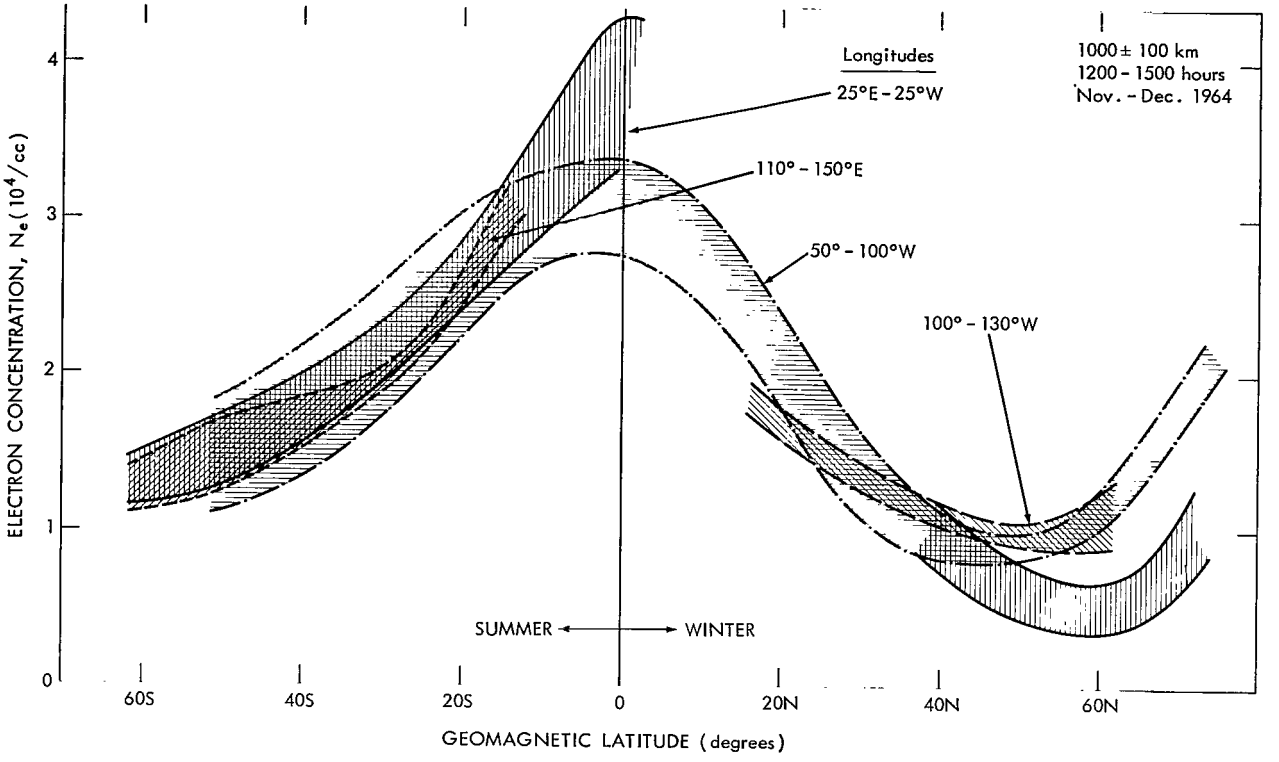


Figure 9—Gross distribution of $N_e$ in the daytime ionosphere.

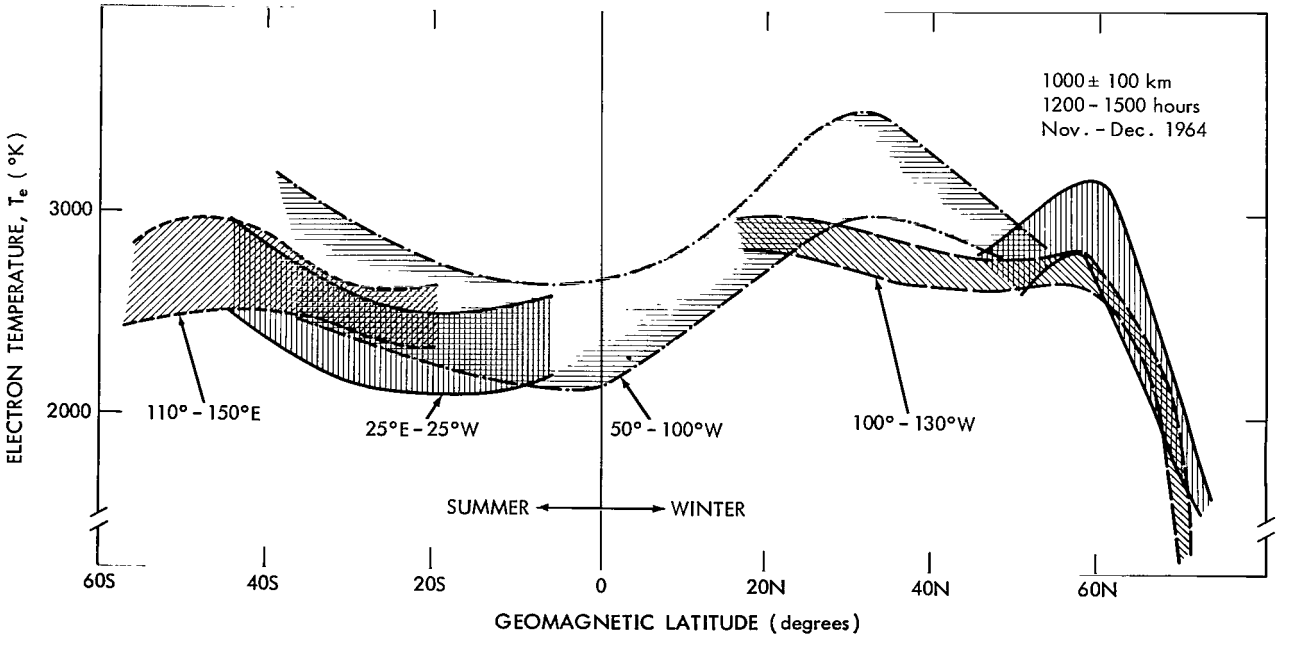


Figure 10—Gross distribution of $T_e$ in the daytime ionosphere.

the extremes of $N_e$ and $T_e$ found in the given longitude ranges and are intended primarily to convey the predominant features of the ionosphere at 1000 ± 100 kilometers during this period.

## The Mean Ion Mass

The ion mass $m_i$ derived from the slope of the ion saturation curves with the associated standard deviations of the values is shown in Figure 11. Since the nighttime $N_e$ is too low to permit the slope to be determined at all latitudes, Figure 11 represents only daytime data. Similar, but preliminary, results have been obtained at midlatitudes at night however.

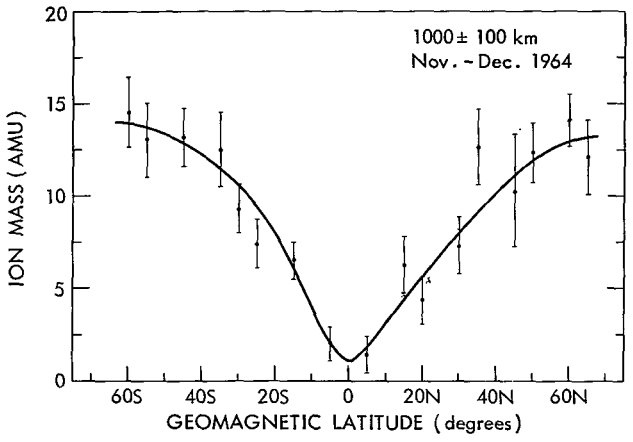


Figure 11—The mean ion mass (AMU) inferred from the slopes of the ion saturation regions of the daytime data.

## Local Time Behavoir of $T_e$ and $N_e$

Although data for a half rotation of the orbit plane (3 months) are not yet analyzed for all stations, it has been possible to analyze enough data to outline the diurnal behavior of the ionosphere at a few locations. The diurnal variation of $T_e$ at midlatitudes near the 75th meridian is given in Figure 12. Most of the spread in the data arises from the wide longitude window employed to obtain sufficient point density. Figure 13 shows, in addition, the corresponding variation of $N_e$. Note that at midlatitudes, the nighttime electron concentration exceeds that found during the day. Figure 14 indicates the corresponding diurnal variation of $T_e$ near the 75th meridian in the northern and southern midlatitudes and at the equator.

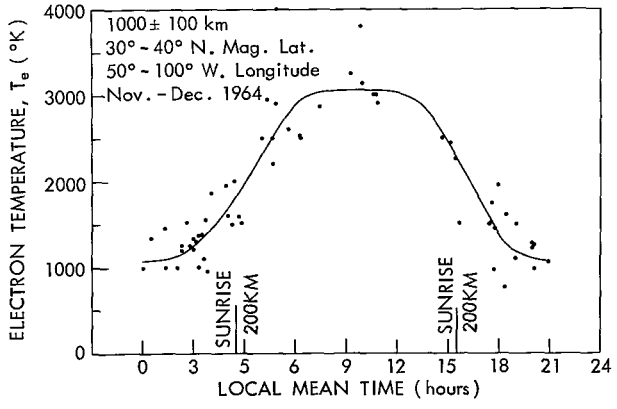


Figure 12—The diurnal variation of $T_e$ at northern midlatitudes.

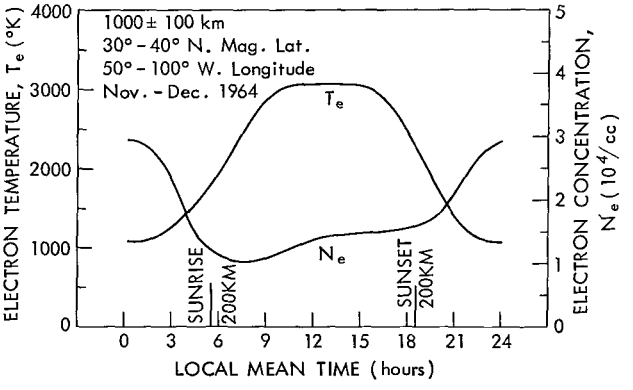


Figure 13—The diurnal variation of $N_e$ and $T_e$ at northern midlatitudes.

## Longitudinal Behavoir

Although the ionosphere at the 1000-kilometer level appears to reflect primarily local time and latitudinal variations, longitudinal variability is also strong in some regions of the globe. The greatest effect is in the 25 degree E - 25 degree W zone where both an equatorial enhancement and a high latitude deficiency are characteristic of the daytime ionosphere. Note that this is in the region just east of the Brazilian magnetic anomaly.

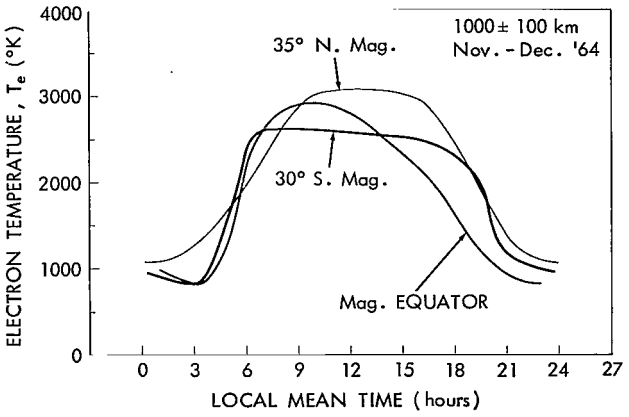


Figure 14—The diurnal variation of $T_e$ at midlatitudes and at the equator at the 75th meridian.

A second longitudinal irregularity occurs at night in the 50 - 100 degree W zone where the southern hemisphere nocturnal maximum is enhanced by nearly a factor of two, and its northern counterpart is depressed and occurs at a somewhat lower latitude. Note that this region is at the western edge of the Brazilian anomaly. It seems probable that these longitudinal irregularities are related to the distortion of the earth's magnetic field in the region of the anomaly and its conjugate.

## Small Scale Irregularities

On many occasions when the satellite was north of the auroral zone, the volt-ampere characteristics exhibited rapid fluctuations of the nature shown in Figure 15. When these small scale current variations occurred, they were visible on both detectors and probes. Since the normal operation of the measurement and telemetry systems is evident from the smoothness of the inflight current calibrations, these fluctuations can only be attributed to small scale variations in $N_e$ along the orbit of the satellite. The horizontal dimensions of these irregularities are of the order of 300 meters and the magnitude may be as great as 30 percent. Figure 16 shows the locations of these occurrences. They are normally found on more than one burst when present at all. With a few exceptions, the irregularities occur above the auroral zone and present statistics suggest that they exist in about 10 percent of the passes, with a strong preference for the early morning hours (0000-0600). There appears to be little correlation with magnetic disturbances which were few during this period.

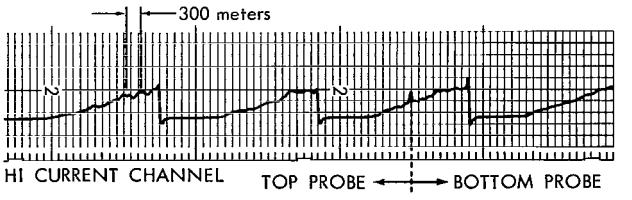


Figure 15—Volt-ampere characteristics exhibiting rapid fluctuations of $N_e$ along the orbital path. Typical fluctuations are 100's of meters in dimension and have magnitudes of up to 30 percent.

## DISCUSSION OF RESULTS

The data reveal that the global structure of the ionosphere at 1000 kilometers exhibits a high degree of variability with respect to latitude, longitude and local time.

### The Electron Concentration

At midday (Figure 9), $N_e$ exhibits a strong maximum at the magnetic equator, a result which is consistent with the Alouette topside sounder data (Lockwood and Nelms, Reference 6). A general decrease in $N_e$ with increasing latitude extends to a minimum at 60 degrees N and S latitude where $N_e$ is about one third its equatorial value.

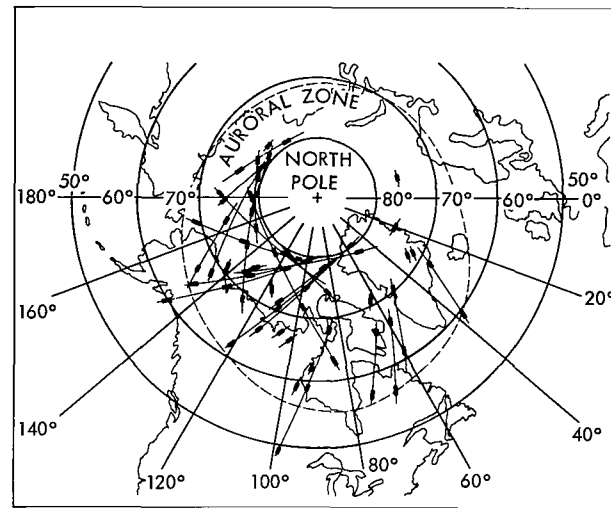


Figure 16—Locations of small scale irregularities. Nearly all occur poleward of the auroral zone and in the early morning hours

At night (Figure 7), the equatorial maximum has given way to a pair of midlatitude maxima at 35 degrees N and 35 degrees S. The value of $N_e$ at the equatorial trough is about one half of that at the maximum. This is not unlike the pattern shown by the Ariel satellite measurement of $N_e$ for this altitude during northern summer of 1962 (Sayers, Reference 7). This may therefore be a permanent feature of the nocturnal ionosphere.

These maxima observed at 35 degrees latitude may be the nighttime counterpart of the equatorial anomaly present in the daytime at lower altitudes (Goldberg and Schmerling, Reference 8). King* has pointed out that the $f_0 F_2$ data from ground-based sounders show a general poleward movement of the maxima, which constitute the anomaly, through the afternoon and evening. Since the double maximum in the daytime anomaly has merged into a single maximum at the altitude of the Explorer XXII observations, we are unable to trace this poleward motion through the day. Instead, the maxima which we observe at 1000 kilometers seem to emerge in their equilibrium position near 35 degrees latitude within a few hours after sunset.

Attempts to explain behavior of the daytime equatorial anomaly have been based on production and diffusion processes in the F region. The identification of this anomaly as a major feature at night at higher altitudes suggests rather that the source of particles is in the protonosphere above the equator. Indeed, the daytime equatorial maximum at 1000 kilometers (Figure 9) assures a huge reservoir of electrons at higher altitudes in the protonosphere. At night this reservoir has nearly disappeared (Figure 7), and there seems little doubt that these electrons have diffused downward along the magnetic field lines to form the midlatitude maxima which are observed.

*King, J. W., Radio and Space Research Station, Slough, England.

At higher latitudes an extraordinarily steep gradient reduces the concentration by nearly two orders of magnitude in less than 20 degrees of latitude. The resulting minimum at 60 degrees North, evident also in Alouette data has been called the "auroral trough" (Muldrew*). This also seems to be a permanent feature of the ionosphere, but is most discernible at night. The fact that the trough occurs at a magnetic latitude of 60 degrees leads one to suspect that this is the same phenomena which produces the "knee whistlers" observed by Carpenter (Reference 9) near magnetic invariant L = 4. The polar cliff, an enhancement north of the auroral trough noted by Muldrew does not seem to be present at all longitudes (Figure 5).

The high degree of symmetry about the magnetic equator which is evident in these $N_e$ data makes it clear that the magnetic field of the earth exercises strong control over the global distribution of electrons, as has been evident to some degree from previous satellite data (References 3, 7 and 10), though the global structure has not been displayed quite so clearly before. The approximate circularity of the orbit combined with its near polar nature, which is a highly advantageous feature of the Explorer XXII, enables a transparent latitudinal exposition of the ionospheric parameters measured without much reduction of the data.

It is interesting that the geomagnetic symmetry remains strong in spite of the extreme declination of the sun which was near the winter solstice during this period. Only a moderate seasonal asymmetry is evident at midlatitudes where $N_e$ is about a factor of two larger in the summer hemisphere.

## The Electron Temperature

A similar and undoubtedly closely related magnetic control is evident in the global distribution of electron temperature. At midday, $T_e$ exhibits broad maxima at 40-50 degrees latitude and a shallow minimum at the equator, variations which are generally inversely related to the variations in $N_e$. This is demonstrated best in Figure 17 which shows the daytime latitudinal behavior of the ionosphere averaged over all longitudes.

At night, the inverse relationship between electron temperature and concentration is limited to the higher latitudes as summarized in Figure 18. Because of the near vertical nature of the magnetic field lines at high latitudes, one expects the same general behavior at lower altitudes also. Explorer XVII data at College, Alaska, indeed show elevated electron temperatures accompanied by depressed electron concentrations in the $F_2$ region (Reference 3), and this is strong evidence for a nocturnal heat source there.

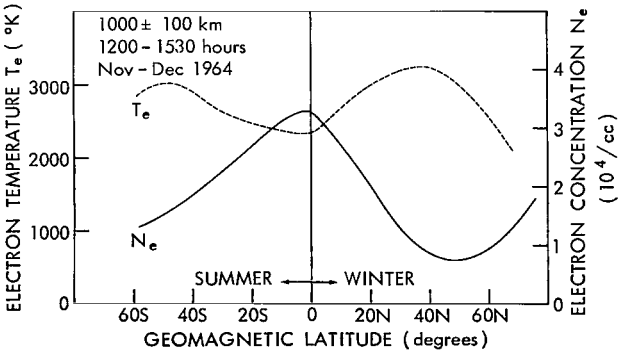


Figure 17—Midday values of $T_e$ and $N_e$, averaged from data at all longitudes.

*Muldrew, D. B., Defense Radio Telecommunications Establishment, Ottawa, Canada.

## Heat Sources

Solar ultraviolet radiation as predicted by References 11 and 12 produces photoelectrons which heat the ambient thermal electrons which in turn conduct their excess energy to neutral particles. In the $F_1$ region and below, the electrons are cooled primarily by their frequent collisions with neutral particles. Near the $F_2$ maximum, the neutral particle concentration is sufficiently low, so that electron cooling to the ions predominates. Geisler and Bowhill (Reference 13) have shown that, in the upper F region and exosphere, heat conduction to lower altitudes within the electron gas predominates the local heat loss.

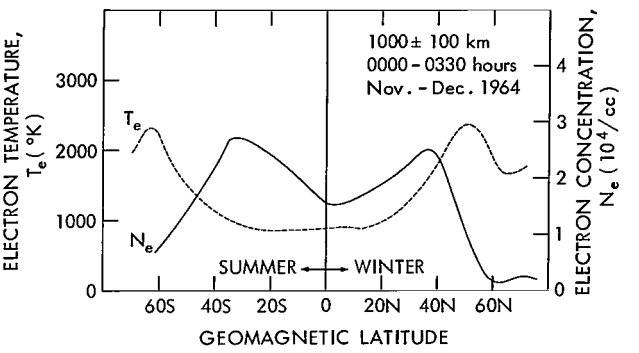


Figure 18—Nighttime values of $T_e$ and $N_e$, averaged from data at all longitudes.

When loss to neutrals predominates ($F_1$ region), the form of the local heating equation is

$$Q_e \propto N_e N_n (T_e - T_n)$$

where $N_n$ and $T_n$ are the neutral particle concentration and temperature respectively, and when loss to ions predominates ($F_2$ region)

$$Q_e \propto N_e^2 (T_e - T_i)/T_e^{3/2} \quad ,$$

and when conductivity controls the cooling rate (upper F region and exosphere) $Q_e$ is independent of $N_e$. Thus one expects $T_e$ and $N_e$ to vary approximately inversely in the $F_1$ region and inversely as the square in the $F_2$ region. In the upper F region, however, there is little local heating. Therefore $T_e$ is controlled by heat conductivity to the lower F region, and $N_e$ is controlled by diffusion and charge transport processes, and the relation between $T_e$ and $N_e$ is not controlled by energy input locally.

## Future Analysis

Further analysis of the data from the sunset and sunrise periods, which have not been stressed here, is expected to expand our understanding of the dynamic response of the upper ionosphere to the elevation of the sun. Data from later orbital plane precession cycles, which have not yet been analyzed or are not yet obtained, will permit us to repeat the profiles given in this paper so as to reveal the seasonal control which may be evident in the global pattern.

## ACKNOWLEDGMENTS

The authors thank James A. Findlay and Tuck Lee for their outstanding efforts in the design and construction of the experiment and its integration into the satellite. We also thank John Sayler, George Dunham, Joseph Johnson and Fred Huie for their dedicated efforts in the reduction of data, and Clyde Freeman, and Don Kennedy for producing the analog records from which the data are reduced.

## REFERENCES

1. "NASA Schedules October launch for Ionospheric Beacon IMP-1," *Aviation Week and Space Technology,* 75(12):30 September 18, 1961.
2. "More Beacon Explorers Soon," *Missiles and Rockets,* 15(16):11 October 19, 1964.
3. Brace, L. H., Spencer, N. W., and Dalgarno, A., "Detailed Behavior of the Midlatitude F Region from Explorer XVII Satellite," to be published in *Planet. Space Sci.,* 1965.
4. Spencer, N. W., Brace, L. H., Carignan, G. R., Taeusch, D. R., and Niemann, H., "Electron and Molecular Nitrogen Temperature and Density in the Thermosphere," *J. Geophys. Res.* 70(11):2665-2698, June 1, 1965.
5. Mott-Smith, H. M., and Langmuir, I., "Theory of Collectors in Gaseous Discharges," *Phys. Rev.* 28:727-763, October 1926.
6. Lockwood, G. E. K., and Nelms, G. L., "Topside Sounder Observations of the Equatorial Anomaly in the 75° Longitude," *J. Atmos. Terr. Phys.* (5):569-580, May 1964.
7. Sayers, J., "The Electron Density Distribution in the Topside Ionosphere. I. Magnetic-Field-Alined Strata," *Proc. Roy. Soc.* 281 A(1387):450-458, 1964.
8. Goldberg, R. A., and Schmerling, E. R., "The Effect of Diffusion on the Equilibrium Electron Density Distribution in the F Region near the Magnetic Equator," *J. Geophys. Res.* 68(7):1927-1936, April 1, 1963.
9. Carpenter, D. C., "Whistler Evidence of a "Knee" in the Magnetospheric Ionization Density Profile," *J. Geophys. Res.* 68(6):1675-1682, March 15, 1963.
10. Bowen, P. J., Boyd, R. L. F., Henderson, C. L., and Willmore, A. P., "Electron Temperature in the Upper F-Region," *Proc. Phys. Soc.* 281 A(1387):526-538, October 6, 1964.
11. Hanson, W. B., "Electron Temperatures in the Upper Atmosphere," in: *Space Research III; Proc. 3rd Internat. Space Sci. Sympos., Washington, D. C., May 2-8, 1962,* ed. by W. Priester, New York: Interscience, 1963 pp. 282-302.
12. Dalgarno, A., McElroy, M. B., and Moffett, R. J., "Electron Temperatures in the Ionosphere," *Planet. Space Sci.* 11(5):463-484, May 1963.
13. Geisler, J. E., and Bowhill, S. A., "An Investigation of Ionosphere-Protonosphere Coupling," Urbana, Illinois: University of Illinois Aeronomy Laboratory, Report Number 5, January 1965.

# ROCKET OBSERVATIONS OF THE STRUCTURE OF THE MESOSPHERE

by
W. Nordberg, L. Katchen,
J. Theon and W. S. Smith
*Goddard Space Flight Center*

Pressure, density, temperature and wind measurements in the upper stratosphere and in the mesosphere resulted from a total of 53 rocket-grenade soundings conducted during the period 1960-1965. Most of the soundings were performed over North America (Wallops Island, 38N and Churchill, 59N) but some results were also obtained over the tropical Atlantic (Ascension Island, 8S) and over Northern Europe (Kronogard, 66N). Soundings were carried out simultaneously at these sites and were coordinated with soundings measuring similar parameters over other areas of the globe.

Seasonal and latitudinal variations in the structure and circulation of this region of the atmosphere were derived from the results. Stratosphere temperatures vary with season and latitude in accordance with solar heating rates and with established circulation models. Temperatures above 65 km are substantially warmer in winter than in summer. Average seasonal temperature differences are about 40°K at 80 km. They are very pronounced at midlatitudes (Wallops Island) and become even more extreme at high latitudes where in summer mesopause temperatures as low as 140°K were observed. Maximum stratopause temperatures were observed during late winter - early summer. At Wallops Island these maxima of about 280°K coincided with the period of transition from winter to summer circulation. Temperature profiles for all seasons at all sites intersect between 60 and 65 km at a temperature range of 230 to 240°K.

The strong westerly flow in winter shows two pronounced cores, one persistent throughout the winter just above the stratopause, the other somewhat weaker and less persistent near 75 km. Deviations from the zonal flow indicate the existence of meteorological circulation cells on a synoptic scale with the average meridional flow at Churchill strongly from the north during both summer and winter and at Wallops Island somewhat weaker from the south during the winter.

## INTRODUCTION

After the successful exploration of the structure of the upper stratosphere with rocket-grenade soundings at White Sands, N. Mex., Churchill, Canada, and Guam, Mariana Islands, during the International Geophysical Year (Reference 1), we conducted a series of soundings at various latitudes

in the Atlantic and North American region during the period of minimum solar activity. Simultaneous, seasonal measurements of temperature, pressure, density and winds were planned at four sites: Point Barrow, Alaska (71N); Churchill, Manitoba, Canada (59N); Wallops Island, Virginia (38N); and Ascension Island (8S). While successful soundings were conducted at each of these locations during 1960-1965, operational difficulties have limited the number of soundings at the various sites, and to date simultaneous observations have been made only at three of the four sites. These took place recently when three successful soundings were conducted each at Pt. Barrow, Wallops Island and Churchill during January and February 1965. Results from this recent series are not yet completely reduced, and only preliminary data from the Pt. Barrow soundings were considered in this analysis. The Point Barrow observations are the first known direct measurements of the structure of the mesosphere north of 70N. Only four successful acoustic grenade soundings were possible at Ascension Island, one each in January and February and two in August 1964. The August observations were made nearly simultaneously with soundings at Churchill, Wallops Island and at Kronogard, Sweden (66N). Data from Kronogard, however, are, as yet, available only for summer 1963, and only preliminary data from the other three sites were considered in this analysis. In addition to the grenade soundings in which temperature, pressure, density, and wind are derived from observations of the soundwaves generated by the exploding rocket-borne grenades, there were three soundings in February and April 1964 at Ascension Island in which pressure, density, and temperature up to 105 km were measured by the pitot-static tube technique. Results of these measurements were reported by Horvarth and Simmons (Reference 2) and are included in this analysis.

Acoustic grenade rocket soundings at Churchill were resumed in December 1962 after a fire had destroyed the launch facility there in 1960. A total of 15 soundings were carried out during December 1962, February and March 1963, January, February, April and August 1964 and January and February 1965. All but one of these soundings were conducted nearly simultaneously with soundings at Wallops Island. Data from all soundings up to August 1964 were included in this analysis, although the August 1964 data are still of a preliminary nature.

By far the largest number of soundings were obtained at Wallops Island, Virginia since that launch site has been available for the longest period. Forty-two successful soundings were conducted at Wallops Island between July 1960 and February 1965. Soundings were taken during every month of the year except October. Results have been analyzed through August 1964.

The times and location of all soundings included in this discussion are summarized in Table 1. Space does not permit the presentation here of the complete data from each sounding. However, complete tabulations and graphic presentations of the data for 1960-1963 have been compiled in a report by W. Smith *et al.* (Reference 3). A similar report for the complete 1964 data is now in preparation.

Only the basic and salient features of the observations will be summarized here with particular emphasis on their latitudinal and seasonal variations and their relationship to the basic physical processes governing the stratosphere and mesosphere. These results are of interest also because they permit a comparison between the structure of the mesosphere observed during the

Table 1

Dates, Times and Locations of GSFC Meteorological Sounding Rocket Experiments, 1960-65.

| Date | Time (GMT) | Location |
|---|---|---|
| 1960 | | |
| 9 July | 0359 | Wallops Island |
| 1961 | | |
| 14 February | 2350 | Wallops Island |
| 17 February | 0226 | Wallops Island |
| 5 April | 1257 | Wallops Island |
| 5 May | 2300 | Wallops Island |
| 6 May | 0454 | Wallops Island |
| 13 July | 2207 | Wallops Island |
| 14 July | 1602 | Wallops Island |
| 20 July | 1030 | Wallops Island |
| 16 September | 2355 | Wallops Island |
| 1962 | | |
| 2 March | 0001 | Wallops Island |
| 2 March | 1115 | Wallops Island |
| 23 March | 2354 | Wallops Island |
| 28 March | 0004 | Wallops Island |
| 18 April | 0928 | Wallops Island |
| 7 June | 0105 | Wallops Island |
| 8 June | 0153 | Wallops Island |
| 1 December | 2125 | Wallops Island |
| 4 December | 0705 | Churchill |
| 6 December | 0532 | Wallops Island |
| 6 December | 0543 | Churchill |
| 1963 | | |
| 20 February | 2334 | Churchill |
| 20 February | 2347 | Wallops Island |
| 28 February | 2147 | Churchill |
| 28 February | 2211 | Wallops Island |
| 9 March | 0001 | Wallops Island |
| 9 March | 0001 | Churchill |
| 7 December | 1312 | Wallops Island |
| 1964 | | |
| 24 January | 0016 | Wallops Island |
| 29 January | 0411 | Wallops Island |
| 29 January | 0417 | Churchill |
| 29 January | 0418 | Ascension Island |
| 4 February | 0135* | Ascension Island |
| 4 February | 0146 | Wallops Island |
| 5 February | 0040 | Churchill |
| 5 February | 0320 | Wallops Island |
| 13 February | 0430 | Wallops Island |
| 13 February | 0430 | Churchill |
| 13 February | 0455 | Ascension Island |
| 7 March | 0245 | Wallops Island |
| 15 April | 0122* | Ascension Island |
| 15 April | 1556* | Ascension Island |
| 18 April | 0039 | Churchill |
| 18 April | 0100 | Wallops Island |
| 7 August | 0600 | Wallops Island |
| 8 August | 1000 | Churchill |
| 12 August | 0149 | Wallops Island |
| 12 August | 0215 | Churchill |
| 16 August | 0315 | Wallops Island |
| 16 August | 0553 | Ascension Island |
| 17 August | 1255 | Ascension Island |
| 18 August | 0115 | Churchill |
| 18 August | 0125 | Wallops Island |
| 1965 | | |
| 27 January | 2132 | Point Barrow |
| 4 February | 0445 | Point Barrow |
| 8 February | 2215 | Point Barrow |

*All soundings were rocket grenade experiments except the pitot-static experiments which are noted with an asterisk (*).

present period of minimum solar activity and during the IGY when solar activity was at its maximum.

Results from the large number of wind observations obtained from Meteorological Rocket Network soundings analyzed by Webb (Reference 4) were also considered as they overlapped our observations at the lower altitudes.

## DISCUSSION OF THE OBSERVATIONAL RESULTS

### The Temperature Structure

In the stratosphere, temperatures are qualitatively in accord with the solar heating rates expected at the various latitudes and seasons. The highest temperatures are generally observed at high latitudes during summer where maximum heating rates are expected, while the lowest temperatures prevail at high latitudes in winter during minimum solar illumination. Quantitatively, however, the observed stratopause temperatures of 255°K near 60N in winter (Churchill Winter 1962-64 in Figure 1) are about 25°C higher than temperatures for the same latitude and season calculated by Leovy (Reference 5) solely on the basis of heating and cooling rates given by the radiative properties of oxygen, ozone and carbon dioxide. At 60N in summer (Churchill Summer 1964 in Figure 1) the observed temperatures of 275K are about 20°C lower than calculated. Thus, the observed seasonal variation in the stratopause temperatures amounts to 20°C (Figure 2),

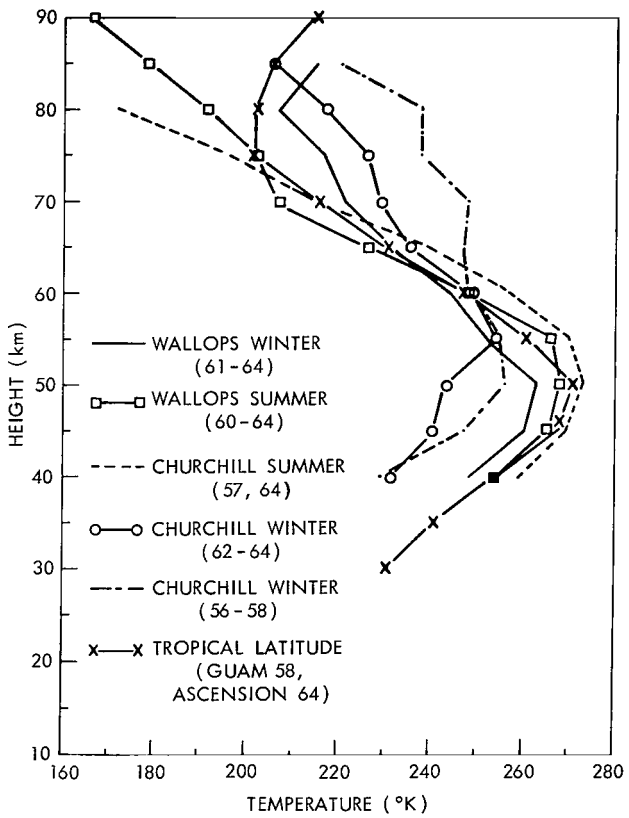


Figure 1—Average 1960-64 summer and winter temperatures for Wallops Island (38N), 1962-64 winter temperatures for Churchill (59N), 1964 summer temperatures for Churchill and winter 1964 temperatures for Point Barrow (71N) are compared to average summer and winter temperatures obtained at Churchill during the IGY (1957-58). The IGY Churchill summer temperatures were quite similar to averages from three summer 1964 soundings in Churchill, thus only one profile is shown. An average temperature profile for tropical latitudes obtained in November 1958 at Guam (13N) and in February 1964 at Ascension Island (8S) is shown for comparison. The average profiles are derived from the following number of individual grenade experiment soundings listed in Table 1: Wallops winter—17, Wallops summer—10, Churchill winter (IGY)—5, Churchill winter (1962-64)—8, High Latitude summer—8, Low Latitude—6 (Guam) plus 7 (Ascension Island). 1962-64 soundings were conducted nearly simultaneously at Churchill and Wallops.

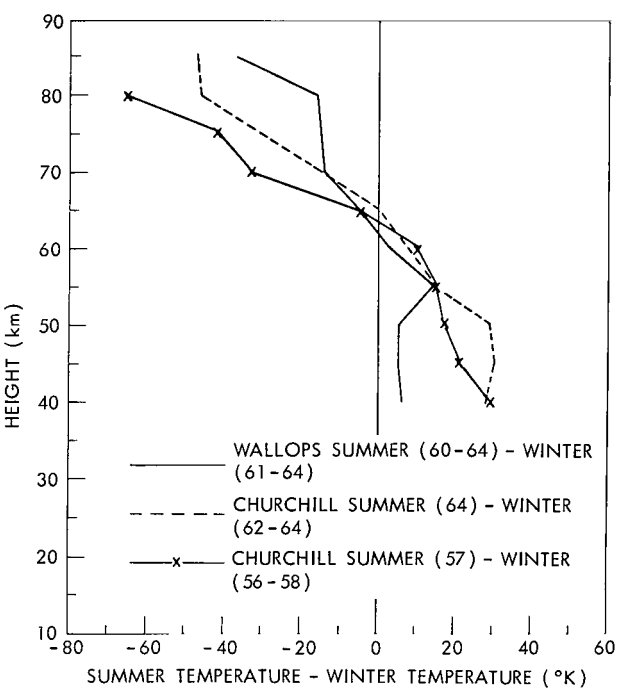


Figure 2—Average summer temperatures minus average winter temperatures for Wallops Island (1960-64) and Churchill (1956-58 and 1962-64) as a function of height.

instead of 65°C calculated from radiative heating and cooling alone. At lower latitudes (Wallops Island) observed average seasonal temperature variations are only about 10°C. Figure 1 shows that latitudinal temperature gradients at the stratopause level are much larger in winter than in summer. This is again in good qualitative agreement with radiatively predicted gradients.

Quantitatively, the discrepancy by about a factor of two between the radiatively predicted and the observed seasonal temperature variations in the stratosphere, especially at high latitudes, requires equatorward and poleward energy transport in the summer and winter hemispheres, respectively. Dynamic processes which carry out this energy transport have been postulated by Murgatroyd and Singleton (Reference 6) on the basis of the IGY temperature observations and more recently by Newell (Reference 7) on the basis of Meteorological Rocket Network wind observations.

The change from cold winter temperatures to warm summer temperatures in the stratosphere takes place very rapidly during the end of each winter season (March-May, Figure 3). Maximum temperatures occur near 45 km, about 5 km lower than during the period of maximum solar heating in midsummer. Furthermore, many temperature profiles during spring exhibit maximum temperatures equal to or exceeding those reached at 50 km later in the year suggesting the stratopause to be warmest and lowest during spring. This phenomenon is obvious at Wallops because of the large number of observations at that site, but results from Churchill are insufficient to confirm its existence there (Figure 4). Indications are that the warm upper stratosphere in late winter exists also at relatively low latitudes in the southern hemisphere (Reference 8). It may be expected that these temperature maxima are dynamically induced and are caused by the final breakdown of the predominantly cyclonic winter circulation which occurs during the same time period. This phenomenon will be considered further in the discussion of the wind observations.

In the lower mesosphere there are practically no seasonal and latitudinal temperature variations in the altitude range of about 60 to 65 km. Indeed, considering the results reported by Groves (Reference 8) for Woomera, Australia (31S), our earlier IGY data (Reference 1) and those shown in Figure 1, one may conclude that temperatures at this altitude range generally between 230 and 240°K over the entire globe during all seasons.

The largest variations in the observed temperature take place in the upper mesosphere and at the mesopause and are especially evident at Churchill and Wallops Island (Figure 2). Average seasonal temperature variations at 80 km during the 1962-64 period are about 45°C at Churchill and about 15°C at Wallops Island. It must be concluded that this variation diminishes at low latitudes since no appreciable seasonal variation can be detected in Groves' (Reference 8) results at Woomera and in our (Reference 1) results at White Sands (33N). At equatorial latitudes, for which an average profile is shown in Figure 1, there have not been sufficient soundings yet to positively deduce any absence of seasonal variations. However, the trend demonstrated in the Churchill, Wallops Island, White Sands and Woomera observations and the fact that at all altitudes the average equatorial temperature profile lies between the summer and winter profiles observed at higher latitudes leaves little doubt that at equatorial latitudes the seasonal variations are at a minimum. It should be noted that the variation at Churchill during 1962-64 was only one half the variation observed during the IGY (Figure 2). More soundings will have to be made during the next solar maximum to determine the possible significance of this result.

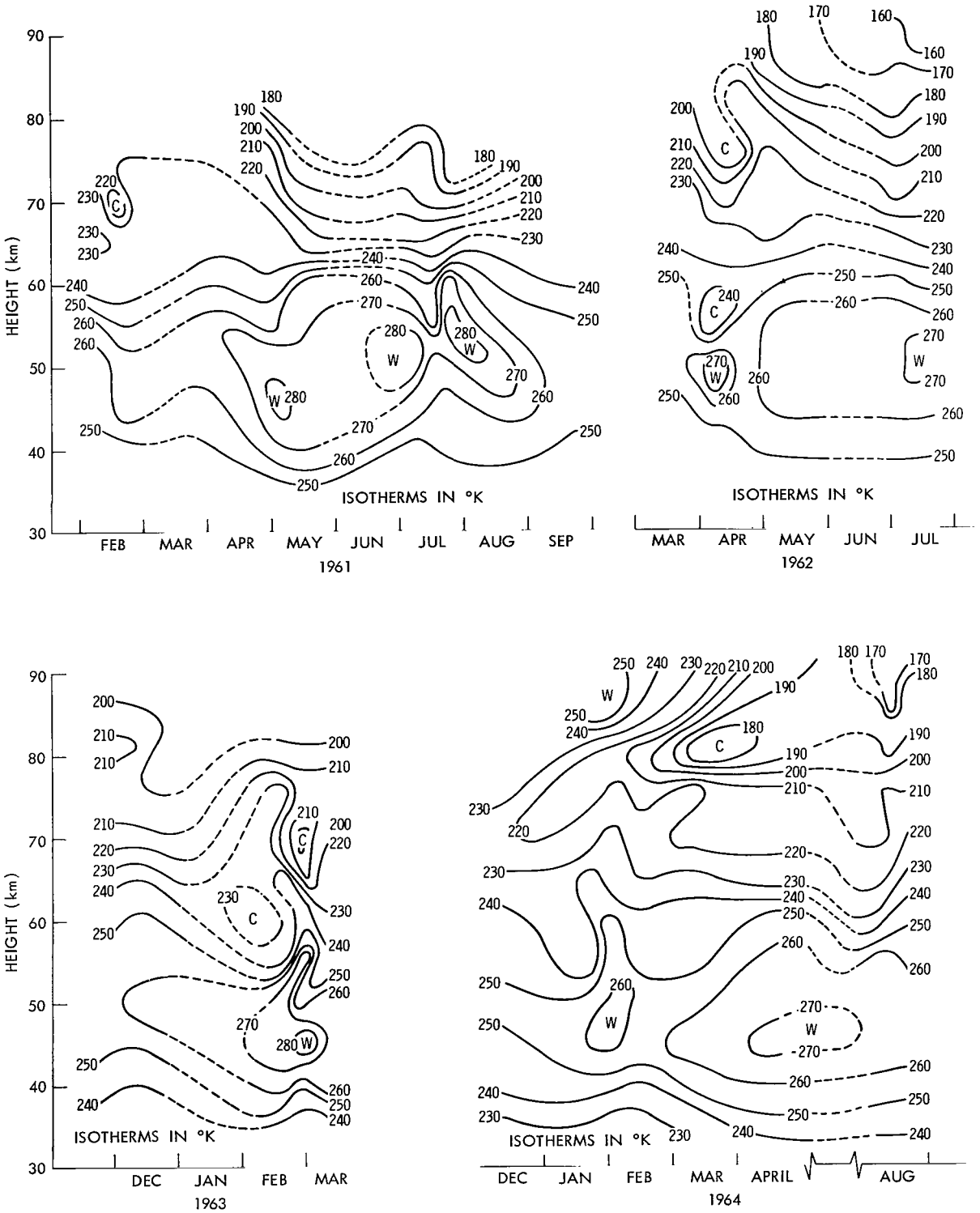


Figure 3—Variation of temperatures in the stratosphere and mesosphere with altitude and season over Wallops Island (38N) during 1961-64. Isotherms are based on 34 grenade soundings listed in Table 1.

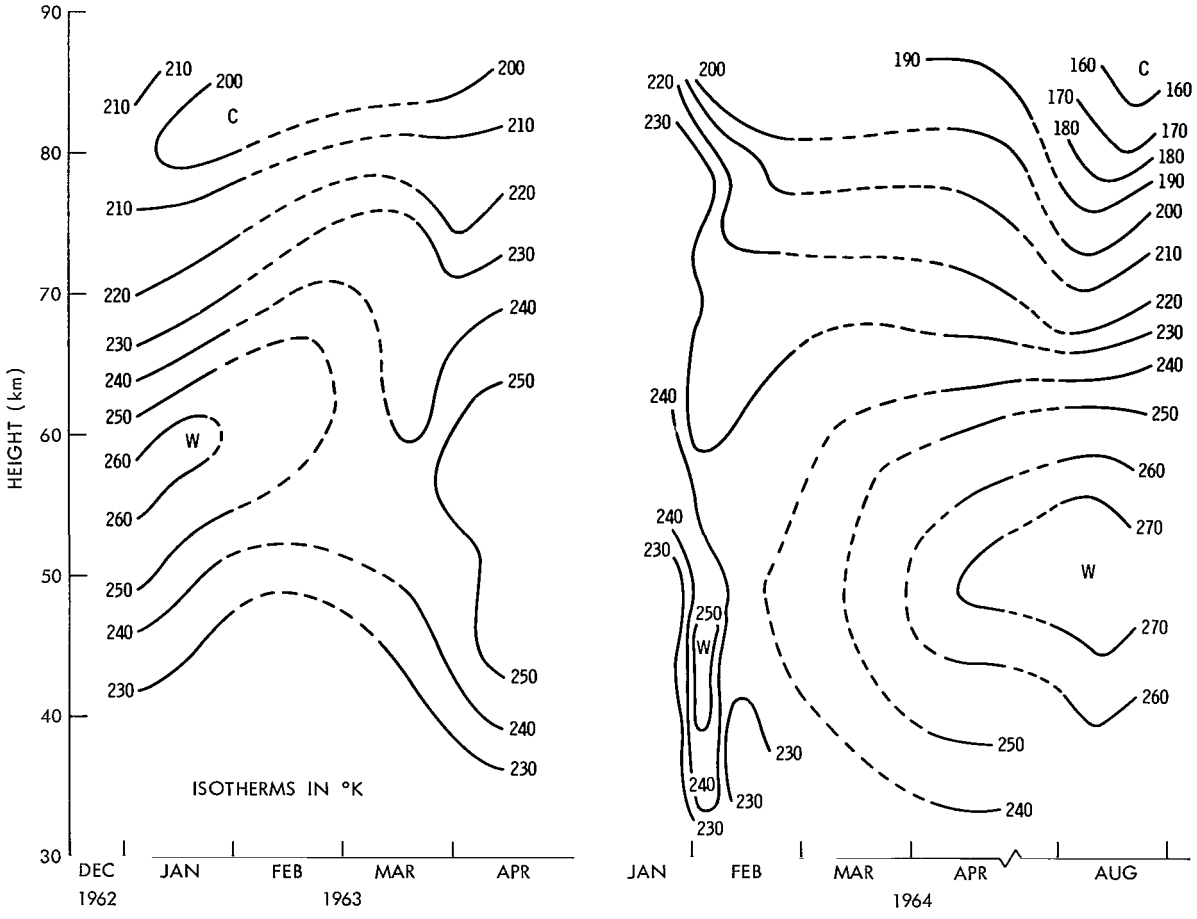


Figure 4—Variation of temperatures in the stratosphere and mesosphere with altitude and season over Churchill (59N) during 1962-64. Isotherms are based on 12 grenade soundings listed in Table 1.

The large average lapse rates found during maximum solar heating (high latitude summer), suggest that a very cold upper mesosphere always occurs in conjunction with a warm and high stratopause. The Swedish grenade soundings made during the summer of 1963 (Reference 9) confirm the existence of a warm stratopause (280°K) occurring with a cold mesopause (140°K) at 66N latitude. On the other hand, during minimum solar heating (high latitude winter), the average lapse rate between 50 and 80 km becomes very small, suggesting that a warm upper mesosphere is always found in conjunction with a cold stratopause. Preliminary data from Point Barrow, Alaska (71°N) during January 1965 (Figure 5) indicate a more nearly isothermal atmosphere from about 40 to 70 km. The seasonal temperature variations which are of opposite sign in the stratosphere and upper mesosphere (Figure 2) seem to pivot around the level of nearly constant temperature between 60 and 65 km. These observations disagree both qualitatively and quantitatively with temperature distributions computed solely on the basis of radiative properties (Reference 5). The computations require a much colder mesosphere in winter. Radiative heating and cooling alone require winter mesospause temperatures of 190°K and summertime temperatures of 230°K at 60°N. Observations (Figure 1) show 170°K in summer and 220°K in winter at the same latitude. This

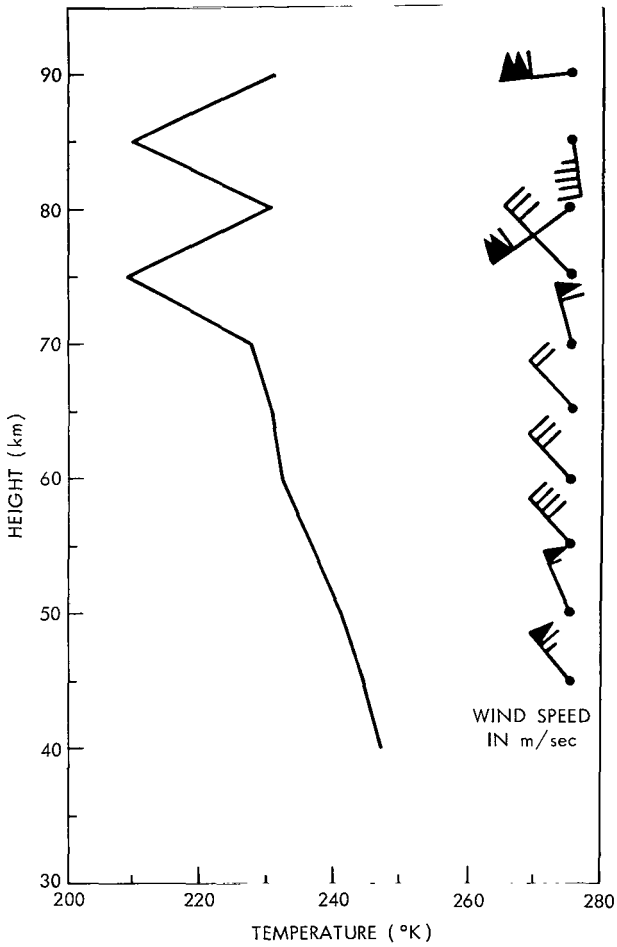


Figure 5—1965 winter stratosphere and mesosphere average temperature and average wind profiles at Point Barrow (preliminary data).

discrepancy again necessitates a large scale dynamic mechanism to transport energy meridionally and vertically. The mechanism of mean meridional and vertical motions postulated by Murgatroyd and Singleton (Reference 6) produces upward motion in the summer mesosphere, downward motion in the winter mesosphere, and meridional motions from summer to winter pole thus, qualitatively at least, explaining the departures of the observed temperatures from radiative equilibrium. Leovy (Reference 10) has developed a quantitative model of such a mean circulation. Our observations agree in general with the temperatures of Leovy's model in the upper mesosphere but disagree quantitatively in the lower mesosphere and at the stratopause. Obviously more sophisticated dynamic models will be needed to conform with the observations.

Heat sources other than solar radiation have been suggested by Kellogg (Reference 11) who pointed out the possibility of heating the polar upper mesosphere by recombination of atomic oxygen transported downward from the ionosphere and by Maeda (Reference 12) who investigated the possibility of heating by auroral particles. The recent simultaneous observations at Churchill and Wallops Island, however, indicate that the warm upper mesosphere is found at both locations and require an explanation which holds at latitudes outside the polar cap as well as inside. Figure 1 indicates that the observations made during the IGY (Churchill winter 1956-58) show considerably higher temperatures than the most recent observations (Churchill winter 1962-64) obtained during low solar activity. Advocates of the auroral heating concept might be tempted to use this finding as evidence for the existence of a heat source depending on solar activity. But, aside from the scarcity of the data sample which invalidates any such evidence, one would still have to explain the observed low summer temperatures which are nearly 100°K colder than those calculated from radiative transfer for 80 km at 60° latitude (Reference 5). Significantly, summer temperatures throughout the mesosphere at Churchill shown in Figure 1 for 1964 are practically the same as those observed during the IGY.

## Pressure Distributions

The average pressure graphs shown in Figure 6 were obtained by integrating the hydrostatic equation for each of the temperature soundings mentioned in Figure 1, and averaging the resulting

pressures at each altitude for the appropriate season and location. A measured pressure (usually by balloon sondes) at the lower boundary of each temperature profile was used as the initial value in the integration. The pressure profiles are very useful to demonstrate the relationship between the seasonal and latitudinal temperature variations and the wind patterns described below.

The stratosphere and mesosphere are dominated by very systematic latitudinal and seasonal pressure variations (Figure 6 and Table 2). These variations are of considerable magnitude throughout the entire region and they converge toward minima at the lower and upper boundaries. Extrapolation of the pressure profiles in Figure 6 to lower altitudes shows that there is a minimum pressure variation in the lower stratosphere, a fact which can also be derived from balloon and Meteorological Rocket Network soundings. It is evident from the data shown in Figure 6 that another minimum exists near the mesopause. Average pressure profiles for all seasons at the three sites seem to converge toward a common value slightly larger than the 1962 U. S. Standard Atmosphere at 90 km.

In winter, throughout most of the stratosphere and mesosphere, pressures at Churchill are more than 20 percent lower than at Wallops Island, and close to 30 percent lower than at equatorial latitudes where the pressure is closest to the standard. The greatest latitudinal pressure gradient in winter occurs near 55 km. The maximum deviation from the standard at all latitudes takes place in winter at Churchill near 65 km.

The variation of the latitudinal pressure gradient with height in winter is plausible on the basis of the temperature profiles. The much colder winter stratosphere and stratopause at high latitudes cause the pressure to

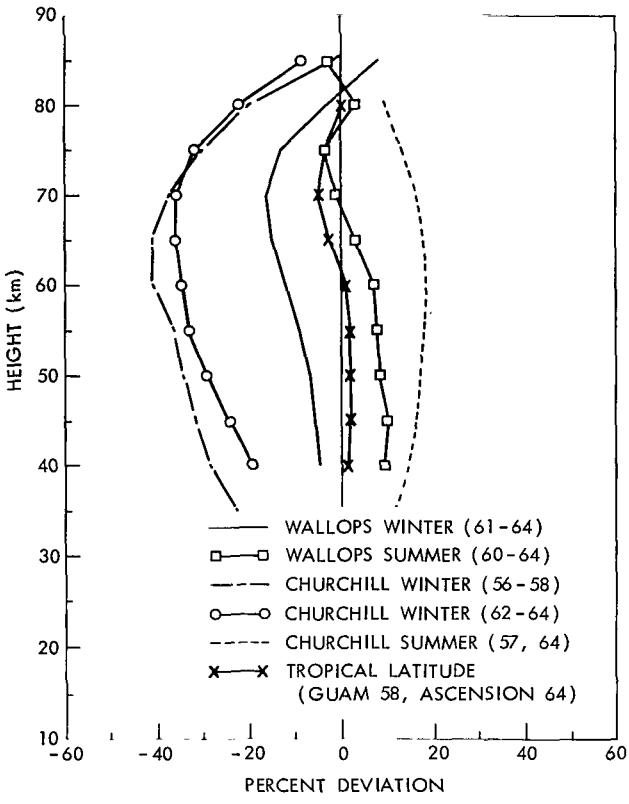


Figure 6—Seasonal pressure averages as a function of height for Wallops Island (38N), Churchill (59N), and equatorial latitudes. Averages are based on the same soundings for which average temperature profiles are shown in Figure 1. Because of their rapid variations with height, observed pressures are shown as deviations from the U. S. Standard Atmosphere, 1962. Absolute values of standard pressures which apply to the zero percent deviation coordinates are shown in Table 2.

Table 2

U. S. Standard Atmosphere 1962, pressure vs. height.

| Altitude (km) | Pressure (newton/m²) |
|---|---|
| 30 | 1197.0 |
| 35 | 574.6 |
| 40 | 287.1 |
| 45 | 149.1 |
| 50 | 79.8 |
| 55 | 42.8 |
| 60 | 22.5 |
| 65 | 11.4 |
| 70 | 5.5 |
| 75 | 2.5 |
| 80 | 1.0 |
| 85 | 0.4 |
| 90 | 0.2 |

decrease with height more rapidly at high latitudes than at low latitudes, resulting in a gradual increase of the latitudinal pressure differences above the level of minimum pressure differences at the lower stratosphere. In the mesosphere the warmer temperatures at the higher latitudes bring about a smaller pressure decrease with height than at lower latitudes causing the latitudinal pressure differences to decrease above 60 km and to reach a second minimum near 90 km.

In summer, pressures are higher at Churchill than at Wallops Island at all latitudes, but differences between the two sites are considerably less than in winter. This is because the high latitude summer stratosphere and stratopause are only moderately warmer than their low latitude counterparts. Pressure differences between Wallops Island and Churchill in summer are about one half of the differences observed in winter. Differences between Wallops Island and tropical latitudes are of about equal magnitude during both seasons.

The large seasonal pressure variations of a factor of two between summer and winter at Churchill which were reported during the IGY (Reference 1) are still prevalent although with a somewhat diminished amplitude (factor of 1.8). At the latitude of Wallops Island, the seasonal variation is considerably less and ranges between a factor of 1.15 and 1.2. At equatorial latitudes, soundings have not been made with sufficient continuity to reach a very definite conclusion, but all observations to date indicate that variations in the average pressure are quite small, generally less than the accuracy of the observations which is better than 5 percent.

## Wind Patterns

Wind observations in the stratosphere and mesosphere have been more numerous than any other type of observation. The basic features of the general circulation in these regions are, therefore, fairly well understood. A number of publications (References 7 and 10) have recently explored these features in greater detail based on our earlier IGY observations and on the large number of meteorological rocket soundings throughout the stratosphere and into the lower mesosphere which have been regularly conducted since 1961. Our observations are summarized in Figures 7 through 12. They confirm that the features observed in the stratosphere by the meteorological network soundings exist throughout the mesosphere, but undergo a major change in the 70 to 80 km region. All observations generally confirm the existence of the expected strong cyclonic circulation around the North Pole in winter and a somewhat weaker anticyclonic motion in summer. Average zonal

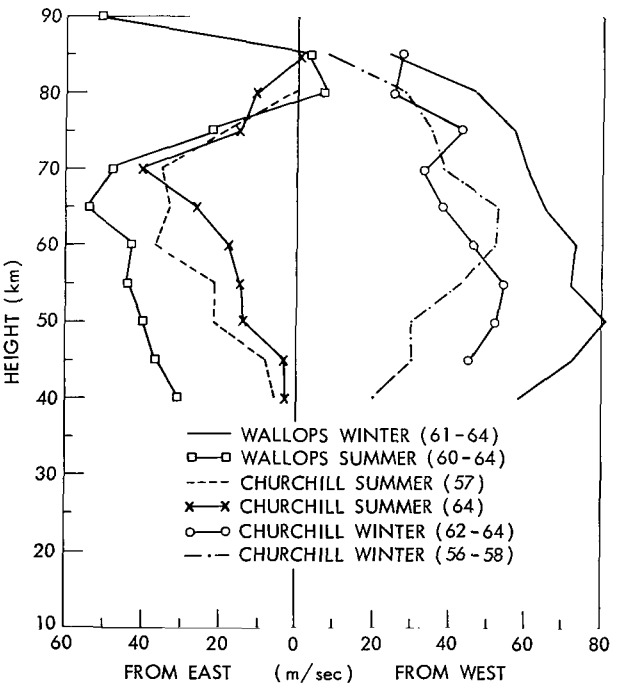


Figure 7—Average zonal wind components vs. altitude for Churchill and Wallops Island. Graphs are based on the same soundings as those shown in Figure 1.

wind speeds are considerably greater at almost all altitudes at Wallops Island than at Churchill, both in winter and summer (Figure 7), although occasionally the maximum wind measured at one given altitude in one given sounding at Churchill may exceed the wind speed measured simultaneously at Wallops Island.

A time cross section of the zonal wind components at Wallops Island (Figure 8) clearly displays two wind maxima during each winter since 1961. One maximum is located very consistently near 55 km in midwinter, but moves gradually to lower altitudes (45 km) toward the end of the winter. This maximum is also obvious in the average zonal wind profile in Figure 7. The second maximum occurs consistently each winter between 70 and 80 km, but it is generally of lesser intensity and shorter duration than the lower altitude maximum. Except for 1962, where no midwinter data exist, the maximum occurs only during January-February. It is for this reason that the upper maximum does not appear in the average profile in Figure 7. The higher wind speeds throughout the *entire* winter season in the lower maximum completely overshadow the upper maximum in the average profile. There is a possibility that the weaker easterlies occurring in summer also form two cores during midsummer, but they are certainly not as pronounced as the two westerly jets. Observations in the mesosphere at this time have not been made with sufficient continuity to determine the persistence in the reversals of the zonal flow from westerly in winter to easterly in summer and vice versa. However, such studies have been made at lower altitudes by Webb (Reference 4) on the basis of Meteorological Rocket Network soundings which showed a very consistent pattern in the seasonal reversals; at low and mid latitudes the reversals always occur during mid-May and September. Figure 8 shows a slope in the springtime zero isotachs from the upper left to the lower right. From this and from the gradual migration of the lower core to lower altitudes, it seems to follow that the winter to summer reversal in the lower cores follows the reversals in the upper cores. Sufficient data do not exist for the fall reversals to draw similar conclusions.

In general, the altitude level of maximum average zonal windspeed is higher in summer than in winter. This is consistent with the height of the maximum latitudinal pressure gradient described above. The comparison of the windspeeds between Wallops Island and Churchill places a steeper latitudinal pressure gradient in the vicinity of Wallops Island than at Churchill. There is complete consistency for the entire region between the average pressures shown in Figure 6 and the average zonal windspeeds in Figure 7. Maximum zonal winds occur at the heights and seasons where maximum latitudinal pressure differences are shown, and the average zonal windspeeds are smallest at those altitudes where the pressure variations are at a minimum.

The time cross section of zonal winds at Wallops Island (Figure 8) also shows that the periods of maximum temperature in the upper stratosphere during late winter and early summer (Figure 3) seem to coincide with the seasonal reversal in the zonal winds. Indeed, during 1961 the maximum temperature occurred exactly when the winter westerlies had dropped to zero. In 1962, measurements were made in April and June showing temperatures of 270°K during both months. Figure 8 shows that in April the westerlies were still pronounced, while in June easterly circulation had already set in and the temperature maximum probably occurred during May again when the zonal winds reversed directions. In 1963, temperatures were already very high in March when

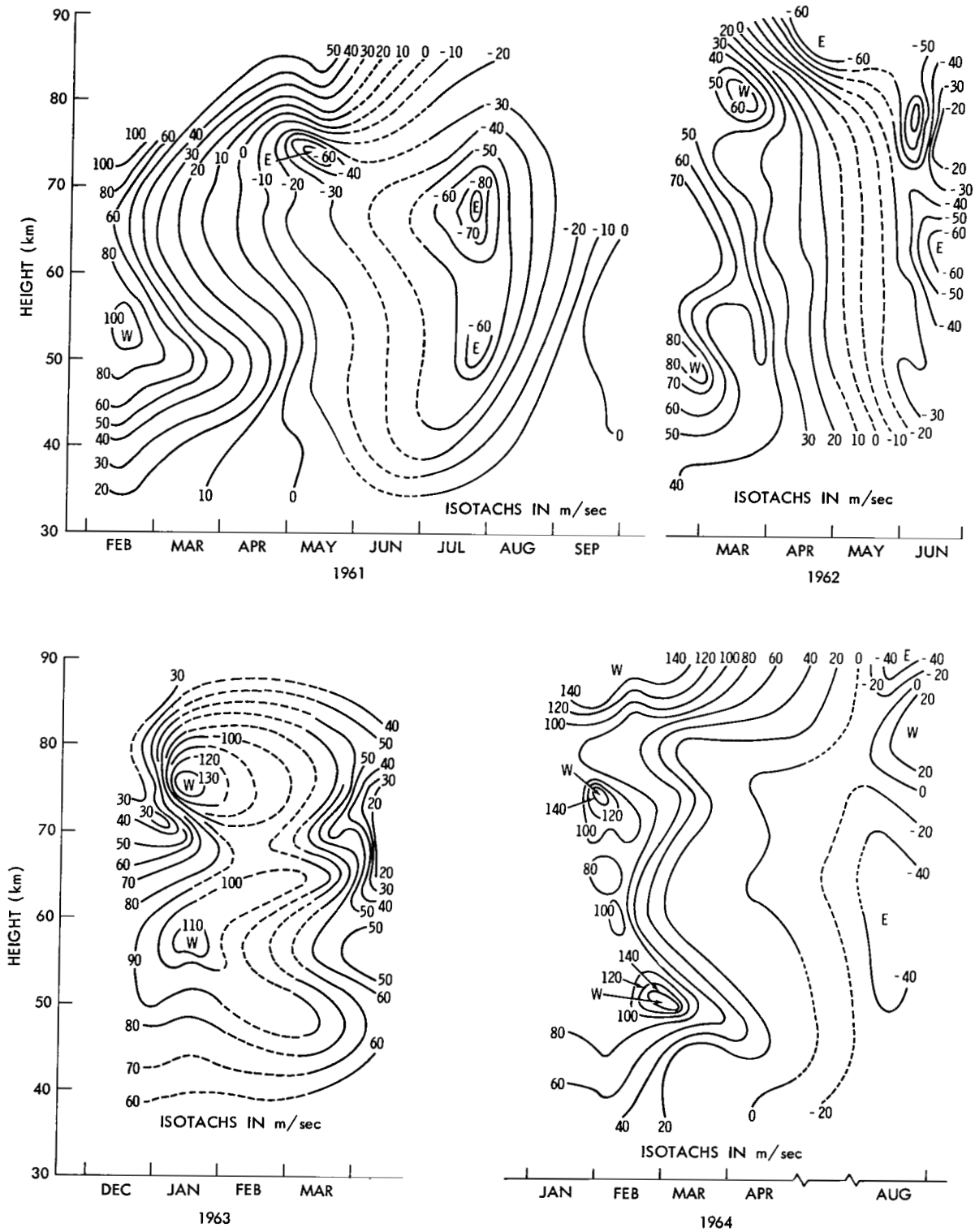


Figure 8—Variation of zonal wind components with altitude and season over Wallops Island, 1961-64.

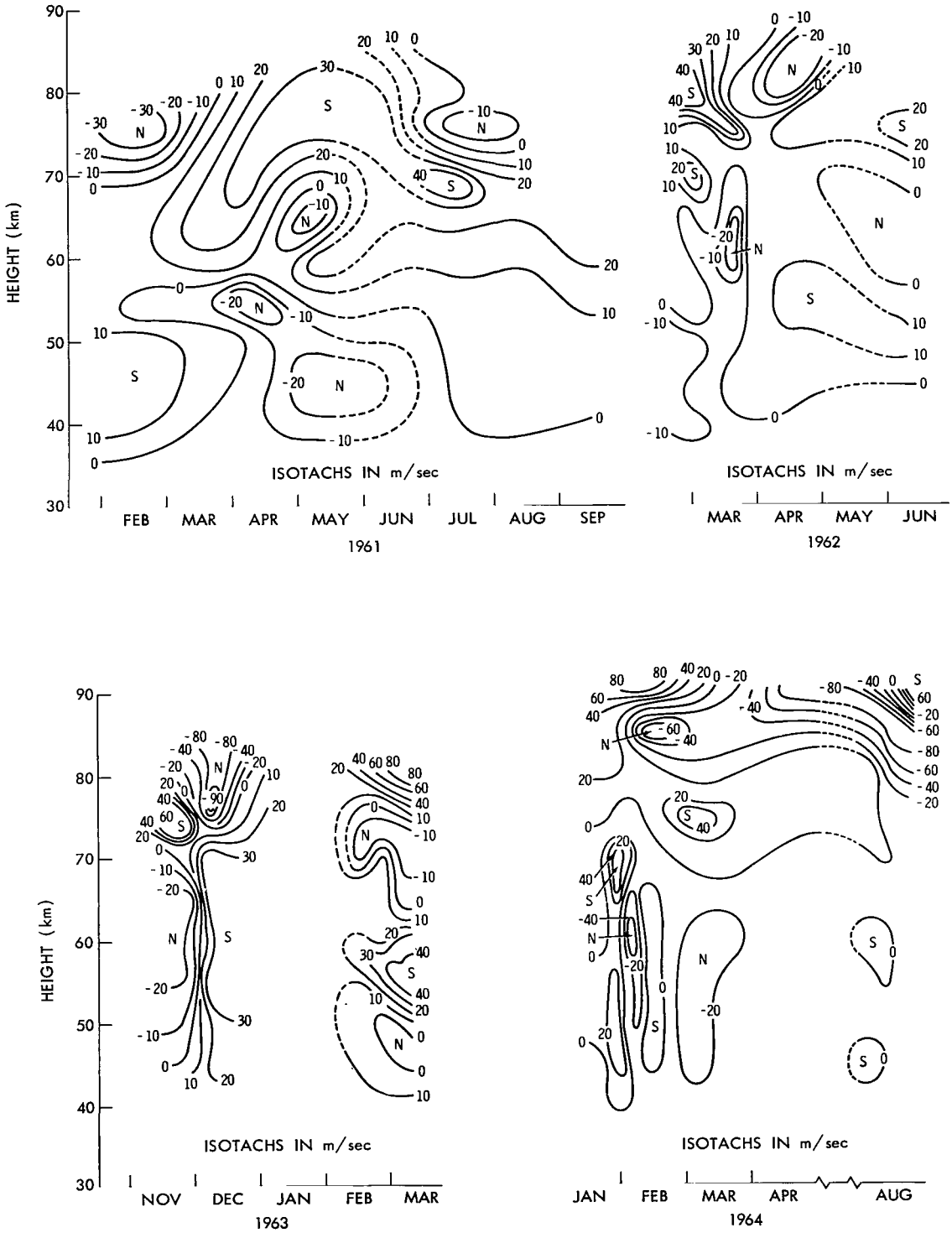


Figure 9—Variation of meridional wind components with altitude and season over Wallops Island, 1961-64.

winds had diminished from their maximum of about 100 m/sec to about 50 m/sec. No temperature measurements exist during April or May for that year, but one may speculate again that the temperature continued to rise until the zonal winds reversed direction in May.

There is no evidence of any increase in the meridional wind components (Figure 9) or of any predominance in either the southerly or northerly component during the time of the high late winter temperatures. Zonal circulation simply undergoes maximum changes during these times. Webb (Reference 4) has analyzed the very large number of wind data near the 50-km level resulting from the Meteorological Rocket Network soundings and has found that except for December, January, and February, the average meridional wind components are very small and show no particular increase in spring.

Webb's analysis also shows that average meridional winds are from the south during the entire year at all low and mid latitude North American stations. Although the meridional flow is not nearly as well organized as the zonal flow, our soundings do show a consistent average component from the south during the winter at all heights up to 70 km at Wallops Island and, with the exception of winter 1957-58, an equally consistent component from the north at Churchill during both summer and winter (Figure 10). These average meridional wind components are much larger than the "mean" meridional winds postulated in models such as Murgatroyd and Singleton (Reference 6). One may therefore conclude that the observed winds reflect large scale pressure disturbances at these longitudes and that the data are too sparse to derive true mean meridional motions. The Churchill meridional winds indicate a more or less permanent position of these pressure disturbances.

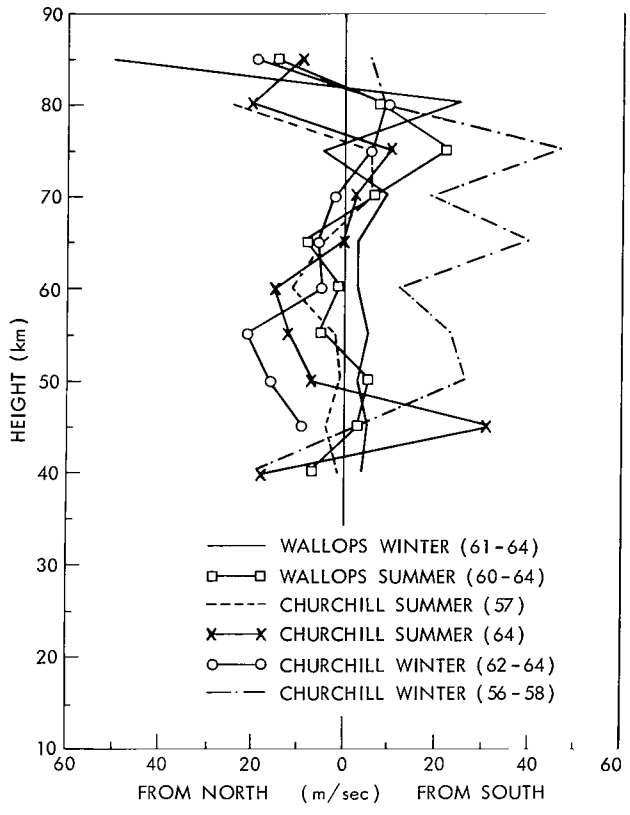


Figure 10—Average meridional wind components vs. altitude for Churchill and Wallops Island. Graphs are based on the same soundings as those shown in Figure 1.

These pressure disturbances are apparently very deep, reaching well into the mesosphere. They are especially pronounced in winter at the very high latitudes. For example, wind data at Wallops indicate a very strong and steady zonal flow from the west during midwinter (Figures 8 and 9), while at the same time at Churchill the westerly wind component is much weaker and a steady northerly component exists in general (Figures 11 and 12). This is also confirmed by the most recent soundings at Point Barrow (Figure 5), suggesting a high pressure cell over the North Pacific and Gulf of Alaska and low pressure over the North Atlantic. This implies that the well-known Aleutian anticyclone may exist up to altitudes of 70 km. A more detailed

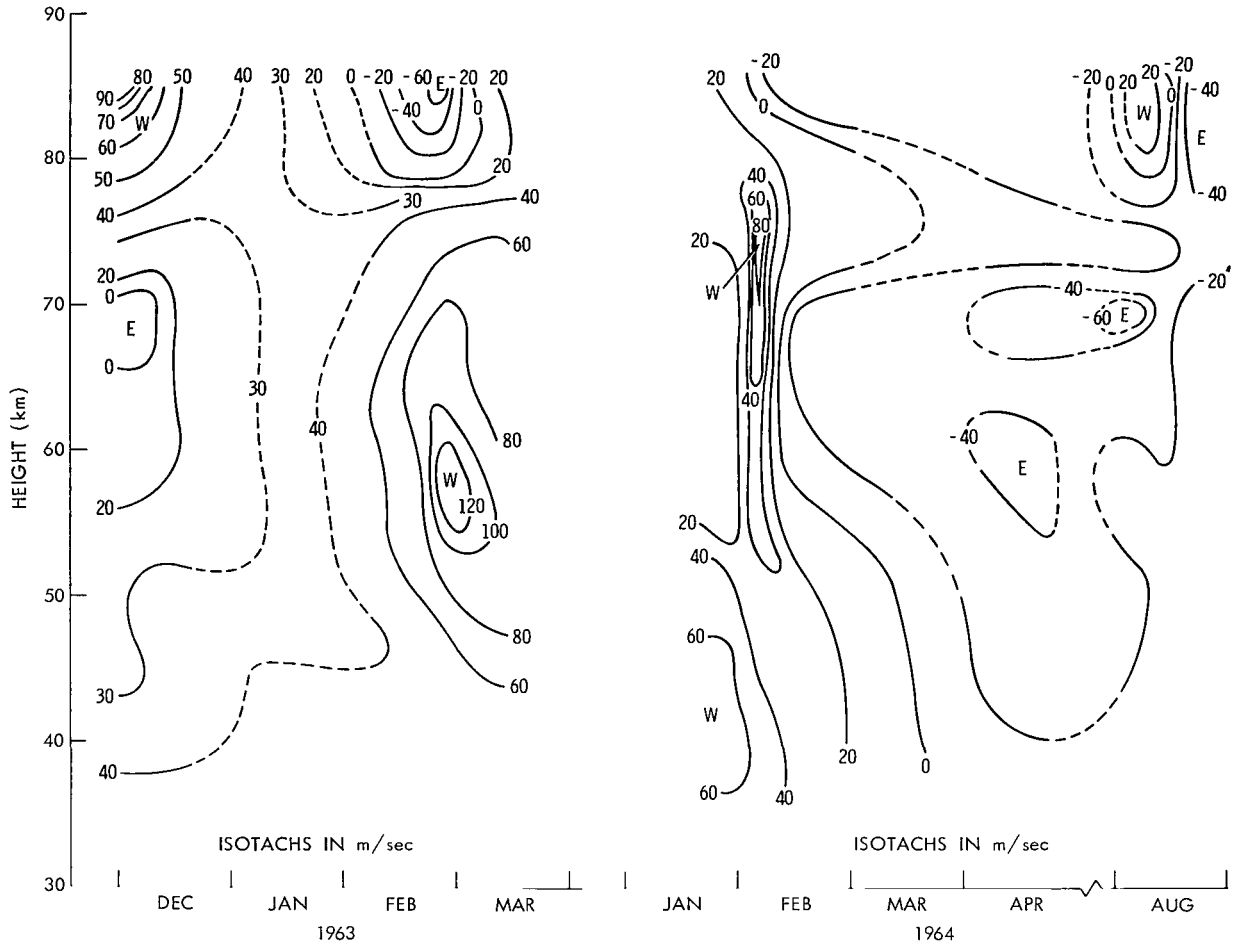


Figure 11—Variation of zonal wind components with altitude and season over Churchill, 1962-64.

analysis of one series of simultaneous soundings at Churchill and Wallops Island by Warnecke and Nordberg (Reference 13) supports this speculation. In contrast to the more recent observations, the averages for the meridional winds for Churchill for 1956-58 show southerly instead of northerly components (Figure 10) because these data are dominated by measurements made during January 1958 when a breakdown in the circulation occurred. During that period the high pressure cell lay to the east and low pressure to the west of Churchill (Reference 14). All observations at Churchill since then have displayed northerly winds, leading to the conclusions that, in general, high pressure is rather stationary to the west of Churchill and low pressure to the east, and that the 1958 measurements specifically reflected the displacement of the pressure cells during "break down" conditions. It seems somewhat surprising, however, that the average meridional wind components at Churchill are from the same direction during both summer and winter, indicating great persistence in the longitudinal position of the pressure cells. Naturally, a much larger number of soundings distributed over a wider range of longitudes would shed some further light on this subject.

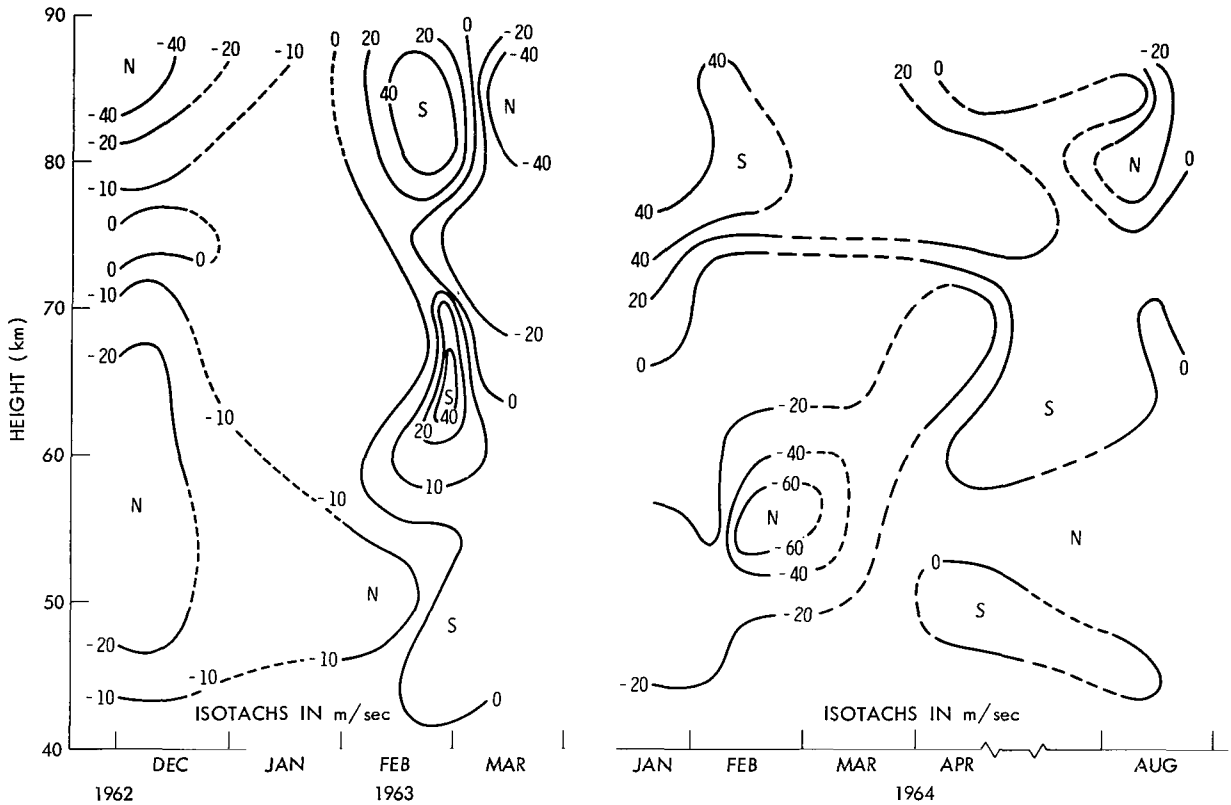


Figure 12—Variation of meridional wind components with altitude and season over Churchill, 1962-64.

The analysis by Warnecke and Nordberg (Reference 13) of a number of the acoustic grenade soundings supplemented by sodium release wind instruments above 70 km showed that the generally accepted circulation patterns cease to exist above about 75 km. Above that altitude the circulation seems to be governed by variations of much smaller time scales than in the stratosphere and mesosphere. Tidal phenomena seem to be of much greater importance at those altitudes than the synoptic scale pressure variations described here for the lower regions.

## CONCLUSIONS

The warm upper mesosphere originally observed at Churchill during the IGY was still present at both Churchill and Wallops Island during the recent years of low solar activity. However, at 80 km, winter temperatures during 1962-64 were only about 45°C warmer than summer temperatures at Churchill and 15°C warmer at Wallops Island, while during the IGY at Churchill, the corresponding temperature difference was 70°C. The possibility that the less intense winter warming of the upper mesosphere over Churchill during the IQSY is associated with the solar cycle cannot be sufficiently substantiated by the small data sample. Summer temperatures at the mesopause at high latitudes were consistently colder than 160°K which does not support the postulation of an additional extraterrestrial heat source to explain the difference between observed and

predicted mesosphere temperatures. Dynamic processes can account better for these differences.

In the stratosphere maximum temperatures occurred at Churchill, Wallops Island and tropical latitudes during the end of the winter season. At that time the stratopause temperatures at 40-45 km were equal to or higher than stratopause temperatures at 50-55 km during midsummer. Wallops Island data suggest that the stratopause is warmest and lowest during early spring. This phenomenon is probably related to the breakdown of the polar vortex which occurs at the same time of year.

A region of minimum seasonal and latitudinal temperature variation exists at 60 km, while minimum pressure variations occur below 25 km and near 85-90 km. There are not sufficient data available to draw any definite conclusions about the seasonal variation of temperature and pressure at the tropics, but indications are that these variations are at a minimum, being probably only a few percent over the entire year.

In midwinter at Wallops Island, the mesophere exhibits two pronounced maxima in the westerly winds at 55 km and 75 km. The upper maximum disapperas usually in February, while the lower maximum migrates toward lower altitudes at the end of the winter. The persistence of meridional flow from the north at Churchill during the entire year indicates fairly permanent large scale pressure systems in the northern latitudes. Preliminary results from Point Barrow show an average temperature profile with the smallest absolute lapse rate yet observed, 0.67°C per km from 40 to 70 km. As at Churchill, a steady northerly component exists, indicating the existence of a high pressure cell over the North Pacific and Gulf of Alaska, and low pressure over the North Atlantic.

## ACKNOWLEDGMENTS

The authors gratefully acknowledge the contribution of Philip C. Swartz of GSFC for processing the data to final form; Superior Engineering Company for fabrication and pre-launch preparations of the payload; New Mexico State University's Physical Science Laboratory for rocket trajectory data; and Texas Western College's Schellenger Research Laboratory for sound ranging support.

## REFERENCES

1. Nordberg, W., and Stroud, W. G., "Seasonal, Latitudinal and Diurnal Variations in the Upper Atmosphere," NASA Technical Note D-703, April 1961.

2. Horvath, J. J., and Simmons, R. W., "Measurements of Upper Atmospheric Parameters by the Pitot-Static Technique," *Trans. Am. Geophys. Union,* 45(4):617, December 1964 (abstract).

3. Smith, W., Katchen, L., Sacher, P., Swartz, P., and Theon, J., "Temperature, Pressure, Density and Wind Measurements with the Rocket Grenade Experiment, 1960-1963," NASA Technical Report R-211, October 1964.

4. Webb, W., "Stratospheric Solar Response," *J. Atmos. Sci.* 21(6):582-591, November 1964.

5. Leovy, C., "Radiative Equilibrium of the Mesosphere," *J. Atmos. Sci.* 21(3):238-248, May 1964.

6. Murgatroyd, R. J., and Singleton, F., "Possible Meridional Circulations in the Stratosphere and Mesosphere," *Quart. Jour. of the Royal Meteorological Society,* 20(3):213-225, May 1963.

7. Newell, R. E., "Preliminary Study of Quasi-Horizontal Eddy Fluxes," *J. Atmos. Sci.* 20(3):213-225, May 1963.

8. Groves, G. V., "Meteorological and Atmospheric Structure Studies with Grenades," in: *Space Research IV: Proceedings of the 4th International Space Science Symposium, Warsaw, Poland, June 1963,* ed. by P. Muller, Amsterdam: North-Holland Pub. Co., 1964, pp. 155-170.

9. Witt, G., Martin-Lof, J., Wilhelm, N., and Smith, W. S., "High Altitude Summer Mesospheric Temperatures and Wind with Particular Regard to Noctilucent Clouds," in: *Space Research V: Proceedings of the 5th International Space Science Symposium, Florence, May 12-15, 1964,* ed. by D. G. King-Hele, P. Muller, and G. Righini, Amsterdam: North Holland Pub. Co., 1965, pp. 820-821.

10. Leovy, C., "Simple Models of Thermally Driven Mesospheric Circulation," *J. Atmos. Sci.* 21(4):327-341, July 1964.

11. Kellogg, W. W., "Chemical Heating Above the Polar Mesosphere in Winter," *J. Meteor.* 18(3):373-381, June 1961.

12. Maeda, K., "On the Heating of Polar Night Mesosphere," in: *Proceedings of the International Symposium on Stratospheric and Mesospheric Circulation, Berlin, Germany, 20 to 31 August 1962,* ed. by R. Scherhag, and G. Warnecke, Berlin: Dietrich Reimer, 1963, pp. 451-506.

13. Warnecke, G., and Nordberg, W., "Inferences of Stratospheric and Mesospheric Circulation Systems from Rocket Experiments," in: *Space Research V: Proceedings of the 5th International Space Science Symposium, Florence, May 12-16, 1964,* ed. by D. G. King-Hele, P. Muller, and G. Righini, Amsterdam: North-Holland Pub. Co., 1965, pp. 1026-1038.

14. Teweles, S., "Time Section and Hodograph Analysis of Churchill Rocket and Radiosonde Winds and Temperatures," *Monthly Weather Review* 89(4):125-136, April 1961.

# THE IN-SITU DETECTION OF THE MID-LATITUDE $S_q$ CURRENT SYSTEM

by
K. Burrows*
and
S. H. Hall
*Geophysics Department, Imperial College*

Two British Skylark research rockets, each carrying a proton magnetometer, were flown from the Woomera Rocket Range, South Australia, in March 1964. The first flight merely recorded an approximately inverse cube law variation of magnetic field with height, but on the second flight a magnetic discontinuity of approximately 24$\gamma$ amplitude was recorded. These results are consistent with ground observations at the times of the two flights and they establish experimentally the existence of an electric current system in the E region of the ionosphere over South Australia. The height and vertical thickness of the current are, however, not in close agreement with theoretical predictions.

## INTRODUCTION

The generally accepted basis for the explanation of the observed daily variations in the earth's magnetic field is to be found in the dynamo theory, first postulated by Balfour Stewart in a famous article in the 1882 edition of the Encyclopaedia Britannica (Reference 1). His suggestion arose from the observation that the amplitude of the daily variations increased by a factor of 2 or more during a sunspot maximum, as compared with that during a sunspot minimum. Since this large factor could not be explained in terms of any known physical changes near the surface of the earth, he concluded that the source of the variations must lie in the upper atmosphere and must, therefore, be an electric current. Schuster (Reference 2), Chapman (Reference 3), and other workers later elaborated the dynamo theory and, using magnetograms recorded at various observatories throughout the world, they were able to represent the complex and changing array of magnetic variations by a relatively simple system of horizontally stratified sheet currents, stationary relative to the sun, but, relative to an observer on the earth, continuously moving westward and varying in intensity with a predominantly 24-hour period.

*Now at the Goddard Space Flight Center, Greenbelt, Maryland.

According to the dynamo theory, the electric currents are initiated and maintained by a combination of the action of solar tidal winds and the effects of solar radiations on the upper atmosphere. As charged particles are transported across the lines of the force of the earth's magnetic field, electromotive forces deflect the positively charged particles in the opposite direction from the negative ones, thereby generating a current. This current rapidly sets up polarization at the boundaries of the conducting region and the electric fields associated with this polarization further modify the current pattern. This current system is identified by the symbol $S_q$ to differentiate it from other proposed currents responsible for lunar (L) variation and storm-time (D) variation. Since the source of the charged particles is to be found in the horizontal layers of the ionosphere, it follows that, on a worldwide scale, the current system must be predominantly horizontal. The overall current density then depends on the velocity of the tidal winds producing the electromotive forces, on the conductivity of the ionized gases, and on the strength and direction of the earth's magnetic field.

Using routine observatory magnetograms, it is possible to estimate the total current flowing above any part of the earth, but a detailed analysis is not possible from ground data alone. In particular, it is difficult to assess such features as the height, vertical thickness, and any possible stratification of the currents.

With the advent of high altitude sounding rockets in 1946, direct *in situ* measurements of atmospheric properties became possible, and Vestine, La Porte, Lange, and Scott (Reference 4) first suggested that rocket-borne magnetometers could be used to investigate the distribution of these electric currents with height. Accurate determinations of the current density as a function of height at several geographical locations would then test the validity of the dynamo theory and assist in its further development.

Assuming for the moment that the electric currents are located in the ionosphere, it follows that their horizontal dimensions must be large compared with their height and thickness; hence, to an observer on the ground, the $S_q$ current system can be approximated by an infinite sheet current. The magnetic field associated with a current of this nature is $2\pi j$ gauss, where $j$ is the current density in absolute amperes per centimeter and it is independent of the height of the current sheet. Thus, if a rocket vehicle is used to carry a magnetometer which is designed to measure the total scalar geomagnetic field F, it should detect a discontinuous change of approximately $4\pi j \cos I \sin\theta$ in passing through the current, where I is the inclination of the geomagnetic field below the horizontal and $\theta$ is the angle between the direction of the current flow and the local magnetic north.

In addition to the measurements of various atmospheric current systems, rocket-borne magnetometers could be used to obtain more detailed information on the morphology of the earth's main magnetic field and secular variations and to check the validity of the various attempts which have been made to describe the geomagnetic field in terms of a spherical harmonic analysis.

A comprehensive summary of the various circumstances in which worthwhile magnetic measurements should be carried out from rockets has been given by Chapman (Reference 5). In addition to his recommendations for flights during magnetic disturbances, he further suggests that

measurements of the current systems be undertaken in low and middle latitudes during periods of magnetic calm in order to confirm the existence of the $S_q$ current system and to investigate its morphology.

The first *in situ* detection of an ionospheric current was made in a pioneering rocket flight by Singer, Maple, and Bowen (Reference 6). They installed a total-field flux-gate magnetometer in an Aerobee rocket which reached a height of 105 kilometers at a point very close to the magnetic equator and succeeded in detecting a magnetic discontinuity of 400 ± 50$\gamma$.

Cahill (Reference 7) has reported a further series of equatorial flights using rockoons which were instrumented with proton magnetometers and were launched from ships. Two flights from the vicinity of Jarvis Island reached heights of 120 and 130 kilometers and detected anomalous departures from a dipole field of -150$\gamma$ and -300$\gamma$, respectively, the experimental error in the observations being ±20$\gamma$. The second flight also indicated some stratification of the electrojet into two layers, though the upper layer was not completely penetrated.

Magnetic anomalies of several hundred gammas associated with localized intense electric currents in auroras have also been detected (Reference 8). A number of other rocket flights have taken place in latitudes away from the geomagnetic equator, but the successful detection of the $S_q$ current system in these latitudes has not been reported (References 9-13).

In consideration of the dynamo theory, the magnetic equator constitutes a special case in which electric fields caused by polarization effects in the ionosphere indirectly result in a considerable enhancement of the current density during the middle daylight period in a band approximately 3° of latitude wide; this results in a magnetic discontinuity of magnitude several hundred gamma as detected by a rocket-borne magnetometer. In midlatitudes, however, the $S_q$ magnetic variations are much smaller, and hence the problem of detecting the postulated ionospheric currents is more difficult.

## ESTIMATED GEOMAGNETIC EFFECTS

A rough estimate of the amplitude of a discontinuity, which might be expected in the total scalar force in passing through the postulated electric current above Woomera, can be made as follows:

The rocket launching site at Woomera, from where British Skylark rockets are normally fired, is at latitude 30°56'S, longitude 136°31'E, geomagnetic latitude -41.0°.

Figure 1 shows the position of Woomera at local midday and midnight relative to the $S_q$ current system, as given by Chapman and Bartels (Reference 14). It is immediately evident that the focus of the southern pattern passes very close to Woomera. In fact the magnetograms recorded at Gnangara in western Australia (latitude 31°47'S) indicate that the focus passes to the north of that observatory on about 60 percent of days, to the south on about 10%, and overhead on about

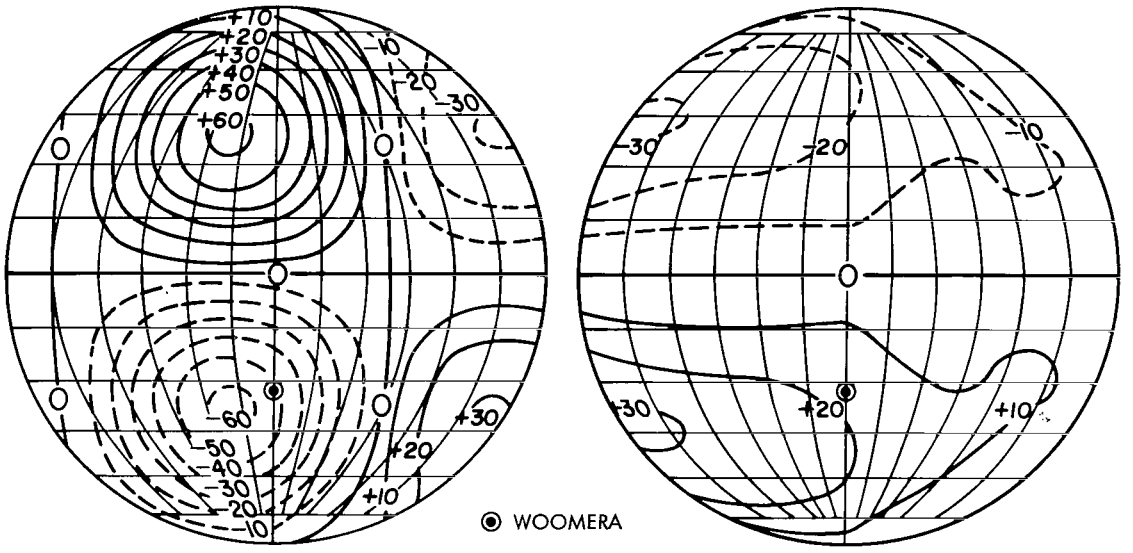


Figure 1—The position of Woomera relative to the $S_q$ current system for the equinox of a sunspot minimum (left) at midday as viewed from the sun, and (right) at midnight as viewed from the night hemisphere (after Chapman and Bartels). The flow between adjacent current lines is 10,000 A.

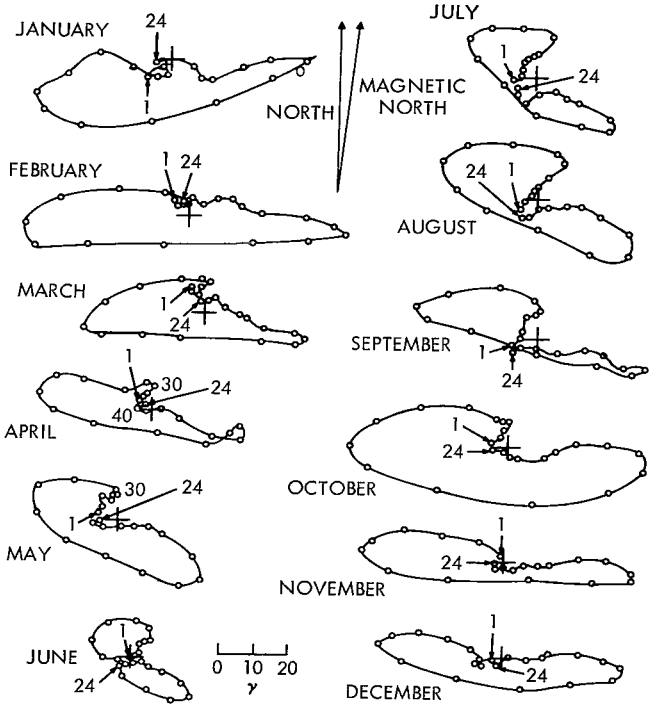


Figure 2—Vectorgrams showing the mean hourly variation in X and Y on the five international quiet days for the months of 1938 at Watheroo, Western Australia. The corresponding monthly means are indicated by crosses.

30 percent.* Normally, therefore, Z, the vertical component of F, shows the greatest diurnal variation at ground level. Z is, however, continuous in passing through the current sheet and so cannot contribute appreciably to any discontinuity.

Figure 2 shows the mean monthly variations in X and Y, the horizontal components of F, for quiet days during 1938 at the Watheroo Magnetic Observatory (30°19'S, 115°53'E, geomagnetic latitude -41.8°, longitude 185.6°). Since the observatory at Watheroo (now removed to Gnangara) was at approximately the same magnetic latitude as Woomera, it is reasonable to assume that the magnetograms from an observatory at Woomera would be very similar at corresponding local times. In Figure 2 the E-W component Y shows maximum variation but, since this component is almost normal to F, it will contribute very little and hence, it is the variation in X which can be expected to be mainly responsible for any discontinuous

*Private communication from P. M. McGregor, Mundaring Geophysical Observatory, Western Australia.

change in F. The maximum value of $\Delta X$ occurs at 0900 ± 1 hours in August, when its value is about $20\gamma$ different from the nighttime value. Since at least 25% of this will be due to induced earth currents, the actual discontinuity in X will be roughly $0.75 \times 2 \times 20 = 30\gamma$, and this leads to an estimated discontinuity in F of $30 \cos 63 = 14\gamma$, since the inclination at Woomera is 63°. Thus the average discontinuity which might be expected in passing through the $S_q$ current over Woomera is about an order of magnitude less than that which has been detected at the geomagnetic equator. The actual effect that might be encountered on any given day could, of course, vary considerably according to the precise location of the focus of the current system and the magnetic conditions prevailing at the time.

## INSTRUMENTATION

The magnetometer and data-processing techniques which were used for these flights have been discussed in detail, together with the results of an instrument-proving flight (Reference 15). Although a horizontal component magnetometer would have simplified the problem of detecting an $S_q$ current discontinuity, the Skylark rocket cannot yet be stabilized to the degree required for useful measurements of magnetic components; a total force instrument was therefore developed using the principle of nuclear free precession (References 16-19). The data from this instrument are in the form of damped sine waves, the frequency of which is an analog of the total scalar magnetic force; it produces approximately one absolute determination of F per second.

In view of the small anticipated magnetic discontinuity, it was essential to remove the sensing head well out of range of the magnetic field perturbations due to various other rocket instrumentation. In a standard Skylark rocket, the two principal sources of magnetic interference are the mild steel tube of the Raven motor and the magnet of the 6-centimeter magnetron used in the Missile Tracking System. Accordingly, the MTS magnetron was enclosed inside a magnetic shield and the magnetometer sensor was mounted on the end of a flexible pneumatic probe.

During the rocket's ascent through the atmosphere, the probe was folded inside a 12-inch diameter canister mounted in the main body of the rocket. After the rocket had passed through the dense atmosphere, the spent motor tube was ejected by means of three pneumatically operated plungers, and the probe was deployed to its full length of 20 feet, at which range the residual magnetic fields associated with the rocket were less than $1\gamma$. This technique considerably simplified the problem of maintaining adequate magnetic cleanliness in other rocket instrumentation.

In the two rocket flights discussed in this paper, the proton magnetometer was classed as a secondary experiment, the primary object of the flights being the measurement of the flux of $\gamma$ rays in the primary cosmic radiation (Southampton University). The rockets also carried sporadic E detectors (University College, London), X-ray cameras (Leicester University), and, for attitude and performance determination, sun slits, flux gates, rate gyroscopes, and accelerometers (Royal Aircraft Establishment, Farnborough).

In conjunction with the rocket flights, a ground proton magnetometer (Reference 20) was operated to record the diurnal variation in F, and a flux-gate instrument, kindly loaned by the

Bureau of Mineral Resources, Melbourne, recorded H, the horizontal component. H was selected as being that component of the $S_q$ variation field which is discontinuous in passing through the postulated current sheet as discussed above.

In flight the rockets were tracked by means of kine-theodolites, radar type FPS 16, and the MTS beacon transmitter, all standard range facilities at Woomera. Each rocket was powered by a combination of a Raven solid fuel motor and a "cuckoo" booster. A full description of the Skylark sounding rocket has been given by Hazell and Dorling (Reference 21).

## DATA PROCESSING

During flight the proton precession signals were relayed via the standard Skylark 465 telemetry system (Reference 22) and recorded, together with a standard 50-kilocycle reference signal and timing code, on an Ampex multichannel tape recorder.

During playback the signal-to-noise ratio of the raw data was improved by means of a manually controlled tracking filter and the signals were mixed with a suitable reference frequency derived from the 50-kilocycle standard recorded on the same tape. By this means variations in precession frequency due to tape speed variations were compensated to first order.

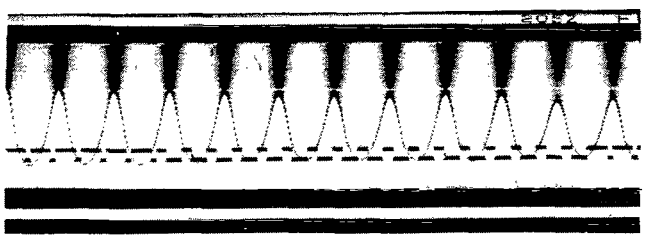

Figure 3—Sample record of beats obtained by processing of raw data (duration of record approximately 0.25 second).

A full description of the apparatus and the data reduction technique has been given by Burrows (Reference 15). Figure 3 shows a sample of the beats obtained on flight SL 129 by this method recorded together with a 1 millisecond timing code.

The precession frequencies, and hence magnetic field readings, were computed manually by counting the number of beats in a time, measured from the timing code, and adding the beat frequency thereby derived to the accurately known reference frequency. The advantage of this manual technique over a fully automatic approach is that, where the signal is of amplitude comparable with noise or interference, the regular beats can be seen and random noise rejected.

## RESULTS

### Ground Data

Figure 4 shows the records of the diurnal variation in F obtained from the ground proton magnetometer at Woomera for seven consecutive days, starting on the date of the first rocket flight. The instrument measures the period of 1024 cycles of the precession signals in units of $10^{-5}$ seconds and records the last two digits; in the ambient field at Woomera this corresponds to a

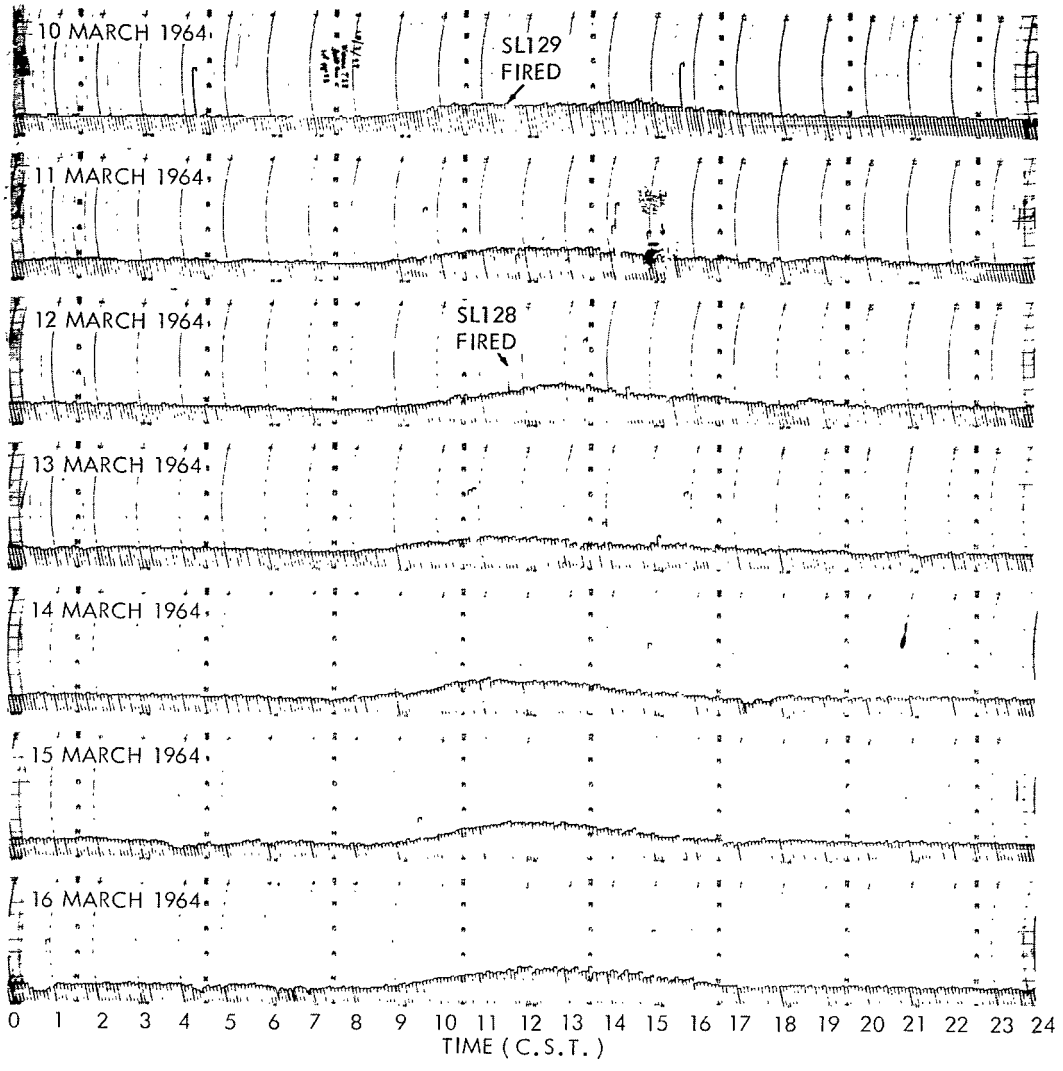


Figure 4—Ground proton magnetometer records, 10-16 March 1964, Woomera. Full-scale deflection of each record is 143$\gamma$. Timing marks are local time at Woomera (U.T.+9 1/2 hours).

full scale deflection of 143$\gamma$. Since the first three digits were invariant at 413, the absolute value of the total force of the geomagnetic field was typically 58,210$\gamma$. In making the records of Figure 4, the instrument was set to take one reading per five minutes. It should be noted that all seven records are similar in general form and amplitude of the peak diurnal variation; indeed all the records taken on magnetically undisturbed days during the three months the instrument was in operation at Woomera are similar in character to those reproduced in Figure 4.

Figure 5 shows the H magnetograms recorded by the flux-gate magnetometer at Woomera on 10 and 12 March 1964, the days of the two rocket flights. A comparison of Figures 4 and 5 indicates that on 10 and 12 March the diurnal variations in F were very similar in amplitude (21$\gamma$ and 24$\gamma$,

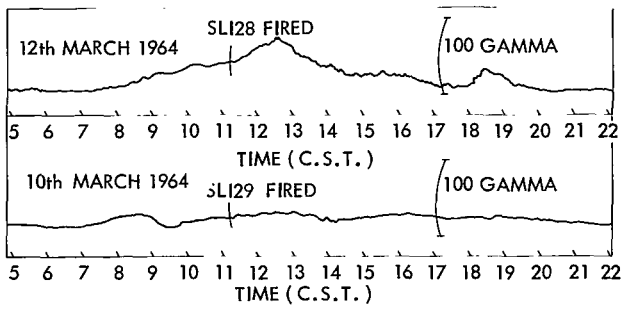


Figure 5—Variation of H on the days of the rocket flights (field strength decreasing upward). Timing marks are local time at Woomera (U.T.+9 1/2 hours).

respectively), whereas there was a much larger negative variation in H on the second day. This suggests that on 10 March the focus of the $S_q$ current pattern passed nearly overhead at Woomera, whereas on 12 March it was at a significantly lower latitude. Therefore, a much more suitable day for the detection of a magnetic discontinuity at Woomera was 12 March.

## Flight Data

Skylark SL 129 was fired at 02:06 Universal Time (1136 Australian Central Standard Time) on 10 March 1964; it reached a height of 175 kilometers and impacted at a point 77 kilometers down range on a bearing of 326.6°T relative to the launcher. Skylark SL 128 was fired at 02:07 Universal Time (1137 ACST) on 12 March 1964; it reached a height of 175 kilometers and impacted at a point 77 kilometers down range on a relative bearing of 285.7°T, approximately 54 kilometers from the impact point of SL 129. On both flights the proton magnetometers functioned satisfactorily and produced data continuously from the time of probe deployment until the sensing head was torn off as the rockets re-entered the earth's atmosphere.

The accuracy of each reading depends on the attitude of the rocket at the time, as a consequence of the variation of signal amplitude with the angle between the axis of the sensing head and the geomagnetic vector (Reference 15); hence, as the rockets tumbled in flight, the scatter of the readings about the mean values varied from less than $1\gamma$ to a maximum of about $10\gamma$. All the readings obtained have, however, been used in the computations and discussions which follow. The first one or two readings of each flight are of dubious value as, at this time, the probes were still being inflated and the sensing heads were probably still under the influence of the rocket's magnetic fields.

It is well known that rotational motions of a proton-sensing head introduce a frequency modulation in the precession signal (References 23 and 24). In practice, however, the flux-gate data showed that Skylarks 129 and 128 precessed with periods of 23 seconds and 35 seconds, respectively; the errors from this cause, though detectable, are small and have been neglected.

The magnetometer data have been compared with values of magnetic total force calculated on the basis of spherical harmonic analyses using coefficients derived by Leaton, Malin, and Evans (Reference 25), Cain, Shapiro, Stolarik, and Heppner (Reference 26), Cain, Hendricks, Daniels and Jensen (Reference 27), and Cain and Hendricks (Reference 28). The values of measured field minus computed field (defined as DEL) which were obtained from two of the reference fields are shown in Figures 6 and 7.

The overall agreement between measured and computed fields depends mainly on the coefficients used, but also there is a second-order difference between the upward and downward sections

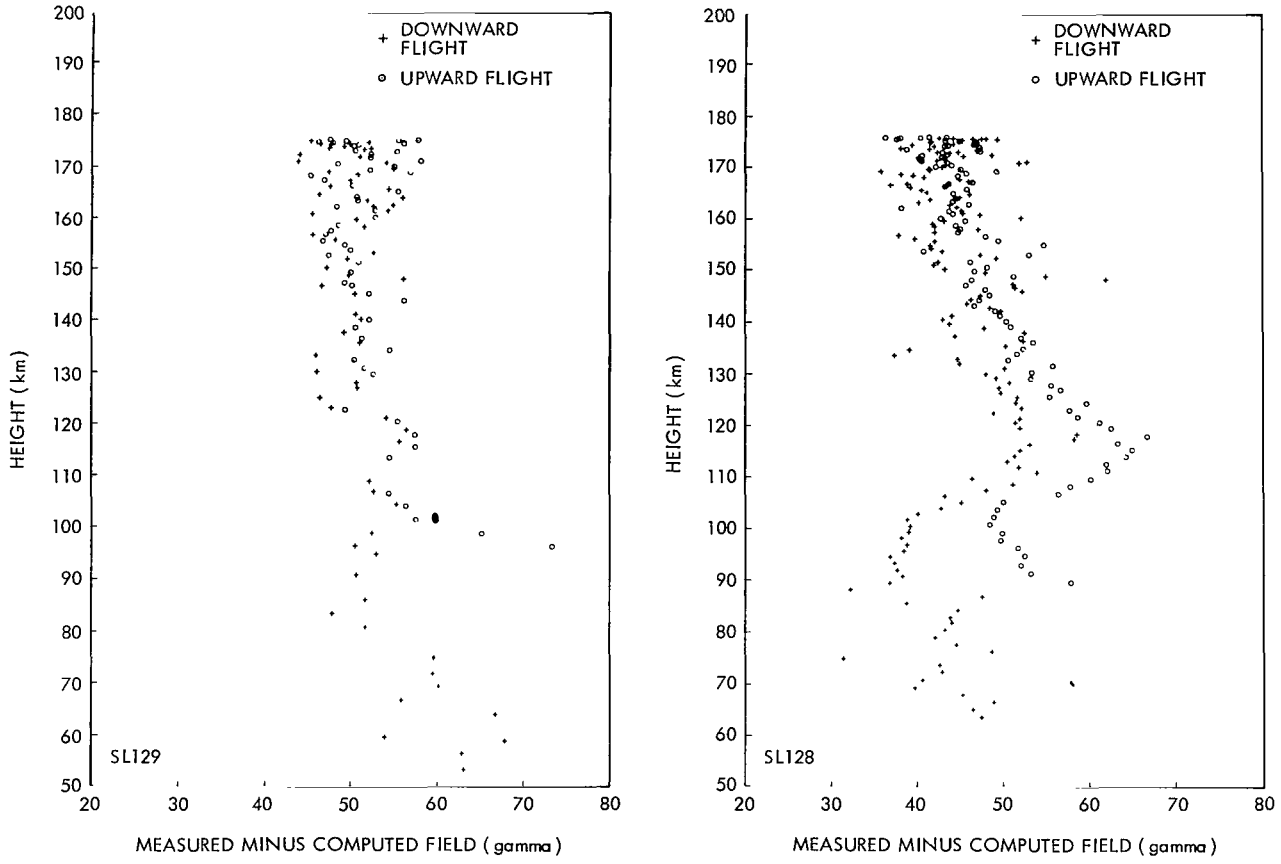


Figure 6—Comparison of measured values of total force with computed values as a function of height: left, SL 129; right, SL 128; Leaton et al. coefficients.

of each flight. Thus when April 1964 coefficients are used, the values of DEL obtained during the upward flight of SL 128 are in close agreement with the downward flight values, but there is a large scatter in the data from flight SL 129; using the Leaton et al. coefficients leads to a better agreement for SL 129, whereas the upward and downward flights can now be resolved in flight SL 128 (Figures 6 and 7). As noted earlier, the trajectories of the two rockets were significantly different, and these secondary discrepancies must reflect the different gradients of the errors in the two computed fields along the tracks of the two rockets.

In order to provide a quantitative comparison between the abilities of the various reference fields accurately to describe the earth's main field at the particular location of Woomera, the values of DEL at the apogee of flight SL 128 are listed below:

| Coefficients | DEL |
|---|---|
| Leaton et al. (Reference 25) | + 44 ± 3$\gamma$ |
| Vanguard A (Reference 26) | - 75 ± 3$\gamma$ |
| April 1964 (Reference 27) | -118 ± 3$\gamma$ |
| Vanguard B (Reference 28) | -992 ± 3$\gamma$ |

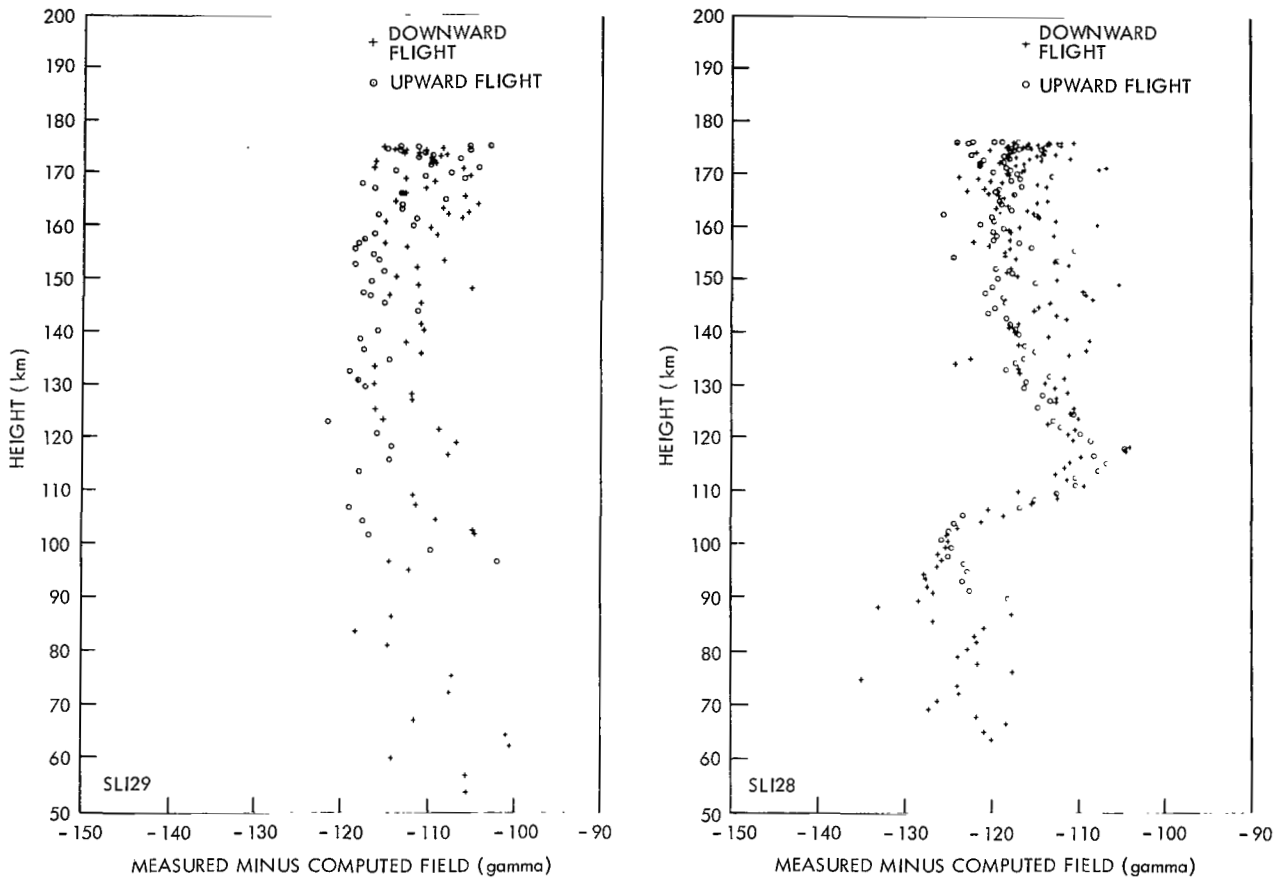


Figure 7—Comparison of measured values of total force with computed values as a function of height: left, SL 129; right, SL 128; April 1964 coefficients (Reference 28).

In spite of these differences in detail as between the flight results using different reference fields, the general form of the variation of DEL with height is consistent, regardless of which coefficients are used in calculating the reference fields.

## IONOSPHERIC CURRENTS

As stated above, Figure 5 shows that the flight of SL 129 took place when the focus of the $S_q$ current system was close to overhead at Woomera and the value of $\Delta H$ recorded at the time of the flight is close to the mean value. It is not therefore surprising that the flight data in Figure 7 (left) do not show any significant discontinuity which could with confidence be attributed to a current sheet.

The flight of SL 128, however, occurred when the magnetic conditions at Woomera were much more favorable for the detection of a discontinuity. As discussed above, at the time of the flight the flux-gate magnetometer recorded a significant departure from the nighttime value (Figure 5).

The $K_p$ index for the appropriate 3-hour period was 4 (Reference 29), but the proton magnetometer record shows that, at Woomera, the diurnal magnetic variation was normal and undisturbed except for minor fluctuations (Figure 4). The reduced data from the rocket-borne magnetometer show an unmistakable change in slope at a height of about 104 kilometers followed by a return to the original slope at about 115 kilometers (Figure 7, right). This indicates that during this time the rocket passed through an electric current and the sign of the discontinuity confirms that the current was flowing in a direction having a westerly component. This anomaly is recorded on both the upward and downward parts of the flight. The absence of any similar discontinuity during the rest of the flight up to apogee indicates that no other current system of comparable magnitude was flowing in this height range at the time of the rocket flight.

In order to measure the amplitude of the magnetic discontinuity and to compare it with that which would be anticipated on the basis of ground data, the upward and downward flight data are each plotted separately in Figure 8, since they constitute two independent measurements. The mean relative displacement of the upper and lower parts of the curves is 24 ± 3$\gamma$. This experimental value can be compared with one calculated on the basis of the ground data, as described above. At the time of the flight, the deviation of H from the undisturbed nighttime value was -35 ± 2$\gamma$, the uncertainty being due to the difficulty in selecting the undisturbed value. This leads to an expected discontinuity in F of between 23 and 26$\gamma$, making the approximations and the assumptions discussed above.

The magnetic discontinuity which was observed in flight therefore agrees very closely, both in amplitude and in sign, with what would be anticipated on the basis of the ground observations at the time. This lends support to the belief that, at the latitude of Woomera, the currents responsible for the normal diurnal magnetic variations are concentrated almost entirely in a single layer extending from approximately 104 kilometers up to approximately 115 kilometers in the E-region of the ionosphere; furthermore, on the basis of the assumption that 25 percent of the observed diurnal variations are due to induced earth currents, these results also imply that any nighttime ionospheric currents must be much smaller than those which have been demonstrated to flow during the daytime.

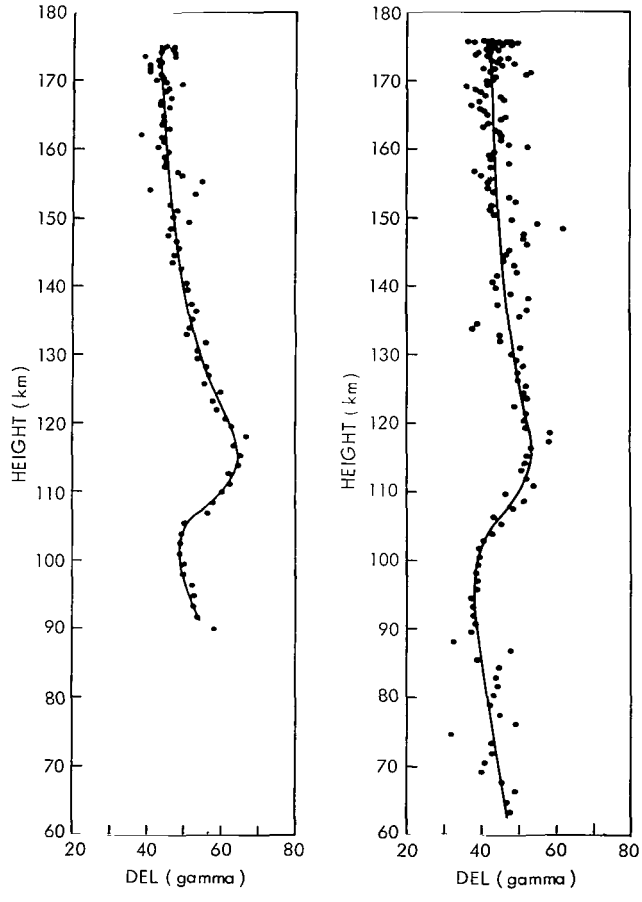


Figure 8—Magnetic discontinuity detected by Skylark SL 128; left, upward flight; right, downward flight.

18. Waters, G. S., and Francis, P. D., "A Nuclear Magnetometer," *J. Sci. Instr.*, 35(3):88-93, March 1958.

19. Burrows, K., " Rocket-borne Magnetometer," *J. Brit. IRE*, 19(12):769-776, December 1959.

20. Burrows, K. "Geomagnetic Measurements in a Rocket Vehicle," Ph.D. thesis, London University, 1963.

21. Hazell, J. F., and Dorling, E. B., "British Sounding Rocket-Skylark," in: *Sounding Rockets*, ed. by H. D. Newell, Jr., New York: McGraw-Hill Book Co., Inc., 1959, pp. 243-251.

22. Rae, W. M., "The Airborne Sender for 24-channel Telemetry," *J. Brit. IRE*, 21(1):57-67, January 1961.

23. Bloom, A. L., "Nuclear Free Precession in a Moving Vehicle," Varian Associates Technical Memorandum, Palo Alto, California, 1955.

24. Hall, S. H., "The Modulation of a Proton Magnetometer Signal Due to Rotation," *Geophys. J.*, 7(1):1-22, September 1962.

25. Leaton, B. R., Malin, S. R. C., and Evans, J. J., "An Analytical Representation of the Estimated Geomagnetic Field and its Secular Change for the Epoch 1965.0," *IAGA Symposium on Magnetism of the Earth's Interior*, Pittsburgh, Pennsylvania, November 1964.

26. Cain, J. C., Shapiro, I. R., Stolarik, J. D., and Heppner, J. P., "Measurements of the Geomagnetic Field by the Vanguard 3 Satellite," NASA Technical Note D-1418, October 1962.

27. Cain, J. C., Hendricks, S., Daniels, W. E., and Jensen, D. C., "Computation of the Main Geomagnetic Field from Spherical Harmonic Expansions," GSFC Document X-611-64-316, October 1964.

28. Cain, J. C., and Hendricks, S., "Comments on the Vanguard 3 Magnetic Field Data and Analysis," *J. Geophys. Res.*, 69(19):4187-4188, October 1, 1964.

29. Lincoln, J., "Geomagnetic and Solar Data," *J. Geophys. Res.*, 69(15):3283-3296, August 1, 1964.

30. Baker, W. G., and Martyn, D. F., "Conductivity of the Ionosphere," *Nature*, 170:1090-1092, December 27, 1962.

31. Fejer, J. A., "Semidiurnal Currents and Electron Drifts in the Ionosphere," *J. Atmospheric Terrest. Phys.*, 4:184-203, December 1953.

32. Chapman, S., "The Electrical Conductivity of the Ionosphere: A Review," *Nuovo Cimento Suppl.* 4(4):1385-1412, 1956.

33. Ratcliffe, J. A., and Weekes, K., "The Ionosphere," in: *Physics of the Upper Atmosphere*, ed. by J. A. Ratcliffe, New York: Academic Press, 1960, pp. 377-470.

34. Maeda, K., and Matsumoto, H., "Conductivity of the Ionosphere and Current System," *Rept. Ionosphere Space Res.* Japan, 16 (Part 1):1-26, March 1962.

35. Kochanski, A., "The Circulation in the Stratosphere, Mesosphere, and Lower Thermosphere," WMO Technical Note, ed. by R. J. Murgatroyd, (in press).

# ROCKET MEASUREMENTS OF MIDLATITUDE $S_q$ CURRENTS

by
T. N. Davis, J. D. Stolarik and J. P. Heppner
*Goddard Space Flight Center*

Rubidium-vapor magnetometers were flown to altitudes near 150 kilometers over Wallops Island, Virginia in four Nike-Apache rockets. Two flights were made at times when no ionospheric current was expected and none was encountered. The other two flights measured a current sheet with lower edge at 105 kilometers and upper edge at 123 kilometers, with the total current being in agreement with that expected from the ground observations.

## INTRODUCTION

Ionospheric currents have been detected by rocket-borne magnetometers flown into the equatorial electroject (References 1 and 2), the auroral electrojet (Reference 3) and in the northern polar cap (Reference 4). Similar attempts to detect midlatitude ionospheric currents have been generally unsuccessful until this year (Reference 5) because of one or more of the following problems: uncertain knowledge of the reference magnetic field, rocket trajectory errors, low precision of the magnetic field measurement, the low current density in the midlatitude ionosphere, and the relative insensitivity of total field magnetometers to the magnetic effects of horizontal sheet currents at high magnetic inclination. This paper presents the results of four rocket flights performed at Wallops Island, Virginia (38 degrees N, 75 degrees W) during the period June-October 1964. In the series, double gas cell rubidium-vapor magnetometers were flown in Nike-Apache rockets to altitudes near 150 kilometers.

The change in magnitude of the total magnetic field ($\Delta F$) measured by a magnetometer on its passage through a horizontal current sheet with height-integrated current J per unit width is given exactly by the law of cosines or with negligible error by $4\pi J \cos I \sin\phi$ where I is the inclination of the main magnetic field and $\phi$ is the horizontal angle between the current direction and the direction of H. Due to the $\sin\phi$ dependence of the measured $\Delta F$, the rocket-borne magnetometer is most sensitive to longitudinal (i.e., east-west) currents. At the surface of the earth these produce variations primarily in H, the horizontal intensity, rather than D, the declination, which is sensitive to meridional currents.

A variation in the horizontal component observed at the ground, $\Delta H_{obs}$, consists of a component $\Delta H_{ex}$, due directly to ionospheric current, and a component $\Delta H_{in}$, due to current induced in the earth.

Assuming the ratio $\Delta H_{ex}/\Delta H_{in}$ is 1.5, then

$$\Delta H_{obs}(\gamma) = 1.67\,\Delta H_{ex} = (1.67)(2\pi J) = (1.67)(2\pi)\left(\frac{\Delta F}{4\pi \cos I}\right)$$

$$= 2.44\,\Delta F(\gamma)$$

where J is the height-integrated current per unit width and the inclination I is taken as 70 degrees; $\Delta F$ is the change in the scalar field as the rocket magnetometer passes through the current sheet.

## INSTRUMENTATION

This study is the first making use of rubidium vapor magnetometers flown in small rockets to study ionospheric currents. In this magnetometer the Zeeman splitting of atomic energy levels in Rb-85 vapor is detected as resonance absorption of light from a Rb-85 source. The frequency of resonance, the Larmor frequency, is a direct measure of the total scalar magnetic field intensity by the relationship

$$f(\text{cps}) = 466744F \pm (K)359\,F^2$$

for a one cell magnetometer where F is in gauss and K, usually <0.5, indicates the fraction of the constant with $F^2$ that appears in a given instrument. Here a self-oscillating, cross-coupled, dual cell arrangement is used to largely eliminate the $F^2$ dependence so that the variation with orientation is small, less than $\pm 2\gamma$ at F = 0.5 gauss. Dual (or single) cell rubidium magnetometers have null regions (regions of low signal amplitude) of conical shape centered on the instrument optical axis and in the form of a zone centered on the plane perpendicular to the optical axis; the instruments flown in this study have conical nulls of half-angle near 10 degrees and zonal nulls of half-width 5 degrees or less.

In each rocket the magnetometer sensor was mounted in the forward end of the nose cone with the magnetometer optical axis inclined 45 degrees to the rocket axis. In this orientation and with the rocket spin-stabilized at 5-6 revolutions per second, null regions were avoided since the magnetic field inclination at Wallops Island, Virginia is 70 degrees.

The Larmor frequency output of each magnetometer was used to phase-modulate a 231.4-megacycle, 2-watt telemetry transmitter fed to a quadrapole antenna located at the base of the payload. Other payload components included a battery pack consisting of 20 HR1 silver cells to supply power for the magnetometer and transmitter, a switching module containing partially-shielded relays for switching operations on the ground, and a DOVAP (doppler) transponder for trajectory determination to supplement and check the radar tracking. The DOVAP transponder was connected to 36.8-megacycle (input) and 73.6-megacycle (output) shroud antennas attached to the Apache rocket motor.

Magnetic materials in the payload components were kept to a minimum and care was used to reduce possible current loops in the payload wiring. The greatest possible separation between the magnetometer sensor and the other payload components was maintained. The structural parts of the payload and the nose cone were constructed primarily of fiberglass to reduce permanent and induced magnetic fields. As a result, the magnetic contribution of each payload was $2\gamma$ or less as measured at the position of the sensor in a zero ambient field.

It is necessary to maintain the magnetometer sensor lamp bulb and absorption cell temperatures within a narrow range for proper operation. The payloads contained circuits allowing measurement and control of the lamp bulb and absorption cell temperatures prior to rocket firing. In flight, the heat output from the lamp together with thermal insulation about the sensor sufficed to maintain operating temperatures within allowable limits.

## DATA RECOVERY AND REDUCTION

On the ground the Larmor frequency-modulated telemetry signal is received and the Larmor frequency is recorded on magnetic tape together with a reference frequency, time-code and tape-recorder speed-lock reference signal. Using a system designed primarily for reduction of satellite data, the rubidium Larmor frequency is counted to an accuracy of one part in $5\times10^6$. This accuracy is achieved by use of the rubidium signal to gate the interval over which a 5-megacycle reference signal is counted. Thus, if a sample period of 0.1 second is desired, the Larmor frequency can be measured sufficiently accurately to allow a 0.5 gauss magnetic field to be determined with a precision of 0.1 gamma. Once the Rb-85 Larmor frequency is counted, a value of the scalar magnetic field is found representing the average field over the sampling interval. In a high-speed computer, radar or DOVAP trajectory data are merged with the magnetometer data. At the midpoint of each sampling interval, the location of the rocket is calculated and for that location a reference magnetic field is computed using the coefficients of a spherical harmonic expansion of the geomagnetic field. The computed reference field ($B_c$) is subtracted from the measured field ($B_m$); the value of $B_m - B_c$ is then available for printing or automatic plotting versus time or spatial parameters.

## PRESENTATION OF DATA

### Magnetic Conditions

Wallops Island, Virginia lies to the north of the focus of the equivalent current system derived from the world-wide $S_q$ magnetic variations. The normal variations on undisturbed days is typified by the reproduction of the Fredericksburg magnetogram in Figure 1 (Fredericksburg is 180 kilometers to the west of Wallops Island). The Z component shows minor variation; eastward and westward declinations appear in the morning and afternoon hours, respectively, and the maximum negative H deviation occurs one to two hours before local noon. Thus the maximum change in the total field $\Delta F$ measured by a rocket-borne magnetometer on its passage through the ionospheric current sheet is expected just prior to noon when $|-\Delta H|$ is greatest.

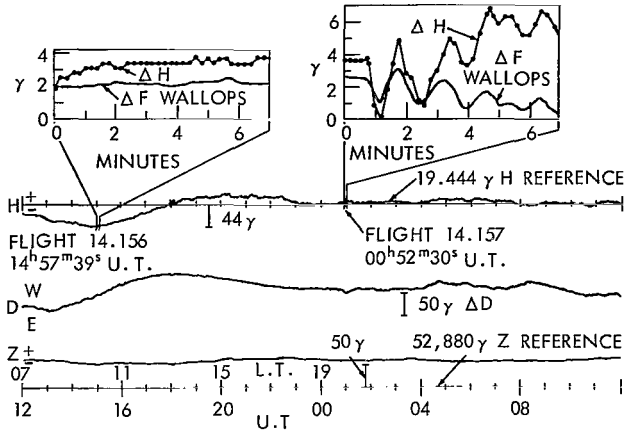


Figure 1—Tracings of the Fredericksburg magnetogram for June 25, 1964 showing the times of flights 14.156 and 14.157. Panel inserts indicate the detailed magnetic variations during each flight: ΔH from the Fredericksburg rapidrun recording; ΔF from a helium magnetometer operated at Wallops Island. Date is given for left-hand portion of the diagram.

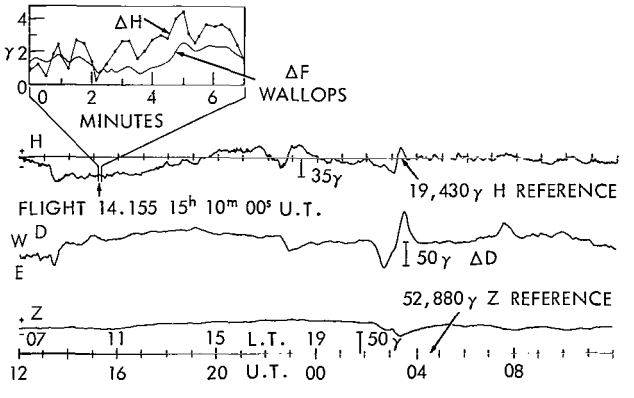


Figure 2—Tracings of the Fredericksburg magnetogram for June 10, 1964 with a panel insert showing the detailed magnetic variations during flight 14.155. See also the title for Figure 1.

One of the flights (Fl. 14.157) was made on the day represented in Figure 1 during an interval in which no ionospheric current was expected on the basis of study of the Fredericksburg magnetic recordings obtained on the several days preceding the flight. The H reference line of Figure 1 represents the value of H deduced for the condition of no overhead current. One minute after the commencement of Fl. 14.157, a small pulsation event occurred; its maximum peak-to-peak amplitude was 5$\gamma$ in H and 2$\gamma$ in F (see the upper right panel of Figure 1).

Flight 14.156 was launched earlier in the same local day at a time when ΔH at the ground was -44$\gamma$, Figure 1. The period represented by Figure 1 was rather quiet magnetically but was not one of the designated 10 quiet days of June 1964; $K_p$ ranged from $1_0$ to $2_0$ and the Fredericksburg K-values were 1 or 2.

A third flight 14.155 was made on June 10, 1964, the most disturbed day in June, Figure 2. At the time of the flight $K_p$ was $3_0$ and the Fredericksburg K-value was 2. As in the case of Fl. 14.156, this flight was made during the pre-noon hours when the maximum westward $S_q$ current was expected. Since the flight occurred during a storm period, the horizontal magnetic field was decreased by $D_{st}$ currents presumed to flow well beyond the ionosphere. Examination of the Fredericksburg magnetograms taken on the days before and after June 10 indicates that the $D_{st}$ depression of H amounted to approximately 14$\gamma$ on that day. That determination accounts for the H reference line on Figure 2 being displaced as compared to that on Figure 1. After removal of the $D_{st}$ depression there remains on Figure 2 a -35$\gamma$ deviation in H which one expects to be caused by westward ionospheric currents and related earth-induced currents.

A fourth flight (Fl. 14.159) was launched on October 8, 1964 in conjunction with a sodium-release rocket flight during morning twilight. The Fredericksburg magnetogram covering the period of this flight is reproduced in Figure 3. Although this was not one of the designated quiet days in October, 1964, the level of magnetic activity was not high during the first half of October 8;

$K_p$ ranged from $2_0$ to $3_0$ and the K-value at Fredericksburg was 2 or 3. At the time of Fl. 14.159, the Fredericksburg H-component trace was within 3$\gamma$ of its quiet-day level so the flight was not expected to encounter ionospheric current.

In summary, Fls. 14.157 and 14.159 occurred at times of minimal $\Delta H$ and were not expected to detect sizable ionospheric current. Flights 14.155 and 14.156 occurred when $\Delta H$ was $-33 \pm 7\gamma$ and $-42.5 \pm 2.5\gamma$, respectively; hence these flights should have encountered detectable ionospheric current.

The horizontal paths of the four rocket flights are indicated on a map (Figure 4) showing the magnitude of the total magnetic field at the earth surface as computed from the coefficients of the spherical harmonic expansion of the geomagnetic field given by Leaton and Evans (References 6 and 7). Actual departures from the computed surface field are indicated in the form of contours drawn at 100$\gamma$ intervals. Although the anomaly contours drawn in the upper-left corner of Figure 4 are based on recent comprehensive data, the anomaly values elsewhere in Figure 4 are derived from very few data points obtained over the past 15 years. Consequently, only the gross features of the anomaly map should be considered as meaningful.

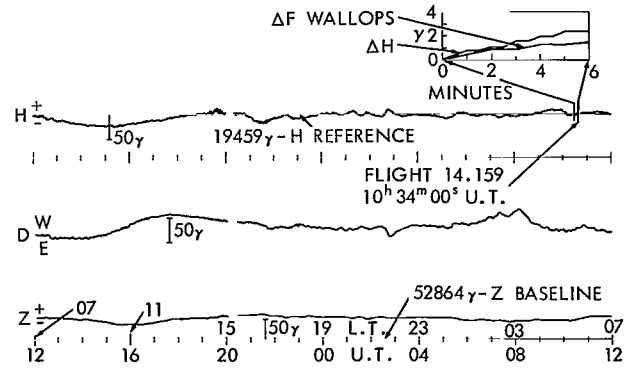


Figure 3—Tracings of the Fredericksburg magnetogram for October 7, 1964 with a panel insert showing the detailed magnetic variations during flight 14.159. See also the title for Figure 1.

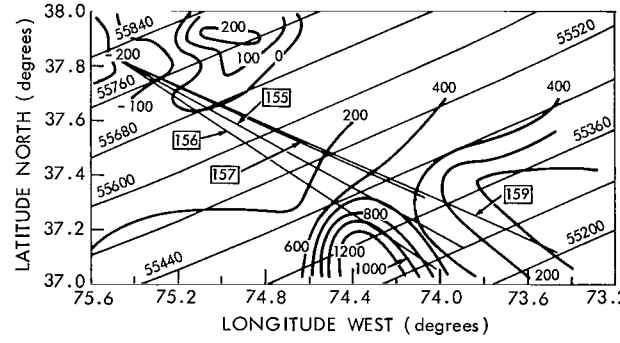


Figure 4—Map showing the horizontal projections of the rocket flights. The parallel lines running from lower left to upper right represent the Leaton and Evans Epoch 1965 reference field at the earth's surface and the curved contours represent the surface anomaly field referenced to the Leaton and Evans field.

The significant features of Figure 4 for our purpose are a generally increasing anomaly field from the launch point (upper left) to the rocket impact points and an isolated region of higher field near the impact point of Fl. 14.156. Relative to the magnetic field computed from the Leaton and Evans coefficients, the rocket magnetometers should measure higher fields near the impact points than measured near the launch point. Flight 14.159 is somewhat of an exception in that its impact point is beyond the main anomalous region.

## Flight Data

The flight data were sampled over a period equal to the appropriate rocket roll period (0.17 to 0.25 seconds). By sampling at this rate, errors which are dependent upon the angular orientation

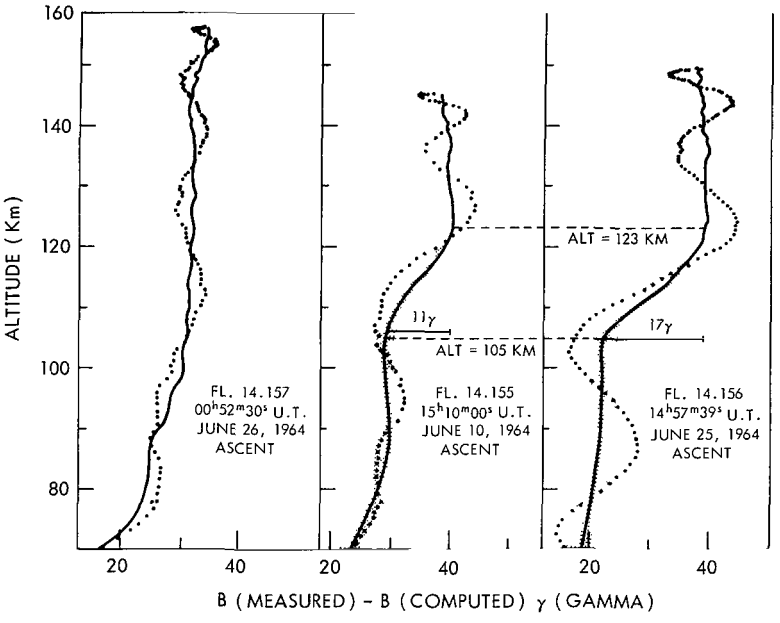


Figure 5—Plots of altitude versus the measured total field minus the computed total field for ascent portions of three flights. Solid lines represent the data corrected for effects due to vehicle precession.

of the rocket measured in the plane perpendicular to its spin axis are averaged out. The result is a measurement of the scalar field independent of the spin and which is precise to within a fraction of $1\gamma$. This measurement gives the magnitude of the vector sum of the local geomagnetic field and the spin-axis component of the rocket's magnetic field. Flight data above altitude 70 kilometers from the ascent portions of Fls. 14.155, 14.156 and 14.157 are shown in Figure 5. (The ascent portion of Fl. 14.159 data is roughly similar to that of Fl. 14.157.)

The data points on Figure 5 exhibit a sinusoidal variation indicating a magnetic contribution along the spin-axis of each rocket and a precessional motion of the rocket with a period near 30 seconds. Although each payload is known to possess a very minor magnetic field ($\leq 2\gamma$), the overall vehicle (payload and attached Apache stage) showed a magnetic field component along the spin axis of 30 to $50\gamma$, as measured during re-entry turn-over. This field was due to magnetic elements within the rocket motor or to currents induced by the high spin rates. Due to the smoothness in the variation of the precession period and angle during the upper portion of each flight, it is possible to apply a precession correction to the data of the form $C \sin \omega t$. The results of such point by point corrections are indicated in Figure 5 by the solid lines drawn through the data points. The shaded regions enclosing the curves for Fls. 14.155 and 14.156 represent a generous estimate of the uncertainty in the precession correction; very little uncertainty exists in the correction applied to Fl. 14.157.

All flight data taken in the region above 80 kilometers are shown in Figure 6 with precession corrections applied. The data obtained below 80 kilometers will be discussed here only to an extent required for the interpretation of the measurements above 80 kilometers. Shortly after launch, when the first stage booster had fallen away, each flight magnetometer measured a field of 100 to $200\gamma$ less than that calculated from the Leaton and Evans reference field. This difference is in accord with that expected from examination of the anomaly map, Figure 4. The ascent portion of each flight shows a steadily increasing value of $B_m - B_c$ with altitude; the rate of increase lessens with altitude to the 90 kilometer level. The lessening rate of increase with altitude evidently reflects the fall-off with distance of the ground anomaly field. Except for Fl. 14.159, the anomaly field appears to have little effect on the ascent data taken above 100 kilometers. As seen in

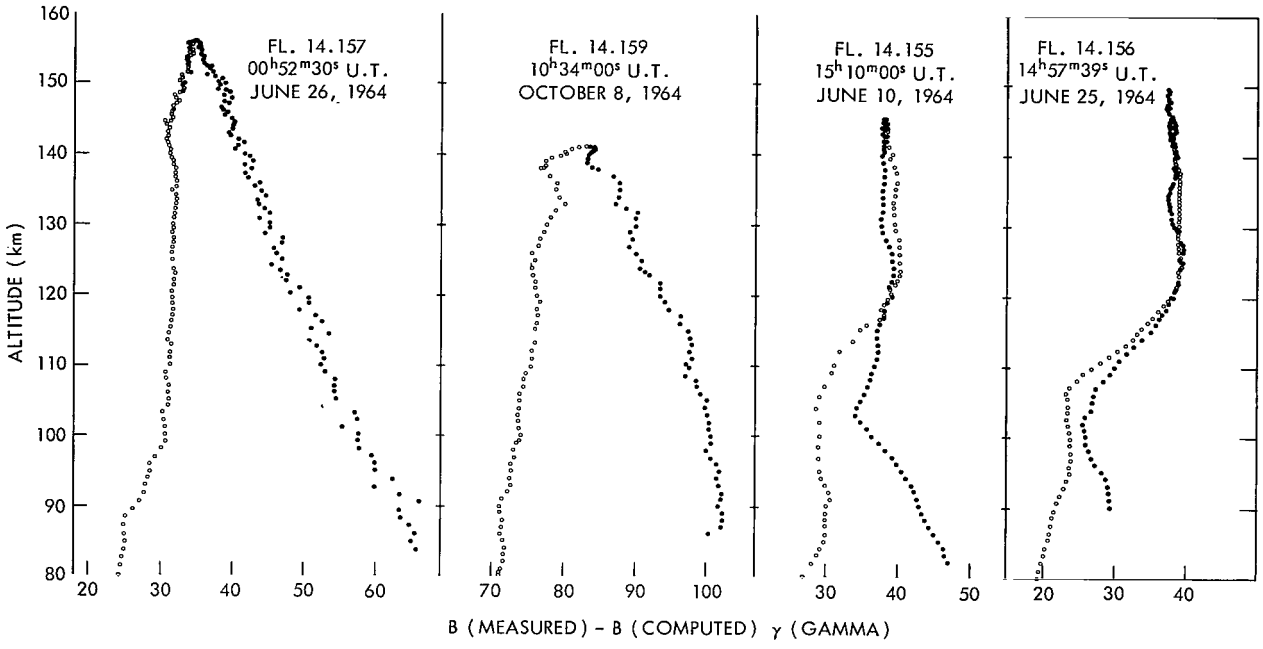


Figure 6—Precession corrected ascent (open-circle) and descent (full-circle) data above altitude 80 km for all flights.

Figure 4, the descent portions of each flight occur over the region of highest surface anomaly field. This is reflected in the measurements at high altitude by the descent $B_m - B_c$ values generally being higher than those measured during ascent (Figure 6).

Below the 100-kilometer level, the descent portions of Fls. 14.155, 14.156 and 14.157 show monotonically increasing $B_m - B_c$ values to rocket impact, at which points the measured fields were $200\gamma$ or more above the Leaton and Evans reference field values. Flight 14.159 passed over the main anomalous region to impact at a point of near-zero surface anomaly and at that point measured a field nearly equal to the reference field value. Flights 14.157 and 14.159 occurred under identical magnetic conditions and along almost identical flight azimuths. The main difference between the flights was the higher apogee and shorter horizontal range of Fl. 14.157 as compared to Fl. 14.159. The characteristics of the high altitude data from these two flights (Figure 6) are very similar. In neither case is there any discontinuity in the region above 80 kilometers that can be attributed to the effect of a current layer in the ionosphere; nor was any expected on the basis of magnetic measurements made on the ground during these flights. In Figure 6, a small change in slope appears near 115 kilometers in the descent portion of the data from Fl. 14.159, but this is the altitude at which the rocket passed over the greatest anomaly measured on its sub-trajectory path. It is not clear whether or not the 14.157 flight magnetometer detected the small pulsation event occurring during the flight but the flight data, especially those taken during the rocket ascent, do indicate that the amplitude of the event could not have been much if any greater at altitude than that observed on the ground.

The ascent data from Fl. 14.155 presented in the central panel of Figure 5 show an increase in $B_m - B_c$ of approximately 11$\gamma$ between the altitudes 105 and 123 kilometers, which indicates the existence of westward current in this height region. The Fl. 14.155 descent data plot, Figure 6, shows a sharp discontinuity at 105 kilometers and possibly one near 125 kilometers, but evidently the effects of the ionospheric current layer are partially masked by the ground anomaly field. For this flight, a deviation of approximately 14$\gamma$ in $|F|$ was predicted from the ground observations on the assumption that 0.6 of the observed $\Delta H$ was due to external currents. Similarly, a deviation in $|F|$ of 17$\gamma$ was predicted for Fl. 14.156. Both the ascent and descent plots, Figures 5 and 6, from this flight show discontinuities at 105 and 123 kilometers. The field change in the upward passage through the current sheet was approximately 17$\gamma$ and the apparent descent field change was near 12$\gamma$. However as in the case of Fl. 14.155, the descent data appear to reflect variations caused both by the ionospheric current and by the ground anomaly.

## SUMMARY AND DISCUSSION

A summary of the results of the four flights together with an estimate of the probable errors, is given in Table 1. An internally consistent interpretation of the flight data requires magnetic

Table 1

Summary of the Results from the Four Flights with an Estimate of the Probable Errors.

| | Flight 14.157<br>$00^h\ 52^m\ 30^s$ U.T.<br>26 June 1964 | Flight 14.159<br>$10^h\ 34^m\ 00^s$ U.T.<br>8 October 1964 | Flight 14.155<br>$15^h\ 10^m\ 00^s$ U.T.<br>10 June 1964 | Flight 14.156<br>$14^h\ 57^m\ 39^s$ U.T.<br>25 June 1964 |
|---|---|---|---|---|
| Observed $\Delta H$ At Ground | $+3.7 \pm 2.5\gamma$ | $-3.0\gamma \pm 2.5\gamma$ | $-33.0 \pm 7\gamma$ | $-42.5 \pm 2.5\gamma$ |
| Predicted $\Delta F$ From Ground Observations, Assuming $f = \frac{\Delta H_{ex}}{\Delta H_{obs}} = 0.6$ | $+1.5 \pm 1\gamma$ | $-1.2 \pm 1\gamma$ | $-13.5 \pm 3\gamma$ | $-17.5\gamma \pm 1\gamma$ |
| $\Delta F$ Observed in Flight | Ascent: $0 \pm 1\gamma$<br>Descent: $0 \pm 2\gamma$ | Ascent: $0 \pm 2\gamma$<br>Descent: $0 \pm 2\gamma$ | Ascent: $-11 \pm 2\gamma$<br>Descent: ? | Ascent: $-17 \pm 2\gamma$<br>Descent: $-12 \pm 2\gamma$ (?) |
| Altitude of Lower Edge of Current Sheet | - | - | Ascent: 105 ± 1km<br>Descent: 104 ± 1km | Ascent: 106 ± 1km<br>Descent: 105 ± 1km |
| Altitude of Maximum Current Density | - | - | Ascent: ~116km (?)<br>Descent: (?) | Ascent: ~110km (?)<br>Descent: ~113km (?) |
| Altitude of Upper Edge of Current Sheet | - | - | Ascent: 123 ± 1km<br>Descent: (?) | Ascent: 123 ± 1km<br>Descent: 123 ± 1km |
| Total Westward Horizontal Current | - | - | Ascent: 25.6 ± 1.5 Amperes/km<br>Descent: (?) | Ascent: 39.4 ± 1.5 Amperes/km<br>Descent: >26 Amperes/km |

contributions from both ionospheric current and ground anomalies. The ground anomaly contribution to the ascent data is minor and poses no interpretative problem. However, the descent portions of all flights pass over an appreciable anomaly which has sufficient magnetic contribution at altitude to prevent a quantitative determination of the ionospheric current contribution from the descent data alone. Since the anomaly magnetic field adds vectorially to the geomagnetic field, a quantitative treatment of its effect on the flight data requires more complete knowledge of the surface anomaly field than is available from the sparse observations now in hand.

The data from the two flights (Fls. 14.155 and 14.156) which penetrated a detectable current layer indicate a simple westward current sheet lying between altitudes 105 and 123 kilometers with the altitude of maximum current density between 110 and 116 kilometers. The total current within the sheet is in good agreement with that expected from the ground measurements.

## ACKNOWLEDGMENTS

We are grateful to Mr. J. C. Seddon for his efforts in providing final trajectories from the DOVAP data. Mr. G. F. Hinton, United States Navy Oceanographic Office, provided total field magnetic data from a helium magnetometer operated at Wallops Island, Virginia.

REFERENCES

1. Singer, F. S., Maple, E., and Bowen, W. A., Jr., "Evidence for Ionospheric Currents from Rocket Experiments Near the Geomagnetic Equator," *J. Geophys. Res.* 56(2):265-281, June 1951.

2. Cahill, L. J., "Investigation of the Equatorial Electrojet by Rocket Magnetometer," *J. Geophys. Res.* 64(5):489-503, May 1959.

3. Meredith, L. H., Davis, L. R., Heppner, J. P., and Berg, O. E., "Rocket Auroral Investigations," *Annals of the IGY*, 12(pt. 2):631-640, 1961.

4. Cahill, L. J., "Detection of an Electrical Current in the Ionosphere above Greenland," *J. Geophys, Res.* 64(10):1377-1380, October 1959.

5. Burrows, K., and Hall, S. H., "*In Situ* Detection of an Ionospheric Electric Current," *Nature*, 204(4960):721-722, November 21, 1964.

6. Leaton, B. R., and Evans, M. J., "An Analytical Representation of the Estimated Geomagnetic Field and Its Secular Change for the Epoch 1965.0," presented at the Symposium on Magnetism of the Earth's Interior, Pittsburgh, Nov. 1964.

7. Cain, J. C., Hendricks, S., Daniels, W. E., and Jensen, D. C., "Computation of the Main Geomagnetic Field from Spherical Harmonic Expansions," GSFC Document X-611-64-316, 1964.

Appendix A

## Glossary of Terms

B — Total scalar magnetic field

D — Declination of the magnetic field

F — Total magnetic field

H — Horizontal intensity component

I — Inclination of the magnetic field

J — Height-integrated current

K — Instrument constant

$S_q$ — Ionospheric current (daily quiet day variation)

# NEUTRON STARS AS X-RAY SOURCES

by
H.-Y. Chiu
*Goddard Institute for Space Studies*

The density of neutron stars is approximately $10^{14}$ g/cm$^3$, with a typical radius of 10 km. At such a high density, the Fermi energy of electrons is of the order of a few hundred Mev, in which the gas is mainly composed of neutrons, thus, nuclei cannot exist. Thought to be a remnant of supernova processes, the neutron star, formed at a temperature $\gtrsim 10^{10}$ °K, cools down, in a matter of a few weeks via neutrino processes, to a temperature of about $5 \times 10^8$ °K. Henceforth, the loss of energy is through surface blackbody emission with a luminosity in the range of 1 $L_\odot$ to $10^3$ $L_\odot$. This corresponds to a surface temperature of $10^6 \rightarrow 10^7$ °K, where most energy is in the wavelength band of 1 Å $\rightarrow$10Å. Neutron stars are, therefore, potential cosmic x-ray emitters if they exist.

The radiation characteristics of neutron star type x-ray sources is also discussed. We have found that the source Scorpius X-1 (ScXR-1) is the most likely selection and further measurements on the angular diameter of this source will be fruitful.

## INTRODUCTION

The existence of neutron stars was first proposed in 1931 by Landau (Reference 1) and Zwicky (Reference 2), in which Zwicky had proposed the formation of neutron stars as a mechanism for supernovae. The theoretical structure of neutron stars was later studied by Oppenheimer and Volkoff (Reference 3).

Today, however, there still remain uncertainties in the theory; the main one stems in the neutrino energy loss rate. J. N. Bahcall and R. A. Wolf have suggested a neutrino process, which, if applicable to the density regime of stable neutron stars, will imply that the surface temperature is below $10^5$ °K and hence, will not penetrate the interstellar medium. The uncertainties in the nuclear many body theory preclude a definite statement if this neutrino loss mechanism will operate in these stars. At present, neutron stars still remain as theoretically postulated objects, although as we shall see, they may be potential cosmic x-ray sources and may be detectable by space x-ray experiments.

## STATIC STRUCTURE OF NEUTRON STARS

The existence of neutron stars follows from the theoretical study of general relativity and nuclear physics. Under ordinary density conditions ($\leq 10^{11}$ g/cm$^3$), neutrons are unstable and will later decay into protons, electrons, and neutrinos with a lifetime of $10^3$ seconds. As the density of matter is increased, the zero-point energy or Fermi energy of the electrons is increased. Thus, at a density of $10^7$g/cm$^3$, the value of the Fermi energy per electron exceeds 1 Mev and the following type of inverse beta reactions,

$$e^- + (Z, A) \rightarrow (Z - 1, A) + \nu \ , \qquad (1)$$

will take place after which the number of electrons will decrease and the nuclei will become more neutron enriched. When a density of $10^{11}$g/cm$^3$ is reached, the Fermi energy of the electrons will be sufficiently increased enough to cause the complete disintegration of all nuclei, leaving only neutrons to exist, as is the case in the stable form of matter. The decay of neutrons is prevented by the presence of a small amount of electrons.

The typical density of a neutron star is of the order of $10^{15}$g/cm$^3$, which is a few times the density of nuclear matter and the radius of one solar mass, corresponding to this density, is around 10 kilometers.

The theory of the formation of these stars is very incomplete because the density is $10^8$ greater than the highest density observed ($\sim 10^6$g/cm$^3$, which is the density of white dwarfs). It is believed that neutron stars are formed during the collapse of a star to become a supernova. This collapse problem must be treated by using the general relativistic hydrodynamical theory. Although no quantitative results are yet available, a few theories have been presented (References 4 and 5).

Because of the high concentration of matter in neutron stars, the space-time curvature is large and the general relativity theory must be used to describe the structure. If the space-time curvature is *too* great, implying too large a mass, then the relativity theory predicts that no light signal may leave the mass concentration. Such a state is referred to as the "Schwarzschild singularity" and as a consequence, the neutron star cannot be observed, hence an upper limit for the mass exists. The numerical value of the upper limit is a very sensitive function of the detailed interaction among neutrons. At a density of approximately $10^{14}$g/cm$^3$, the average distance between neutrons is about $10^{-13}$cm, or equivalent to the size of a neutron, thus this interaction cannot be neglected. Figure 1 shows two structures of neutron stars obtained by Cameron* by use of two equations of state. These are obtained by two different empirical fits to low energy, nuclear interaction data, within the experimental error. The mass of the neutron star in Figure 1 is expressed as a function of the central density.

*A. G. W. Cameron, private communication.

## OBSERVABLE FEATURES OF NEUTRON STARS

The observational features of neutron stars are not sensitive to their internal structure and can be predicted. The internal temperature upon its formation is approximately $10^{10}$ °K. Because of neutrino processes, this temperature is reduced quickly, in a matter of a few weeks, to a value of the order of $5 \times 10^{8}$ °K. The main neutrino processes are (Reference 6) the Plasma process

$$\gamma \rightarrow \nu_e + \bar{\nu}_e \ , \qquad (2)$$

and the URCA process

$$n + n \rightarrow n + p + e^- + \nu_\mu \ , \qquad (3)$$

and at the density of interest, the process (Reference 7)

$$\pi + n \rightarrow \mu^- + n + \nu_e \ . \qquad (4)$$

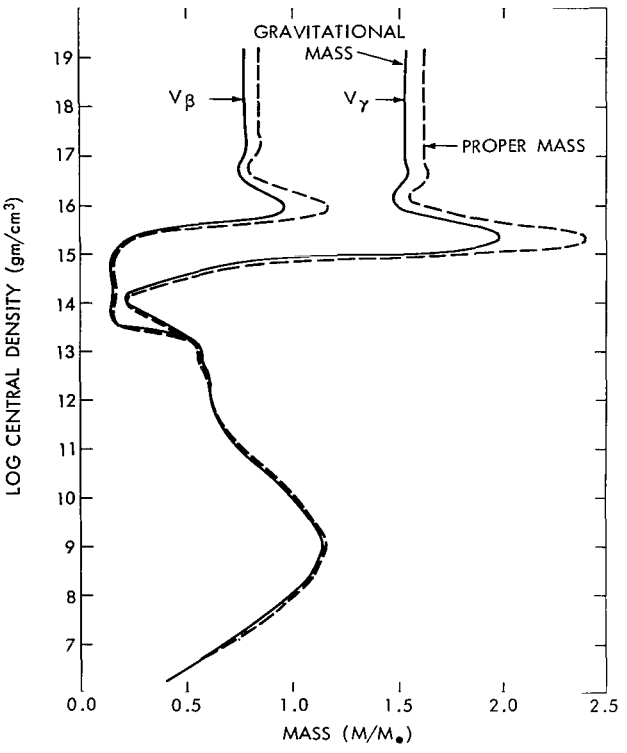


Figure 1 — Central density-mass relationship.

Process 4 is a very rapid one and is important in neutron stars as the rate of cooling would be so great that these stars could not be observed, in which case, $\pi$-mesons would be created at a high density ($10^{14}$ to $10^{18}$ g/cm$^3$). Because $\pi$-mesons interact strongly with the neutron gas, their effective mass (rest mass plus interactive energy) is different from their rest mass. At present, both the sign and the value of the interaction energy (denoted by $E_{int}$) is not known. If $E_{int}$ is > 0, $\pi$-mesons will be created at a density much greater than that of neutron stars and this process will not be of importance. If $E_{int} < -34$ Mev, process 4 cannot take place because of energetic reasons and is replaced by the process

$$\pi^- + n \rightarrow n + e^- + \bar{\nu}_e \ . \qquad (5)$$

The rate of Process 5 is slower than Process 4 by a factor of $10^{-5}$ and if Process 5 is to take place instead of Process 4, the cooling rate is determined by the main neutrino processes and is almost unaffected by Process 5. If $0 < E_{int} < -34$ Mev, then Process 4 would be very important and neutron stars would be unobservable.

Assuming that Process 4 is not important, the most likely internal temperature of neutron stars is of the order of $5 \times 10^{8}$ °K. The surface temperature is around 1/100 of the internal temperature and this value is hardly affected by the detailed structure of the neutron star (References 8 and 9),

thus, the surface temperature is about 8 x $10^6$ °K and the lifetime of a neutron star at this surface temperature is approximately $10^4$ years. The thickness of the outer layer of neutron stars that supports the temperature gradient is approximately 1 meter. Figure 2 shows the typical temperature-age relationship for these stars of two masses (Reference 11).

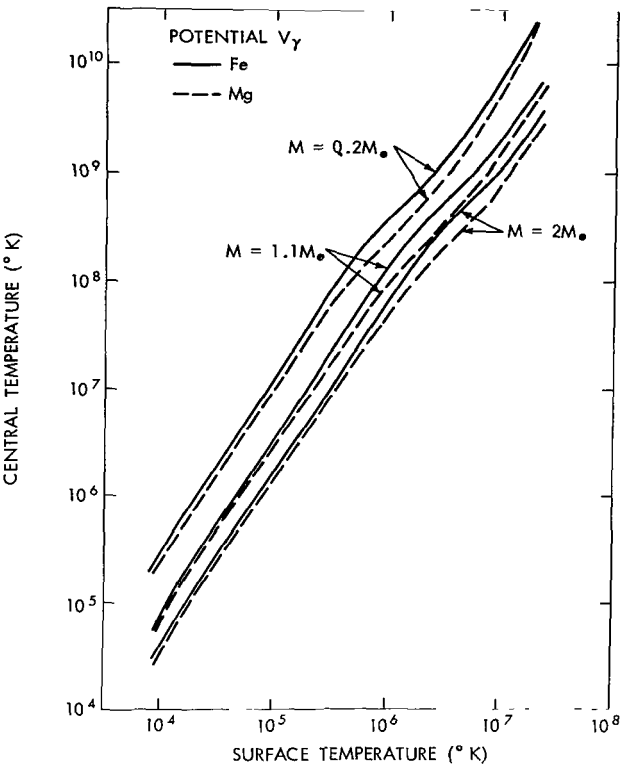


Figure 2 — Typical temperature-age relationship.

## CONCLUDING REMARKS

At present, there exists a large uncertainty as to whether neutron stars are x-ray sources, and this uncertainty may be resolved either by a better theoretical study of the properties of nuclear matter or by observation.

Of the 20 odd x-ray sources already discovered, most can be excluded from being neutron stars (Reference 10). Observationally, one expects to find the following characteristics of such a star:

1. An angular diameter below the resolution limit of any instrument. The angular diameter of a neutron star is $\lesssim 10^{-10}$ seconds of an arc.
2. Most of the energy is in the 1Å – 10Å band region with temperatures of 1 to 8 x $10^6$ °K.
3. A neutron star x-ray source is *not necessarily* accompanied by any visible nebulosity, or any radio source.

Of all sources discovered, the only possible candidate is Scorpius X-1. With a radius of less than 7 minutes of arc, Scorpius X-1 has no radio source or any visible nebulosity associated with it.

As long as our knowledge of nuclear physics is not complete enough to exclude or include (Process 4), the case of neutron stars as x-ray sources is still not closed.

## REFERENCES


1. Landau, L., "On the Theory of Stars," *Physik. Z. Sowjetunion*, 3(1):285-288, January 1932.
2. Zwicky, F., "On Collapsed Neutron Stars," *Astrophysical J.* 88(4):522-525, November 1938.
3. Oppenheimer, J. R., and Volkoff, G. M., "On Massive Neutron Cores," *Phys. Rev.* 55(4):374-381, Feburary 1939.

4. Chiu, H. Y., "Supernovae, Neutrinos and Neutron Stars," *Annals of Physics,* 26(3):364-410, February 1964.

5. Colgate, S. A., and Johnson, M. H., "Hydrodynamic Origin of Cosmic Rays," *Phys. Rev. Letters,* 5(6):235-238, September 1960.

6. Chiu, H. Y., and Salpeter, E. E., "Surface X-ray Emission from Neutron Stars," *Phys. Rev. Letters,* 12(15):413-415, April 1964.

7. Bahcall, J. N., and Wolf, R. A., "Neutron Stars," *Phys. Rev. Letters,* 14(10):343-346, March 1965.

8. Morton, D., "Neutron Stars as X-ray Sources," *Nature,* 201(4926):1308-1309, March 1964.

9. Morton, D. C., "Neutron Stars as X-ray Sources," *Astrophysical J.* 140(2):460-469, August 1964.

10. Finzi, A., "Cooling of a Neutron Star by the 'URCA' Process," *Phys. Rev.* 137(2B):B472, January 1965.

11. Cameron, A. G. W. and Tsuruta, S., Private communication.

*"The aeronautical and space activities of the United States shall be conducted so as to contribute . . . to the expansion of human knowledge of phenomena in the atmosphere and space. The Administration shall provide for the widest practicable and appropriate dissemination of information concerning its activities and the results thereof."*

—NATIONAL AERONAUTICS AND SPACE ACT OF 1958

# NASA SCIENTIFIC AND TECHNICAL PUBLICATIONS

TECHNICAL REPORTS: Scientific and technical information considered important, complete, and a lasting contribution to existing knowledge.

TECHNICAL NOTES: Information less broad in scope but nevertheless of importance as a contribution to existing knowledge.

TECHNICAL MEMORANDUMS: Information receiving limited distribution because of preliminary data, security classification, or other reasons.

CONTRACTOR REPORTS: Technical information generated in connection with a NASA contract or grant and released under NASA auspices.

TECHNICAL TRANSLATIONS: Information published in a foreign language considered to merit NASA distribution in English.

SPECIAL PUBLICATIONS: Information derived from or of value to NASA activities. Publications include conference proceedings, monographs, data compilations, handbooks, sourcebooks, and special bibliographies.

TECHNOLOGY UTILIZATION PUBLICATIONS: Information on technology used by NASA that may be of particular interest in commercial and other nonaerospace applications. Publications include Tech Briefs; Technology Utilization Reports and Notes; and Technology Surveys.

***Details on the availability of these publications may be obtained from:***

**SCIENTIFIC AND TECHNICAL INFORMATION DIVISION**

**NATIONAL AERONAUTICS AND SPACE ADMINISTRATION**

**Washington, D.C. 20546**